United States
Environmental Protection
Agency

Environmental Sciences Research
Laboratory
Research Triangle Park NC 27711

EPA-600/3-78-059
June 1978

Research and Development

EPA

Computer Modeling of Simulated Photochemical Smog

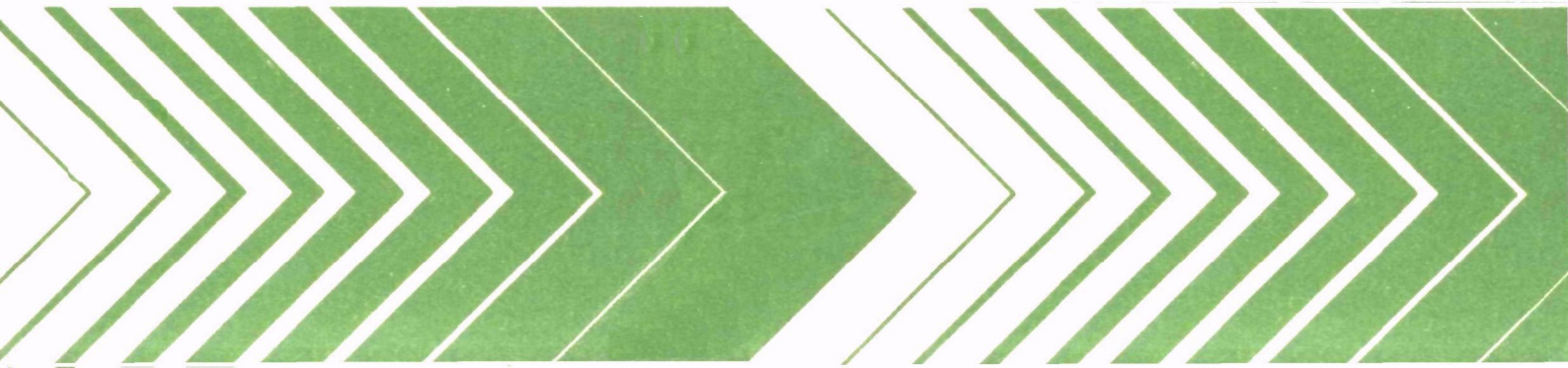

RESEARCH REPORTING SERIES

Research reports of the Office of Research and Development, U.S. Environmental Protection Agency, have been grouped into nine series. These nine broad categories were established to facilitate further development and application of environmental technology. Elimination of traditional grouping was consciously planned to foster technology transfer and a maximum interface in related fields. The nine series are:

1. Environmental Health Effects Research
2. Environmental Protection Technology
3. Ecological Research
4. Environmental Monitoring
5. Socioeconomic Environmental Studies
6. Scientific and Technical Assessment Reports (STAR)
7. Interagency Energy-Environment Research and Development
8. "Special" Reports
9. Miscellaneous Reports

This report has been assigned to the ECOLOGICAL RESEARCH series. This series describes research on the effects of pollution on humans, plant and animal species, and materials. Problems are assessed for their long- and short-term influences. Investigations include formation, transport, and pathway studies to determine the fate of pollutants and their effects. This work provides the technical basis for setting standards to minimize undesirable changes in living organisms in the aquatic, terrestrial, and atmospheric environments.

This document is available to the public through the National Technical Information Service, Springfield, Virginia 22161.

EPA-600/3-78-059
June 1978

COMPUTER MODELING OF SIMULATED PHOTOCHEMICAL SMOG

by

D. G. Hendry, A. C. Baldwin, J. R. Barker,
and D. M. Golden

SRI International
333 Ravenswood Avenue
Menlo Park, California 94025

Contract No. 68-02-2427

Project Officer

Marcia C. Dodge
Atmospheric Chemistry and Physics Division
Environmental Sciences Research Laboratory
Research Triangle Park, North Carolina 27711

ENVIRONMENTAL SCIENCES RESEARCH LABORATORY
OFFICE OF RESEARCH AND DEVELOPMENT
U.S. ENVIRONMENTAL PROTECTION AGENCY
RESEARCH TRIANGLE PARK, NORTH CAROLINA 27711

DISCLAIMER

This report has been reviewed by the Environmental Sciences Research Laboratory, U.S. Environmental Protection Agency, and approved for publication. Approval does not signify that the contents necessarily reflect the views and policies of the U.S. Environmental Protection Agency, nor does mention of trade names or commercial products constitute endorsement or recommendation for use.

ABSTRACT

The photochemical smog chemistries of ethene, propene, butene-1, trans-butene-2, n-butane, 2,3-dimethylbutane, and toluene NO_x systems have been developed and tested with smog chamber data collected at the University of California, Riverside. The mechanisms are composed of critically evaluated kinetic data for the individual reactions to the extent possible. Where data on specific reactions were not available or were not at the appropriate temperature and pressures, thermochemical techniques were used to estimate or extrapolate exising data to obtain the desired rate data. Whenever thermochemical data were estimated to predict rate constants, error bounds were assigned to the estimates and the resulting rate constants. In only a relatively few cases was it necessary to vary the estimated rate constants within the error limits in order to optimize the agreement between computed and experimental concentration-time profiles. Given the kinetic information currently available this general approach minimizes the need for adjustment of rate constants and produces mechanisms that are valid representations of the homogeneous gas-phase chemistry of each of these hydrocarbons in photochemical smog formation.

CONTENTS

FIGURES

FIGURES

FIGURES

FIGURES

FIGURES

TABLES

TABLES

1. INTRODUCTION

To assist the United States Environmental Protection Agency in developing models that describe photochemical smog formation in urban atmospheres, SRI International is continuing to develop explicit mechanisms describing smog forming chemistry of individual hydrocarbons. This report discusses our efforts during the past year to develop mechanisms describing the chemistry of ethene, propene, butene-1, trans-butene-2, n-butane, 2,3-dimethylbutane, and toluene/NO_x systems. Smog chamber data obtained through EPA's laboratory research program at the Statewide Air Pollution Research Center (SAPRC), University of California, Riverside, have been used to test and verify these models.[1]

Our approach to computer modeling is to use critically evaluated kinetic data wherever possible for the individual reactions incorporated in the mechanisms. Where data on specific reactions are not available or are not at the appropriate temperature and pressures, we used thermochemical techniques to estimate the desired rate data. Whenever thermochemical data are estimated to predict rate constants, we assign reasonable error bounds to the estimates and the resulting rate constants. If needed, we vary the estimated rate constants within our error limits to optimize the agreement between computed and experimental concentration-time profiles. One danger of this procedure is that inaccuracies in the model may be artificially compensated for under smog chamber conditions, thereby reducing the reliability of the model when extrapolated to practical atmospheric conditions. By considering the mechanisms for different hydrocarbons together, and only adjusting rate constants as groups within our evaluations, we use the maximum possible data base to guard against fortuitous compensations obscuring difficiencies in the mechansims. We feel that, given the kinetic information currently available, our approach minimizes the need for adjustment of rate constants and produces mechanisms that are a good representation of homogeneous gas-phase smog formation.

Considerable effort has been made to develop detailed models to describe photochemical smog chemistry of individual hydrocarbons. Demerjian, Kerr, and Calvert[2] and Niki, Daby, and Weinstock[3] first attempted to analyze in detail the chemistry of a few systems. Hecht, Seinfeld, and Dodge[4] constructed a more compact mechanism while maintaining important details by attempting to generalize certain reactions. Most recent is the work of Whitten[5] to develop detailed mechanisms for propene and n-butane. At each stage the improvements have been mainly due to better kinetic information about individual reactions.

During this year, the following four major developments in laboratory data set our effort apart from the earlier modeling programs.

(1) It was observed that the reaction

$$HO_2\cdot + NO_2 \longrightarrow HNO_2 + O_2$$

does not occur at a significant rate. Previously the inclusion of this reaction in the models ensured a source of hydroxy radicals throughout a simulation because HNO_2 is readily photolyzed to form OH.

(2) A much higher value was reported for the rate constant of the reaction

$$HO_2 + NO \longrightarrow OH + NO_2$$

than used previously. This change becomes important as NO_x becomes very small late in a smog chamber simulation.

(3) Peroxyacyl nitrates were observed to be thermally labile, according to the reaction

$$RC(O)OONO_2 \longrightarrow RC(O)OO\cdot + NO_2 \quad .$$

This reaction can lead to enhanced ozone formation late in the simulation; it also suggests that there is a whole family of

peroxynitrates, $ROONO_2$, that may affect the overall rate of smog formation.

(4) A breakthrough in the modeling of toluene has resulted from data on the initial products of the reaction of OH and toluene under conditions applicable to the atmosphere. These data make it possible, for the first time, to formulate a detailed mechanism describing chemistry of aromatic/NO_x systems.

2. CONCLUSIONS AND RECOMMENDATIONS

The photochemical smog chemistries of ethene, propene, butene-1, trans-butene-2, n-butane, 2,3-dimethylbutane, and toluene have been developed and tested using SAPRC chamber data. Each mechanism uses the best kinetic data available and is chemically consistent with the others. Some adjustment of unknown rate constants was necessary to give good agreement between simulation and smog chamber experiments. However, relatively few parameters have been adjusted, and although better overall agreement could undoubtedly be obtained by further fitting, it would not necessarily improve the predictability of the models. We believe our present results best represent the current understanding of these complex systems.

Since the ultimate goal of this program is a set of mechanisms that may be reliably extrapolated to conditions other than those where they have been tested, we have attempted to ensure that the reactions represent smog chemistry on an elementary molecular level. Our principal objective was chemical consistency between the different hydrocarbon mechanisms, and particularly between individual experimental runs. We have thus used only one empirical parameter that can vary on a run-to-run basis--the postulated amount of initial nitrous acid. We have adequately simulated most of the experimental runs for seven different hydrocarbons, using consistent chemical mechanisms, rate constants that are thermochemically consistent, and photolysis rate constants that vary only in accordance with reported spectral changes.

For the simulations of single alkene, the computed ozone values average 20.4% high with a range of 33% low to 50% high compared with the observed values. For various alkene mixtures, the calculated ozone averages 7.1% high with a range of 23% low to 90% high (two extreme points dropped). The alkane mechanisms predict ozone values

that average 5.9% high with a range of 30% low to 30% high. For propene-butane mixtures, the computed ozone values are 12.1% low with a range from 36% low to the observed value. The toluene mechanism predicts ozone an average of 20.2% high with a range of 50% low to 90% high.

We believe that chamber uncertainties contribute to the variation in fit between the calculated and observed results. Propene experiments that have been run over a three-year period appear to indicate a variability that is not predicted when variations in known light intensities are taken into account. The effect is one where an experimental run proceeds more slowly the later it occurs in the program. Earlier, where there were insufficient spectral data, the effect was interpreted as aging of the light source. However, in the runs since that time, where there are ample spectral data to correct for any spectral changes, the effect is still occurring. Thus, we believe that either there is variability associated with the ability of the chamber walls to effect the radical concentrations during runs or there are gross errors in spectral data for recent chamber runs, which seems unlikely.

Thus, the most important need in the modeling program is to determine to what degree the chamber walls affect the results in chambers, and whether the effects change gradually with time or whether they change significantly from run to run. In addition, to improve the reliability of the models, more complete data are needed on the products of each of the hydrocarbon reactions. For example, because of lack of product data, we have assigned a fraction of the alkene plus OH reaction to form hydroxycarbonyl compounds. Although the presence of such pathways does not appear to have any large effect on our results, it will significantly affect long-term runs where appreciable amounts of such compounds can become a major source of carbon. Similar uncertainties concerning the products exist in the alkane and toluene mechanisms.

Some of the individual reactions that need further clarification are the alkoxy rearrangement reactions, the photolysis of the various carbonyl compounds in the presence of oxygen, and the reactions of intermediate products from the various systems with OH and ozone.

3. DETAILED CHEMISTRY

3.1 INORGANIC REACTIONS

The inorganic reactions, excluding photolytic reactions, that are used in all the mechanisms are shown in Table 1. This set of reactions is in general well established and has been extensively used.[5,6] Some notable changes to certain rate constants have been made based on recent measurements. The rates of reaction of OH radicals with NO and NO_2 to form HONO and HNO_3 have been increased to 1.0×10^4 ppm^{-1} min^{-1} and 1.5×10^4 ppm^{-1} min^{-1}, respectively.[7,8] Howard[9] has measured the rate of reaction of HO_2 radicals with NO and NO_2 at low pressures ($\sim$ 1 torr) using a flow system with laser magnetic resonance detection. The reaction with NO is not pressure-dependent and we have used the measured rate of 1.2×10^4 ppm^{-1} min^{-1} in our mechanisms. The reaction with NO_2 to form HONO and O_2 was found to be very slow (< 5 ppm^{-1} min^{-1}) and has been omitted from the mechanisms. The rate of formation of peroxynitric acid from HO_2 and NO_2 is more complex, being pressure-dependent, and this is discussed in detail along with the reactions of alkylperoxy radicals with NO_2 (see Section 3.2).

3.2 PEROXYNITRATES

The reaction of peroxy radicals with NO_2 to form peroxynitrates,

$$RO_2 + NO_2 + M \rightleftarrows RO_2NO_2 + M$$

and the reverse reactions are potentially very important in smog chemistry. These reactions may act either as sources or sinks of RO_2 and NO_2, depending on how the concentrations of RO_2 and NO_2 vary during the experiment. Very few experimental data are available on these reactions; however, we have attempted to estimate the rates of the association and the decomposition reactions and their pressure dependence on the basis of what is known.

TABLE 1. INORGANIC REACTIONS

No.	Reaction	Rate Constant[a]	Reference
1-1	$O(^3P) + O_2 + M \rightarrow O_3 + M$	2.0×10^{-5} [b]	10
1-2	$O(^3P) + NO_2 \rightarrow NO + O_2$	1.3×10^{4}	11
1-3	$O_3 + NO \rightarrow NO_2 + O_2$	2.5×10^{1}	12
1-4	$O(^1D) + M \rightarrow O(^3P) + M$	8.6×10^{4}	13
1-5	$O(^1D) + H_2O \rightarrow 2OH$	5.1×10^{5}	13
1-6	$O_3 + OH \rightarrow HO_2 + O_2$	8.7×10^{1}	14
1-7	$O_3 + HO_2 \rightarrow OH + 2O_2$	1.2	13,14
1-8	$O_3 + NO_2 \rightarrow NO_3 + O_2$	5.0×10^{-2}	13,12
1-9	$O_3 \rightarrow$ wall	1.0×10^{-3} [c]	10
1-10	$NO_3 + NO \rightarrow 2NO_2$	1.3×10^{4}	15
1-11	$NO_3 + NO_2(+ M) \rightarrow N_2O_5(+ M)$	5.6×10^{3}	13
1-12	$N_2O_3 + H_2O \rightarrow 2HNO_3$	5.0×10^{-6}	16
1-13	$N_2O_5(+ M) \rightarrow NO_2 + NO_3(+ M)$	2.4×10^{1} [c]	13
1-14	$NO + NO_2 + H_2O \rightarrow 2HONO$	2.2×10^{-9} [b]	17
1-15	$2HNO_2 \rightarrow NO + NO_2 + H_2O$	1.3×10^{-3}	17
1-16	$NO_2 + OH(+ M) \rightarrow HNO_3(+ M)$	1.5×10^{4}	8
1-17	$NO + OH(+ M) \rightarrow HONO (+ M)$	1.0×10^{4}	18,7
1-18	$NO + HO_2 \rightarrow NO_2 + OH$	1.2×10^{4}	9
1-19	$NO_2 + HO_2 \rightarrow HO_2NO_2$	3.0×10^{3}	d
1-20	$HO_2NO_2 \rightarrow HO_2 + NO_2$	0.2[c]	d
1-21	$HO_2 + HO_2 \rightarrow H_2O_2 + O_2$	2.0×10^{9}	19
1-22	$CO + OH \rightarrow HO + CO$	2.1×10^{2}	13,20

[a] Units in ppm^{-1} min^{-1} unless otherwise indicated.

[b] Units in ppm^{-2} min^{-1}.

[c] Units in min^{-1}.

[d] See Section 3.2.

The only direct measurement of the rate of these reactions is by Howard,[9] who measured the rate of combination of HO_2 and NO_2 in the third-order low-pressure limit (M = N_2).

$$HO_2 + NO_2 + N_2 \rightleftarrows HO_2NO_2 + N_2 \quad . \qquad (1,-1)$$

Our procedure has been to estimate the rate of combination of HO_2 with NO_2; assuming this has no activation energy, we calculate the A-factor for the decomposition from the overall entropy change, using the known entropies of HO_2 and NO_2 and a reasonable estimate for HO_2NO_2. We then estimate the bond strength $D(HO_2-NO_2)$, which gives us a complete set of rate parameters in the high-pressure limit. By performing an RRKM calculation, we calculate the pressure dependence of the rates and the low-pressure limit rate, which may be compared with Howard's measurement.

Since E_1 is assigned as zero, k_{1_∞} the high pressure limit of k_1 must equal A_{1_∞}. An estimate of A_{1_∞} based on the analogous reaction of of alkyl (ethyl + isopropyl) radicals using the geometric mean rule[21] yields $k_{1_\infty} = A_{1\infty} = 10^{10.2}\ M^{-1}\ s^{-1}$. Howard[10] has measured the rate of reaction of HO_2 with NO as $10^{9.7}\ M^{-1}\ s^{-1}$; the rate with NO_2 should be similar or a little slower. Batt et al.[22] have measured the rate of decomposition of methyl nitrate, from which they calculate the rate of combination of methoxy radicals (isoelectronic with HO_2) and NO_2 to be $10^{9.7\pm.6}\ M^{-1}\ s^{-1}$.

An absolute upper limit must be $k_1\infty = 10^{10.5}\ M^{-1}\ s^{-1}$ and a reasonable lower limit on the basis of the foregoing estimates would be $10^{9.5}\ M^{-1}\ s^{-1}$. The entropy of HO_2NO_2 can be estimated with reasonable accuracy to be 71.6 e.u., based on a measured value for $MeONO_2$. This yields A_{-1} in the high-pressure limit [assuming reaction (1) has no activation energy] to be between $10^{16.4}$ and $10^{17.4}\ s^{-1}$, requiring $E_{-1} = 23.0$ kcal mol^{-1} to fit the low-pressure limit data. The best estimate for E_{-1} is 27.0 kcal mol^{-1}, based on $D(CH_3C(O)O_2-NO_2)$ measured by Hendry and Kenley,[23] which requires that A_{-1} be between $10^{17.0}$ and $10^{18.0}\ s^{-1}$, and $S_o(HO_2NO_2) = 69.0$ e.u. to fit the low-pressure data.

The above rate parameters with the corresponding pressure dependences are summarized in Table 2; note that the falloff behavior depends only on k_1 as k_{-1} in the high-pressure limit is adjusted to yield the measured value of the rate in the low-pressure limit. The details of the RRKM calculation are also summarized in Table 2. For each limit of k_1^∞, two sets of parameters for k_{-1}^∞ are derived by fitting the low pressure data. Each set of parameters leads to the same falloff corrections once k_1^∞ is defined.

TABLE 2. PRESSURE DEPENDENCE OF THE DECOMPOSITION OF PEROXYNITRIC ACID

	$k_1^\infty = 10^{9.5}$[a] Hindrance = 98%		$k_1^\infty = 10^{10.5}$[a] Hindrance = 80%	
$S^0(HO_2NO_2)$/e.u.	71.6	69.0	71.6	69.0
E_{-1}^∞/kcal mol^{-1}	23.0	27.0	23.0	27.0
$\log_{10} A_{-1}^\infty$/s^{-1}	16.4	17.0	17.4	18.0
P/torr	k_1/k_1^∞ or k_{-1}/k_{-1}^∞		k_1/k_1^∞ or k_{-1}/k_{-1}^∞	
0.1	1.4×10^{-4}		1.4×10^{-4}	
1.0	1.1×10^{-3}		1.4×10^{-3}	
5.0	5.1×10^{-3}		6.1×10^{-3}	
20.0	1.7×10^{-2}		2.2×10^{-2}	
100.0	6.2×10^{-2}		9.5×10^{-2}	
760.0	2.4×10^{-1}		5.1×10^{-1}	
1000.0	2.8×10^{-1}		6.3×10^{-1}	

[a] Units in M^{-1} s^{-1}.

Collisional efficiency = 0.4; Temperature = 300 K.

The RRKM calculation used a hindered rotational Gorin model for the transistion state.[24] The percentage hindrance used is given in Table 2.

The other parameters for HO_2 and NO_2 in the transition state were taken from the JANAF tables.[19] Vibrational frequencies of HO_2NO_2 were taken from data of Niki et al.[25] or were estimated from H_2O_2 and HNO_3. From the data in Table 2, the value of k_1 can range from 2000 to 4000 ppm^{-1} min^{-1}, whereas k_{-1} can range from 0.01 to 10 min^{-1}. In developing the models, we have used k_1 = 3000 ppm^{-1} min^{-1} and k_{-1} = 0.2 min^{-1}. Subsequent to our work, Pitts has obtained k_{-1} = 9 min^{-1}. Using this value in place of the value that was used has relatively little effect. The largest effect is at the high concentrations of the more reactive hydrocarbons, where ozone may increase by 10 to 20%.

The rates of reaction of alkylperoxy radicals with NO_2 are expected to be similar to HO_2 and NO_2; k_1 may be slightly slower with large alkyl groups. At 300 K and 1 atmosphere, even the smallest alkylperoxy radicals should be close to their high-pressure limit rate. The actual rate constants used in the mechanisms were determined empirically to give the best fit to the propylene data, and are listed in Table 7.

3.3 ALKOXY RADICALS

Alkoxy radicals are extremely important intermediates in smog chemistry because most of the reacted hydrocarbon appears as alkoxy radicals before undergoing further reactions. Alkanes react by abstraction to form alkyl radicals, and alkenes react by addition to form hydroxyalkyl radicals. The alkyl radicals so formed undergo a fast addition reaction with oxygen to form alkylperoxy radicals, which react with NO to form alkoxy radicals and NO_2,

$$R\cdot + O_2 \rightarrow RO_2\cdot \qquad (2)$$

$$RO_2\cdot + NO \rightarrow RO\cdot + NO_2 \quad . \qquad (3)$$

Reaction (2) is assumed to be very fast so that any R· formed is immediately converted to RO_2·. The rate of reaction (3) is assumed to be 1 x 10^4 ppm^{-1} min^{-1} for all alkylperoxy radicals based on Howard's[10] measurement for hydroperoxy radicals. All alkyl radicals are assumed to undergo reactions (2) and (3) in all the mechanisms described.

Once formed, alkoxy radicals undergo three major types of reaction: decomposition, isomerization, and reaction with oxygen. The rates of these reactions for a wide variety of alkoxy radicals have been evaluated[26,27] based on available experimental data and standard estimation techniques.[28] The results are summarized in Tables 3 to 5. Isomerization by intramolecular hydrogen abstraction is only important in radicals that have a hydrogen atom such that a six-membered cyclic transition state can be formed. The resulting alkyl radical will add oxygen and then react with NO to form an alkoxy radical again. Thus, the net result of isomerization is hydroxy substitution of the radical accompanied by the oxidation of NO to NO_2.

Alkoxy radicals may also decompose to form an aldehyde and an alkyl radical, and subsequent photolysis of the aldehyde may yield two radicals. Thus, the decomposition of alkoxy radicals is eventually a source of radicals in smog chemistry. As shown in Table 3, the rate of decomposition of alkoxy radicals depends significantly on the carbon chain length and structure, the rate being fastest for long chains and branched structures.

Oxygen molecules will abstract hydrogen from alkoxy radicals to form HO_2 radicals and carbonyl compounds. Again, photolysis of the carbonyl compounds may yield two radicals, so this reaction also leads to additional radical formation. The rate of reaction of alkoxy radicals with oxygen is much less sensitive to structure than the rate of decomposition, as seen in Table 4.

The reactions of alkoxy radicals in the atmosphere can thus be summarized as follows: Those radicals having a hydrogen atom six atoms away will undergo isomerization; those that do not will largely decompose if they have branched structures, and if not branched, they will react with oxygen. Because all the estimated rate parameters in Tables 3 to 5 have uncertainties associated with them, the reported rate constants may have uncertainties as large as a factor of ten larger or smaller. This is a reflection of the lack of good experimental data on

TABLE 3. ESTIMATED RO· DECOMPOSITION RATES

Radical [a]	ΔH_R^o	ΔS_R^o	log A_r [b]	log $A(s^{-1})$	E_{est} [c]	k/k_∞ [d]	$k(min^{-1})$ [f]
C-CO·	12.4	33.4	8.2	13.7	21.6	0.003	2.1×10^{-3}
CC-CO·	9.4	35.0	8.0	13.8	19.5	0.6	1.7×10^{1}
C-CC (O·)	7.1	37.8	8.2	14.6	17.8	0.5	1.6×10^{2}
CCC-CO·	8.9	36.3	7.5	13.6	19.1	0.8	2.9×10^{1}
CC-CC (O·)	2.6	37.7	8.0	14.4	14.6	0.7	2.9×10^{5}
C-CO·-C (C)	4.3	41.2	8.0	15.2	15.9	0.5	1.5×10^{5}
HOC-CC (O·)	6.8 (3.5)[e]	38.0	8.0	14.5	17.6 (15.3)[e]	0.8	2.8×10^{3} (2.2×10^{5})[e]
HOCCC-CO·	8.7	36.6	7.1	13.3	19.0	1.0	2.1×10^{2}
HOCCC-COH (O·)	−9.7	39.2	7.1	13.8	12.8	1.0	2.1×10^{6}
$(HO)_2CCC$-COH (O·)	−9.6	39.2	6.8	13.5	12.8	1.0	1.0×10^{6}
$(HO)_2CCC$-C$(OH)_2$ (O·)	−30.9	37.7	6.8	13.2	12.8	1.0	5.2×10^{5}
$(HO)_3CCC$-C$(OH)_2$ (O·)	−24.5	37.7	6.5	12.9	12.8	1.0	2.6×10^{5}
HOC-CO·-C (C)	11.4 (8.2)[e]	37.7	7.5	13.9	20.9 (18.6)[e]	0.9	3.6×10^{0} (2.2×10^{2})[e]
CC-CC (O·, O)	-5.1	40.3	7.5	14.5	12.8	0.8	8.2×10^{6}

[a] Notation: HOC-CC (O·) represents $HOCH_2\dot{C}HCH_3 \rightarrow HO\dot{C}H_2 + H\dot{C}CH_3$, etc.

[b] A-factor for analogous alkyl radical + alkene association reaction.

[c] $E_{est} = 12.8 + 0.71\ \Delta H_R^o$ (kcal/mole).

[d] Falloff estimated from RRK Tables for 1 atm, 300 K.

[e] Based on Group Additivity, not on experimental ΔH_f^o for propane-1,2-diol.

[f] Rate constants for 300 K and 1 atm air.

TABLE 4. ESTIMATED RO· ISOMERIZATION REACTION RATES

Reaction[a]	log A(s^{-1})	E(kcal/mole)	k (min^{-1})
$\cdot OCCCC \rightarrow HOCCCC\cdot$	11.4	7.7	3.7×10^{7}
$\overset{\overset{\cdot}{O}}{\underset{|}{C}}CCC \rightarrow \overset{\overset{OH}{|}}{C}CCC\cdot$	11.7	13.1	8.6×10^{3}
$HOCCCCO\cdot \rightarrow HO\dot{C}CCCOH$	11.2	6.5	1.9×10^{8}
$HO\overset{O\cdot}{\underset{|}{C}}CCCOH \rightarrow (HO)_2C\dot{C}COH$	11.2	6.5	1.9×10^{8}
$(HO)_2\overset{O\cdot}{\underset{|}{C}}CCOH \rightarrow (HO)_2\dot{C}CC(OH)_2$	10.9	4.6	2.2×10^{9}
$(HO)_2\overset{O\cdot}{\underset{|}{C}}CC(OH)_2 \rightarrow (HO)_3C\dot{C}C(OH)_2$	10.9	4.6	2.2×10^{9}
$\overset{\overset{OH}{|}}{C}CCO\cdot \rightarrow \cdot\overset{\overset{OH}{|}}{C}CCOH$	11.4	7.7	3.0×10^{8}

[a]Notation: $\overset{\overset{OH}{|}}{C}CCO\cdot \rightarrow \cdot\overset{\overset{OH}{|}}{C}CCOH$ represents $CH_3\overset{\overset{OH}{|}}{C}HCH_2CH_2O\cdot \rightarrow \cdot CH_2\overset{\overset{OH}{|}}{C}HCH_2CH_2OH$

TABLE 5. ESTIMATES FOR REACTIONS OF RO· + O_2

Reaction	$\log (A)_{est}$	I $E_a = 4.0$	II $E_a = 10.6 + 0.25 \times (\Delta H_R^o)$	III $E_a = 11.5 + 0.29 \times (\Delta H_R^o)$
		k (min^{-1})	k (min^{-1})	k (min^{-1})
$CH_3O + O_2$	8.5	2.0×10^5	2.0×10^5	2.0×10^5
$EtO + O_2$	8.3	1.3×10^5	8.2×10^5	1.3×10^6
$n\text{-}PrO + O_2$	8.3	1.3×10^5	8.2×10^5	1.3×10^6
$i\text{-}PrO + O_2$	8.0	6.7×10^4	1.5×10^6	3.7×10^6
$n\text{-}BuO + O_2$	8.3	1.3×10^5	3.5×10^5	5.8×10^5
$s\text{-}BuO + O_2$	8.0	6.7×10^4	1.1×10^6	2.2×10^6

[a]Effective first-order rate constants at 300 K in air (2.1×10^5 ppm O_2).

the reactions of alkoxy radicals. The actual rate constants used in the mechanisms are given for each hydrocarbon in the appendices.

A further reaction common to all alkoxy radicals is reaction with NO_2 to form an alkyl nitrate or an aldehyde, and nitrous acid:

$$RO\cdot + NO_2 \rightarrow RONO_2 \qquad (4)$$

$$RO\cdot + NO_2 \rightarrow R'CHO + HNO_2 \quad . \qquad (5)$$

These reactions have been considered in detail by Barker and Golden,[27] and their results are summarized in Table 6. The results are based on an experimental measurement[29] for the reactions of methoxy radicals and NO_2.

TABLE 6. $RO\cdot + NO_2$ REACTIONS

Reaction	k_5 (ppm^{-1} min^{-1})[a]	k_4 (ppm^{-1} min^{-1})
$CH_3O\cdot + NO_2$	4.4×10^3	1.5×10^4
$EtO\cdot + NO_2$	2.9×10^3	1.5×10^4
$n\text{-}C_3H_7O\cdot + NO_2$	2.9×10^3	1.5×10^4
$i\text{-}C_3H_7O\cdot + NO_2$	1.5×10^3	1.5×10^4
$n\text{-}C_4H_3O\cdot + NO_2$	2.9×10^3	1.5×10^4
$s\text{-}C_4H_3O\cdot + NO_2$	1.5×10^3	1.5×10^4
$t\text{-}C_4H_9O\cdot + NO_2$	0	1.5×10^4

[a] $\log k_d/M^{-1}\ s^{-1} = 9.3 + \log n$.

3.4 TERMINATION REACTIONS AND RADICAL-RADICAL REACTIONS

The major termination steps in our mechanisms are the reactions of alkylperoxy radicals and acylperoxy radicals with HO_2:

$$RO_2\cdot + HO_2\cdot \rightarrow ROOH + O_2 \qquad (6)$$

$$R\overset{O}{\overset{\|}{C}}O_2\cdot + HO_2\cdot \rightarrow R\overset{O}{\overset{\|}{C}}OOH + O_2 \quad . \tag{7}$$

There are no experimental measurements on these classes of reactions; we have estimated $k_6 = 2.0 \times 10^3$ ppm^{-1} min^{-1} by analogy with the rate of reaction of two HO_2 radicals, and $k_7 = 4.0 \times 10^3$ ppm^{-1} min^{-1} because we expect this rate to be a little faster.

We have also included the following radical-radical reactions:

$$RO_2\cdot + RO_2\cdot \rightarrow RO\cdot + RO\cdot + O_2 \tag{8}$$

$$R\overset{O}{\overset{\|}{C}}O_2\cdot + R\overset{O}{\overset{\|}{C}}O_2\cdot \rightarrow RO_2\cdot + RO_2\cdot + 2CO_2 + O_2 \quad . \tag{9}$$

We have set $k_8 = 2.0 \times 10^2$ ppm^{-1} min^{-1} based on experiments by Parkes[30] on the combination of methylperoxy radicals, and $k_9 = 2.4 \times 10^3$ ppm^{-1} min^{-1} as a reasonable value based on solution phase data.[31]

3.5 ALDEHYDES

The chemistry of aldehydes is an important part of the smog chemistry of all hydrocarbons. In addition to the thermal reactions considered in this section, the photochemical reactions discussed in the following section are also very critical. Table 7 summarizes the reactions for formaldehyde and the generalized aldehyde $(R\overset{O}{\overset{\|}{C}}H)$, which represents acetaldehyde and higher analogs. Benzaldehyde is considered in the discussion of toluene chemistry in Section 3.9.

Besides the photolysis, which is discussed in the following section, the reaction of aldehydes with OH (reaction 7-1 in Table 7) controls their participation in photochemical smog. The literature sets the value for the rate constants in the range of 1 to 2 x 10^4 ppm^{-1},[32,33] although the preferred value is the upper limit.[13] Because of this uncertainty, we have experimented with the rate constant for reaction 7-1 prior to our final runs and elected to use 2 x 10^4 ppm^{-1} min^{-1} for all aldehydes. However, the overall results are not highly sensitive to this rate constant, and the upper limit value has only a slight advantage when all alkene and alkane models are considered.

TABLE 7. ALDEHYDE CHEMISTRY

No.	Reaction	Rate Constant[a]	Reference
7-1	$RCH(=O) + OH \xrightarrow{O_2} RCO_2\cdot(=O)$	2×10^4	13
7-2	$RCO_2\cdot(=O) + NO_2 \longrightarrow RCO_2NO_2(=O)$	1.5×10^3	23
7-3	$RCO_2NO_2(=O) \longrightarrow RCO_2\cdot(=O) + NO_2$	4.0×10^{-2}[b,c]	23
7-4	$RCO_2\cdot(=O) + NO \longrightarrow RCO\cdot(=O) + NO_2$	5.4×10^3	23
7-5	$RCO\cdot(=O) \xrightarrow{O_2} RO_2\cdot + CO_2$	1.3×10^3	34
7-6	$RO_2\cdot + NO_2 \longrightarrow RO_2NO_2$	6×10^3	Sec. 3.2
7-7	$RO_2NO_2 \longrightarrow RO_2\cdot + NO_2$	0.5[b,d]	Sec. 3.2
7-8	$RO_2\cdot + NO \longrightarrow RO\cdot + NO_2$	1×10^4	Sec. 3.2
7-9	$HCH(=O) + OH \longrightarrow HC\cdot(=O)$	2×10^4	13
7-10	$HC\cdot(=O) + O_2 \longrightarrow HCO_2\cdot(=O)$	80	Sec. 3.2
7-11	$HC\cdot(=O) + O_2 \longrightarrow HO_2\cdot + CO$	1.0×10^4	36

[a] Units in ppm^{-1} min^{-1} unless otherwise indicated.

[b] Units in min^{-1}

[c] $\log k_3 = 18.0 - 27000/4.576\ T$.

[d] $\log k_7 = 17.68 - 25000/4.576\ T$.

The acyl radical formed from the reaction of acetaldehyde and higher analogs with OH rapidly adds oxygen to form the acylperoxy radical. This radical reacts rapidly with both NO and NO_2 (reactions 7-2 and 7-4).[23] The peroxyacyl nitrate slowly regenerates peroxy radical and NO_2 (reaction 7-3). We have used values for the rate constants for these reactions as reported for acetylperoxy radical[23] for all acylperoxy reactions.

The acylperoxy radical decarboxylates rapidly and yields the corresponding alkylperoxy radical,[34] which also reacts rapidly with NO_2 (Section 3.2) and NO (Section 3.3). The rate constant for reaction 7-8 has been assumed to be independent of the R alkyl group and the value in Table 7 has been obtained by adjusting the rate constant to give the best fit in the propene simulations.

Formaldehyde reacts with OH (reaction 7-9) to yield the formyl radical. The reactions of formyl radical with oxygen (reactions 7-10 and 7-11) are the most controversial. Recent work of Niki[25] indicates that oxidation of formaldehyde at low concentrations gives CO with no evidence of formic acid; however, at high concentrations (> 1 ppm), formic acid is detected. At 1 atmosphere, k_{10} is estimated to be about 0.01 of the high pressure using the method of Emanuel.[35] Since the high pressure limit is expected to be about $10^{9.5}$ M^{-1} s^{-1}, k_{10} is 3 x 10^7 M^{-1} s^{-1} or 80 ppm^{-1} min^{-1}. The value of k_{11} has recently been measured at room temperature by Martinez[36] as approximately 1.0 x 10^4 ppm^{-1} min^{-1}, which is consistent with the extrapolation of data obtained at high temperatures.[37] Thus k_{11} is much greater than k_{10}, and we have not included reaction 10 in our models. This conclusion is consistent with Niki's experiments with low formaldehyde concentrations;[25] however, at higher concentrations, other reactions must account for the formation of formic acid in his system.

3.6 PHOTOLYTIC REACTIONS

The photolytic reactions used in the mechanisms are shown in Table 8. The rates of photolysis were calculated from the absorption

cross sections given in the references in the table. The quantum yields for most of the processes were assumed to be unity; the photolysis of ozone was assumed to yield $O(^1D)$ atoms with unit quantum yield at wavelengths below 308 nm, and $O(^3P)$ atoms with unit quantum yield above 308 nm.[13] Recent work on the photolysis of formaldehyde in air at 1 atmosphere by Moortgat et al.[38] has established the branching ratio for the molecular and radical pathways, at wavelengths between 276 and 366 nm, assuming the total quantum yield is unity.

TABLE 8. PHOTOLYTIC REACTIONS

No.	Reaction	Reference
8-1	$NO_2 + h\nu \rightarrow NO + O(^3P)$	41
8-2	$HONO + h\nu \rightarrow OH + NO$	42, 43
8-3	$H_2O_2 + h\nu \rightarrow 2OH$	44
8-4	$O_3 + h\nu \rightarrow O(^1D) + O_2$	45, 46
8-5	$O_3 + h\nu \rightarrow O(^3P) + O_2$	45, 46
8-6	$CH_2O + h\nu \rightarrow \dot{C}HO + H\cdot$	47
8-7	$CH_2O + h\nu \rightarrow CO + H_2$	47
8-8	$CH_3CHO + h\nu \rightarrow \dot{C}HO + \dot{C}H_3$	48
8-9	$CH_3CH_2CHO + h\nu \rightarrow \dot{C}HO + CH_3\dot{C}H_2$	48
8-10	$CH_3CH_2CH_2CHO + h\nu \rightarrow \dot{C}HO + CH_3CH_2\dot{C}H_2$ (rad.)	48
8-11	$CH_3CH_2CH_2CHO + h\nu \rightarrow CH_3CHO + C_2H_4$ (molec.)	48
8-12	$CH_3CH_2C(O)CH_3 + h\nu \rightarrow CH_3\dot{C}O + CH_3\dot{C}H_2$	48

The SAPRC data include relative light intensity measurements as a function of wavelength for each individual run after EC-106. For these runs, relative photolysis rate constants were calculated for each run by summation at 1-nm intervals over the range 380 to 420 nm, using linear interpolation between the reported relative intensities (usually 10-nm intervals). These relative rates were changed

to an absolute basis using the reported rate constant for the photodecomposition of NO_2. For runs EC-1 to EC-86, the photolysis rate is based on a spectrum obtained immediately before EC-95. The spectrum obtained with the new lamp was used for runs EC-95 to EC-106. There is some doubt as to the exact spectral distribution or the reproducibility from run to run in the early runs, and thus the uncertainty associated with the calculated photolytic rate constants is unknown.

Many of the species in Table 8 absorb strongly only in the short wavelength region around 280 to 300 nm where the intensities are lowest and most difficult to measure. Very small changes in the measured relative intensities in this region produce large changes in the relative rates for these species compared with NO_2, which absorbs over the whole range. Since the measured rate of photodecomposition of NO_2 is used to arrive at the absolute rates for all other species, it is imperative that the short wavelength relative intensity measurements be made as accurately as possible.

The formaldehyde branching ratio calculated from the relative quantum yields described above is also critically dependent on the short wavelength intensity measurements, but, on the average, this ratio is about equal for the two channels. A quantum yield of 0.5 was assigned for radical production from acetaldehyde.[39,40]

The actual photolytic rate constants used in each simulation are tabulated in the Appendices.

3.7 ALKENES

The reactions of alkenes in photochemical smog are predominantly with OH and O_3 but reactions with $O(^3P)$ and NO_3 can be important under some conditions and are included in the mechanism. The principal reactions occurring in the propylene mechanism are shown in Figure 1. Detailed mechanisms for this species as well as ethene, 1-butene, and trans-2-butene are included in Appendix A. (The mechanisms in the appendix are complete

except for the inorganic thermal reactions, which are given in Table 1.

The rate constants for the reactions of OH,[49-51] O_3,[52] $O(^3P)$,[53-55] and NO_3[56] with simple olefins have received considerable attention and are relatively well known. There are much less data on the products from these reactions. We have applied the basic mechanism proposed by Niki et al.[57] to all the olefins. We have added irreversible formation of the peroxy nitrate as discussed in Section 3.2. The decomposition rate values for the two hydroperoxynitrates shown in Figure 1 are assumed to be equal and were adjusted in the final stages of the model devleopment to optimize fit of hydrocarbon, NO, and NO_2 data for the propene simulations. For each case, the rate constants for the competing reactions of the hydroalkoxy radical, $HOCH_2CH(O_2\cdot)CHCH_3$, were selected to reflect both the range of values in Section 3.3 and the fact that a significant amount of cleavage occurs according to the chamber data. Thus, for each alkene, significant amounts of hydroxy carbonyl compound, $HOCH_2C(=O)CH_3$, are predicted although these compounds have not been detected. Unfortunately, the measurements of the aldehydes formed as the result of cleavage are not sufficiently accurate to verify this competing route by difference. Because of the low reactivity of the hydroxy carbonyl compound (relative to the reactivity of the alkenes), the reaction of this compound with OH has not been included in the alkene mechanism.

The proposed products of the alkene-O_3 reactions are consistent with the O'Neal-Blumstein mechanism.[58] Recent data by Herron and Huie[59] give support to the general types of products expected, although for ethylene the radical yield appears to be only 9% of postulated reaction yield. Although over the entire chamber run OH accounts for most of the alkene consumption, once the ozone maximum is reached ozone reactions with the alkenes can dominate, and these ozone reactions can be a significant source of radicals. For the reactions of $O(^3P)$, we have followed the reaction channels proposed by Whitten.[5] The $O(^3P)$ reactions,

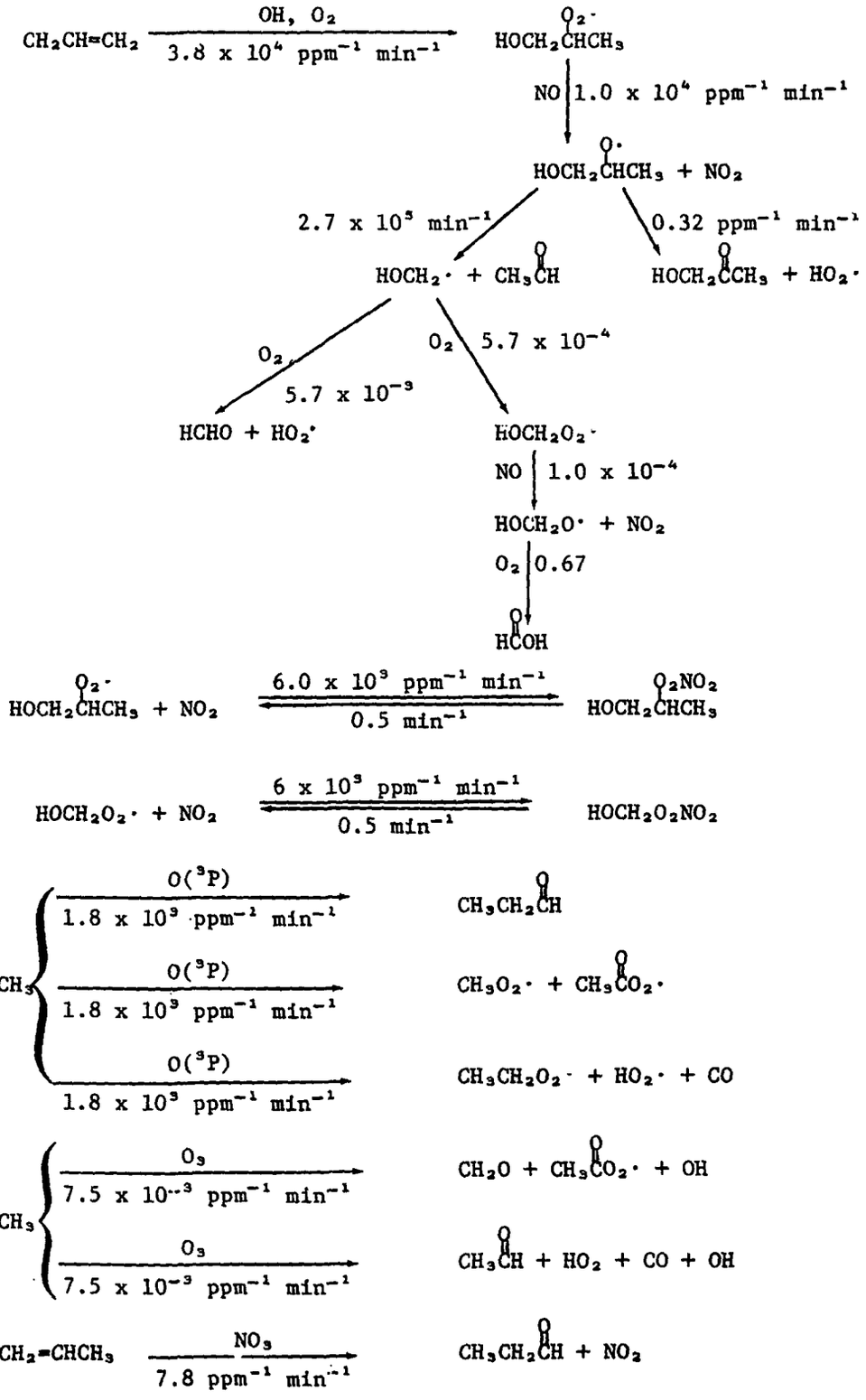

FIGURE 1. PROPENE REACTIONS.

although they do not contribute significantly to the alkene consumption, can be a small but significant source of radicals at early stages in the reaction.

3.8 ALKANES

SAPRC has reported data for two alkane-NO_x systems--an extensive set for n-butane, and a very limited set for 2,3-dimethylbutane. Alkanes react primarily with OH radicals[60,61] that abstract hydrogen to give alkyl radicals and hence alkoxy radicals (see Section 3.3). Butane contains only primary and secondary hydrogens and hence yields normal and secondary alkoxy radicals; 2,3-dimethylbutane contains only primary and tertiary hydrogens, and yields the corresponding alkoxy radicals. Since reaction with OH is faster at the secondary or tertiary position than at the primary position, the formation of primary alkoxy radicals is the more minor pathway in both systems. The reaction of alkanes with $O(^3P)$ atoms,[62] although it does not contribute significantly to alkane oxidation, has been included in these mechanisms.

n-Butane--The principal reactions of the hydrocarbon species in the butane system are shown in Figure 2 and are tabulated in detail in Appendix B. The majority of the reacted hydrocarbon ($\sim$ 86%) forms secondary butoxy radicals that do not have hydrogen atoms in position to allow rapid intramolecular isomerization. These radicals may react with oxygen to form 2-butanone, or may decompose to form acetaldehyde and ethoxy radicals that will react principally with oxygen to give more acetaldehyde. As described in Section 3.3, the rates of decomposition of alkoxy radicals can be estimated with reasonable accuracy, whereas the rates of reaction of alkoxy radicals with oxygen are much less certain. In the n-butane mechanism, we have used the rates of alkoxy radical decomposition given in Table 3 and the rate of reaction of alkoxy radicals with oxygen given in Table 5, column I, except for secondary butoxy and oxygen. Here we used a value of 8.8×10^5 min^{-1} for the pseudo first-order rate constant; this value is higher than the value in column I, but well within the estimated range for this reaction (columns II and III). This rate constant was arrived at empirically

to simulate the correct amounts of 2-butanone and acetaldehyde in the products; it is very approximate and depends on the accuracy with which these products were measured. There is now some question as to the accuracy of the acetaldehyde measurements.

The remaining hydrocarbon (∿ 14%) forms normal butoxy radicals. These do have hydrogen atoms in position for intramolecular rearrangement, and on the basis of our estimated rates, should undergo rapid reaction to form polyhydroxy-substituted radicals with the oxidation of NO to NO_2. Figure 2 shows the course of these reactions with the competing reactions (decomposition or reaction with oxygen) at each step. As can be seen, isomerization is much faster than either competing reaction until the terminal carbon atoms are completely hydroxy substituted. The ultimate fate of this hydroxy-substituted compound is not known, but it is a minor route for the consumption of hydrocarbon. However, because each molecule isomerizes several times, converting an NO molecule to an NO_2 molecule each time, isomerization is an important process in the NO_x cycle.

2,3-Dimethylbutane--The principal reactions of the hydrocarbon species in the 2,3-dimethylbutane system are shown in Figure 3, and are tabulated in detail in Appendix B. The mechanism is precisely analogous to that already described for n-butane, except that the majority of the reacted hydrocarbon (∿ 88%) forms tertiary alkoxy radicals. However, in common with s-butoxy radicals, these radicals are postulated to decompose (reaction with oxygen is not possible) to form acetone and isopropoxy radicals. The isopropoxy radicals will react principally with oxygen to yield more acetone.

The remaining hydrocarbon (∿ 12%) forms normal alkoxy radicals which have hydrogen in position for isomerization. These are expected to isomerize repeatedly (there are 11 abstractable hydrogens), oxidizing NO to NO_2. The fates of the polyhydroxylated products are not known, but again, this is a minor route for the consumption of hydrocarbon, although it is very important in the NO_x cycle. Details of all the estimations on the rates of reaction of the primary and tertiary radicals derived

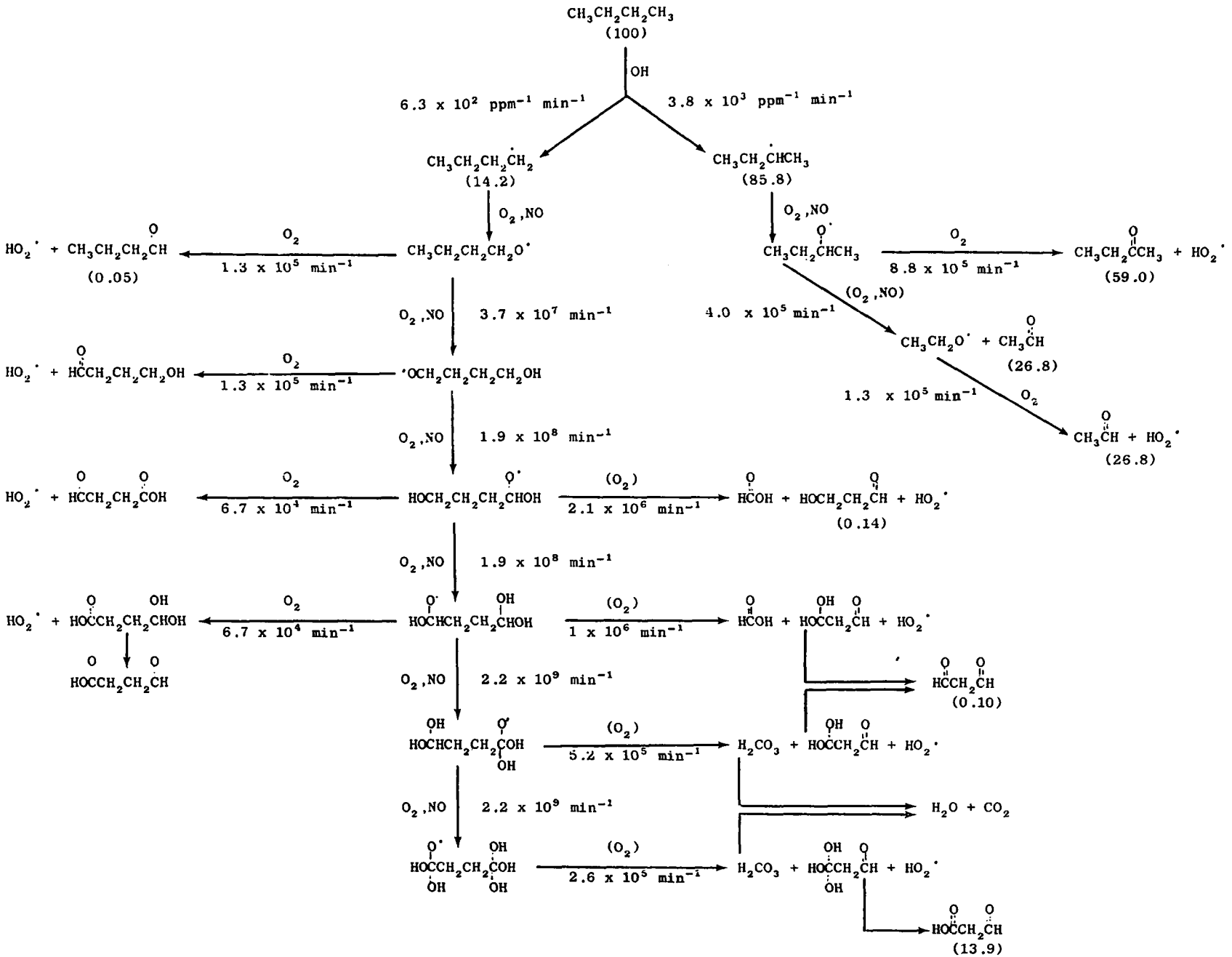

FIGURE 2 n-BUTANE REACTIONS

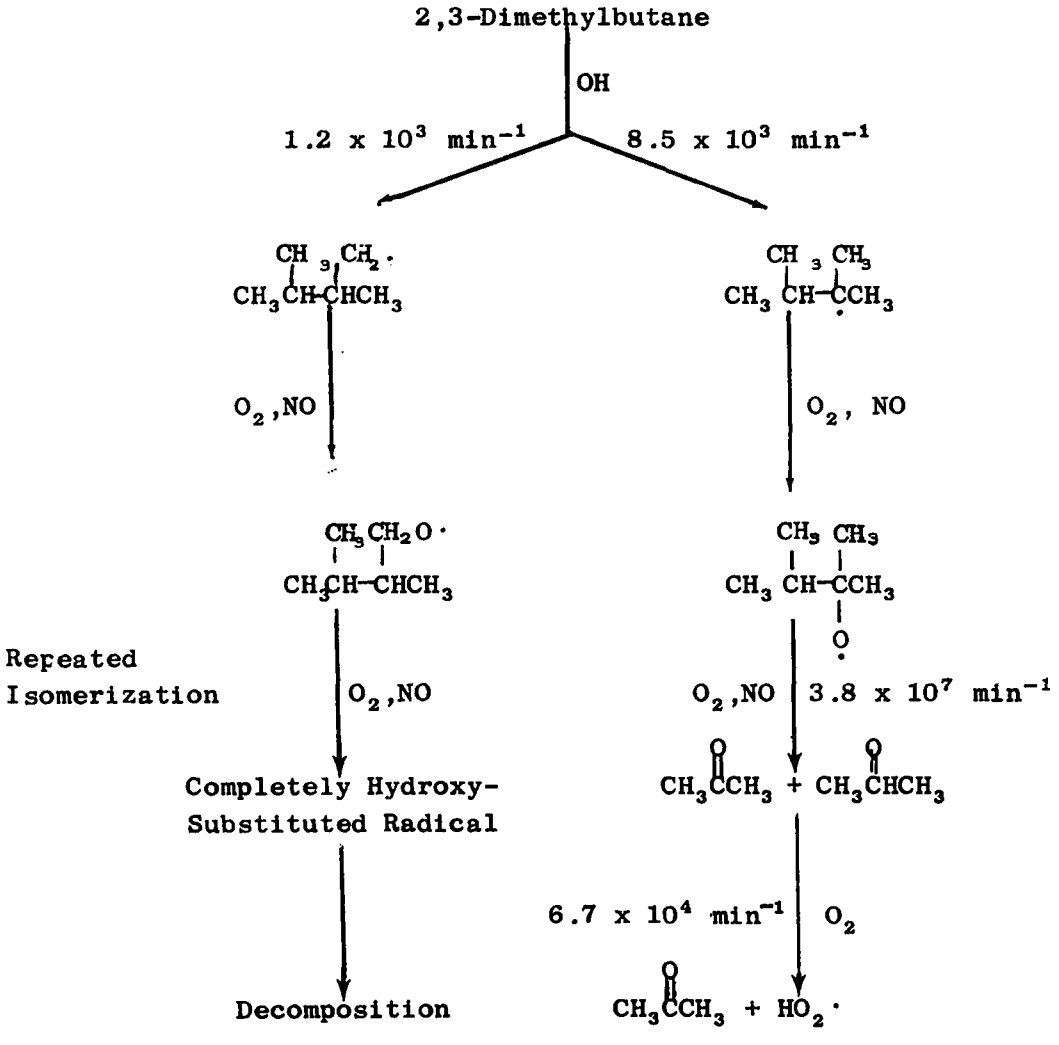

FIGURE 3 2,3-DIMETHYLBUTANE REACTIONS

from 2,3-dimethylbutane are shown in Tables 9 to 11. The estimation methods used were described earlier in Section 3.3. The detailed mechanism for this alkane is tabulated in Appendix B.

3.9 TOLUENE

Toluene and other aromatic hydrocarbons are significant constituents of the hydrocarbon fraction of the urban atmosphere and yet there has been no information available on their fate. Smog chamber data using toluene as the hydrocarbon fuel, are available, but no attempt to model the chemistry has been successful. Therefore, one of the major goals of this study is to develop a mechanism to describe the chemistry of toluene and its products using the limited amount of available experimental data.

The loss of toluene in the atmosphere is due predominantly to reaction with OH. Toluene, as well as most simple aromatic compounds, is stable to troposphere radiation and to ozone. Although toluene is capable of reacting with $O(^3P)$, the combination of a relatively low $O(^3P)$ concentration and only a moderately fast rate constant[63] prevents the reaction from competing favorably with the OH reactions.

Excellent agreement exists on the reported rate constant for reaction of toluene with OH obtained by following OH decay using resonance fluorescence. The two basic pathways suggested for the reaction are:
Abstraction:

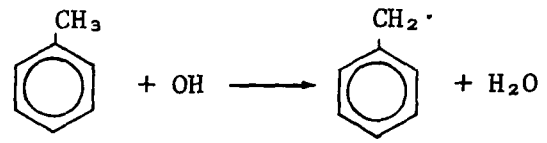

(10)

Addition:

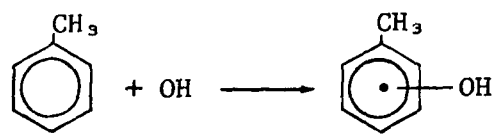

(11)

TABLE 9. ESTIMATED RATE OF DECOMPOSITION OF THE p- and t-ALKOXY RADICALS DERIVED FROM 2,3-DIMETHYLBUTANE

Radical	ΔH_R^o	ΔS_R^o	log A_r (M^{-1} s^{-1})	log A (s^{-1})	E_{est}	k (min^{-1})
Primary	6.25	38.71	7.53	14.16	17.24	2.4×10^3
Tertiary	−1.6	43.26	7.5	15.12	12.8	3.8×10^7

TABLE 10. ESTIMATED RATES OF ISOMERIZATION OF THE ALKOXY RADICALS DERIVED FROM 2,3-DIMETHYLBUTANE

Radical	E	log A/s^{-1}	k (min^{-1})
Tertiary	13.1	11.7	8.6×10^3
Primary	7.7	11.4	3.7×10^7
Primary $(OH)^a$	6.5	11.2	1.7×10^8
Primary $(OH)_2^a$	4.6	10.9	2.1×10^9

[a]A primary alkoxy radical abstracting hydrogen from a 4-carbon containing OH substituent.

TABLE 11. ESTIMATED RATE OF REACTION OF OXYGEN WITH ALKOXY RADICALS DERIVED FROM 2,3-DIMETHYLBUTANE

Radical	log A/s^{-1}	E_A		k (min^{-1})	
		I[a]	II[b]	I[a]	II[b]
Tertiary		no reaction possible			
Primary	8.3	4.0	2.4	1.3×10^5	1.8×10^6

[a]Estimation method I (Section 3.3).

[b]Estimation method II (Section 3.3).

From pressure dependence studies, Davis et al.[64] concluded that at 298 K, $k_1/(k_1 + k_2)$ is less than 0.5. From temperature dependence studies, Perry et al.[65] deduced that at 298 K, this ratio is 0.14 ± 0.06. In our own laboratory we have investigated this reaction primarily to determine what products would be formed under atmospheric conditions.[66] In the range of 6 to 15 torr we have found, based on product analysis, that $k_1/(k_1 + k_2) = 0.15 \pm 0.02$ *independent of total pressure.* The products isolated from reaction (1) are benzaldehyde and benzyl alcohol, which result from the reactions

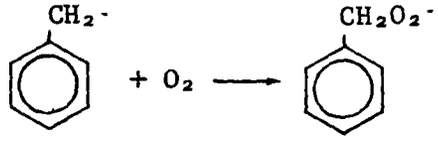

(12)

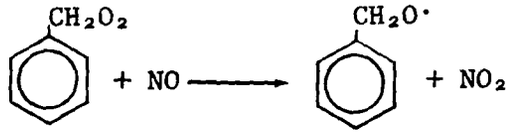

(13)

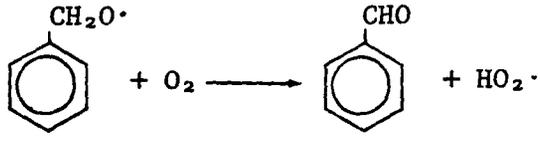

(14)

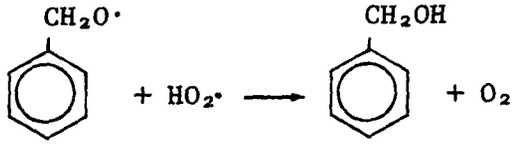

(15)

Benzyl alcohol is not expected to be an important product in the atmosphere or in smog chambers because of a very low $[HO_2\cdot]/[O_2]$ ratio obtained under these conditions. The products obtained from reaction (11) were a mixture of o,p,m-cresol and m-nitrotoluenes. The reactions are (showing only those for the o-addition product)

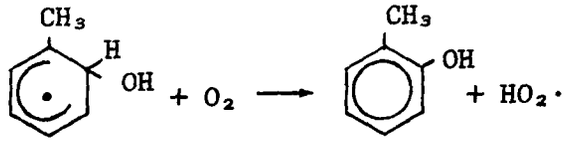

(16)

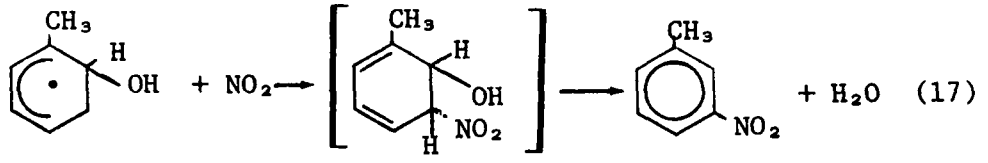

From the $[NO_2]/[O_2]$ dependence of cresol-nitrotoluene products, k_{17}/k_{16} has been estimated to be 4.4×10^3. Therefore, under atmospheric conditions and in the SAPRC smog chamber experiments, where $[NO_2]/[O_2]$ is less than 10^{-5}, reaction (16) will account for essentially all the toluene consumed in reaction (11). All these reactions are included in Table 12 along with the other reactions that make up the complete mechanism.

Data on the fate of benzaldehyde and the cresols are much more limited than for toluene. Unpublished chamber data seem to indicate that the benzaldehyde and cresols formed initially from toluene react rapidly so that high concentrations are not found.[67] For benzaldehyde we have included both abstraction of the aldehydic hydrogen (reaction 12-11, Table 12) similar to other aldehydes (Section 3.5) and addition to the ring (reaction 12-19) similar to toluene. The first pathway leads to reaction (12-12) to (12-18). The second and minor pathway leads to hydroxylated benzaldehyde, which we have assumed to react with OH (reaction 12-29).

The fate of cresol has been assumed to be determined by reaction with OH and O_3. Perry et al.[68] have reported rate constants for the reaction of OH plus cresol. Following the analogy of toluene,[65] they believe they have identified both an abstraction and an addition reaction. Therefore, we have included both pathways (reactions 12-20 and 12-27). The reactions that result from radical products of reaction 12-20 are expected to be complex and to involve a number of parallel pathways. We have assumed that the radical can react with O_2 and NO to form a series of intermediates only four of which react with NO (X1, X2, X3, and X4). These reactions result in the breakdown of the ring with formation of glyoxal $HC(=O)C(=O)H$, methylglyoxal $CH_3C(=O)C(=O)H$, and formaldehyde (reactions 12-21 to 26).

TABLE 12. TOLUENE MECHANISM

No.	Reaction	Rate Constant[a]	Reference
12-1	$PhCH_3 + OH \longrightarrow$ 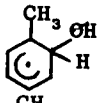 (I)	7.4×10^3	64, 65, 66
12-2	$I + O_2 \longrightarrow$ 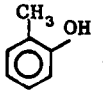 $+ HO_2\cdot$	0.7	66
12-3	$I + NO_2 \longrightarrow \longrightarrow$ 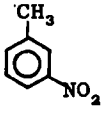 $+ H_2O$	1.5×10^3	66
12-4	$PhCH_3 + OH \xrightarrow{O_2} PhCH_2O_2\cdot + HOH$	1.6×10^3	64, 65
12-5	$PhCH_2O_2\cdot + NO \longrightarrow PhCH_2O\cdot + NO_2$	1.0×10^4	Section 3.3
12-6	$PhCH_2O\cdot + O_2 \longrightarrow PhCHO + HO_2$	0.6	3.3
12-7	$PhCH_2O\cdot + NO_2 \longrightarrow PhCH_2ONO_2$	1.5×10^4	3.3
12-8	$PhCH_2O\cdot + NO_2 \longrightarrow PhCHO + HNO_2$	3.0×10^3	3.3
12-9	$PhCH_2O_2\cdot + NO_2 \longrightarrow PhCH_2O_2NO_2$	5.0×10^3	3.2
12-10	$PhCH_2O_2NO_2 \longrightarrow PhCH_2O_2\cdot + NO_2$	0.53	3.2
12-11	$PhCHO + OH \xrightarrow{O_2} PhC(O)O_2\cdot$	1×10^4	3.5
12-12	$PhC(O)O_2\cdot + NO \longrightarrow PhC(O)O + NO_2$	2×10^3	3.5
12-13	$PhC(O)O_2\cdot + NO_2 \longrightarrow PhC(O)O_2NO_2$	1.5×10^3	3.5
12-14	$PhC(O)O_2NO_2 \longrightarrow PhC(O)O_2\cdot + NO_2$	0.042	3.5
12-15	$PhC(O)O\cdot + NO_2 \longrightarrow PhC(O)ONO_2$	1.5×10^4	3.3
12-16	$PhC(O)O\cdot \xrightarrow{O_2} PhO_2 + CO_2$	5.2×10^4	70
12-17	$PhO_2\cdot + NO \longrightarrow PhO\cdot + NO_2$	1.0×10^4	Section 3.3
12-18	$PhO\cdot + NO_2 \longrightarrow PhONO_2$	6.0×10^3	3.3
12-19	$PhCHO + OH \xrightarrow{O_2}$ 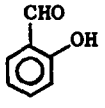 $+ HO\cdot$	6.3×10^3	3.9
12-20	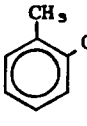 $+ OH \xrightarrow{O_2} X1 + H_2O$	6.0×10^3	Section 3.9
12-21	$X1 + NO \longrightarrow X_2 + NO_2$	1.0×10^4	Section 3.9
12-22	$X1 + NO \longrightarrow X_2 + NO_2 + CH_2O$	1.0×10^4	3.9

Continued...

Table 12 (continued)

No.	Reaction	Rate Constant[a]	Reference
12-23	X1 + NO_2 ⟶ X1PN	6.0×10^3	Section 3.2
12-24	X1PN ⟶ X1 + NO_2	0.53	Section 3.2
12-25	X2 + NO ⟶ X3 + NO_2 + 1/3 $CH_3C(=O)CH(=O)$ + 2/3 $HC(=O)C(=O)H$	1.0×10^4	Section 3.9
12-26	X3 + NO ⟶ (O_2) 1/3 $CH_3C(=O)CH(=O)$ + 2/3 $HC(=O)C(=O)H$ + CH_2O + NO_2 + HO_2·	1.0×10^4	Section 3.9
12-27	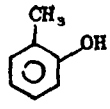 + OH ⟶ (O_2) 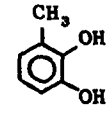 (+ isomers) + HO_2·	4.4×10^4	68
12-28	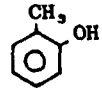 + O_3 ⟶ X1 + HO_2·	2.5×10^{-2}	69
12-29	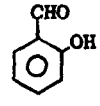 + OH ⟶ X1 + H_2O	2.5×10^4	
12-30	$CH_3C(=O)O_2$· + NO ⟶ (O_2) CH_3O_2· + CO_2 + NO_2	5.3×10^3	Section 3.5
12-31	$CH_3C(=O)O_2$· + NO_2 ⟶ $CH_3C(=O)O_2NO_2$	1.5×10^3	3.5
12-32	$CH_3C(=O)O_2NO_2$ ⟶ $CH_3C(=O)O_2$· + NO_2	4.2×10^{-2}	3.5
12-33	CH_3O_2· + NO ⟶ CH_3O· + NO_2	1.0×10^4	3.5
12-34	CH_3O· + O_2 ⟶ HCHO + HO_2·	2.0×10^3	3.3
12-35	CH_3O· + NO_2 ⟶ CH_3ONO_2	2.0×10^4	3.3
12-36	CH_3O· + NO_2 ⟶ HCHO + HNO_2	2.2×10^3	3.3
12-37	$PhCH_2O_2$· + HO_2 ⟶ $PhCH_2O_2H$	2.0×10^3	3.4
12-38	$PhCH_2O$· + HO_2· ⟶ $PhCH_2OH$	2.0×10^3	3.4
12-39	$PhC(=O)O_2$· + HO_2· ⟶ $PhC(=O)O_2H$	2.0×10^3	3.4

Continued...

Table 12 (continued)

No.	Reaction	Rate Constant[a]	Reference
12-40	$PhC(=O)\cdot + HO_2\cdot \longrightarrow PhC(=O)OH$	2.0×10^9	3.4
12-41	$PhO_2\cdot + HO_2\cdot \longrightarrow PhO_2H$	2.0×10^9	3.4
12-42	$PhO\cdot + HO_2\cdot \longrightarrow PhOH$	2.0×10^9	3.4
12-43	$CH_3O_2\cdot + HO_2\cdot \longrightarrow CH_3O_2H$	2.0×10^9	3.4
12-44	$X1 + HO_2\cdot \longrightarrow X1\text{-}H$	2.0×10^9	3.4
12-45	$X2 + HO_2\cdot \longrightarrow X2\text{-}H$	2.0×10^9	3.4

Based on very limited data we have included a reaction of cresol with O_3.[69] This reaction is assumed to generate a HO_2 radical and the same intermediates as formed from the reaction of cresol with OH.

Included in the mechanism is the photolysis of the aldehydic products: benzaldehyde, glyoxal, methylglyoxal, and formaldehyde. Based on limited uv spectra we have set upper limits for these photolysis rates and have then adjusted the values.

Because of the degree of uncertainties for the reactions of cresols with O_3 and OH as well as the proposed photolysis reactions, the mechanism must be considered somewhat speculative and probably less quantitative than desired. However, judging from the results in the following section, it serves as a very good starting point that can be improved further as the needed information becomes available.

4. RESULTS AND DISCUSSION

4.1 NONHOMOGENEOUS RADICAL SOURCES

In all attempts to simulate data from the SAPRC evacuable chamber,[5,71] it has been found that a mechanism based solely on homogeneous gas-phase chemistry predicts both a rate of decomposition of the hydrocarbon and a rate of conversion of NO to NO_2 that are considerably slower than rates indicated by the experimental data. In addition, the experimental data on the rate of initial disappearance of the hydrocarbon indicate that the concentration of radicals increases extremely rapidly as soon as the chamber is irradiated. This behavior is inconsistent with the radical supply mechanism from the photolysis of secondary carbonyl products in our mechanism. Thus, we have postulated nonhomogeneous sources of radicals that can be formed rapidly upon irradiation. Experimental evidence is inconclusive, but indicates two reasonable sources--radicals produced from the chamber walls, and the photolysis of nitrous acid formed during the loading of the chamber.

Regarding the first case, there is a certain amount of qualitative evidence that the walls of the chamber are active in producing radicals during irradiation; however, as yet no quantitative information is available. Under irradiation, larger quantities of CO are produced in the chamber than can be explained by the homogeneous mechanisms. In fact, CO is formed even if no hydrocarbon is present (runs EC-9, EC-38)[1] so long as the chamber is irradiated; no CO is formed in the dark (EC-1, EC-40).[1] The excess CO cannot be due to the unpurified makeup air, which could contain more CO than the original purified air, because recent experiments (EC-216, EC-217)[1] using purified makeup air also show the large increase in CO. Since irradiation apparently produces CO from a photochemical process, which probably involves materials absorbed on the chamber wall, it is most likely that other species including free radicals are also being formed.

Other evidence for the action of the chamber walls is provided by the observation of the "aldehyde memory effect."[1] Reactions EC-46 and EC-49 have the same initial aldehyde concentrations as Run EC-41, but were run after experiments that had high aldehyde concentrations (due to aldehydes being added initially). In these runs a much enhanced reactivity was observed, compared with Run EC-41 (see Section 4.4 and Appendix B). This effect was observed despite the fact that the chamber was subjected to an extended pumpdown between the runs and the analysis showed no evidence of excess aldehydes. The increased reactivity is seen as a perturbation of the "standard" behavior of the system after exposure of the chamber to high concentrations of aldehyde. Aldehydes are always present as products of the photooxidation of hydrocarbons; in the propylene system the concentrations of aldehydes that are produced are often as high as those used to produce the "memory effect" in the butane runs. Even with butane, the amounts of aldehyde formed are as much as one-third of the amount that causes the "memory effect." Thus, we assume that the "standard" reactivity observed reflects some contribution from adsorbed aldehydes from pervious runs. We believe that this effect as well as the formation of CO are due to the photolysis of these adsorbed species. Although a memory effect has been demonstrated only for aldehydes, other photochemically active species may act similarly.

The second nonhomogeneous source of radicals is the formation and photolysis of HNO_2 formed in equlibrium with NO, NO_2, and water:

$$NO + NO_2 + H_2O \rightleftarrows HNO_2 \quad . \tag{9}$$

Given the concentrations of NO and NO_2 present in the chamber and the humidity of the air, the equilibrium concentration of nitrous acid would be significant. However, the homogeneous rate of formation of nitrous acid is very slow at concentrations used in the runs, so that even though the reactants are left in the chamber in the dark for about one hour before the experiments are begun, an insignificant amount of nitrous acid should be formed homogeneously. Chan et al.[17] observed the formation of nitrous acid during the loading of a large chamber with NO and NO_2.

This may be due to heterogeneous reactions, or to high concentrations of NO and NO_2 around the injection area that produce an amount of nitrous acid closer to equilibrium than would be formed from the homogeneous process alone. Using present experimental data, it is impossible to predict the amount of nitrous acid formed. This amount may depend critically on the method and timing of the NO and NO_2 injections, which may vary substantially from run to run.

In attempting to simulate the SAPRC data, we found that postulating only an initial amount of nitrous acid would not fit all the data satisfactorily. In a number of cases postulating an initial concentration of nitrous acid would give the desired initial rate but once the nitrous acid was consumed (about 1 hour) the computed rates for all reactants dropped below the oberved value. Clearly, what is needed is an additional radical source that is effective throughout the reaction. This problem was most important for the less reactive systems such as n-butane, although propene and toluene also gave evidence of this problem at the lowest concentrations. We believe that at high concentrations of propene and toluene, this problem does not occur because the photolysis of the carbonyl compounds formed in the reaction generates more radicals than are produced from the wall reaction.

To simulate those runs where initial nitrous acid was insufficient to fit the rates late in the run, we found that a continuous source of radicals, representing wall contributions, was much more effective. Since there are probably radicals from both nitrous acid and the walls, we have adopted the following, somewhat artitrary conditions to represent the nonhomogeneous radical sources. In all the simulations described in this report, we have assumed a standard constant influx of HO_2 radicals of 2×10^{-4} ppm^{-1} min^{-1}. In practice, the results of representing the influx as OH or HO_2 radicals are identical due to the rapid equilibrium between the two species. The radical influx is almost certainly not due to one species; however, the above procedure represents a workable approximation. The above rate was arrived at such that no simulation had a rate of hydrocarbon consumption

exceeding the experimental data with only the radical influx. In runs that showed a slow initial rate of consumption of hydrocarbon, an amount of initial nitrous acid (1 to 50 ppb) was postulated to increase the reactivity. The level of nitrous acid assumed for each run is tabulated in the appendices. Control experiments on the SAPRC chamber are needed to elucidate the quantitative nature of nonhomogeneous radical sources.

4.2 GENERAL APPROACH TO DEVELOPMENT OF MECHANISMS

Initially, we developed the mechanisms for propene, n-butane, and toluene independently of each other using the preliminary work done by others as a starting point but adding the new laboratory data and estimations where appropriate. The mechanisms for the reactions of ethene, 1-butene, and trans-2-butene then were prepared using propene as a model, whereas the 2,3-dimethylbutane mechanism was developed using the n-butane work. Once the individual models were constructed, we attempted to make them consistent. Because of the wide range of propene data, most changes were first tested using a block of propene experiments with as wide a range of conditions as possible. Then the effects of changes were tested on the various mechanisms to ensure that changes would be compatible with each mechanism. Once the mechanisms were compatible, adjustments were made in the decomposition of peroxynitric acid and peroxyalkyl nitrates and in the OH + aldehyde rate constants. All simulations were carried out using the Systems Applications, Inc. routine CHEMK on either the CDC-6400 computer at SRI International or the CDC-7600 at the Lawrence Berkeley Laboratory of the University of California, Berkeley.

After the individual mechanisms were complete, they were combined as needed to model the chamber data for the various mixtures and tested with representative mixtures. When these results proved to be satisfactory, simulations were carried out for all the conditions for which there were smog chamber experiments.

4.3 ALKENES

The mechanism developed for each alkene is given in Appendix A, Tables A-3 to A-6. The starting conditions for each SAPRC chamber reaction to which the models have been applied are summarized in Tables A-1 and A-2. The photolysis rate constants that have been used are summarized in Tables A-7 and A-8 and have been obtained as discussed in Section 3.6. The concentration-time plots for all the runs that have been computed are given in Appendix A. For more careful analysis we have redrawn representative runs for each alkene, ethene, propane, butene-1, and trans-butene-2, as shown in Figures 4 to 10. In these figures the simulation concentrations are represented by the solid lines and the experimental concentrations by the points.

The four propene experiments reflect a wide range of initial concentrations and ratios of hydrocarbon to NO_x. For runs EC-60 and EC-17, the initial [propene]/[NO_x] = 1.0, whereas the concentration of propene for EC-60 is ten times that for EC-17. For runs EC-21 and EC-11, [propene]/[NO_x] = 0.2 and 5.0, respectively. In general the agreement between our simulated curves and the experimental points is very good. The largest differences show up in the data for formaldehyde, acetaldehyde, and peroxyacetyl nitrate--components for which the experimental data are the most uncertain.

The experiments shown for ethene (Figure 8), 1-butene (Figure 9), and trans-2-butene (Figure 10) are at [RH]/[NO_x] ratios of about 0.4. The good agreement between simulation and chamber data indicates the validity of the alkene mechanism in general and its applicability to specific alkenes. The mechanism is the least reliable for ethene where ozone is underpredicted. The components that show the poorest agreement in general are the peroxyacylnitrates and aldehydes, for which the laboratory data are the most uncertain.

Examples of the results with mixtures are shown in Figure 11 for ethene-propene; Figure 12 for propene-1-butene; and Figure 13 for ethene, propene, 1-butene, and trans-2-butene. The agreement in these mixtures

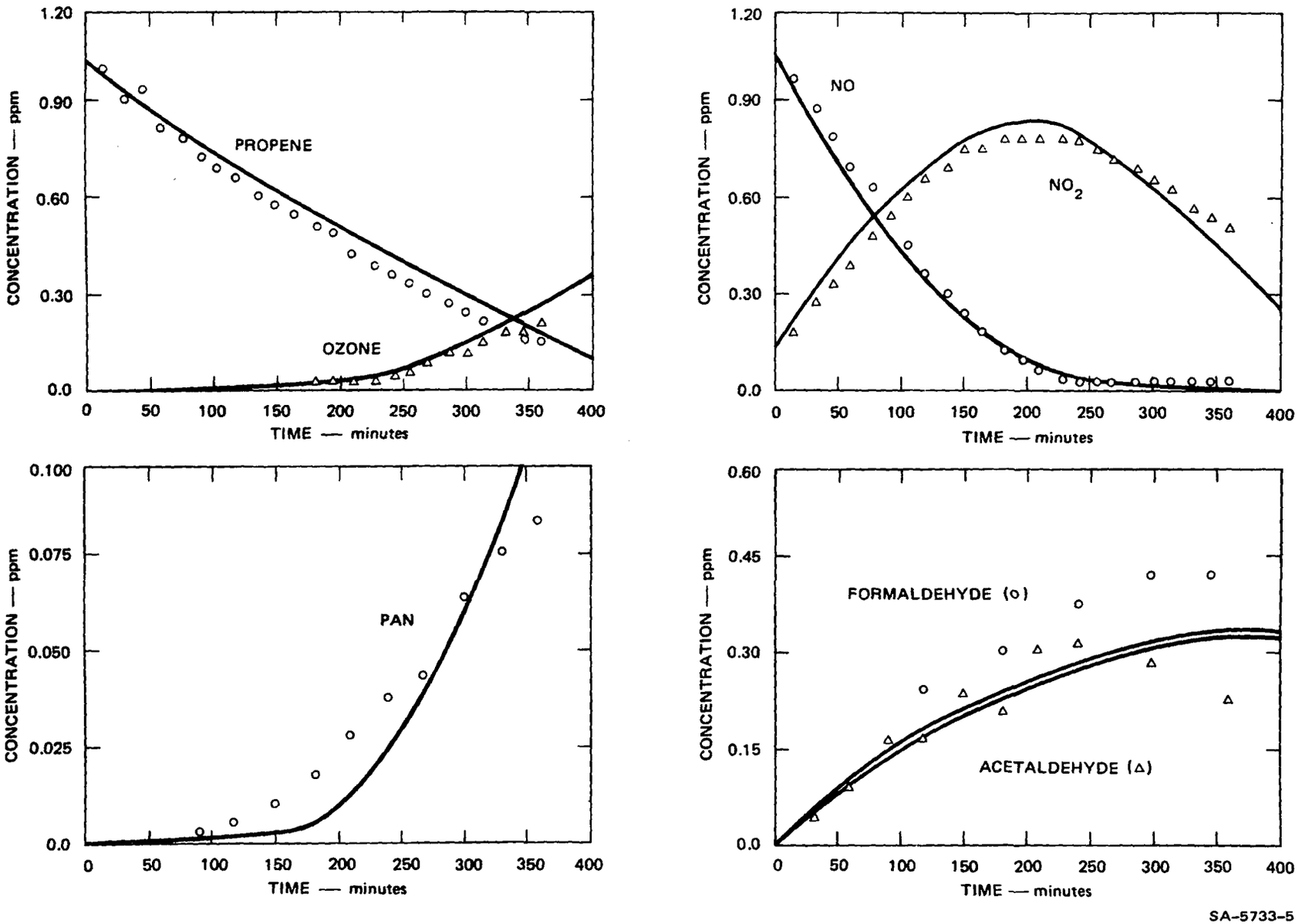

Figure 4. Simulation of SAPRC EC-60: 1.04 ppm Propene and 1.25 ppm NO_x.

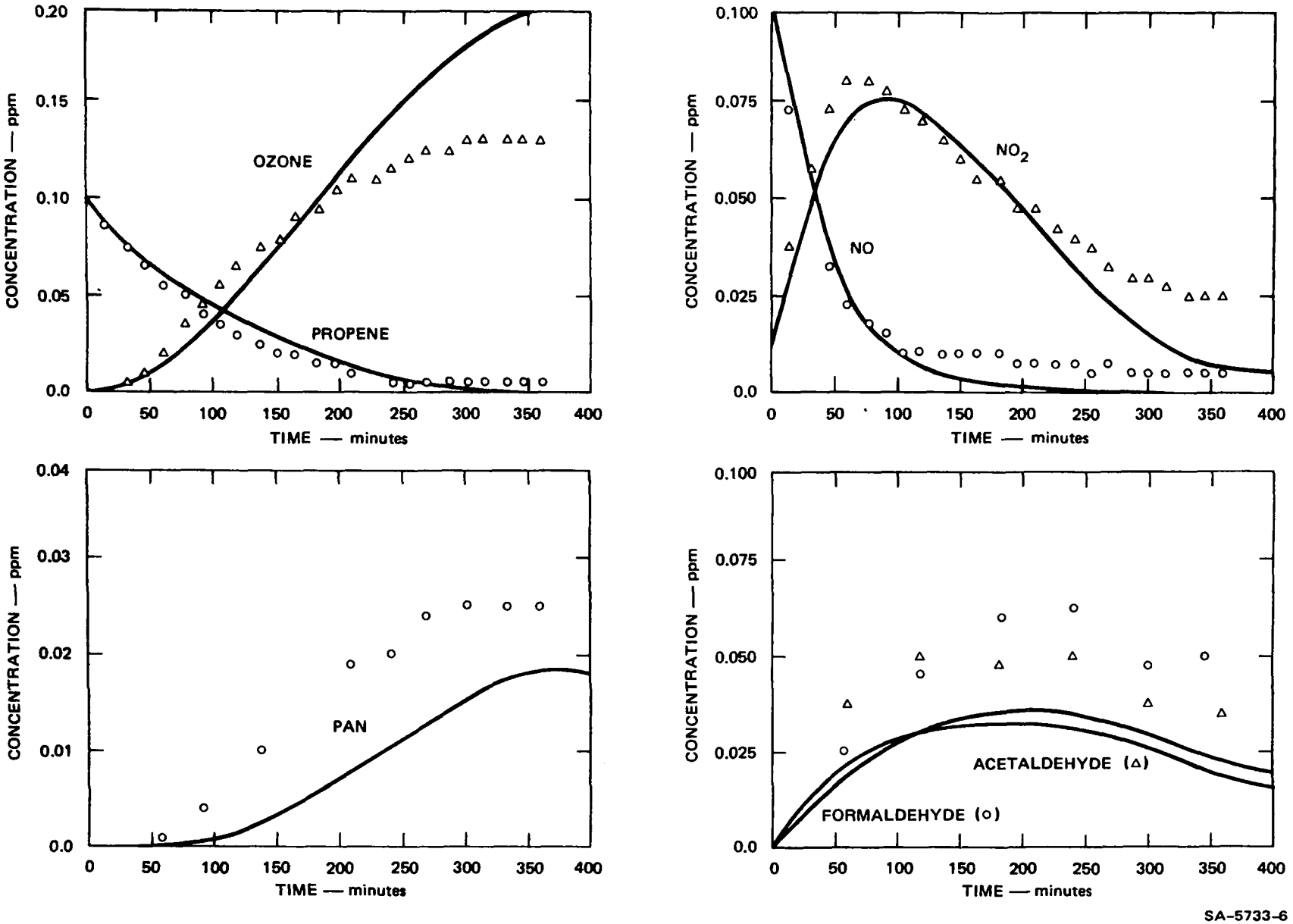

Figure 5. Simulation of SAPRC EC-17: 0.103 ppm Propene and 0.106 ppm NO_x.

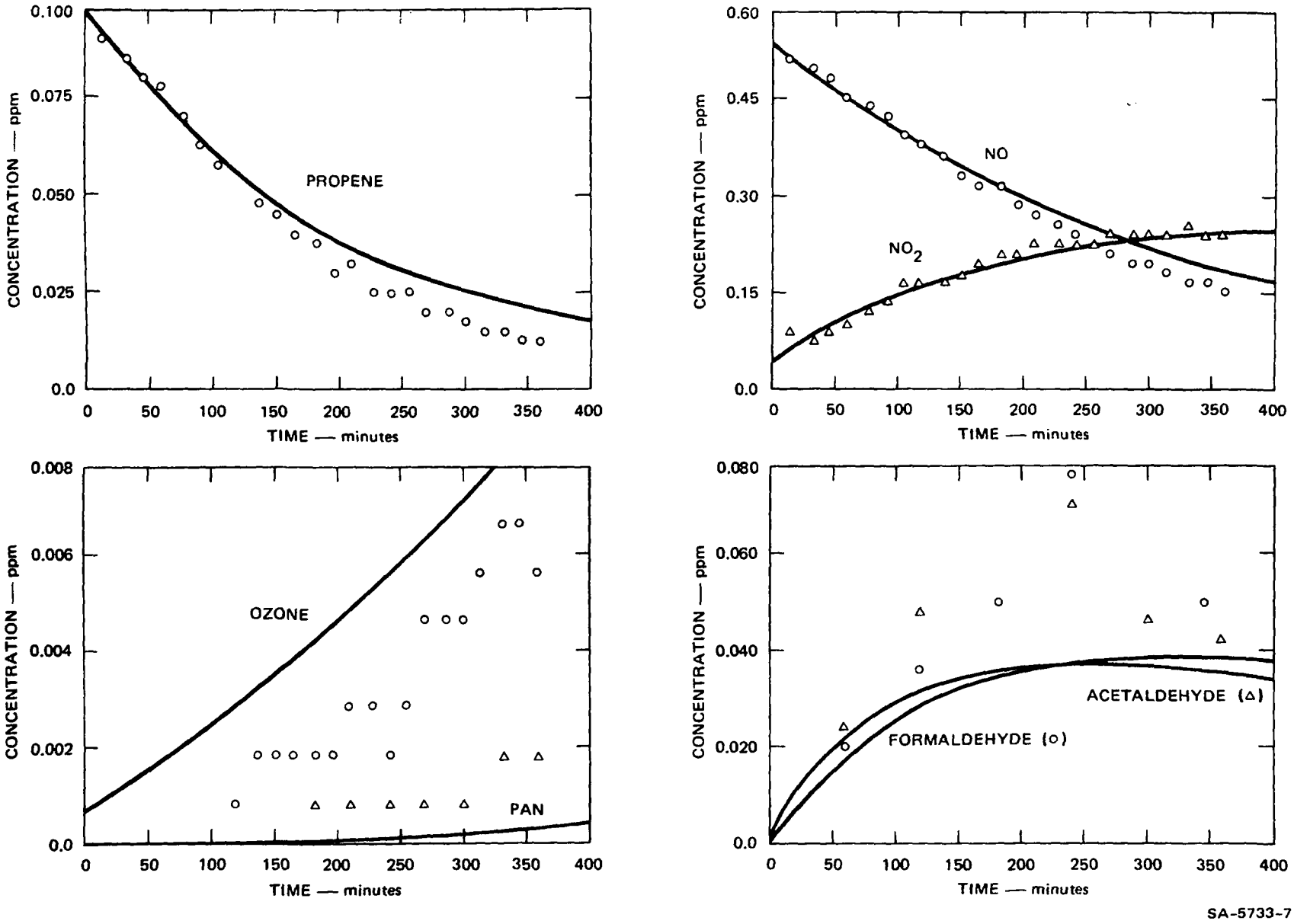

Figure 6. Simulation of SAPRC EC-21: 0.104 ppm Propene and 0.624 ppm NO_x.

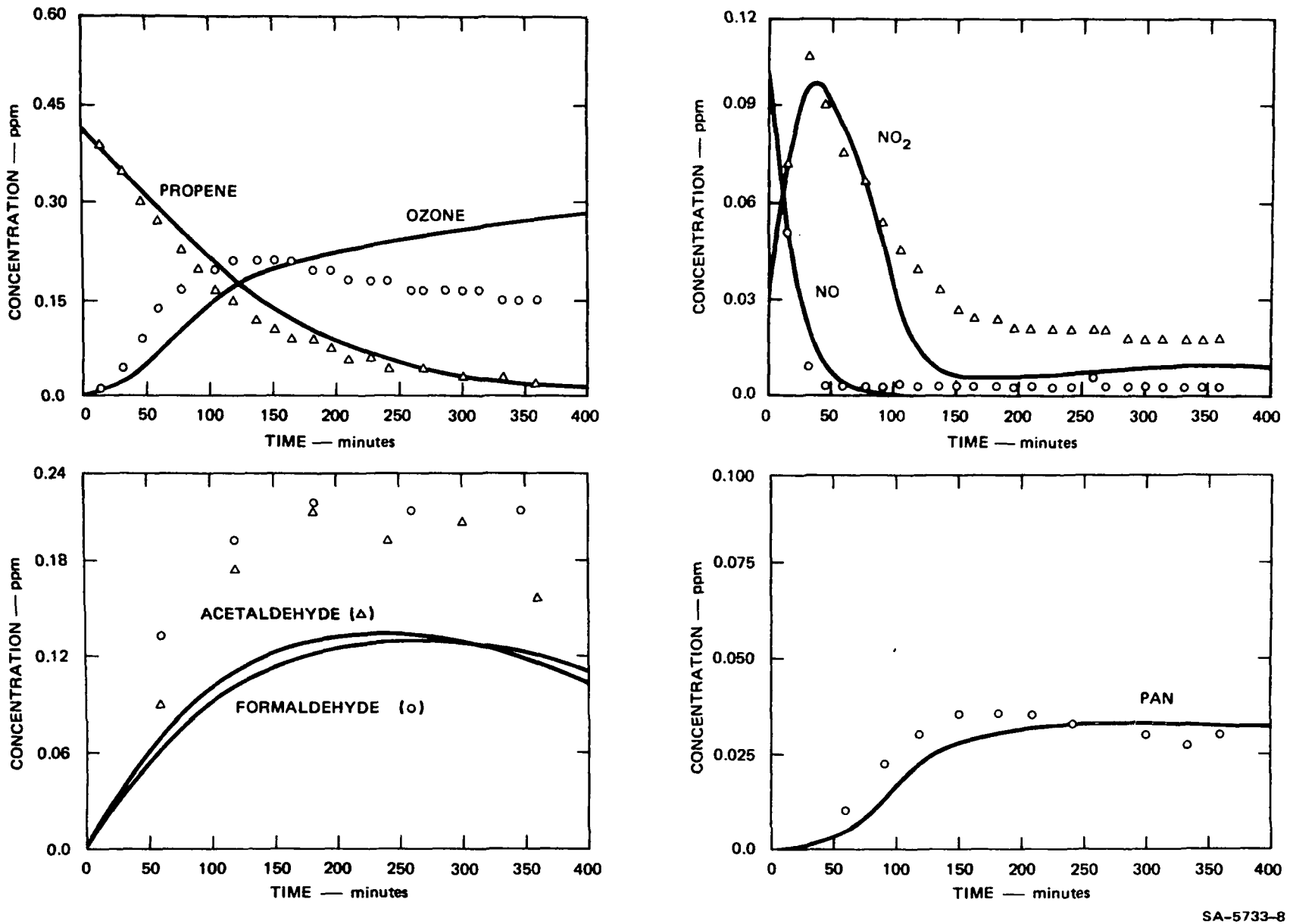

Figure 7. Simulation of SAPRC EC-11: 0.447 ppm Propene and 0.135 ppm NO_x.

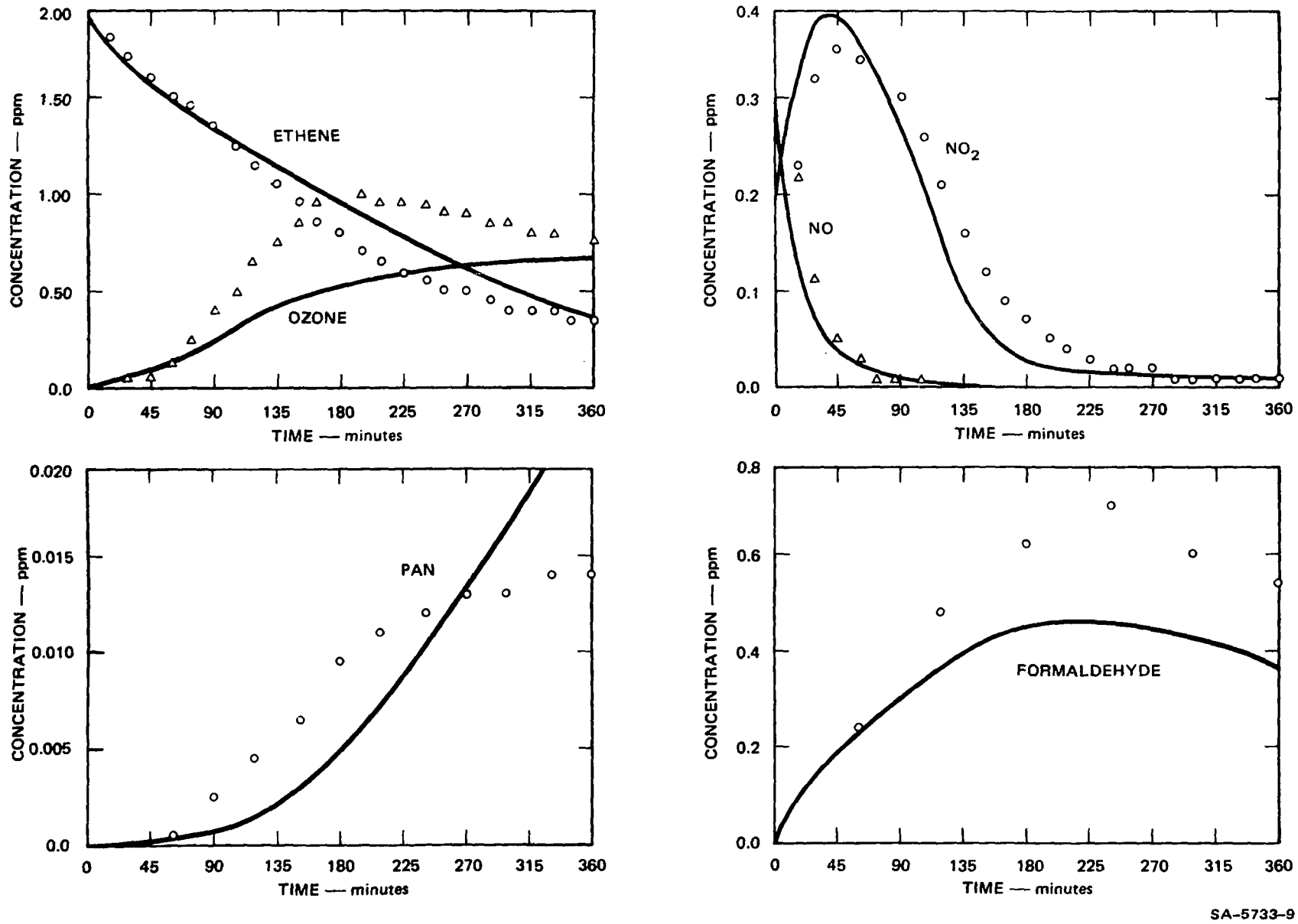

Figure 8. Simulation of SAPRC EC-156: 2.00 ppm Ethene and 0.501 ppm NO_x.

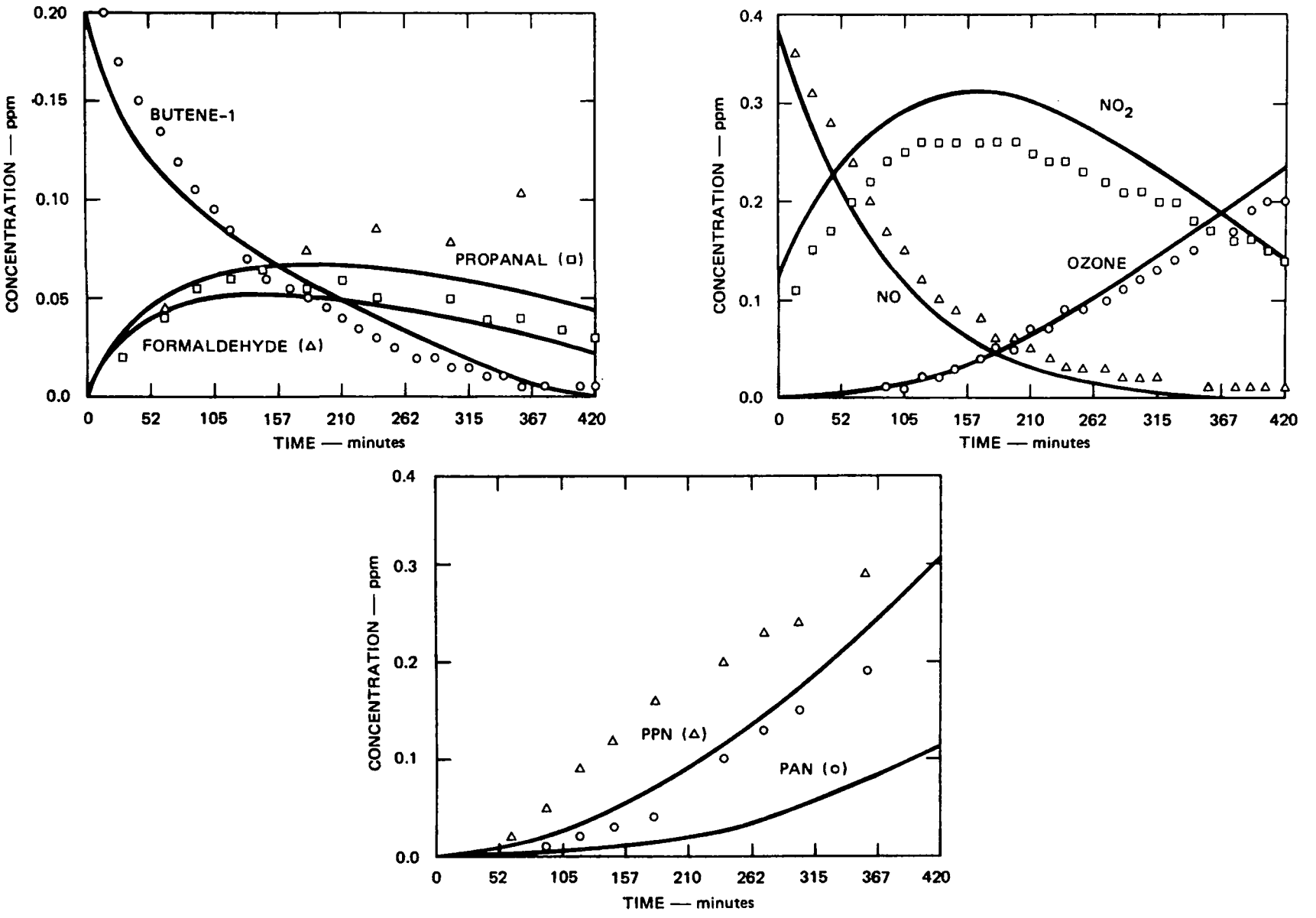

Figure 9. Simulation of SAPRC EC-122: 0.217 ppm Butene-1 and 0.500 ppm NO_x.

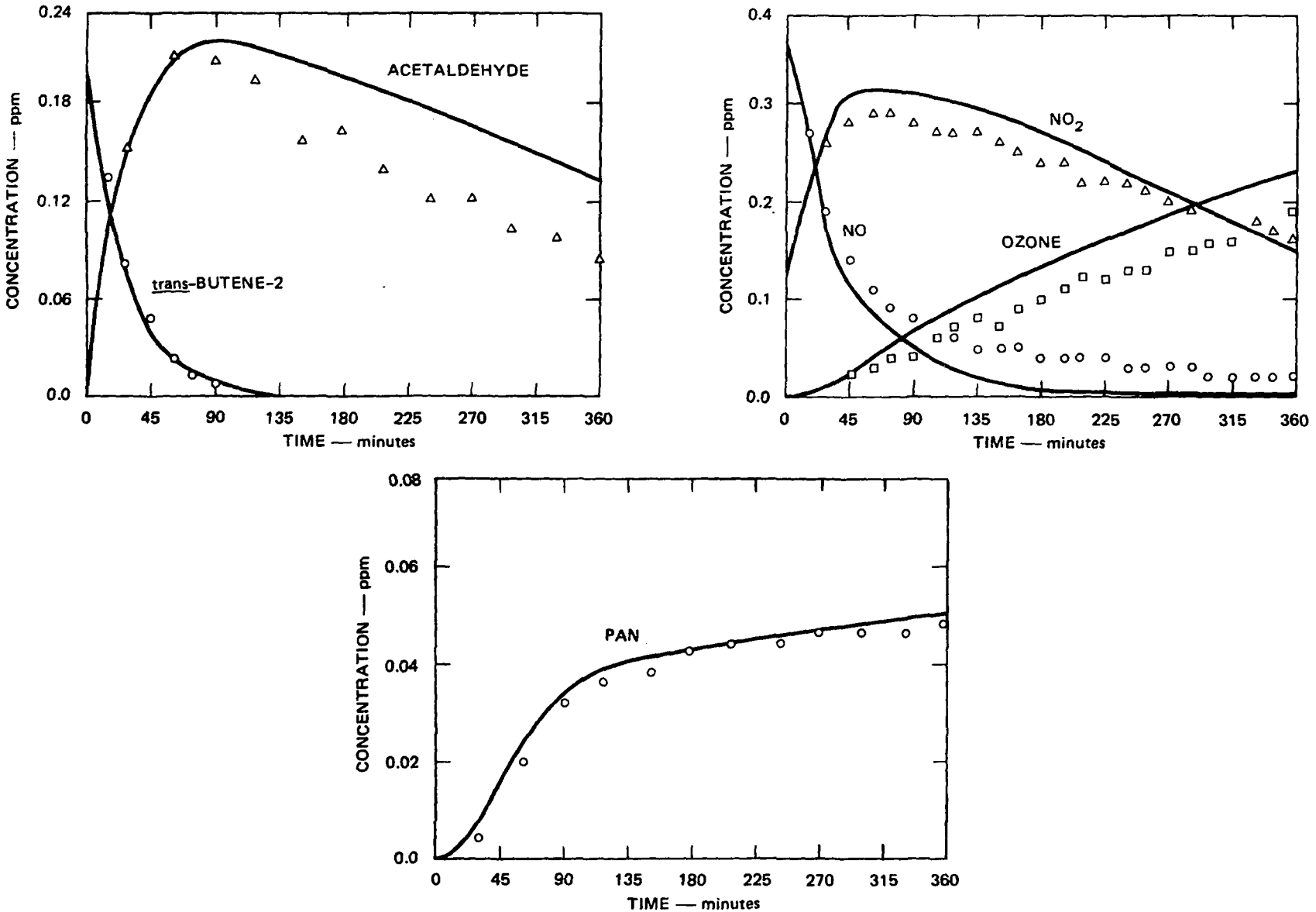

Figure 10. Simulation of SAPRC EC-157: 0.216 ppm trans-Butene-2 and 0.525 ppm NO_x.

is good and indicates that the individual mechanisms are additive with no synergistic effect being apparent.

Analysis of the simulation of all the alkene runs summarized in Appendix A shows that the fits for some runs are far from satisfactory. The reason for the variation of these experiments from the computed data cannot be easily ascertained. However, the effect cannot be related to initial reactant concentrations since in most cases the concentrations are matched in other runs where the fits are good. In general, data trends suggest that the calculated simulations of the early chamber runs tend to be slower than observed while those calculated for the later runs tend to be faster than observed. For example, chamber runs EC-13, -55, and -216 were carried out with about 0.5 ppm of propene and 0.5 ppm of NO_x; although there is a variation in the light intensity that the model takes into consideration, the computed curves are slower than those observed for EC-13, about the same for EC-55, and faster than those for EC-216. In the absence of light intensity data at various wavelengths, the fact that EC-55 was slower than EC-13 was assumed by Whitten and Hugo[5] to have resulted from a faster deterioration of the solar simulator output in the short wavelength region where ozone and aldehyde selectively absorb than at the longer wavelengths where NO_2 predominantly absorbs. Thus, photolysis of ozone and aldehydes was assumed to be slower in EC-55 due to deterioration of the light source. However, the very recent propene runs (for example 216), where the relative light intensities have been measured and where there can be little question as to photolysis rates, continue the trend of lower chamber reactivity with time. Thus, while light source deterioration may account for some of the effect in the early runs, it clearly cannot be the cause of the problem in the later runs.

There are other important factors that we believe are related to the ability of chambers to produce radicals along the lines discussed in Section 4.1. Therefore, in addition to the simulation in Appendix A using the standard conditions that assume an input of radicals of 2 x

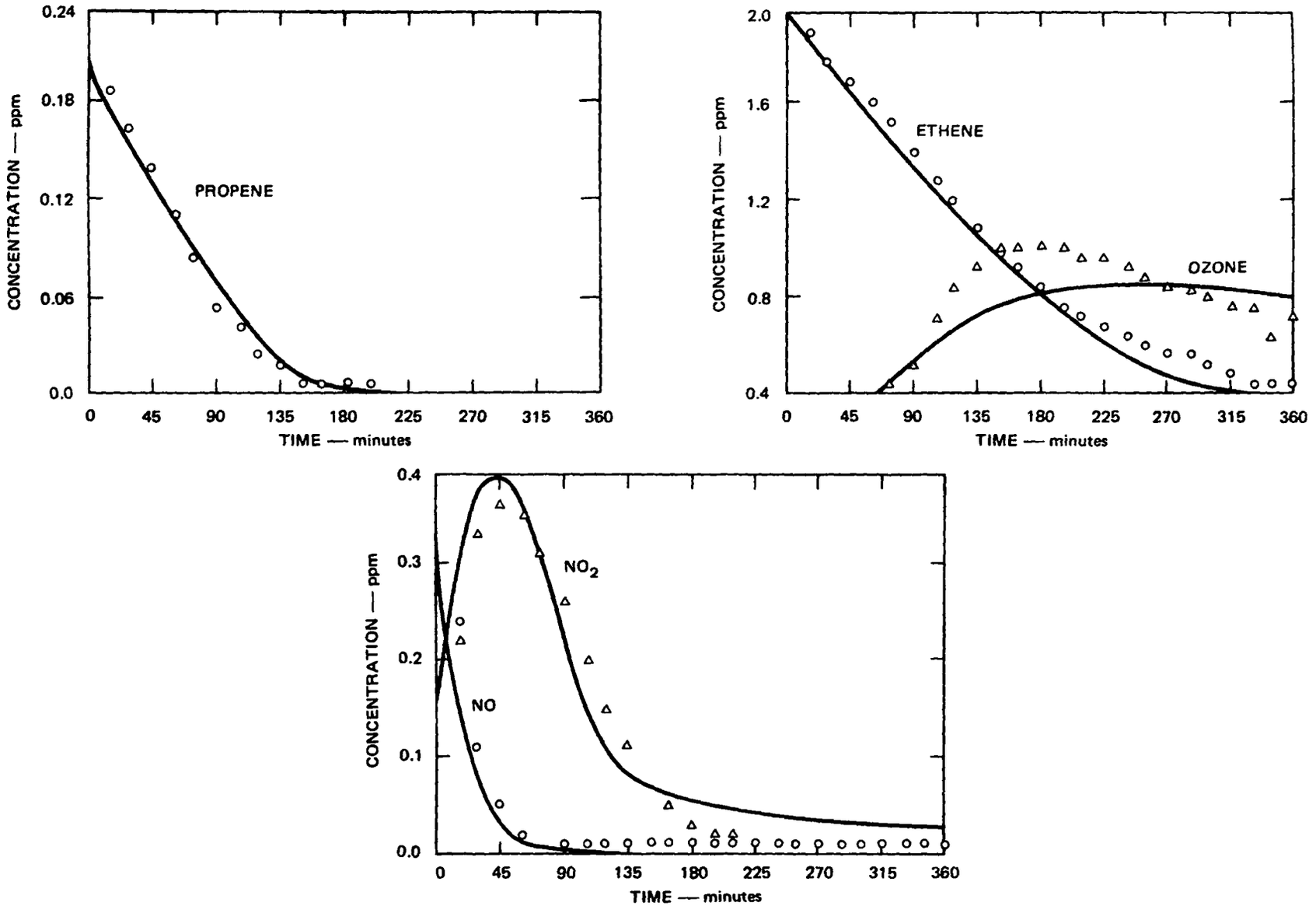

Figure 11. Simulation of SAPRC EC-144: 2.03 ppm Ethene, 0.221 ppm Propene, and 0.509 ppm NO_x.

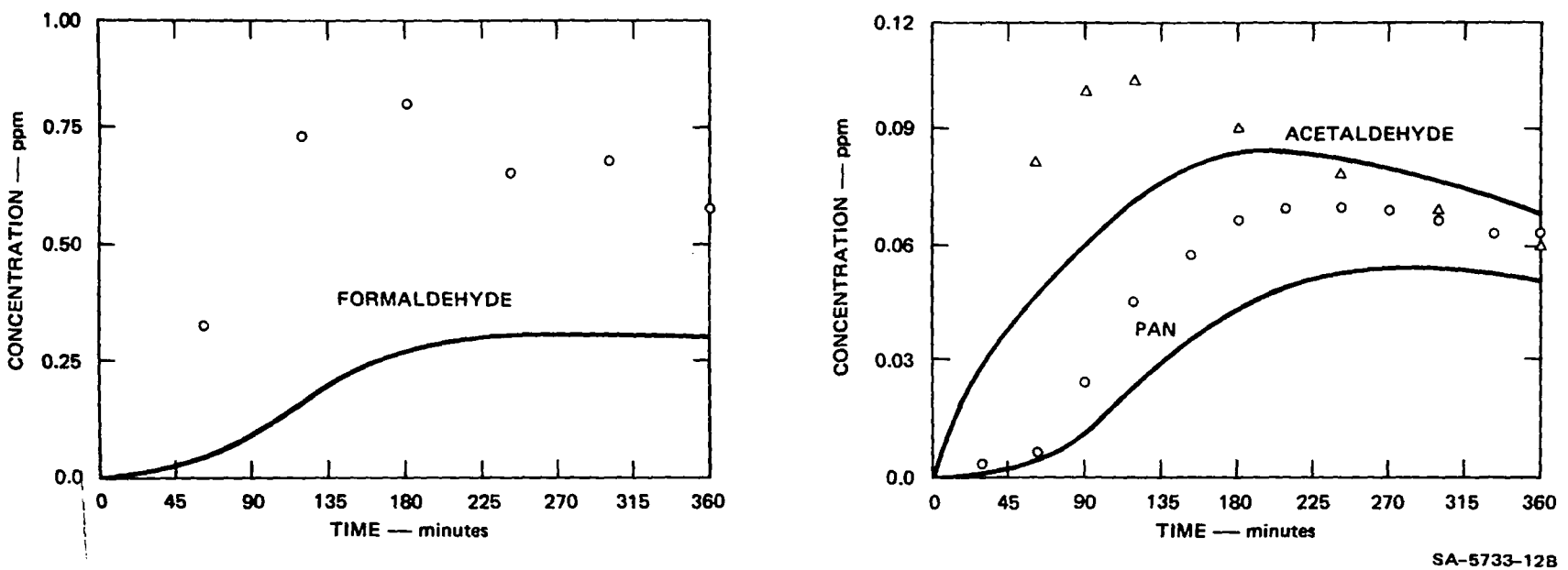

Figure 11. Simulation of SAPRC EC-144: 2.03 ppm Ethene, 0.221 ppm Propene, and 0.509 ppm NO_x (Concluded).

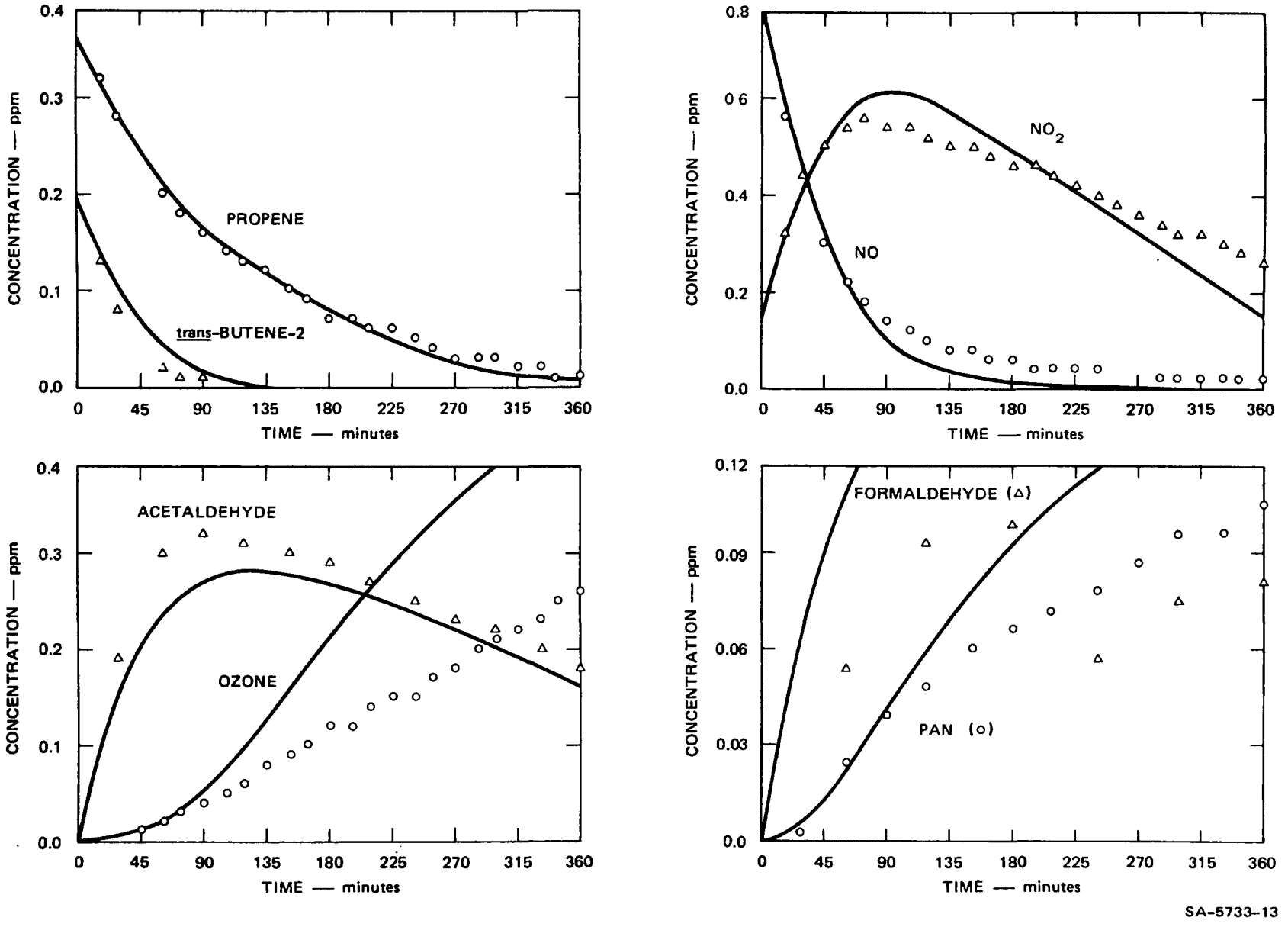

Figure 12. Simulation of SAPRC EC-149: 0.384 ppm Propene, 0.209 ppm trans-Butene-2, and 0.989 ppm NO_x.

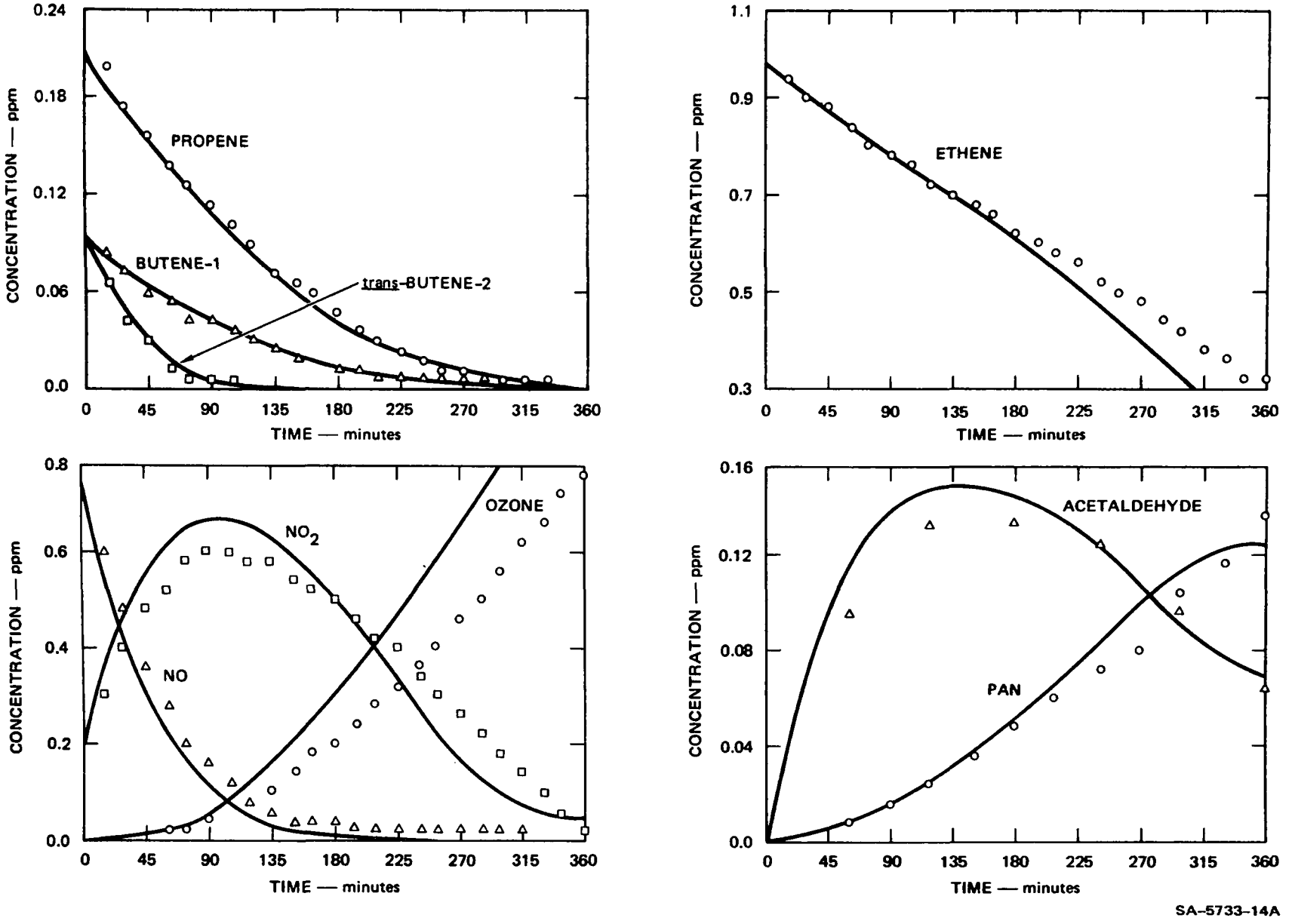

Figure 13. Simulation of SAPRC EC-150: 1.01 ppm Ethene, 0.224 ppm Propene, 0.097 ppm Butene-1, 0.093 ppm trans-Butene-2, and 0.998 ppm NO_x.

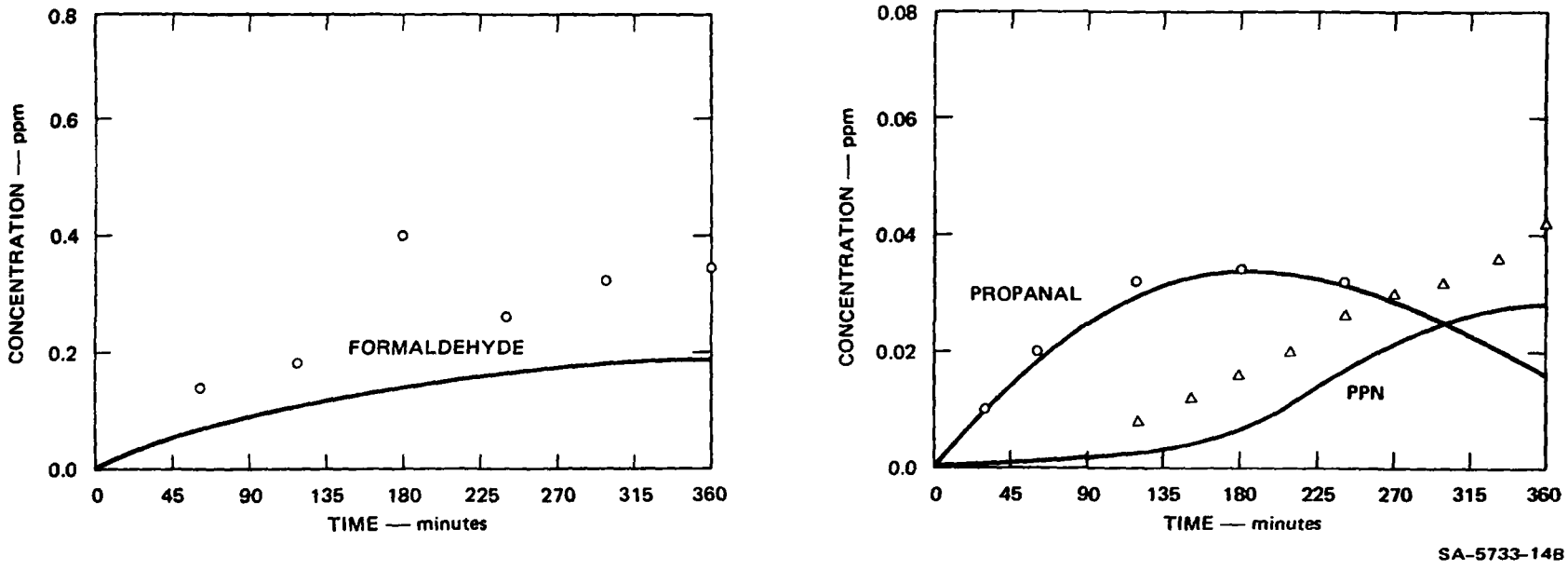

Figure 13. Simulation of SAPRC EC-150: 1.01 ppm Ethene, 0.224 ppm Propene, 0.097 ppm Butene-1, 0.093 ppm trans-Butene-2, and 0.998 ppm NO_x (Concluded).

10^{-4} ppm^{-1} min^{-1}, we have included simulations where we have altered this radical input rate for several runs. It is necessary to increase the radical addition rate to improve the fit for the earlier runs EC-13, 16, -53, and -54, and to reduce it to zero for the later runs EC-216 and EC-217. The implication is that an aging process has occurred with the SAPRC chamber so that there are essentially no chamber sources of radicals in the most recent runs. However, initially there were sources of radicals in the chamber, and these sources apparently varied depending on such factors as previous chemical history of the chamber and clean-out procedures. The effect of removing the heterogeneous source of radicals in runs EC-216 and EC-217 is small, although it is a step in the right direction. The possibility exists that the chamber wall may be actually consuming radicals rather than generating radicals or remaining passive. Such processes have been invoked in many experimental programs, but further experiments are necessary to determine whether these processes may be important in smog chambers.

4.4 ALKANES AND ALKANE-ALKENE MIXTURES

The available SAPRC data on alkanes consist of an extensive series of runs using n-butane, and three runs using 2,3-dimethylbutane. Appendix B describes the results of the simulations for each run, using the mechanisms tabulated in Tables B-3 and B-4, along with the initial conditions and photolytic rate constants. Some typical runs are described and discussed below. SAPRC has also reported data on propene-n-butane mixtures. A mixture of propene and n-butane is often used to represent the hydrocarbons present in the polluted troposphere. These runs allow the testing of the mechanisms developed for individual hydrocarbons under conditions somewhat different from those for which the mechanisms were developed, and somewhat closer to the conditions where they may be used in a practical predictive manner.

The results of the simulations for each run, using the mechanisms described previously (see Section 3.8), are presented in Appendix B, along with the initial conditions and photolysis rate constants. Some typical runs are described and discussed below.

n-Butane--Figures 14 through 16 show the results of simulating SAPRC runs EC-42, -39, and -178. Runs EC-42 and EC-178 have the lowest (0.64) and highest (19.8) hydrocarbon to NO_x ratios in the n-butane-NO_x series. EC-39 has a hydrocarbon to NO_x ratio (3.8) typically used in many experiments. The results are, in general, very good; the simulations reproduce well the experimentally observed concentration-time profiles. In run EC-42, the ozone concentrations are not accurately matched; however, extremely low levels of ozone ($\sim$ 5 ppb) were observed, and the experimental measurement is probably unreliable at these levels. In EC-178, the computed PAN concentration is too low by about a factor of 2; this result is seen in several other runs in the n-butane set (see Appendix B). PAN is formed only in relatively small amounts in n-butane systems and is difficult to measure because in the gas chromatographic analysis used its peak overlaps that of butyl nitrate. Thus, the experimental measurements may contain a systematic error. Alternatively, if the experimental measurements are accurate, then the computer-simulated level of acylperoxy radicals is too low. In the simulations, acylperoxy radicals are produced primarily by hydroxy radical abstraction from acetaldehyde; therefore, this rate may be too slow. The mechanism may be missing some alternative route to acylperoxy radicals, or the amount of acetaldehyde present may be too low.

Apart from the PAN concentrations described above, there appear to be no systematic discrepancies between the computed and experimental concentrations in the n-butane systems. It is encouraging that the same mechanism can simulate the results of experiments with initial

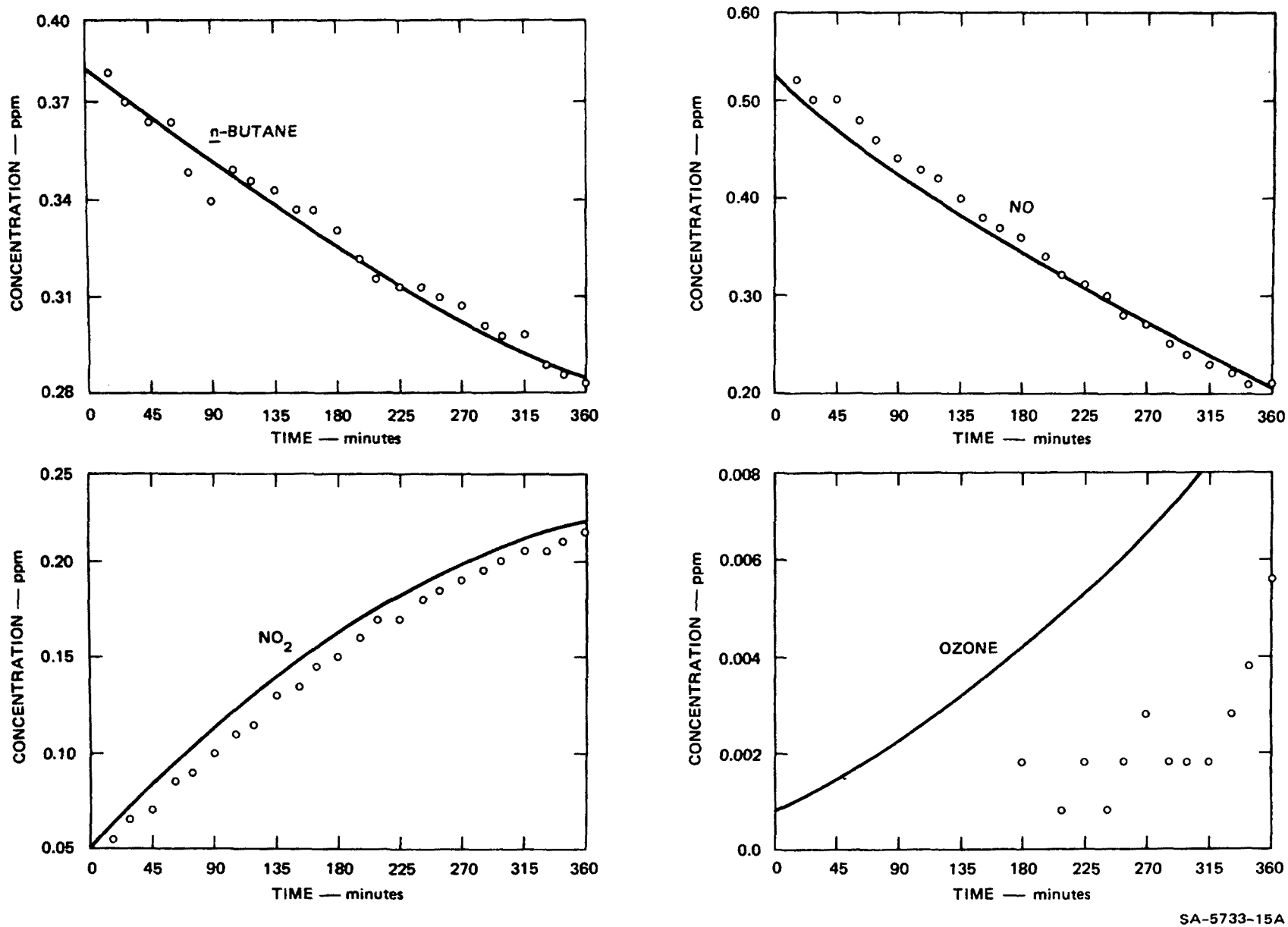

Figure 14. Simulation of SAPRC EC-42: 0.385 ppm n-Butane and 0.601 ppm NO_x.

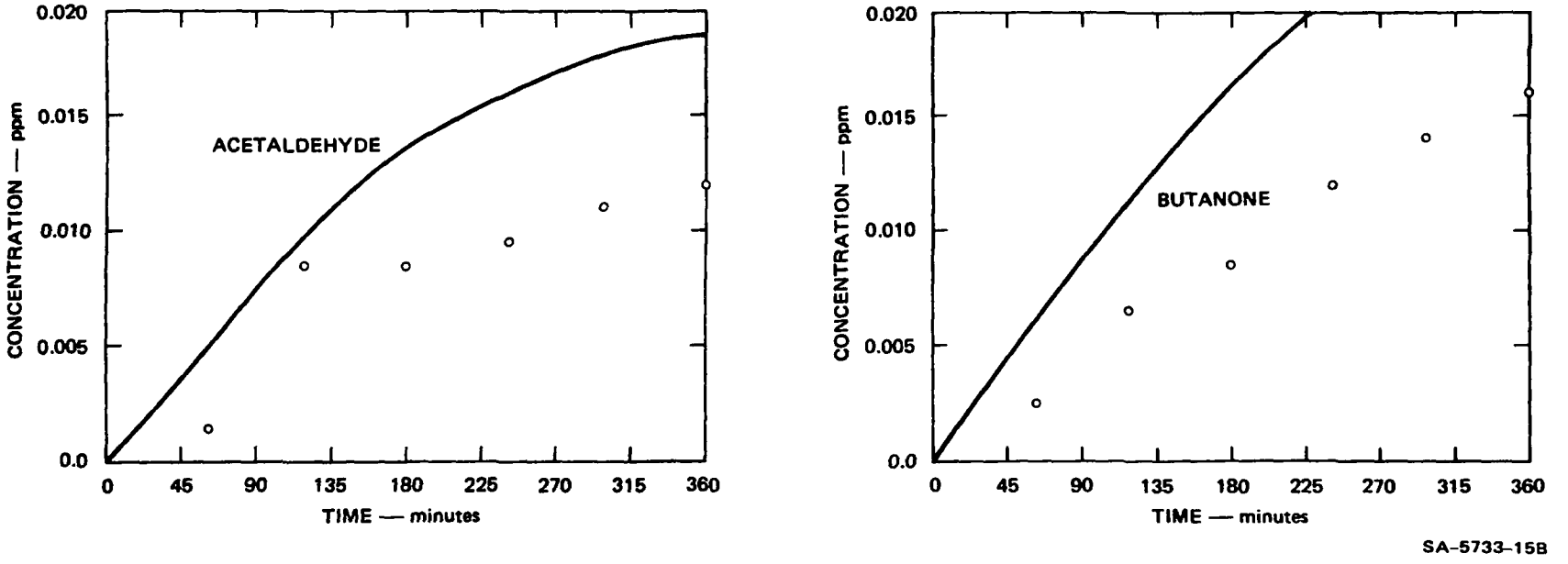

Figure 14. Simulation of SAPRC EC-42: 0.385 ppm n-Butane and 0.601 ppm NO_x (Concluded).

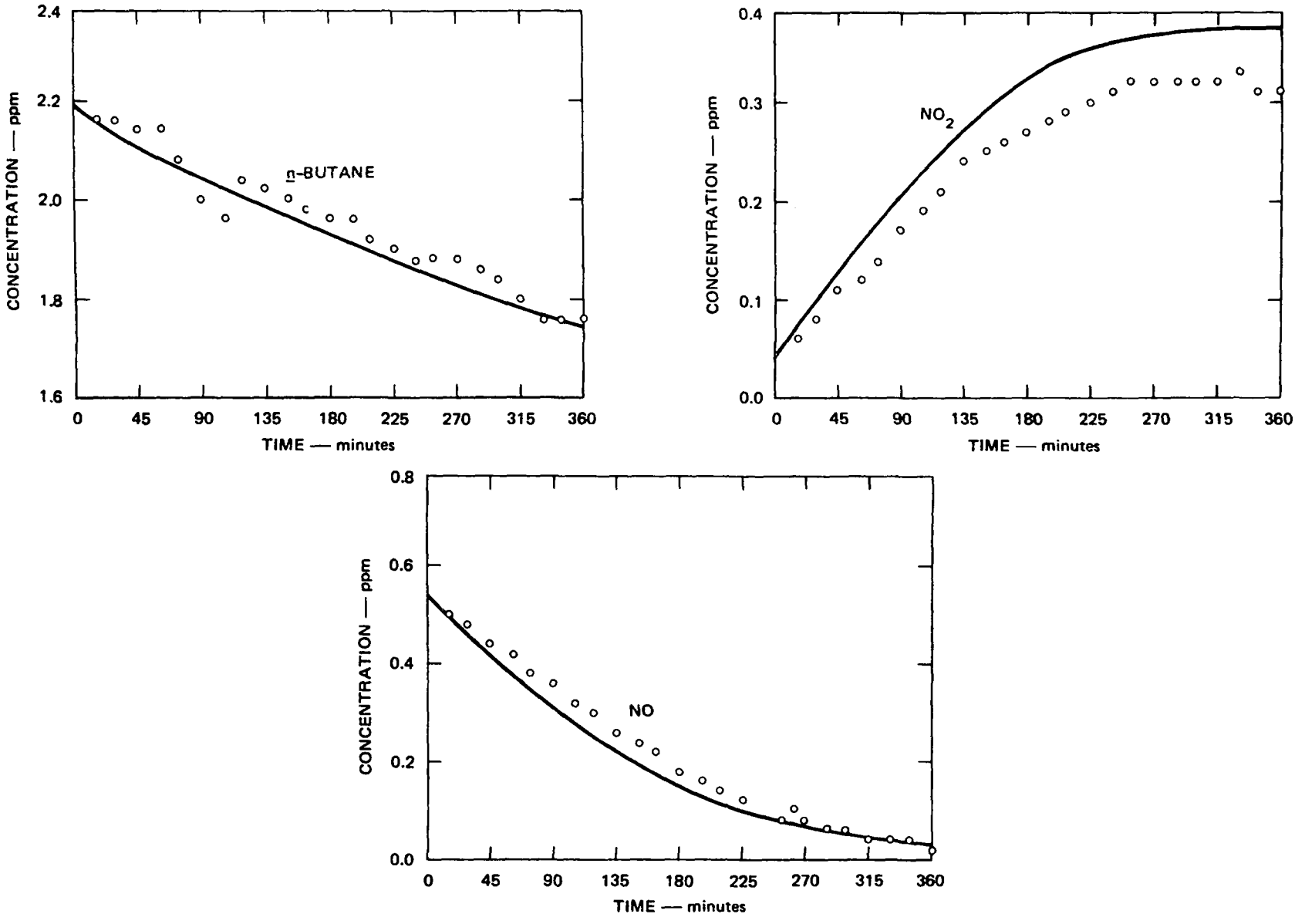

Figure 15. Simulation of SAPRC EC-39: 2.2 ppm n-Butane and 0.61 ppm NO_x.

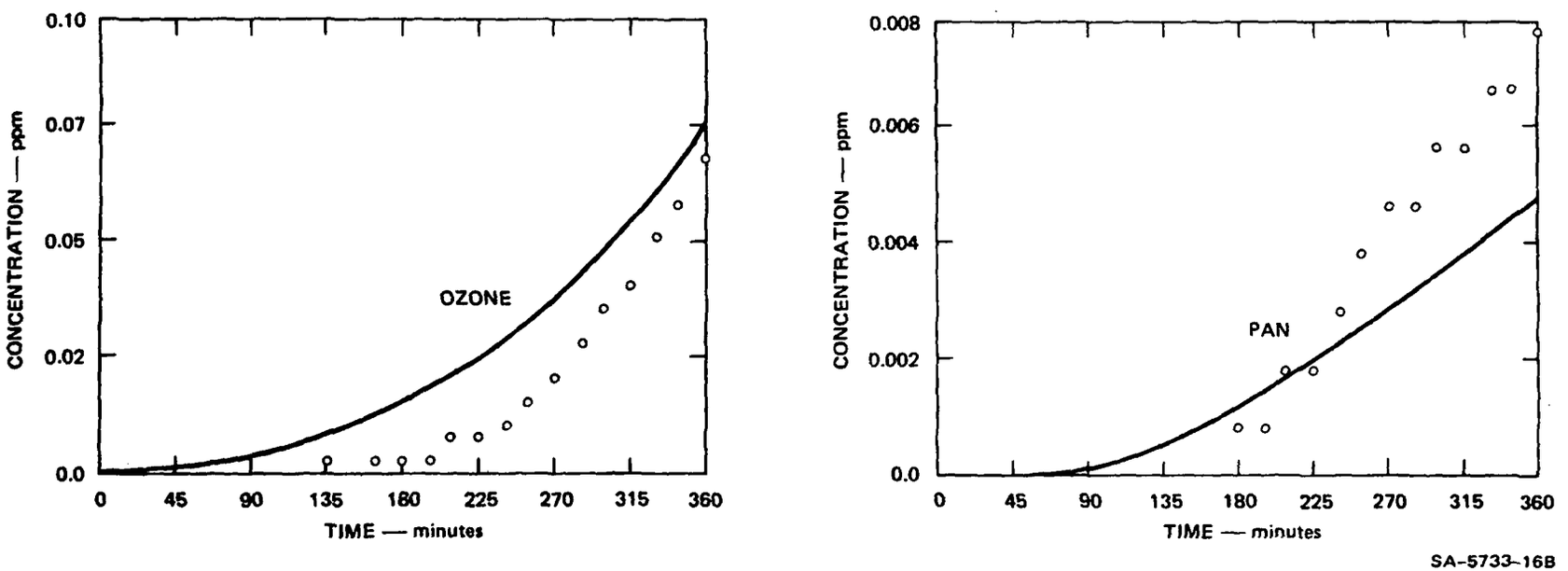

Figure 15. Simulation of SAPRC EC-39: 2.2 ppm n-Butane and 0.61 ppm NO_x (Concluded).

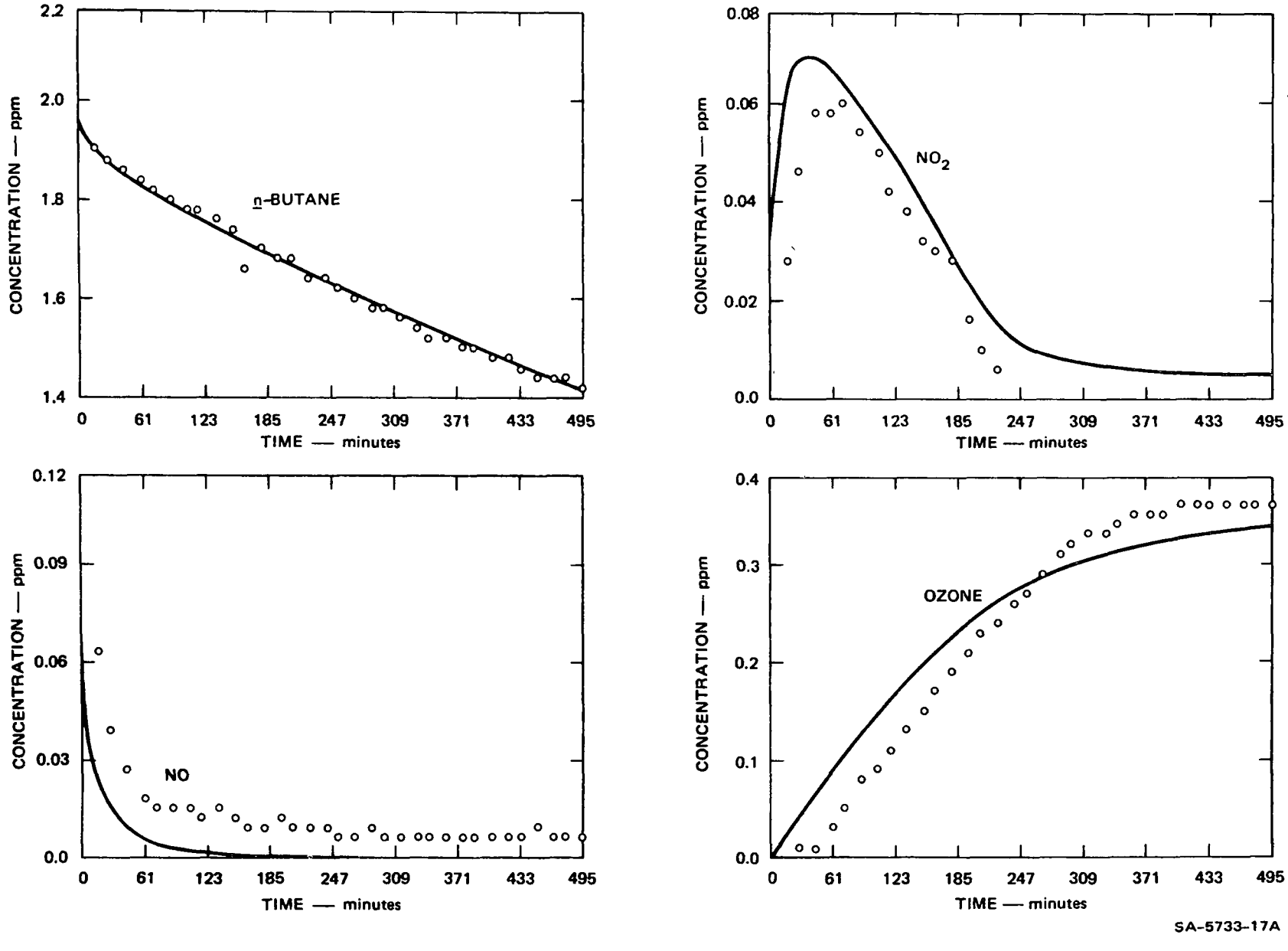

Figure 16. Simulation of SAPRC EC-178: 1.96 ppm n-Butane and 0.099 ppm NO_x.

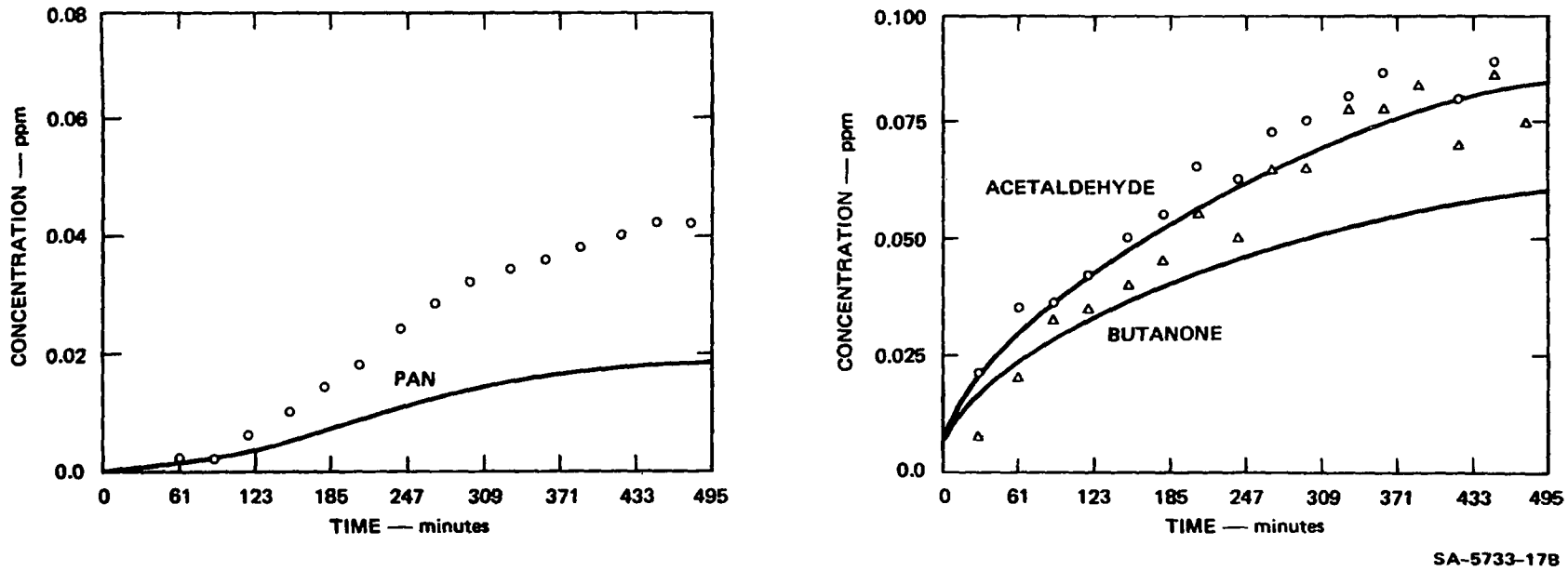

Figure 16. Simulation of SAPRC EC-178: 1.96 n-Butane and 0.099 ppm NO_x (Concluded).

hydrocarbon to NO_x ratios varying by a factor of 30, using only one adjustable parameter--the amount of initial nitrous acid.

In Appendix B, two simulations are shown for EC-46 and EC-49--the "aldehyde memeory effect" runs (see Section 4.1). The second simulation shows the effect of increasing the influx of radicals by 50%. In both cases, these results show much better agreement between computed and experimental data.

2,3-Dimethylbutane--Figure 17 shows the simulation of SAPRC run EC-169. This run has the intermediate hydrocarbon-NO_x ratio of the three reported runs. The agreement between the computed and experimental concentration-time profiles are not as good as in the n-butane system; however, in general they show the correct qualitative behavior. This is to be expected, as there are few measured rate constants for the system and much reliance had to be placed on estimations.

Propene-n-Butane Mixtures--Runs made with mixtures composed of propene and n-butane were simulated using a mechanism that was a combination of the individual mechanisms for propene and n-butane without modification. The results of applying this mechanism to runs EC-106 and EC-115 are shown in Figures 18 and 19; these runs are typical of the seven reported. The results are generally good, comparable with those obtained using individual hydrocarbon runs. The ability of the mechanism to reproduce experiments under different conditions than those for which it was developed is good evidence that the overall chemistry is essentailly correct and contains a minimum of fortuitous compensations. This is particularly true of the n-butane mechanism, as it was developed for use in runs where the radical level is quite low. In the runs with propene, the radical level is much higher; yet the mechanism still seems to be able to reproduce the experimental results.

4.5 TOLUENE

The toluene mechanism, which is composed of reactions from Tables 1 and 12, has been used to simulate SAPRC chamber reactions. The initial

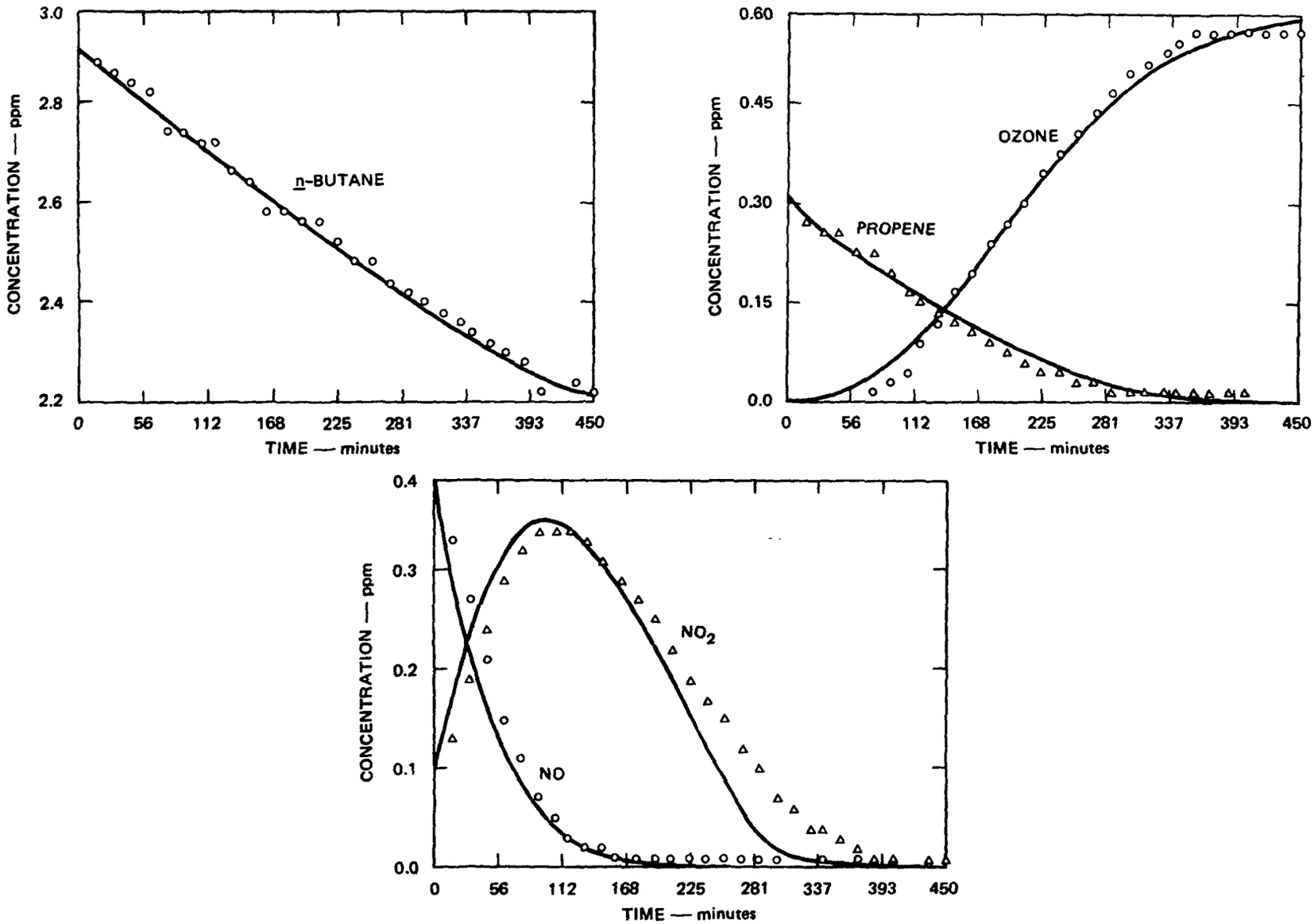

Figure 17. Simulation of SAPRC EC-115; 0.310 ppm *Propene*, 2.94 *ppm* n-Butane, and 0.506 ppm NO_x.

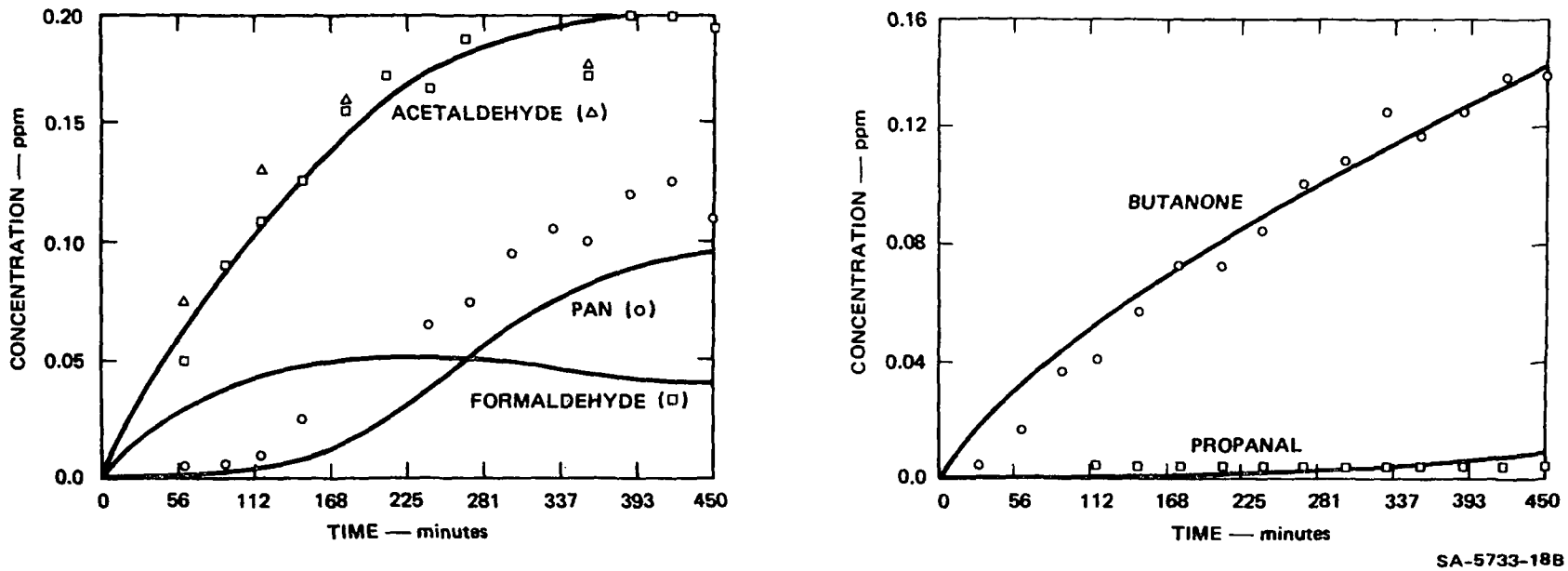

Figure 17. Simulation of SAPRC EC-115: 0.310 ppm Propene, 2.94 ppm n-Butane, and 0.506 ppm NO_x (Concluded).

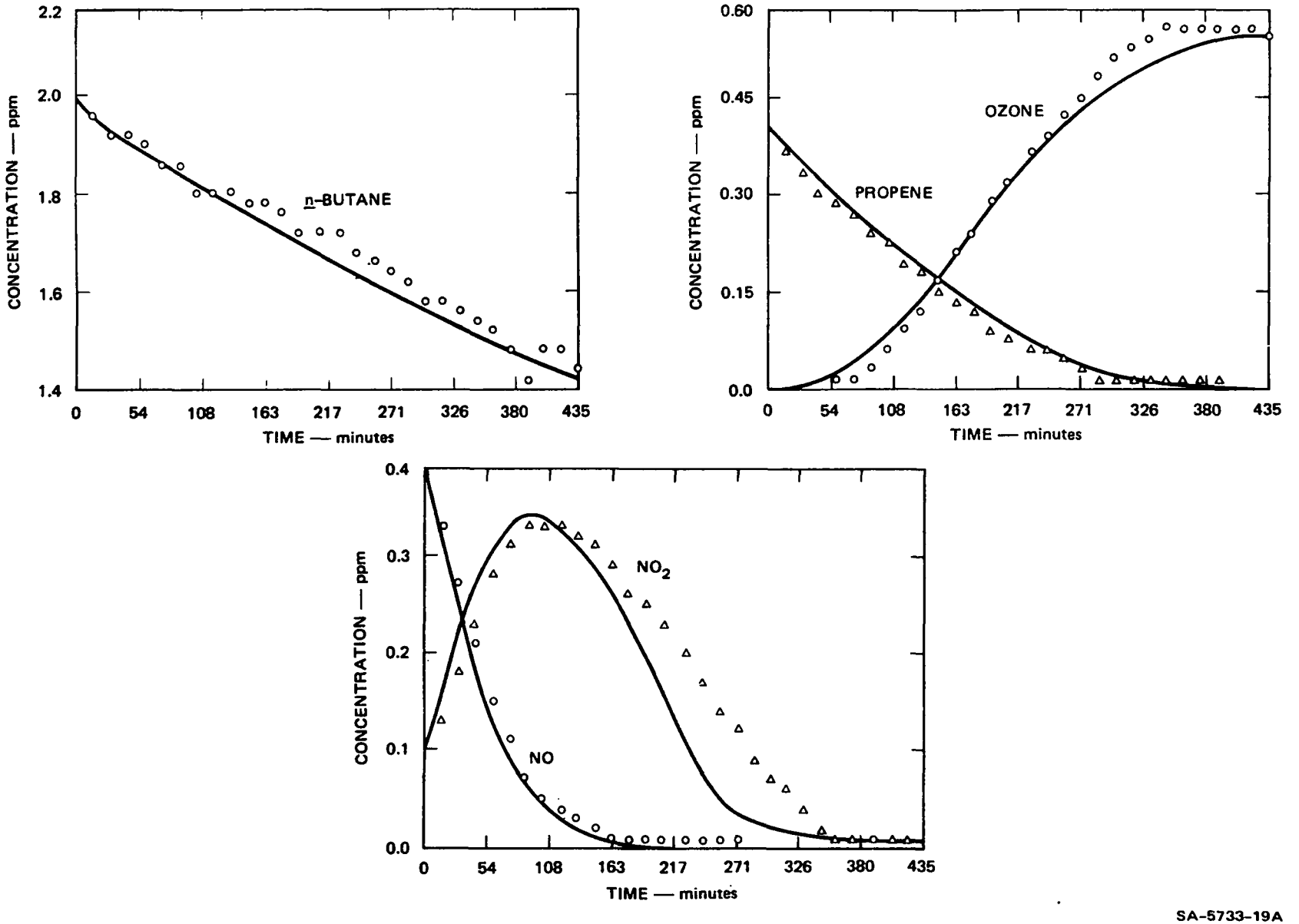

Figure 18. Simulation of SAPRC EC-106: 0.402 ppm Propene, 2.00 ppm n-Butane, and 0.500 ppm NO_x.

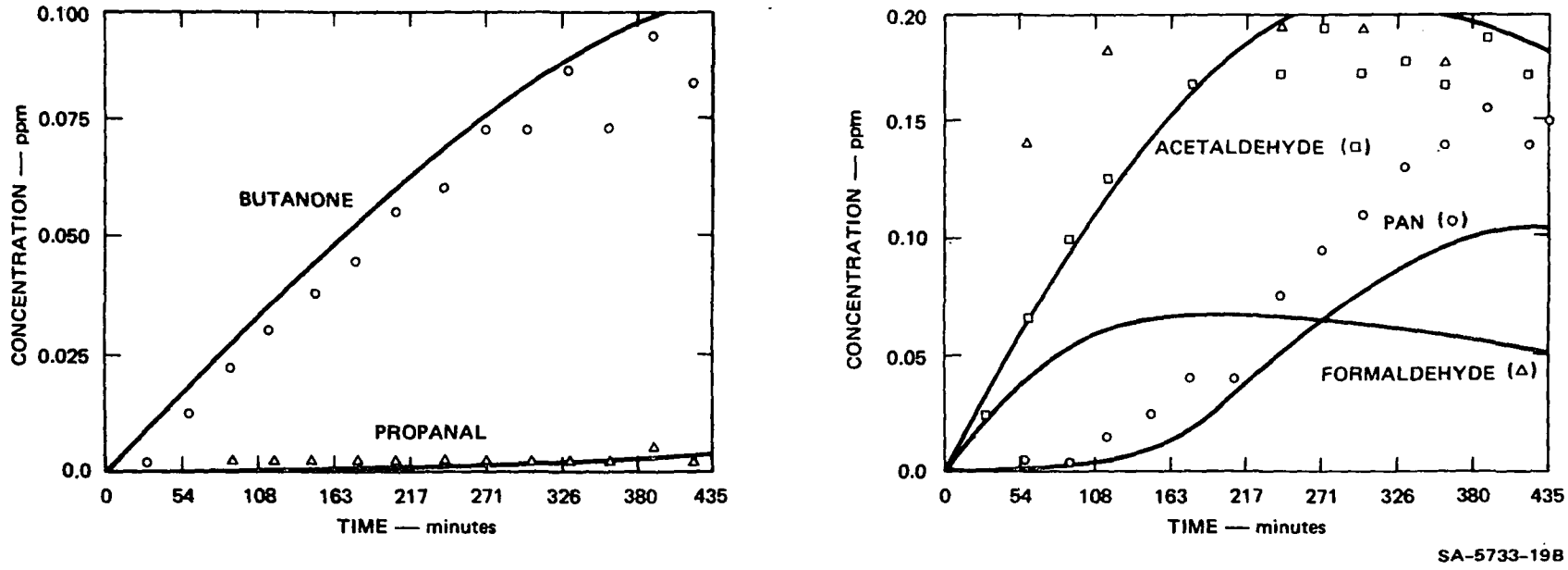

Figure 18. Simulation of SAPRC EC-106: 0.402 ppm Propene, 2.00 ppm n-Butane, and 0.500 ppm NO_x (Concluded).

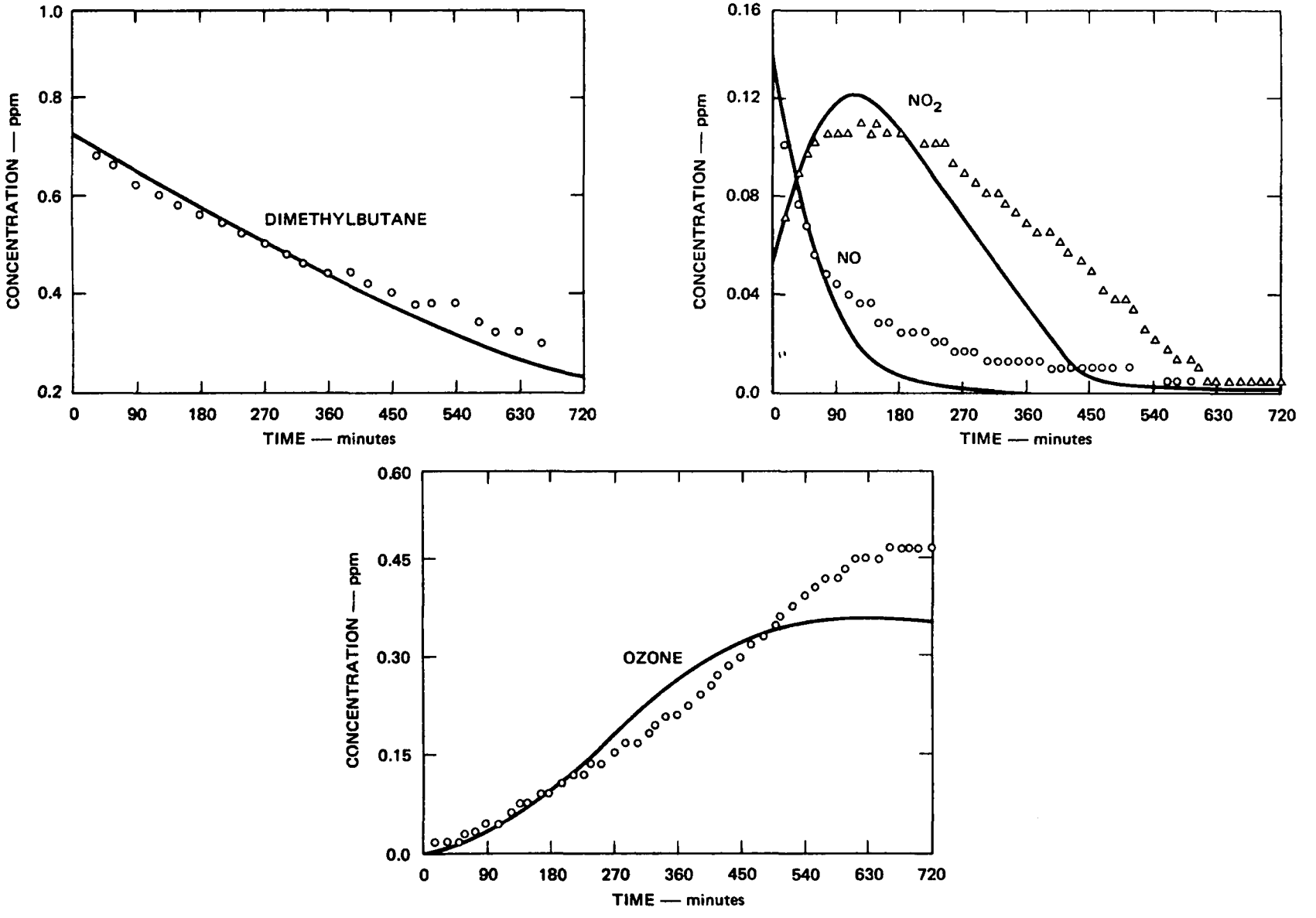

Figure 19. Simulation of SAPRC EC-169: 0.74 ppm Dimethylbutane and 0.191 ppm NO_x.

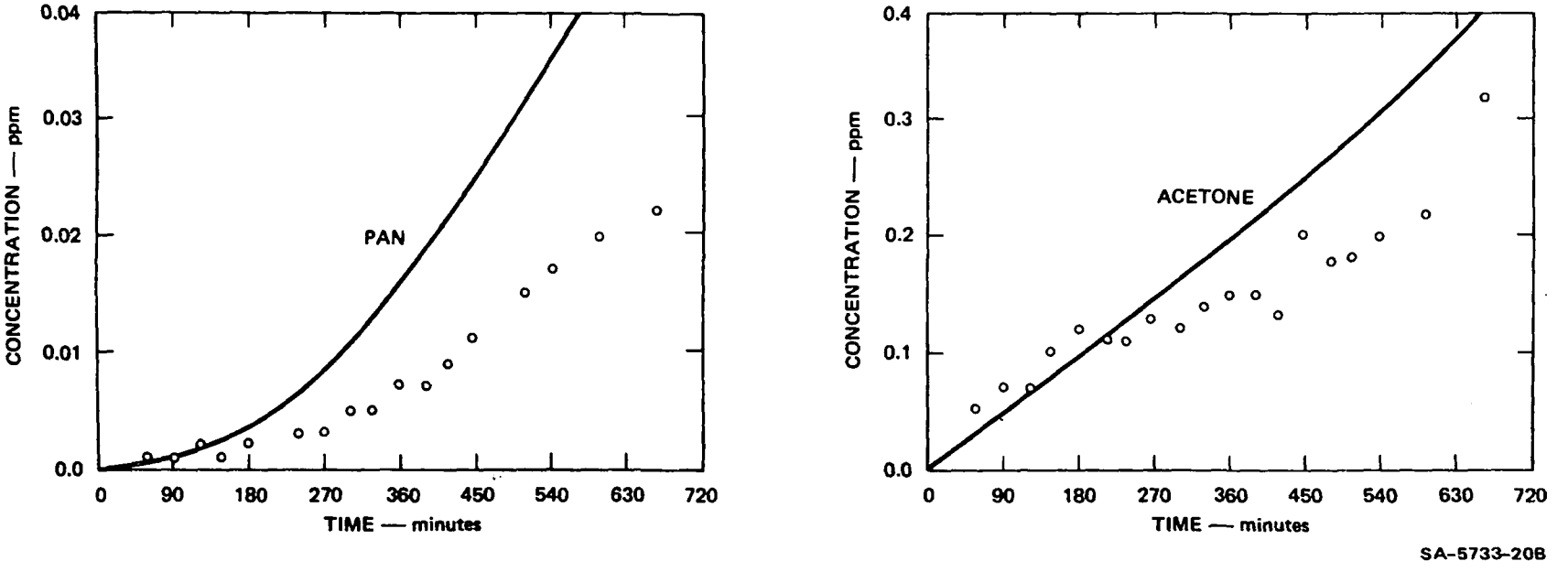

Figure 19. Simulation of SAPRC EC-169: 0.74 ppm Dimethylbutane and 0.191 ppm NO_x (Concluded).

conditions used are summarized in Tables C-1 and C-2 of Appendix C. Copies of all the concentration-time plots for all the simulations are included in Appendix C; however runs EC-77 and EC-86 have been re-plotted in Figures 20 and 21, as representative runs for more careful consideration. These two runs were selected because they are at different [toluene]/[NO_x] ratios--0.48 and 2.63, respectively. In addition, EC-86 has 0.161 ppm of formaldehyde present initially.

From the data in Figures 20 and 21 we can see that the toluene model computes the chamber data well. Again the major problem is with the aldehydes, for which there may be sizable experimental uncertainty associated with the data. Inspection of the runs in Appendix C indicates that in some runs, such as EC-80, the computation underestimates the experimental data in the last half of the run. This effect may be due to an increase in the chamber temperature since the temperature monitoring and refrigeration unit was not in operation for the toluene experiment block.

Even though the toluene mechanism is at a preliminary stage of development, in Table 13 we have summarized the toluene products predicted by the model at 100-min intervals. We see that cresol is predicted to be the major product, accounting for 44% of the consumed toluene at 100 min and 17% at 400 min. The model predicts significant amounts of dihydroxytoluene and phenylnitrate; however, this is because the model does not include their chemistry for reasons of simplicity, although these compounds should be very reactive. The dihydroxytoluene should be more reactive than cresol, whereas phenyl nitrate is expected to readily hydrolyze heterogeneously to form phenol, which again would be reactive like cresol.

All other products except for benzaldehyde, which was analyzed at concentrations consistent with the model, are in the sub-ppb region. Thus, the inability to find toluene reaction products should not be surprising. The possible exception is cresol, which should be present largely as the ortho and para isomers; however, the material is very

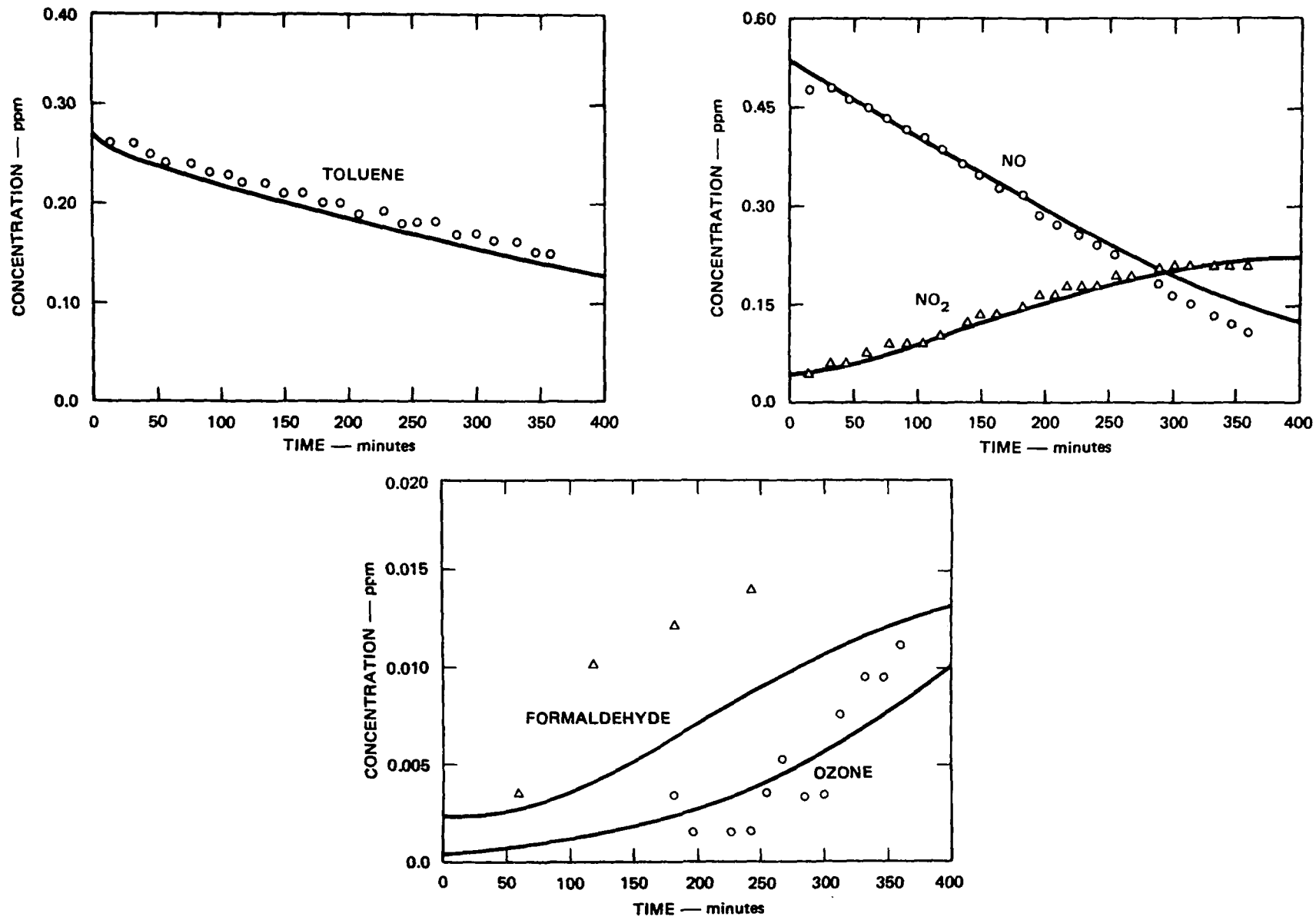

Figure 20. Simulation of SAPRC EC-77: 0.276 ppm Toluene and 0.574 ppm NO_x.

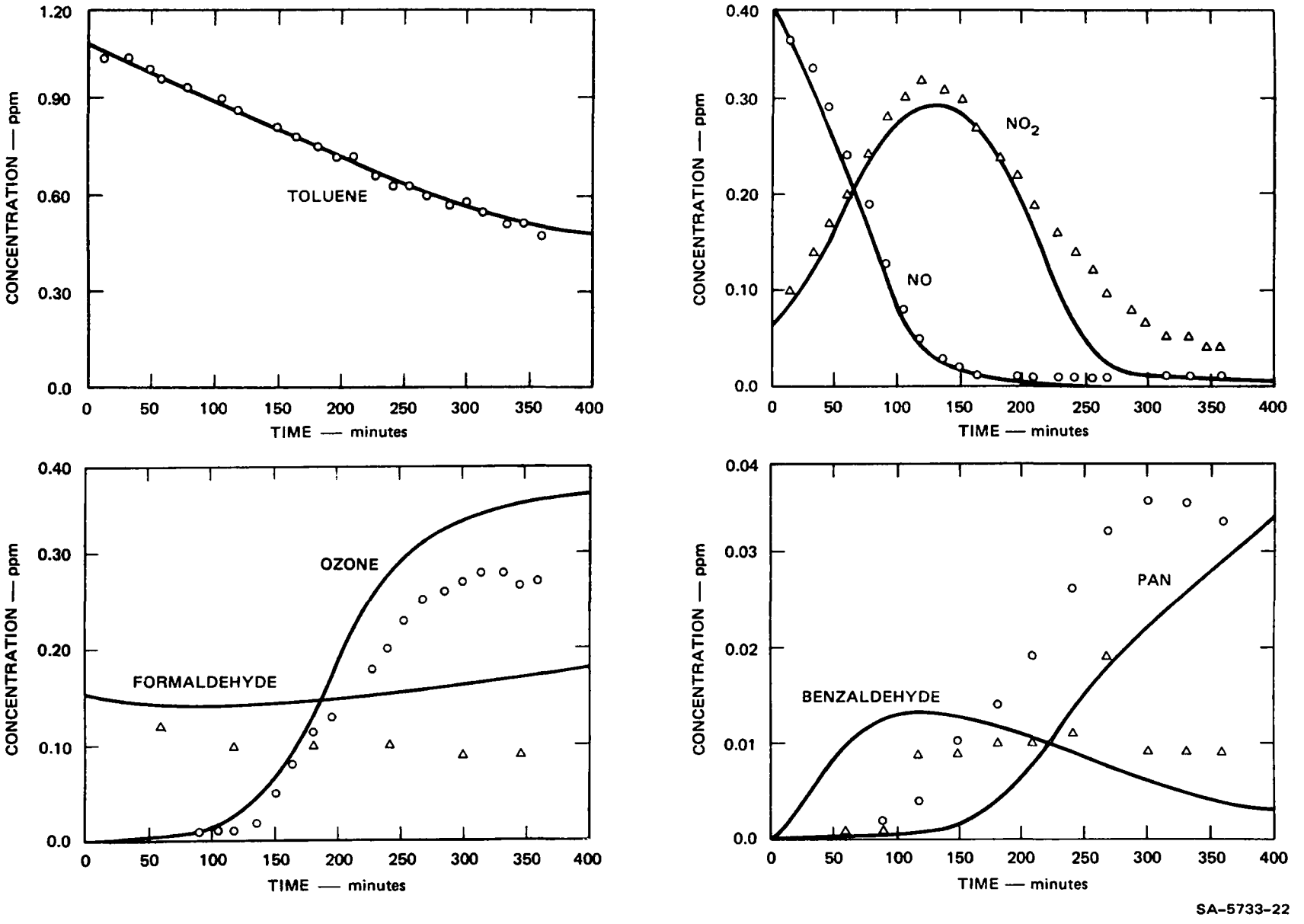

Figure 21. Simulation of SAPRC EC-86: 1.09 ppm Toluene, 0.486 ppm NO_x, and 0.161 ppm Formaldehyde.

TABLE 13. PREDICTED TOLUENE REACTION PRODUCTS (EC-77)[a]

Products	Concentration-ppm			
	Time (min)			
	100	200	300	400
Benzaldehyde	0.0033	0.0052	0.0050	0.0043
Cresol	0.0163	0.0245	0.0245	0.0227
$PhCO_2NO_2$	0.0001	0.0003	0.0005	0.0006
$PhCH_2O_2NO_2$	0.0001	0.0003	0.0004	0.0004
$PhONO_2$	0.0009	0.0040	0.0062	0.0083
HCCH	0.0004	0.0006	0.0005	0.0005
Hydroxybenzaldehyde	0.0001	0.0005	0.0007	0.0007
Dihydroxytoluene	0.0046	0.0220	0.0328	0.0428
Nitrotoluene	0.00002	0.00005	0.00008	0.0001
Δ Toluene	0.0374	0.0774	0.1077	0.1299

[a]Concentrations include correction for dilution.

polar and may be extremely difficult to analyze. Care must be taken to ensure that reactive compounds like cresols and other phenols do not react with NO_x in the process of trapping them out from sample streams.

4.6 FUTURE MODELING EFFORTS

Model development is continuing during the following year. The major emphasis will be to apply and test the current mechanisms using new data being obtained at the SAPRC facility. Special consideration will be given to the further development of the toluene mechanisms and

to evaluating the effect of peroxynitric acid and the closely related peroxyalkyl nitrates on the overall chemistry, especially ozone formation.

APPENDIX A

Simulations of SAPRC Alkene and Alkene Mixture Data

TABLE A-1. INITIAL CONDITIONS OF PROPENE CHAMBER RUNS

E.C. Number	INITIAL CONCENTRATION (ppm)					
	Propene	NO	NO_2	HNO_2	HCHO	CH_3CHO
5	0.970	0.551	0.047	0.020	0.0	0.003
11	0.447	0.115	0.020	0.010	0.0	0.002
12	0.082	0.106	0.012	0.000	0.0	0.001
13	0.500	0.504	0.078	0.020	0.038	0.005
16	1.036	1.122	0.156	0.040	0.015	0.007
17	0.103	0.106	0.014	0.001	0.0	0.002
18	0.972	0.106	0.014	0.020	0.0	0.003
21	0.104	0.558	0.066	0.010	0.003	0.008
51	0.552	0.516	0.049	0.010	0.0	0.004
53[a]	0.551	0.552	0.077	0.030	0.0	0.001
54[a]	0.514	0.527	0.060	0.015	0.0	0.003
55	0.545	0.480	0.121	0.020	0.005	0.003
56	0.531	0.311	0.283	0.030	0.0	0.002
59	0.530	0.124	0.481	0.010	0.001	0.004
60	1.082	1.105	0.145	0.020	0.0	0.002
95	0.504	0.365	0.092	0.020	0.010	0.005
121	0.483	0.410	0.101	0.030	0.0	0.005
177	0.493	0.364	0.099	0.005	0.010	0.001
216	0.503	0.412	0.104	0.000	0.030	0.002
217	0.099	0.241	0.238	0.000	0.003	0.146

[a]All runs were at 302 ± 1 K, except runs 53 and 54, which were at 311 and 289 K, respectively.

TABLE A-2. INITIAL CONDITIONS OF ALKENE CHAMBER RUNS

E.C. Number	INITIAL CONCENTRATION (ppm)								
	Ethene	Propene	Butene-1	trans-Butene-2	NO	NO_2	HNO_2	H_2CO	CH_3CHO
142	0.949	0	0	0	0.322	0.158	0.050	0.050	0.005
143	2.027	0	0	0	0.390	0.110	0.050	0.0	0.002
156	1.995	0	0	0	0.376	0.124	0.050	0.027	0.001
122	0	0	0.217	0	0.398	0.103	0.030	0.0	0.002
123	0	0	0.404	0	0.401	0.106	0.030	0.0	0.001
124	0	0	0.424	0	0.608	0.385	0.030	0.0	0.001
146	0	0	0	0.231	0.385	0.124	0.030	0.0	0.002
147	0	0	0	0.417	0.782	0.200	0.030	0.010	0.002
157	0	0	0	0.216	0.397	0.129	0.020	0.010	0.001
144	2.027	0.221	0	0	0.398	0.111	0.030	0.020	0.005
145	0.210	0.428	0	0	0.745	0.246	0.030	0.004	0.003
160	1.014	0.400	0	0	0.752	0.241	0.030	0.004	0.002
149	0	0.384	0	0.209	0.813	0.176	0.030	0.0	0.002
150	1.014	0.224	0.097	0.093	0.774	0.222	0.030	0.050	0.001
151	0.975	0.441	0.209	0.190	1.466	0.590	0.030	0.0	0.001
152	1.015	0.116	0.222	0.102	0.398	0.104	0.030	0.0	0.002
153	1.923	0.109	0.415	0.193	0.774	0.197	0.030	0.0	0.003
161	0.908	0.102	0.189	0.088	0.386	0.123	0.030	0.0	0.002

TABLE A-3. PROPENE MECHANISM

No.			Rate Constants[a]
1	$CH_2{=}CHCH_3 + OH \xrightarrow{O_2}$	$HOCH_2CH_2(\dot{O}_2)CH_3$	3.8×10^4
2	$CH_2{=}CHCH_3 + O(^3P) \rightarrow$	CH_3CH_2CHO	1.8×10^3
3	$CH_2{=}CHCH_3 + O(^3P) \rightarrow$	$CH_3\dot{O}_2 + CH_2C(O)\dot{O}_2$	1.8×10^3
4	$CH_2{=}CHCH_3 + O(^3P) \rightarrow$	$CH_3CH_2\dot{O}_2 + HO_2$	1.8×10^3
5	$CH_2{=}CHCH_3 + O_3 \rightarrow$	$CH_3CHO + HO_2 + OH + CO$	7.5×10^{-3}
6	$CH_2{=}CHCH_3 + O_3 \rightarrow$	$CH_2O + CH_3C(O)\dot{O}_2 + OH$	7.5×10^{-3}
7	$CH_2{=}CHCH_3 + NO_3 \rightarrow$	$CH_3CH_2CHO + NO_2$	7.8
8	$HOCH_2CH(\dot{O}_2)CH_3 + NO \rightarrow$	$HOCH_2CH(\dot{O})CH_3 + NO_2$	1.0×10^4
9	$CH_3CH_2\dot{O}_2 + NO \rightarrow$	$CH_3CH_2\dot{O} + NO_2$	1.0×10^4
10	$CH_3\dot{O}_2 + NO \rightarrow$	$CH_3\dot{O} + NO_2$	1.0×10^4
11	$CH_3C(O)\dot{O}_2 + NO \rightarrow$	$CH_3\dot{O}_2 + NO_2 + CO_2$	5.4×10^3
12	$CH_3CH_2C(O)\dot{O}_2 + NO \rightarrow$	$CH_3CH_2\dot{O}_2 + NO_2 + CO_2$	5.4×10^3
13	$CH_2(OH)\dot{O}_2 + NO \rightarrow$	$CH_2(OH)\dot{O} + NO_2$	1.0×10^4
14	$HOCH_2CH(\dot{O})CH_3 \xrightarrow{O_2}$	$CH_3CHO + \dot{C}H_2OH$	$^*2.7 \times 10^5$
15	$HOCH_2CH(\dot{O})CH_3 + O_2 \rightarrow$	$HOCH_2C(O)CH_3 + HO_2$	$^*6.7 \times 10^4$
16	$CH_3CH_2\dot{O} + O_2 \rightarrow$	$CH_3CHO + HO_2$	$^*2.0 \times 10^9$
17	$CH_3\dot{O} + O_2 \rightarrow$	$CH_2O + HO_2$	$^*2.0 \times 10^9$
18	$\dot{C}H_2OH + O_2 \rightarrow$	$CH_2(OH)\dot{O}_2$	$^*1.2 \times 10^8$
19	$\dot{C}H_2OH + O_2 \rightarrow$	$CH_2O + HO_2$	$^*1.2 \times 10^9$
20	$CH_2(OH)\dot{O} + O_2 \rightarrow$	$HC(O)OH + HO_2$	$^*1.4 \times 10^9$
21	$CH_3CH_2CHO + h\nu \rightarrow$	$CH_3CH_2\dot{O}_2 + CO_2 + HO_2$	
22	$CH_3CHO + h\nu \rightarrow$	$CH_3\dot{O}_2 + CO_2 + HO_2$	
23	$CH_2O + h\nu \rightarrow$	$CO + H_2$	
24	$CH_2O + h\nu \rightarrow$	$CO + HO_2 + HO_2$	
25	$HOCH_2C(O)CH_3 + h\nu \rightarrow$	$CH_3C(O)\dot{O}_2 + \dot{C}H_2OH$	
26	$CH_3CH_2CHO + OH \xrightarrow{O_2}$	$CH_3CH_2C(O)\dot{O}_2 + H_2O$	2.0×10^4
27	$CH_3CHO + OH \xrightarrow{O_2}$	$CH_3C(O)\dot{O}_2 + H_2O$	2.0×10^4
28	$CH_2O + OH \xrightarrow{O_2}$	$HO_2 + CO$	2.0×10^4
29	$HO_2 + NO_2 \rightarrow$	HO_2NO_2	3.0×10^3
30	$HO_2NO_2 \rightarrow$	$HO_2 + NO_2$	$^*2.0 \times 10^{-1}$
31	$CH_2(OH)\dot{O}_2 + NO_2 \rightarrow$	$CH_2(OH)O_2NO_2$	6.0×10^3
32	$CH_2(OH)O_2NO_2 \rightarrow$	$CH_2(OH)\dot{O}_2 + NO_2$	$^*1.0$
33	$CH_2(OH)CH(\dot{O}_2)CH_3 + NO_2 \rightarrow$	$CH_2(OH)CH(O_2NO_2)CH_3$	6.0×10^3
34	$CH_2(OH)CH(O_2NO_2)CH_3 \rightarrow$	$CH_2(OH)CH(\dot{O}_2)CH_3 + NO_2$	$^*1.0$
35	$CH_3C(O)O_2 + NO_2 \rightarrow$	$CH_3C(\dot{O})O_2NO_2$	1.5×10^{-3}
36	$CH_3C(O)O_2NO_2 \rightarrow$	$CH_3C(O)\dot{O}_2 + NO_2$	$^*4.0 \times 10^{-4}$

continued...

Propene Mechanism (concluded)

37	$CH_3CH_2C(O)\dot{O}_2 + NO_2$	→	$CH_3CH_2C(O)O_2NO_2$	1.5×10^3
38	$CH_3CH_2C(O)O_2NO_2$	→	$CH_3CH_2C(O)\dot{O}_2 + NO_2$	$^*4.0 \times 10^{-2}$
39	$CH_3\dot{O} + NO_2$	→	CH_3ONO_2	2.0×10^4
40	$CH_3\dot{O} + NO_2$	→	$CH_2O + HNO_2$	2.2×10^3
41	$CH_3CH_2\dot{O} + NO_2$	→	$CH_3CH_2ONO_2$	2.0×10^4
42	$CH_3CH_2\dot{O} + NO_2$	→	$CH_3CHO + HNO_2$	2.2×10^3
43	$CH_2(OH)CH(\dot{O})CH_3 + NO_2$	→	$CH_2(OH)CH(ONO_2)CH_3$	2.0×10^4
44	$CH_2(OH)CH(\dot{O})CH_3 + NO_2$	→	$CH_2(OH)C(O)CH_3 + HNO_2$	2.2×10^3
45	$CH_3\dot{O}_2 + NO_2$	→	$CH_3O_2NO_2$	6.0×10^3
46	$CH_3O_2NO_2$	→	$CH_3\dot{O}_2 + NO_2$	$^*1.0$
47	$CH_3CH_2C(O)\dot{O}_2 + HO_2$	→	$CH_3CH_2C(O)OOH$	4.0×10^3
48	$CH_3C(O)\dot{O}_2 + HO_2$	→	$CH_3C(O)OOH$	4.0×10^3
49	$CH_2(OH)\dot{O}_2 + HO_2$	→	$CH_2(OH)OOH$	4.0×10^3
50	$CH_2(OH)CH_2CH_2\dot{O}_2 + HO_2$	→	$CH_2(OH)CH_2CH_2OOH$	2.0×10^3
51	$CH_3CH_2\dot{O}_2 + HO_2$	→	CH_3CH_2OOH	2.0×10^3
52	$CH_3C(O)\dot{O}_2 + CH_3C(O)\dot{O}_2$	→	$CH_3\dot{O}_2 + CH_3\dot{O}_2 + 2CO_2$	2.4×10^3
53	$CH_2(OH)CH_2CH_2\dot{O}_2 + CH_2(OH)CH_2CH_2\dot{O}_2$	→	$CH_2(OH)CH_2CH_2\dot{O} + CH_2(OH)CH_2CH_2\dot{O} + O_2$	2.5×10^2

[a]Units ppm^{-1} min^{-1} except * min^{-1}.

TABLE A-4. ETHENE MECHANISM

No.			Rate Constants[a]
1	$CH_2CH_2 + OH \xrightarrow{O_2}$	$HOCH_2CH_2\dot{O}_2$	1.2×10^4
2	$CH_2CH_2 + O(^3P) \rightarrow$	CH_3CHO	6.0×10^2
3	$CH_2CH_2 + O(^3P) \rightarrow$	$CH_3\dot{O}_2 + HO_2 + CO$	6.0×10^2
4	$CH_2CH_2 + NO_3 \rightarrow$	$CH_3CHO + NO_2$	1.4
5	$CH_2CH_2 + O_3 \rightarrow$	$CH_2O + HO_2 + CO + OH$	2.8×10^{-3}
6	$HOCH_2CH_2\dot{O}_2 + NO \rightarrow$	$HOCH_2CH_2\dot{O} + NO_2$	1.0×10^4
7	$CH_3\dot{O}_2 + NO \rightarrow$	$CH_3O + NO_2$	1.0×10^4
8	$CH_3C(O)\dot{O}_2 + NO \rightarrow$	$CH_3\dot{O}_2 + NO_2 + CO_2$	2.0×10^3
9	$HOCH_2CH_2\dot{O} + O_2 \rightarrow$	$HOCH_2CHO + HO_2$	$^*1.3 \times 10^4$
10	$CH_3O\cdot + O_2 \rightarrow$	$CH_2O + HO_2$	$^*2.0 \times 10^3$
11	$CH_2O + h\nu \xrightarrow{O_2}$	$HO_2 + HO_2 + CO$	
12	$CH_2O + h\nu \rightarrow$	$CO + H_2$	
13	$CH_3CHO + h\nu \xrightarrow{O_2}$	$CH_3\dot{O}_2 + CO + HO_2$	
14	$CH_2O + OH \xrightarrow{O_2}$	$CO + HO_2 + H_2O$	2.0×10^4
15	$CH_3CHO + OH \xrightarrow{O_2}$	$CH_3C(O)\dot{O}_2 + H_2O$	2.0×10^4
16	$HOCH_2CHO + OH \xrightarrow{O_2}$	$CH_2O + HO_2 + CO$	2.0×10^4
17	$CH_3O_2\cdot + HO_2 \rightarrow$	$CH_3OOH + O_2$	2.0×10^3
18	$HOCH_2CH_2\dot{O}_2 + HO_2 \rightarrow$	$HOCH_2CH_2OOH + O_2$	2.0×10^3
19	$CH_3C(O)\dot{O}_2 + HO_2 \rightarrow$	$CH_3C(O)OOH + O_2$	4.0×10^3
20	$CH_3C(O)\dot{O}_2 + NO_2 \rightarrow$	$CH_3C(O)O_2NO_2$	1.5×10^3
21	$CH_3C(O)O_2NO_2 \rightarrow$	$CH_3C(O)\dot{O}_2 + NO_2$	$^*4.1 \times 10^{-3}$
22	$HO_2 + NO_2 \rightarrow$	HO_2NO_2	3.0×10^3
23	$HO_2NO_2 \rightarrow$	$HO_2 + NO_2$	$^*2.0 \times 10^{-1}$
24	$CH_3\dot{O}_2 + NO_2 \rightarrow$	$CH_3O_2NO_2$	6.0×10^3
25	$CH_3O_2NO_2 \rightarrow$	$CH_3O_2 + NO_2$	$^*1.0$
26	$HOCH_2CH_2\dot{O}_2 + NO_2 \rightarrow$	$HOCH_2CH_2O_2NO_2$	6.0×10^3
27	$HOCH_2CH_2O_2NO_2 \rightarrow$	$HOCH_2CH_2\dot{O}_2 + NO_2$	$^*1.0$
28	$CH_3C(O)\dot{O}_2 + CH_3C(O)\dot{O}_2 \rightarrow$	$CH_3\dot{O}_2 + CH_3\dot{O}_2 + 2CO_2 + O_2$	2.4×10^3
29	$CH_3\dot{O}_2 + CH_3\dot{O}_2 \rightarrow$	$CH_3\dot{O} + CH_3\dot{O} + O_2$	2.0×10^2
30	$HOCH_2CH_2\dot{O}_2 + HOCH_2CH_2\dot{O}_2 \rightarrow$	$HOCH_2CH_2O + HOCH_2CH_2\dot{O} + O_2$	2.0×10^2
31	$HOCH_2CH_2\dot{O} \xrightarrow{O_2}$	$CH_2O + CH_2O + HO_2$	$^*1.0 \times 10^4$
32	$CH_2CH_2 + O_3 \rightarrow$	$CH_3CHO + O_2$	2.0×10^{-4}

[a]Units ppm^{-1} min^{-1} except * min^{-1}

TABLE A-5. 1-BUTENE MECHANISM

No.		Rate Constant[a]
1	$CH_2{=}CHCH_2CH_3 + OH \xrightarrow{O_2} CH_2(OH)CH(\dot{O}_2)CH_2CH_3$	3.8×10^4
2	$CH_2{=}CHCH_2CH_3 + O(^3P) \rightarrow CH_3CH_2CH_2C(O)H$	1.8×10^3
3	$CH_2{=}CHCH_2CH_3 + O(^3P) \xrightarrow{O_2} CH_3\dot{O}_2 + CH_3CH_2C(O)\dot{O}_2$	1.8×10^3
4	$CH_2{=}CHCH_2CH_3 + O(^3P) \xrightarrow{O_2} CH_3CH_2CH_2\dot{O}_2 + HO_2 + CO$	1.8×10^3
5	$CH_2{=}CHCH_2CH_3 + O_3 \xrightarrow{O_2} CH_2O + CH_3CH_2C(O)\dot{O}_2 + OH$	3.8×10^{-1}
6	$CH_2{=}CHCH_2CH_3 + NO_3 \rightarrow CH_3CH_2CH_2C(O)H + NO_2$	12.0
7	$CH_2(OH)CH(\dot{O}_2)CH_2CH_3 + NO \rightarrow CH_2(OH)CH(\dot{O})CH_2CH_3 + NO_2$	1.0×10^4
8	$CH_3CH_2CH_2\dot{O}_2 + NO \rightarrow CH_3CH_2CH_2\dot{O} + NO_2$	1.0×10^4
9	$CH_3CH_2\dot{O}_2 + NO \rightarrow CH_3CH_2\dot{O} + NO_2$	1.0×10^4
10	$CH_3\dot{O}_2 + NO \rightarrow CH_3\dot{O} + NO_2$	1.0×10^4
11	$HOCH_2\dot{O}_2 + NO \rightarrow HOCH_2\dot{O} + NO_2$	1.0×10^4
12	$CH_3CH_2CH_2\dot{O} + O_2 \rightarrow CH_3CH_2CHO + HO_2$	
13	$CH_3CH_2\dot{O} + O_2 \rightarrow CH_3CHO + HO_2$	
14	$CH_3\dot{O} + O_2 \rightarrow HO_2 + HO_2 + CO$	
15	$HOCH_2\dot{O} + O_2 \rightarrow HC(O)OH + HO_2$	
16	$CH_2(OH)CH(\dot{O})CH_2CH_3 + O_2 \rightarrow CH_2(OH)C(O)CH_2CH_3 + HO_2$	$^*6.7 \times 10^4$
17	$CH_2(OH)CH(\dot{O})CH_2CH_3 \xrightarrow{O_2} CH_3CH_2CHO + H\dot{O}CH_2$	$^*2.7 \times 10^3$
18	$H\dot{O}CH_2 + O_2 \rightarrow CH_2O + HO_2$	5.7×10^{-3}
19	$H\dot{O}CH_2 + O_2 \rightarrow HOCH_2\dot{O}_2$	5.7×10^{-4}
20	$CH_2O + h\nu \xrightarrow{O_2} HO_2 + HO_2 + CO$	
21	$CH_2O + h\nu \rightarrow CO + H_2$	
22	$CH_3CHO + h\nu \xrightarrow{O_2} CH_3\dot{O}_2 + CO + HO_2$	
23	$CH_3CH_2CHO + h\nu \xrightarrow{O_2} CH_3CH_2\dot{O}_2 + CO + HO_2$	
24	$CH_3CH_2CH_2CHO + h\nu \xrightarrow{O_2} CH_3CH_2CH_2\dot{O}_2 + CO + HO_2$	
25	$CH_3CH_2CH_2CHO + h\nu \rightarrow CH_3CHO + C_2H_4$	
26	$HOCH_2C(O)CH_2CH_3 + h\nu \xrightarrow{O_2} H\dot{O}CH_2 + CH_3CH_2C(O)\dot{O}_2$	
27	$CH_2O + OH \xrightarrow{O_2} CO + HO_2 + H_2O$	2.0×10^4
28	$CH_3CHO + OH \xrightarrow{O_2} CH_3C(O)\dot{O}_2 + H_2O$	2.0×10^4
29	$CH_3CH_2CHO + OH \xrightarrow{O_2} CH_3CH_2C(O)\dot{O}_2 + H_2O$	2.0×10^4
30	$CH_3CH_2CH_2CHO + OH \xrightarrow{O_2} CH_3CH_2CH_2C(O)\dot{O}_2 + H_2O$	2.0×10^4
31	$HO_2 + NO_2 \rightarrow HO_2NO_2$	3.0×10^3
32	$HO_2NO_2 \rightarrow HO_2 + NO_2$	$^*2.0 \times 10^{-1}$
33	$CH_3\dot{O}_2 + NO_2 \rightarrow CH_3O_2NO_2$	6.0×10^3
34	$CH_3O_2NO_2 \rightarrow CH_3\dot{O}_2 + NO_2$	$^*1.0$
35	$CH_3CH_2\dot{O}_2 + NO_2 \rightarrow CH_3CH_2O_2NO_2$	6.0×10^3

continued...

1-Butene (concluded)

36	$CH_3CH_2O_2NO_2$	→ $CH_3CH_2\dot{O}_2 + NO_2$	*1.0
37	$CH_2(OH)CH(\dot{O}_2)CH_2CH_3 + NO_2$	→ $CH_2(OH)CH(O_2NO_2)CH_2CH_3$	6.0×10^3
38	$CH_2(OH)CH(O_2NO_2)CH_2CH_3$	→ $CH_2(OH)CH(\dot{O}_2)CH_2CH_3 + NO_2$	*1.0
39	$CH_3C(O)\dot{O}_2 + NO$	→ $CH_3\dot{O}_2 + NO_2 + CO_2$	2.0×10^3
40	$CH_3CH_2C(O)\dot{O}_2 + NO$	→ $CH_3CH_2\dot{O}_2 + NO_2 + CO_2$	2.0×10^3
41	$CH_3CH_2CH_2C(O)\dot{O}_2 + NO$	→ $CH_3CH_2CH_2\dot{O}_2 + NO_2 + CO_2$	2.0×10^3
42	$CH_3C(O)\dot{O}_2 + NO_2$	→ $CH_3C(O)O_2NO_2$	1.5×10^3
43	$CH_3C(O)O_2NO_2$	→ $CH_3C(O)\dot{O}_2 + NO_2$	*4.0×10^{-2}
44	$CH_3CH_2C(O)\dot{O}_2 + NO_2$	→ $CH_3CH_2C(O)O_2NO_2$	1.5×10^3
45	$CH_3CH_2C(O)O_2NO_2$	→ $CH_3CH_2C(O)\dot{O}_2 + NO_2$	*4.0×10^{-2}
46	$CH_3CH_2CH_2C(O)\dot{O}_2 + NO_2$	→ $CH_3CH_2CH_2C(O)O_2NO_2$	1.5×10^3
47	$CH_3CH_2CH_2C(O)O_2NO_2$	→ $CH_3CH_2CH_2C(O)\dot{O}_2 + NO_2$	*4.0×10^{-2}
48	$CH_3\dot{O} + NO_2$	→ CH_3ONO_2	1.5×10^4
49	$CH_3\dot{O} + NO_2$	→ $CH_2O + HNO_2$	4.4×10^3
50	$CH_3CH_2\dot{O} + NO_2$	→ $CH_3CH_2ONO_2$	1.5×10^4
51	$CH_3CH_2\dot{O} + NO_2$	→ $CH_3CHO + HNO_2$	2.9×10^3
52	$CH_3CH_2CH_2\dot{O} + NO_2$	→ $CH_3CH_2CH_2ONO_2$	1.5×10^4
53	$CH_3CH_2CH_2\dot{O} + NO_2$	→ $CH_3CH_2CHO + HNO_2$	2.9×10^3
54	$CH_3CH_2CH_2C(O)\dot{O}_2 + HO_2$	→ $CH_3CH_2CH_2C(O)OOH + O_2$	4.0×10^3
55	$CH_3CH_2C(O)\dot{O}_2 + HO_2$	→ $CH_3CH_2C(O)OOH + O_2$	4.0×10^3
56	$CH_3C(O)\dot{O}_2 + HO_2$	→ $CH_3C(O)OOH + O_2$	4.0×10^3
57	$CH_2(OH)CH(\dot{O}_2)CH_2CH_3 + HO_2$	→ $CH_2(OH)CH(OOH)CH_2CH_3 + O_2$	2.0×10^3
58	$CH_3CH_2CH_2\dot{O}_2 + HO_2$	→ $CH_3CH_2CH_2OOH + O_2$	2.0×10^3
59	$CH_3CH_2\dot{O}_2 + HO_2$	→ $CH_3CH_2OOH + O_2$	2.0×10^3
60	$CH_3\dot{O}_2 + HO_2$	→ $CH_3OOH + O_2$	2.0×10^3
61	$CH_2(OH)CH(\dot{O}_2)CH_2CH_3 + CH_2(OH)CH(\dot{O}_2)CH_2CH_3$	→ $CH_2(OH)CH(\dot{O})CH_2CH_3 + CH_2(OH)CH(\dot{O})CH_2CH_3 + O_2$	4.0×10^3
62	$CH_3C(O)\dot{O}_2 + CH_3C(O)\dot{O}_2$	→ $CH_3\dot{O}_2 + CH_3\dot{O}_2 + 2CO_2 + O_2$	2.4×10^3

[a]Units $ppm^{-1}\ min^{-1}$, except * min^{-1} .

TABLE A-6. TRANS-2-BUTENE MECHANISM

No.		Rate Constant[a]
1	$CH_3CH{=}CHCH_3 + OH \xrightarrow{O_2} CH_3CH(OH)CH(\dot{O}_2)CH_3$	7.2×10^4
2	$CH_3CH{=}CHCH_3 + O(^3P) \rightarrow CH_3CH_2C(O)CH_3$	9.0×10^3
3	$CH_3CH{=}CHCH_3 + O(^3P) \xrightarrow{O_2} CH_3CH_2\dot{O}_2 + CH_3C(O)\dot{O}_2$	1.8×10^4
4	$CH_3CH{=}CHCH_3 + NO_3 \rightarrow CH_3CH_2C(O)CH_3 + NO_2$	2.1×10^2
5	$CH_3CH{=}CHCH_3 + O_3 \xrightarrow{O_2} CH_3CHO + CH_3C(O)\dot{O}_2 + OH$	3.8×10^1
6	$CH_3CH(OH)CH(\dot{O}_2)CH_3 + NO \rightarrow CH_3CH(OH)CH(\dot{O})CH_3 + NO_2$	1.0×10^4
7	$CH_3\dot{O}_2 + NO \rightarrow CH_3\dot{O} + NO_2$	1.0×10^4
8	$CH_3CH_2\dot{O}_2 + NO \rightarrow CH_3CH_2\dot{O} + NO_2$	1.0×10^4
9	$CH_3CH(OH)\dot{O}_2 + NO \rightarrow CH_3CH(OH)\dot{O} + NO_2$	1.0×10^4
10	$CH_3CH(\dot{O}_2)C(O)CH_3 + NO \rightarrow CH_3CH(\dot{O})C(O)CH_3 + NO_2$	1.0×10^4
11	$CH_3C(O)\dot{O}_2 + NO \xrightarrow{O_2} CH_3\dot{O}_2 + NO_2 + CO_2$	2.0×10^3
12	$CH_3CH(OH)CH(\dot{O})CH_3 \rightarrow CH_3CHO + CH_3\dot{C}HOH$	$^*2.7 \times 10^5$
13	$CH_3CH(OH)CH(\dot{O})CH_3 + O_2 \rightarrow CH_3CH(OH)C(O)CH_3 + HO_2$	$^*6.7 \times 10^4$
14	$CH_3\dot{O} + O_2 \rightarrow CH_2O + HO_2$	$^*2.0 \times 10^3$
15	$CH_3CH_2\dot{O} + O_2 \rightarrow CH_3CHO + HO_2$	$^*1.3 \times 10^3$
16	$CH_3CH(OH)\dot{O} + O_2 \rightarrow CH_3C(O)OH + HO_2$	$^*1.4 \times 10^3$
17	$CH_3\dot{C}HOH + O_2 \rightarrow CH_3CH(OH)\dot{O}_2$	$^*1.2 \times 10^2$
18	$CH_3\dot{C}HOH + O_2 \rightarrow CH_3CHO + HO_2$	$^*1.2 \times 10^3$
19	$CH_2O + h\nu \rightarrow CO + H_2$	
20	$CH_2O + h\nu \rightarrow CO + HO_2 + HO_2$	
21	$CH_3CHO + h\nu \rightarrow CH_3\dot{O}_2 + HO_2 + CO$	
22	$CH_3CH(OH)C(O)CH_3 + h\nu \rightarrow CH_3C(O)\dot{O}_2 + CH_3CH(OH)\dot{O}_2$	
23	$CH_3CH_2C(O)CH_3 + h\nu \rightarrow CH_3C(O)\dot{O}_2 + CH_3CH_2\dot{O}_2$	
24	$CH_2O + OH \rightarrow CO + HO_2 + H_2O$	2.0×10^4
25	$CH_3CHO + OH \rightarrow CH_3C(O)\dot{O}_2 + H_2O$	2.0×10^4
26	$CH_3CH_2C(O)CH_3 + OH \rightarrow CH_3CH(\dot{O}_2)C(O)CH_3 + H_2O$	5.0×10^3
27	$HO_2 + NO_2 \rightarrow HO_2NO_2$	3.0×10^3
28	$HO_2NO_2 \rightarrow HO_2 + NO_2$	$^*2.0 \times 10^{-1}$
29	$CH_3\dot{O}_2 + NO_2 \rightarrow CH_3O_2NO_2$	6.0×10^3
30	$CH_3O_2NO_2 \rightarrow CH_3\dot{O}_2 + NO_2$	$^*1.0$
31	$CH_3CH(OH)CH(\dot{O}_2)CH_3 + NO_2 \rightarrow CH_3CH(OH)CH(O_2NO_2)CH_3$	6.0×10^3
32	$CH_3CH(OH)CH(O_2NO_2)CH_3 \rightarrow CH_3CH(OH)CH(\dot{O}_2)CH_3 + NO_2$	$^*1.0$
33	$CH_3CH_2\dot{O}_2 + NO_2 \rightarrow CH_3CH_2O_2NO_2$	6.0×10^3
34	$CH_3CH_2O_2NO_2 \rightarrow CH_3CH_2\dot{O}_2 + NO_2$	$^*1.0$
35	$CH_3C(O)\dot{O}_2 + NO_2 \rightarrow CH_3C(O)O_2NO_2$	1.5×10^3
36	$CH_3C(O)O_2NO_2 \rightarrow CH_3C(O)\dot{O}_2 + NO_2$	$^*4.0 \times 10^{-2}$

continued . . .

trans-2-Butene Mechanism (concluded)

37	$CH_3\dot{O} + NO_2 \rightarrow CH_3ONO_2$		1.5×10^4
38	$CH_3\dot{O} + NO_2 \rightarrow CH_2O + HNO_2$		4.4×10^3
39	$CH_3CH_2\dot{O} + NO_2 \rightarrow CH_3ONO_2$		1.5×10^4
40	$CH_3CH_2\dot{O} + NO_2 \rightarrow CH_3CHO + HNO_2$		4.4×10^3
41	$CH_3CH(OH)CH(\dot{O})CH_3 + NO_2 \rightarrow CH_3CH(OH)CH(ONO_2)CH_3$		1.5×10^4
42	$CH_3CH(OH)CH(\dot{O})CH_3 + NO_2 \rightarrow CH_3CH(OH)C(O)CH_3 + HNO_2$		4.4×10^3
43	$CH_3C(O)\dot{O}_2 + HO_2 \rightarrow CH_3C(O)OOH$		4.0×10^3
44	$CH_3\dot{O}_2 + HO_2 \rightarrow CH_3OOH$		2.0×10^3
45	$CH_3CH_2\dot{O}_2 + HO_2 \rightarrow CH_3CH_2OOH$		2.0×10^3
46	$CH_3CH(OH)CH(\dot{O}_2)CH_3 + HO_2 \rightarrow CH_3CH(OH)CH(OOH)CH_3$		2.0×10^3
47	$CH_3C(O)\dot{O}_2 + CH_3C(O)\dot{O}_2 \rightarrow CH_3\dot{O}_2 + CH_3\dot{O}_2 + 2CO_2 + O_2$		2.4×10^3
48	$CH_3CH(OH)CH(\dot{O}_2)CH_3 + CH_3CH(OH)CH(\dot{O}_2)CH_3 \rightarrow CH_3CH(OH)CH(\dot{O})CH_3 + CH_3(CH(OH)CH(\dot{O})CH_3 + O_2$		4.0×10^3

[a]Units ppm^{-1} min^{-1}; except * min^{-1} .

TABLE A-7. PHOTOLYSIS RATE CONSTANTS FOR PROPENE CHAMBER RUNS (min^{-1})

E.C. Number	NO_2	HNO_2	H_2O_2	$O_3(^1D)$	$O_3(^3P)$	H_2CO (rad.)	H_2CO (molec.)	CH_3CHO	C_2H_5CHO	$HOCH_2C(O)CH_3$
5	0.24	0.066	4.9×10^{-4}	10.0×10^{-4}	3.0×10^{-4}	6.3×10^{-4}	1.2×10^{-3}	3.0×10^{-4}	3.0×10^{-4}	1.8×10^{-4}
11	0.23	0.063	4.7	9.6	2.8	6.0	1.1	2.8	2.9	1.8
12	0.22	0.060	4.5	9.2	2.7	5.7	1.1	2.7	2.8	1.7
13	0.22	0.060	4.5	9.2	2.7	5.7	1.1	2.7	2.8	1.7
16	0.21	0.058	4.3	8.8	2.6	5.5	1.0	2.6	2.7	1.6
17	0.21	0.58	4.3	8.8	2.6	5.5	1.0	2.6	2.7	1.6
18	0.20	0.055	4.1	8.3	2.5	5.2	1.0	2.5	2.5	1.5
21	0.19	0.052	3.9	7.9	2.4	5.0	0.9	2.4	2.4	1.5
51	0.22	0.060	4.5	9.2	2.8	5.8	1.2	2.7	2.8	1.7
53-56	0.21	0.058	4.3	8.7	2.6	5.5	1.0	2.6	2.6	1.6
59,60	0.20	0.055	4.1	8.3	2.5	5.0	.90	2.5	2.5	1.5
95	0.35	0.11	8.6	50.0	19	14.0	2.3	7.5	8.0	6.1
121	0.30	0.089	6.6	34.0	13.0	10.0	1.7	10.0	11.0	3.6
177	0.33	0.098	7.8	15.0	19.0	13.0	2.3	13.0	14.0	4.8
216,217	0.43	0.13	9.9	18.0	23.0	16.0	2.8	16.0	17.0	5.4

TABLE A-8. PHOTOLYSIS RATE CONSTANTS FOR ALKENE CHAMBER RUNS (min^{-1})

E.C. Number	NO_2	HNO_2	H_2O_2	$O_3(^1D)$	$O_3(^3P)$	H_2CO (rad.)	H_2CO (molec.)	CH_3CHO	C_2H_5CHO	C_3H_7CHO (rad.)	C_3H_7CHO (molec.)	$C_2H_5C(O)CH_3$
						Ethene						
142,143	0.33	0.095	6.0×10^{-4}	11.0×10^{-4}	12.0×10^{-4}	9.0×10^{-4}	17.0×10^{-4}	4.4×10^{-4}	7.5×10^{-4}	5.8×10^{-4}	2.8×10^{-4}	2.0×10^{-4}
156	0.32	0.096	6.1	11.0	12.0	8.2	17.0	4.4	7.8	6.0	3.0	2.2
						Butene-1						
122	0.29	0.087	6.5	35.0	14.0	9.9	17.0	5.4	12.0	8.3	4.1	4.1
123	0.28	0.084	6.3	34.0	13.0	9.7	16.0	5.0	11.0	8.0	4.0	4.0
124	0.27	0.081	6.0	32.0	13.0	9.5	15.0	4.8	11 0	7.8	4.0	4.0
						trans-Butene-2						
146	0.33	0.092	5.6	15.0	7.8	7.5	18.0	3.1	6.4	4.8	2.5	2.0
147	0.34	0.097	6.5	25.0	12.0	8.8	17.0	4.4	9.3	6.6	3.3	3.3
157	0.33	0.096	6.1	25.0	12.0	8.8	17.0	4.4	7.8	6.0	3.0	2.2
						Ethene/Propene						
144	0.33	0.095	6.0	3.6	11.0	7.9	17.0	3.7	7.5	5.8	2.8	2.0
145	0.34	0.098	6.5	13.0	12.0	9.3	18.0	4.5	9.4	8.0	4.0	3.1
160	0.34	0.096	6.1	6.9	11.0	8.2	17.0	3.8	7.8	6.0	3.0	2.2
						Propene/trans-Butene-2						
149	0.33	0.092	5.6	15.0	7.8	7.5	18.0	3.1	6.4	4.8	2.5	2.0
						Ethene/Propene/Butene-1/trans-Butene-2						
150	0.33	0.098	6.4	10.0	12.0	8.4	17.0	4.0	8.6	6.4	3.0	2.5
151,152	0.35	0.099	6.4	10.0	12.0	8.8	17.0	4.2	8.8	6.6	3.3	2.7
153	0.34	0.097	6.3	10.0	12.0	8.4	17.0	4.0	8.6	6.2	3.0	2.5
161	0.34	0.096	6.1	6.9	11.0	8.2	17.0	3.8	7.8	6.0	3.0	2.2

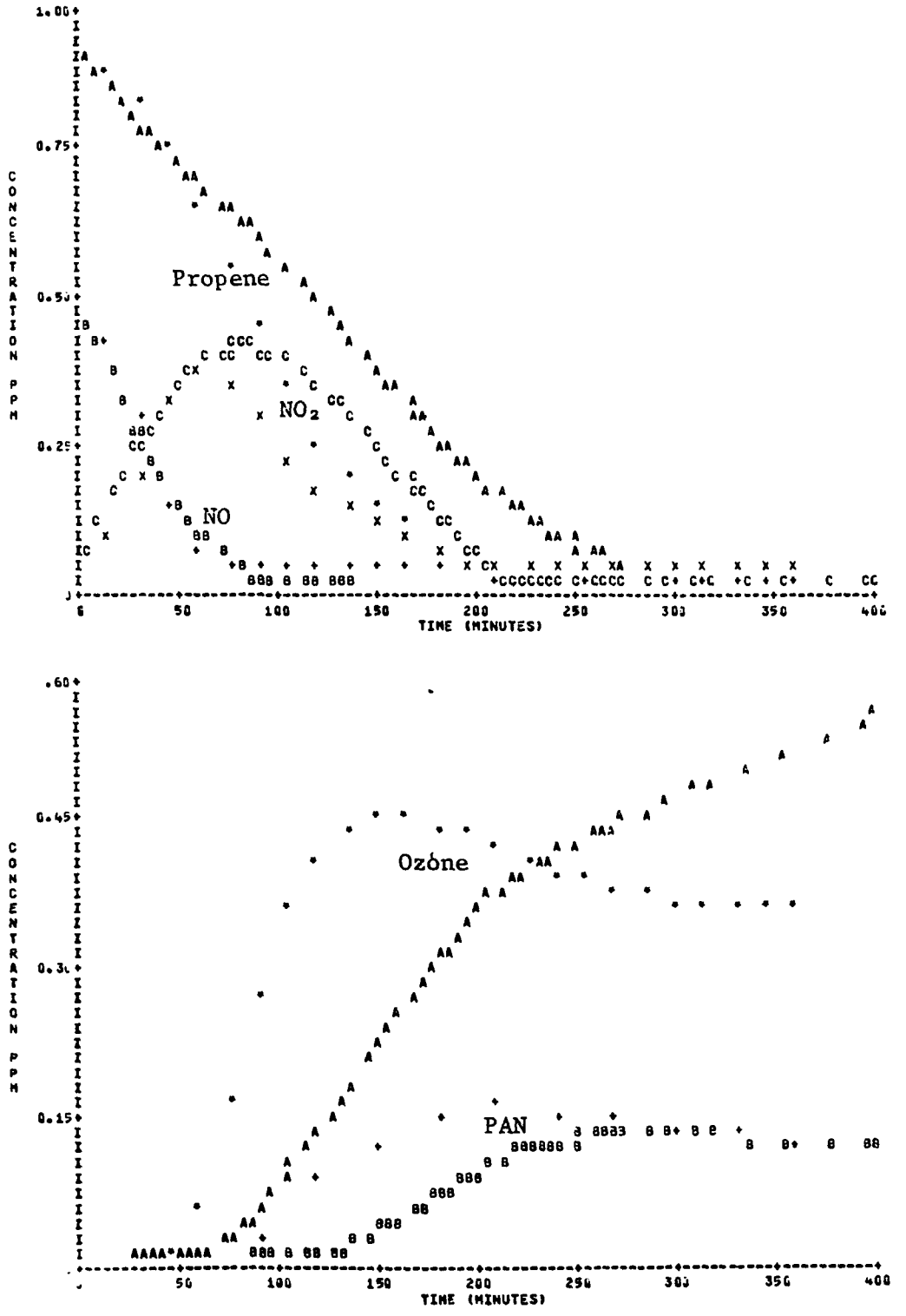

Figure A-1. Simulation of SAPRC EC-5.

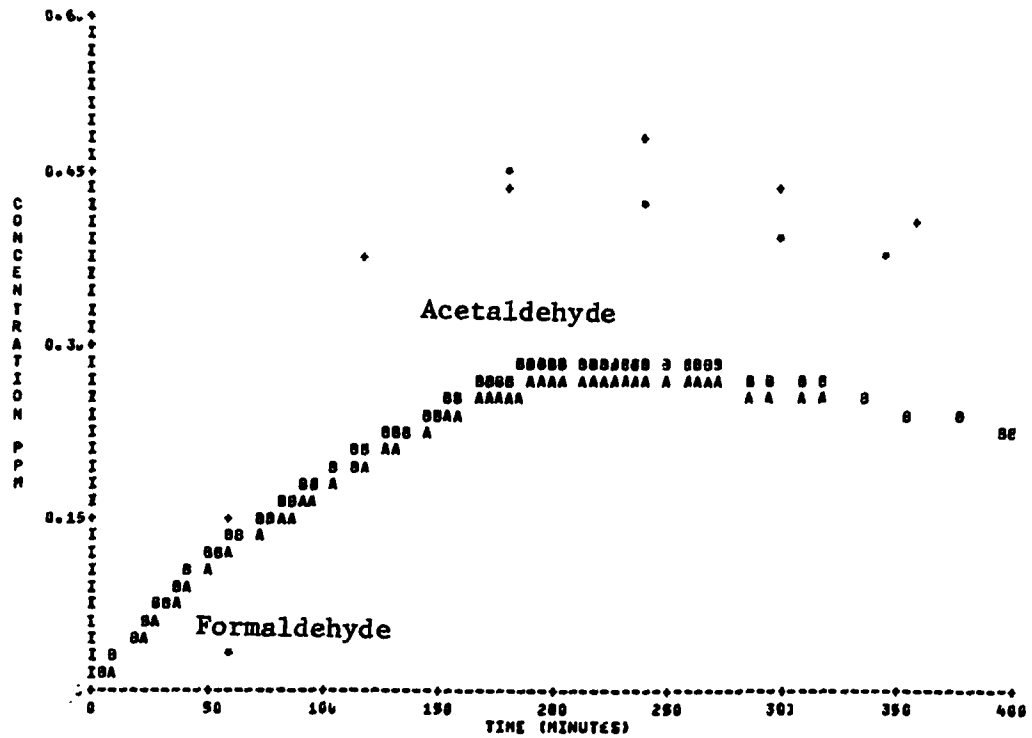

Figure A-1. Simulation of SAPRC EC-5 (Concluded).

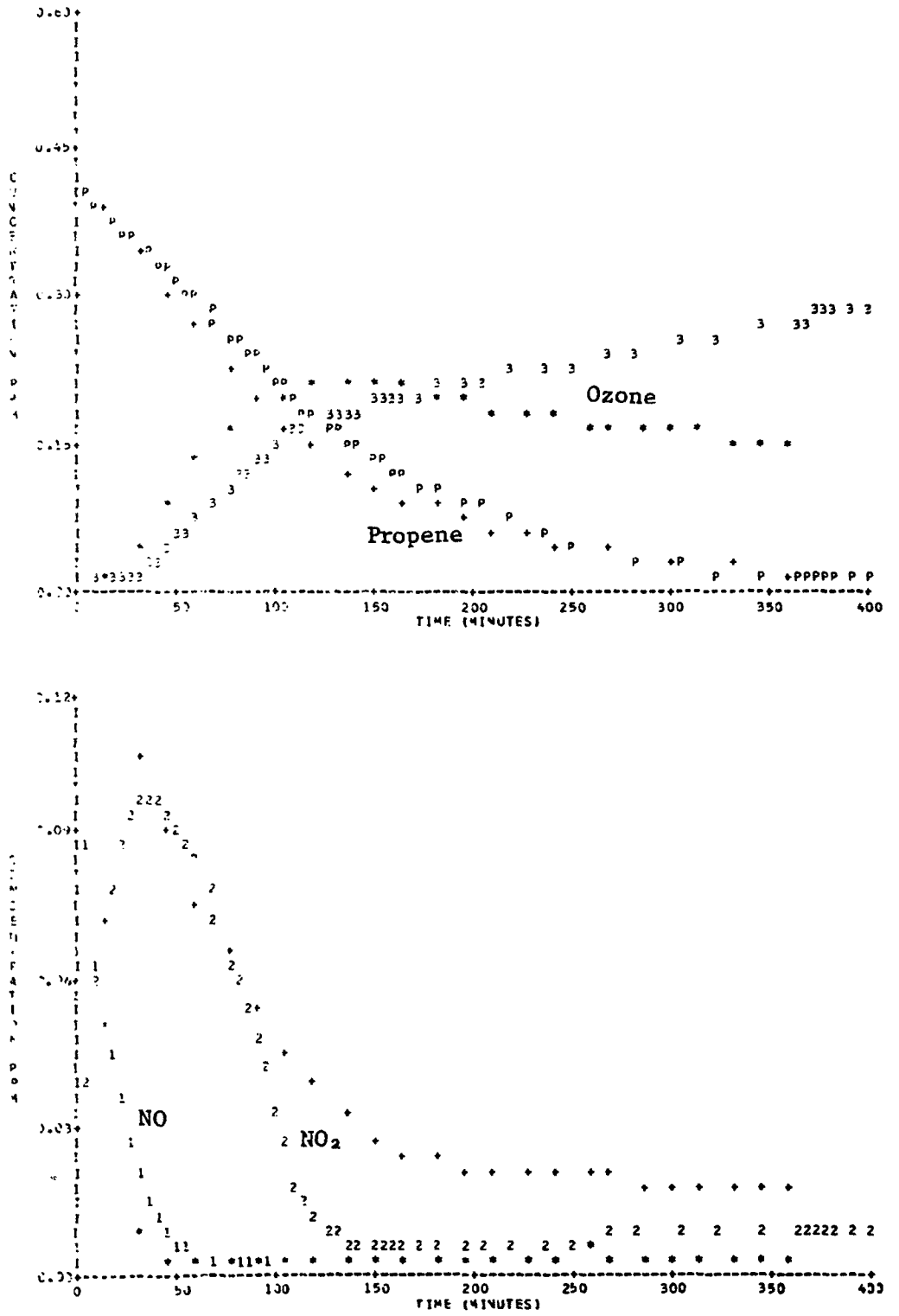

Figure A-2. Simulation of SAPRC EC-11.

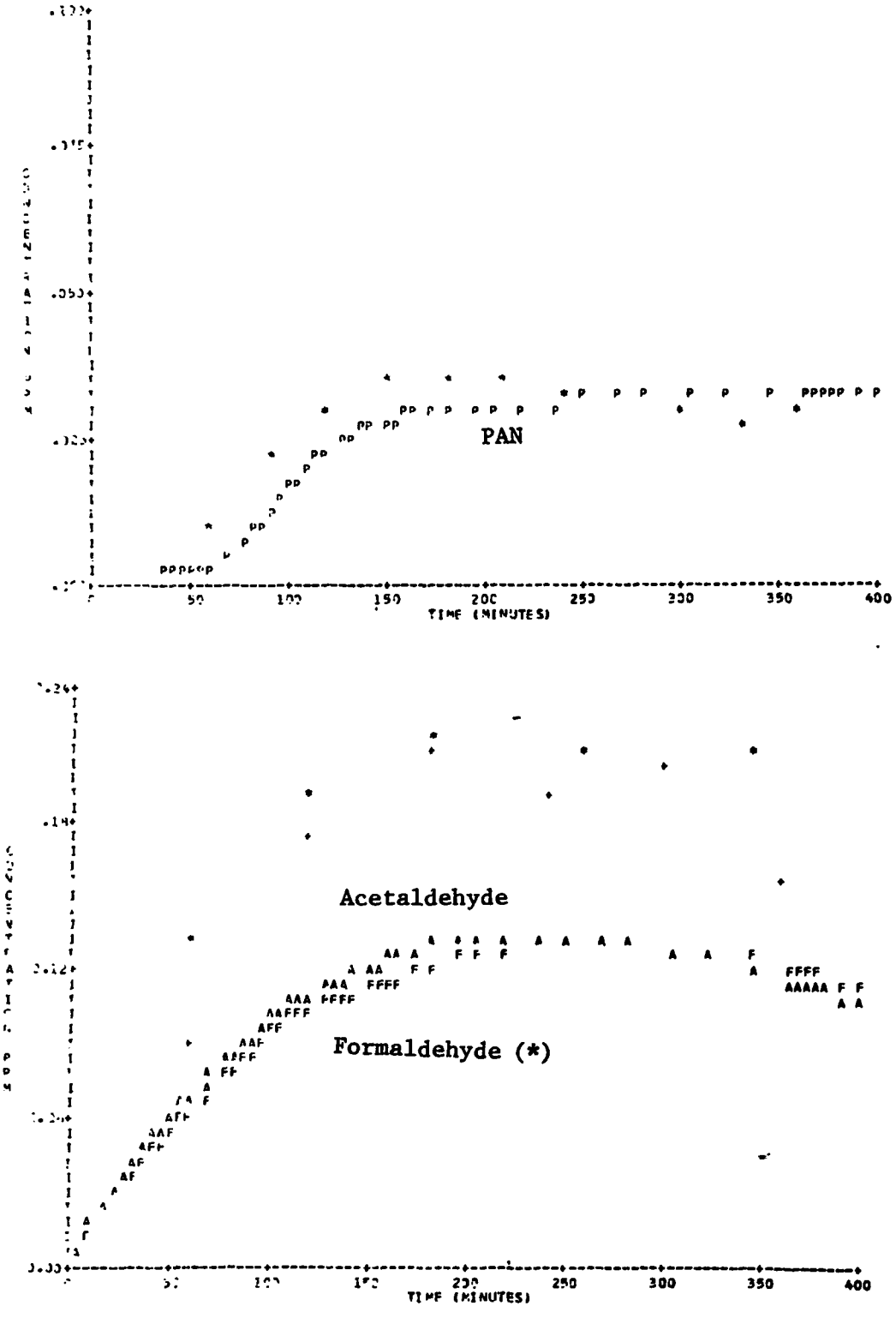

Figure A-2. Simulation of SAPRC EC-11 (Concluded).

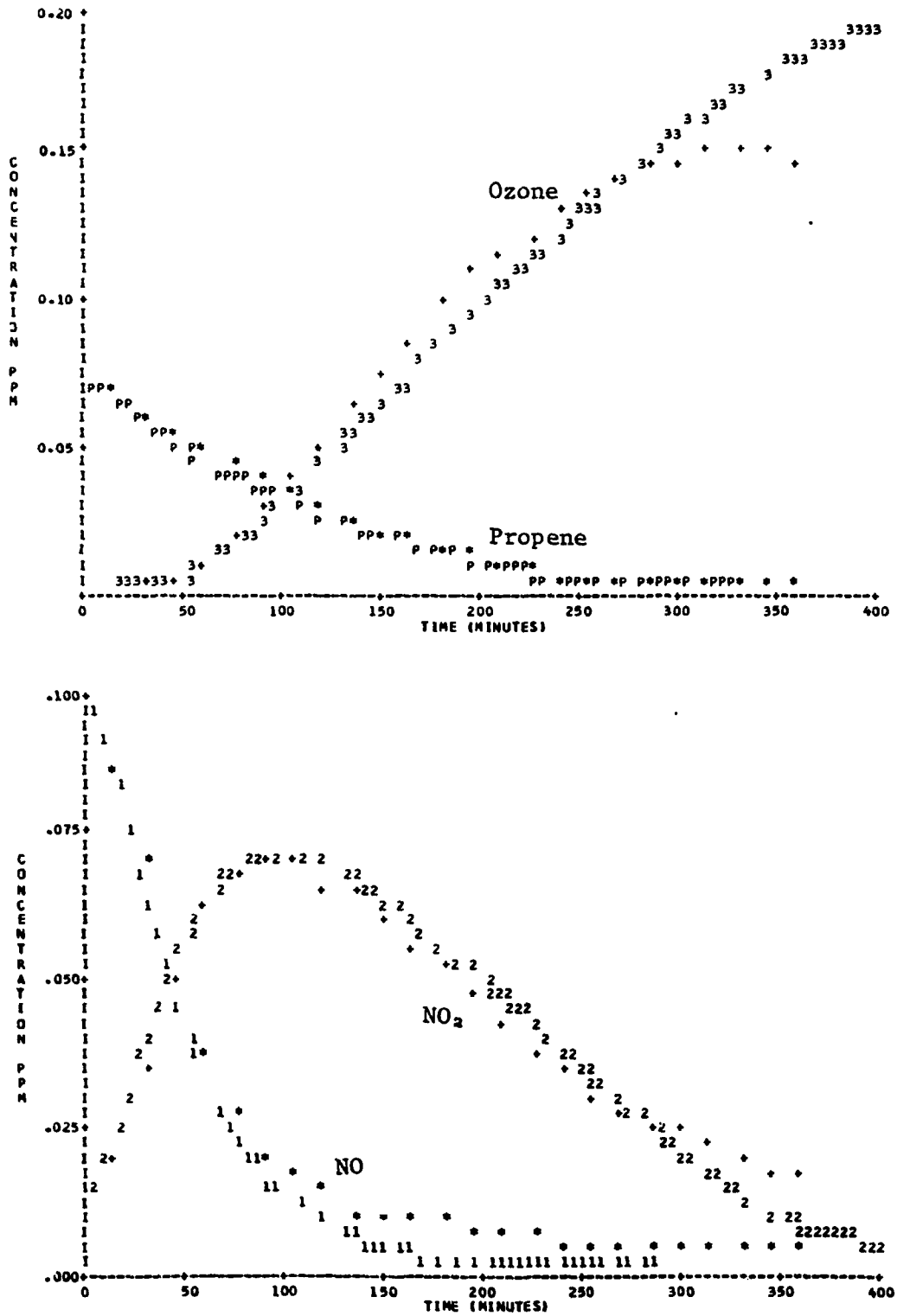

Figure A-3. Simulation of SAPRC EC-12.

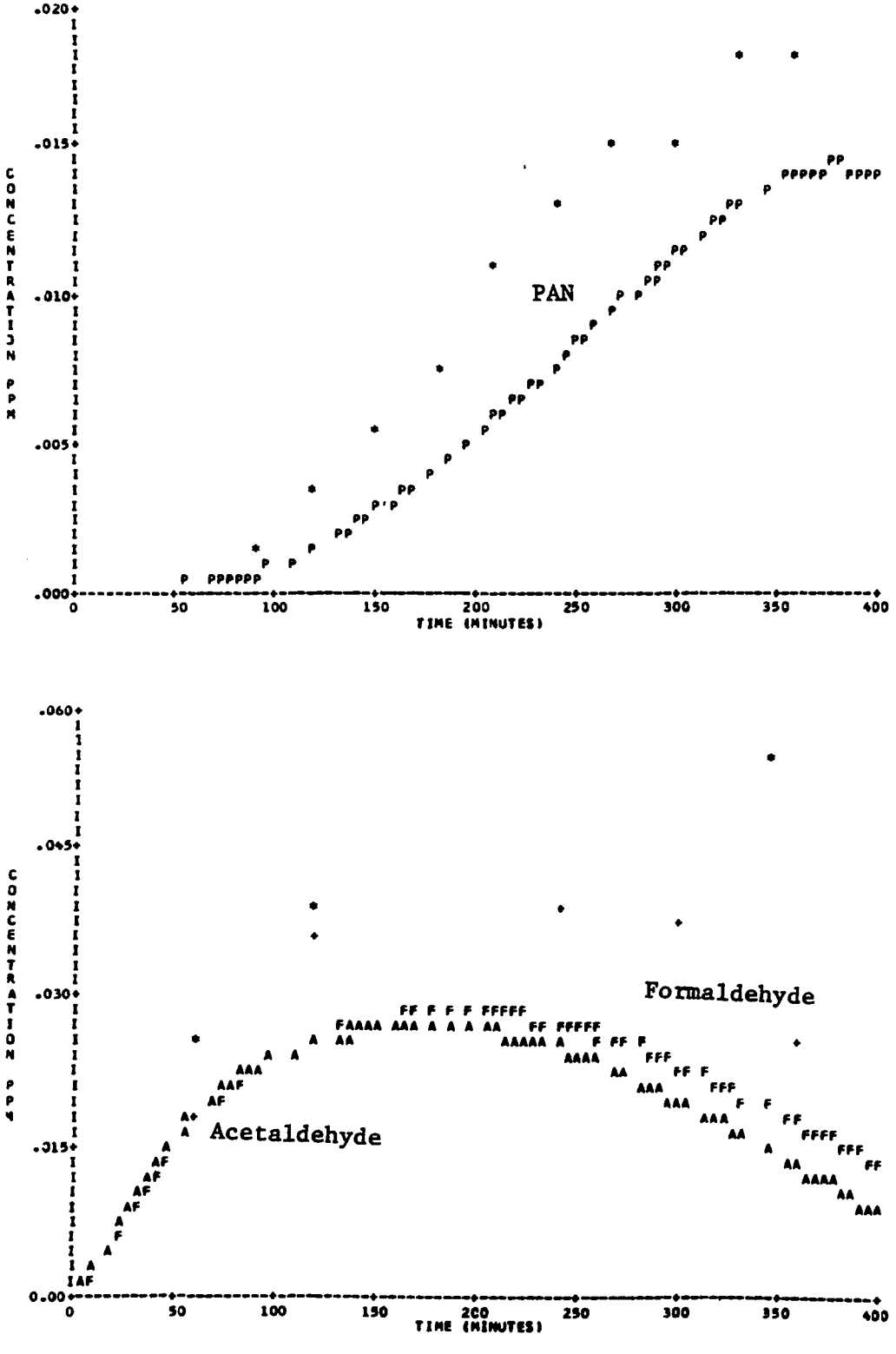

Figure A-3. Simulation of SAPRC EC-12 (Concluded).

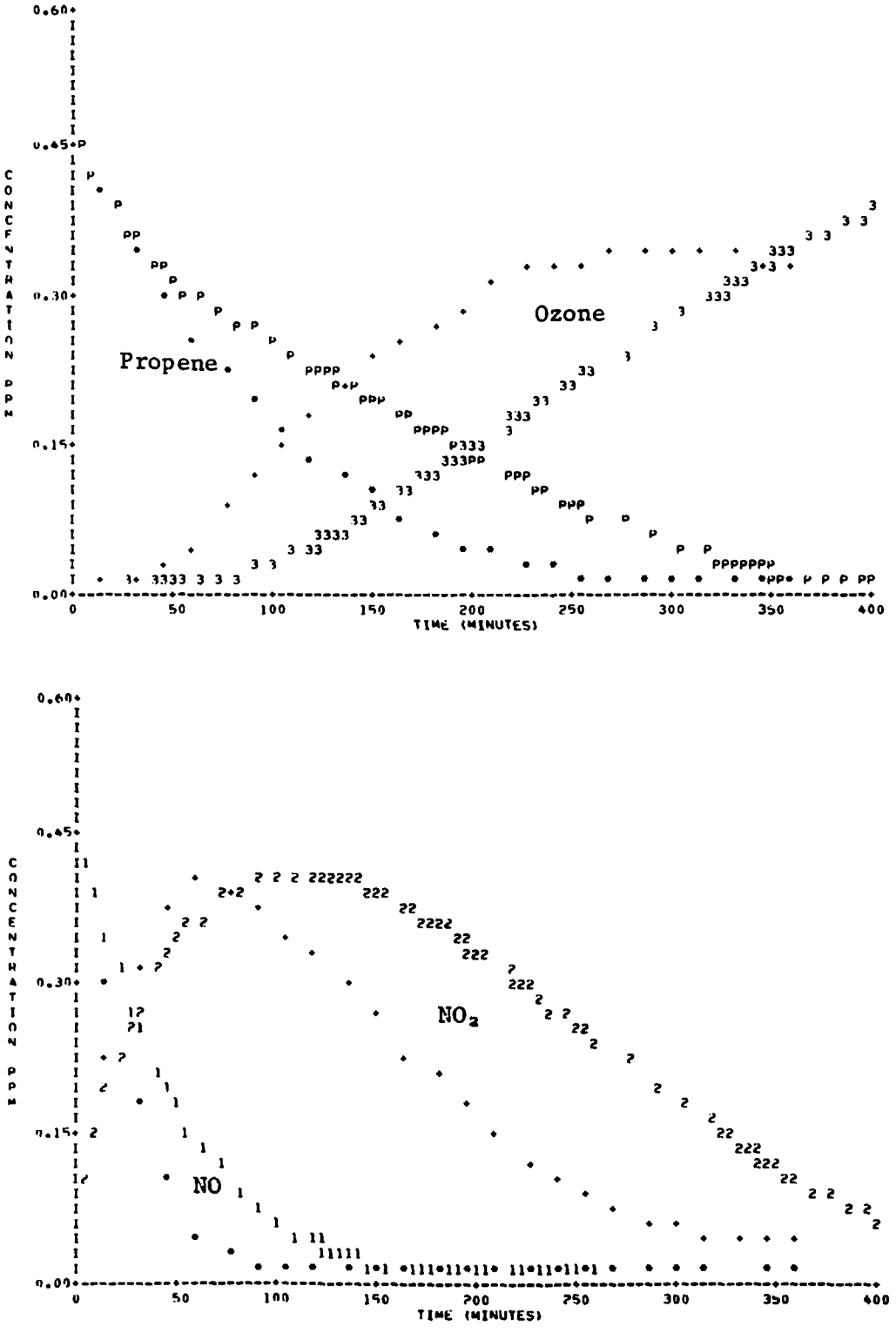

Figure A-4. Simulation of SAPRC EC-13.

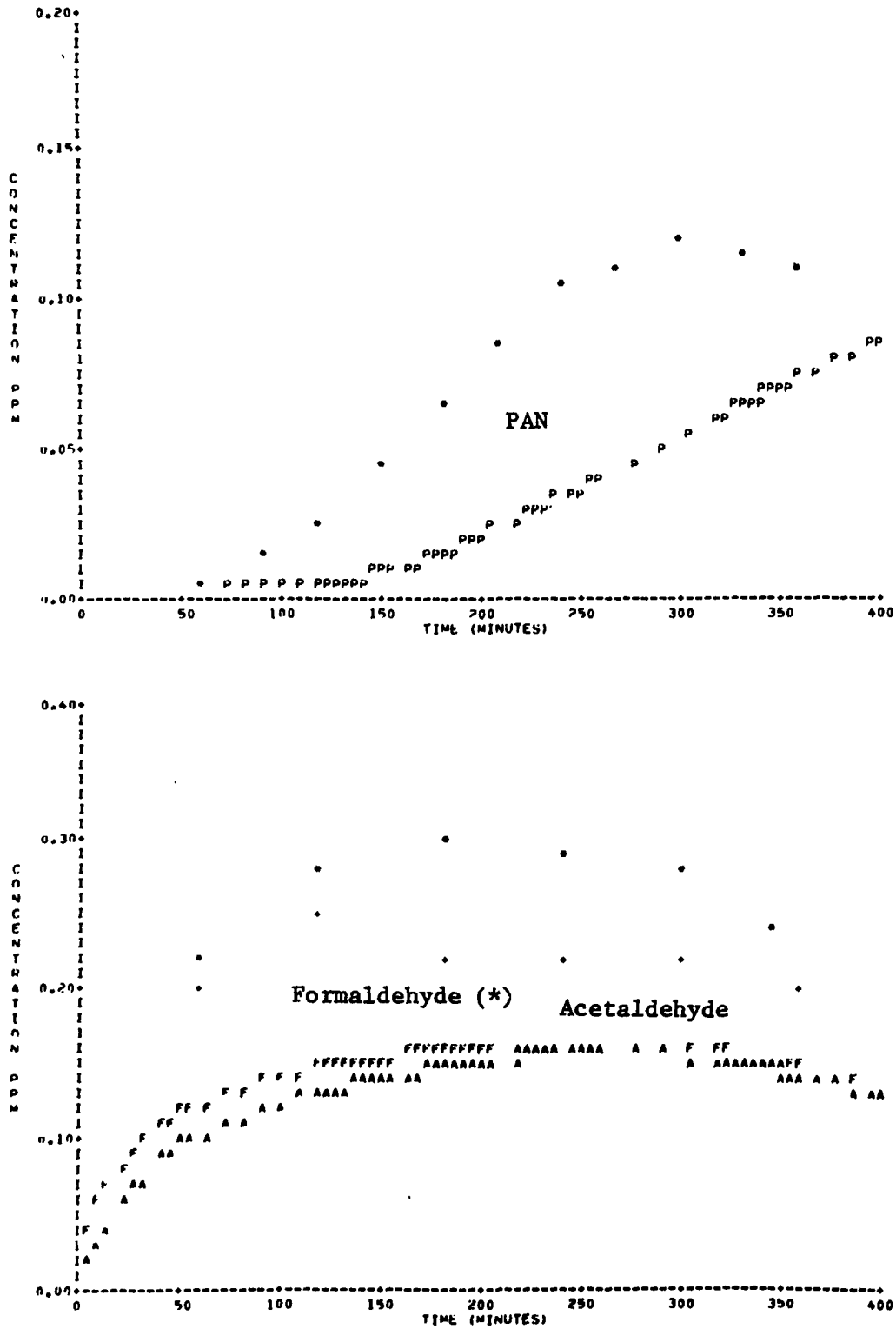

Figure A-4. Simulation of SAPRC EC-13 (Concluded).

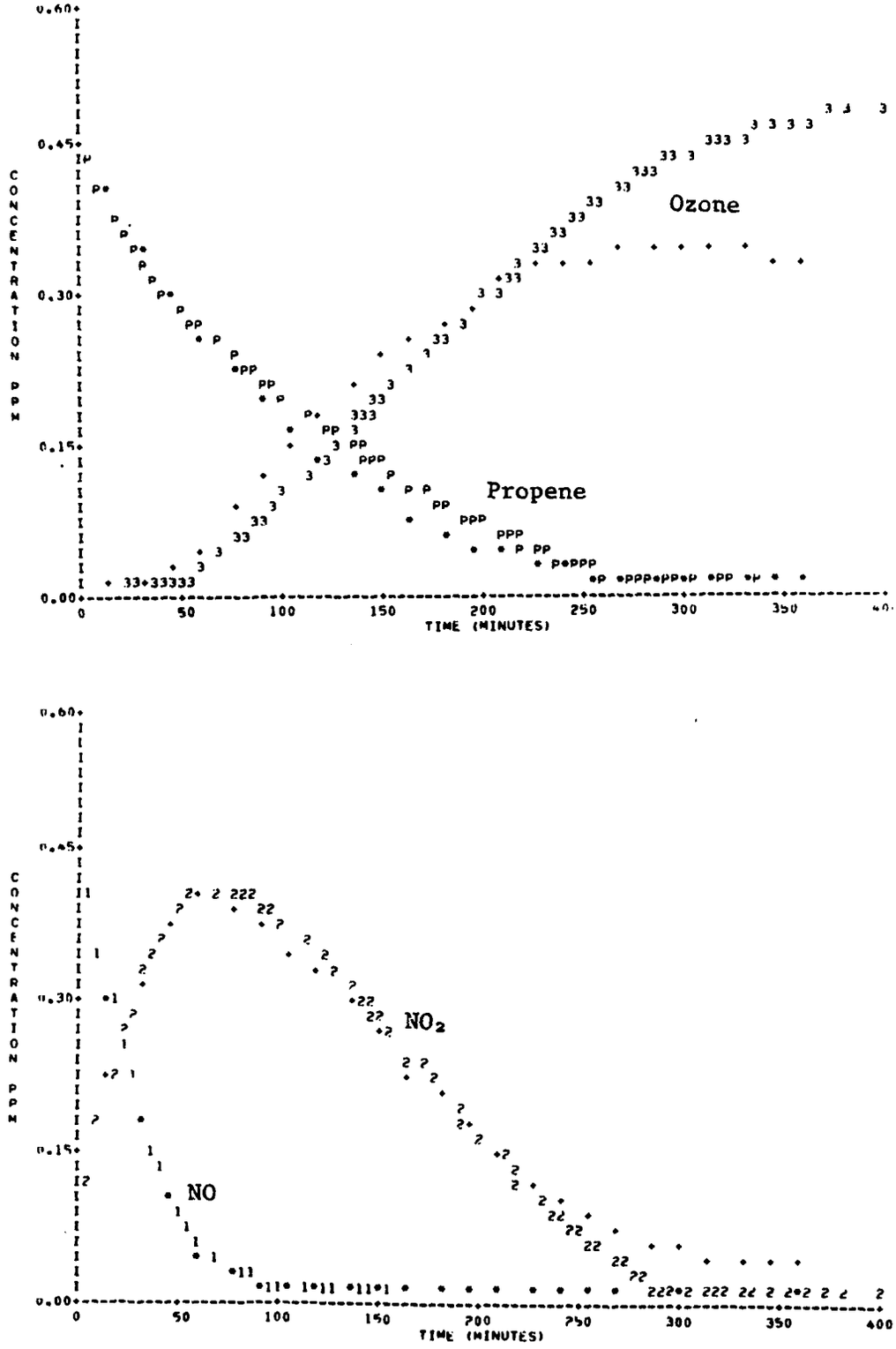

Figure A-4A. Simulation of SAPRC EC-13.
(Radical Addition Rate = 8.0 x 10^{-4} min^{-1})

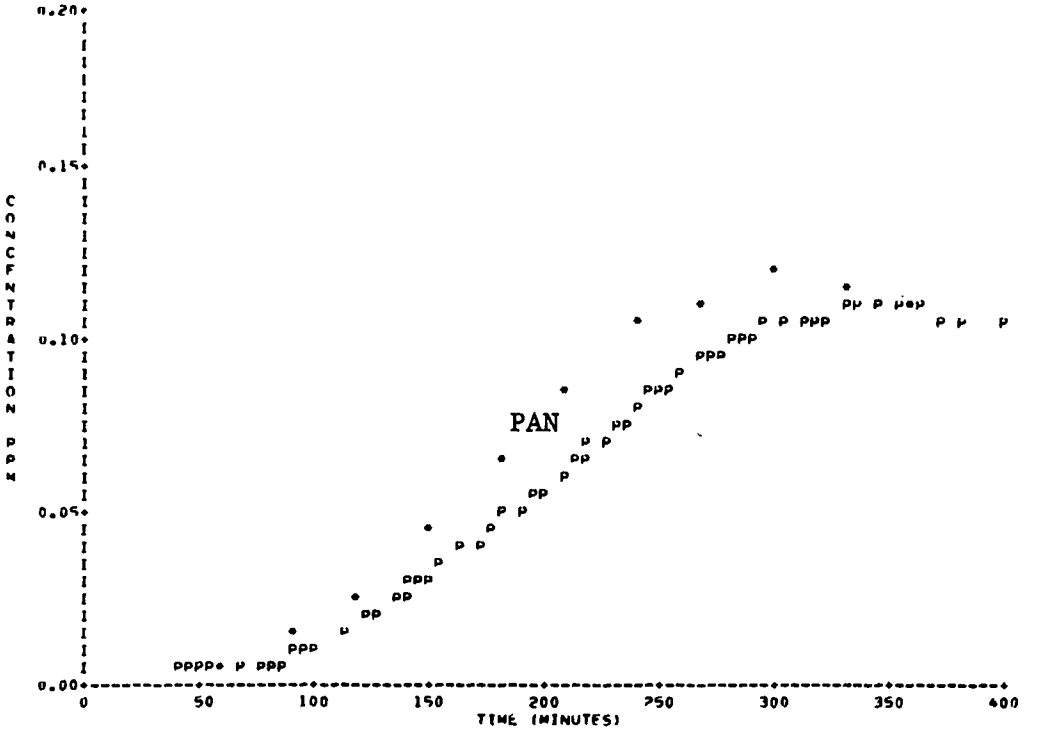

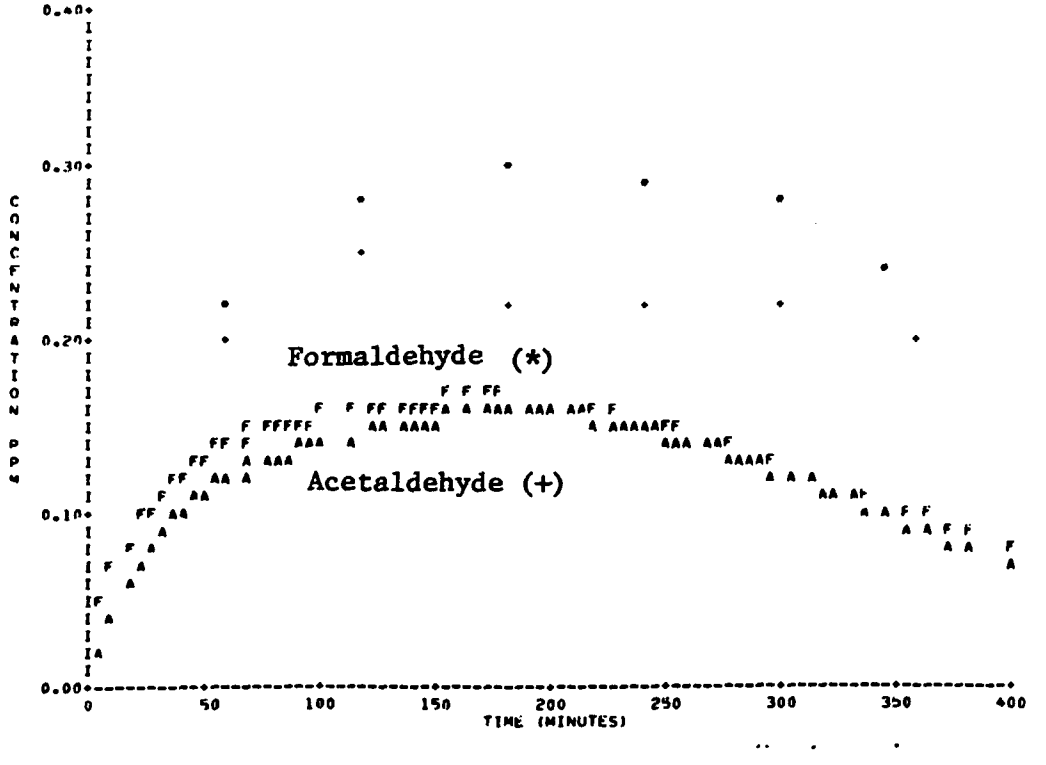

Figure A-4A. Simulation of SAPRC EC-13.
(Radical Addition Rate = 8.0 x 10^{-4} min^{-1}) (Concluded).

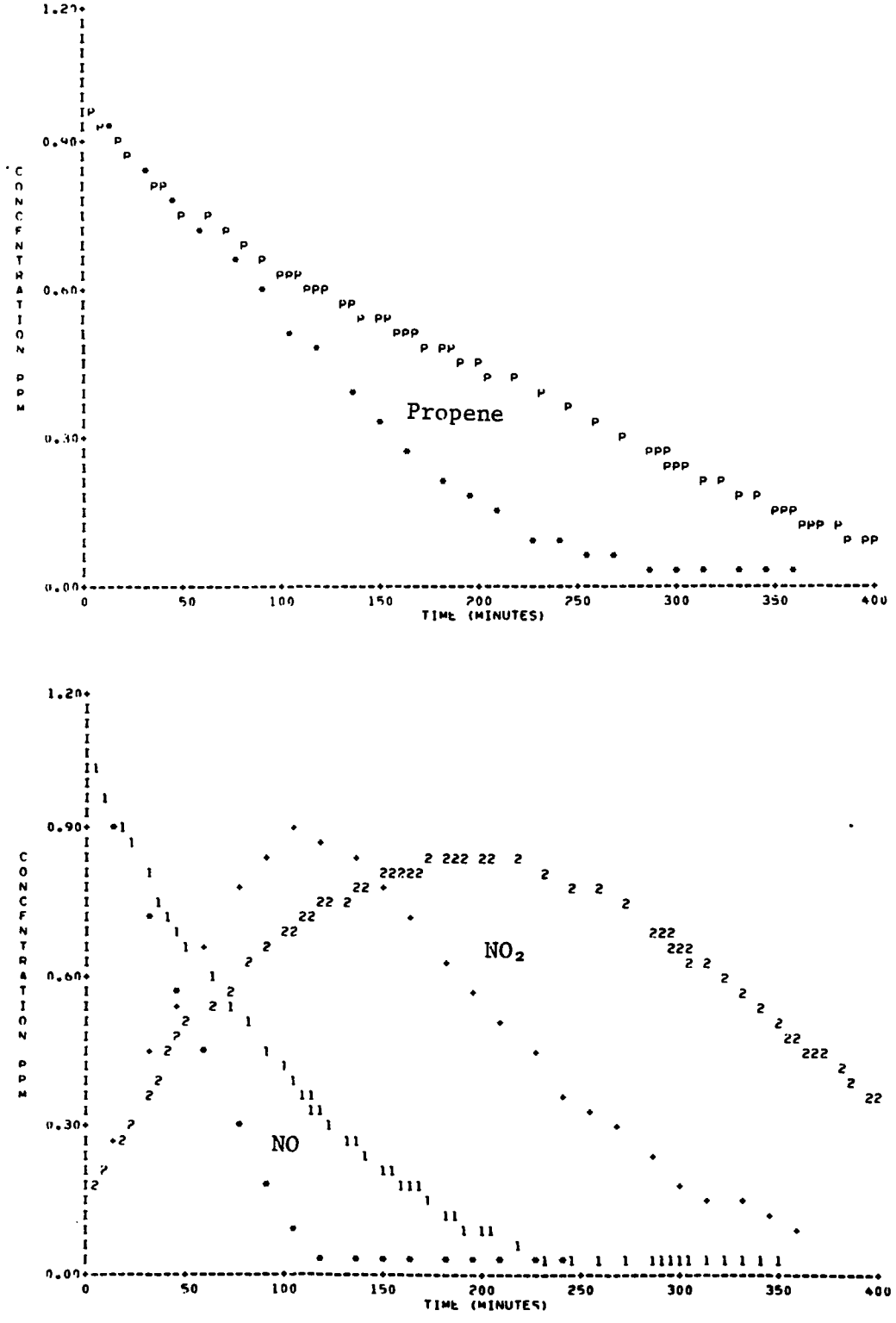

Figure A-5. Simulation of SAPRC EC-16.

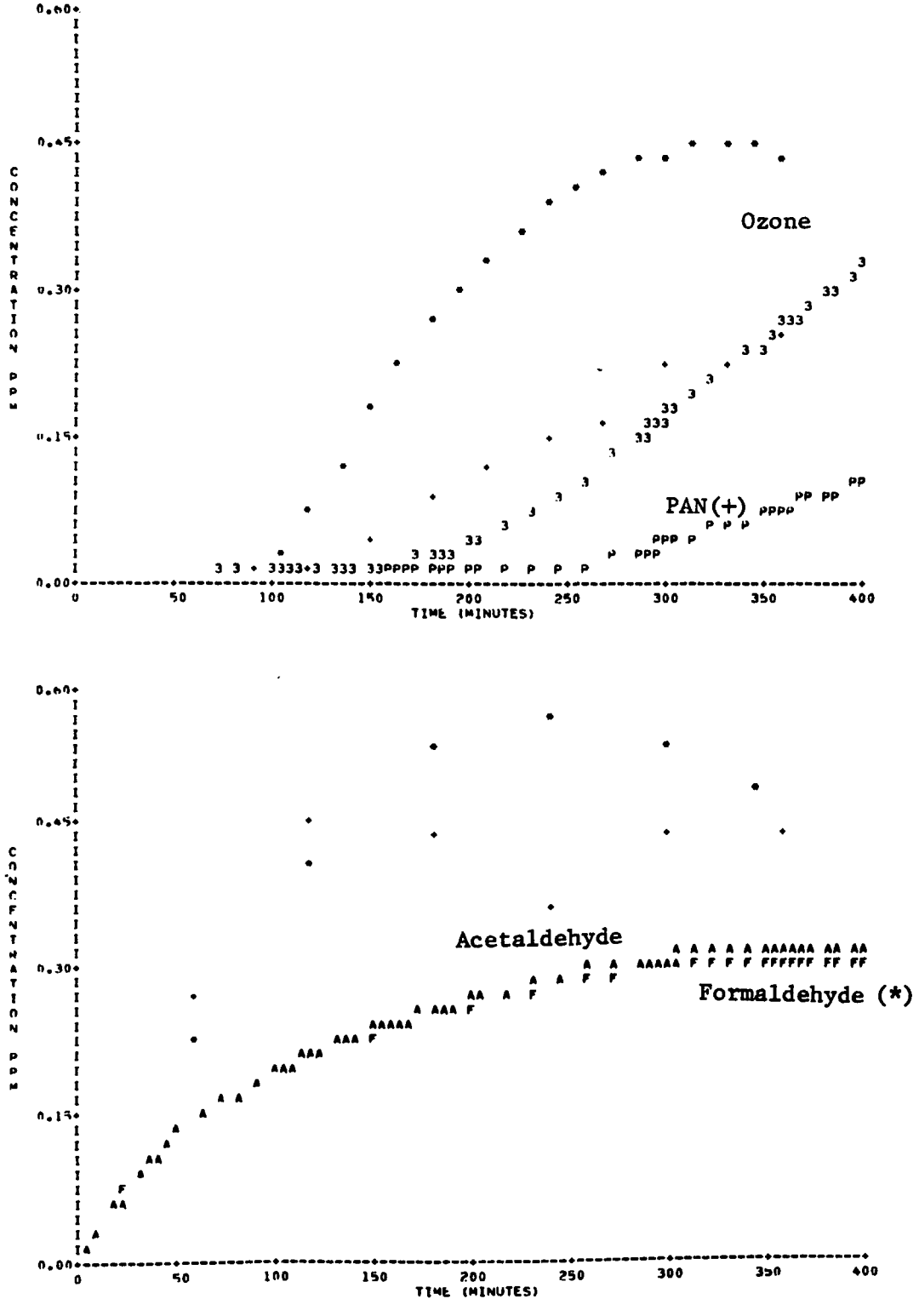

Figure A-5. Simulation of SAPRC EC-16 (Concluded).

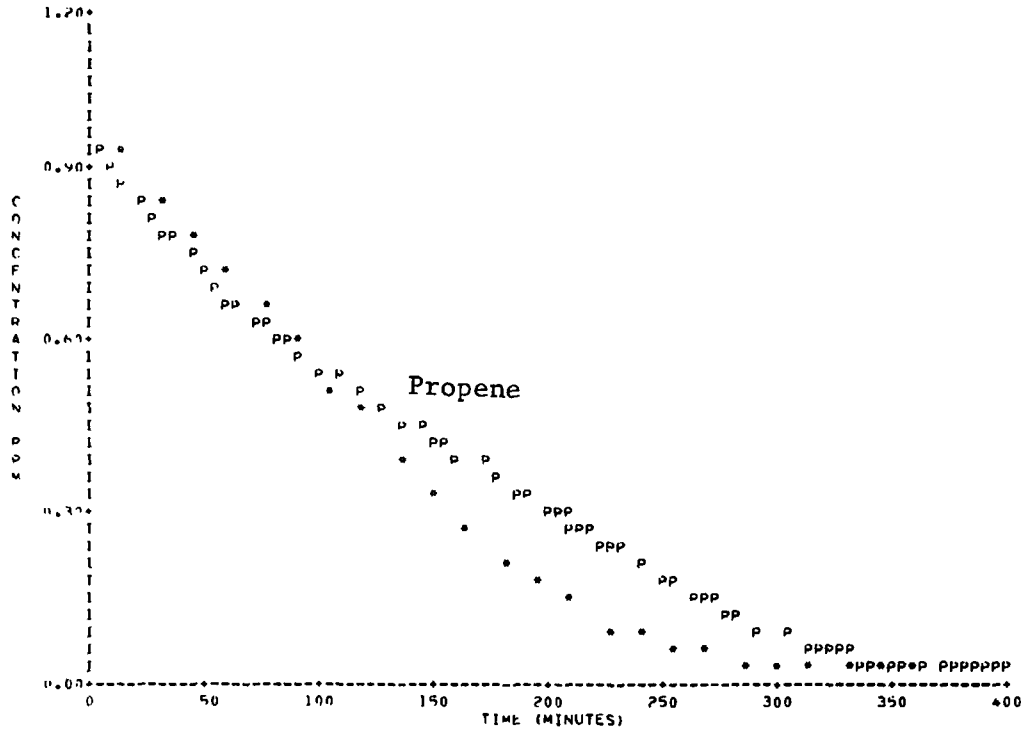

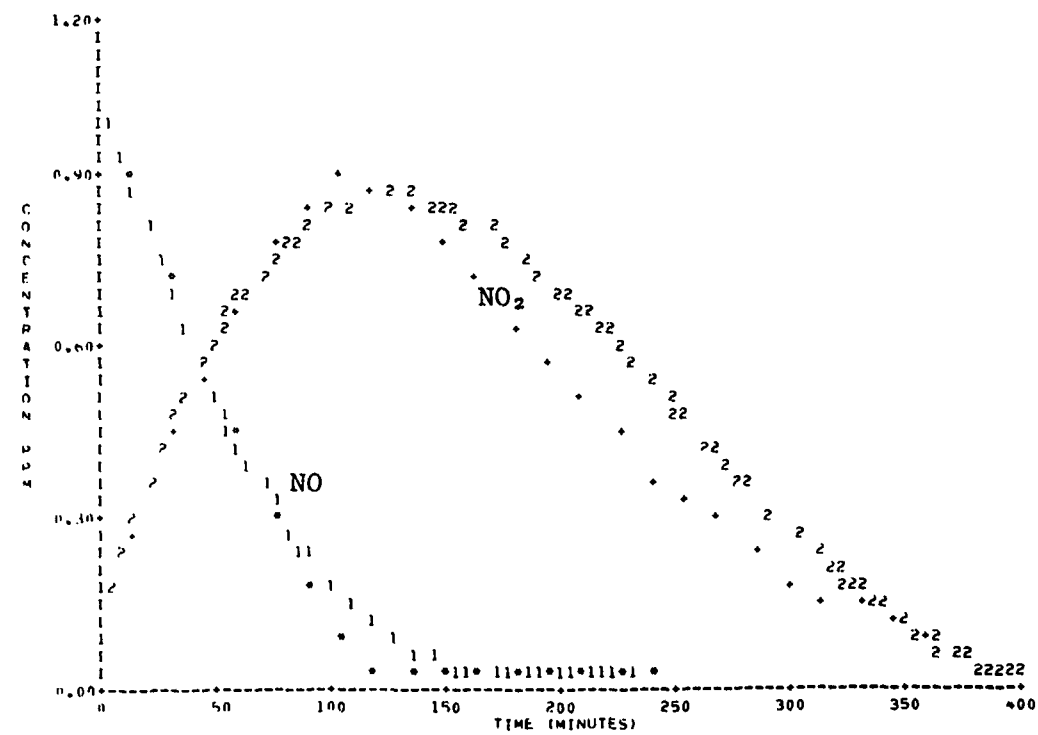

Figure A-5A. Simulation of SAPRC EC-16.
(Radical Addition Rate = 6 x 10^{-4} min^{-1})

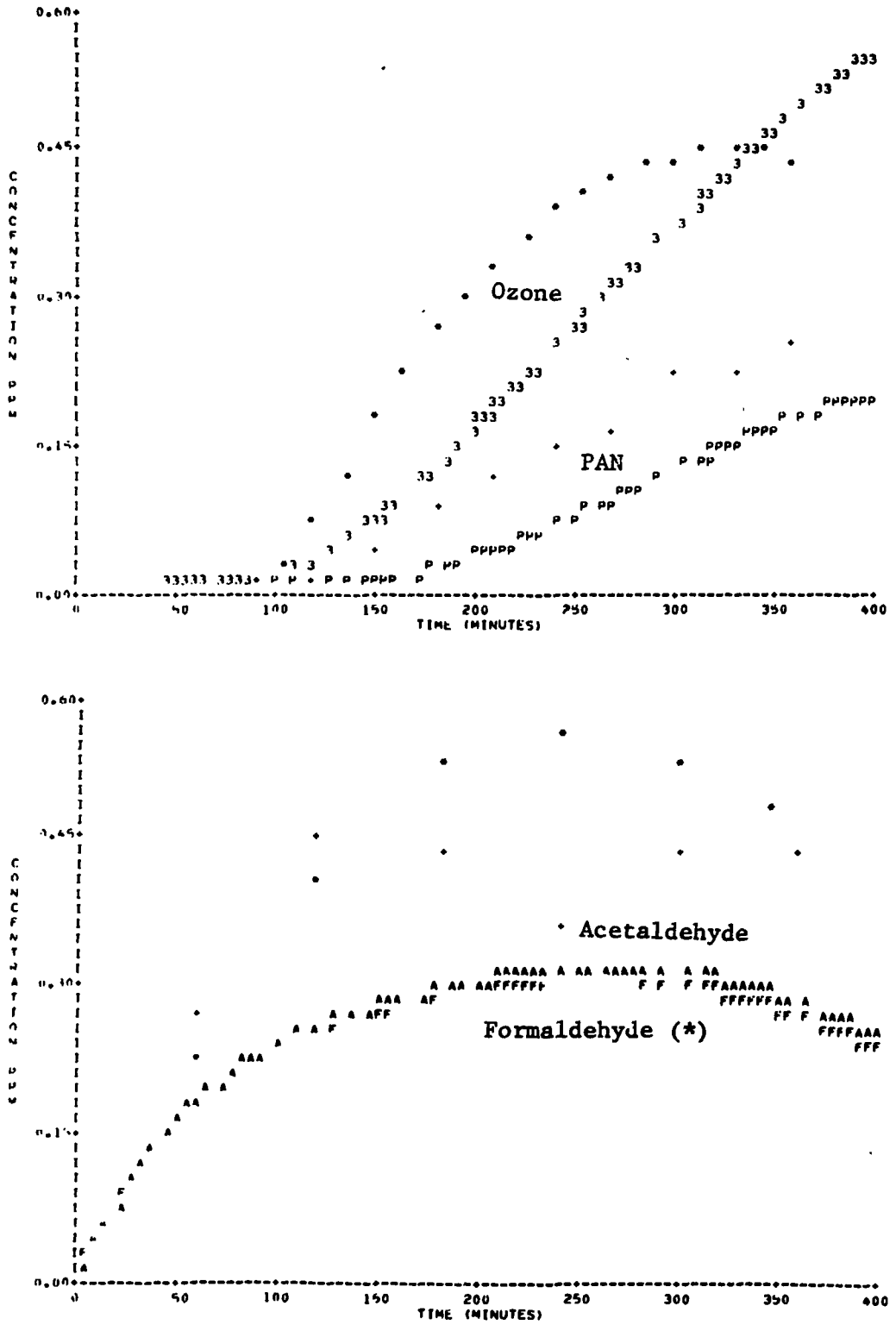

Figure A-5A. Simulation of SAPRC EC-16.
(Radical Addition Rate = 6 x 10^{-4} min^{-1}) (Concluded).

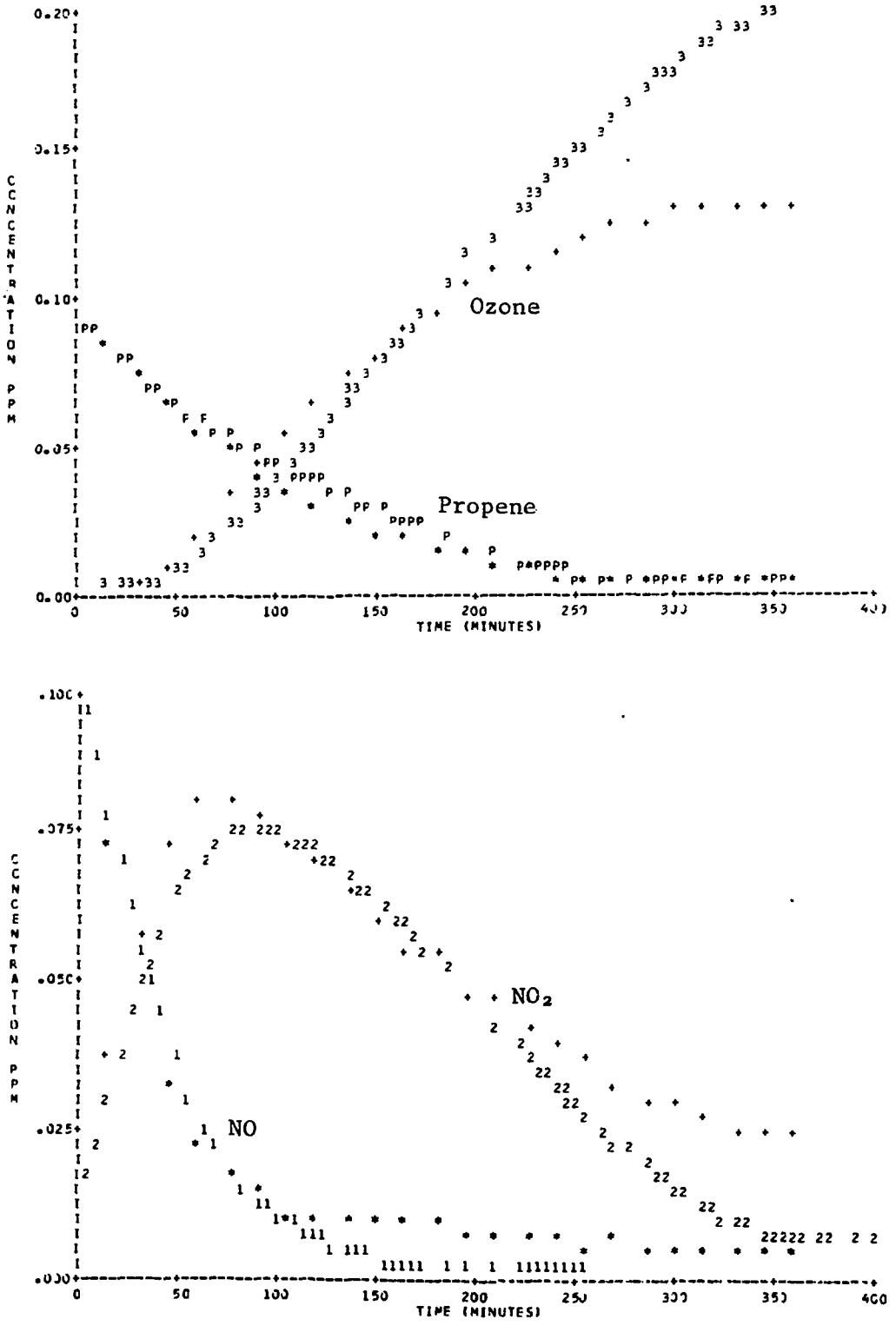

Figure A-6. Simulation of SAPRC EC-17.

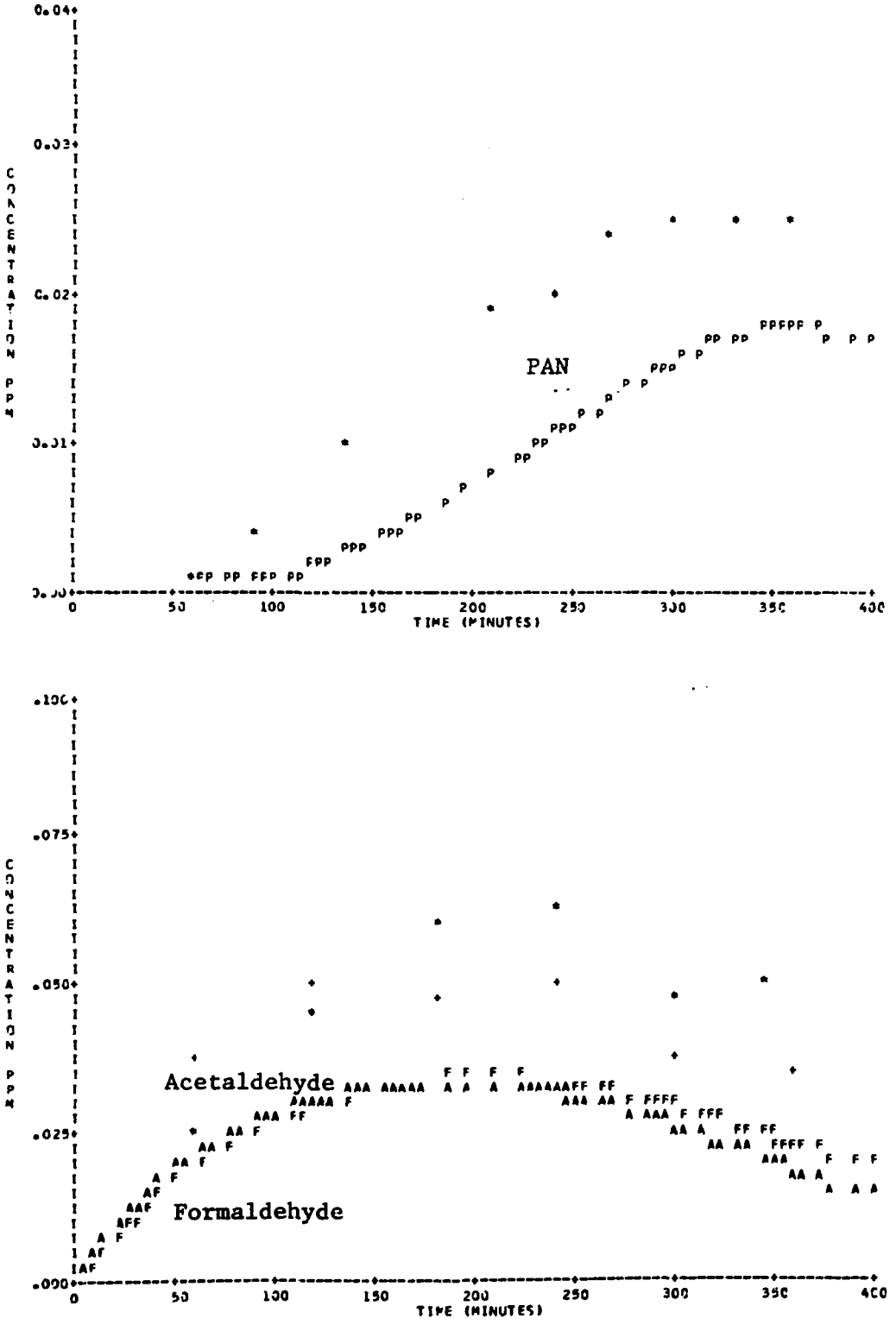

Figure A-6. Simulation of SAPRC EC-17 (Concluded).

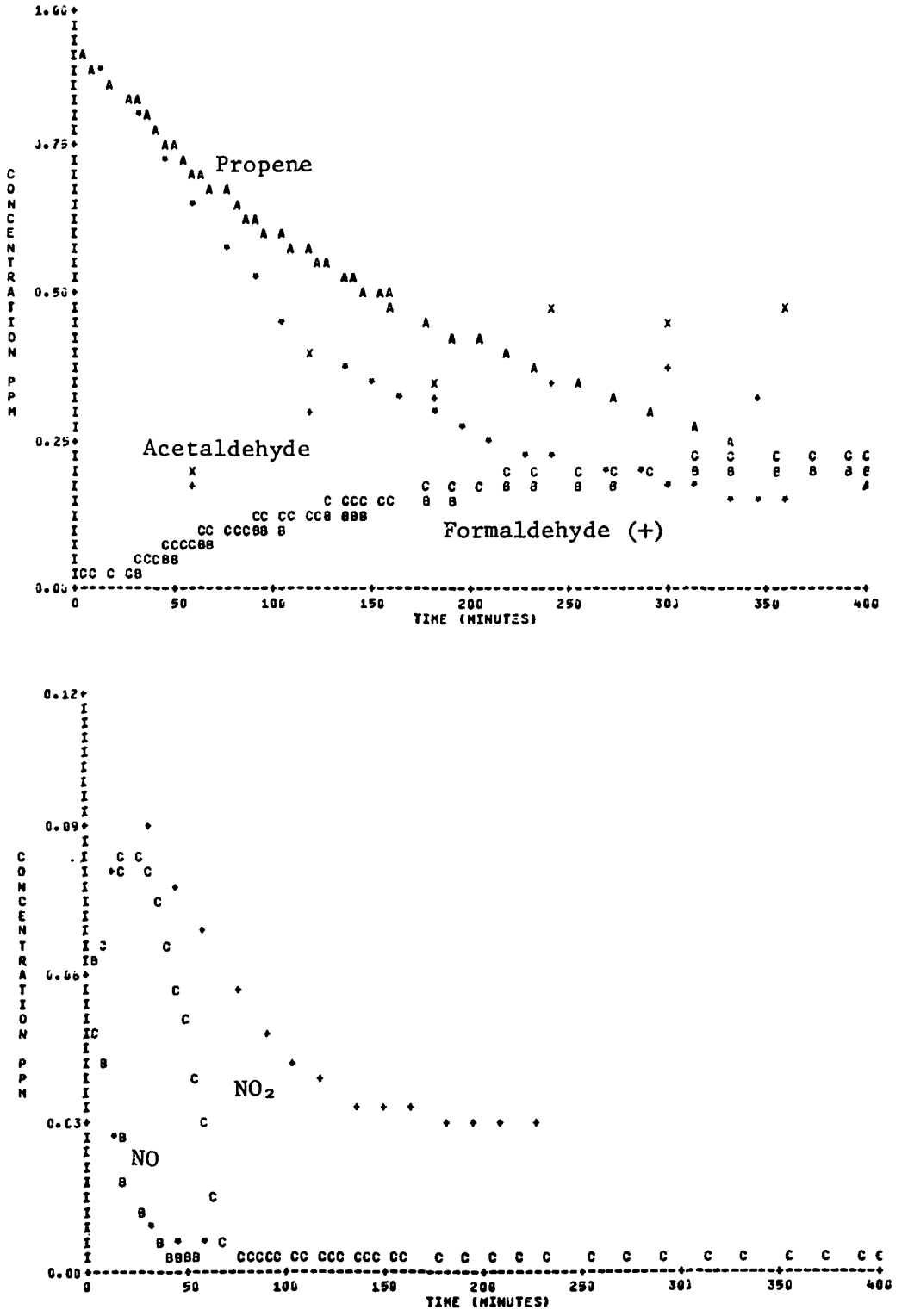

Figure A-7. Simulation of SAPRC EC-18.

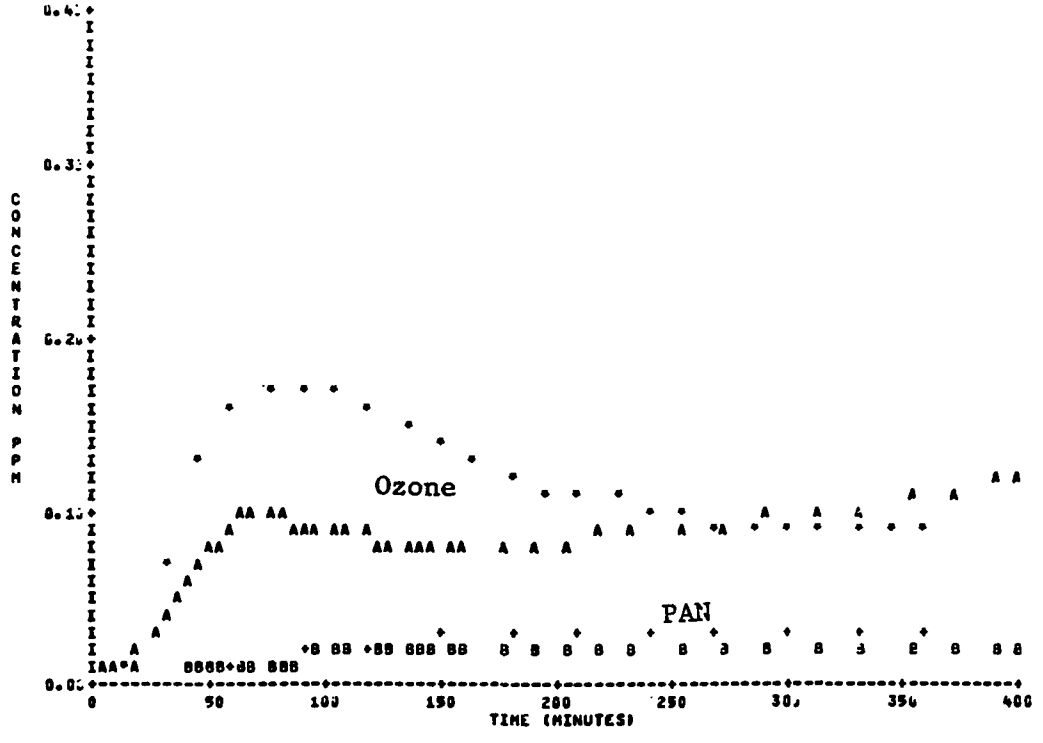

Figure A-7. Simulation of SAPRC EC-18 (Concluded).

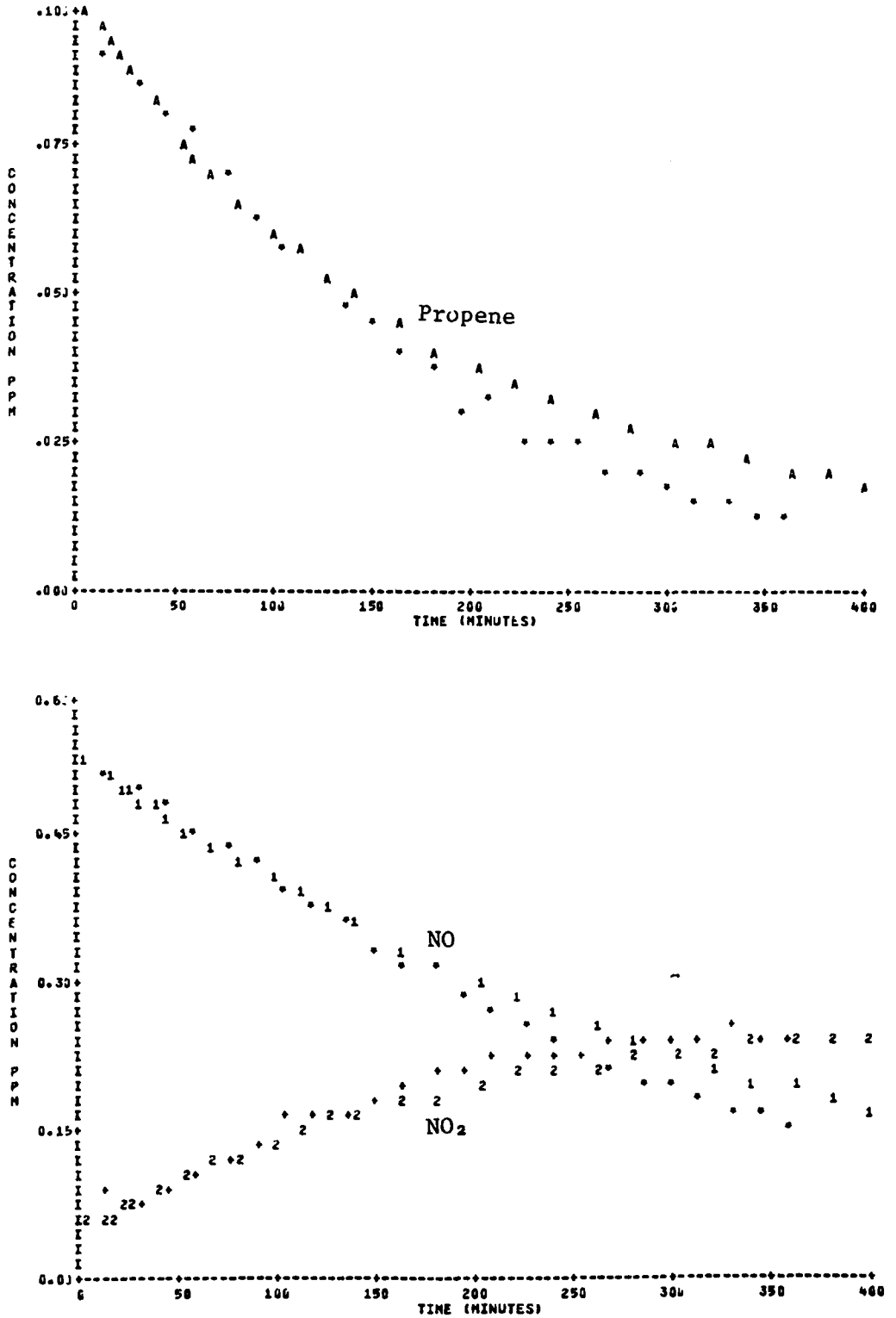

Figure A-8. Simulation of SAPRC EC-21.

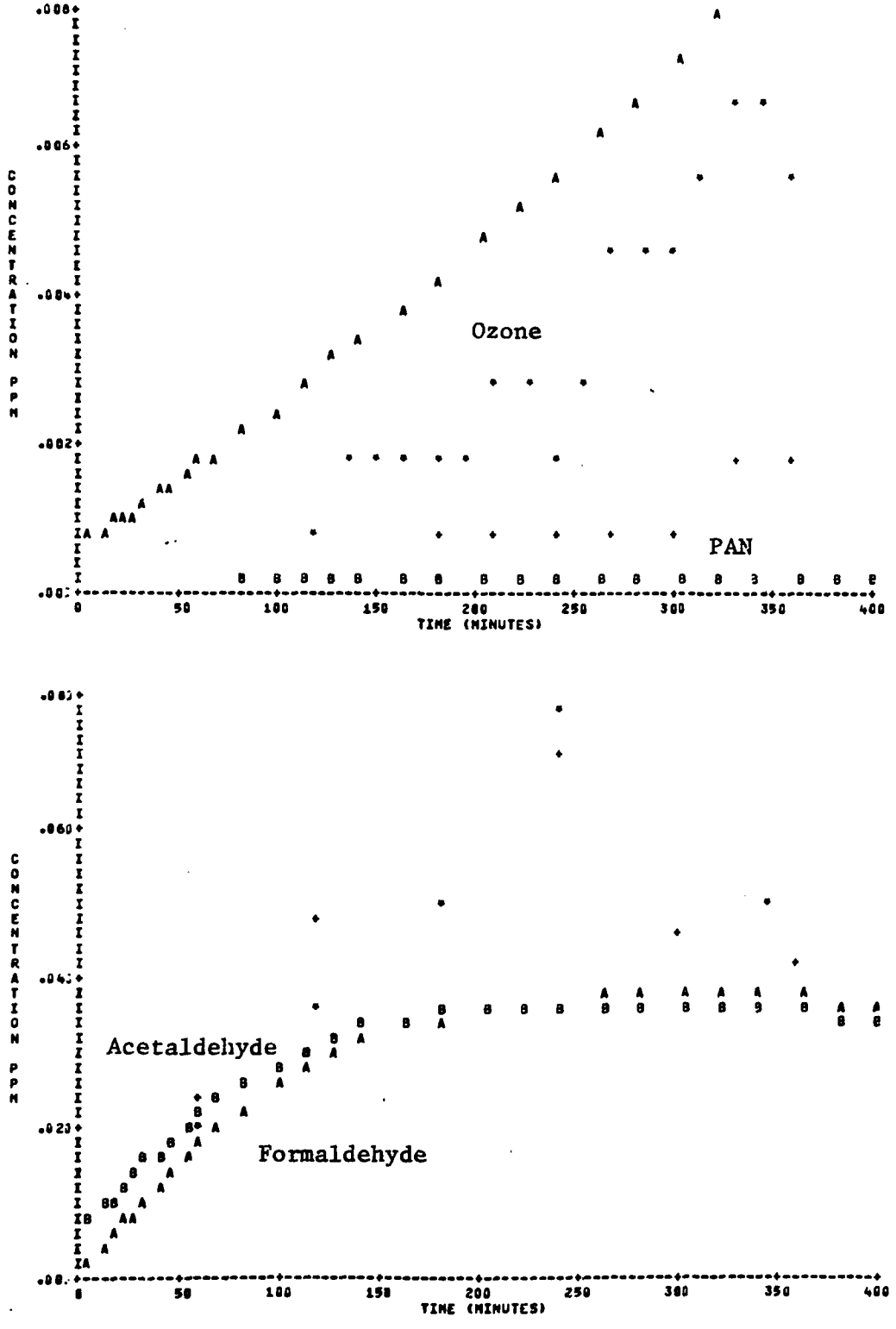

Figure A-8. Simulation of SAPRC EC-21 (Concluded).

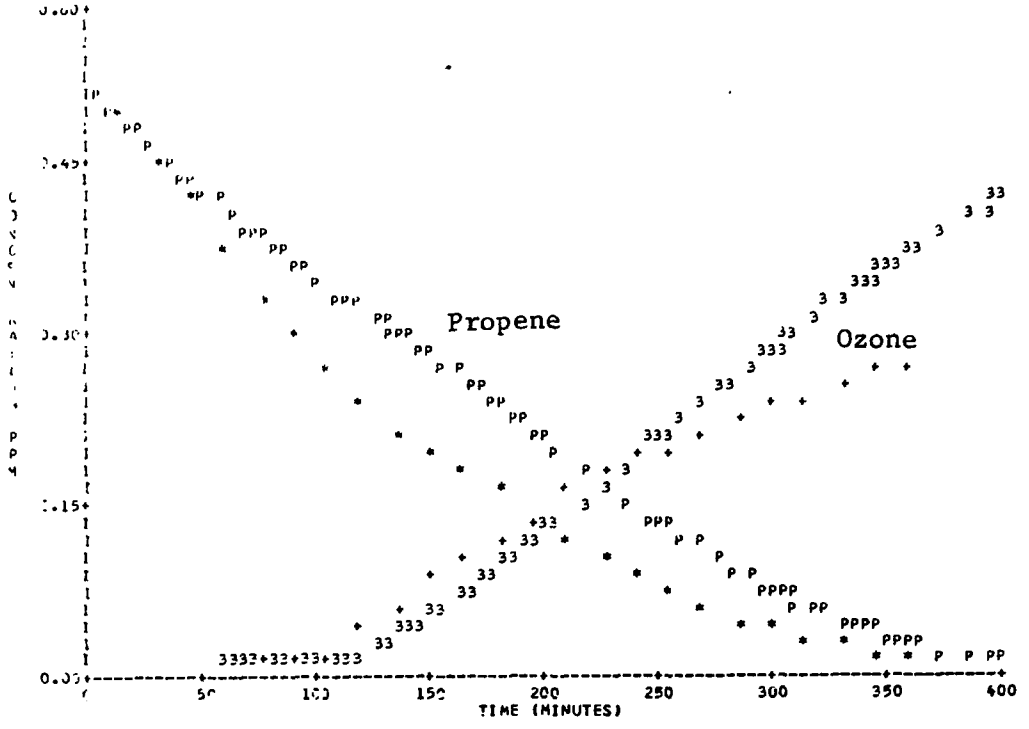

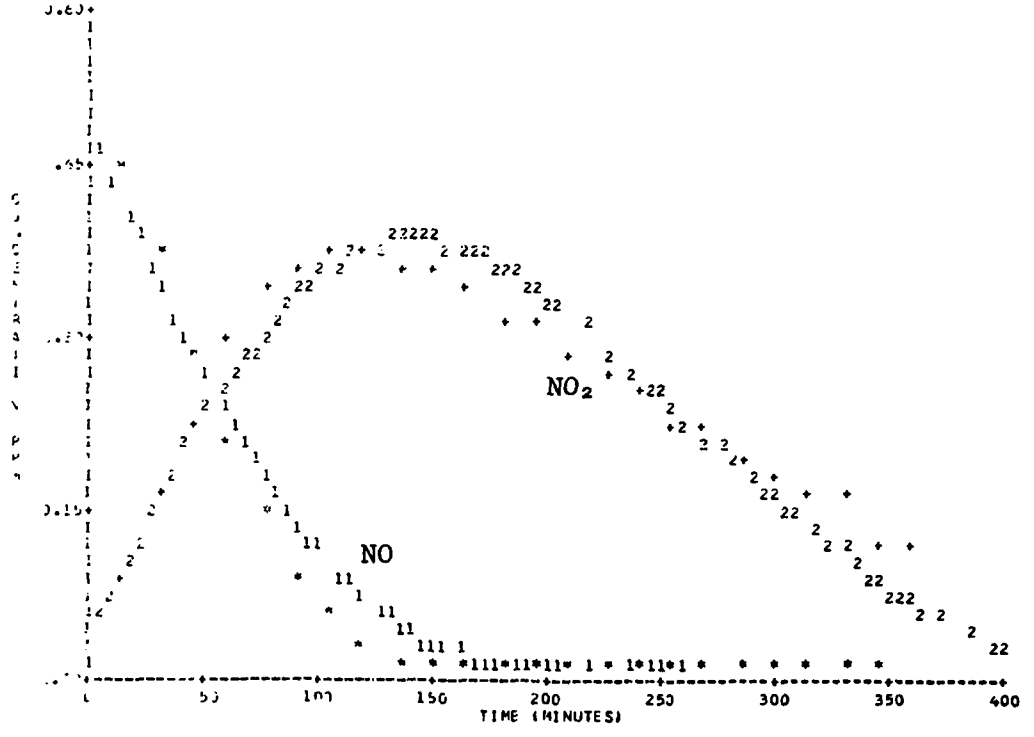

Figure A-9. Simulation of SAPRC EC-51.

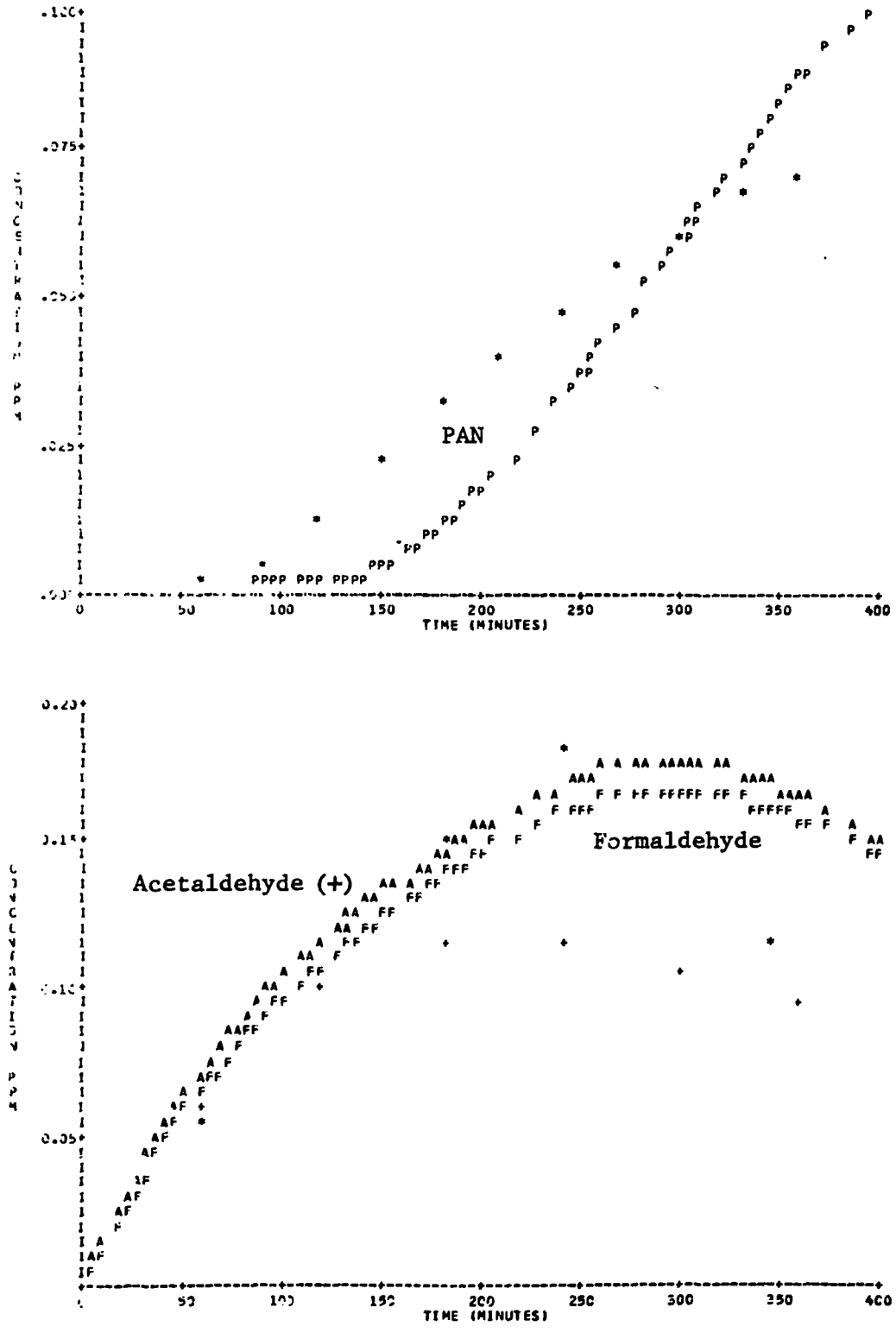

Figure A-9. Simulation of SAPRC EC-51 (Concluded).

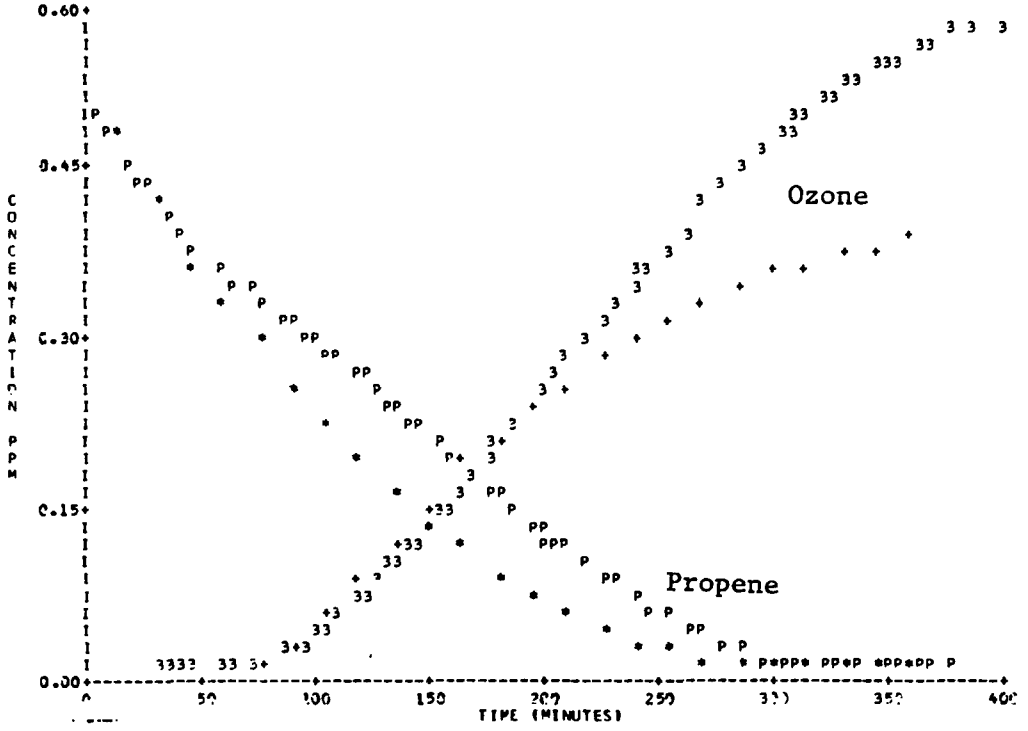

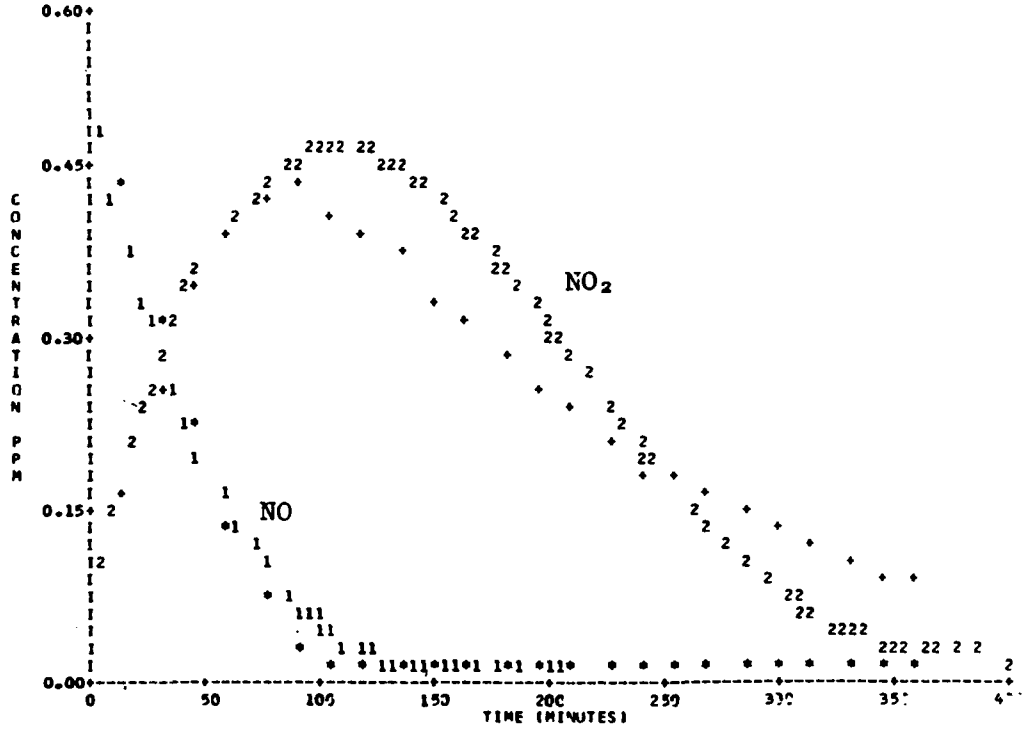

Figure A-10. Simulation of SAPRC EC-53.

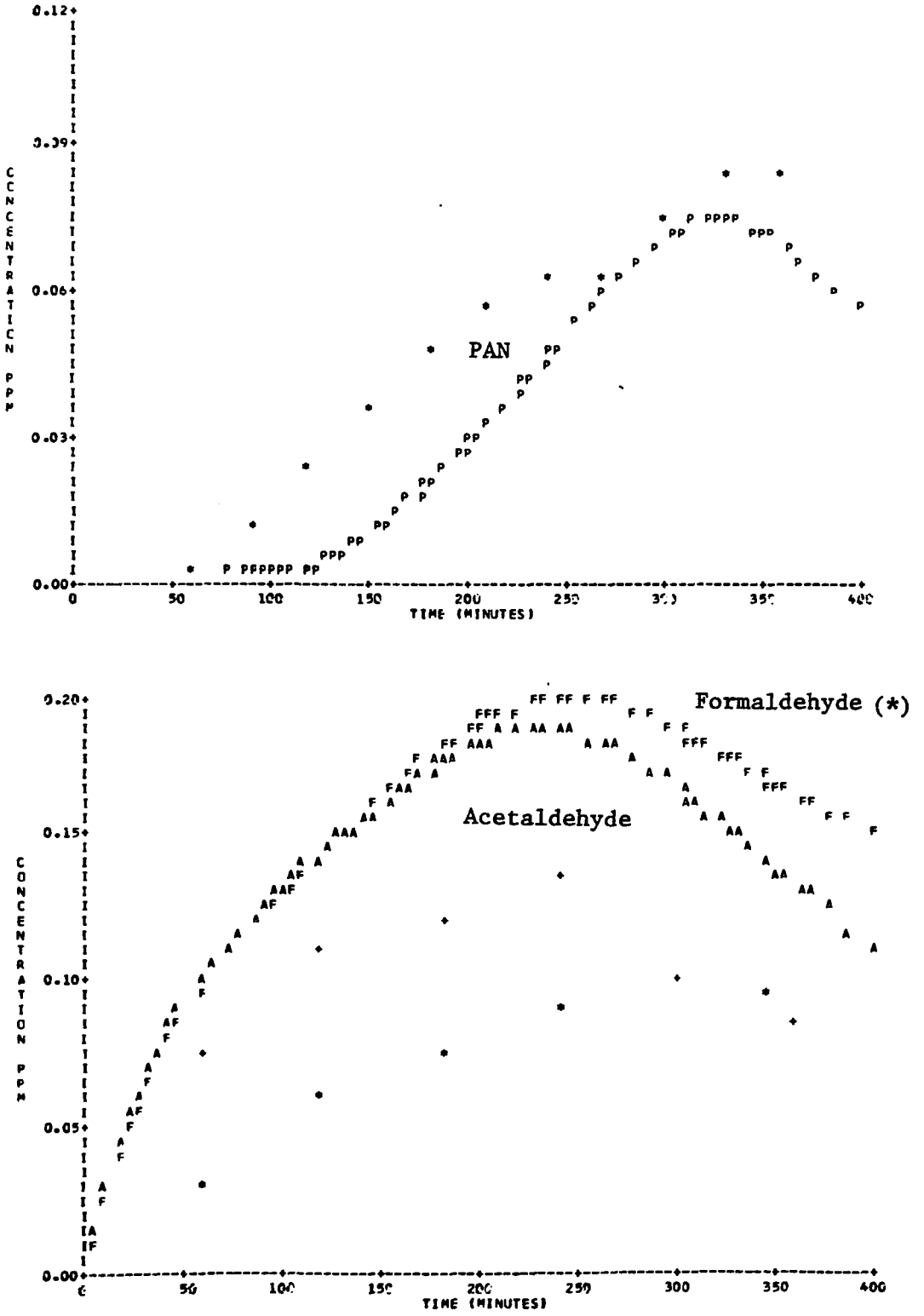

Figure A-10. Simulation of SAPRC EC-53 (Concluded).

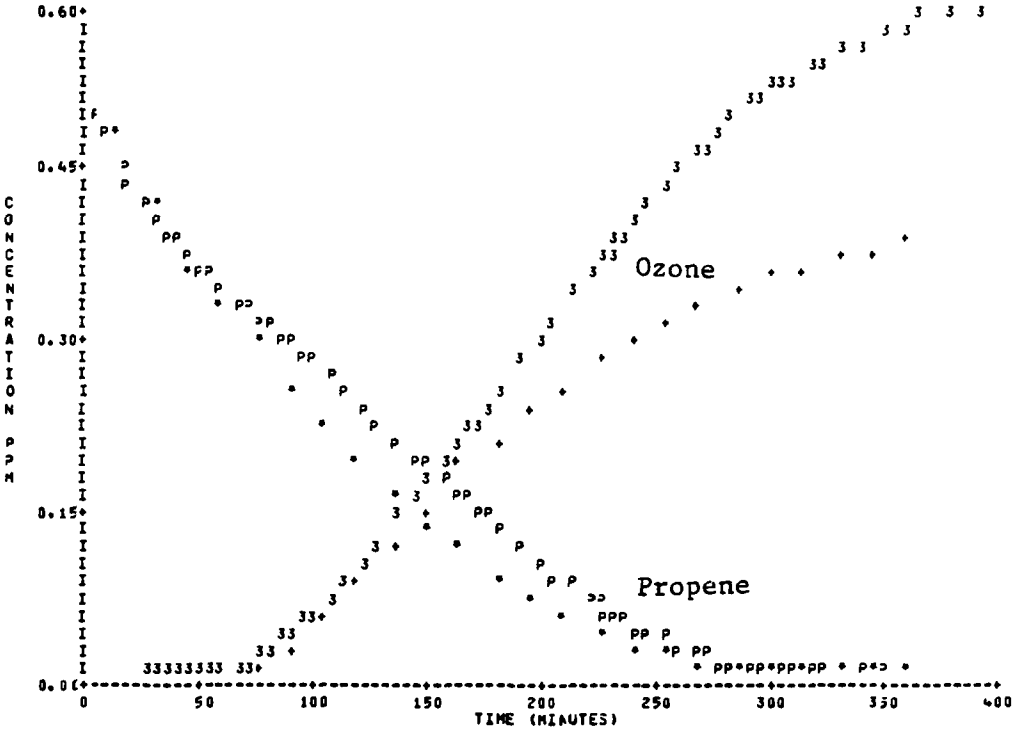

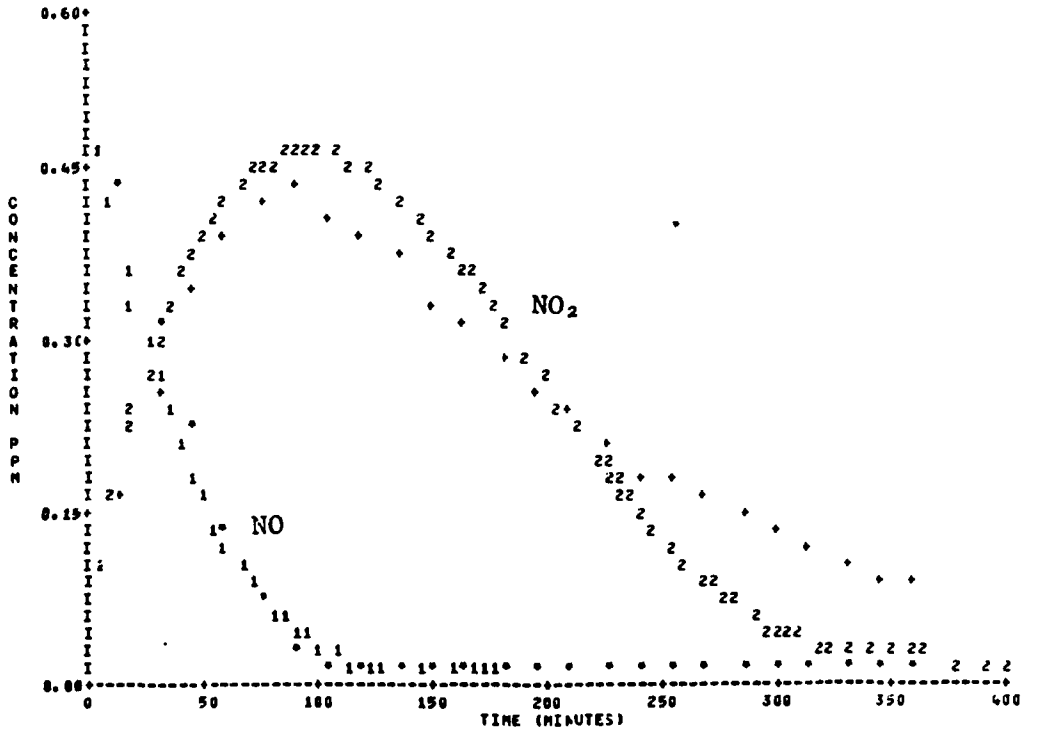

Figure A-10A. Simulation of SAPRC EC-53.
(Radical Addition Rate = 3 x 10^{-4} min^{-1})

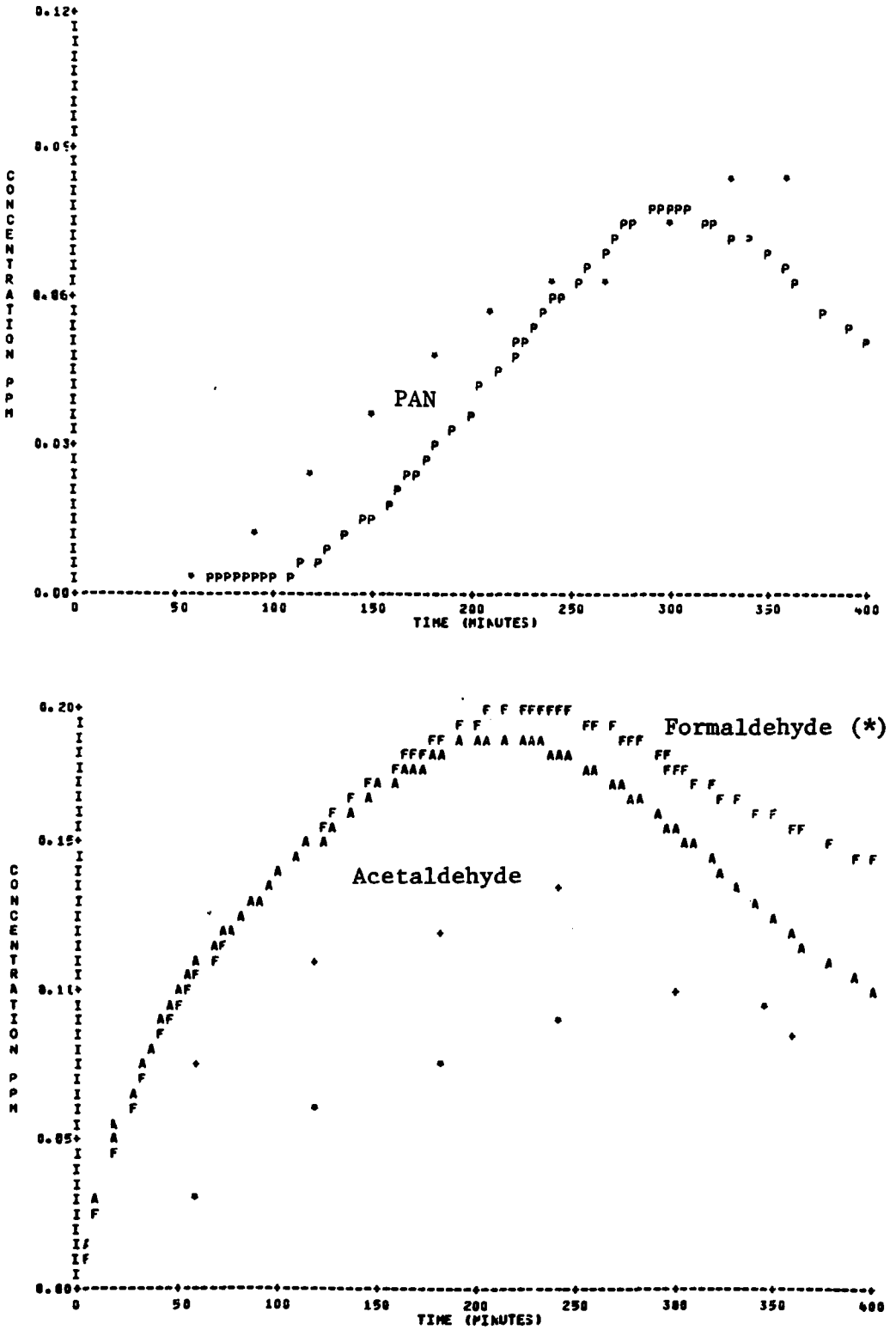

Figure A-10A. Simulation of SAPRC EC-53.
(Radical Addition Rate = 3 x 10^{-4} min^{-1}) (Concluded).

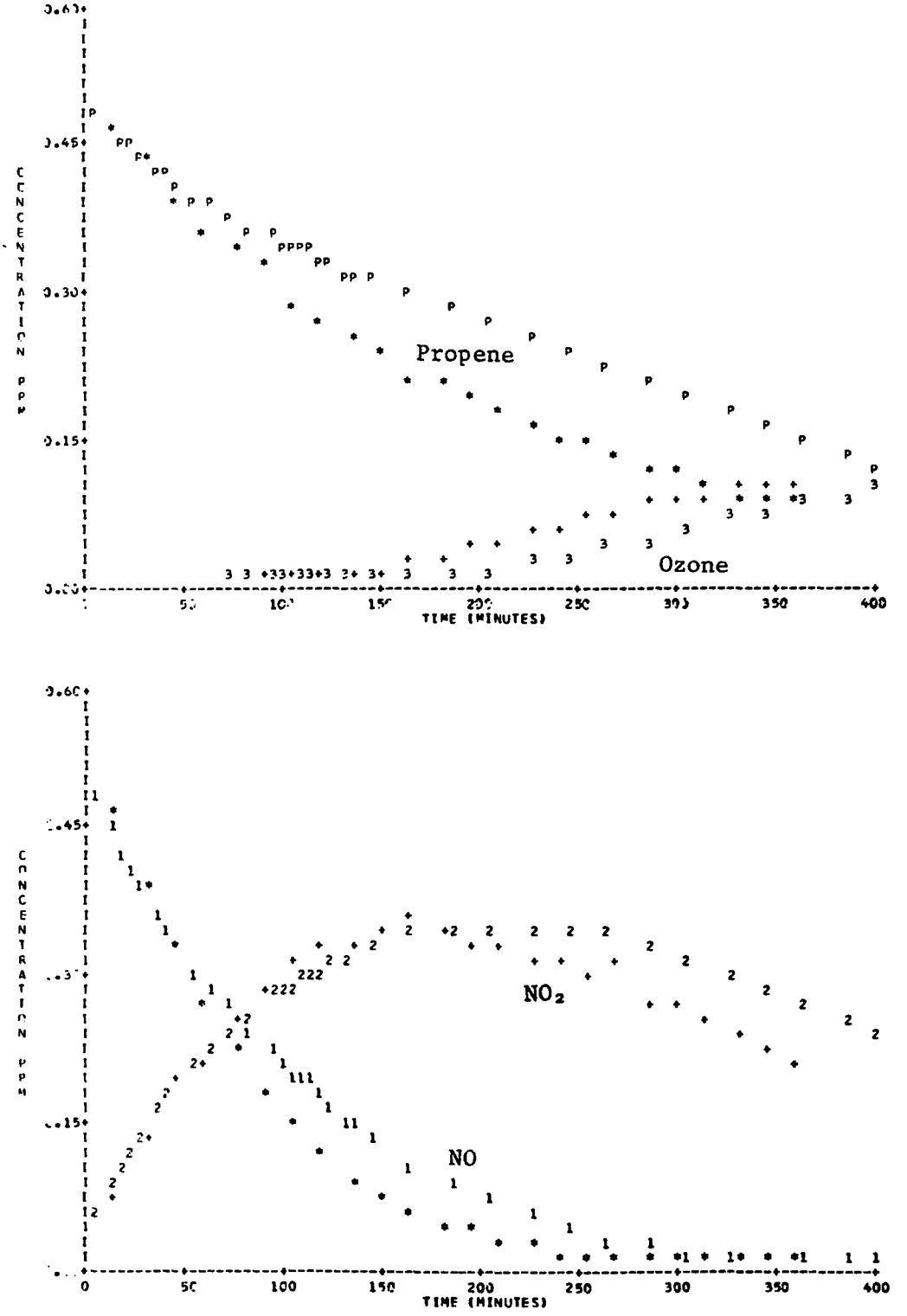

Figure A-11. Simulation of SAPRC EC-54.

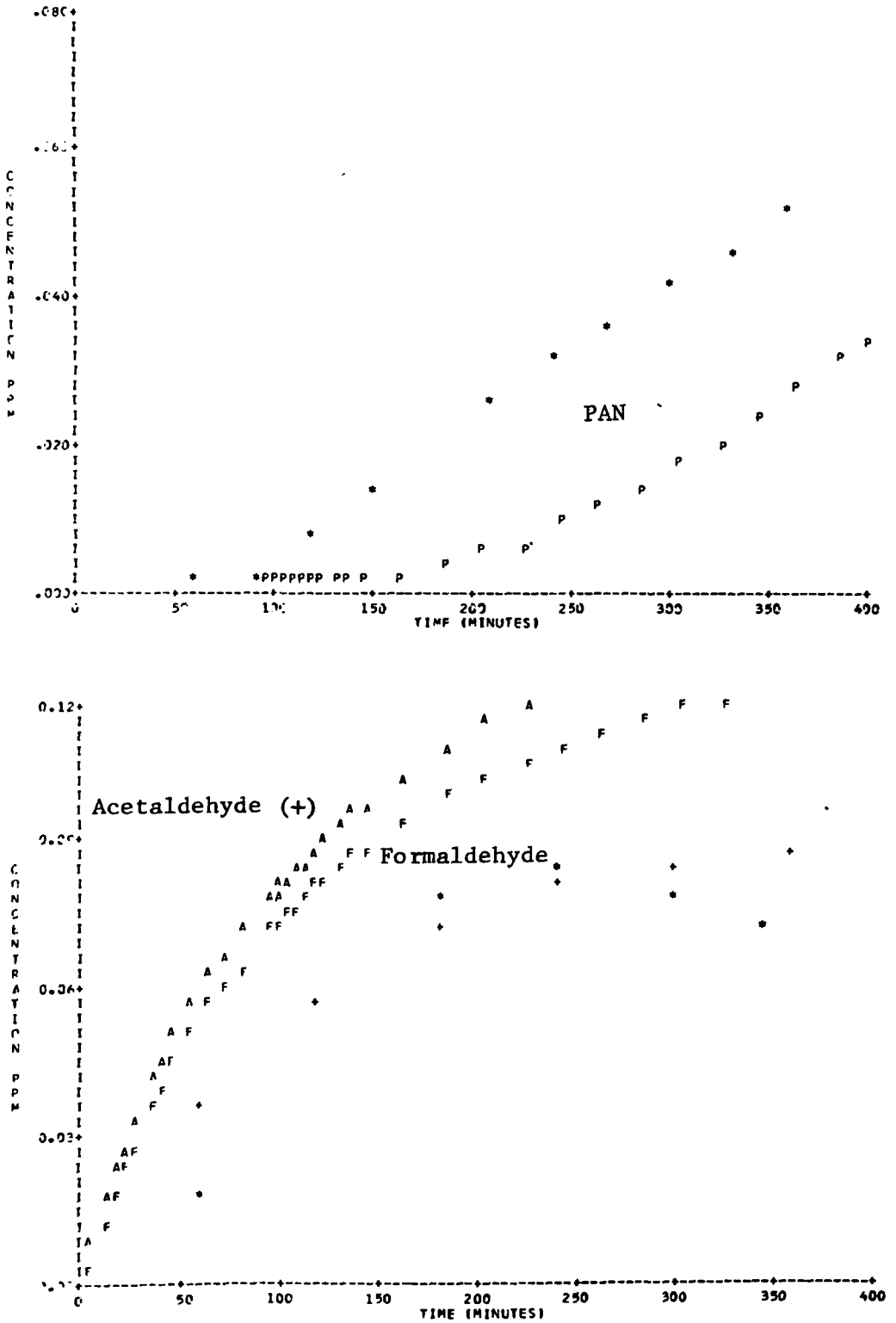

Figure A-11. Simulation of SAPRC ED-54 (Concluded).

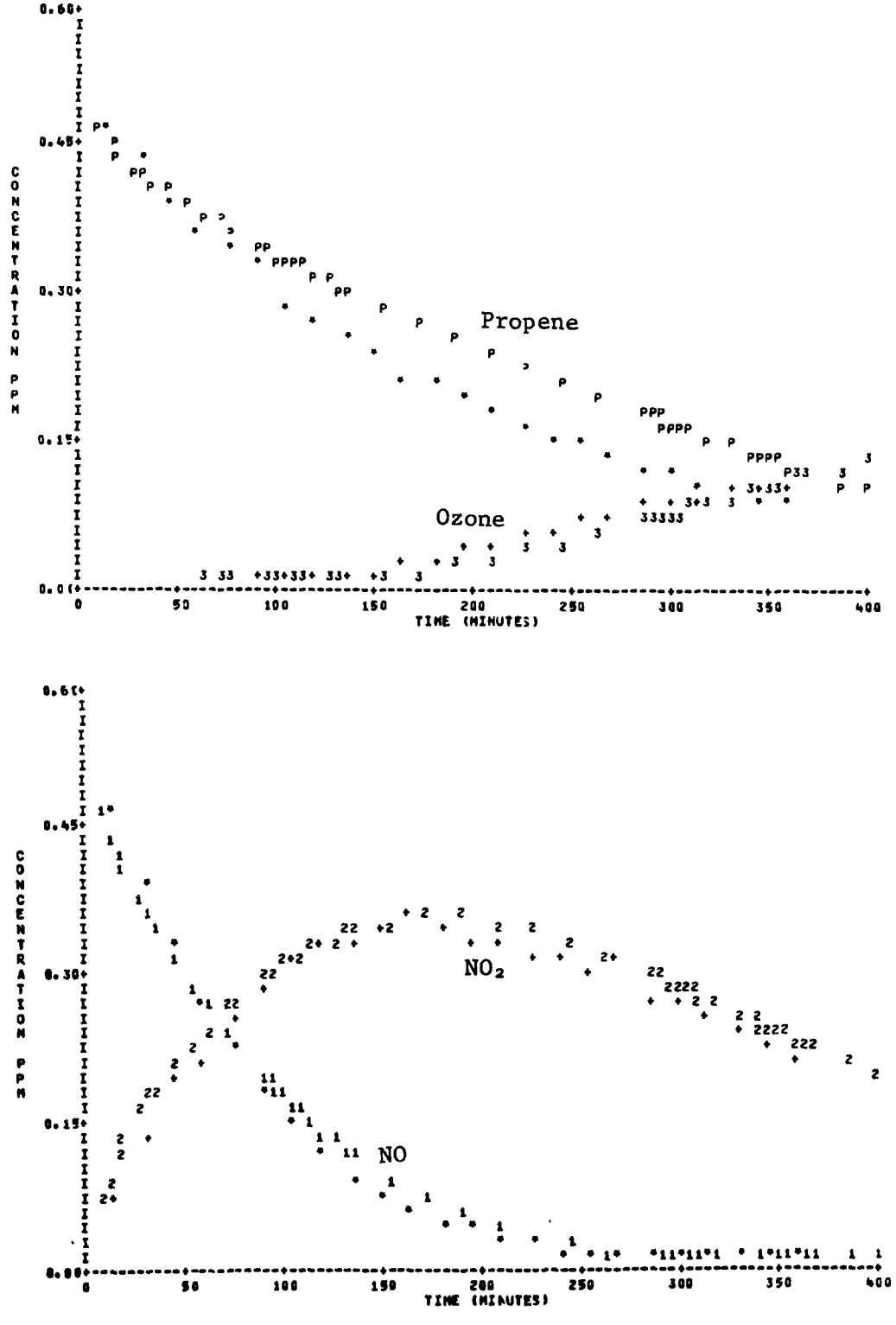

Figure A-11A. Simulation of EC-54.
(Radical Addition Rate = 3 x 10^{-4} min^{-1})

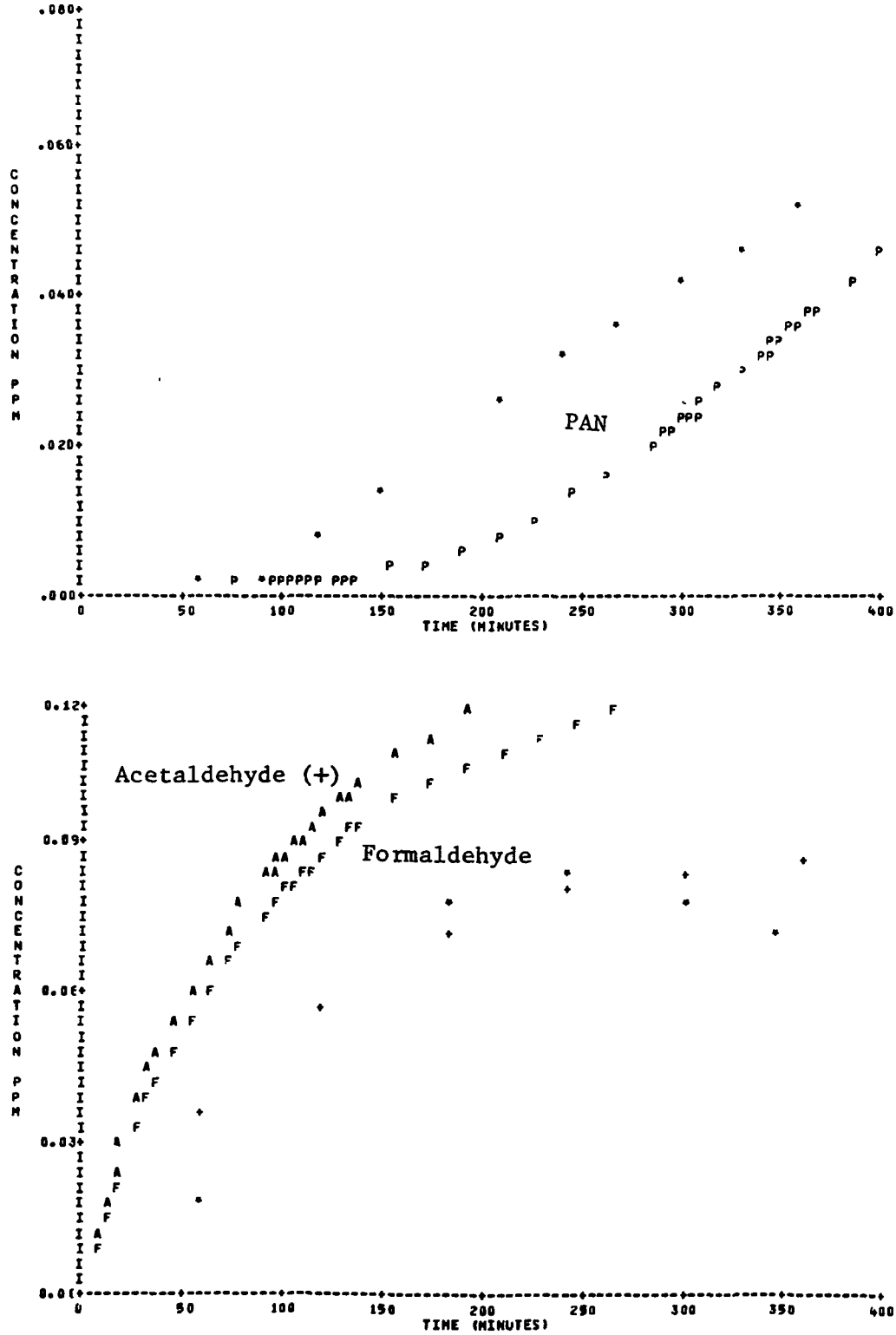

Figure A-11A. Simulation of SAPRC EC-54.
(Radical Addition Rate = 3 x 10^{-4} min^{-1}) (Concluded).

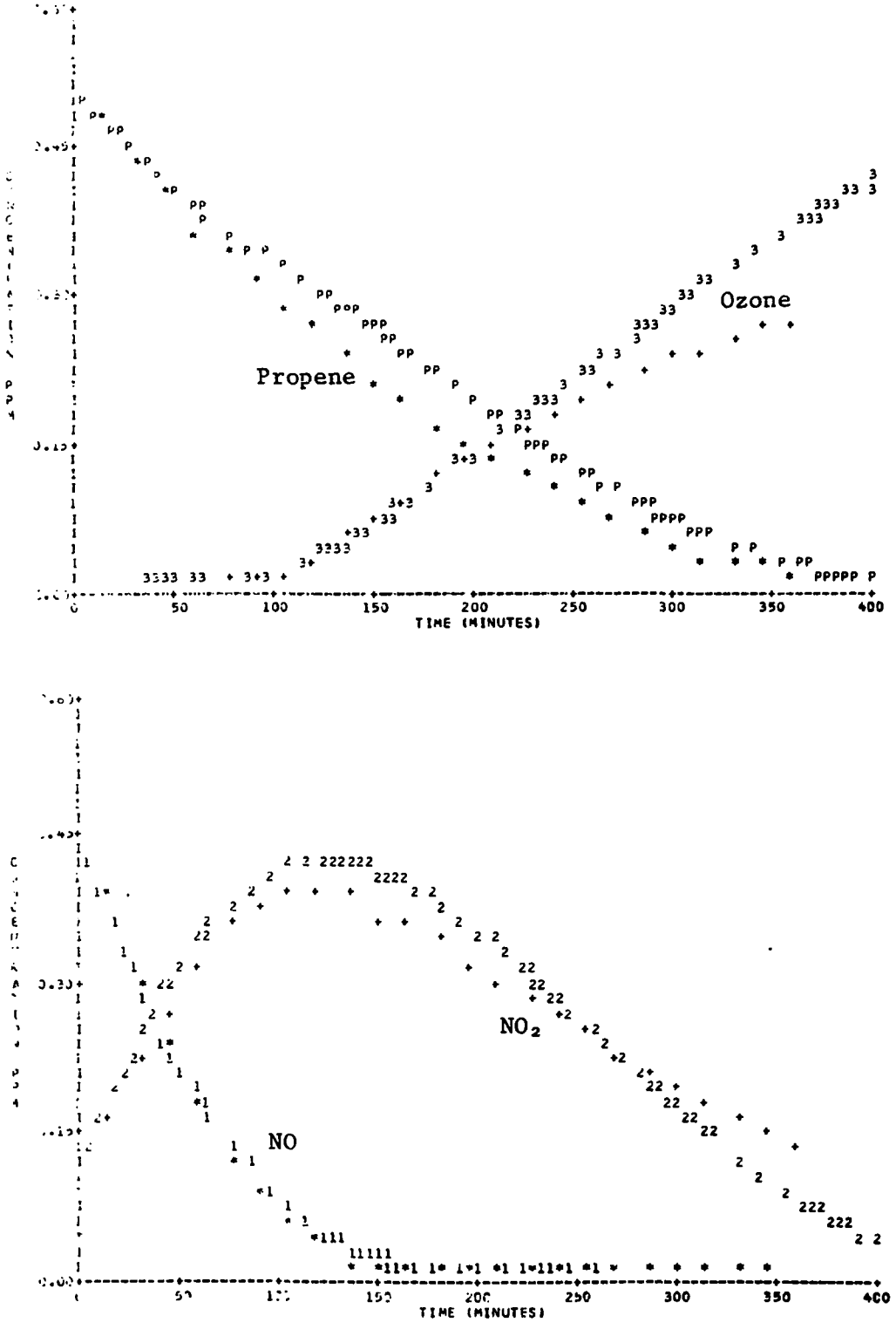

Figure A-12. Simulation of SAPRC EC-55.

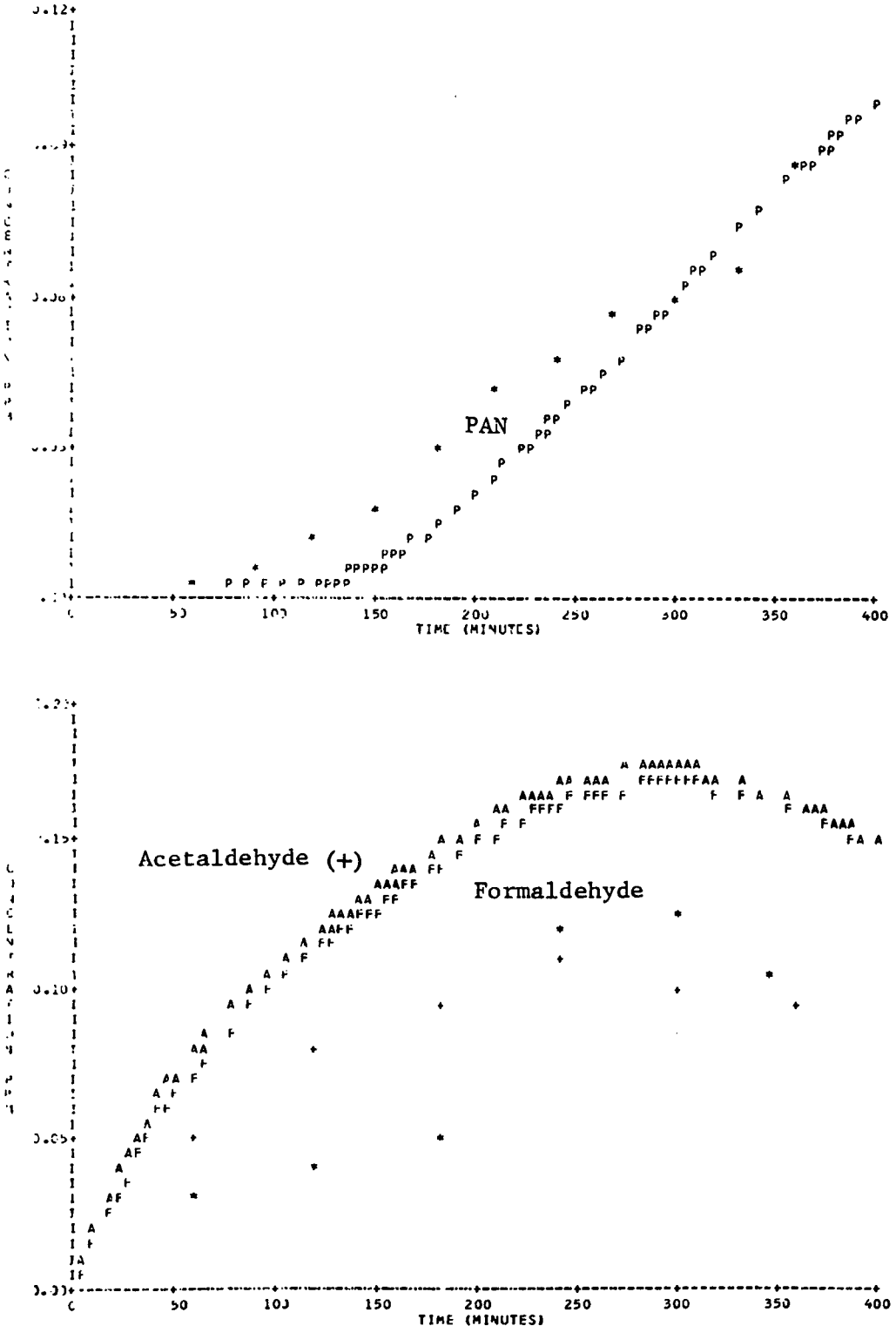

Figure A-12. Simulation of SAPRC EC-55 (Concluded).

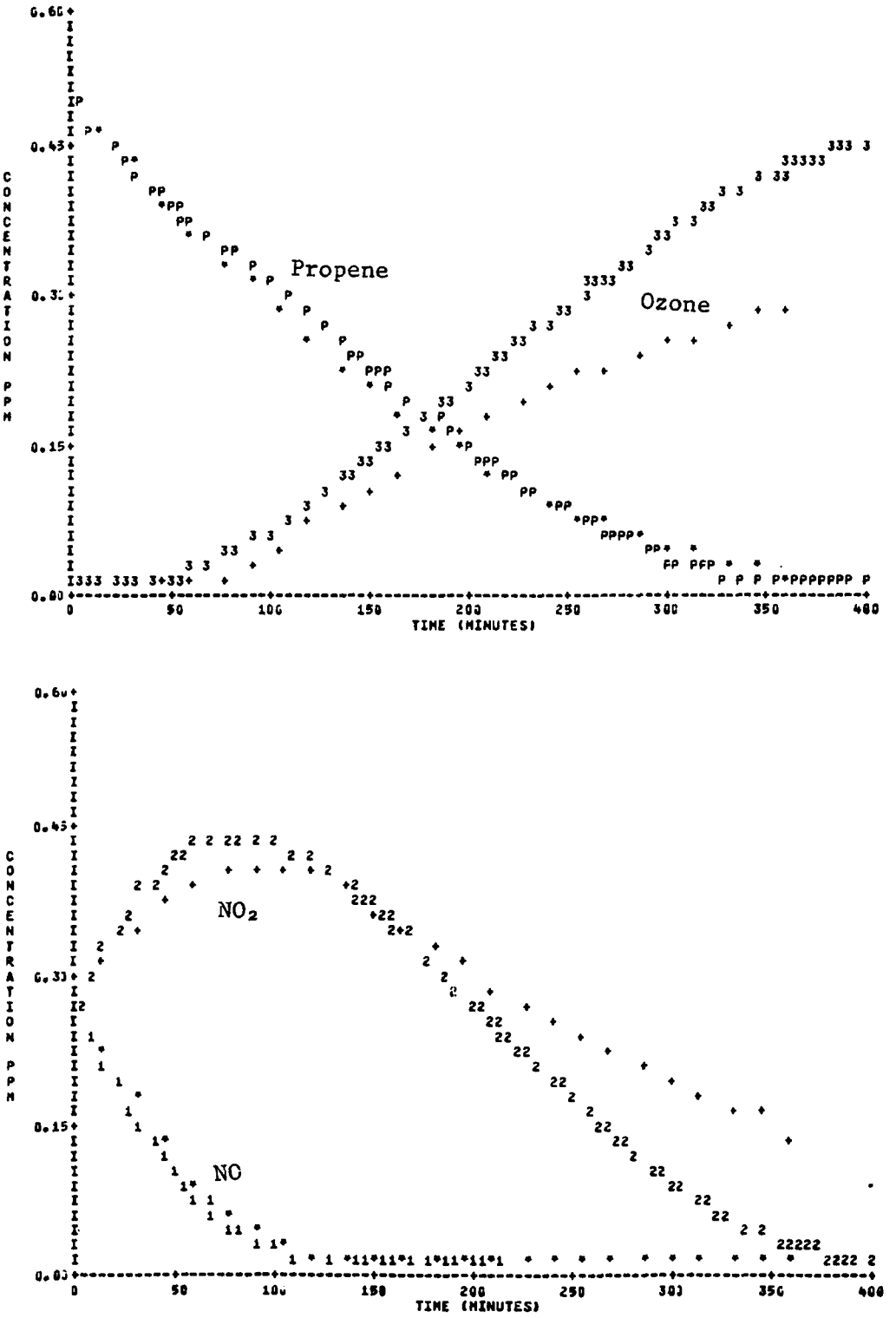

Figure A-13. Simulation of SAPRC EC-56.

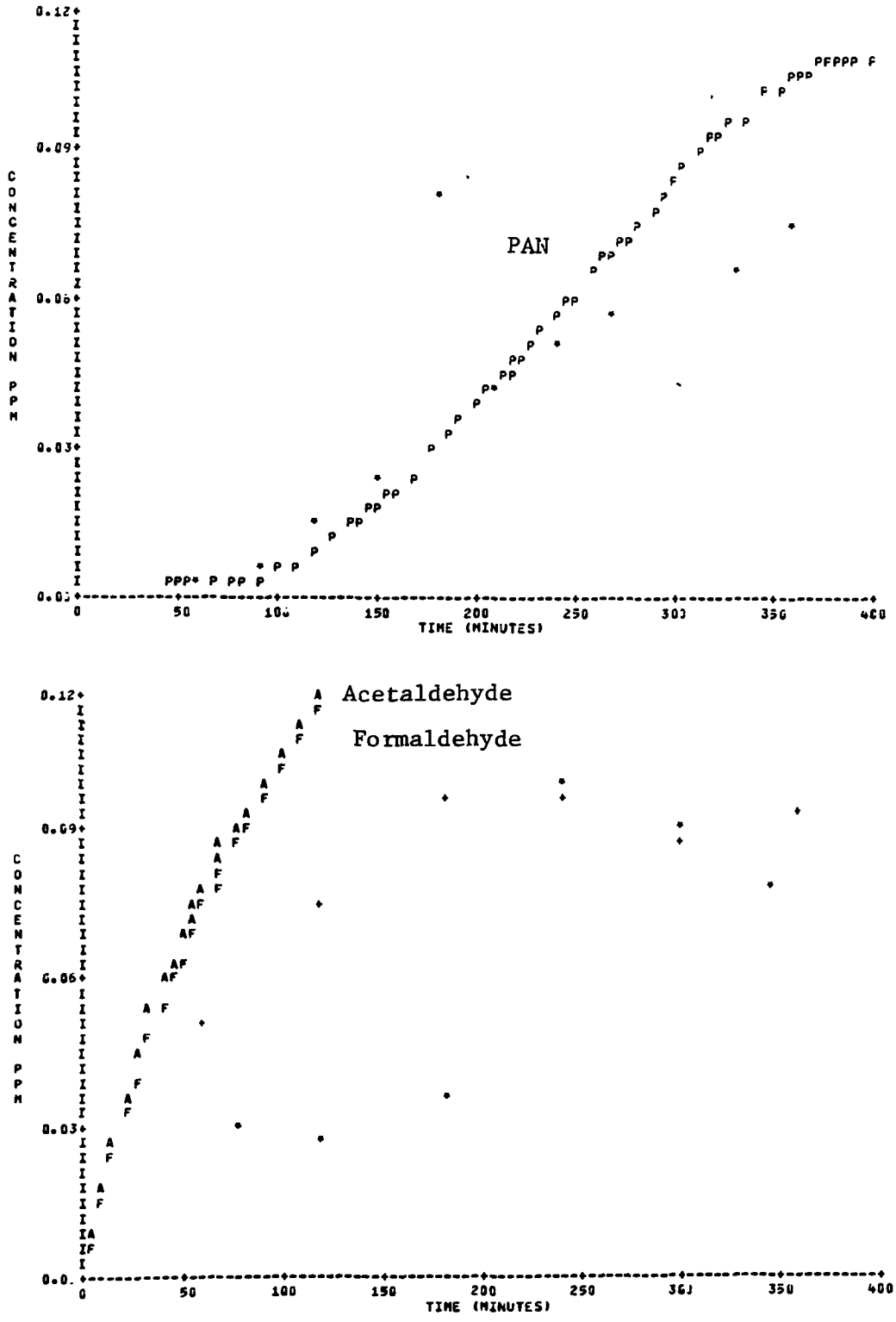

Figure A-13. Simulation of SAPRC EC-56 (Concluded).

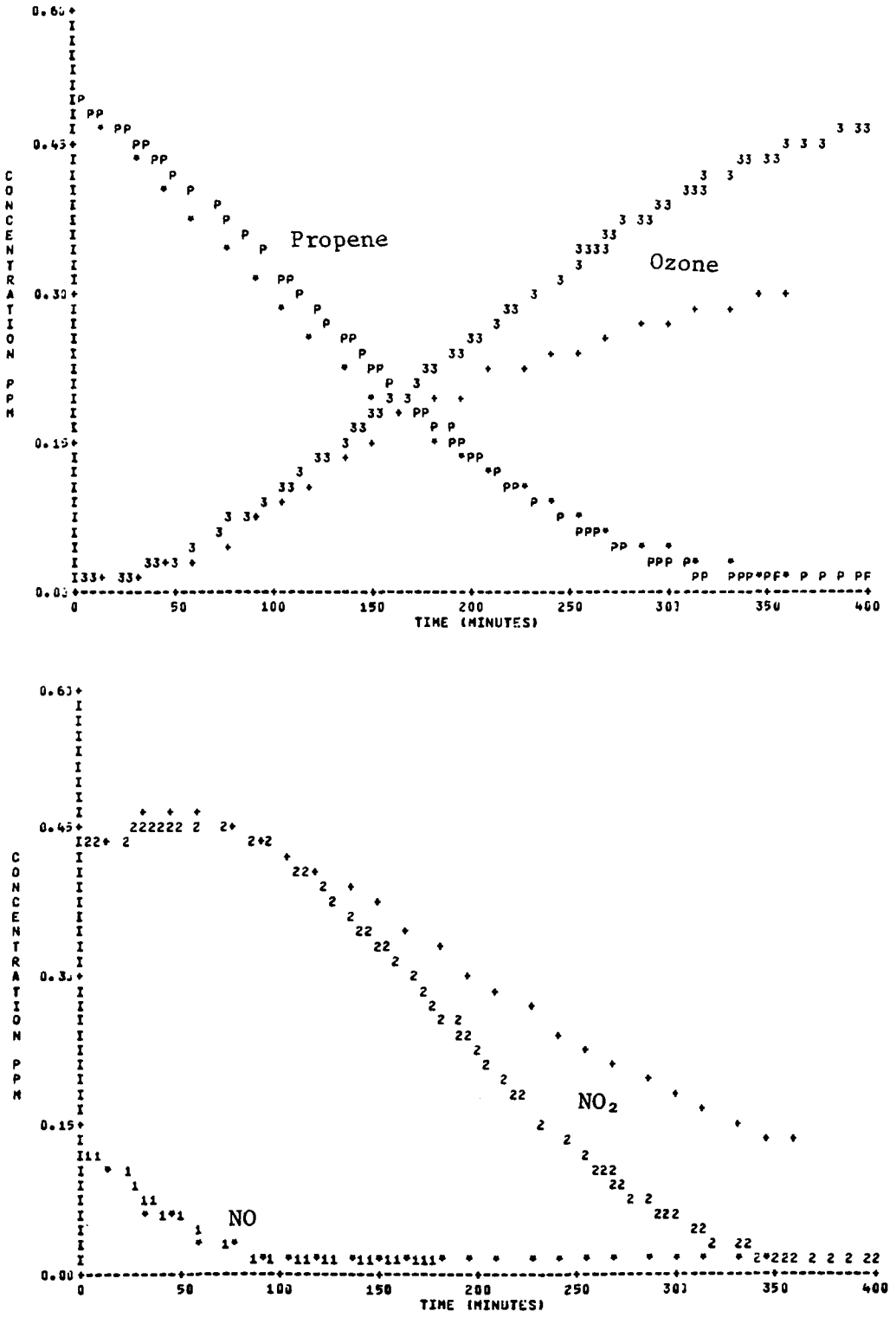

Figure A-14. Simulation of SAPRC EC-59.

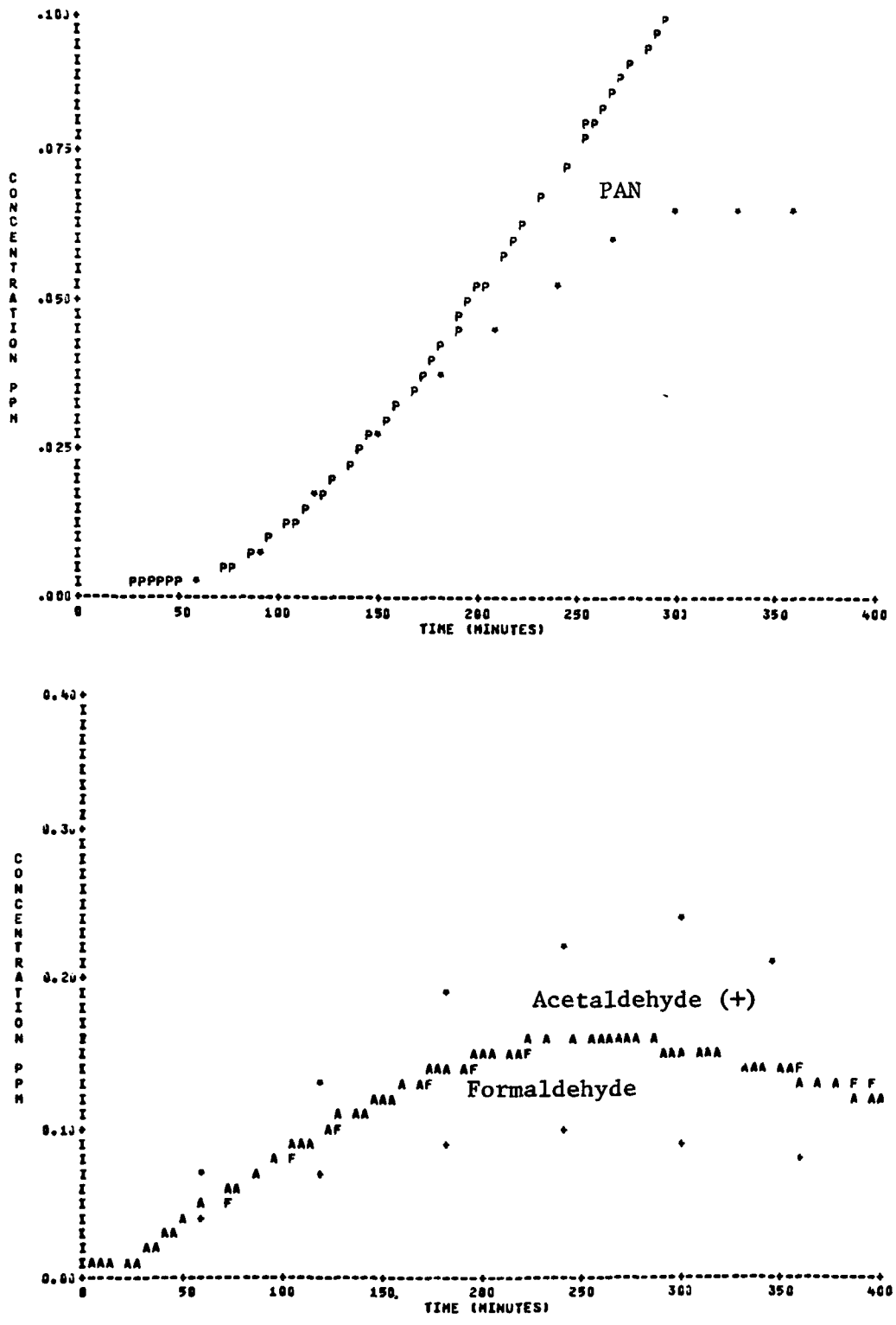

Figure A-14. Simulation of SAPRC EC-59 (Concluded).

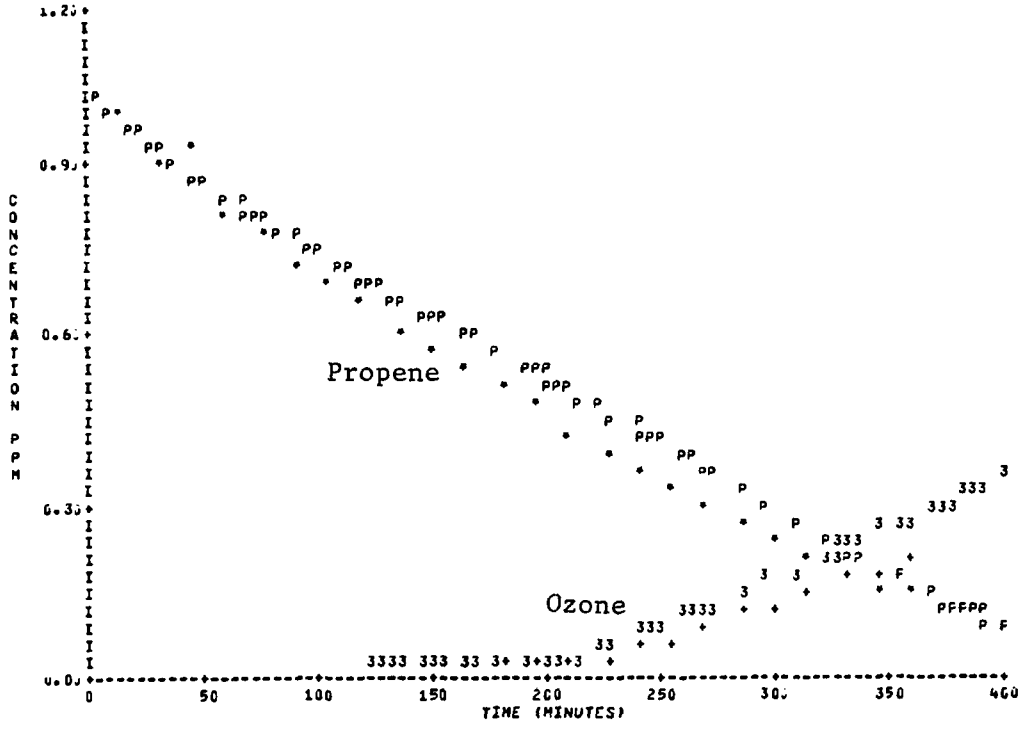

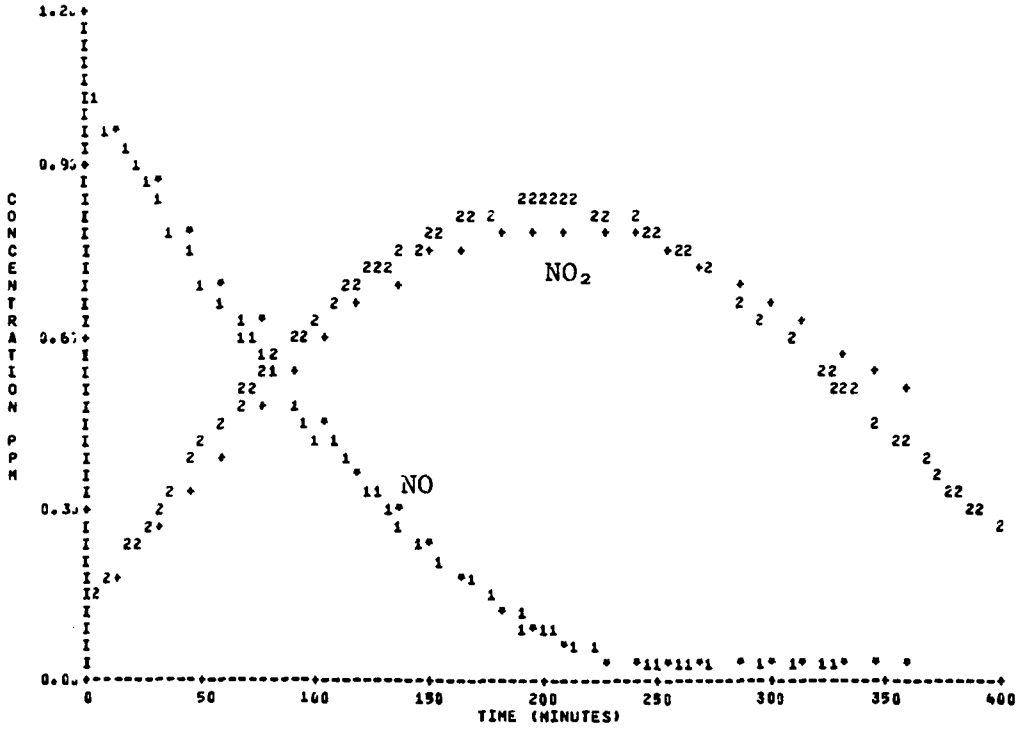

Figure A-15. Simulation of SAPRC EC-60.

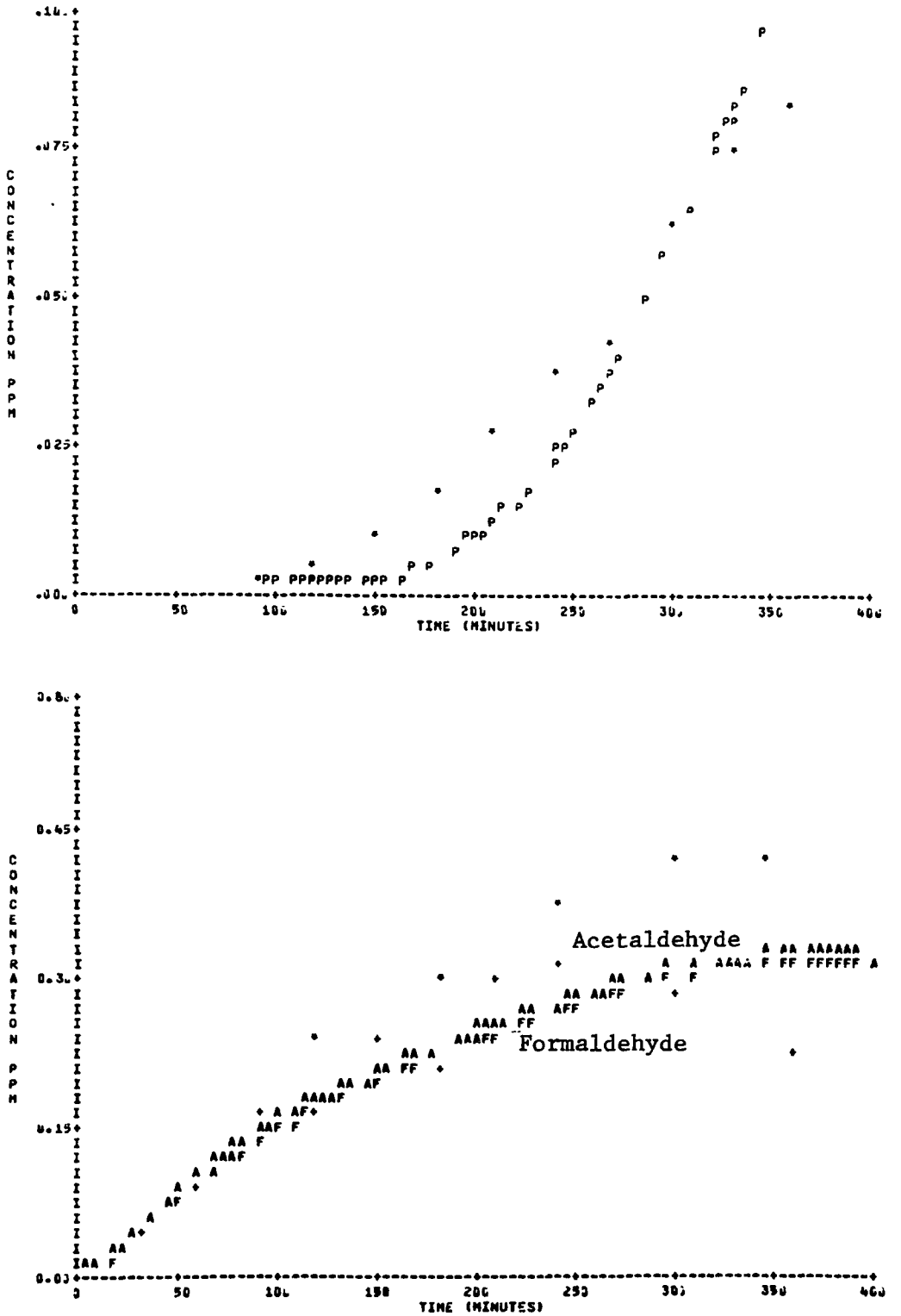

Figure A-15. Simulation of SAPRC EC-60 (Concluded).

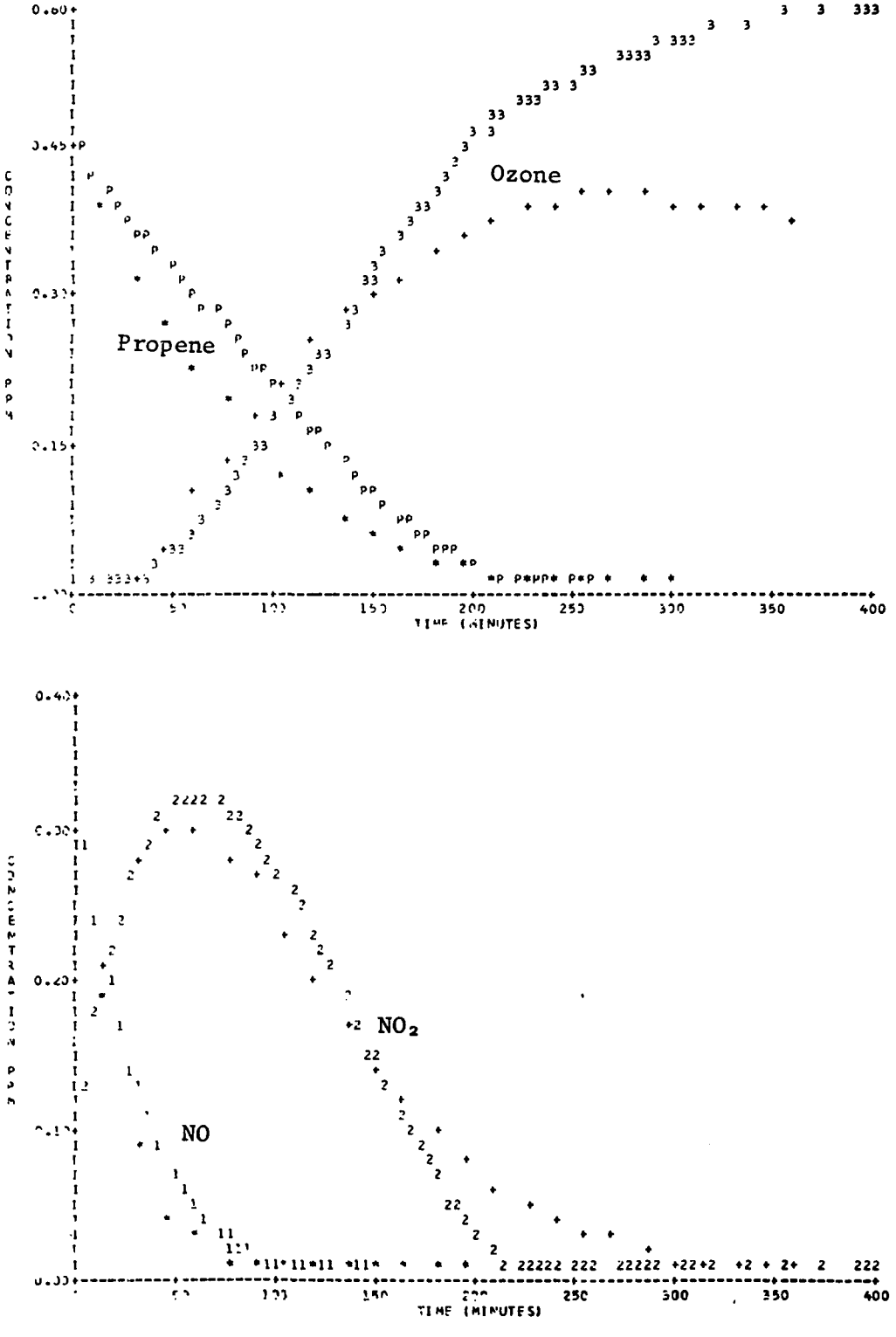

Figure A-16. Simulation of SAPRC EC-95.

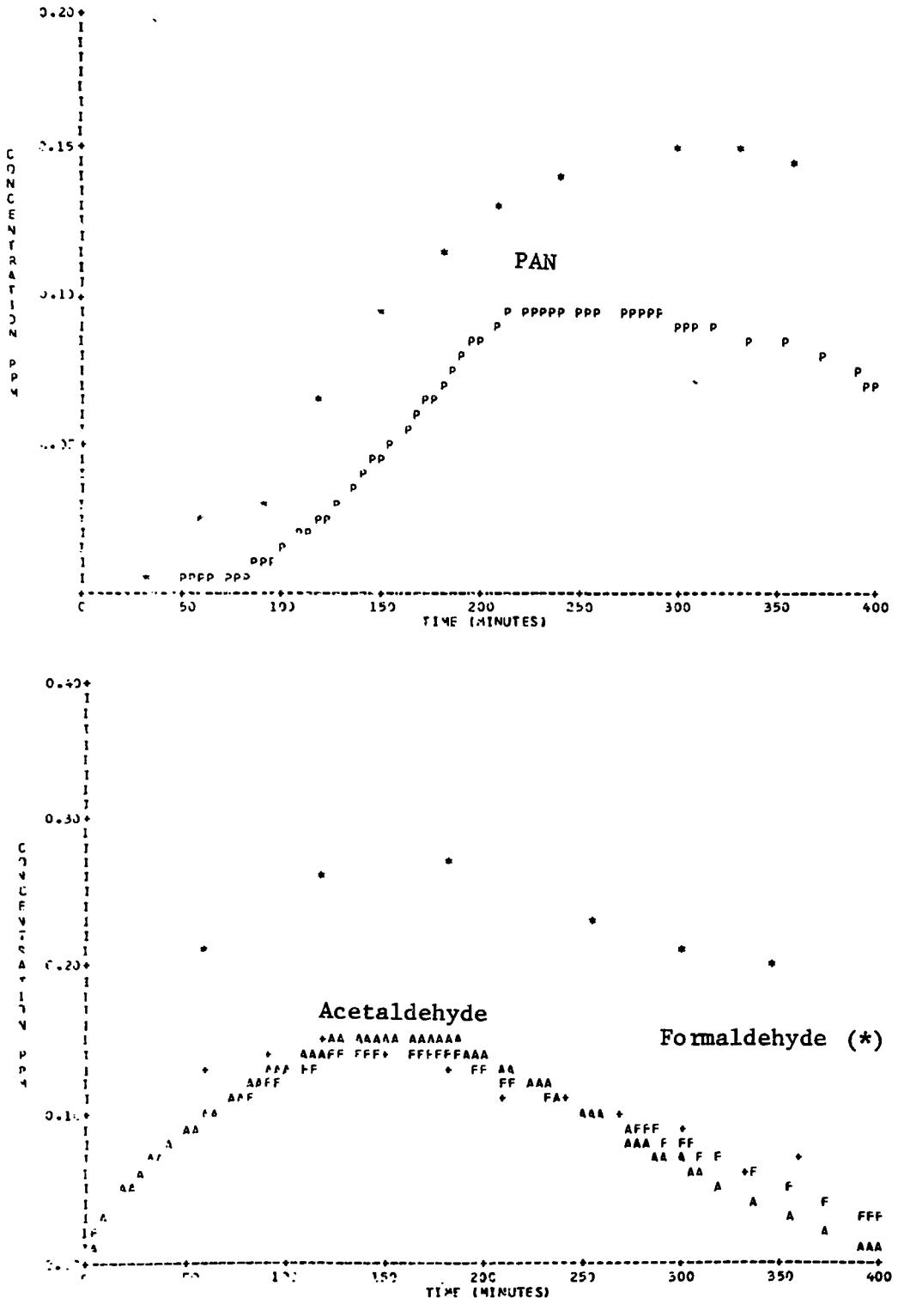

Figure A-16. Simulation of SAPRC EC-95 (Concluded).

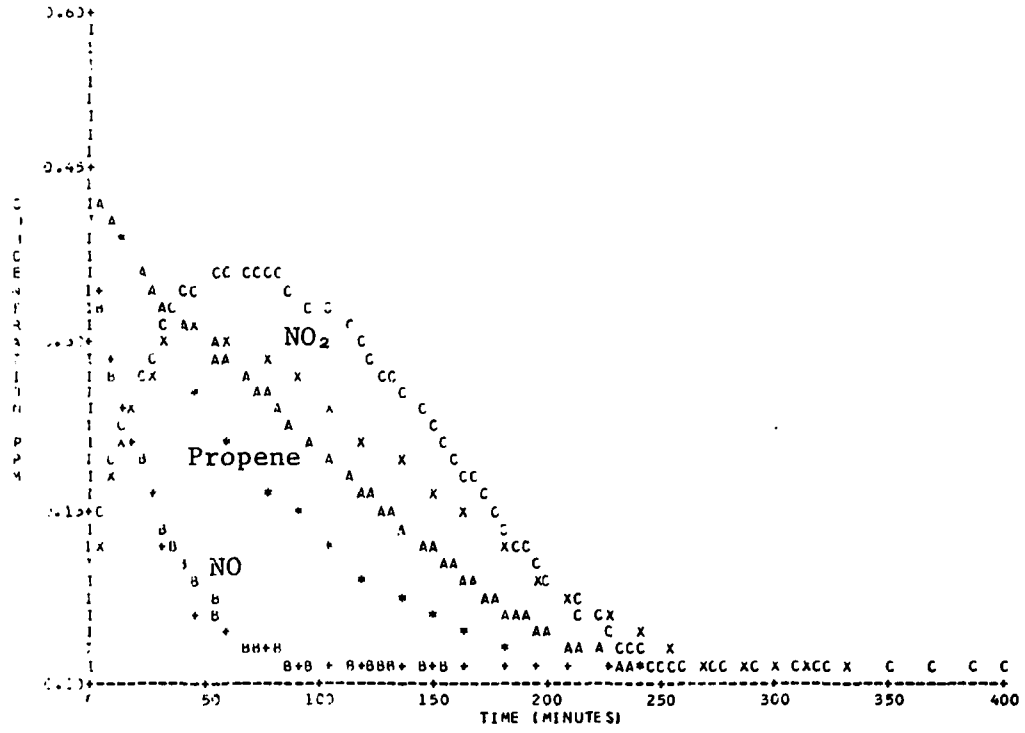

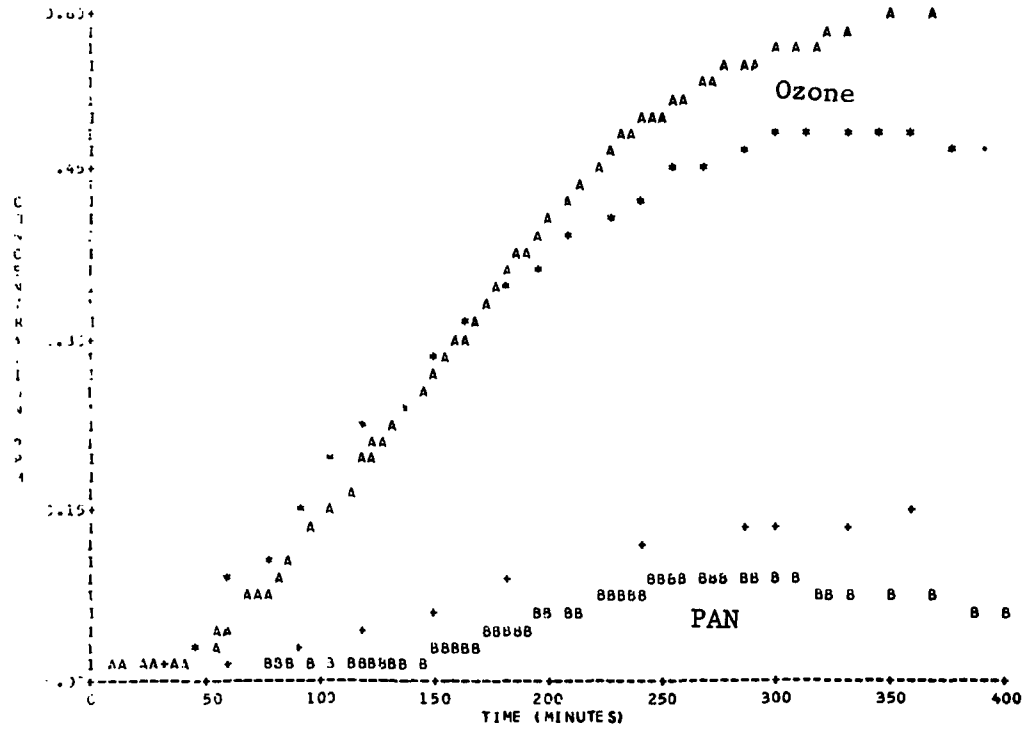

Figure A-17. Simulation of SAPRC EC-121.

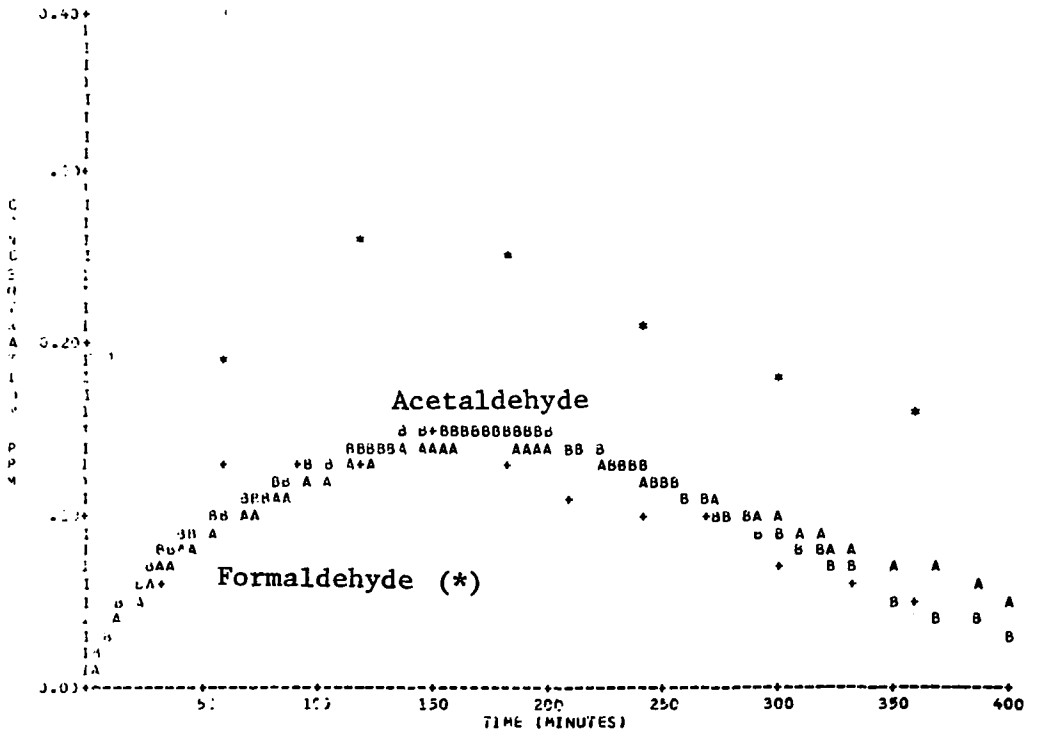

Figure A-17. Simulation of SAPRC EC-121 (Concluded).

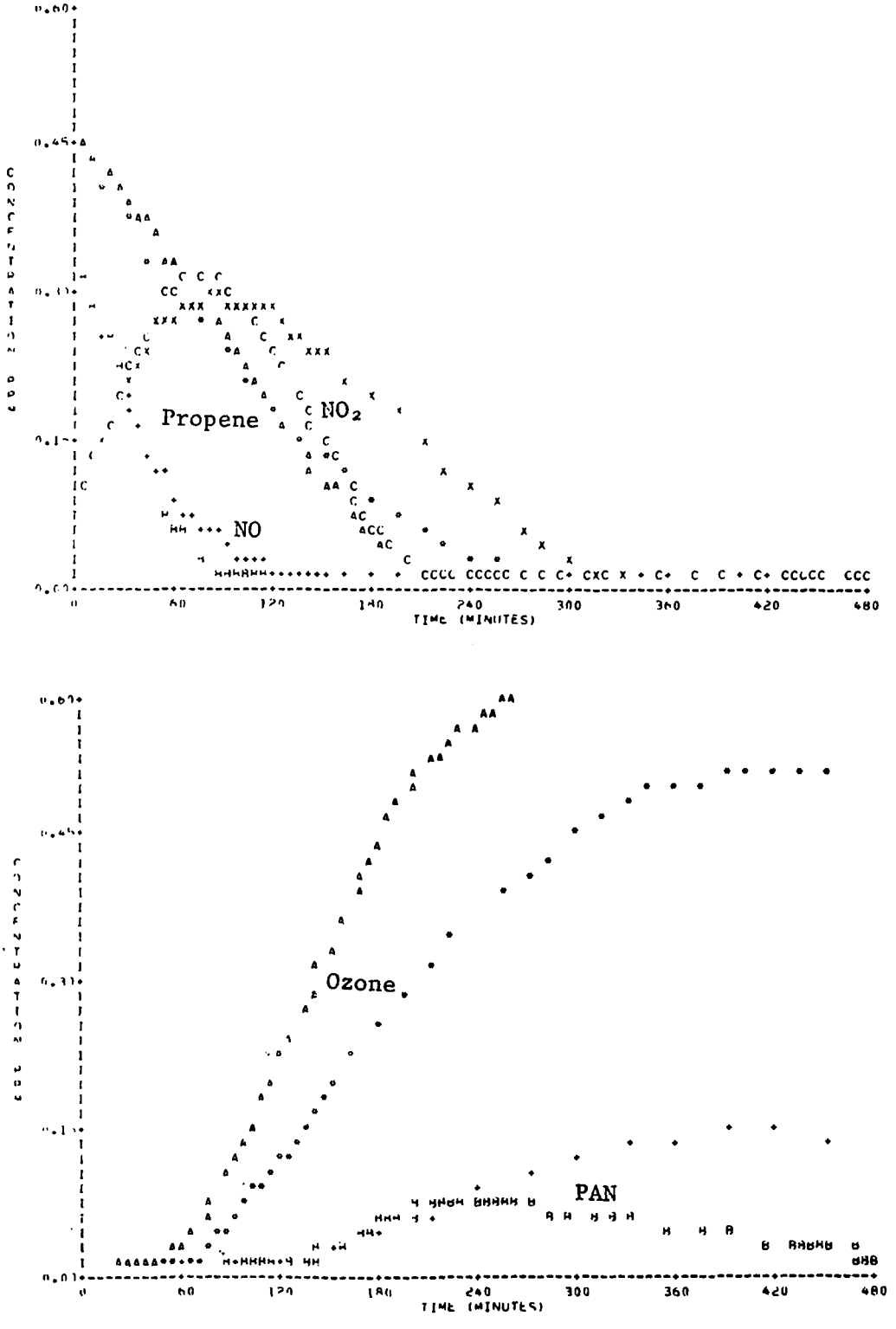

Figure A-18. Simulation of SAPRC EC-177.

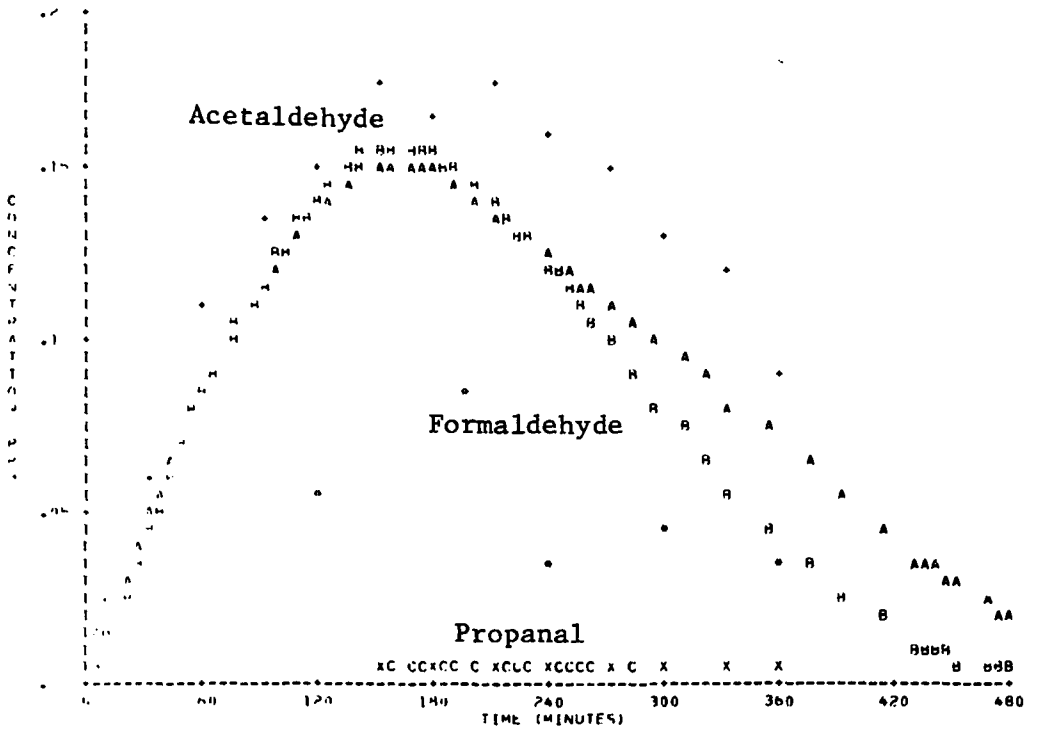

Figure A-18. Simulation of SAPRC EC-177 (Concluded).

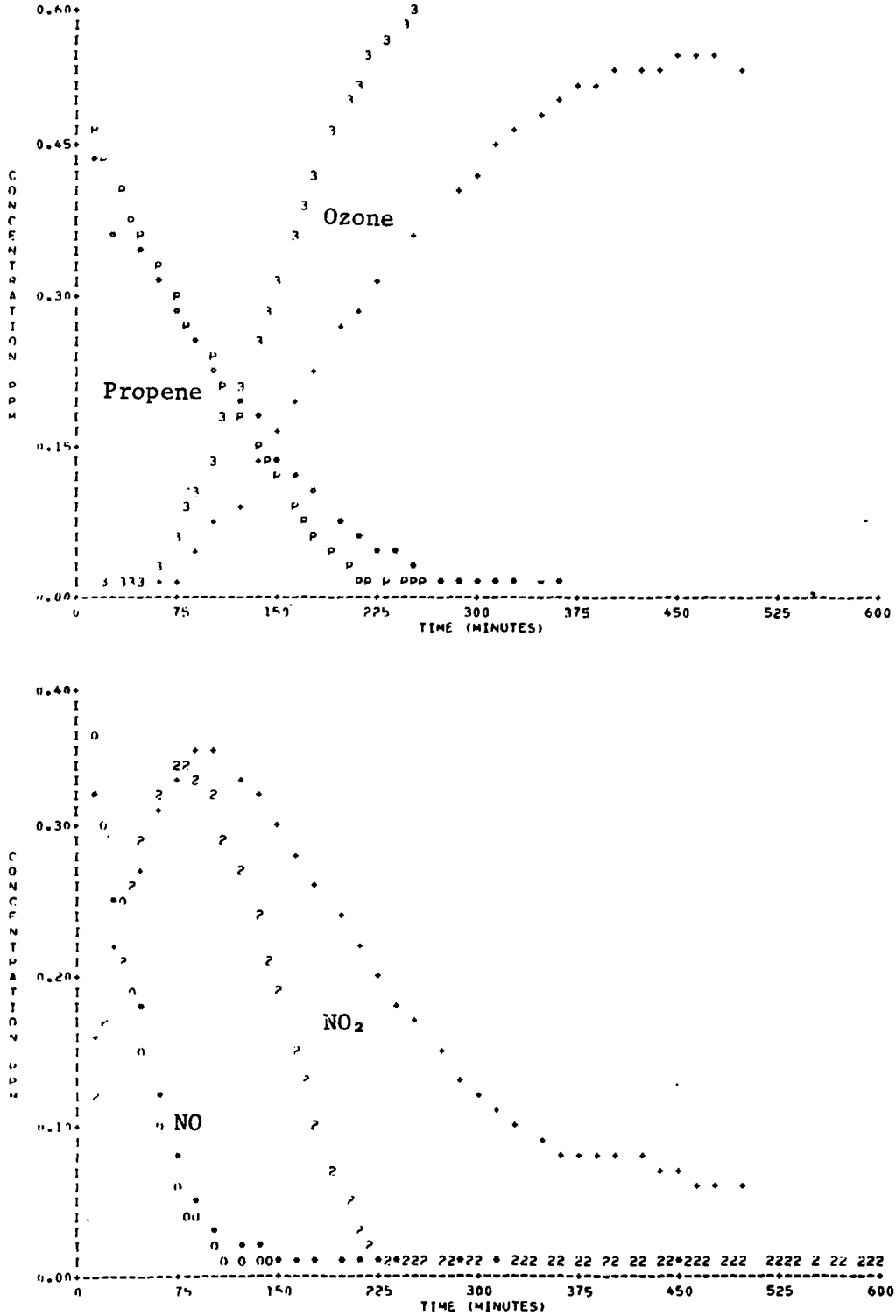

Figure A-19. Simulation of SAPRC EC-216.

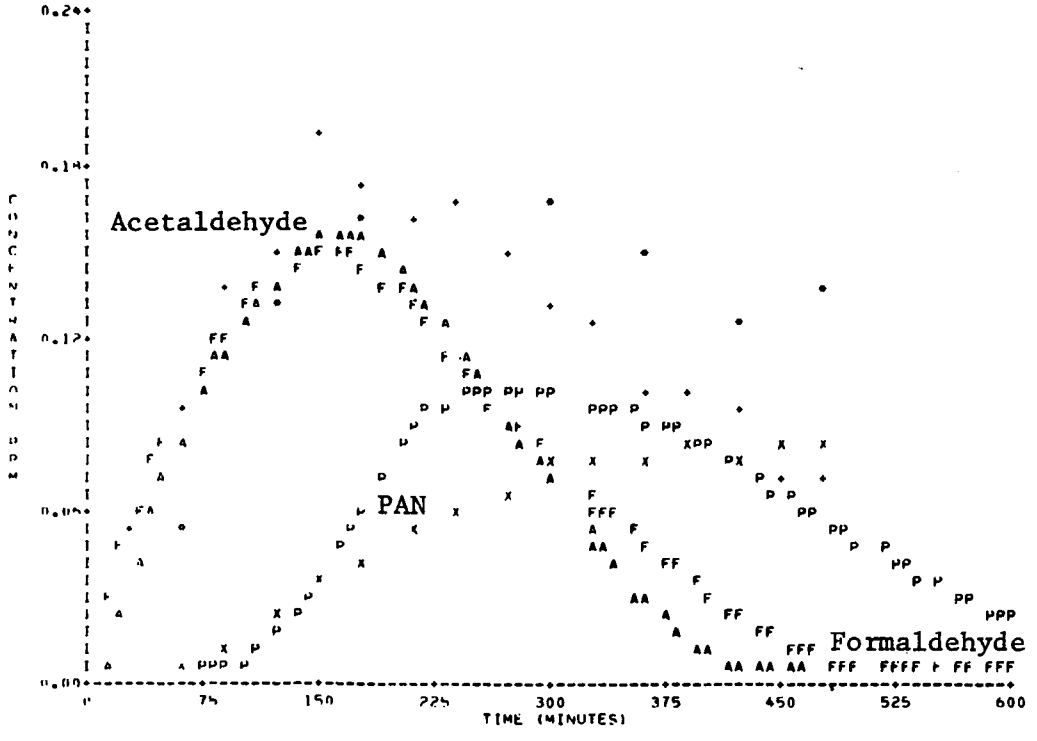

Figure A-19. Simulation of SAPRC EC-216 (Concluded).

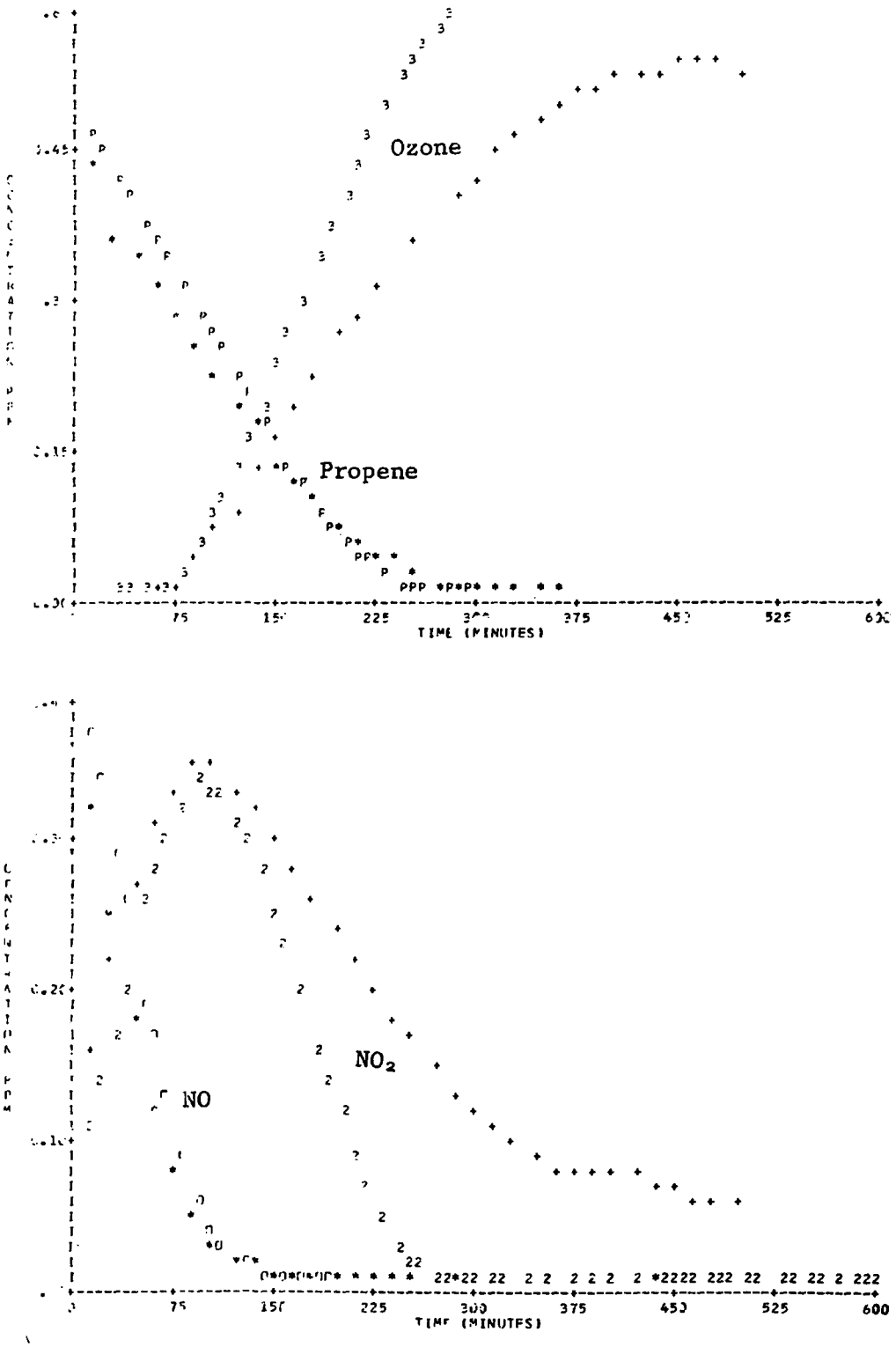

Figure A-19A. Simulation of SAPRC EC-216
(Radical Addition Rate = zero)

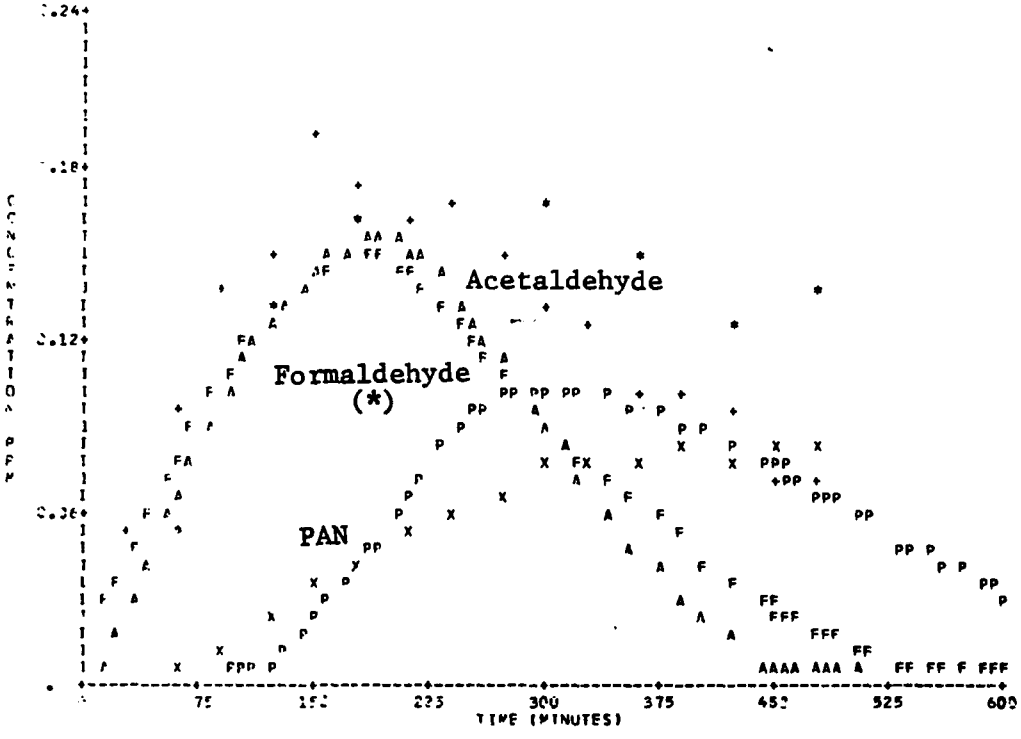

FigureA-19. Simulation of SAPRC EC-216.
(Radical Addition Rate = zero) (Concluded).

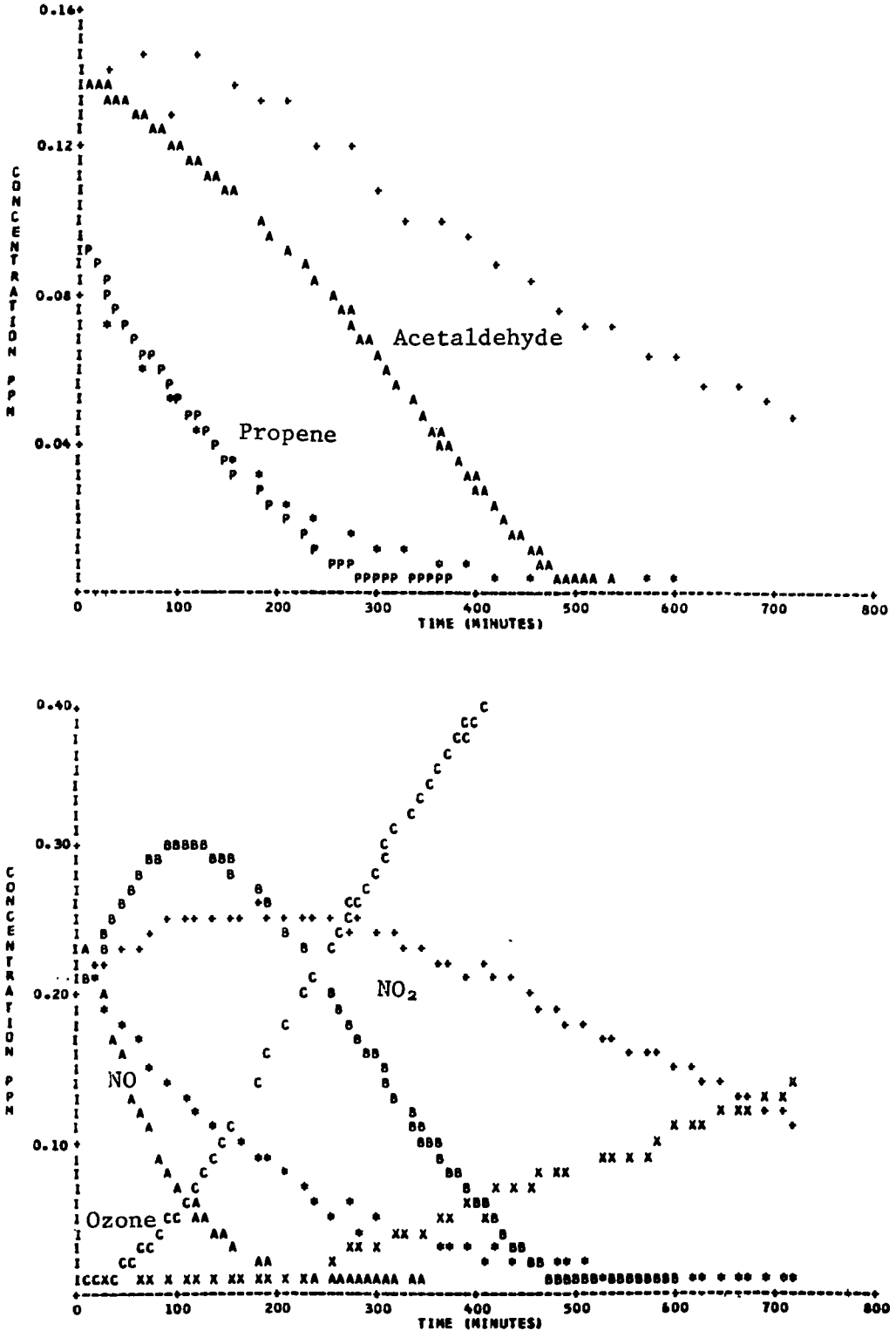

Figure A-20. Simulation of SAPRC EC-217.

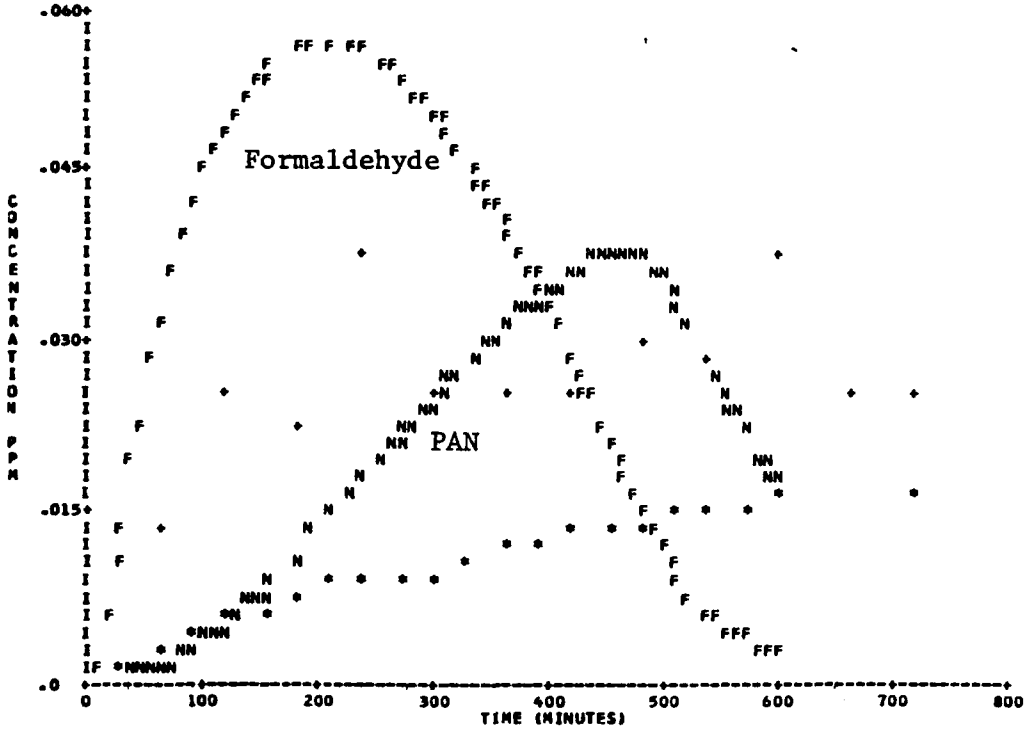

Figure A-20. Simulation of SAPRC EC-217 (Concluded).

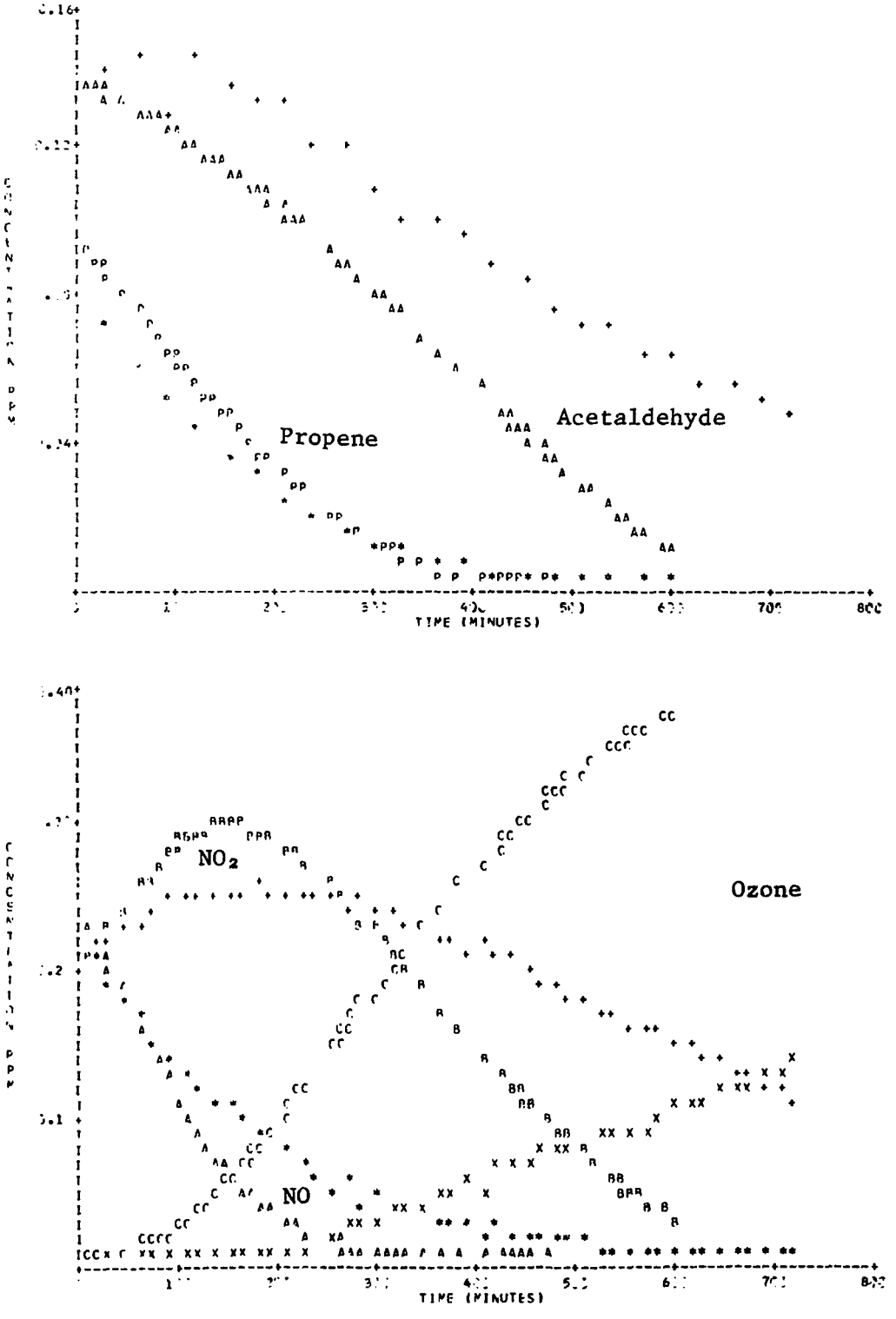

Figure A-20A. Simulation of SAPRC EC-217.
(Radical Addition Rate = zero)

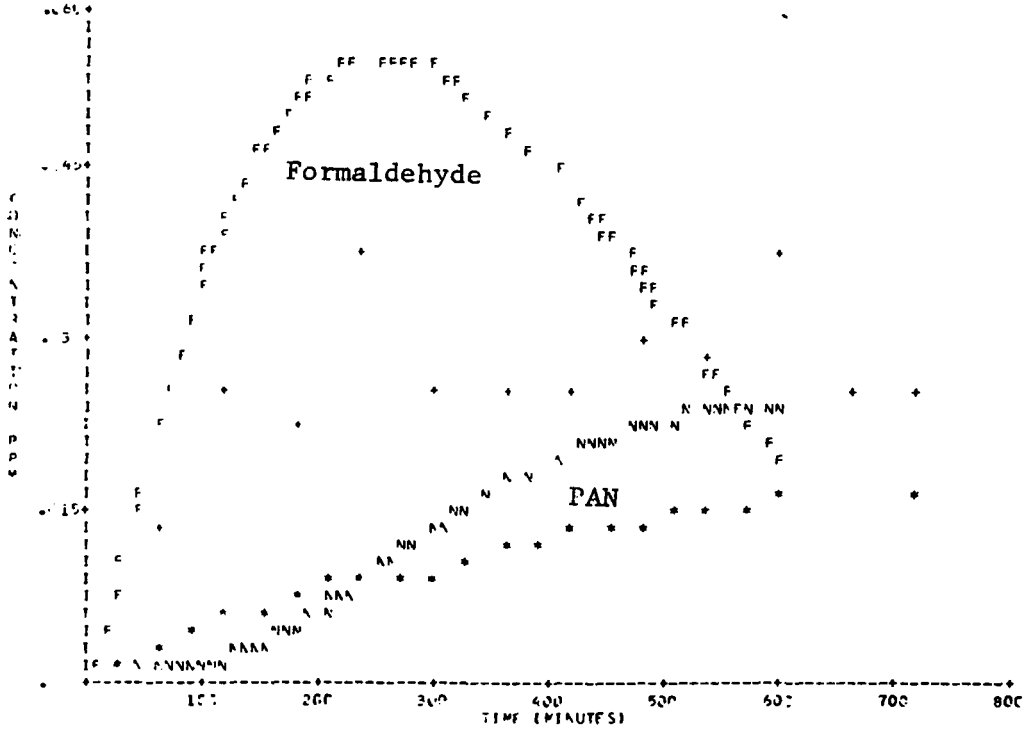

Figure A-20A. Simulation of SAPRC EC-217. (Radical Addition Rate = zero) (Concluded).

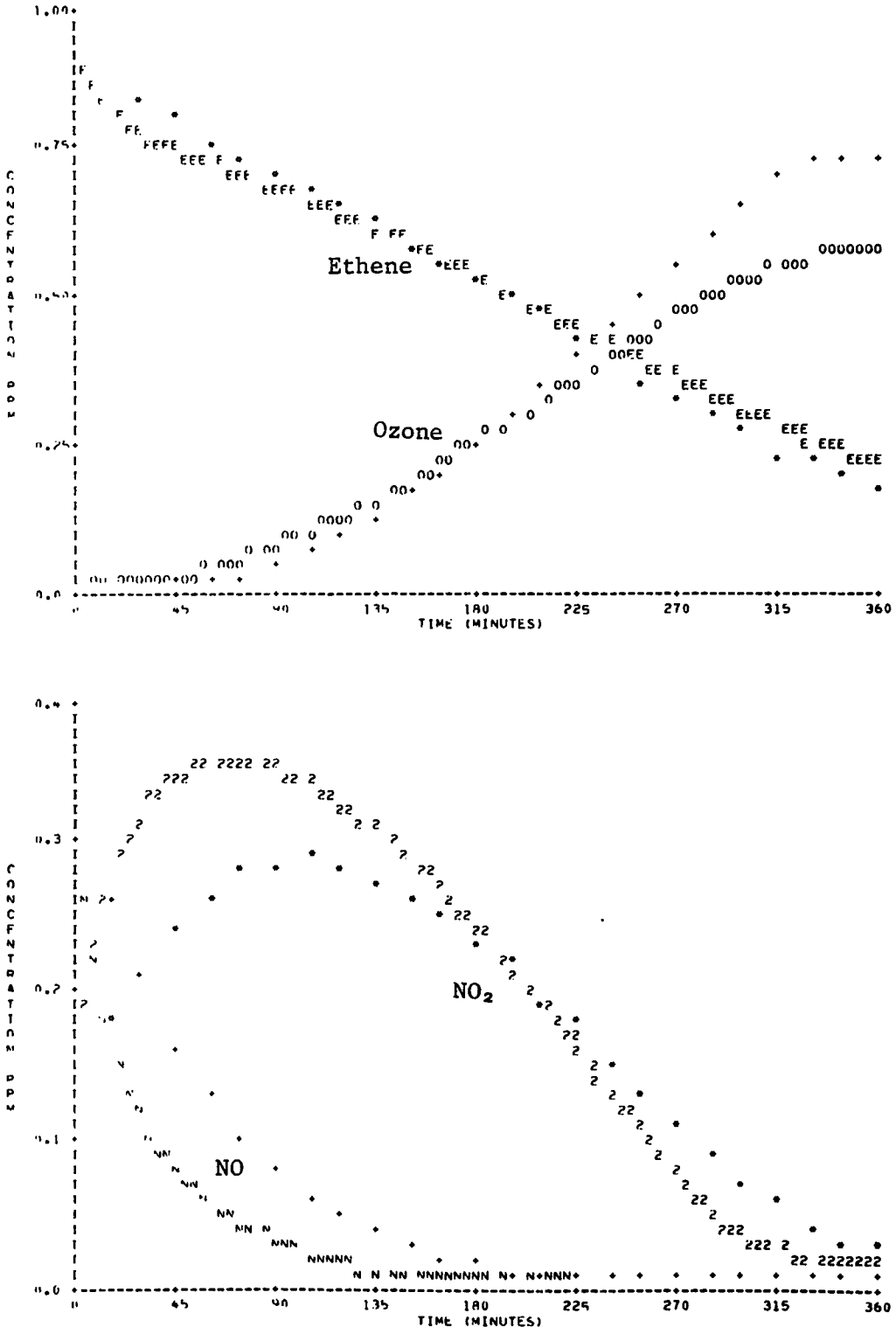

Figure A-21. Simulation of SAPRC EC-142.

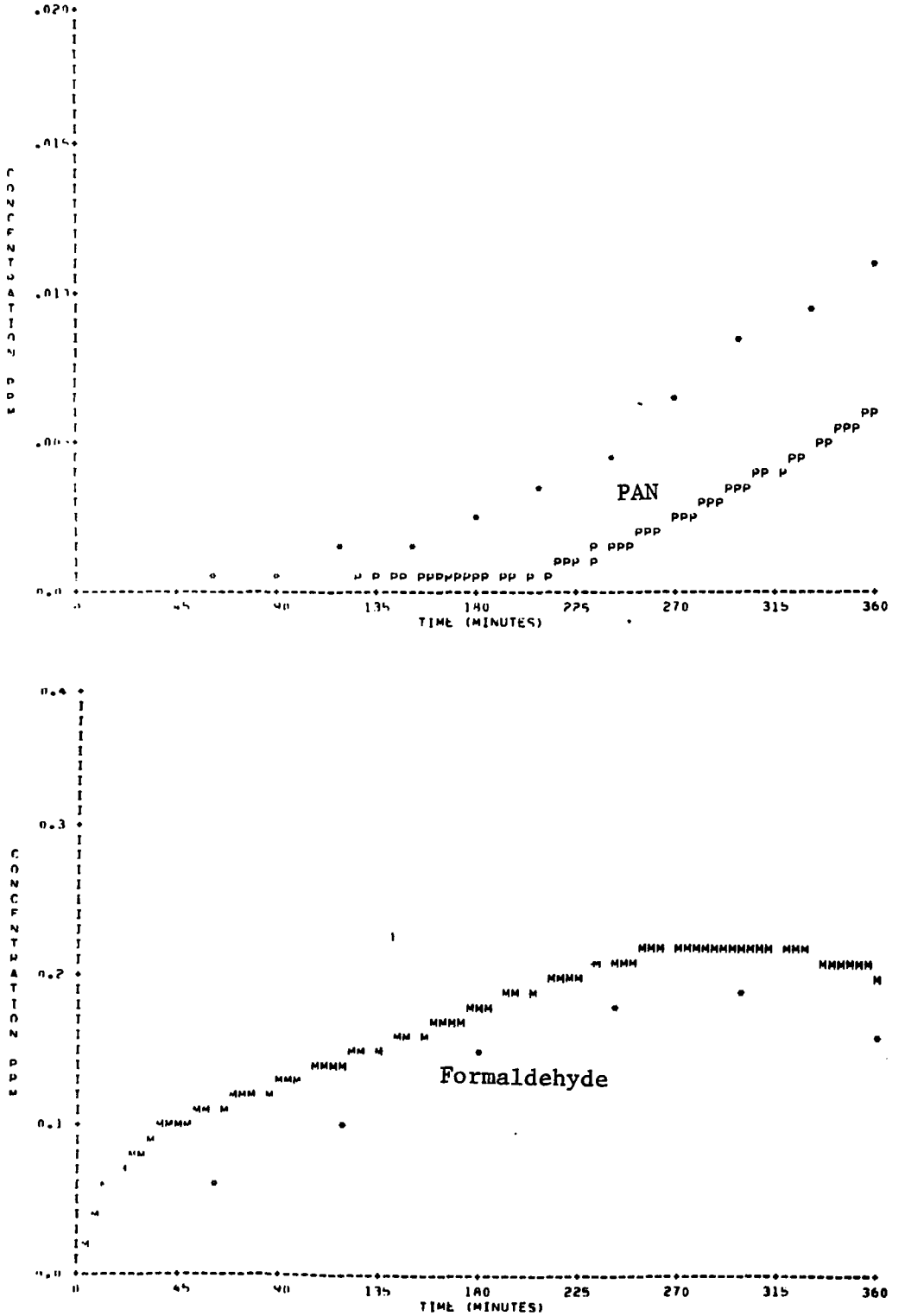

Figure A-21. Simulation of SAPRC EC-142 (Concluded).

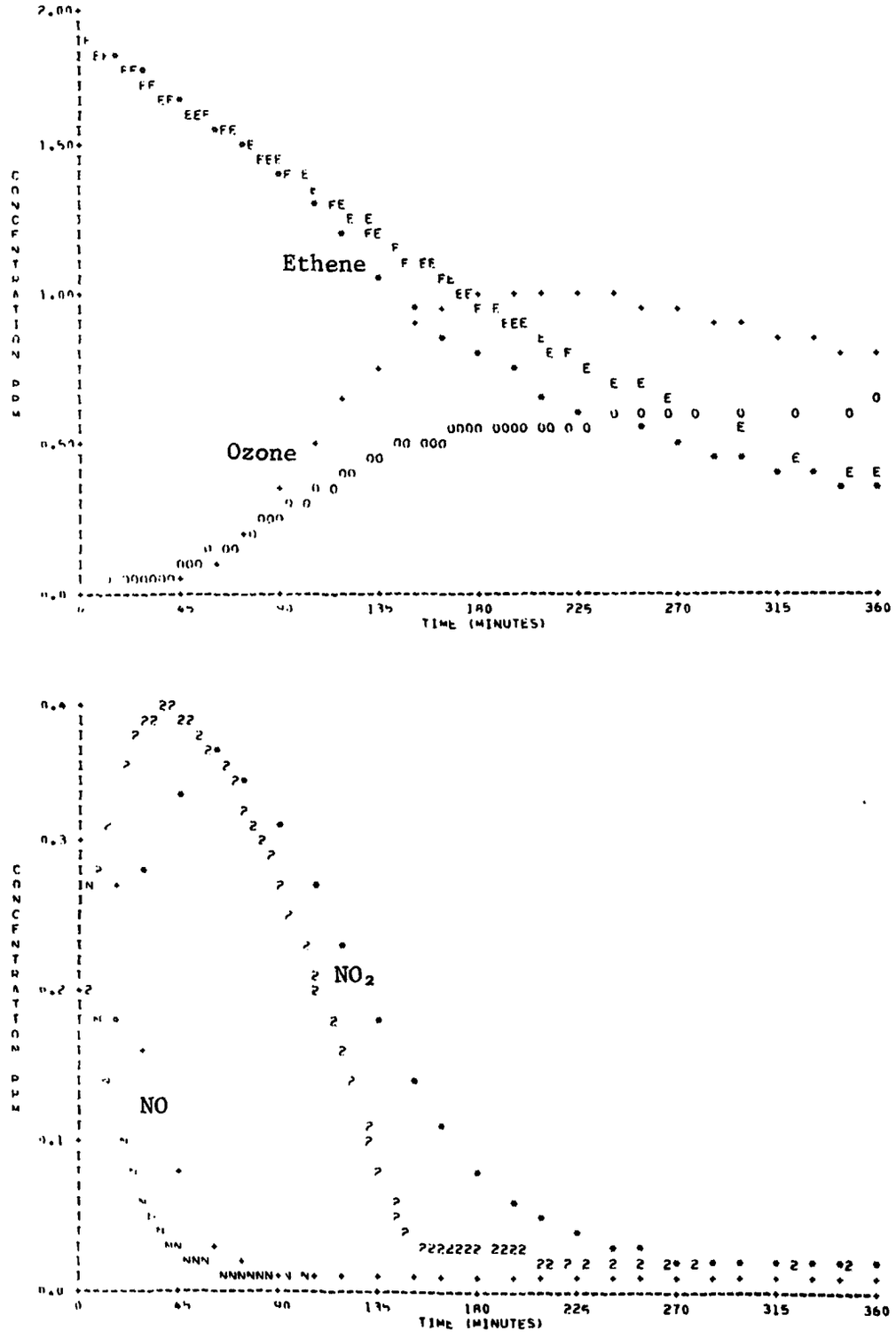

Figure A-22. Simulation of SAPRC EC-143.

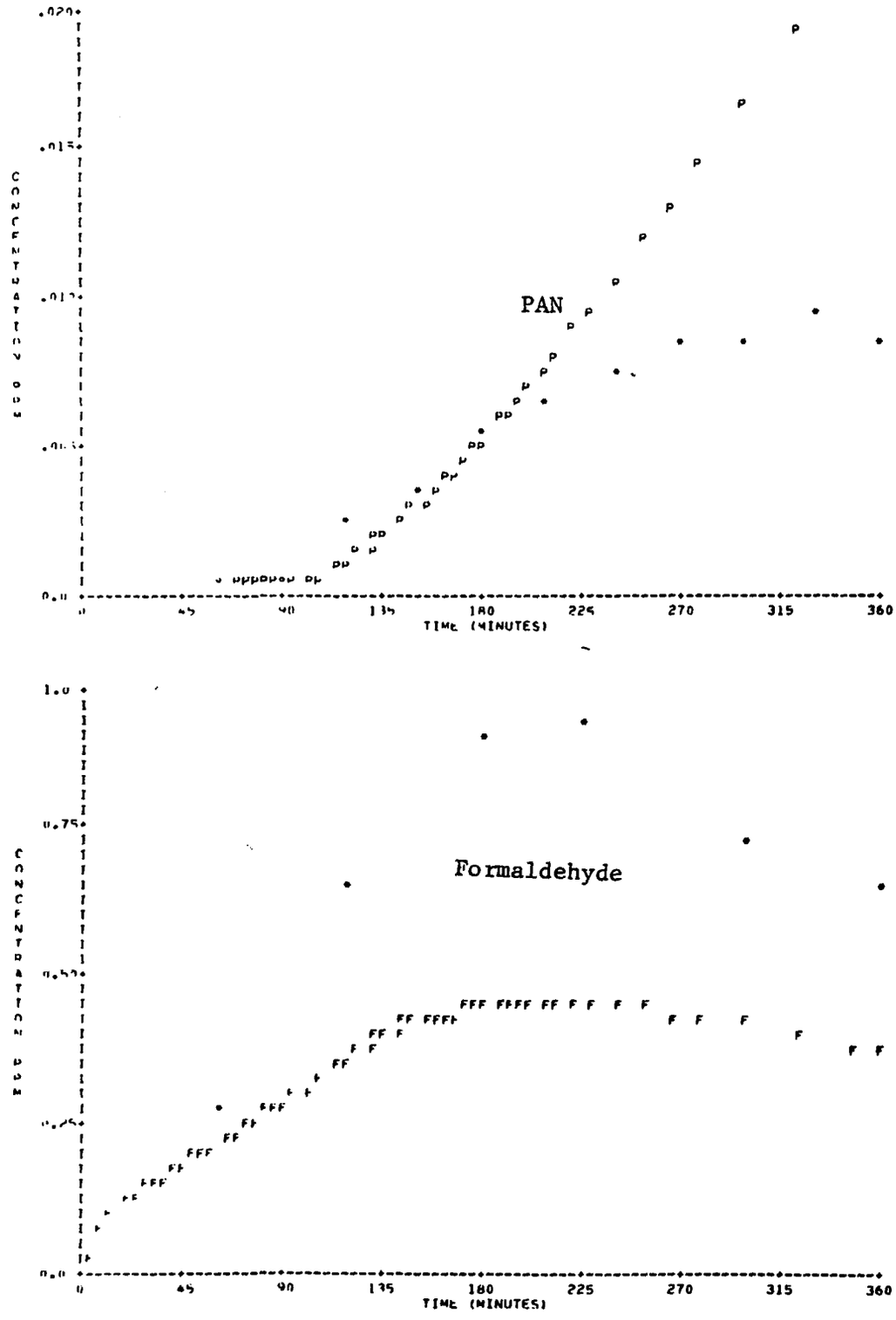

Figure A-22. Simulation of SAPRC EC-143 (Concluded).

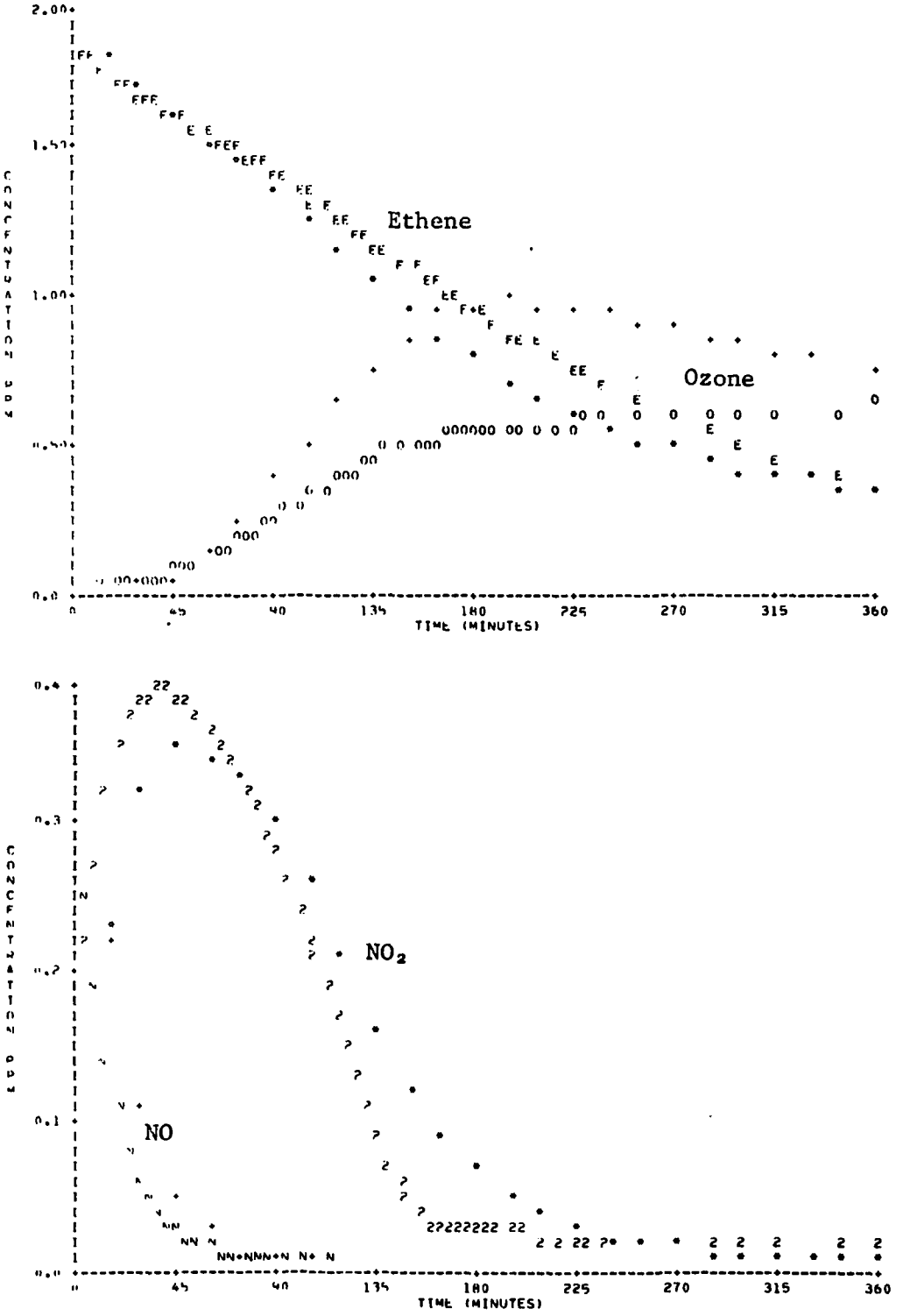

Figure A-23. Simulation of SAPRC EC-156.

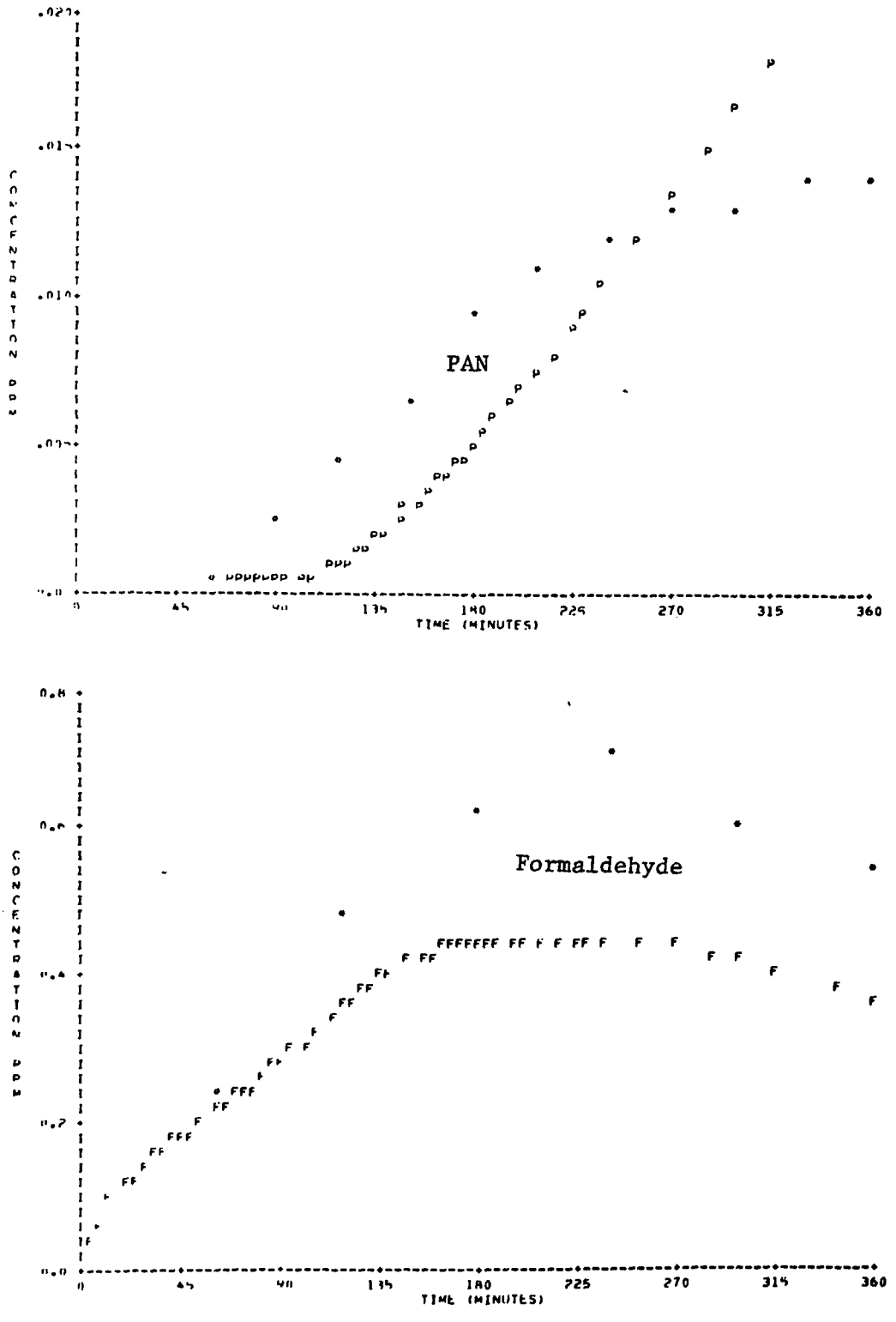

Figure A-23. Simulation of SAPRC EC-156 (Concluded).

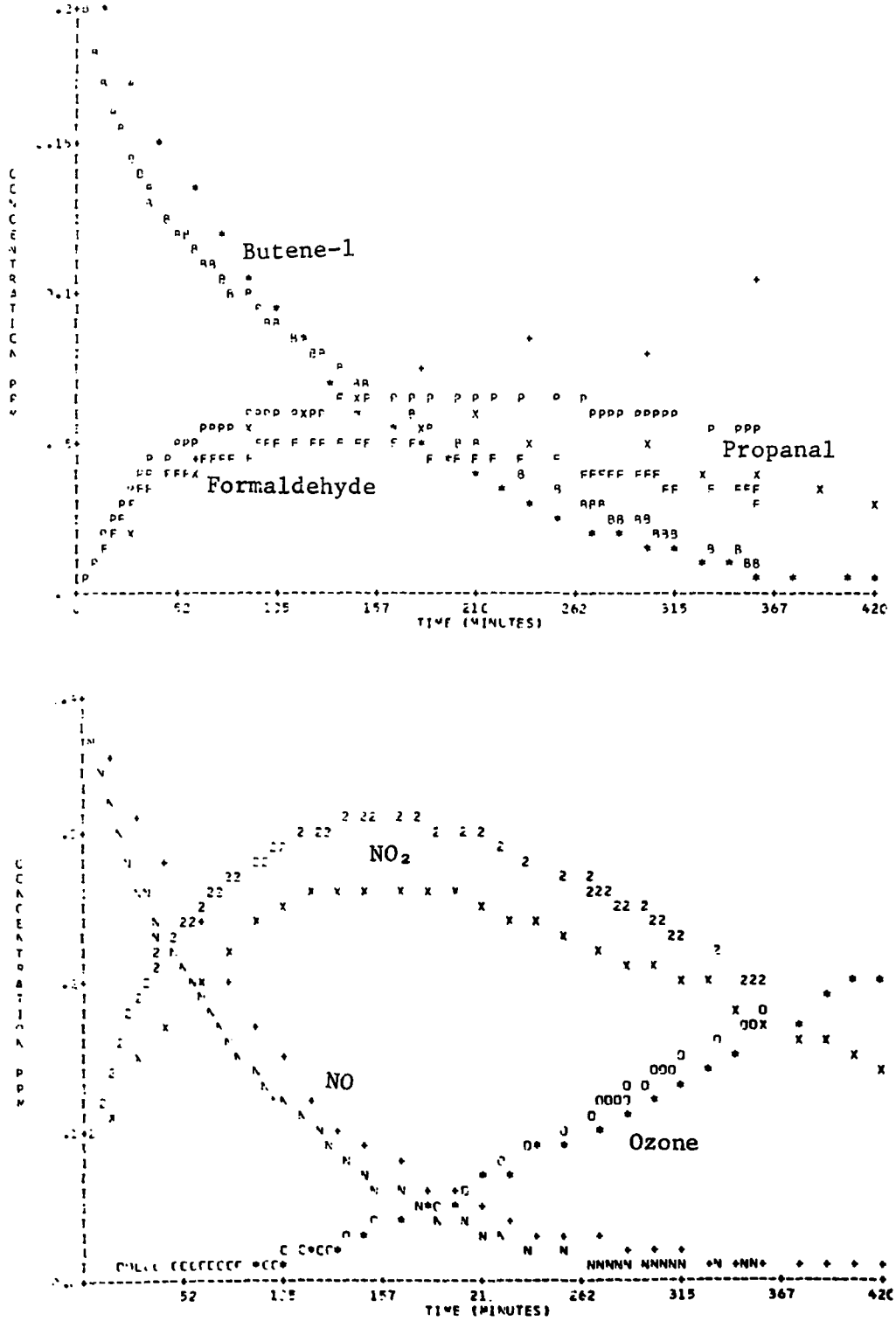

Figure A-24. Simulation of SAPRC EC-122.

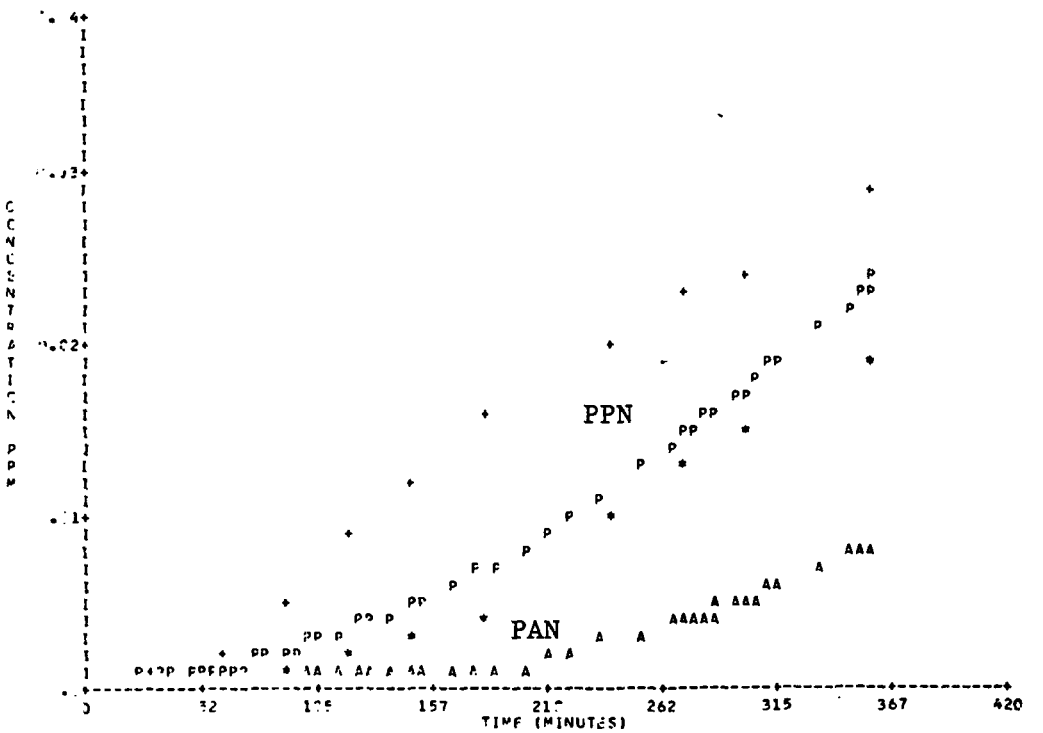

Figure A-24. Simulation of SAPRC EC-122 (Concluded).

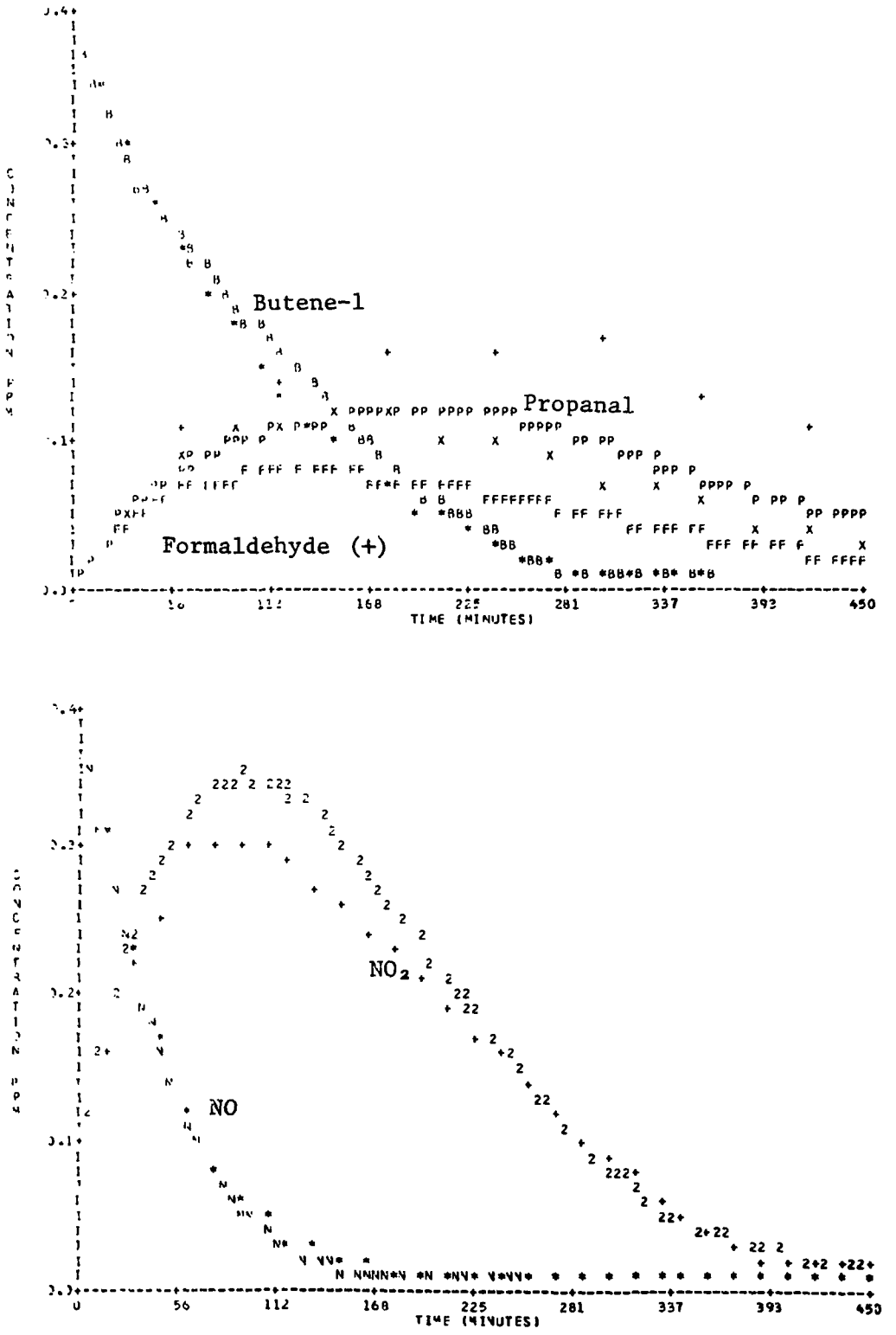

Figure A-25. Simulation of SAPRC EC-123.

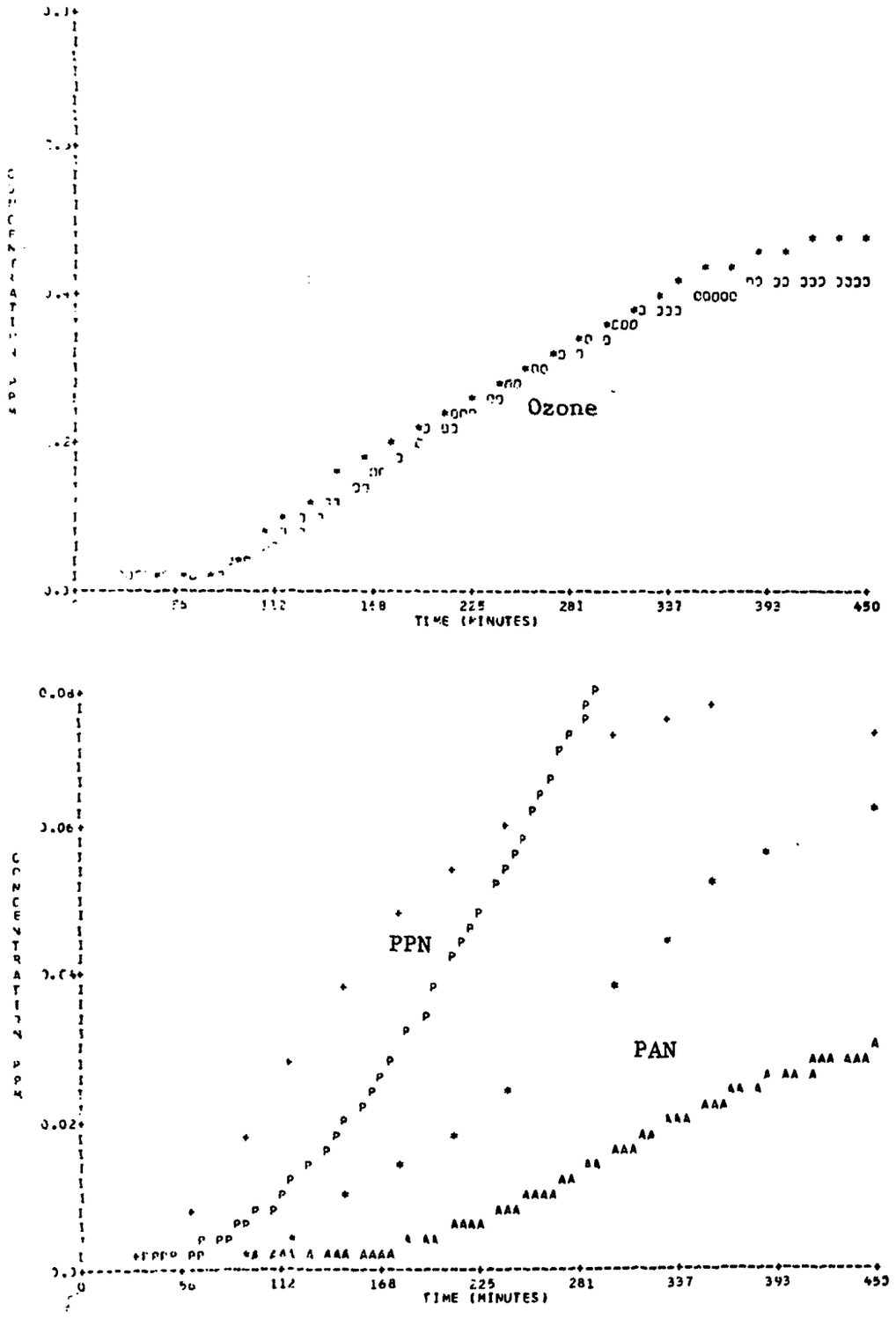

Figure A-25. Simulation of SAPRC EC-123 (Concluded).

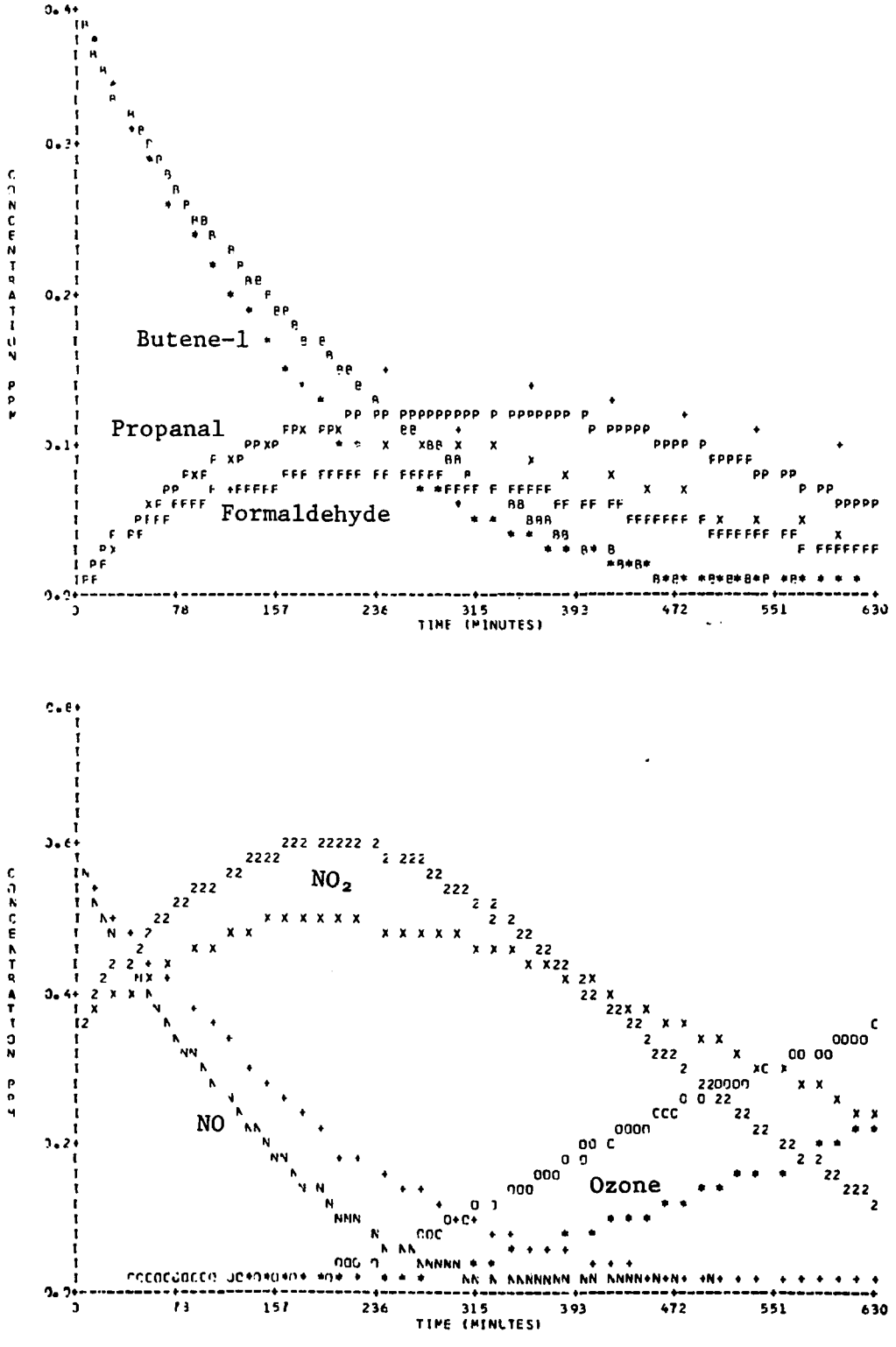

Figure A-26. Simulation of SAPRC EC-124.

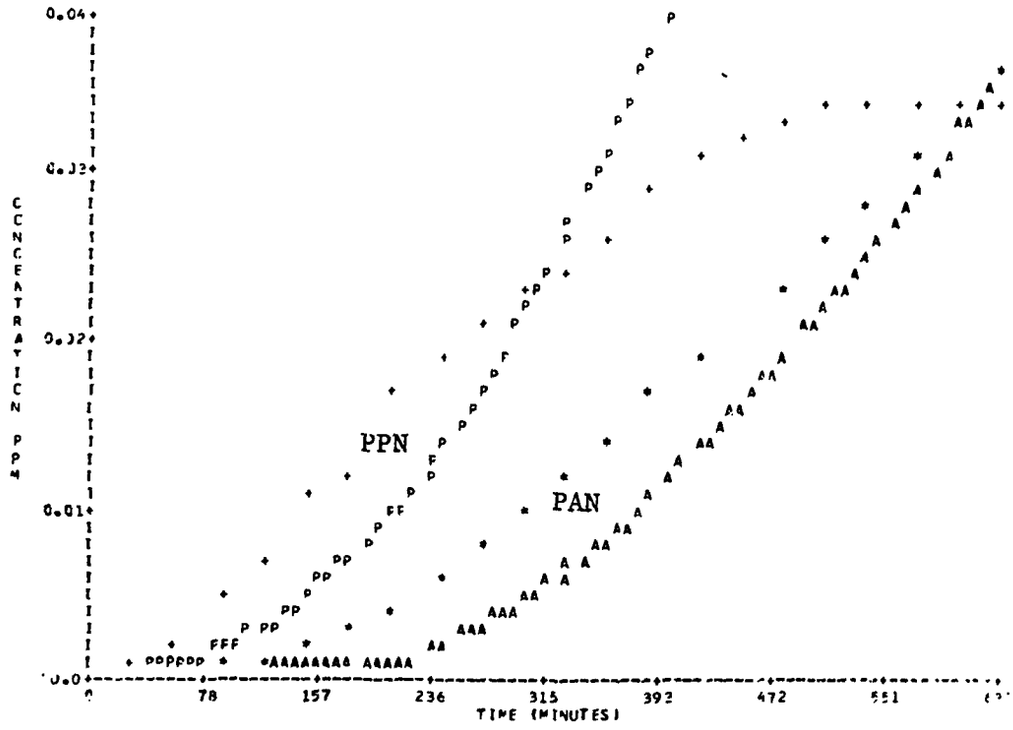

Figure A-26. Simulation of SAPRC EC-124 (Concluded).

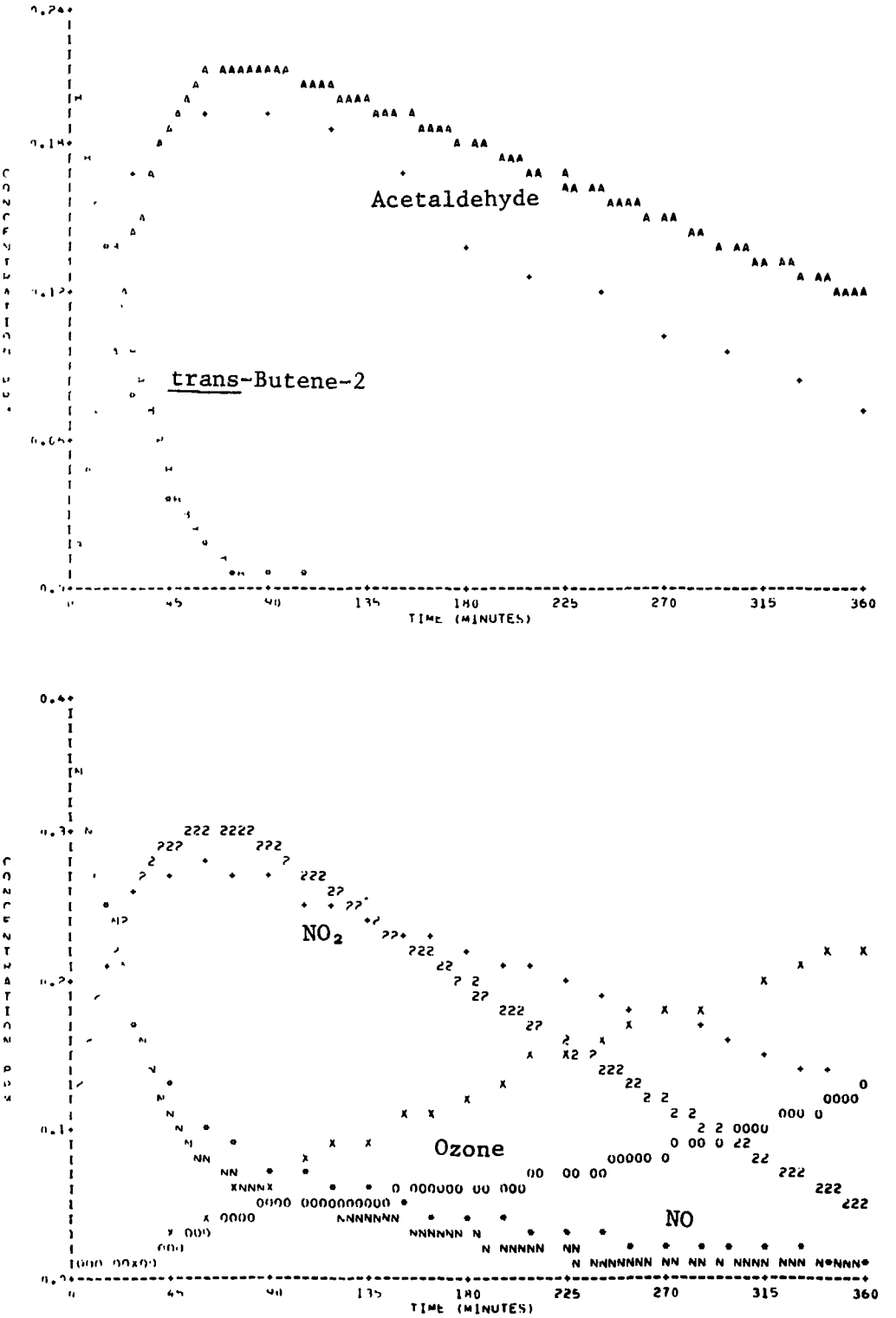

Figure A-27. Simulation of SAPRC EC-146.

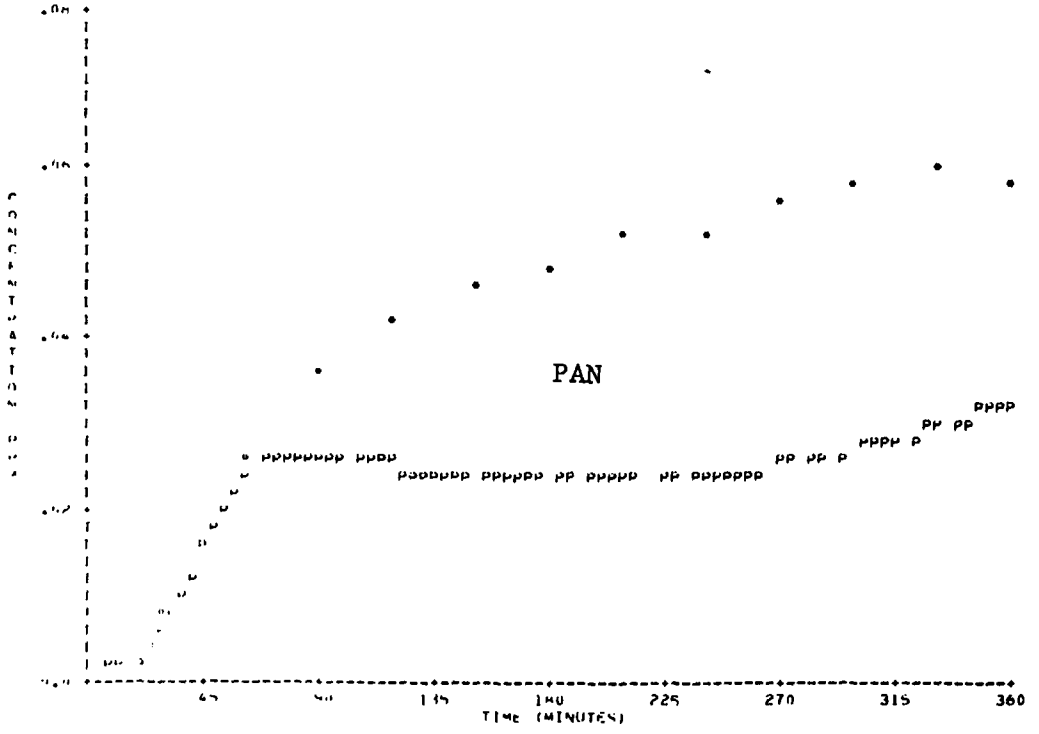

Figure A-27. Simulation of SAPRC EC-146 (Concluded).

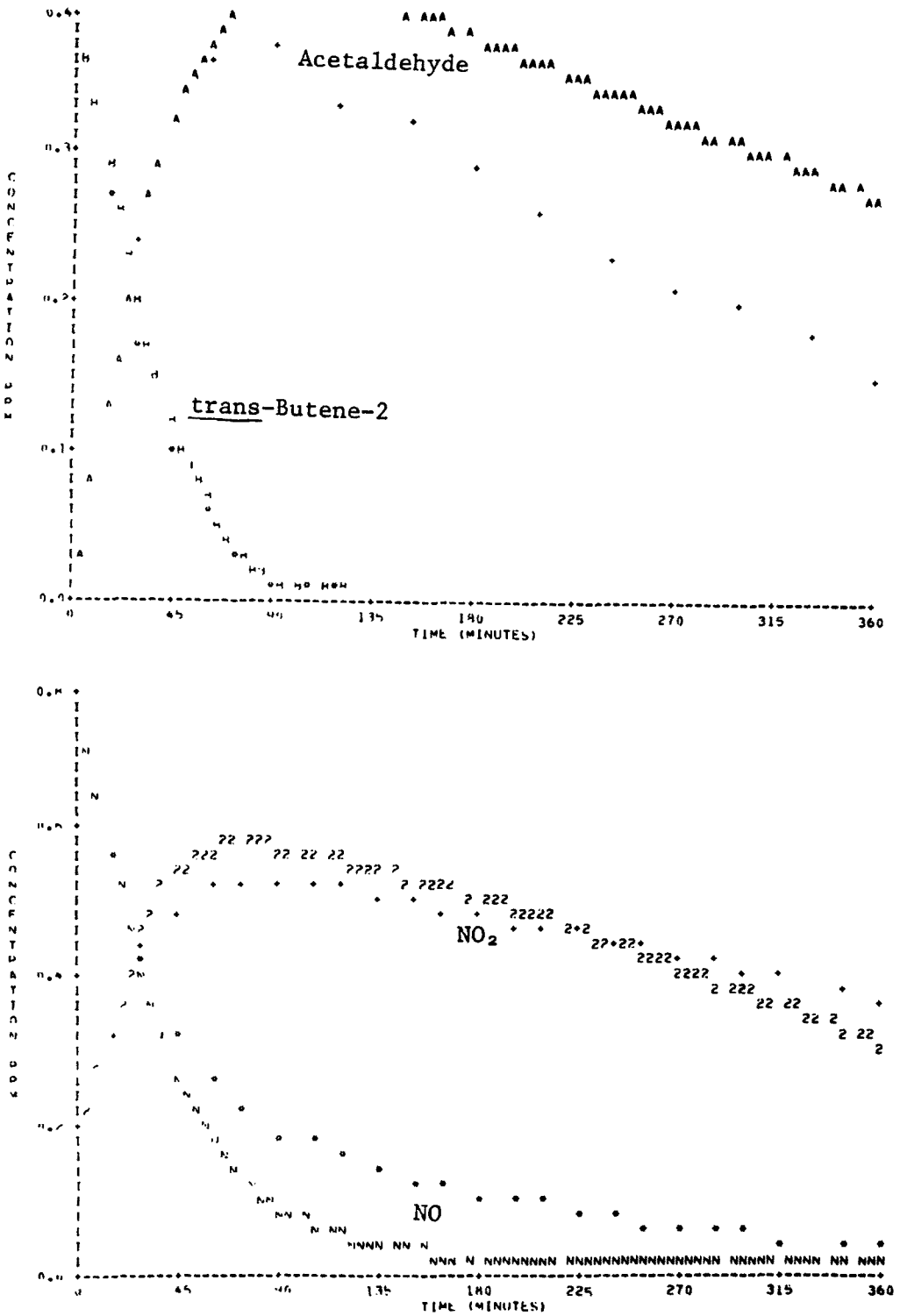

Figure A-28. Simulation of SAPRC EC-147.

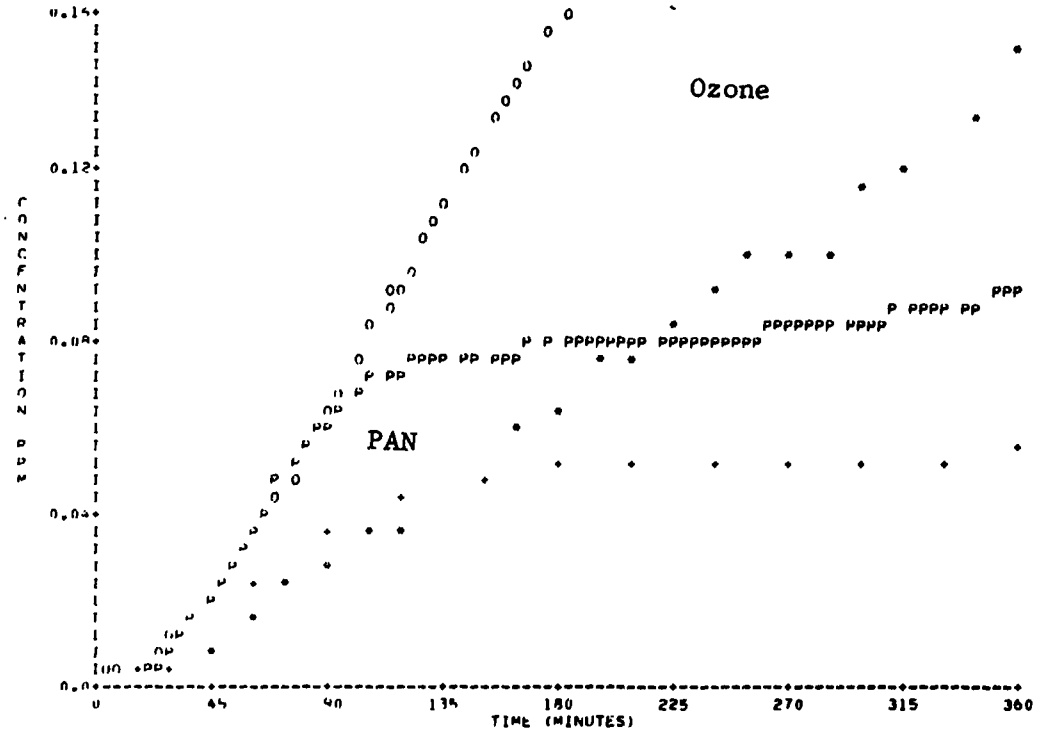

Figure A-28. Simulation of SAPRC EC-147 (Concluded).

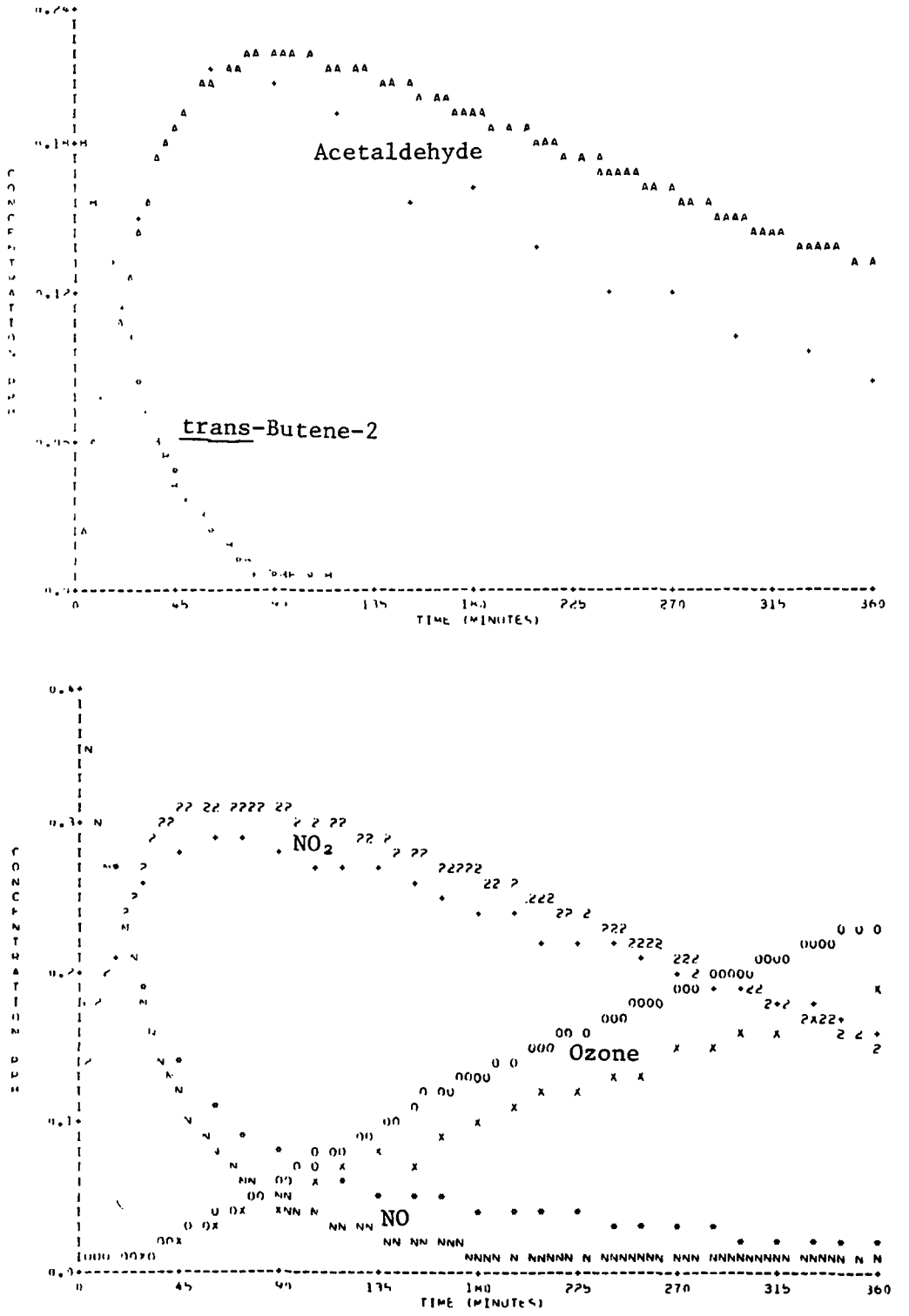

Figure A-29. Simulation of SAPRC EC-157.

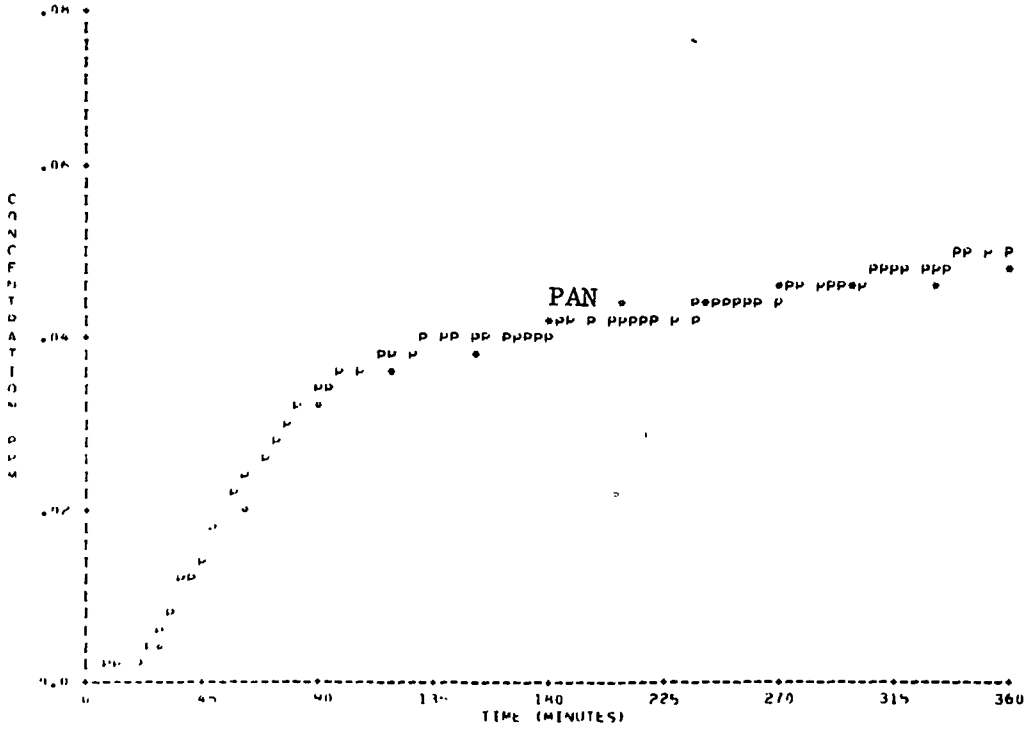

Figure A-29. Simulation of SAPRC EC-157 (Concluded).

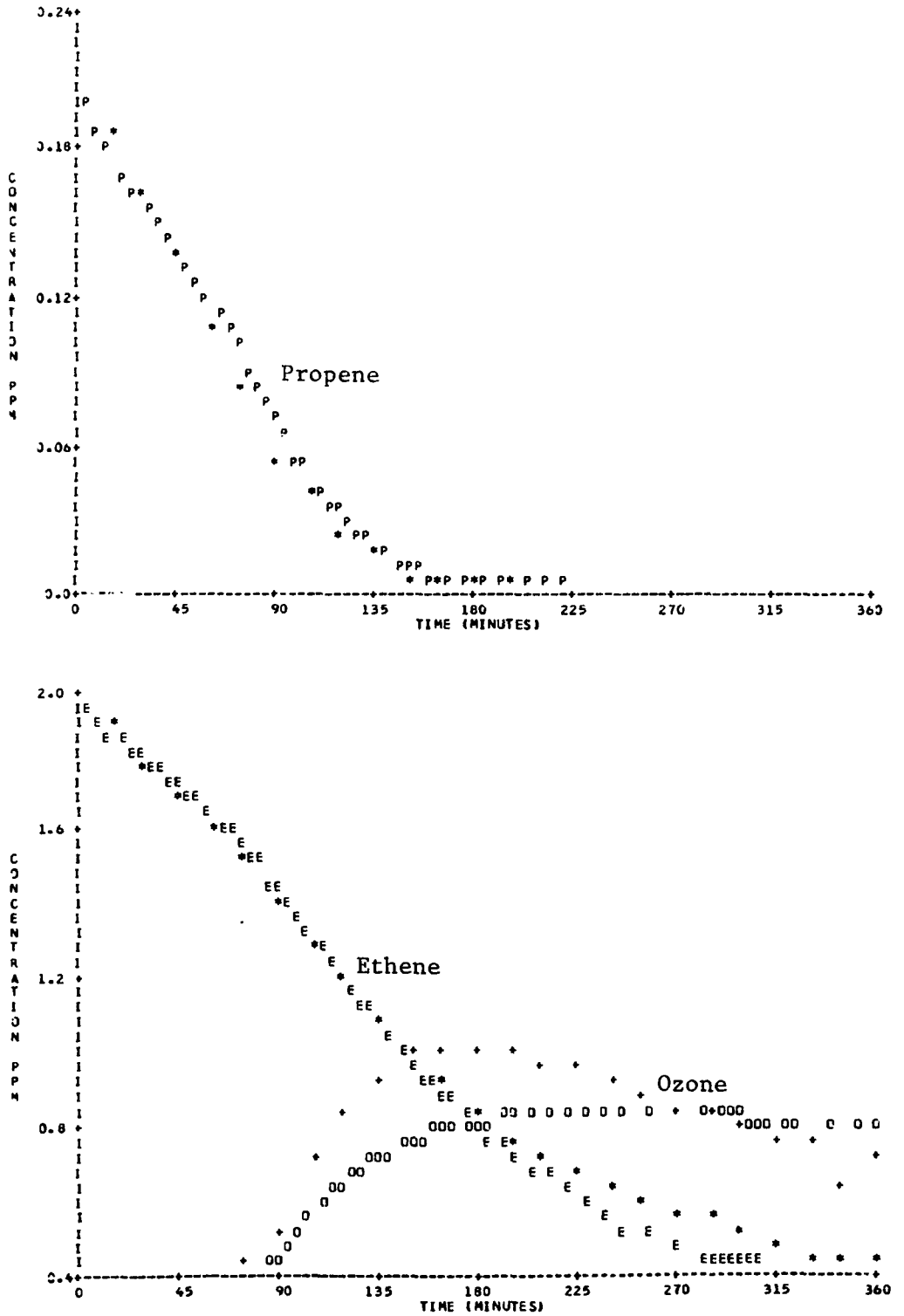

Figure A-30. Simulation of SAPRC EC-144.

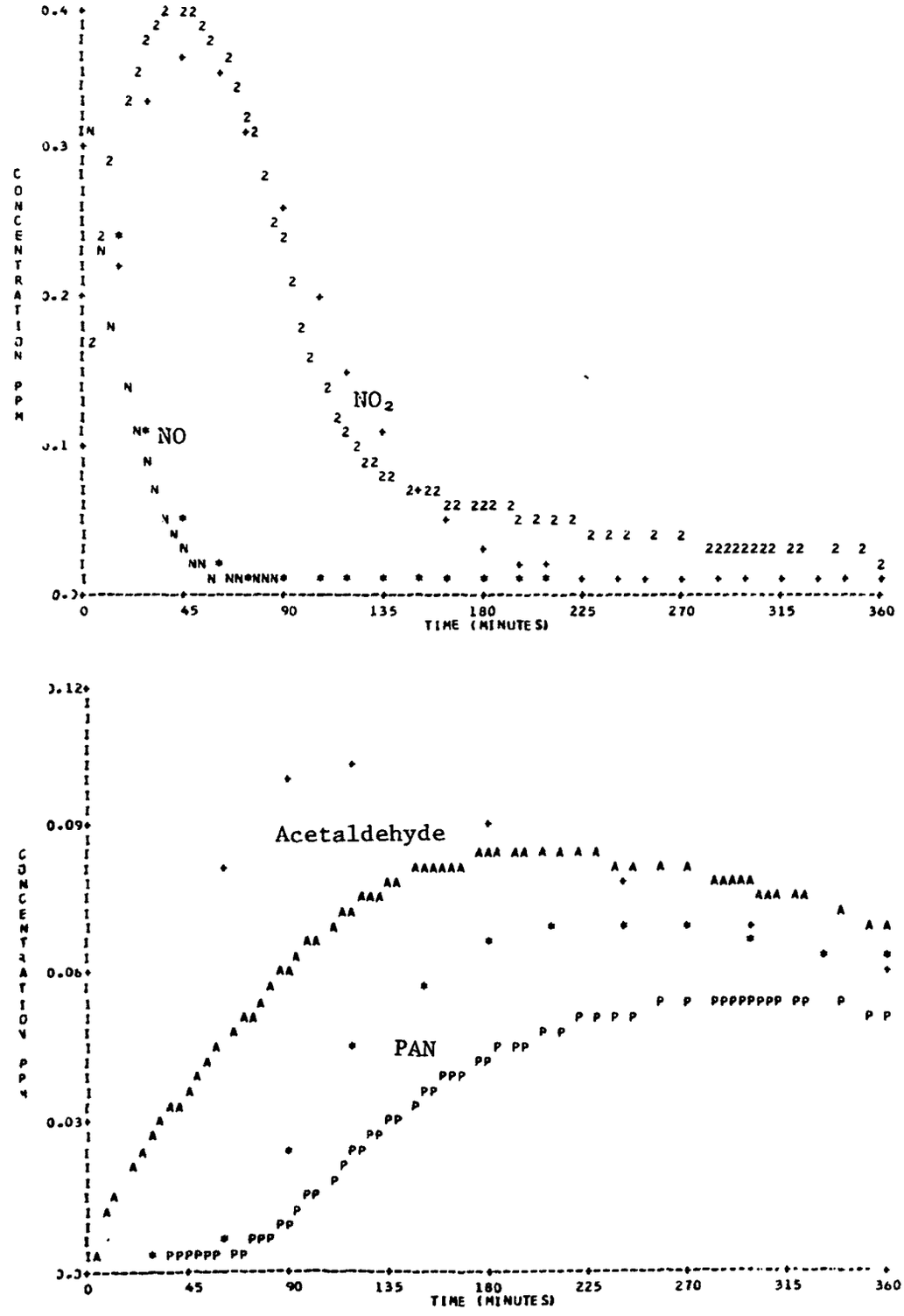

Figure A-30. Simulation of SAPRC EC-144 (Continued).

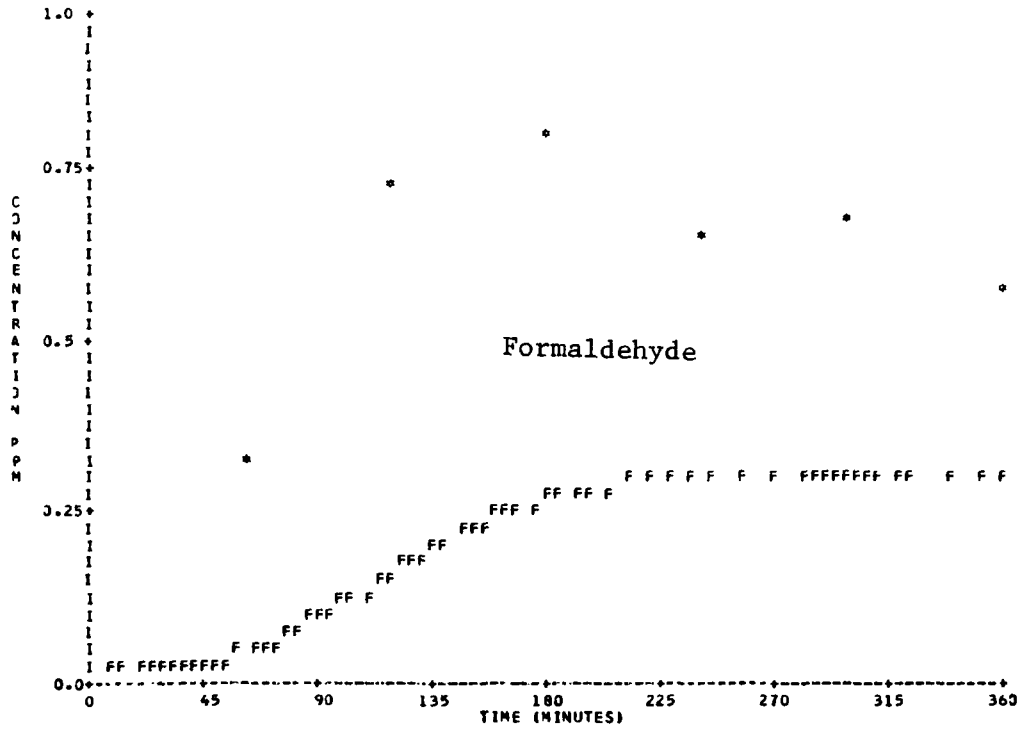

Figure A-30. Simulation of SAPRC EC-144 (Concluded).

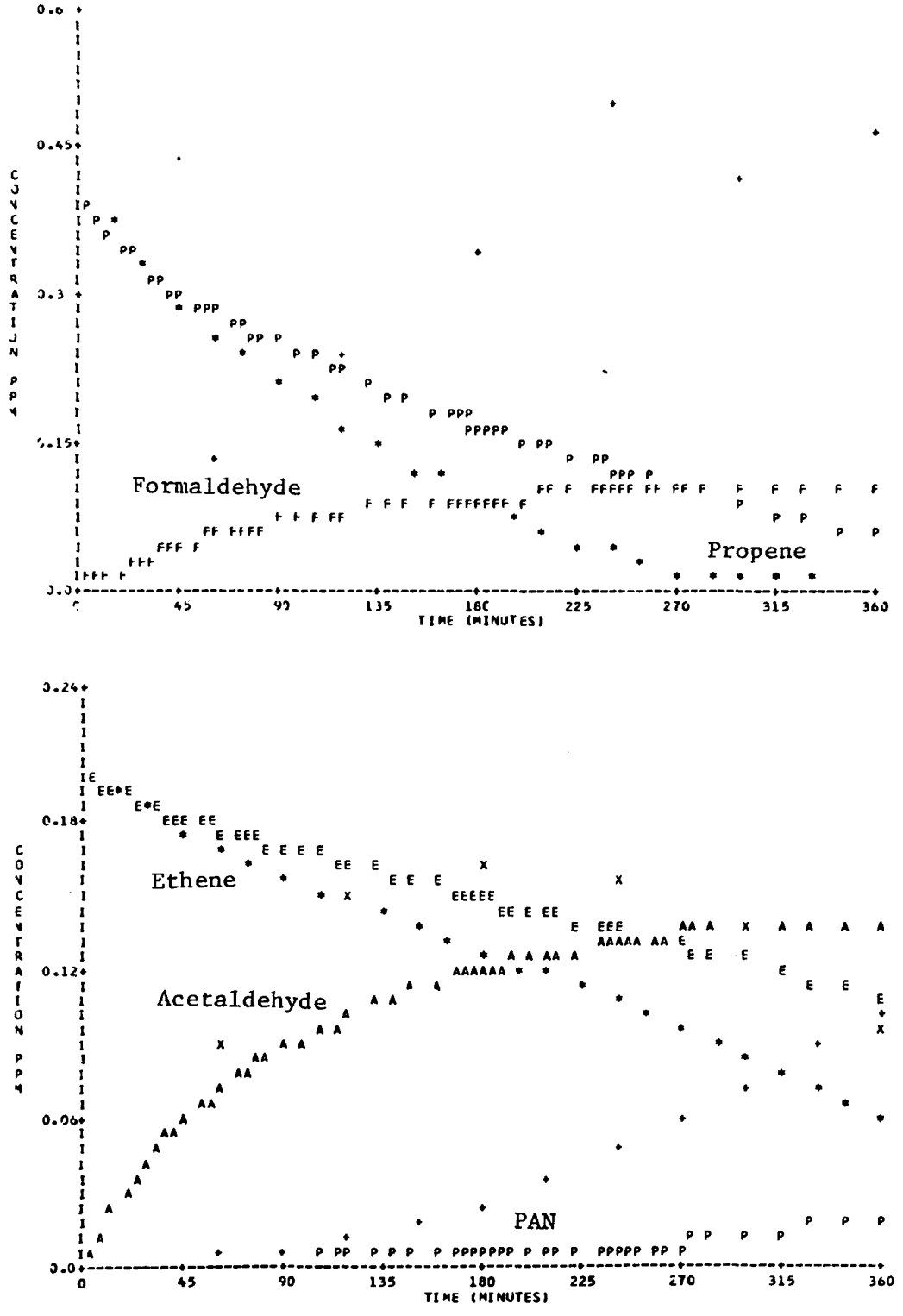

Figure A-31. Simulation of SAPRC EC-145.

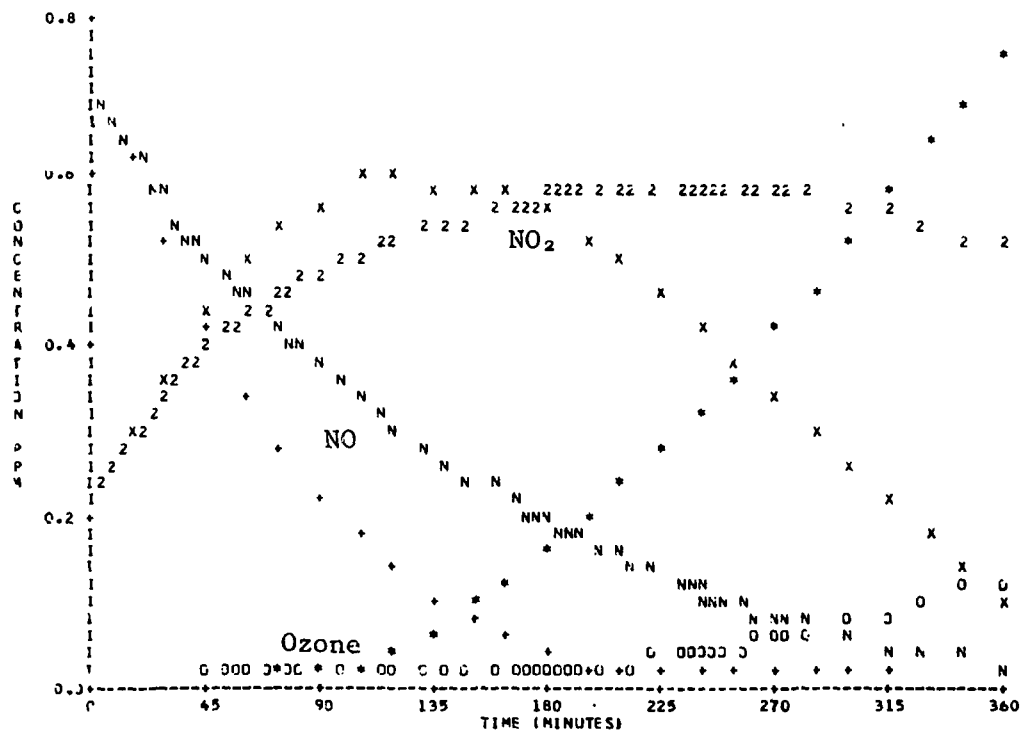

Figure A-31. Simulation of SAPRC EC-145 (Concluded).

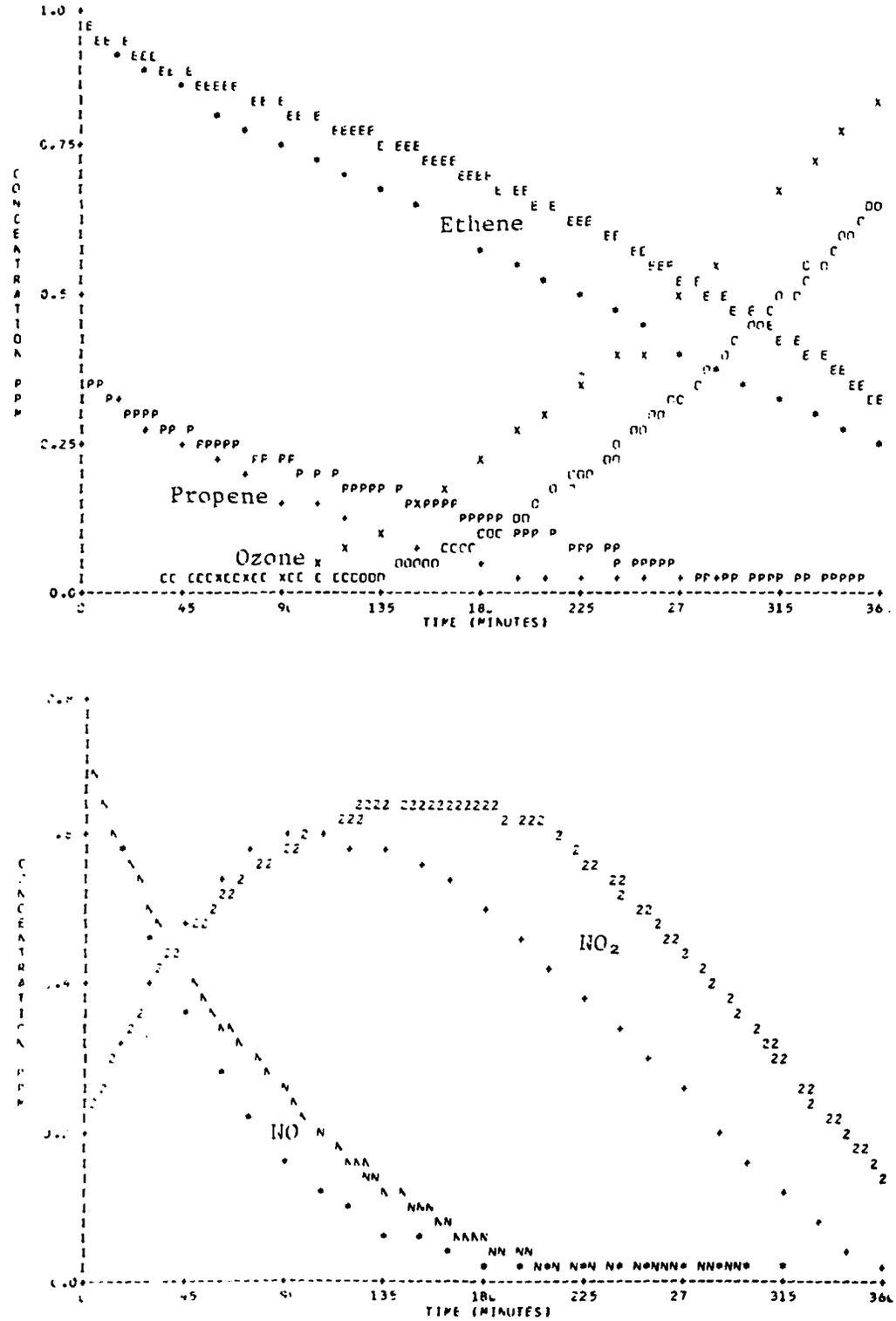

Figure A-32. Simulation of SAPRC EC-160.

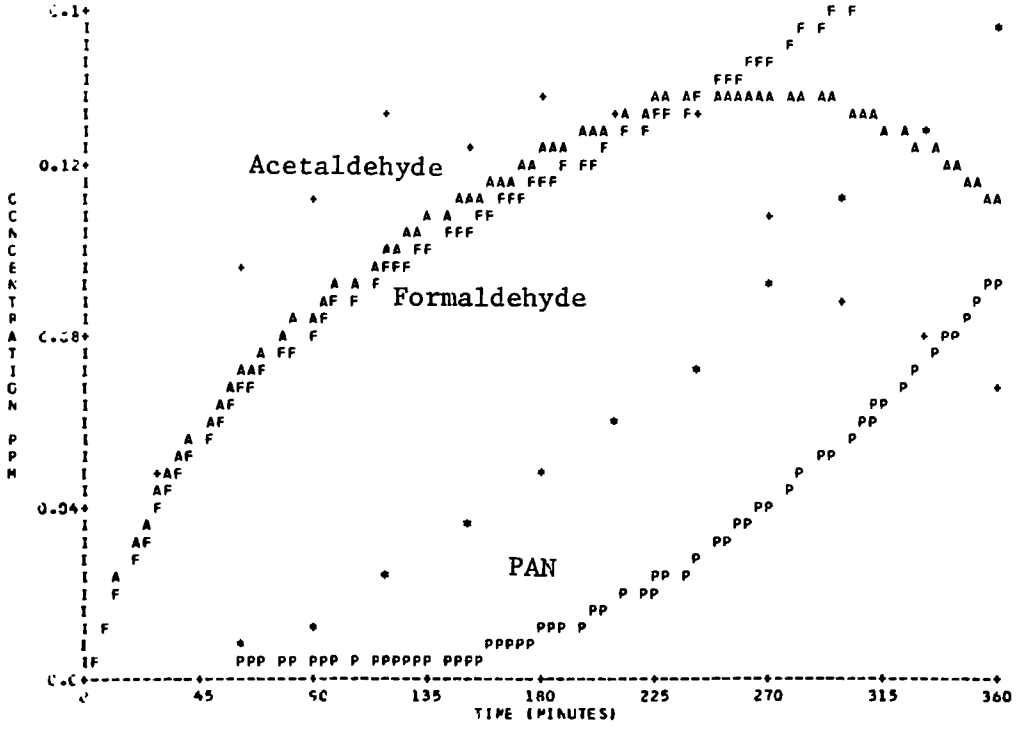

Figure A-32. Simulation of SAPRC EC-160 (Concluded).

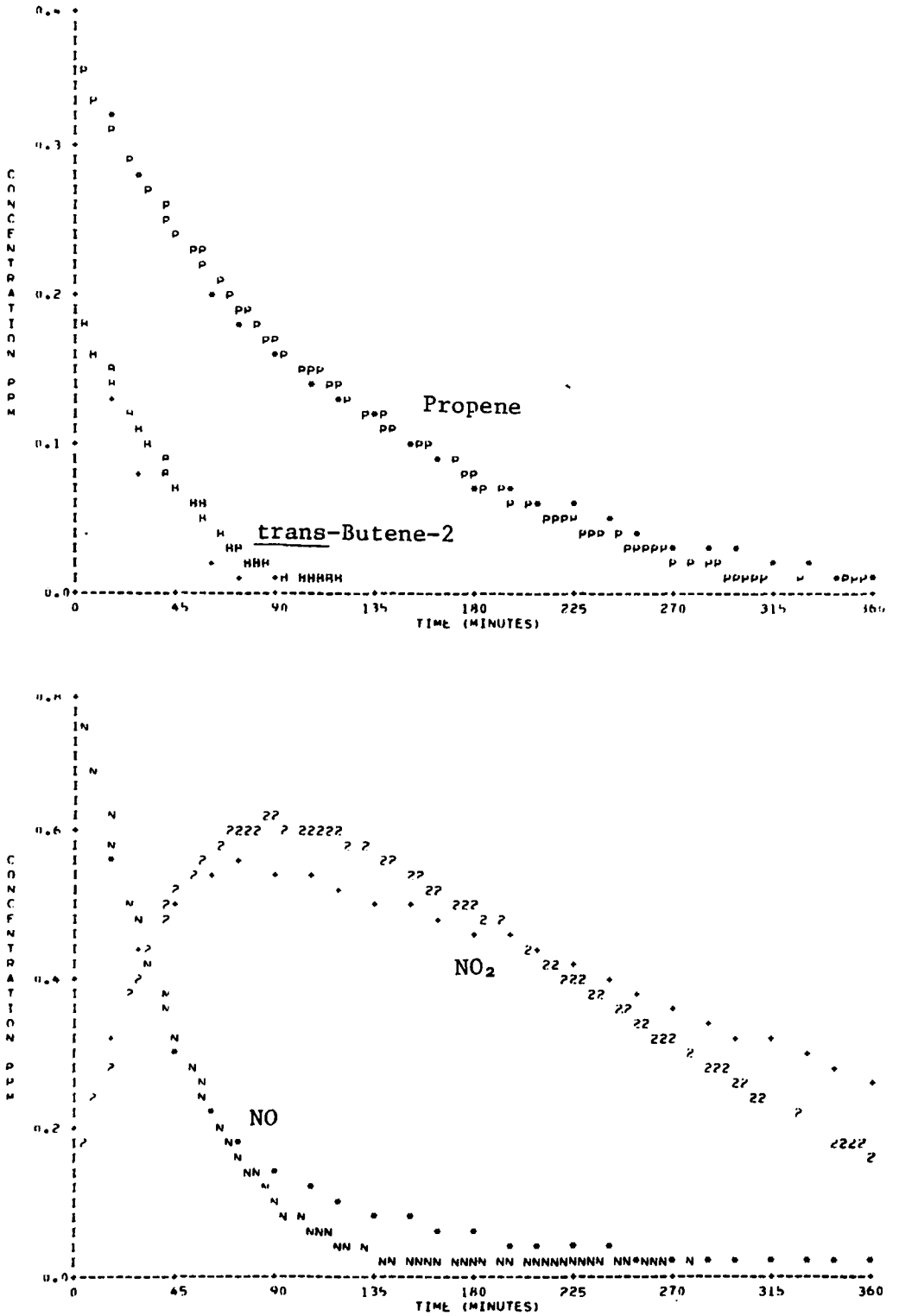

Figure A-33. Simulation of SAPRC EC-149.

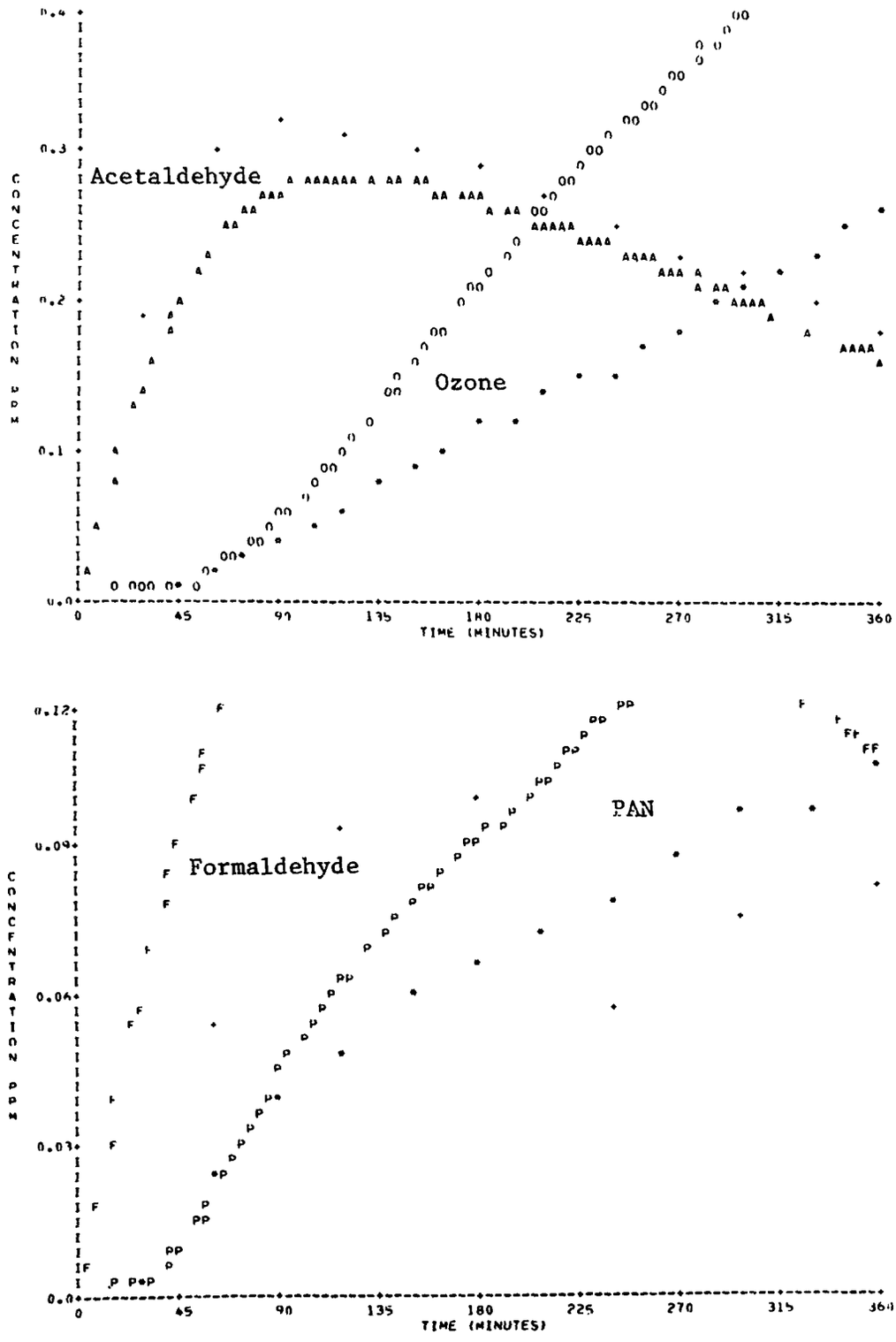

Figure A-33. Simulation of SAPRC EC-149 (Concluded).

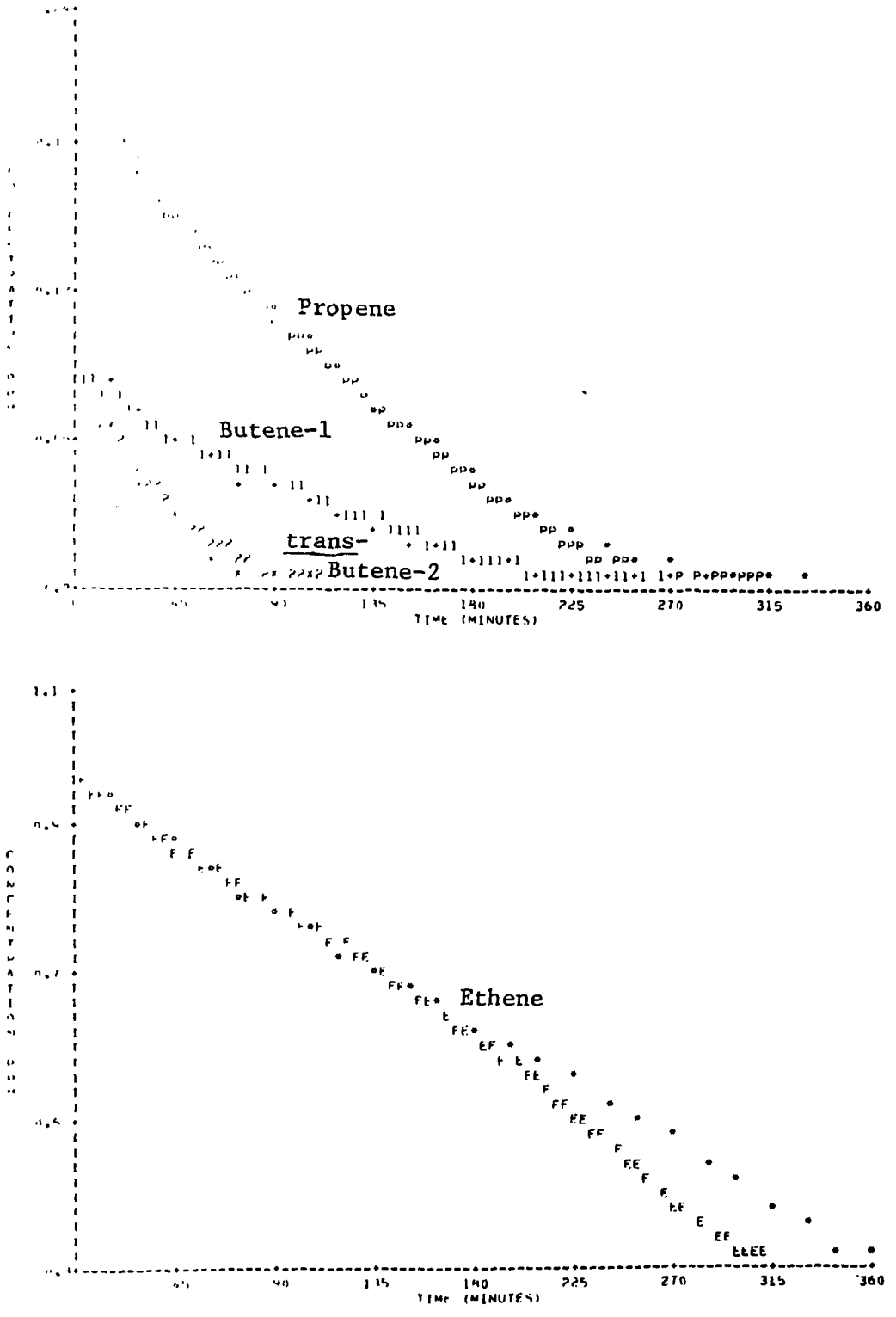

Figure A-34. Simulation of SAPRC EC-150.

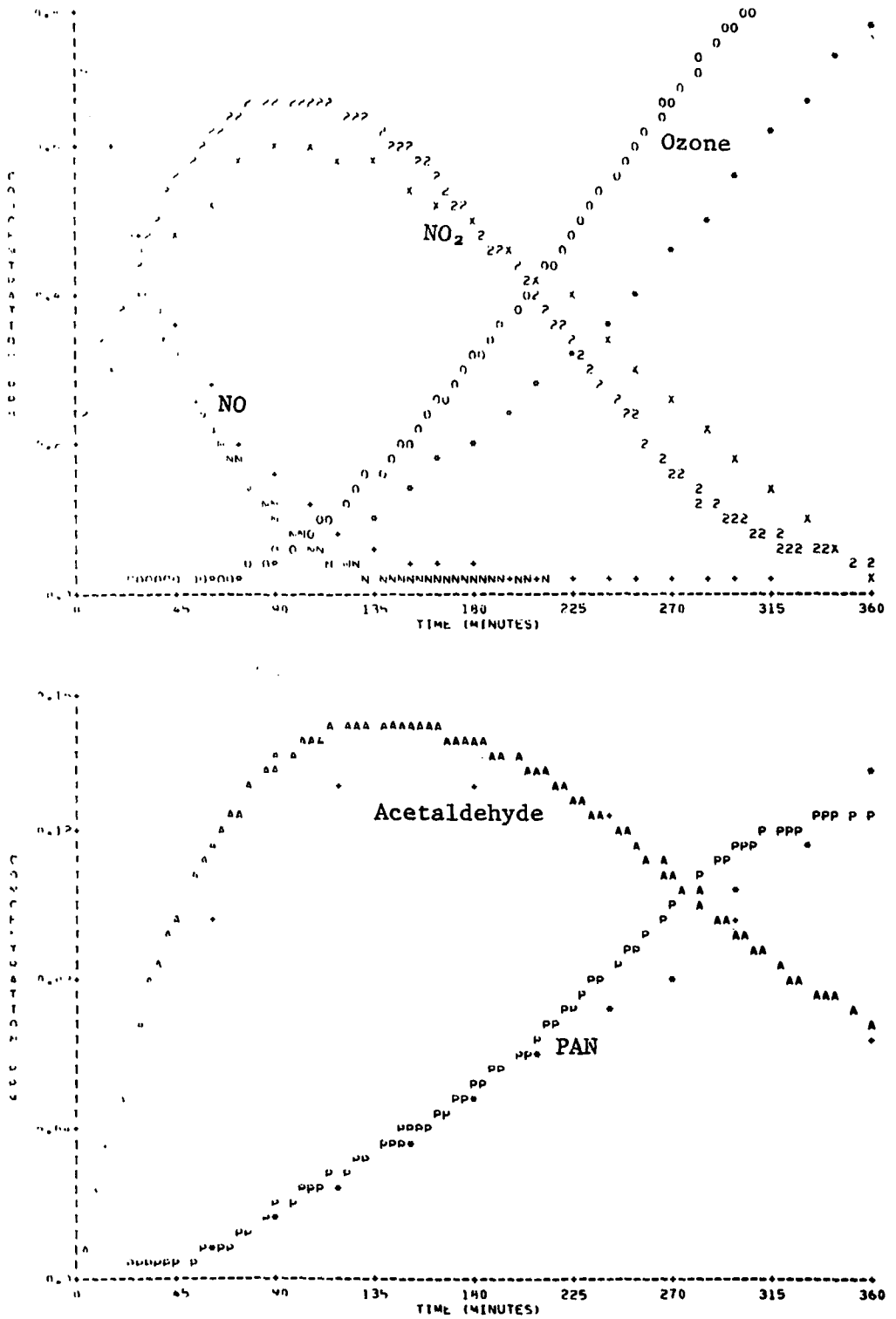

Figure A-34. Simulation of SAPRC EC-150 (Continued).

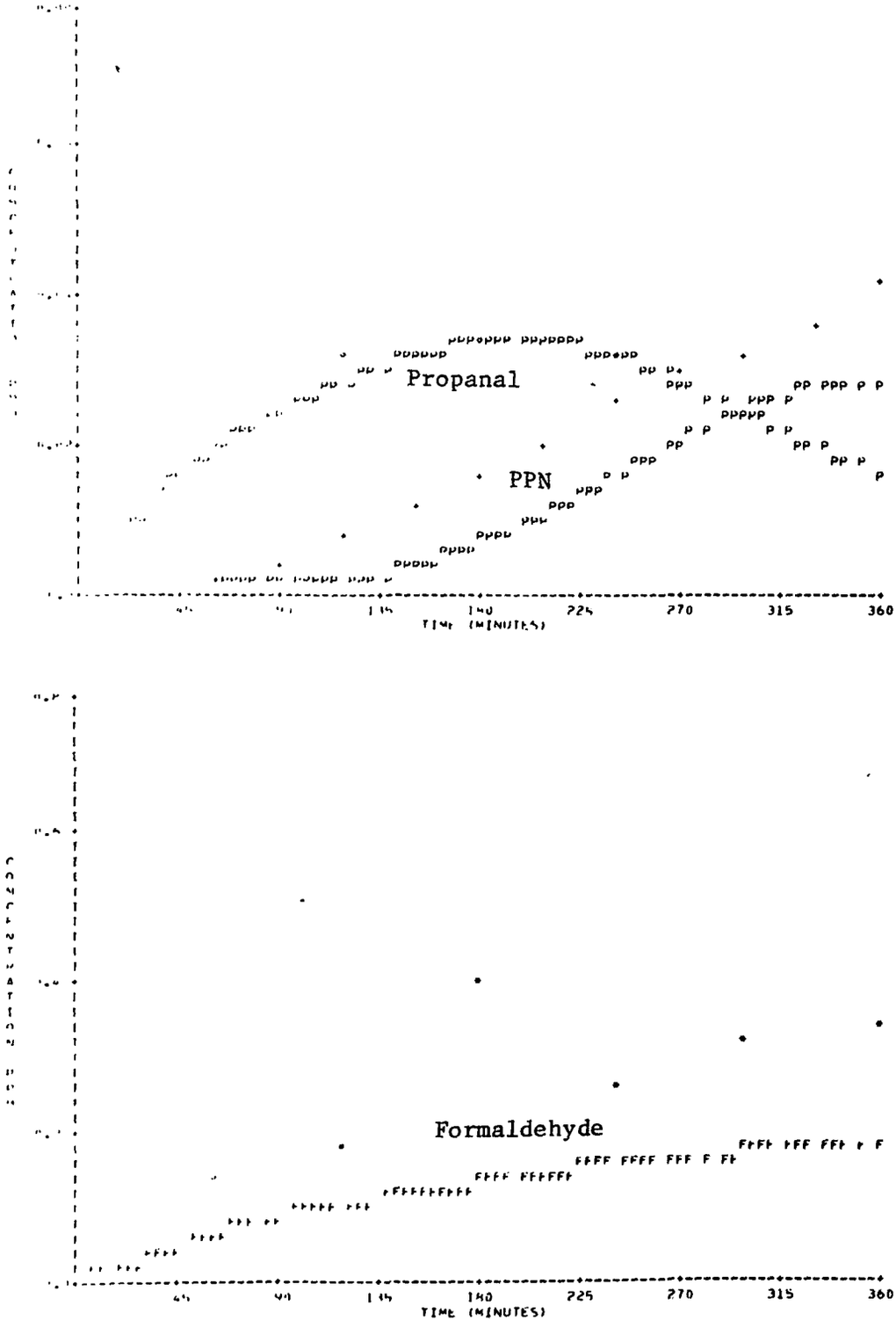

Figure A-34. Simulation of SAPRC EC-150 (Concluded).

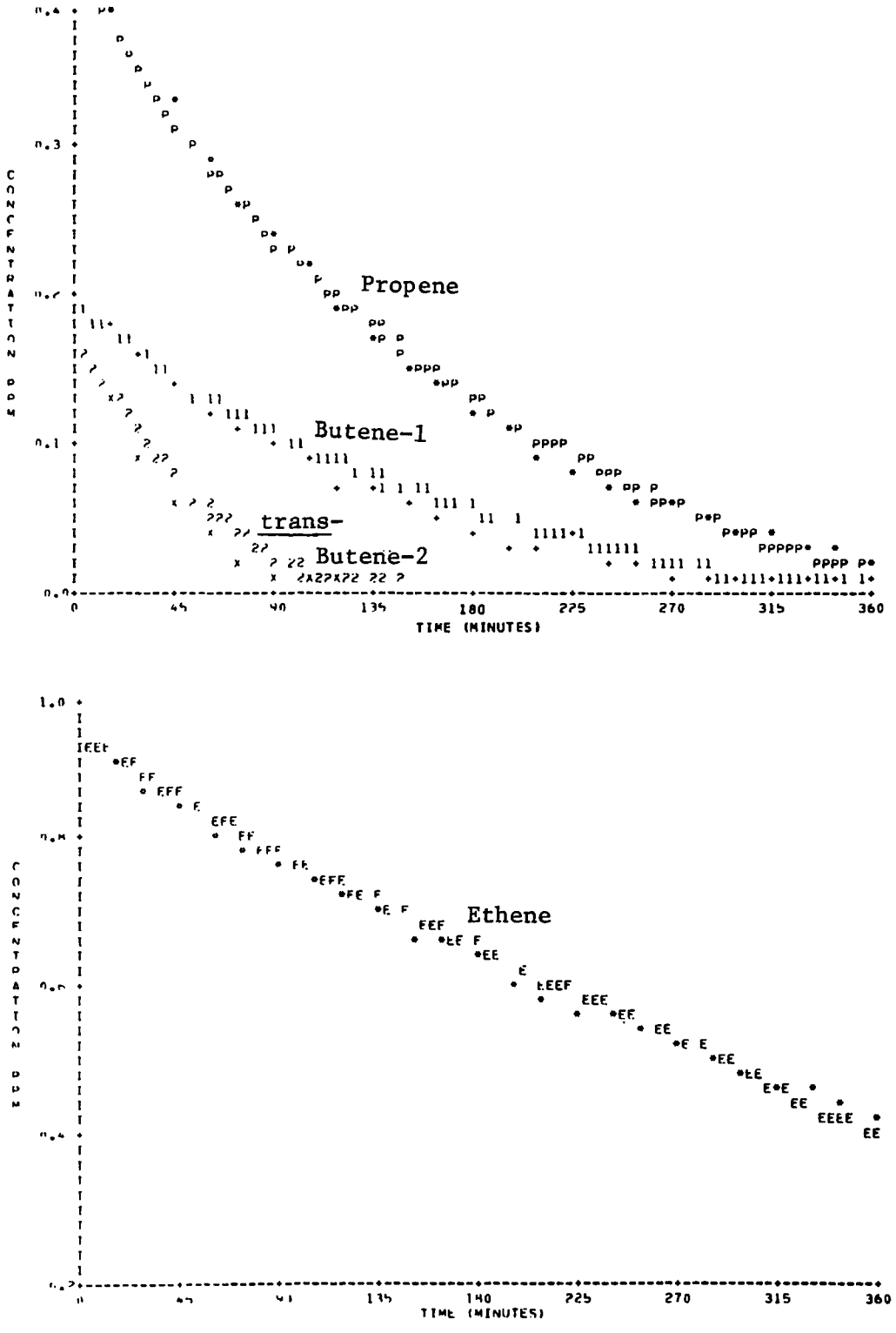

Figure A-35. Simulation of SAPRC EC-151.

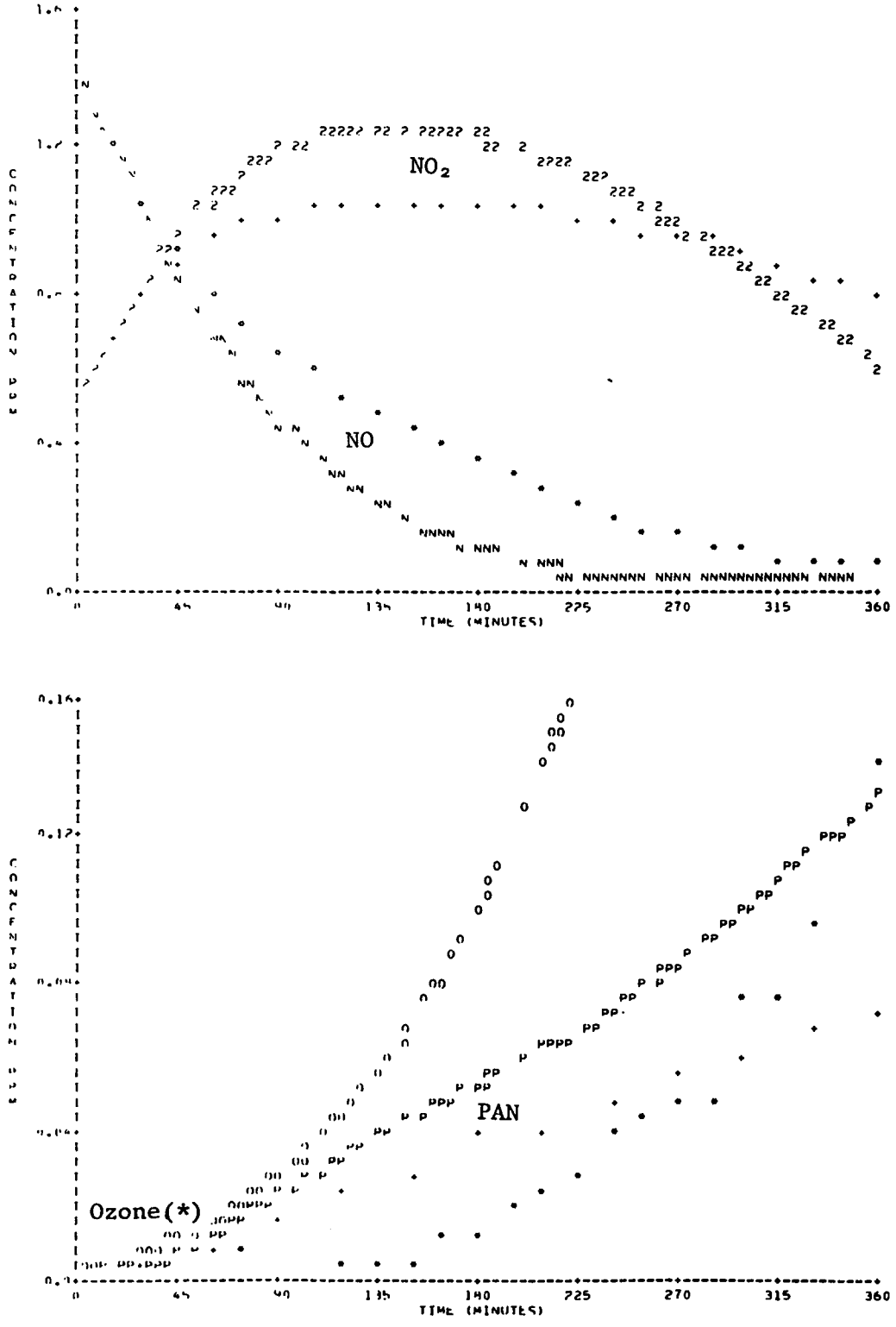

Figure A-35. Simulation of SAPRC EC-151 (Continued).

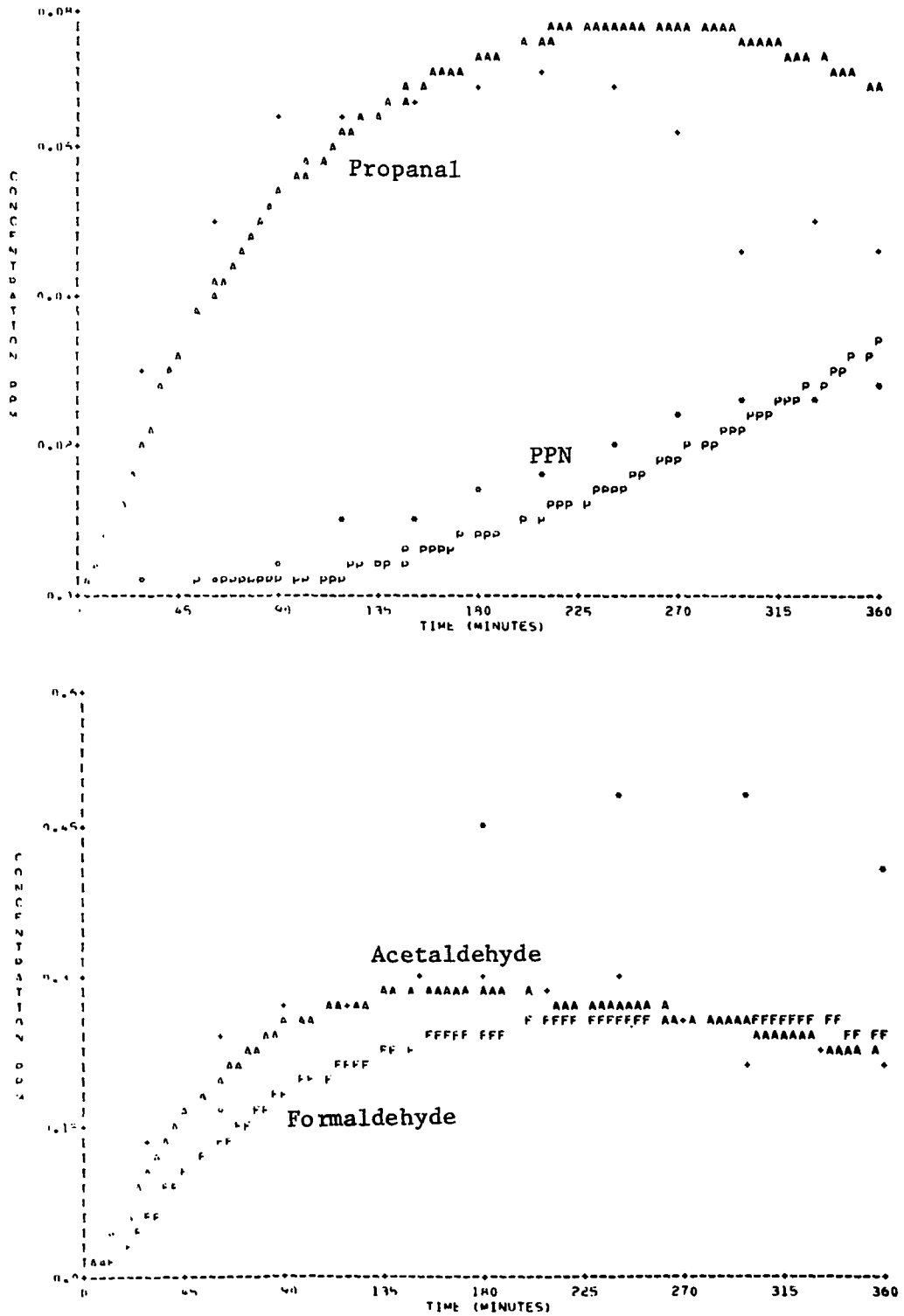

Figure A-35. Simulation of SAPRC EC-151 (Concluded).

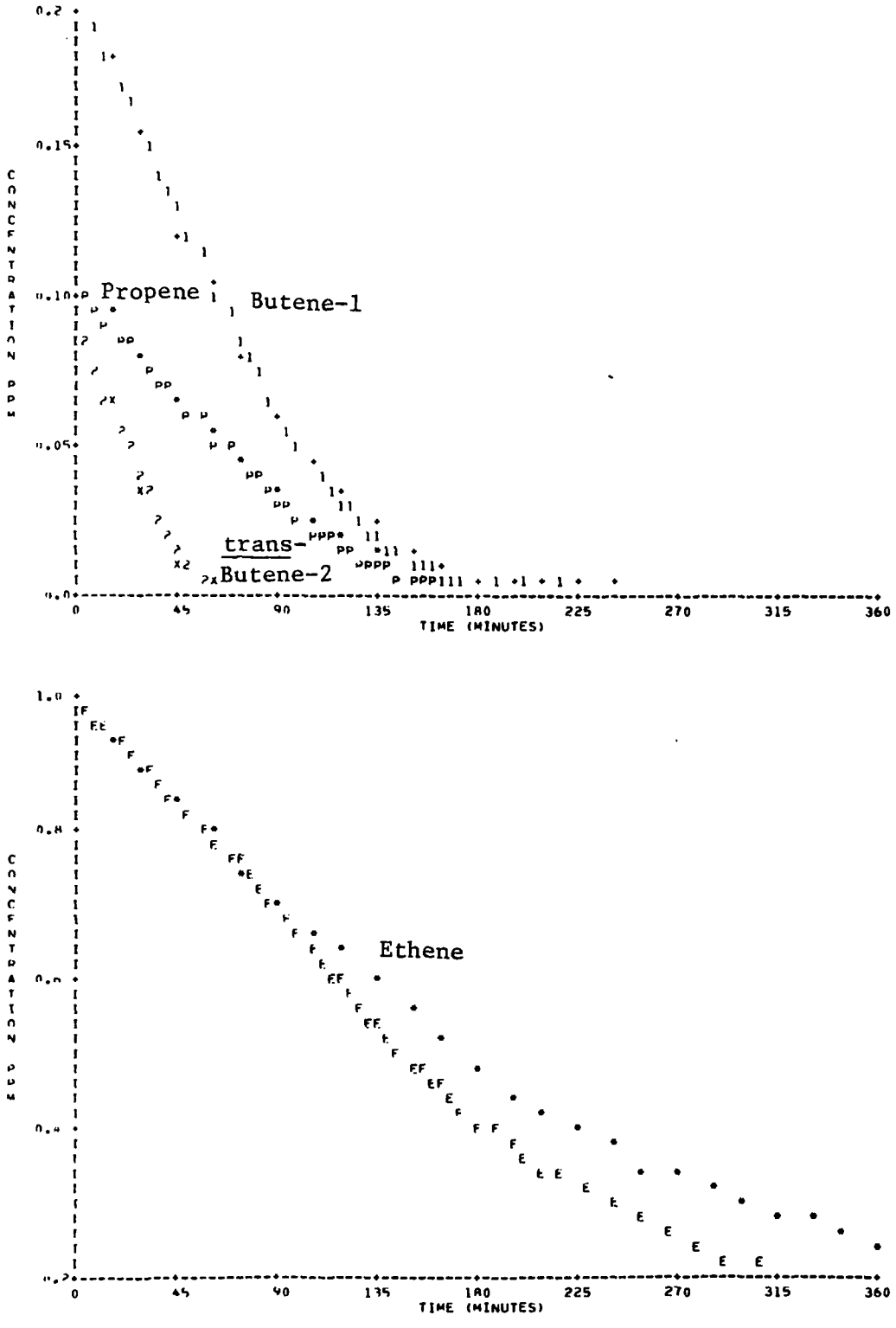

Figure A-36. Simulation of SAPRC EC-152.

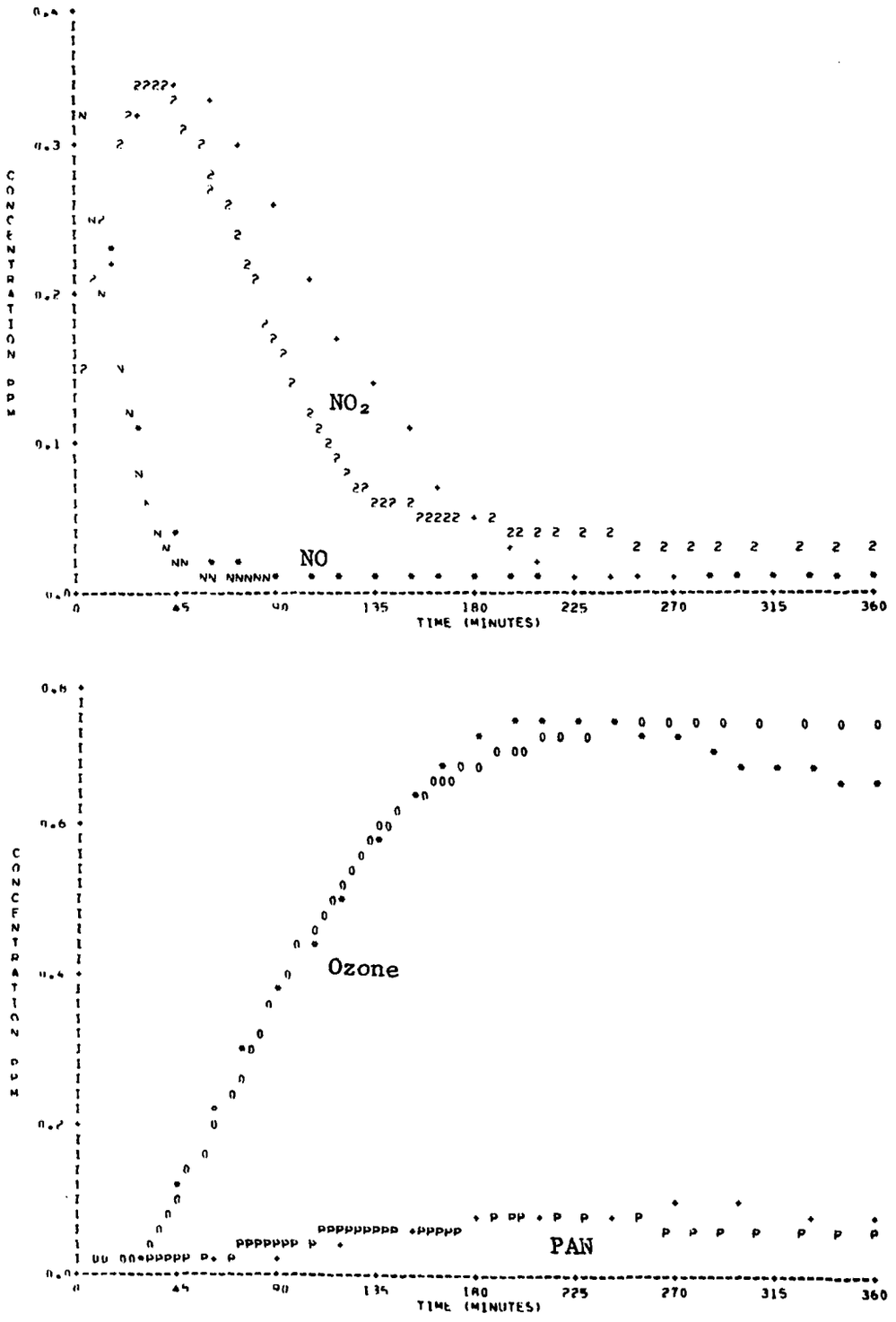

Figure A-36. Simulation of SAPRC EC-152 (Continued).

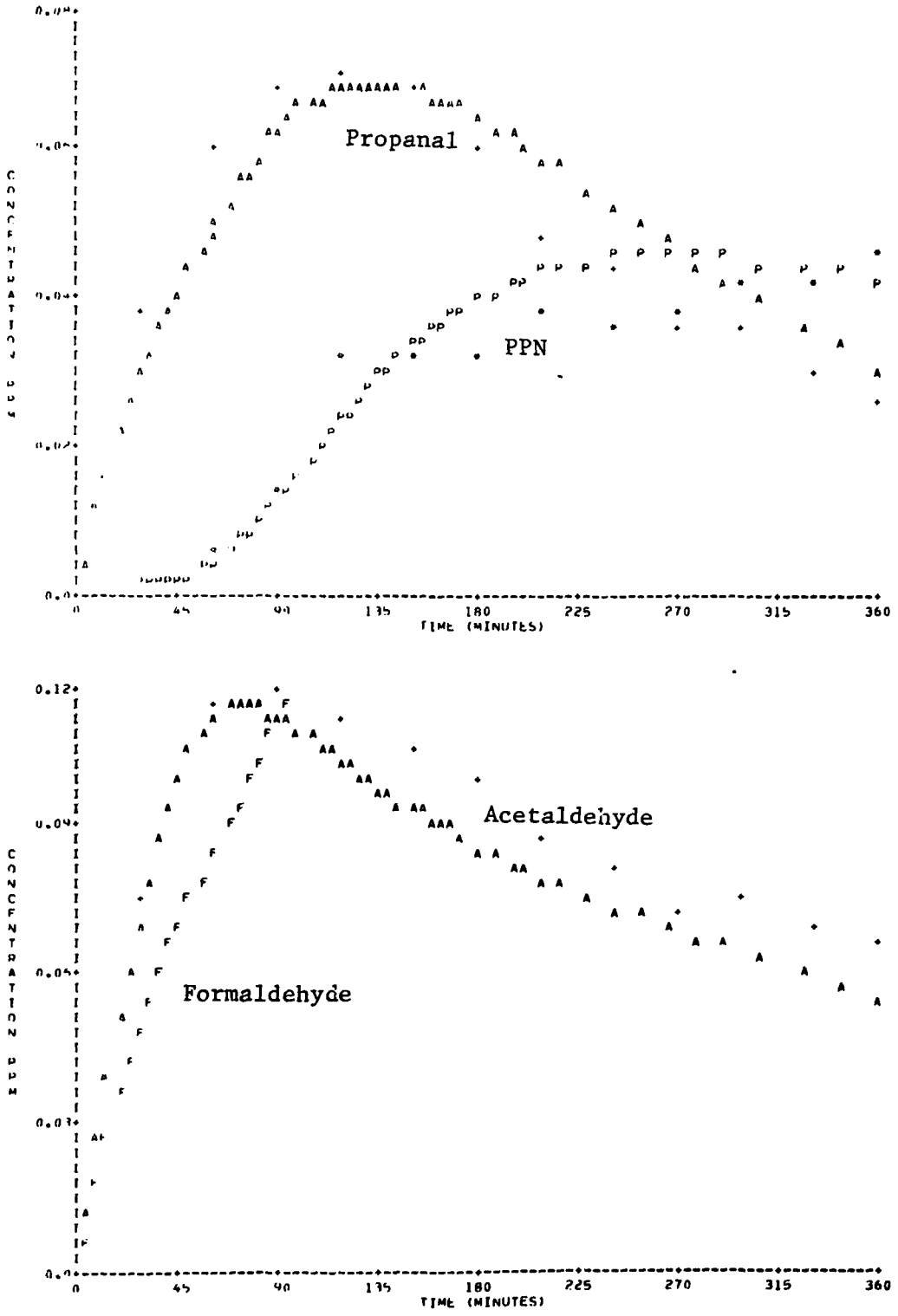

Figure A-36. Simulation of SAPRC EC-152 (Concluded).

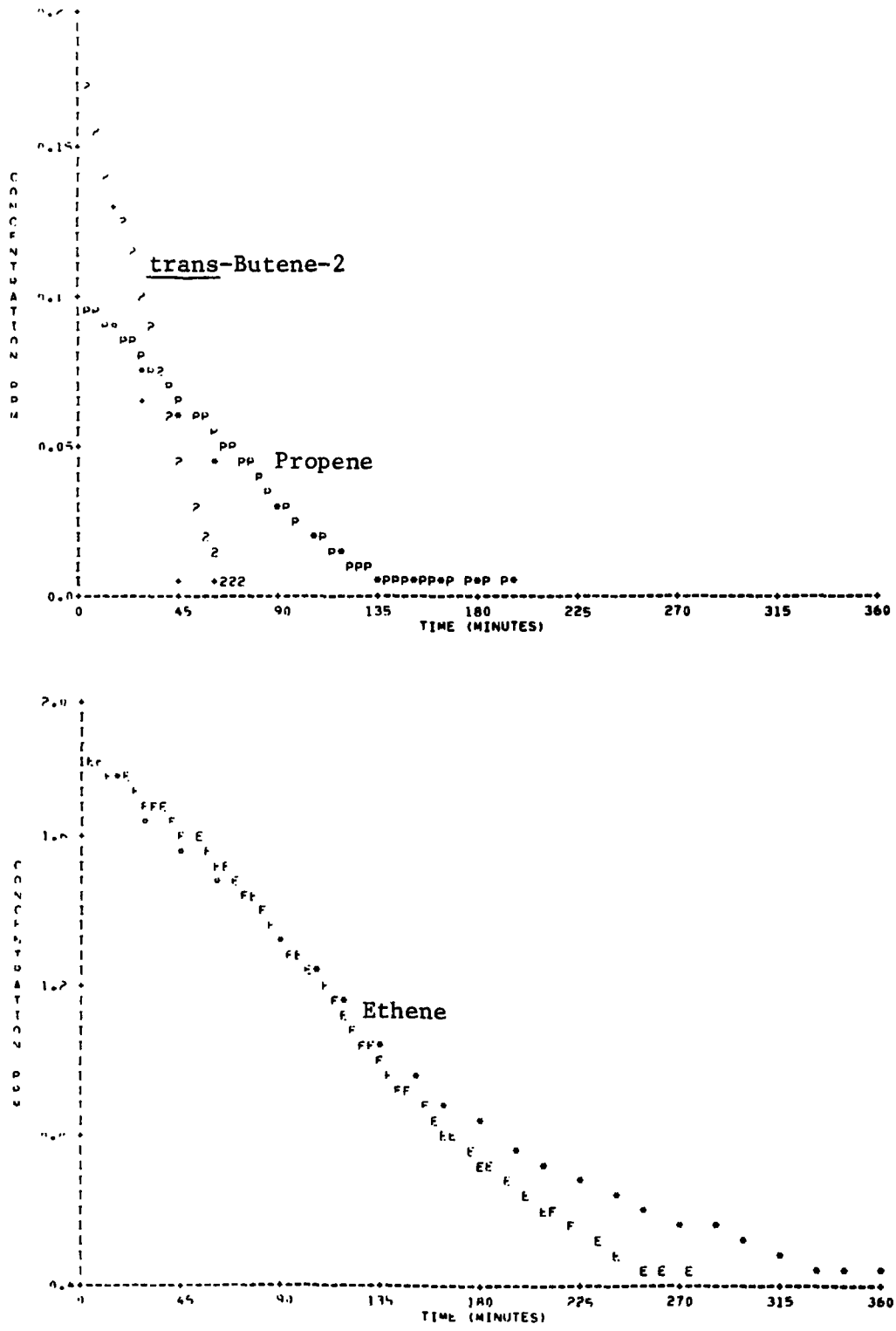

Figure A-37. Simulation of SAPRC EC-153.

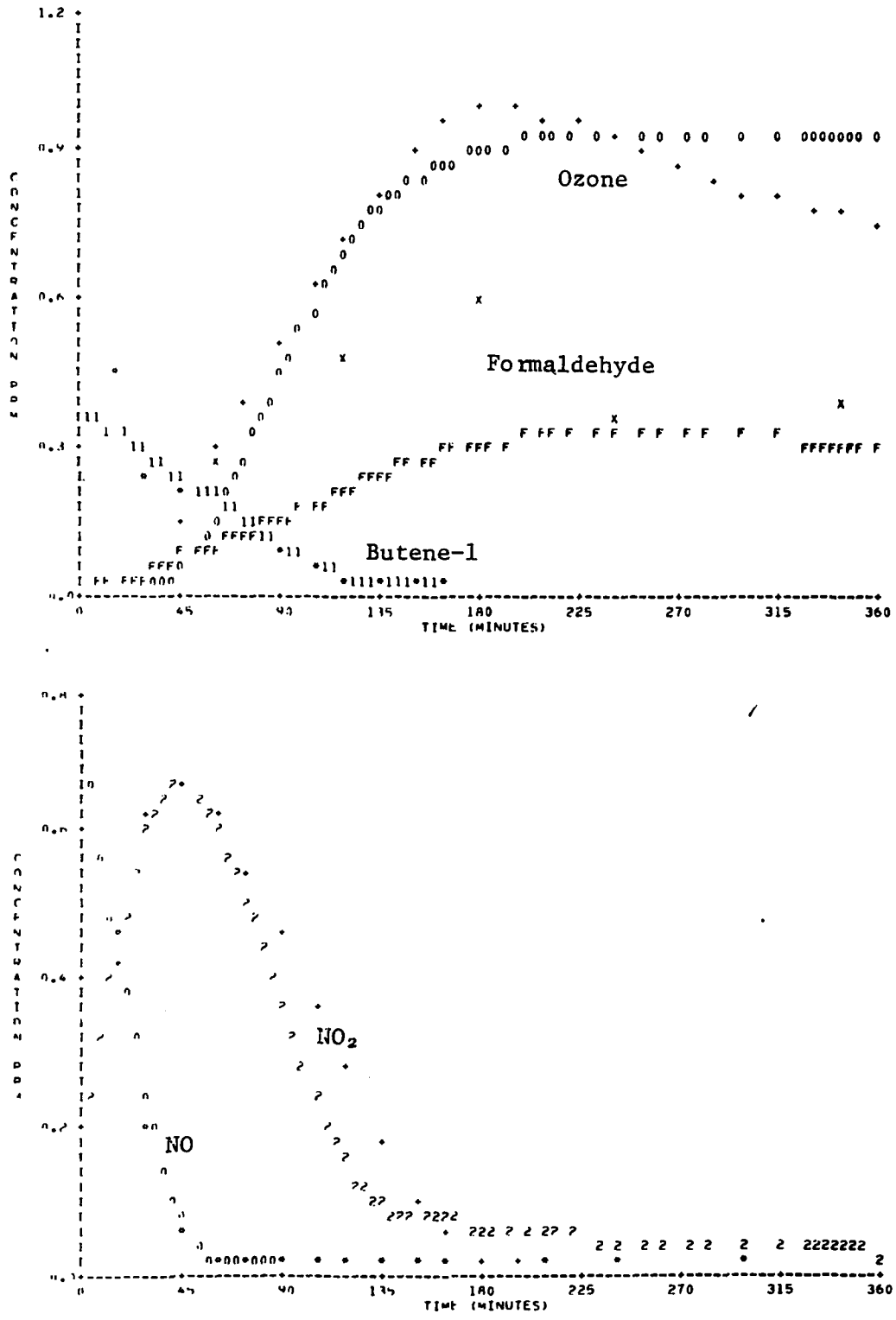

Figure A-37. Simulation of SAPRC EC-153 (Continued).

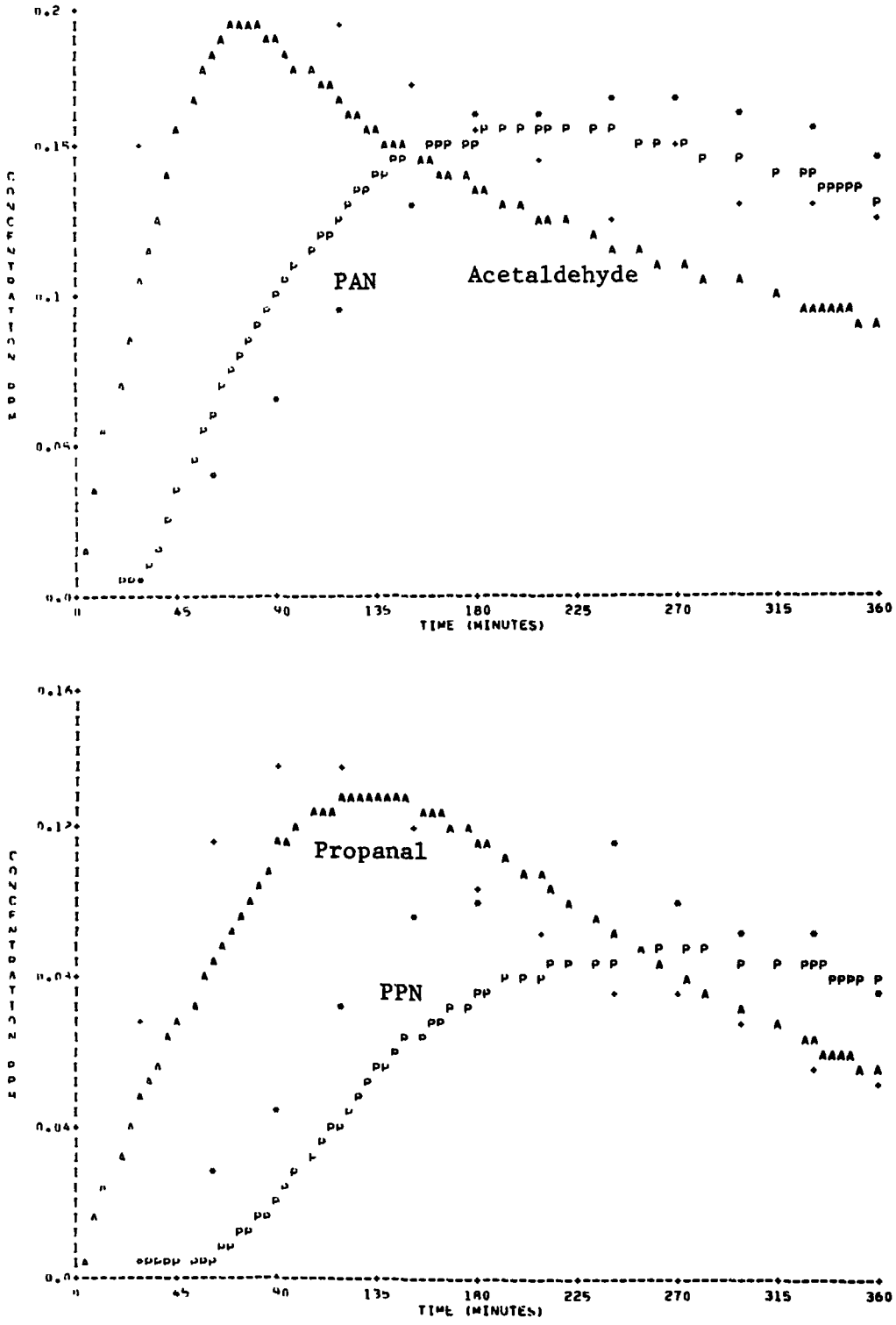

Figure A-37. Simulation of SAPRC EC-153 (Concluded).

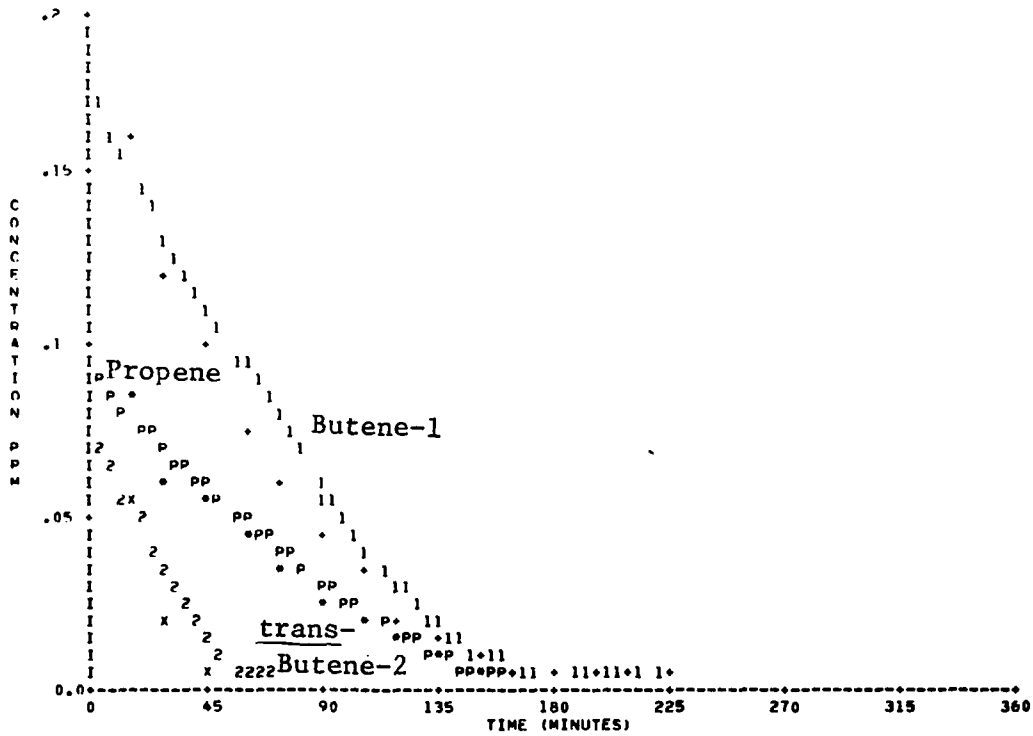

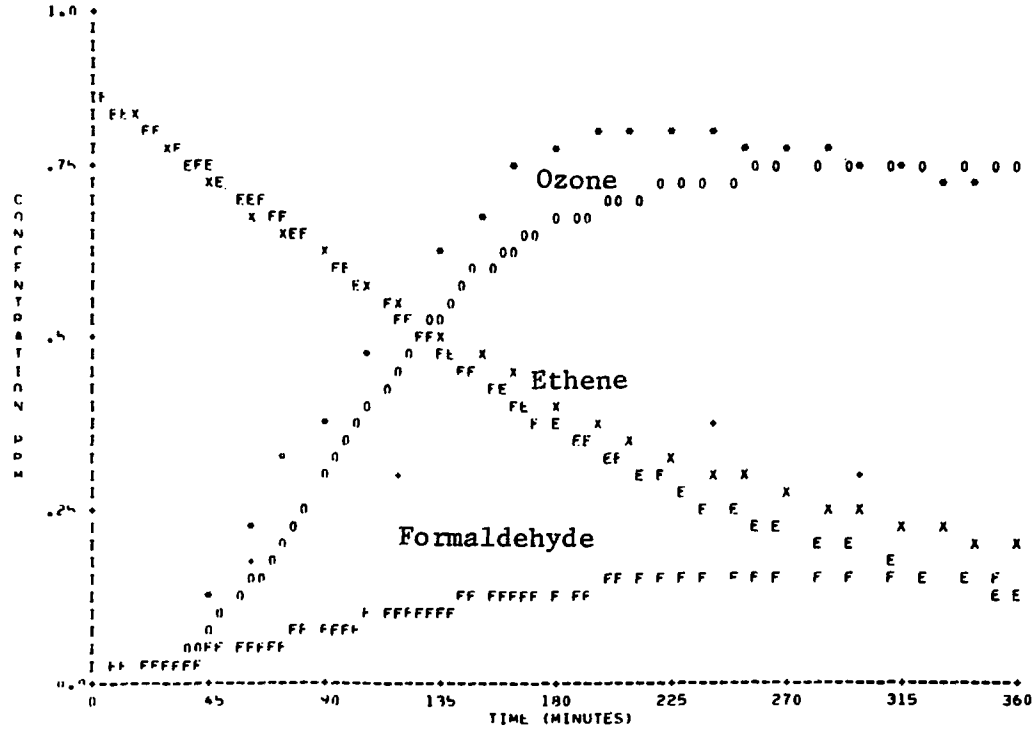

Figure A-38. Simulation of SAPRC EC-161.

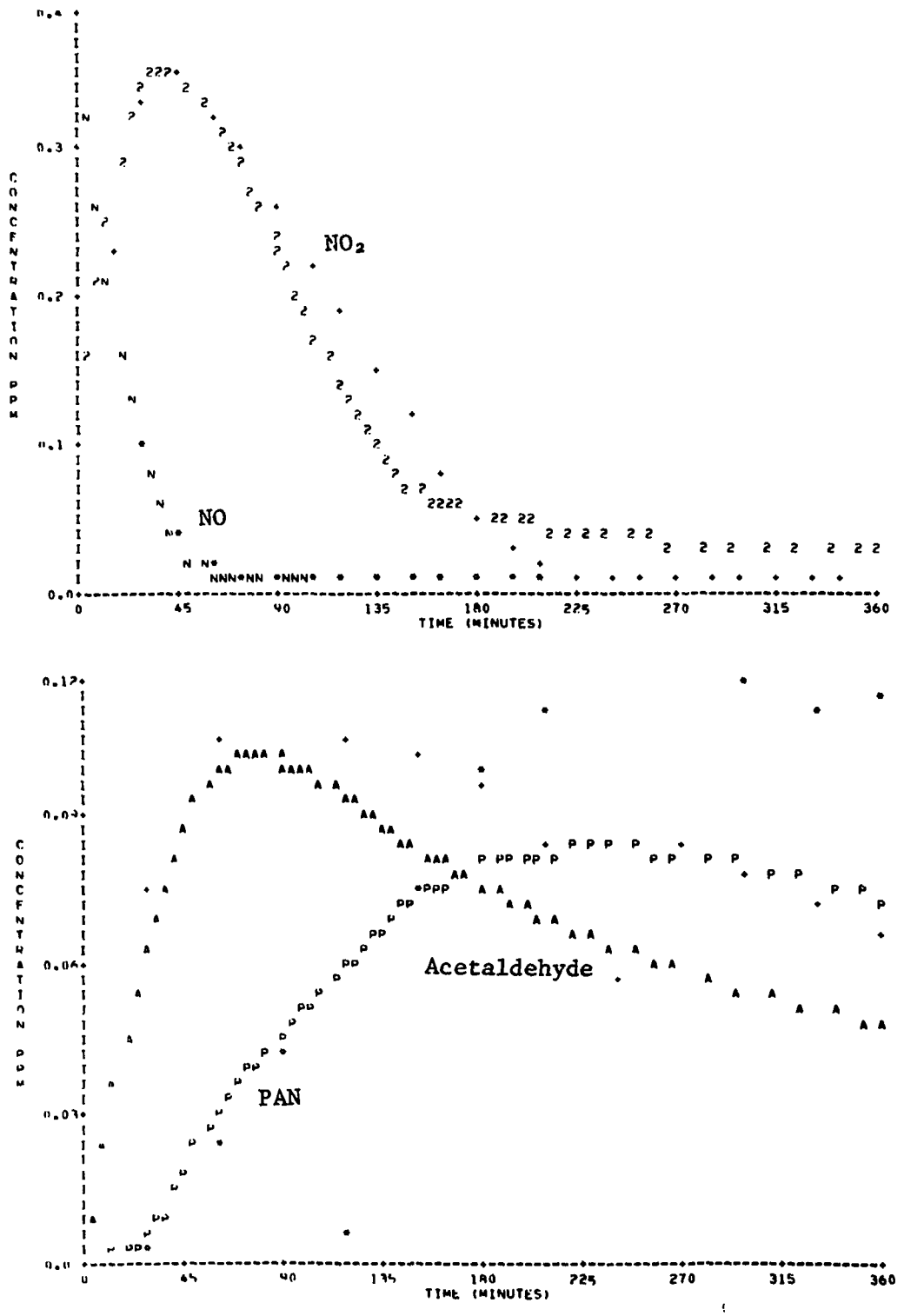

Figure A-38. Simulation of SAPRC EC-161 (Continued).

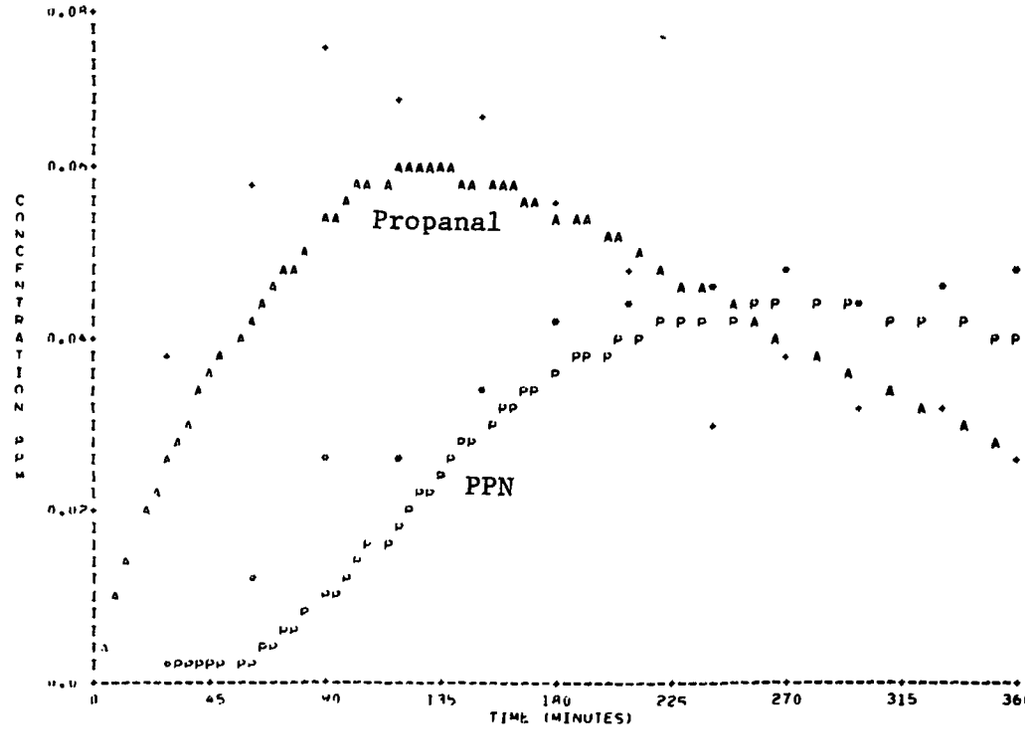

Figure A-38. Simulation of SAPRC EC-161 (Concluded).

APPENDIX B

Simulations of SAPRC Alkane and Alkane-Propene Mixture Data

TABLE B-1. INITIAL CONDITIONS FOR ALKANE CHAMBER RUNS

E.C. Number	INITIAL CONCENTRATION (ppm)					
	Butane	NO	NO_2	HNO_2	HCHO	CH_3CHO
39	2.200	0.547	0.060	0	0.001	0.001
41	4.030	0.524	0.063	0.01	0	0.002
42	0.385	0.542	0.059	0.005	0.007	0.002
43	0.380	0.126	0.013	0	0.001	0.005
44	3.920	1.140	0.132	0	0.02	0.001
45	1.940	0.552	0.062	0	0.129*	0.002
46	3.990	0.527	0.061	0	0.013	0.002
47	3.900	0.534	0.062	0	0.0	0.002
48	1.940	0.535	0.054	0	0.0	0.245*
49	4.120	0.553	0.059	0	0.0	0.005
162	2.050	0.383	0.122	0.03	0.02	0.014
163	1.978	0.377	0.113	0.03	0.0	0.526*
168	1.961	0.327	0.166	0.01	0.101*	0.029
178	1.961	0.087	0.011	0.015	0.0	0.001

* Initial aldehyde added.

	2,3-Dimethyl-butane					
165	1.885	0.088	0.011	0	0	0
169	0.740	0.127	0.064	0	0	0
171	0.586	0.086	0.013	0	0	0.002

TABLE B-2. INITIAL CONDITIONS FOR n-BUTANE-PROPENE MIXTURE RUNS

E.C. Number	INITIAL CONCENTRATION (ppm)						
	Butane	Propene	NO	NO_2	HNO_2	HCHO	CH_3CHO
97	2.040	0.500	0.397	0.088	0.01	0.004	0.001
99	2.000	0.400	0.407	0.090	0.01	0	0.001
106	2.000	0.402	0.401	0.102	0.01	0.012	0.001
113	2.040	0.410	0.091	0.020	0.02	0	0
114	3.660	0.766	0.794	0.204	0.01	0.008	0
115	2.940	0.310	0.402	0.104	0.01	0.012	0
116	4.000	0.824	0.391	0.104	0.01	0.005	0

TABLE B-3. n-BUTANE MECHANISM

No.		Rate Constants[a]
1	$CH_3CH_2CH_2CH_3 + OH \xrightarrow{O_2} CH_3CH_2CH_2CH_2\dot{O}_2 + H_2O$	6.3×10^2
2	$CH_3CH_2CH_2CH_3 + OH \xrightarrow{O_2} CH_3CH_2CH(\dot{O}_2)CH_3 + H_2O$	3.8×10^3
3	$CH_3CH_2CH_2CH_3 + O(^3P) \xrightarrow{O_2} CH_3CH_2CH_2CH_2\dot{O}_2 + OH$	6.4×10^1
4	$CH_3CH_2CH_2CH_2\dot{O}_2 + NO \rightarrow CH_3CH_2CH_2CH_2\dot{O} + NO_2$	1.0×10^4
5	$CH_3CH_2CH(\dot{O}_2)CH_3 + NO \rightarrow CH_3CH_2CH(\dot{O})CH_3 + NO_2$	1.0×10^4
6	$CH_3CH_2CH_2C(O)\dot{O}_2 + NO \xrightarrow{O_2} CH_3CH_2\dot{O}_2 + NO_2 + CO_2$	2.0×10^3
7	$CH_3CH_2C(O)\dot{O}_2 + NO \xrightarrow{O_2} CH_3CH_2\dot{O}_2 + NO_2 + CO_2$	2.0×10^3
8	$CH_3C(O)\dot{O}_2 + NO \xrightarrow{O_2} CH_3\dot{O}_2 + NO_2 + CO_2$	2.0×10^3
9	$CH_3CH_2(\dot{O}_2)C(O)CH_3 + NO \xrightarrow{O_2} NO_2 + HO_2 + CH_3C(O)C(O)CH_3$	2.0×10^3
10	$HOCH_2CH_2CH_2CH_2\dot{O}_2 + NO \rightarrow HOCH_2CH_2CH_2CH_2\dot{O} + NO_2$	1.0×10^4
11	$CH_3CH_2CH_2\dot{O}_2 + NO \rightarrow CH_3CH_2CH_2\dot{O} + NO_2$	1.0×10^4
12	$CH_3CH_2\dot{O}_2 + NO \rightarrow CH_3CH_2\dot{O} + NO_2$	1.0×10^4
13	$CH_3\dot{O}_2 + NO \rightarrow CH_3\dot{O} + NO$	1.0×10^4
14	$CH_3CH_2CH(\dot{O})CH_3 \xrightarrow{O_2} CH_3CH_2\dot{O}_2 + CH_3CHO$	$^*2.9 \times 10^5$
15	$CH_3CH_2CH_2CH_2\dot{O} \xrightarrow{O_2} CH_2(\dot{O}_2)CH_2CH_2CH_2OH$	$^*3.7 \times 10^7$
16	$CH_3CH_2CH(\dot{O})CH_3 + O_2 \rightarrow CH_3CH_2CH(O)CH_3 + HO_2$	$^*8.8 \times 10^3$
17	$CH_3CH_2CH_2CH_2\dot{O} + O_2 \rightarrow CH_3CH_2CH_2CHO + HO_2$	$^*1.3 \times 10^3$
18	$CH_3CH_2CH_2\dot{O} + O_2 \rightarrow CH_3CH_2CHO + HO_2$	$^*1.3 \times 10^3$
19	$CH_3CH_2\dot{O} + O_2 \rightarrow CH_3CHO + HO_2$	$^*1.3 \times 10^3$
20	$CH_3\dot{O} + O_2 \rightarrow CH_2O + HO_2$	$^*1.9 \times 10^3$
21	$CH_2O + h\nu \xrightarrow{2O_2} HO_2 + HO_2 + CO$	
22	$CH_2O + h\nu \rightarrow H_2 + CO$	
23	$CH_3CHO + h\nu \xrightarrow{2O_2} CH_3\dot{O}_2 + HO_2 + CO$	
24	$CH_3CH_2CHO + h\nu \xrightarrow{2O_2} CH_3CH_2\dot{O}_2 + HO_2 + CO$	
25	$CH_3CH_2CH_2CHO + h\nu \xrightarrow{2O_2} CH_3CH_2CH_2\dot{O}_2 + HO_2 + CO$	
26	$CH_3CH_2CH_2CHO + h\nu \rightarrow CH_3CHO + C_2H_4$	
27	$CH_3CH_2C(O)CH_3 + h\nu \xrightarrow{2O_2} CH_3C(O)\dot{O}_2 + CH_3CH_2\dot{O}_2$	
28	$CH_2O + OH \xrightarrow{O_2} CO + HO_2 + H_2O$	2.0×10^4
29	$CH_3CHO + OH \xrightarrow{O_2} CH_3C(O)\dot{O}_2 + H_2O$	2.0×10^4
30	$CH_3CH_2CHO + OH \xrightarrow{O_2} CH_3CH_2C(O)\dot{O}_2 + H_2O$	2.0×10^4
31	$CH_3CH_2CH_2CHO + OH \xrightarrow{O_2} CH_3CH_2CH_2C(O)\dot{O}_2 + H_2O$	2.0×10^4
32	$CH_3CH_2C(O)CH_3 + OH \xrightarrow{O_2} CH_3CH(\dot{O}_2)C(O)CH_3 + H_2O$	5.2×10^3
33	$CH_3CH_2CH_2C(O)\dot{O}_2 + HO_2 \rightarrow CH_3CH_2CH_2C(O)OOH + O_2$	4.0×10^3
34	$CH_3CH_2C(O)\dot{O}_2 + HO_2 \rightarrow CH_3CH_2C(O)OOH + O_2$	4.0×10^3
35	$CH_3C(O)\dot{O}_2 + HO_2 \rightarrow CH_3C(O)OOH + O_2$	4.0×10^3
36	$HOCH_2CH_2CH_2CH_2\dot{O}_2 + HO_2 \rightarrow HOCH_2CH_2CH_2CH_2OOH + O_2$	2.0×10^3
37	$CH_3CH(\dot{O}_2)C(O)CH_3 + HO_2 \rightarrow CH_3CH(OOH)C(O)CH_3 + O_2$	2.0×10^3
38	$CH_3CH_2CH(\dot{O}_2)CH_3 + HO_2 \rightarrow CH_3CH_2CH(CH_3)OOH + O_2$	2.0×10^3
39	$CH_3CH_2CH_2CH_2\dot{O}_2 + HO_2 \rightarrow CH_3CH_2CH_2CH_2OOH + O_2$	2.0×10^3
40	$CH_3CH_2CH_2\dot{O}_2 + HO_2 \rightarrow CH_3CH_2CH_2OOH + O_2$	2.0×10^3
41	$CH_3CH_2\dot{O}_2 + HO_2 \rightarrow CH_3CH_2OOH + O_2$	2.0×10^3
42	$CH_3\dot{O}_2 + HO_2 \rightarrow CH_3OOH + O_2$	2.0×10^3
43	$CH_3CH_2CH_2C(O)\dot{O}_2 + NO_2 \rightarrow CH_3CH_2CH_2C(O)O_2NO_2$	1.5×10^3
44	$CH_3CH_2C(O)\dot{O}_2 + NO_2 \rightarrow CH_3CH_2C(O)O_2NO_2$	1.5×10^3

45	$CH_3C(O)\dot{O}_2$	→ $CH_3C(O)O_2NO_2$	1.5×10^3
46	$CH_3CH_2CH_2C(O)O_2NO_2$	→ $CH_3CH_2CH_2C(O)\dot{O}_2 + NO_2$	$^*4.1 \times 10^{-2}$
47	$CH_3CH_2C(O)O_2NO_2$	→ $CH_3CH_2C(O)\dot{O}_2 + NO_2$	$^*4.1 \times 10^{-2}$
48	$CH_3C(O)O_2NO_2$	→ $CH_3C(O)\dot{O}_2 + NO_2$	$^*4.1 \times 10^{-2}$
49	$CH_3\dot{O} + NO_2$	→ CH_3ONO_2	1.5×10^4
50	$CH_3\dot{O} + NO_2$	→ $CH_2O + HNO_2$	4.4×10^3
51	$CH_3CH_2\dot{O} + NO_2$	→ $CH_3CH_2ONO_2$	1.5×10^4
52	$CH_3CH_2\dot{O} + NO_2$	→ $CH_3CHO + HNO_2$	2.9×10^3
53	$CH_3CH_2CH_2\dot{O} + NO_2$	→ $CH_3CH_2CH_2ONO_2$	1.5×10^4
54	$CH_3CH_2CH_2\dot{O} + NO_2$	→ $CH_3CH_2CHO + HNO_2$	2.9×10^3
55	$CH_3CH_2CH_2CH_2\dot{O} + NO_2$	→ $CH_3CH_2CH_2CH_2ONO_2$	1.5×10^4
56	$CH_3CH_2CH_2CH_2\dot{O} + NO_2$	→ $CH_3CH_2CH_2CHO + HNO_2$	1.5×10^3
57	$CH_3CH_2CH(\dot{O})CH_3 + NO_2$	→ $CH_3CH_2CH(ONO_2)CH_3$	1.5×10^4
58	$CH_3CH_2CH(\dot{O})CH_3 + NO_2$	→ $CH_3CH_2C(O)CH_3 + HNO_2$	1.5×10^4
59	$HO_2 + NO_2$	→ HO_2NO_2	3.0×10^3
60	HO_2NO_2	→ $HO_2 + NO_2$	$^*2.0 \times 10^{-1}$
61	$CH_3\dot{O}_2 + NO_2$	→ $CH_3O_2NO_2$	6.0×10^3
62	$CH_3O_2NO_2$	→ $CH_3\dot{O}_2 + NO_2$	$^*1.0$
63	$CH_3CH_2\dot{O}_2 + NO_2$	→ $CH_3CH_2O_2NO_2$	6.0×10^3
64	$CH_3CH_2O_2NO_2$	→ $CH_3CH_2\dot{O}_2 + NO_2$	$^*1.0$
65	$CH_3CH_2CH_2\dot{O}_2 + NO_2$	→ $CH_3CH_2CH_2O_2NO_2$	6.0×10^3
66	$CH_3CH_2CH_2O_2NO_2$	→ $CH_3CH_2CH_2\dot{O}_2 + NO_2$	$^*1.0$
67	$CH_3CH_2CH_2CH_2\dot{O}_2 + NO_2$	→ $CH_3CH_2CH_2CH_2O_2NO_2$	6.0×10^3
68	$CH_3CH_2CH_2CH_2O_2NO_2$	→ $CH_3CH_2CH_2CH_2\dot{O}_2 + NO_2$	$^*1.0$
69	$CH_3CH_2CH(O_2)CH_3 + NO_2$	→ $CH_3CH_2CH(O_2NO_2)CH_3$	6.0×10^3
70	$CH_3CH_2CH(O_2NO_2)CH_3$	→ $CH_3CH_2CH(\dot{O}_2)CH_3 + NO_2$	$^*1.0$
71	$CH_3CH_2CH(\dot{O}_2)CH_3 + CH_3CH_2CH(\dot{O}_2)CH_3$	→ $CH_3CH_2CH(\dot{O})CH_3 + CH_3CH_2CH(\dot{O})CH_3 + O_2$	2.0×10^3
72	$CH_3CH_2CH_2CH_2\dot{O}_2 + CH_3CH_2CH_2CH_2\dot{O}_2$	→ $CH_3CH_2CH_2CH_2\dot{O} + CH_3CH_2CH_2CH_2\dot{O} + O_2$	2.0×10^2
73	$CH_3CH_2CH_2\dot{O}_2 + CH_3CH_2CH_2\dot{O}_2$	→ $CH_3CH_2CH_2\dot{O} + CH_3CH_2CH_2\dot{O} + O_2$	2.0×10^2
74	$CH_3CH_2\dot{O}_2 + CH_3CH_2\dot{O}_2$	→ $CH_3CH_2\dot{O} + CH_3CH_2\dot{O} + O_2$	2.0×10^2
75	$CH_3\dot{O}_2 + CH_3O_2$	→ $CH_3\dot{O} + CH_3\dot{O} + O_2$	2.0×10^2
76	$CH_3C(O)\dot{O}_2 + CH_3C(O)\dot{O}_2$	→ $CH_3\dot{O}_2 + CH_3\dot{O}_2 + 2CO_2 + O_2$	2.4×10^3
77	$CH_2(\dot{O})CH_2CH_2CH_2OH$	$\xrightarrow{O_2}$ $CH_2(OH)CH_2CH_2CH(OH)\dot{O}_2$	$^*1.9 \times 10^0$
78	$CH_2(OH)CH_2CH_2CH(OH)\dot{O}_2 + NO$	→ $CH_2(OH)CH_2CH_2CH(OH)\dot{O} + NO_2$	2.0×10^4
79	$CH_2(OH)CH_2CH_2CH(OH)\dot{O}_2 + HO_2$	→ stable product	4.0×10^3
80	$CH_2(OH)CH_2CH_2CH(OH)\dot{O}$	$\xrightarrow{O_2}$ $CH(OH)(\dot{O}_2)CH_2CH_2CH(OH)_2$	$^*1.9 \times 10^0$
81	$CH(OH)(\dot{O}_2)CH_2CH_2CH_2(OH)_2 + NO$	→ $CH(OH)(\dot{O})CH_2CH_2CH(OH)_2$	2.0×10^4
82	$CH(OH)(\dot{O}_2)CH_2CH_2CH_2(OH)_2 + HO_2$	→ stable product	4.0×10^3
83	$CH(OH)(\dot{O})CH_2CH_2CH(OH)_2$	$\xrightarrow{O_2}$ $CH(OH)_2CH_2CH_2C(OH)_2\dot{O}_2$	$^*2.2 \times 10^0$
84	$CH(OH)_2CH_2CH_2C(OH)_2\dot{O}_2 + NO$	→ $CH(OH)_2CH_2CH_2C(OH)\dot{O}$	2.0×10^4
85	$CH(OH)_2CH_2CH_2C(OH)_2\dot{O}_2 + HO_2$	→ stable product	4.0×10^3
86	$CH(OH)_2CH_2CH_2C(OH)_2\dot{O}$	$\xrightarrow{O_2}$ $C(OH_2)(\dot{O}_2)CH_2CH_2C(OH)_3$	$^*2.2 \times 10^0$
87	$C(OH)_2(\dot{O}_2)CH_2CH_2C(OH)_3 + NO$	→ $C(OH_2)(\dot{O})CH_2CH_2C(OH)_3$	2.0×10^4
88	$C(OH)_2(\dot{O}_2)CH_2CH_2C(OH)_3 + HO_2$	→ stable products	4.0×10^3

[a]Units ppm^{-1} min^{-1}, except * units min^{-1} .

TABLE B-4. 2,3-DIMETHYLBUTANE MECHANISM

No.		Rate Constant[a]
1	$CH_3CH(CH_3)CH(CH_3)CH_3 + OH \xrightarrow{O_2} CH_3CH(CH_3)CH(CH_3)CH_2\dot{O}_2 + H_2O$	1.2×10^3
2	$CH_3CH(CH_3)CH(CH_3)CH_3 + OH \xrightarrow{O_2} CH_3CH(CH_3)C(CH_3)(\dot{O}_2)CH_3 + H_2O$	8.5×10^3
3	$CH_3CH(CH_3)CH(CH_3)CH_3 + O(^3P) \xrightarrow{O_2} CH_3CH(CH_3)C(CH_3)(\dot{O}_2)CH_3 + OH$	3.4×10^2
4	$CH_3CH(CH_3)CH(CH_3)CH_2\dot{O}_2 + NO \rightarrow CH_3CH(CH_3)CH(CH_3)CH_2\dot{O} + NO_2$	1.0×10^4
5	$CH_3CH(CH_3)C(CH_3)(\dot{O}_2)CH_3 + NO \rightarrow CH_3CH(CH_3)C(CH_3)(\dot{O})CH_3 + NO_2$	1.0×10^4
6	$CH_3CH(\dot{O}_2)CH_3 + NO \rightarrow CH_3CH(\dot{O})CH_3 + NO_2$	1.0×10^4
7	$CH_3CH_2\dot{O}_2 + NO \rightarrow CH_3CH_2\dot{O} + NO_2$	1.0×10^4
8	$CH_3C(O)\dot{O}_2 + NO \xrightarrow{O_2} CH_3\dot{O}_2 + NO_2 + CO_2$	2.0×10^3
9	$CH_3CH(CH_3)CH(CH_3)\dot{O}_2 + NO \rightarrow CH_3CH(CH_3)CH(CH_3)\dot{O} + NO_2$	1.0×10^4
10	$CH_3CH(CH_3)CH(CH_3)CH_2\dot{O}_2 + O_2 \rightarrow CH_3CH(CH_3)CH(CH_2)CHO + HO_2$	1.8×10^4
11	$CH_3CH(CH_3)C(CH_3)(O)CH_3 \xrightarrow{O_2} CH_3C(O)CH_3 + CH_3CH(\dot{O}_2)CH_3$	3.8×10^7
12	$CH_3CH(\dot{O})CH_3 + O_2 \rightarrow CH_3C(O)CH_3 + HO_2$	6.7×10^4
13	$CH_3CH(CH_3)CH(CH_3)CHO + h\nu \rightarrow CH_3CH_2CHO + CH_2CHCH_3$	
14	$CH_3CH(CH_3)CH(CH_3)CHO + h\nu \xrightarrow{O_2} CH_3CH(CH_3)CH(CH_3)\dot{O}_2HO_2 + CO$	
15	$CH_3CH_2CHO + h\nu \xrightarrow{O_2} CH_3CH_2\dot{O}_2 + HO_2 + CO$	
16	$CH_3C(O)CH_3 + h\nu \xrightarrow{2O_2} CH_3\dot{O}_2 + CH_3C(O)\dot{O}_2$	
17	$CH_3CH(CH_3)CH(CH_3)CH_2\dot{O}_2 + HO_2 \rightarrow CH_3CH(CH_3)CH(CH_3)CH_2OOH + O_2$	2.0×10^3
18	$CH_3CH(CH_3)C(CH_3)(\dot{O}_2)CH_3 + HO_2 \rightarrow CH_3CH(CH_3)C(CH_3)(OOH)CH_3 + O_2$	2.0×10^3
19	$CH_3CH(\dot{O}_2)CH_3 + HO_2 \rightarrow CH_3CH(OOH)CH_3 + O_2$	2.0×10^3
20	$CH_3CH_2\dot{O}_2 + HO_2 \rightarrow CH_3CH_2OOH + O_2$	2.0×10^3
21	$CH_3C(O)O_2 + HO_2 \rightarrow CH_3C(O)OOH + O_2$	4.0×10^3
22	$CH_3CH(CH_3)CH(CH_3)\dot{O}_2 + HO_2 \rightarrow CH_3CH(CH_3)CH(CH_3)OOH + O_2$	2.0×10^3
23	$CH_3CH(CH_3)C(CH_3)(\dot{O})CH_3 + NO_2 \rightarrow CH_3CH(CH_3)C(CH_3)(ONO_2)CH_3$	2.0×10^4
24	$CH_3CH(CH_3)CH(CH_3)CH_2\dot{O} + NO_2 \rightarrow CH_3CH(CH_3)CH(CH_3)CH_2ONO_2$	2.0×10^4
25	$CH_3CH(CH_3)CH(CH_3)CH_2\dot{O} + NO_2 \rightarrow CH_3CH(CH_3)CH(CH_3)CHO + HNO_2$	2.0×10^3
26	$CH_3CH(\dot{O})CH_3 + NO_2 \rightarrow CH_3CH(ONO_2)CH_3$	2.0×10^4
27	$CH_3CH(\dot{O})CH_3 + NO_2 \rightarrow CH_3COCH_3 + HNO_2$	2.0×10^4
28	$CH_3C(O)\dot{O}_2 + NO_2 \rightarrow CH_3C(O)O_2NO_2$	1.5×10^3
29	$CH_3C(O)O_2NO_2 \rightarrow CH_3C(O)\dot{O}_2 + NO_2$	$^*4.0 \times 10^{-2}$
30	$HO_2 + NO_2 \rightarrow HO_2NO_2$	3.0×10^3
31	$HO_2NO_2 \rightarrow HO_2 + NO_2$	$^*2.0 \times 10^{-1}$
32	$CH_3CH(\dot{O}_2)CH_3 + NO_2 \rightarrow CH_3CH(O_2NO_2)CH_3$	6.0×10^3
33	$CH_3CH(O_2NO_2)CH_3 \rightarrow CH_3CH(\dot{O}_2)CH_3 + NO_2$	$^*1.0$
34	$CH_3CH(CH_3)C(CH_3)(\dot{O}_2)CH_3 + NO_2 \rightarrow CH_3CH(CH_3)C(CH_3)(O_2NO_2)CH_3$	6.0×10^3
35	$CH_3CH(CH_3)C(CH_3)(O_2NO_2)CH_3 \rightarrow CH_3CH(CH_3)C(CH_3)(\dot{O}_2)CH_3 + NO_2$	$^*1.0$

continued . . .

2,3-Dimethylbutane Mechanism (concluded)

36	$CH_3CH(CH_3)CH(CH_3)CH_2\dot{O}_2 + NO_2$	→	$CH_3CH(CH_3)CH(CH_3)CH_2O_2NO_2$	6.0×10^3
37	$CH_3CH(CH_3)CH(CH_3)CH_2O_2NO_2$	→	$CH_3CH(CH_3)CH(CH_3)CH_2\dot{O}_2 + NO_2$	*1.0
38	$CH_3C(O)\dot{O}_2 + CH_3C(O)\dot{O}_2$	→	$CH_3\dot{O}_2 + CH_3\dot{O}_2 + 2CO_2 + O_2$	2.4×10^9
39	$CH_3CH(\dot{O}_2)CH_3 + CH_3CH(\dot{O}_2)CH_3$	→	$CH_3CH(\dot{O})CH_3 + CH_3CH(\dot{O})CH_3 + O_2$	2.0×10^2
40	$2CH_3CH(CH_3)CH(CH_3)CH_2\dot{O}_2$	→	$2CH_3CH(CH_3)CH(CH_3)CH_2\dot{O} + O_2$	2.0×10^2
41	$2CH_3CH(CH_3)C(CH_3)(\dot{O}_2)CH_3$	→	$2CH_3CH(CH_3)C(CH_3)(\dot{O})CH_3 + O_2$	2.0×10^2
42	$CH_3CH(CH_3)CH(CH_3)CH_2\dot{O}$	O_2	$CH_2(\dot{O}_2)CH(CH_3)CH(CH_3)CH_2OH$	*1.7×10^8
43	$CH_2(\dot{O}_2)CH(CH_3)CH(CH_3)CH_2OH + NO$	→	$CH_2(\dot{O})CH(CH_3)CH(CH_3)CH_2OH$	1.0×10^4
44	$CH_2(\dot{O})CH(CH_3)CH(CH_3)CH_2OH$	O_2	$CH_2(OH)CH(CH_3)CH(CH_3)CH(\dot{O}_2)OH$	*1.7×10^8
45	$CH_2(OH)CH(CH_3)CH(CH_3)CH(\dot{O}_2)OH + NO$	→	$CH_2(OH)CH(CH_3)CH(CH_3)CH(\dot{O})OH$	1.0×10^4
46	$CH_2(OH)CH(CH_3)CH(CH_3)CH(\dot{O})OH$	O_2	$CH(OH)(\dot{O}_2)CH(CH_3)CH(CH_3)CH(OH)_2$	*2.1×10^9
47	$CH(OH)(\dot{O}_2)CH(CH_3)CH(CH_3)CH(OH)_2 + NO$	→	$CH(OH)(\dot{O})CH(CH_3)CH(CH_3)CH(OH)_2$	1.0×10^4
48	$CH(OH)(\dot{O})CH(CH_3)CH(CH_3)CH(OH)_2$	O_2	$CH(OH)_2CH(CH_3)CH(CH_3)C(OH)_2(\dot{O}_2)$	*2.1×10^9
49	$CH(OH)_2CH(CH_3)CH(CH_3)C(OH)_2(\dot{O}_2) + NO$	→	$CH(OH)_2CH(CH_3)CH(CH_3)C(OH)_2(\dot{O})$	1.0×10^4
50	$CH(OH)_2CH(CH_3)CH(CH_3)C(OH)_2(\dot{O})$	O_2	$C(OH_2)(\dot{O}_2)CH(CH_3)CH(CH_3)C(OH)_3$	*2.1×10^9
51	$C(OH_2)(\dot{O}_2)CH(CH_3)CH(CH_3)C(OH)_3 + NO$	→	$C(OH_2)(\dot{O})CH(CH_3)CH(CH_3)C(OH)_3$	1.0×10^4
52	$C(OH_2)(\dot{O})CH(CH_3)CH(CH_3)C(OH)_3$	O_2	$C(OH)_3CH(CH_3)CH(CH_2\dot{O}_2)C(OH_3)$	*3.7×10^7
53	$C(OH)_3CH(CH_3)CH(CH_2\dot{O}_2)C(OH)_3 + NO$	→	$C(OH)_3CH(CH_3)CH(CH_2\dot{O})C(OH)_3$	1.0×10^4
54	$C(OH)_3CH(CH_3)CH(CH_2\dot{O})C(OH)_3$	O_2	$C(OH)_3CH(CH_2\dot{O}_2)CH(CH_2OH)C(OH)_3$	*3.7×10^7
55	$C(OH)_3CH(CH_2\dot{O}_2)CH(CH_2OH)C(OH)_3 + NO$	→	$C(OH)_3CH(CH_2\dot{O})CH(CH_2OH)C(OH)_3$	1.0×10^4
56	$C(OH)_3CH(CH_2\dot{O})CH(CH_2OH)C(OH)_3$	O_2	$C(OH)_3CH(CH_2OH)CH(CH(OH)\dot{O}_2)C(OH)_3$	*1.7×10^8
57	$C(OH)_3CH(CH_2OH)CH(CH(OH)\dot{O}_2)C(OH)_3 + NO$	→	$C(OH)_3CH(CH_2OH)CH(CH(OH)\dot{O})C(OH)_3$	1.0×10^4
58	$C(OH)_3CH(CH_2OH)CH(CH(OH)\dot{O})C(OH)_3$	O_2	$C(OH)_3CH(CH(OH)\dot{O}_2)CH(CH(OH)_2)C(OH)_3$	*1.7×10^8
59	$C(OH)_3CH(CH(OH)\dot{O}_2)CH(CH(OH)_2)C(OH)_3 + NO$	→	$C(OH)_3CH(CH(OH)\dot{O})CH(OH)_2)C(OH)_3$	1.0×10^4
60	$C(OH)_3CH(CH(OH)\dot{O})CH(OH)_2)C(OH)_3$	O_2	$C(OH)_3CH(CH(OH)_2)CH(C(OH)_2\dot{O}_2)C(OH)_3$	*2.1×10^9
61	$C(OH)_3CH(CH(OH)_2)CH(C(OH)_2\dot{O}_2)C(OH)_3 + NO$	→	$C(OH)_3CH(CH(OH)_2)CH(C(OH)_2\dot{O})C(OH)_3$	1.0×10^4
62	$C(OH)_3CH(CH(OH)_2)CH(C(OH)_2\dot{O})C(OH)_3$	O_2	$C(OH)_3CH(C(OH)_2\dot{O}_2)CH(C(OH)_3)C(OH)_3$	*2.1×10^9
63	$C(OH)_3CH(C(OH)_2\dot{O}_2)CH(C(OH)_3)C(OH)_3 + NO$	→	$C(OH)_3CH(C(OH)_2\dot{O})CH(C(OH_3))C(OH)_3$	1.0×10^4

[a]Units $ppm^{-1}\ min^{-1}$, except * min^{-1} .

TABLE B-5. PHOTOLYSIS RATE CONSTANTS FOR ALKANE CHAMBER RUNS (min^{-1})

E.C. Number	NO_2	HNO_2	H_2O_2	$O_3(^1D)$	$O_3(^3P)$	H_2CO (rad)	H_2CO (molec)	CH_3CHO	C_2H_5CHO	C_3H_7CHO (rad)	C_3H_7CHO (molec)	$C_2H_5C(O)CH_3$
						n-Butane						
39	0.24	6.6×10^{-2}	4.9×10^{-4}	1.0×10^{-3}	3.0×10^{-4}	6.3×10^{-4}	1.2×10^{-3}	3.0×10^{-4}	6.0×10^{-4}	4.6×10^{-4}	2.3×10^{-4}	1.0×10^{-4}
41	0.24	6.6×10^{-2}	4.9×10^{-4}	1.0×10^{-3}	3.0×10^{-4}	6.3×10^{-4}	1.2×10^{-3}	3.0×10^{-4}	6.0×10^{-4}	4.6×10^{-4}	2.3×10^{-4}	1.0×10^{-4}
42	0.24	6.6×10^{-2}	4.9×10^{-4}	1.0×10^{-3}	3.0×10^{-4}	6.3×10^{-4}	1.2×10^{-3}	3.0×10^{-4}	6.0×10^{-4}	4.6×10^{-4}	2.3×10^{-4}	1.0×10^{-4}
43	0.23	6.3×10^{-2}	4.7×10^{-4}	9.6×10^{-4}	2.9×10^{-4}	6.0×10^{-4}	1.2×10^{-3}	2.9×10^{-4}	5.8×10^{-4}	4.4×10^{-4}	2.2×10^{-4}	1.8×10^{-4}
44	0.23	6.3×10^{-2}	4.7×10^{-4}	9.6×10^{-4}	2.9×10^{-4}	6.0×10^{-4}	1.2×10^{-3}	2.9×10^{-4}	5.8×10^{-4}	4.4×10^{-4}	2.2×10^{-4}	1.8×10^{-4}
45	0.23	6.3×10^{-2}	4.7×10^{-4}	9.6×10^{-4}	2.9×10^{-4}	6.0×10^{-4}	1.2×10^{-3}	2.9×10^{-4}	5.8×10^{-4}	4.4×10^{-4}	2.2×10^{-4}	1.8×10^{-4}
46	0.23	6.3×10^{-2}	4.7×10^{-4}	9.6×10^{-4}	2.9×10^{-4}	6.0×10^{-4}	1.2×10^{-3}	2.9×10^{-4}	5.8×10^{-4}	4.4×10^{-4}	2.2×10^{-4}	1.8×10^{-4}
47	0.22	6.1×10^{-2}	4.5×10^{-4}	9.2×10^{-4}	2.8×10^{-4}	5.8×10^{-4}	1.1×10^{-3}	2.8×10^{-4}	5.5×10^{-4}	4.2×10^{-4}	2.1×10^{-4}	1.7×10^{-4}
48	0.22	6.1×10^{-2}	4.5×10^{-4}	9.2×10^{-4}	2.8×10^{-4}	5.8×10^{-4}	1.1×10^{-3}	2.8×10^{-4}	5.5×10^{-4}	4.2×10^{-4}	2.1×10^{-4}	1.7×10^{-4}
49	0.22	6.1×10^{-2}	4.5×10^{-4}	9.2×10^{-4}	2.8×10^{-4}	5.8×10^{-4}	1.1×10^{-3}	2.8×10^{-4}	5.5×10^{-4}	4.2×10^{-4}	2.1×10^{-4}	1.7×10^{-4}
162	0.35	9.4×10^{-2}	5.7×10^{-4}	1.2×10^{-3}	8.9×10^{-4}	4.5×10^{-4}	1.5×10^{-3}	3.3×10^{-4}	6.8×10^{-4}	5.1×10^{-4}	2.6×10^{-4}	2.1×10^{-4}
163	0.34	9.1×10^{-2}	5.5×10^{-4}	1.2×10^{-3}	8.6×10^{-4}	6.3×10^{-4}	1.5×10^{-3}	3.2×10^{-4}	6.6×10^{-4}	5.0×10^{-4}	2.5×10^{-4}	2.0×10^{-4}
168	0.33	9.8×10^{-2}	7.7×10^{-4}	1.7×10^{-3}	1.9×10^{-3}	2.1×10^{-4}	1.3×10^{-3}	6.5×10^{-4}	1.4×10^{-3}	1.0×10^{-3}	6.0×10^{-4}	4.7×10^{-4}
178	0.33	9.8×10^{-2}	7.7×10^{-4}	1.7×10^{-3}	1.9×10^{-3}	2.1×10^{-4}	1.3×10^{-3}	6.5×10^{-4}	1.4×10^{-3}	1.0×10^{-3}	6.0×10^{-4}	4.7×10^{-4}
						2,3-Dimethylbutane						
165	0.33	9.0×10^{-2}	5.4×10^{-4}	1.2×10^{-3}	3.5×10^{-4}	6.1×10^{-4}	1.5×10^{-3}	3.1×10^{-4}	6.4×10^{-4}	4.3×10^{-4}	2.5×10^{-4}	2.0×10^{-4}
169	0.33	9.8×10^{-2}	7.7×10^{-4}	1.7×10^{-3}	1.9×10^{-3}	2.1×10^{-4}	1.3×10^{-3}	6.5×10^{-4}	1.6×10^{-4}	1.4×10^{-3}	6.4×10^{-4}	4.7×10^{-4}
171	0.33	9.8×10^{-2}	7.7×10^{-4}	1.7×10^{-3}	1.9×10^{-3}	2.1×10^{-4}	1.3×10^{-3}	6.5×10^{-4}	1.6×10^{-4}	1.4×10^{-3}	6.4×10^{-4}	4.7×10^{-4}
						n-Butane/Propene						
97	0.35	1.1×10^{-1}	8.6×10^{-4}	5.0×10^{-3}	1.9×10^{-3}	1.4×10^{-3}	2.3×10^{-3}	7.5×10^{-4}	1.6×10^{-3}	1.2×10^{-3}	6.0×10^{-4}	6.1×10^{-4}
99	0.35	1.1×10^{-1}	8.6×10^{-4}	5.0×10^{-3}	1.9×10^{-3}	1.4×10^{-3}	2.3×10^{-3}	7.5×10^{-4}	1.6×10^{-3}	1.2×10^{-3}	6.0×10^{-4}	6.1×10^{-4}
106	0.35	1.1×10^{-1}	8.6×10^{-4}	5.0×10^{-3}	1.9×10^{-3}	1.4×10^{-3}	2.3×10^{-3}	7.5×10^{-4}	1.6×10^{-3}	1.2×10^{-3}	6.0×10^{-4}	6.1×10^{-4}
113	0.35	1.0×10^{-1}	8.0×10^{-4}	4.8×10^{-3}	1.7×10^{-3}	1.1×10^{-3}	2.1×10^{-3}	6.5×10^{-4}	1.4×10^{-3}	1.1×10^{-3}	5.0×10^{-4}	5.5×10^{-3}
114	0.35	1.0×10^{-1}	8.0×10^{-4}	4.8×10^{-3}	1.7×10^{-3}	1.1×10^{-3}	2.1×10^{-3}	6.5×10^{-4}	1.4×10^{-3}	1.1×10^{-3}	5.0×10^{-4}	5.5×10^{-3}
115	0.35	1.0×10^{-1}	8.0×10^{-4}	4.8×10^{-3}	1.7×10^{-3}	1.1×10^{-3}	2.1×10^{-3}	6.5×10^{-4}	1.4×10^{-3}	1.1×10^{-3}	5.0×10^{-4}	5.5×10^{-3}
116	0.35	1.0×10^{-1}	8.0×10^{-4}	4.8×10^{-3}	1.7×10^{-3}	1.1×10^{-3}	2.1×10^{-3}	6.5×10^{-4}	1.4×10^{-3}	1.1×10^{-3}	5.0×10^{-4}	5.5×10^{-3}

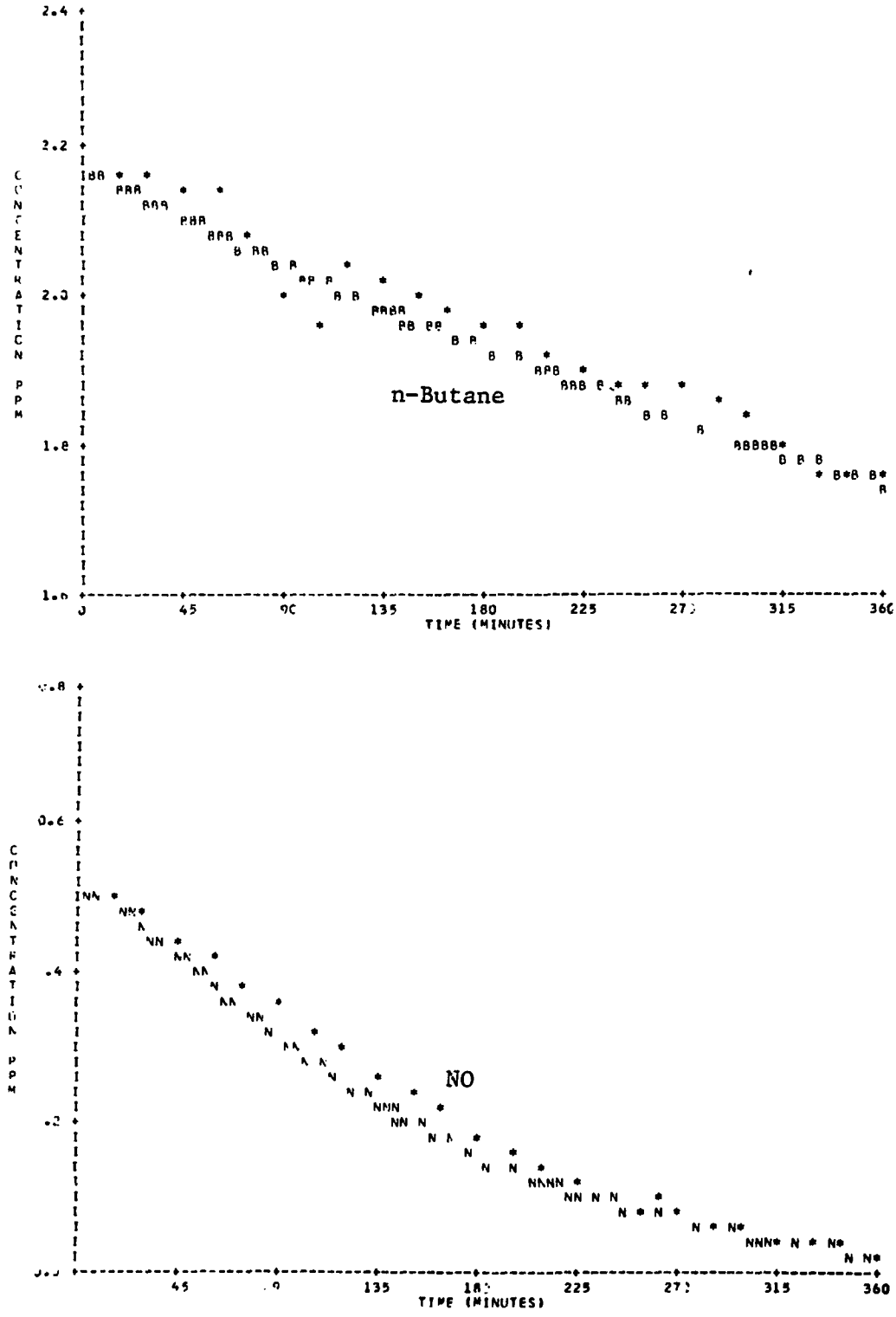

Figure B-1. Simulation of SAPRC EC-39.

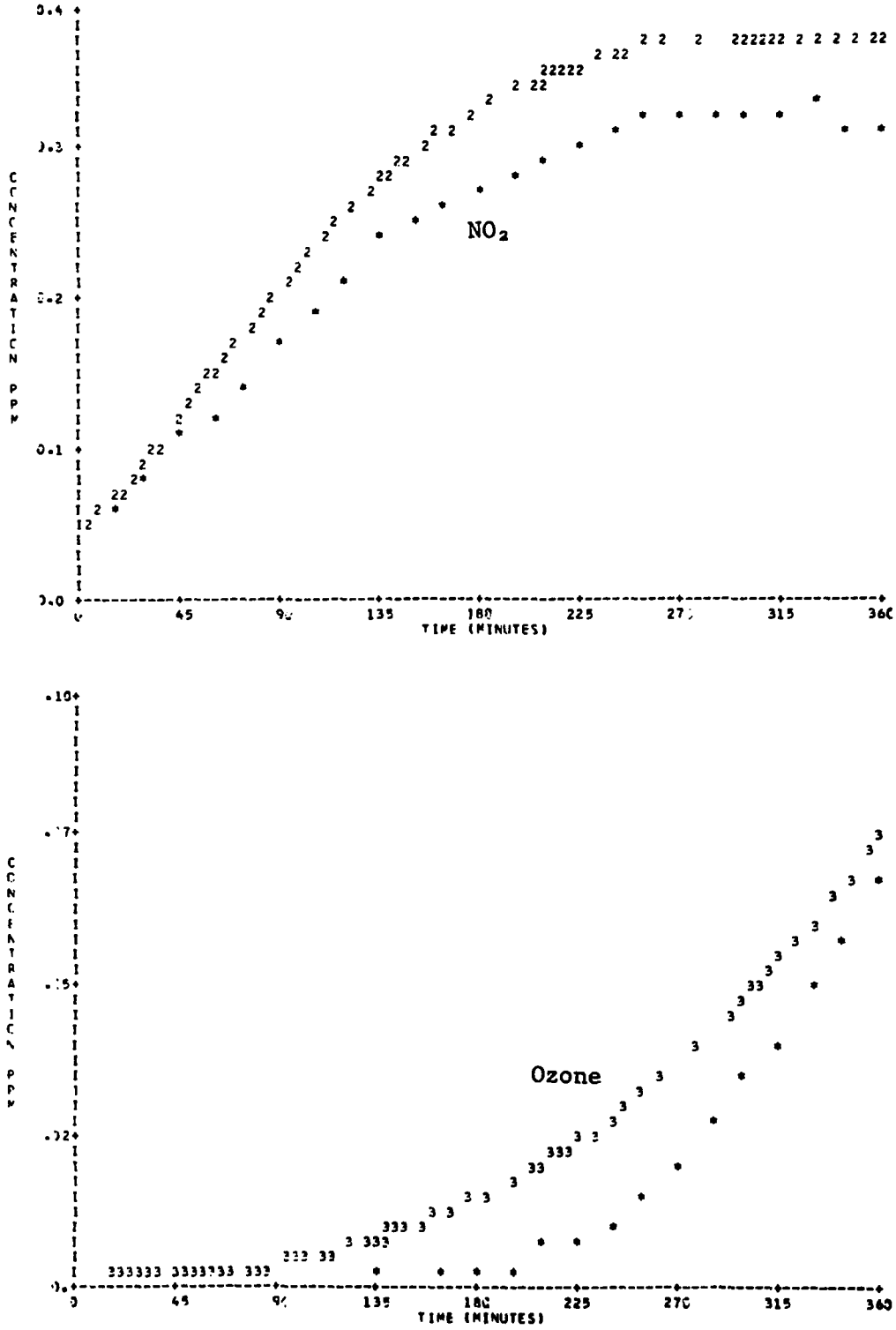

Figure B-1. Simulation of SAPRC EC-39 (Continued).

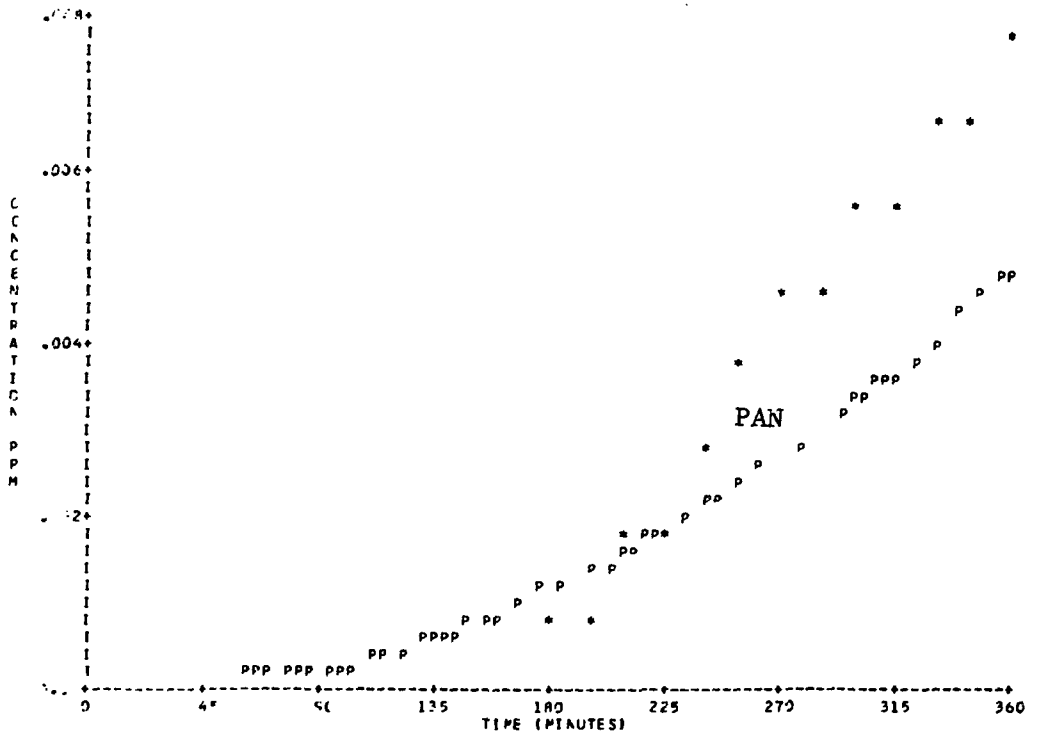

Figure B-1. Simulation of SAPRC EC-39 (Concluded).

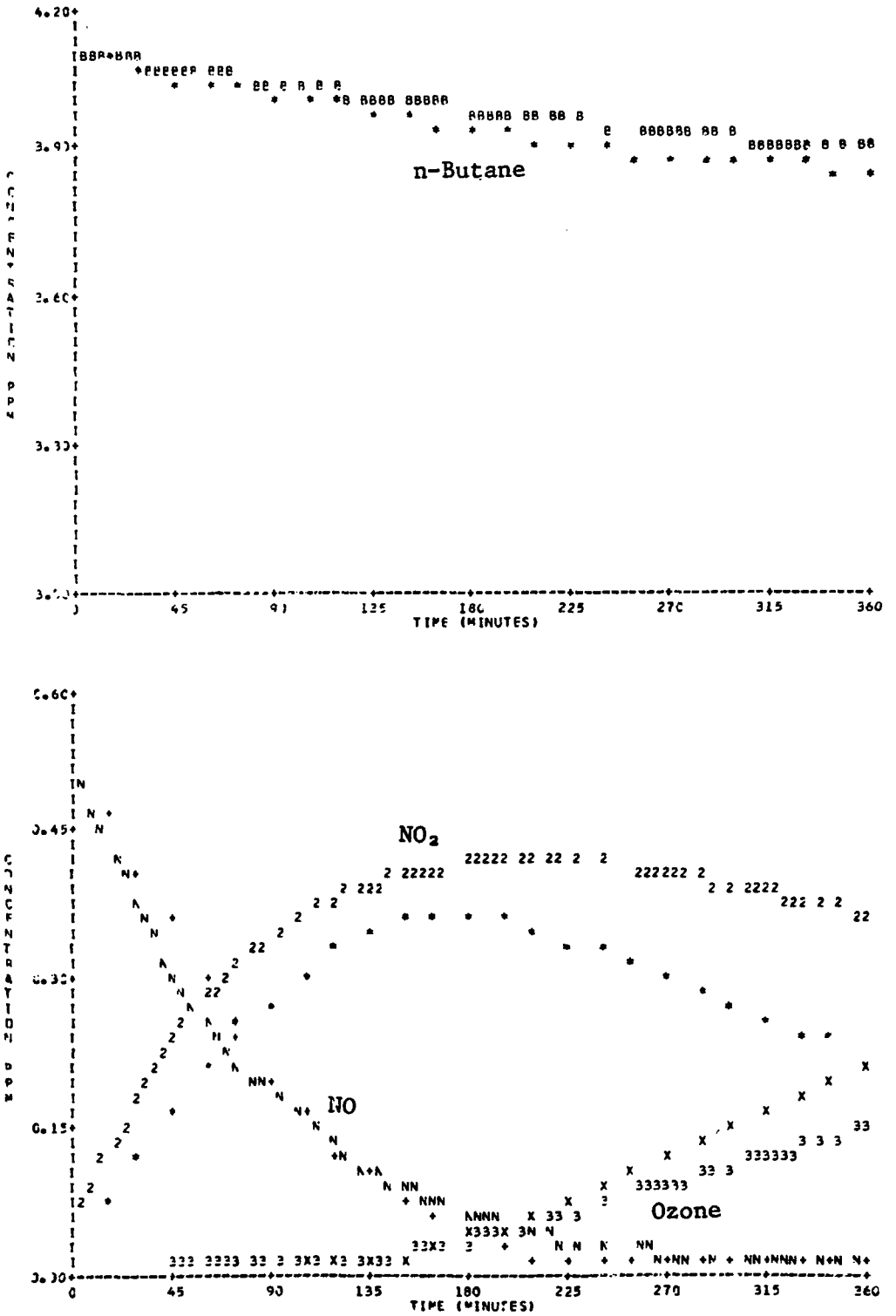

Figure B-2. Simulation of SAPRC EC-41.

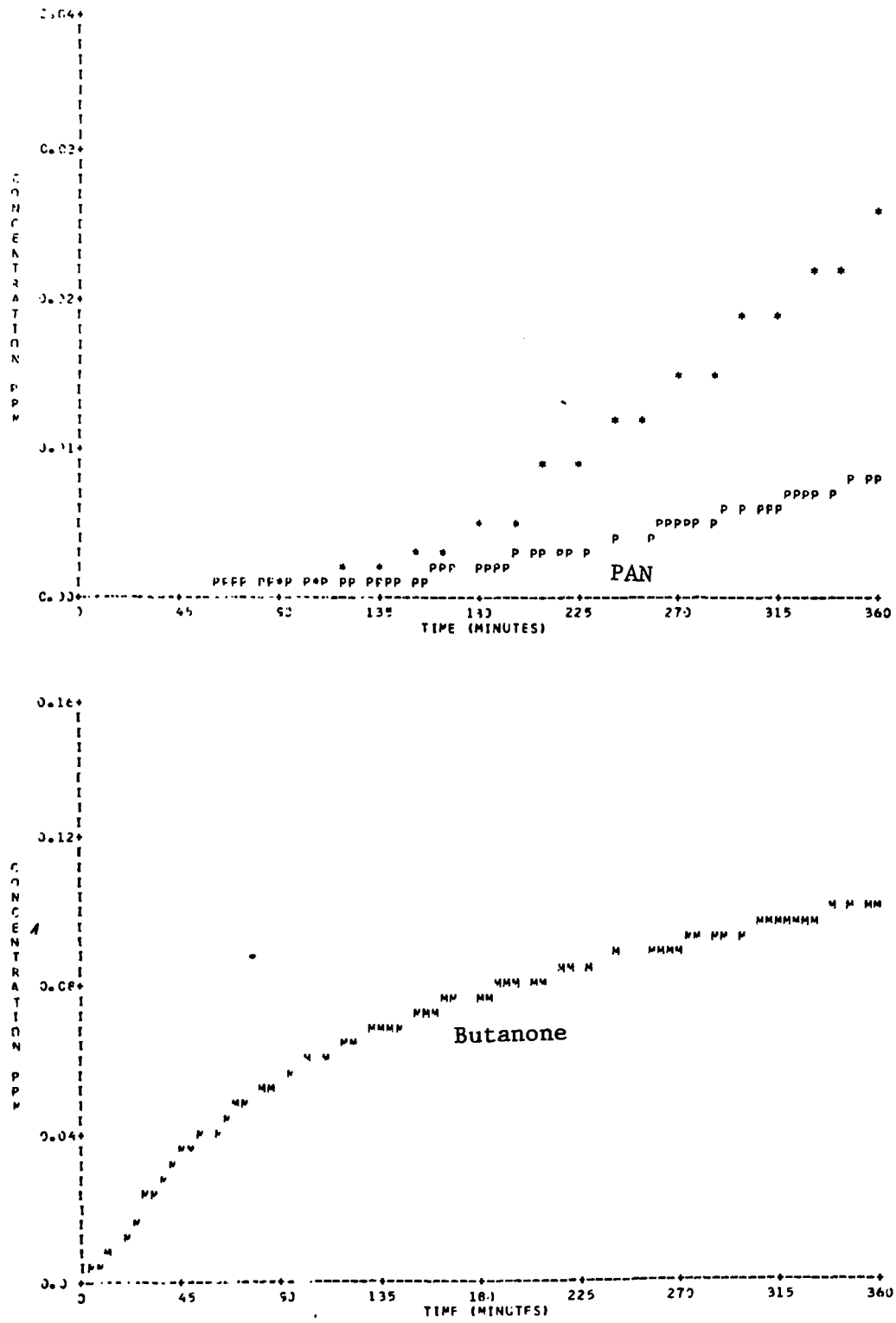

Figure B-2. Simulation of SAPRC EC-41 (Concluded).

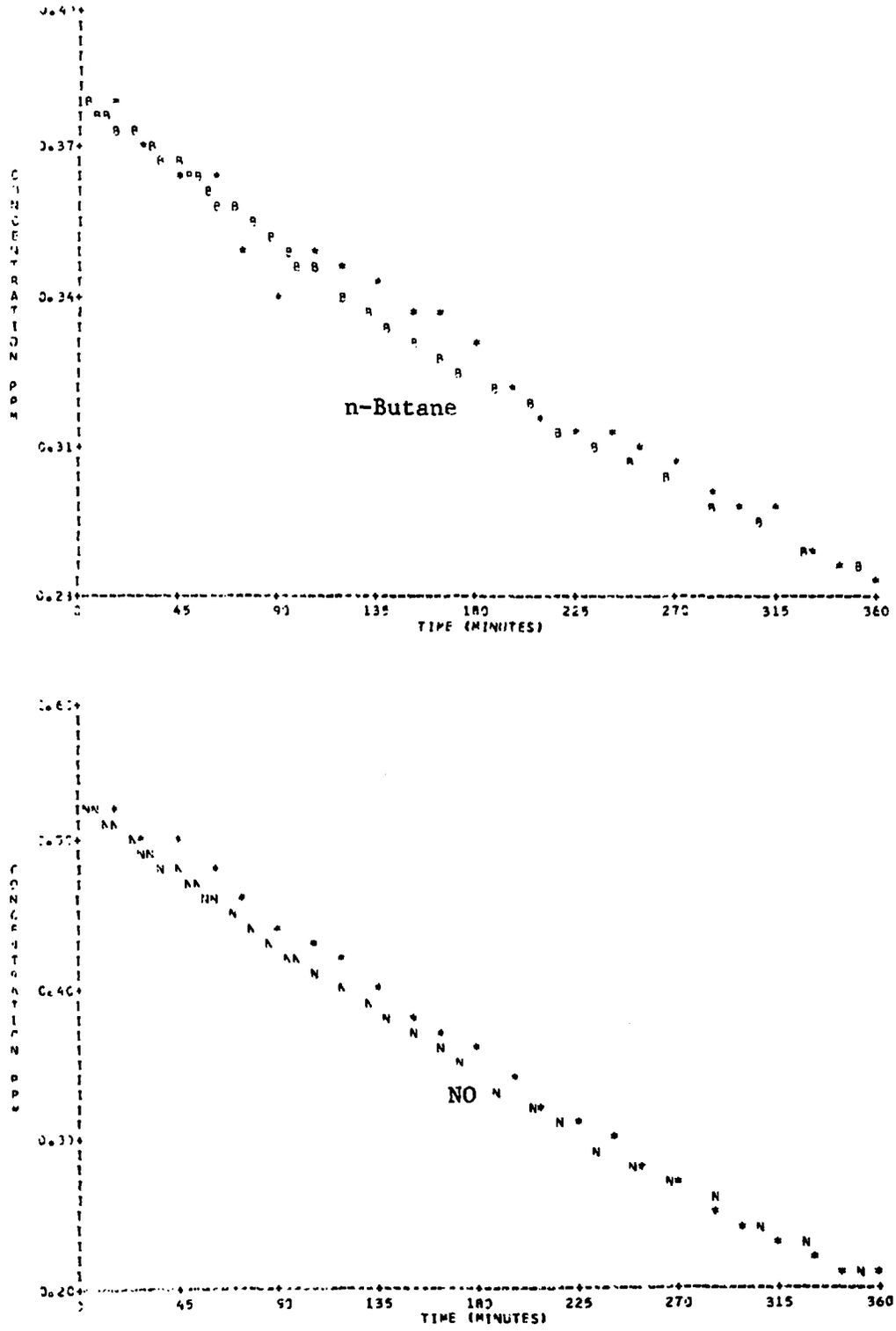

Figure B-3. Simulation of SAPRC EC-42.

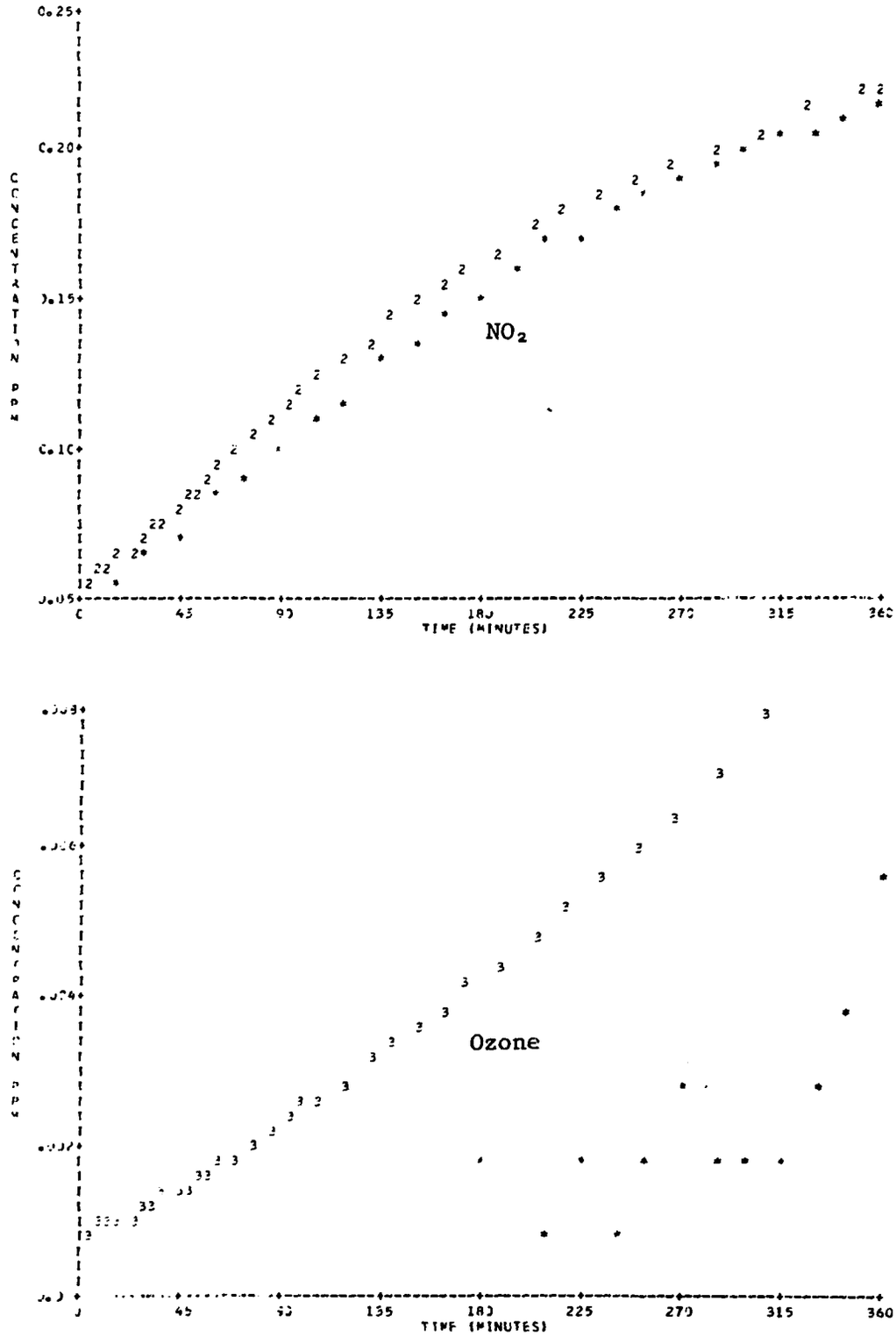

Figure B-3. Simulation of SAPRC EC-42 (Continued).

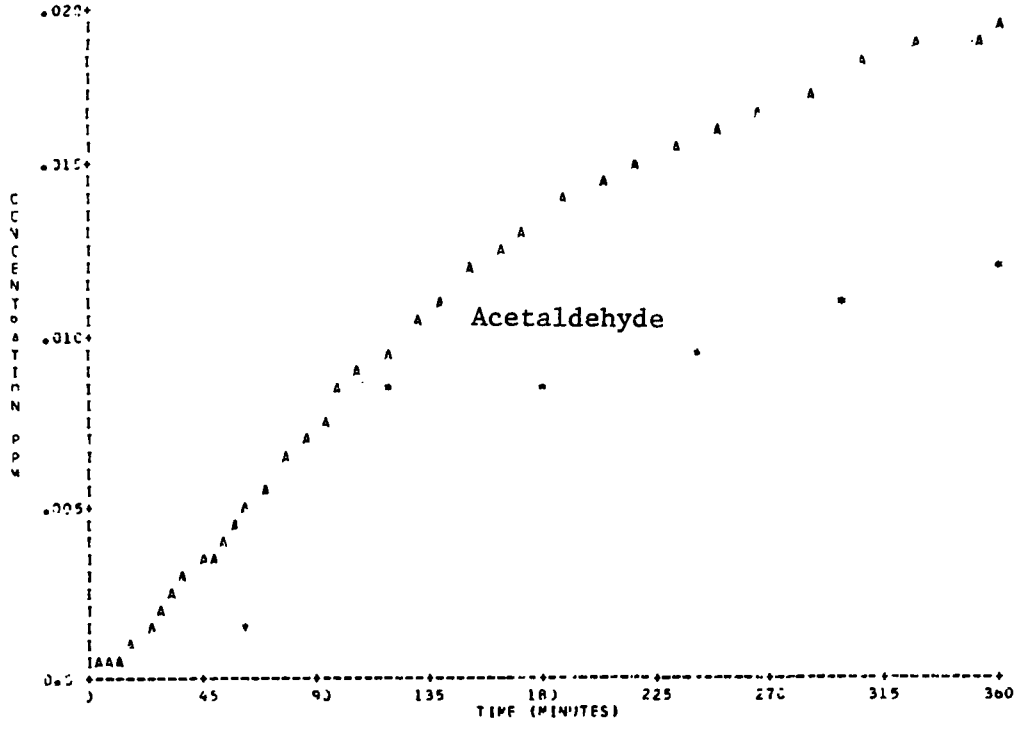

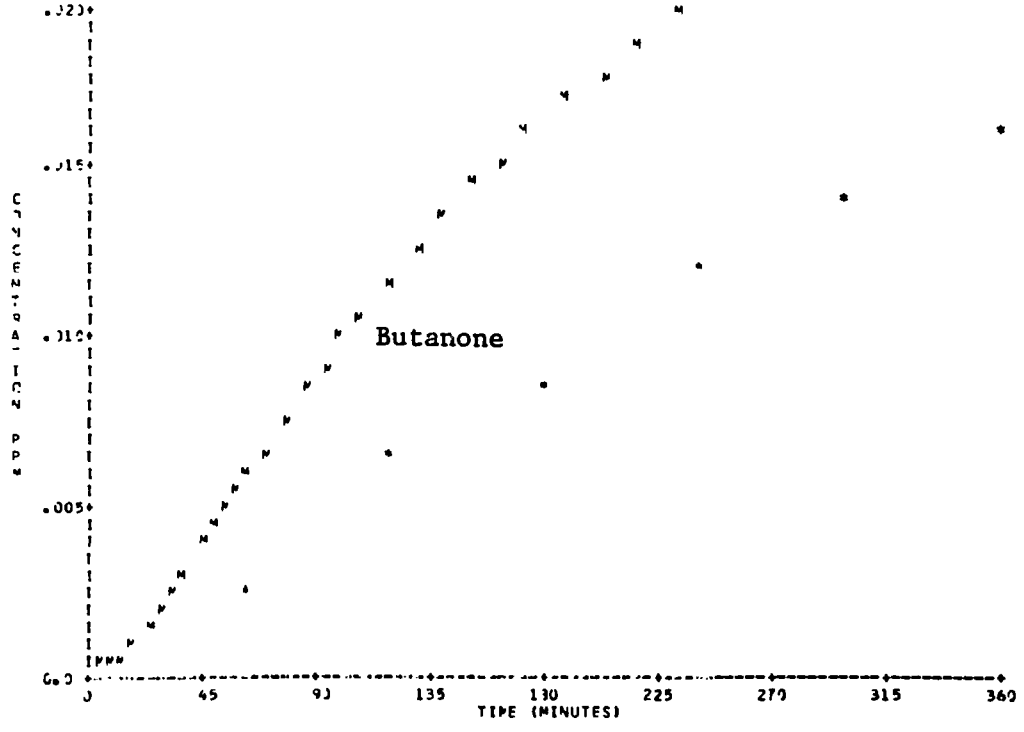

Figure B-3. Simulation of SAPRC EC-42 (Continued).

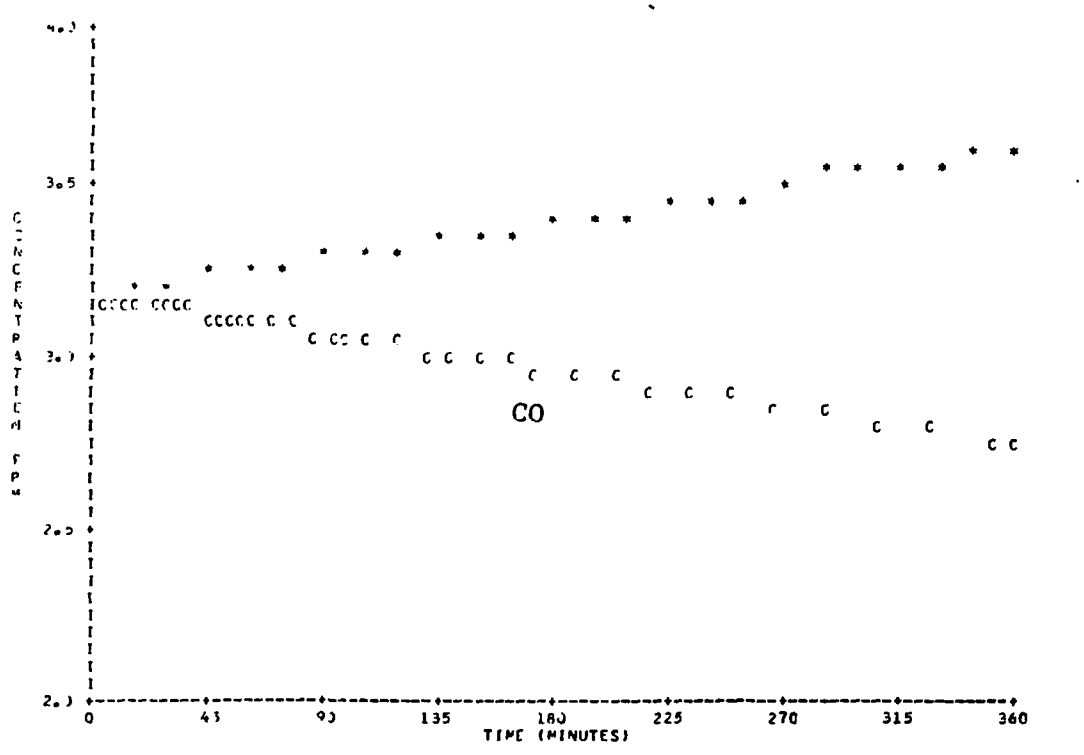

Figure B-3. Simulation of SAPRC EC-42 (Concluded).

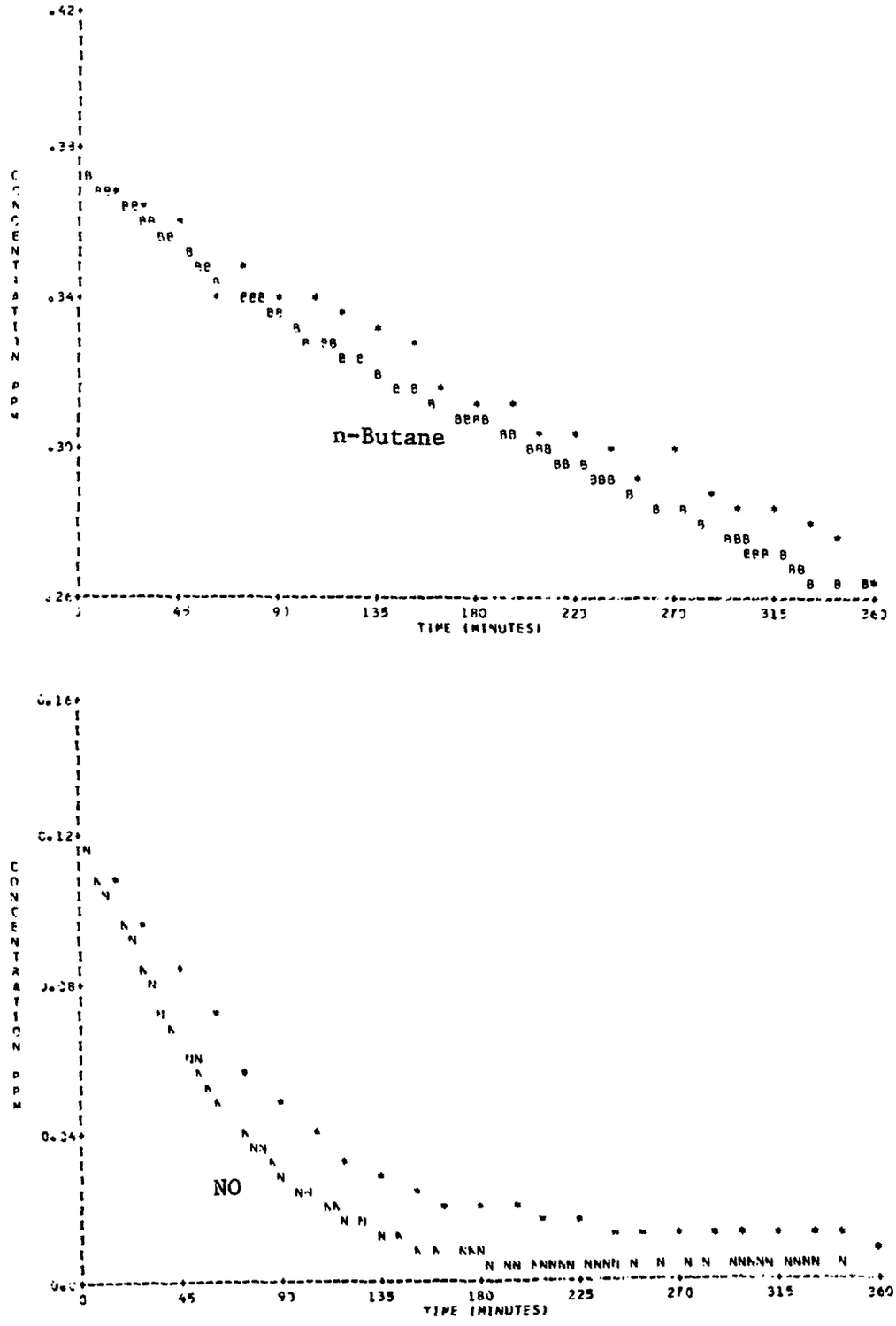

Figure B-4. Simulation of SAPRC EC-43.

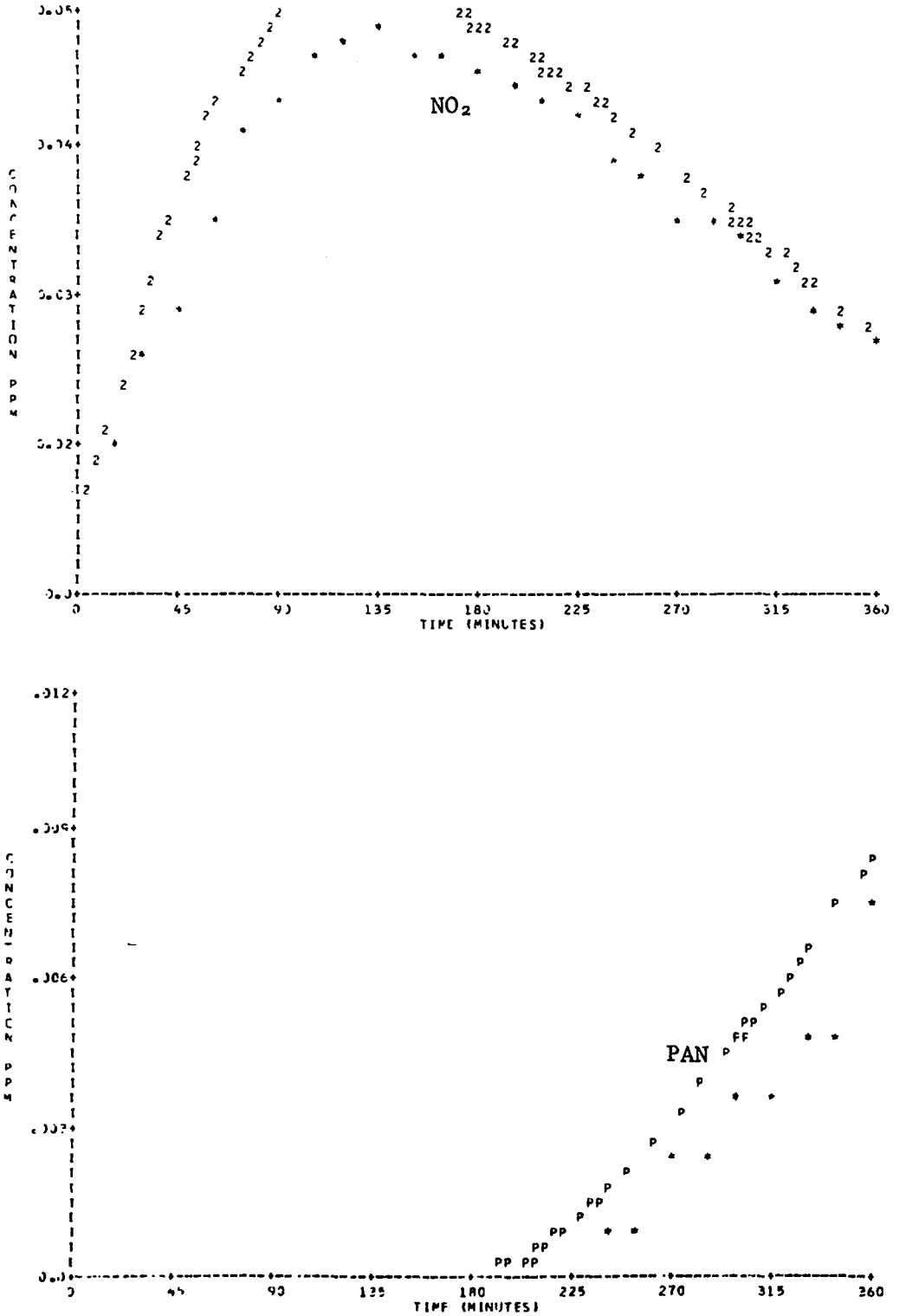

Figure B-4. Simulation of SAPRC EC-43 (Continued).

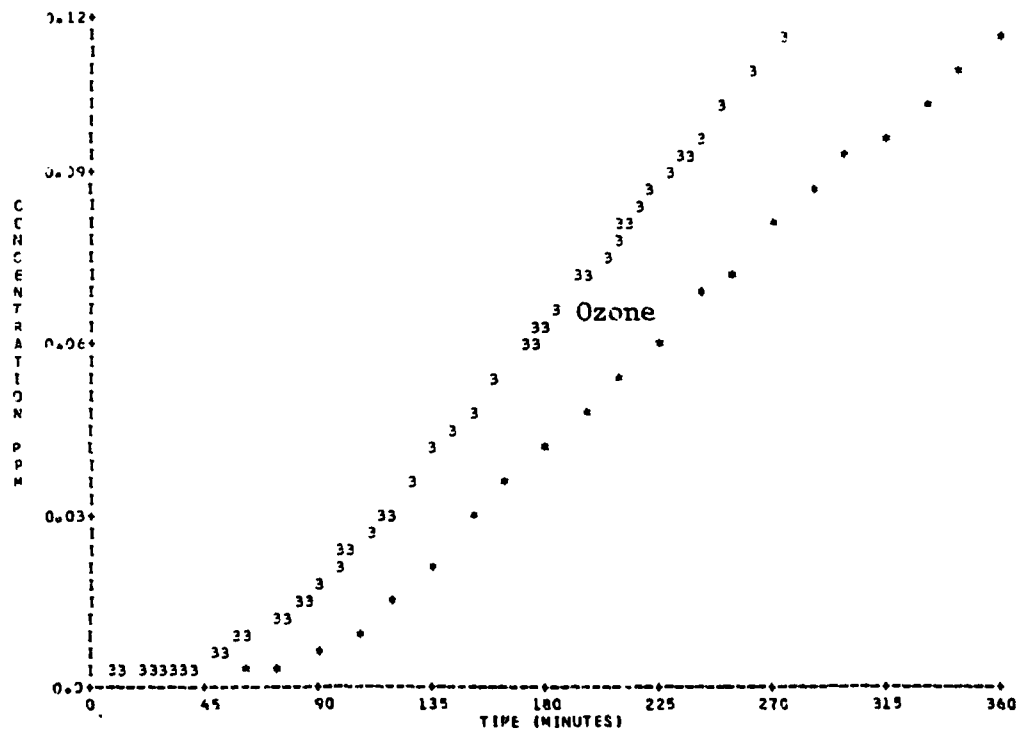

Figure B-4. Simulation of SAPRC EC-43 (Concluded).

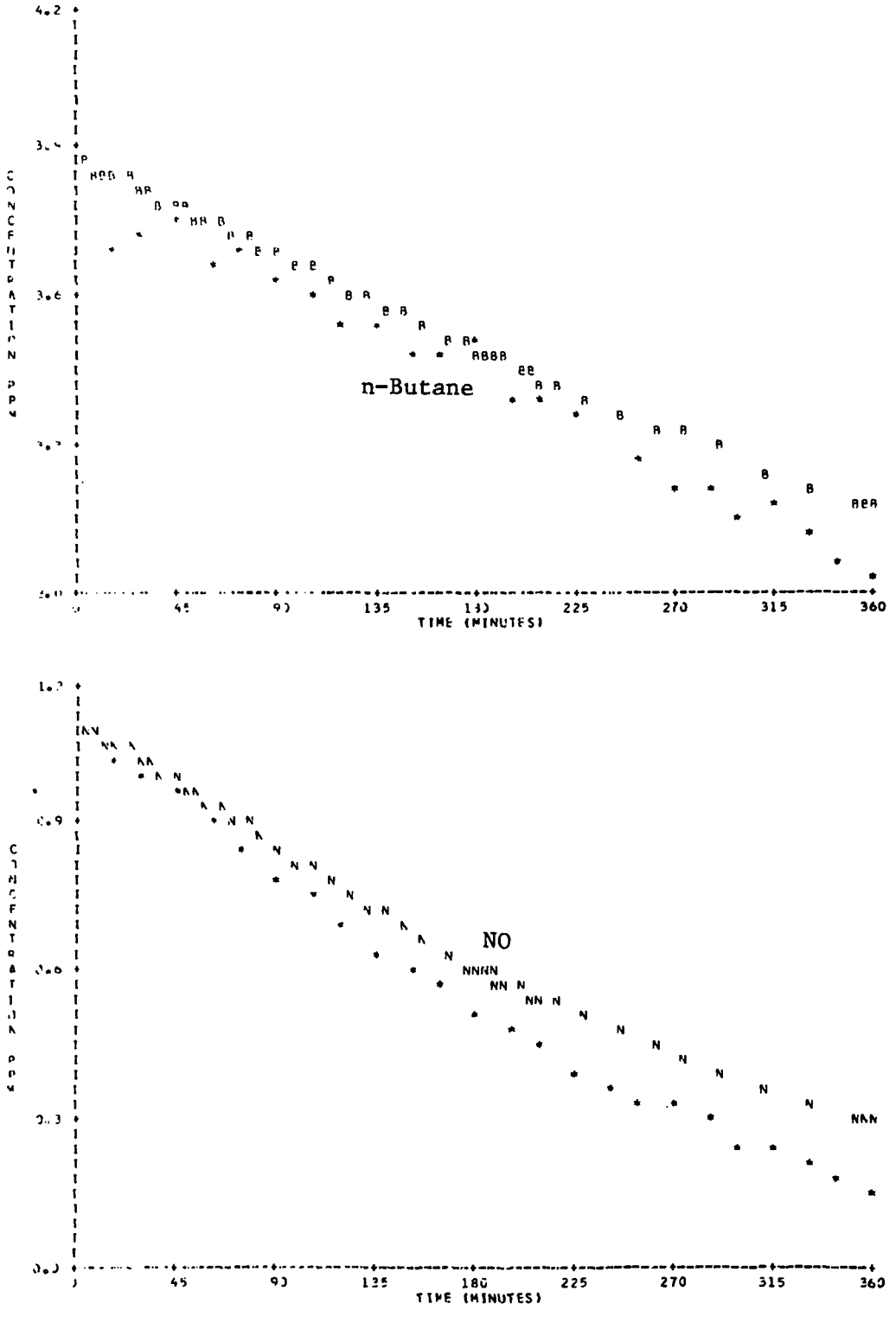

Figure B-5. Simulation of SAPRC EC-44.

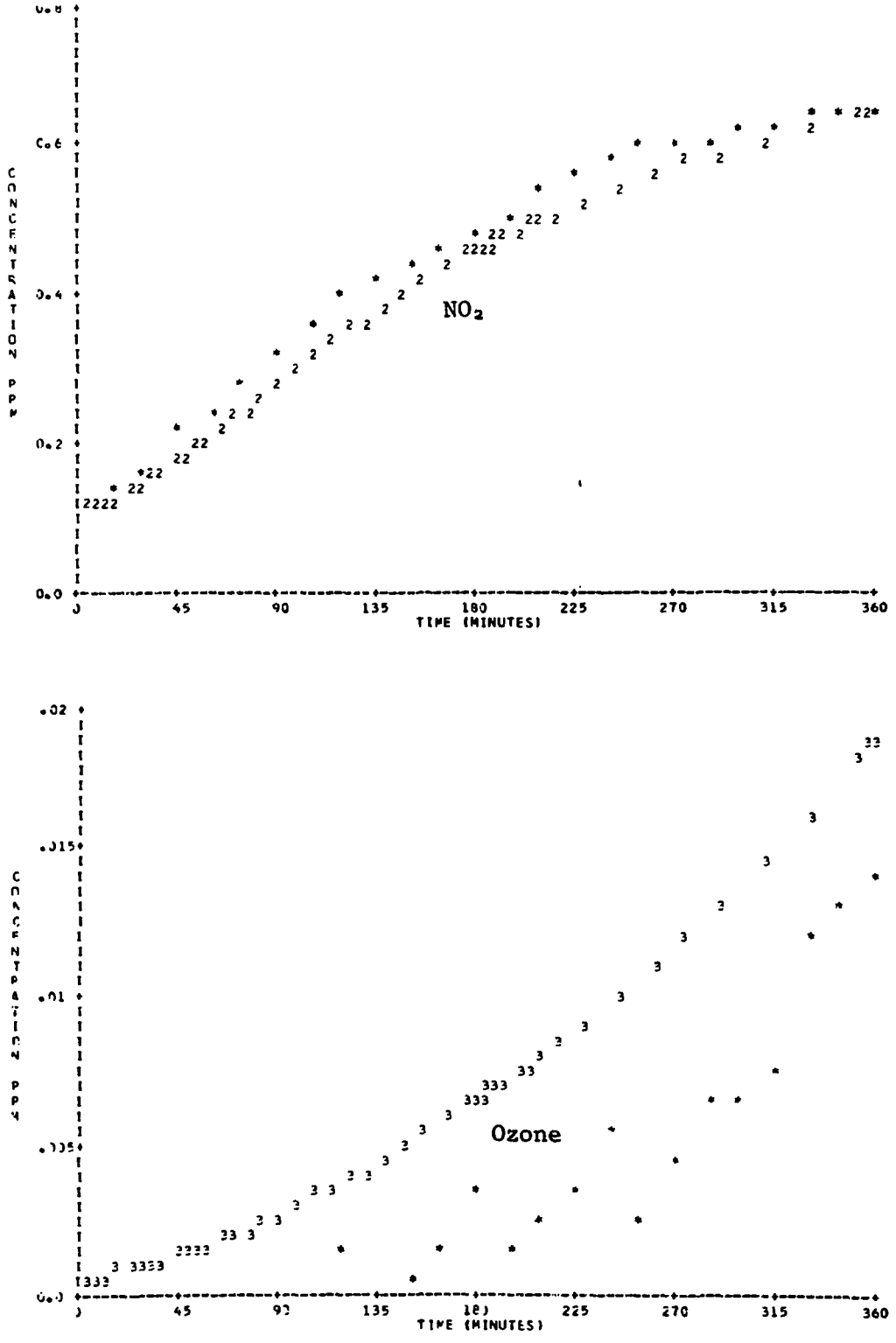

Figure B-5. Simulation of SAPRC EC-44 (Continued).

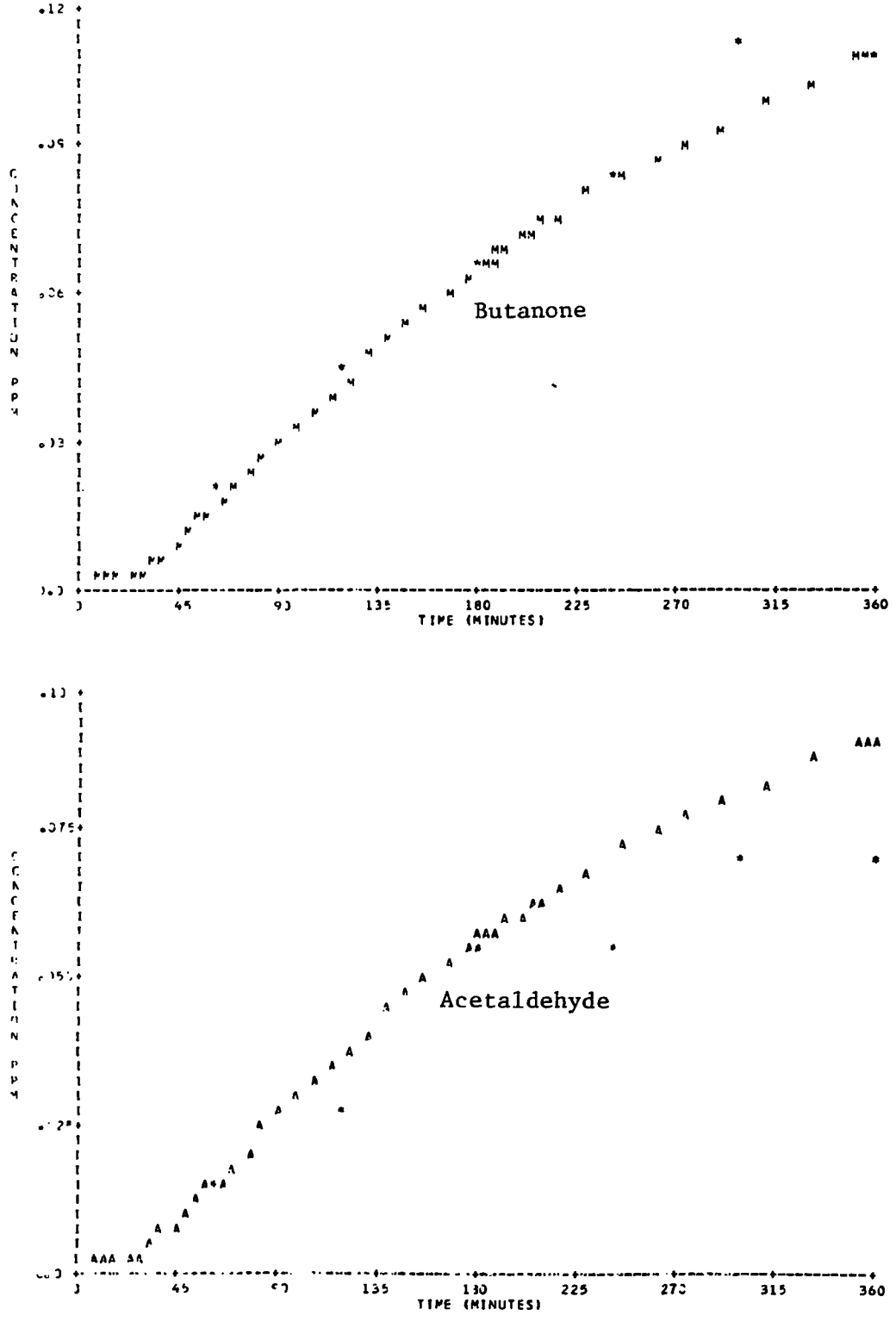

Figure B-5. Simulation of SAPRC EC-44 (Concluded).

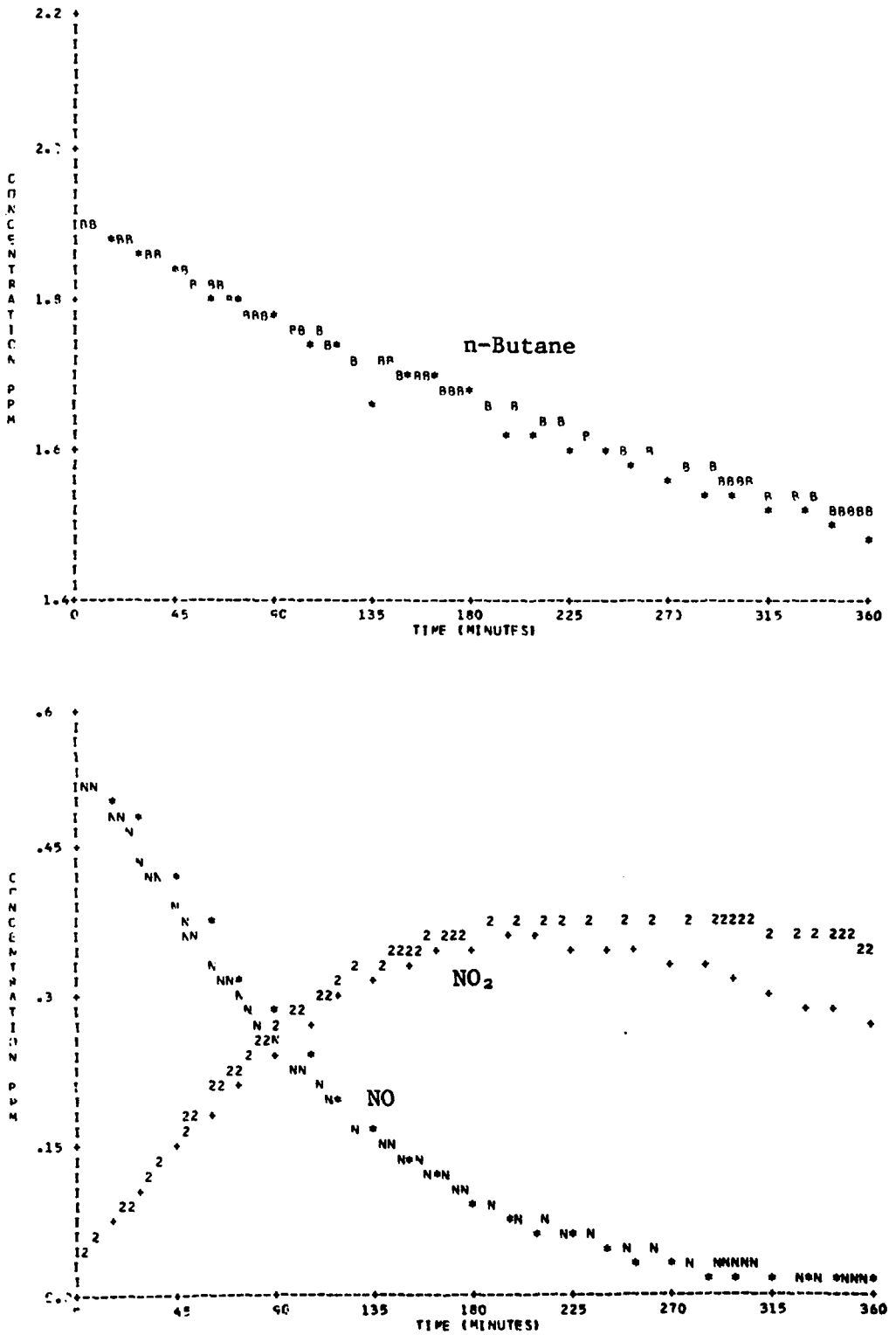

Figure B-6. Simulation of SAPRC EC-45.

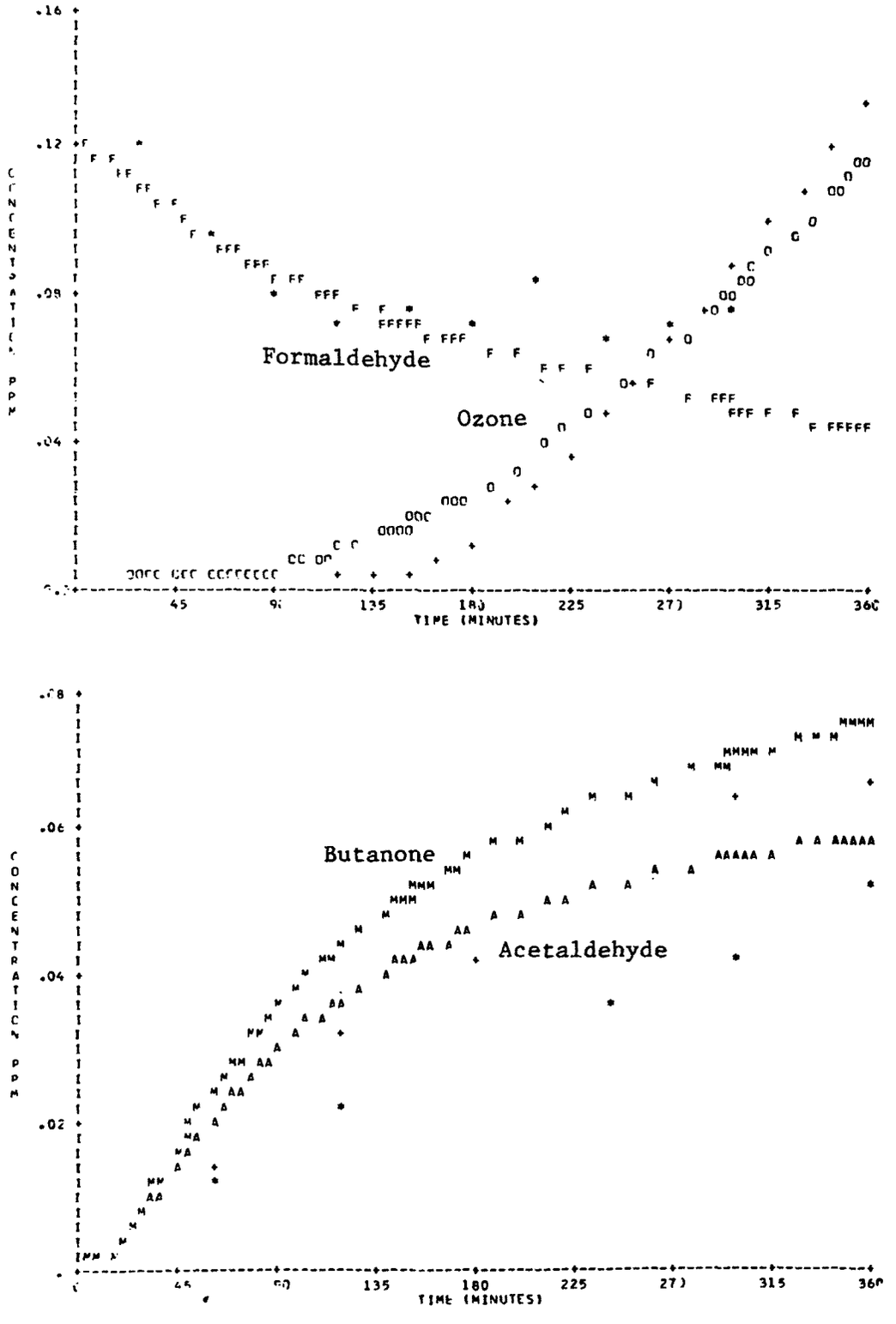

Figure B-6. Simulation of SAPRC EC-45 (Continued).

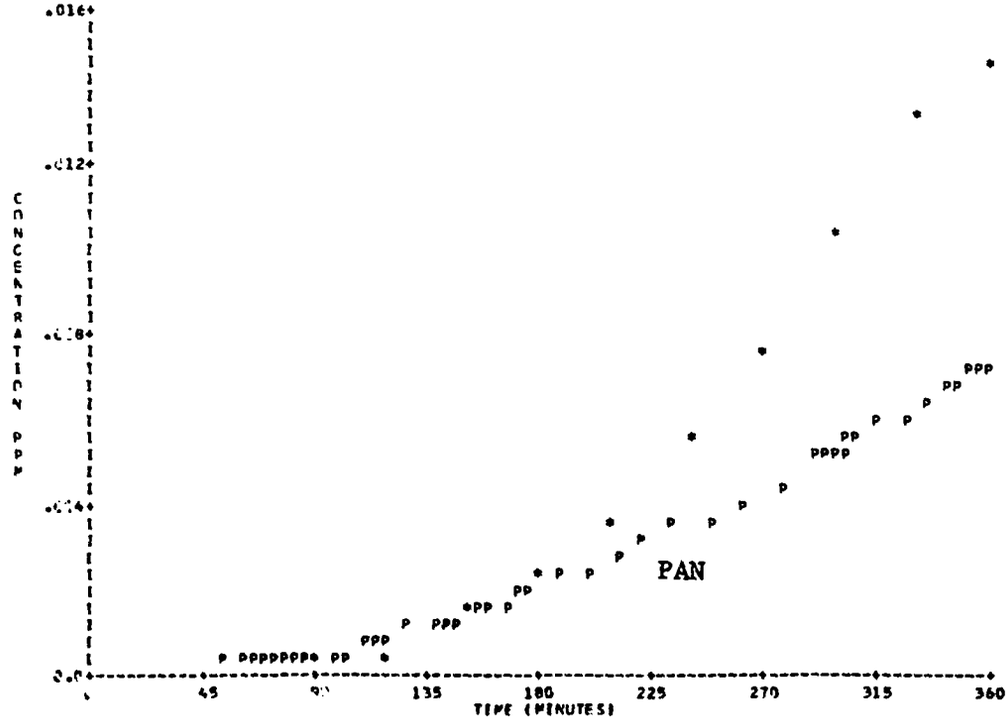

Figure B-6. Simulation of SAPRC EC-45 (Concluded).

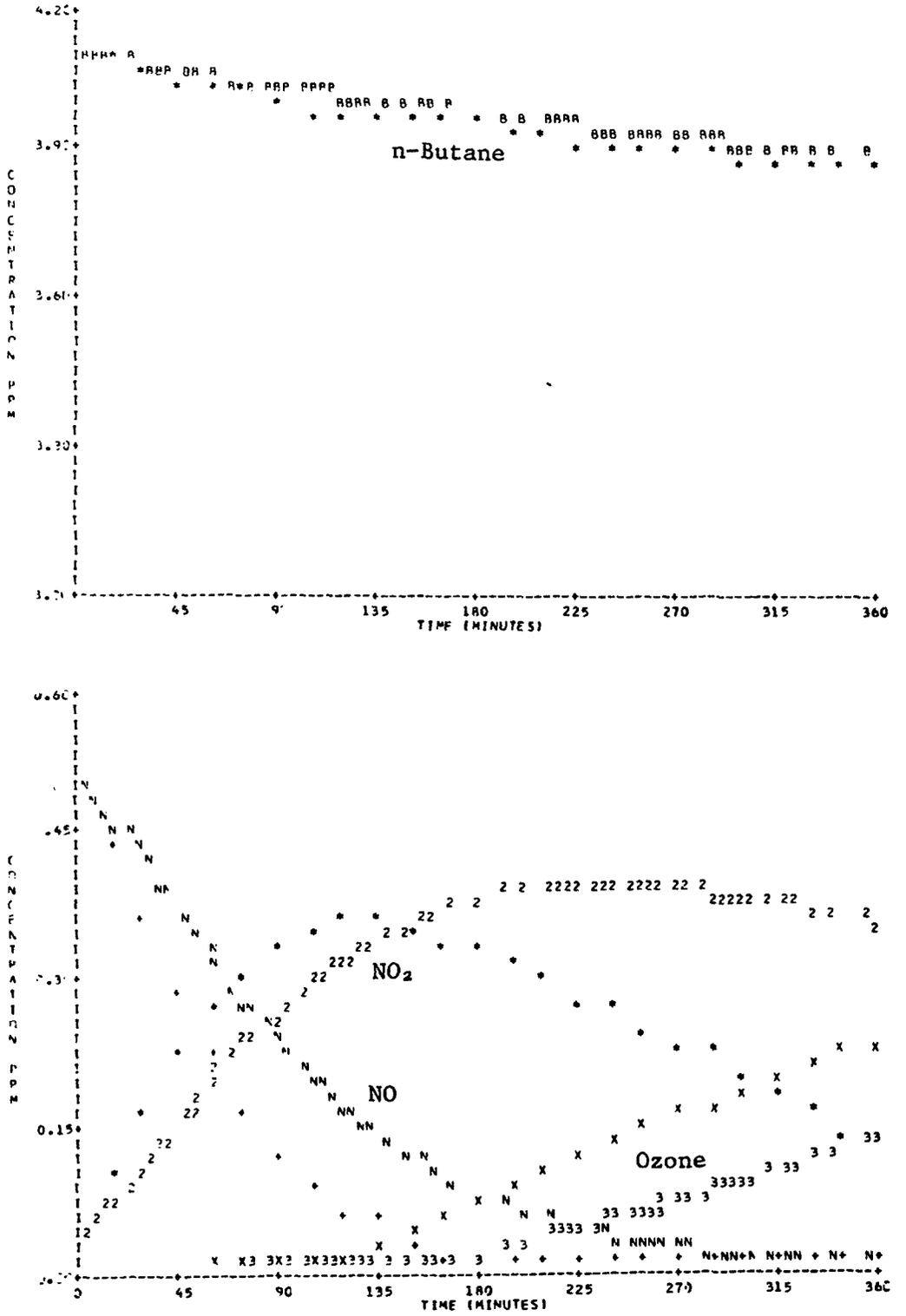

Figure B-7. Simulation of SAPRC EC-46.

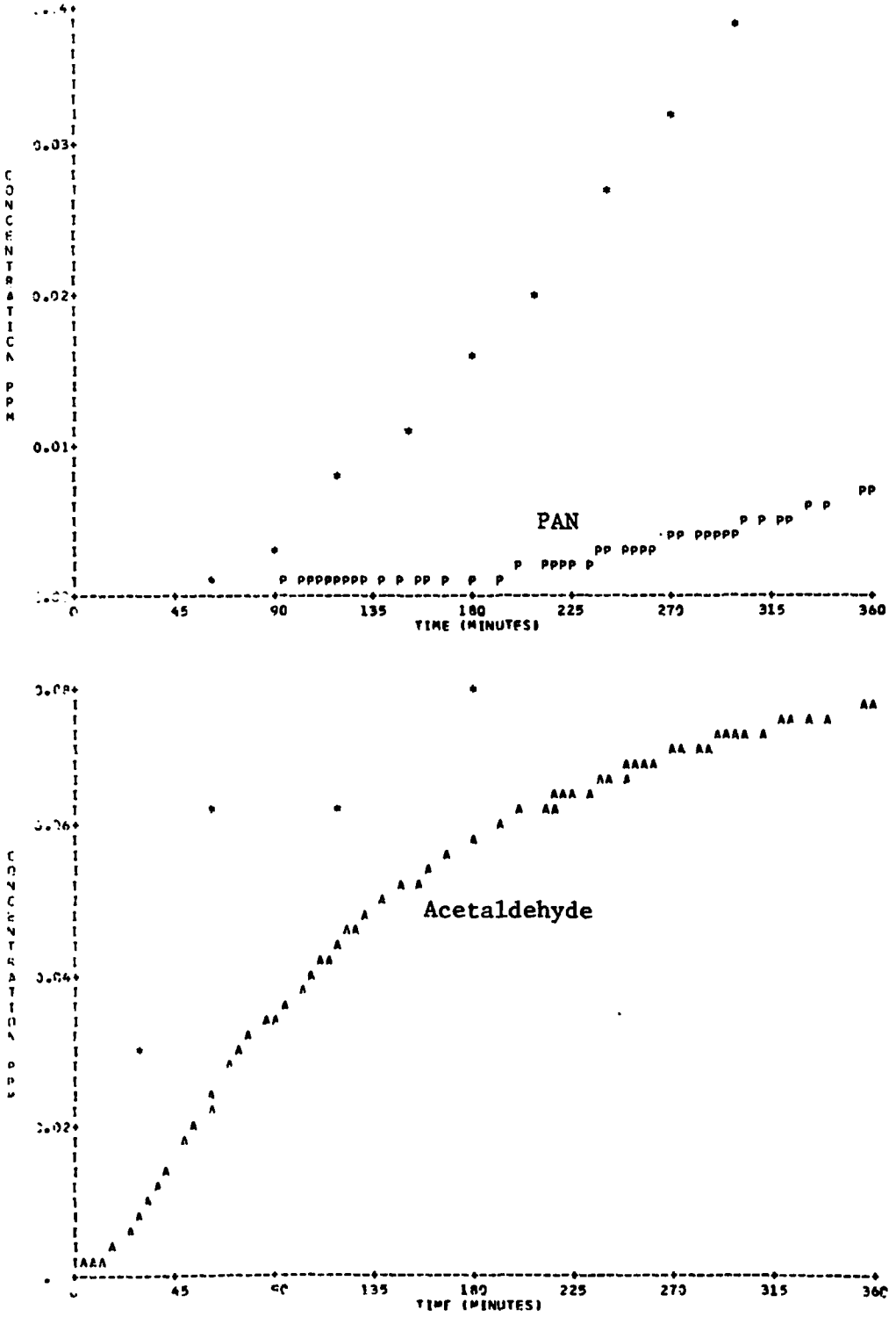

Figure B-7. Simulation of SAPRC EC-46 (Continued).

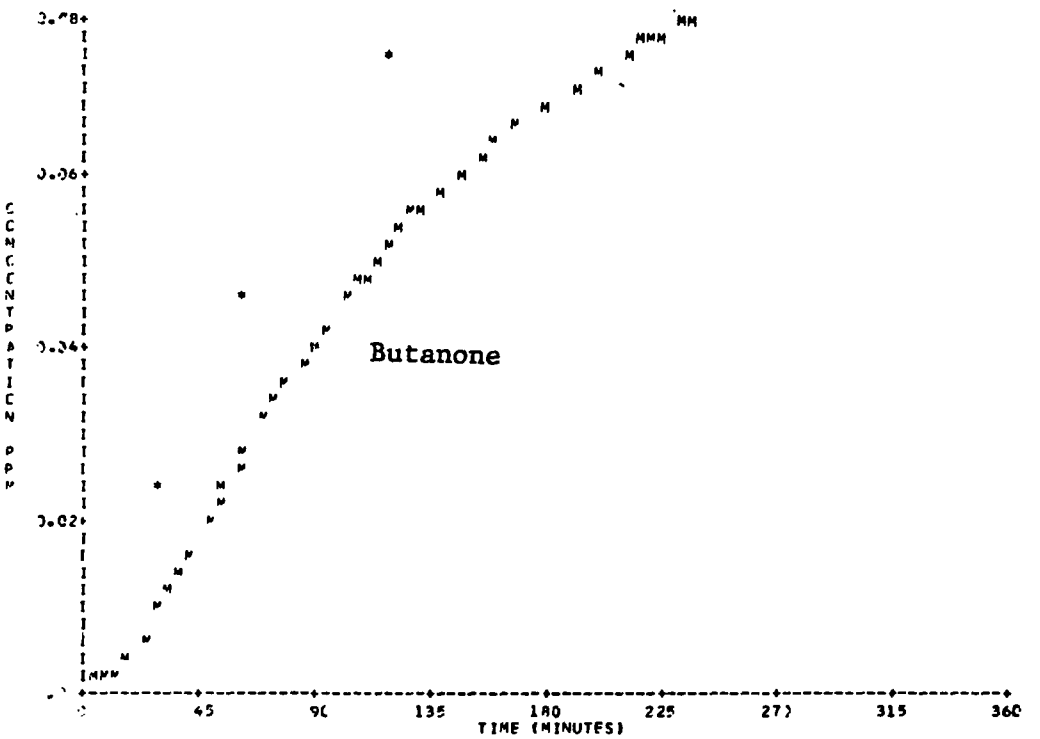

Figure B-7. Simulation of SAPRC EC-46 (Concluded).

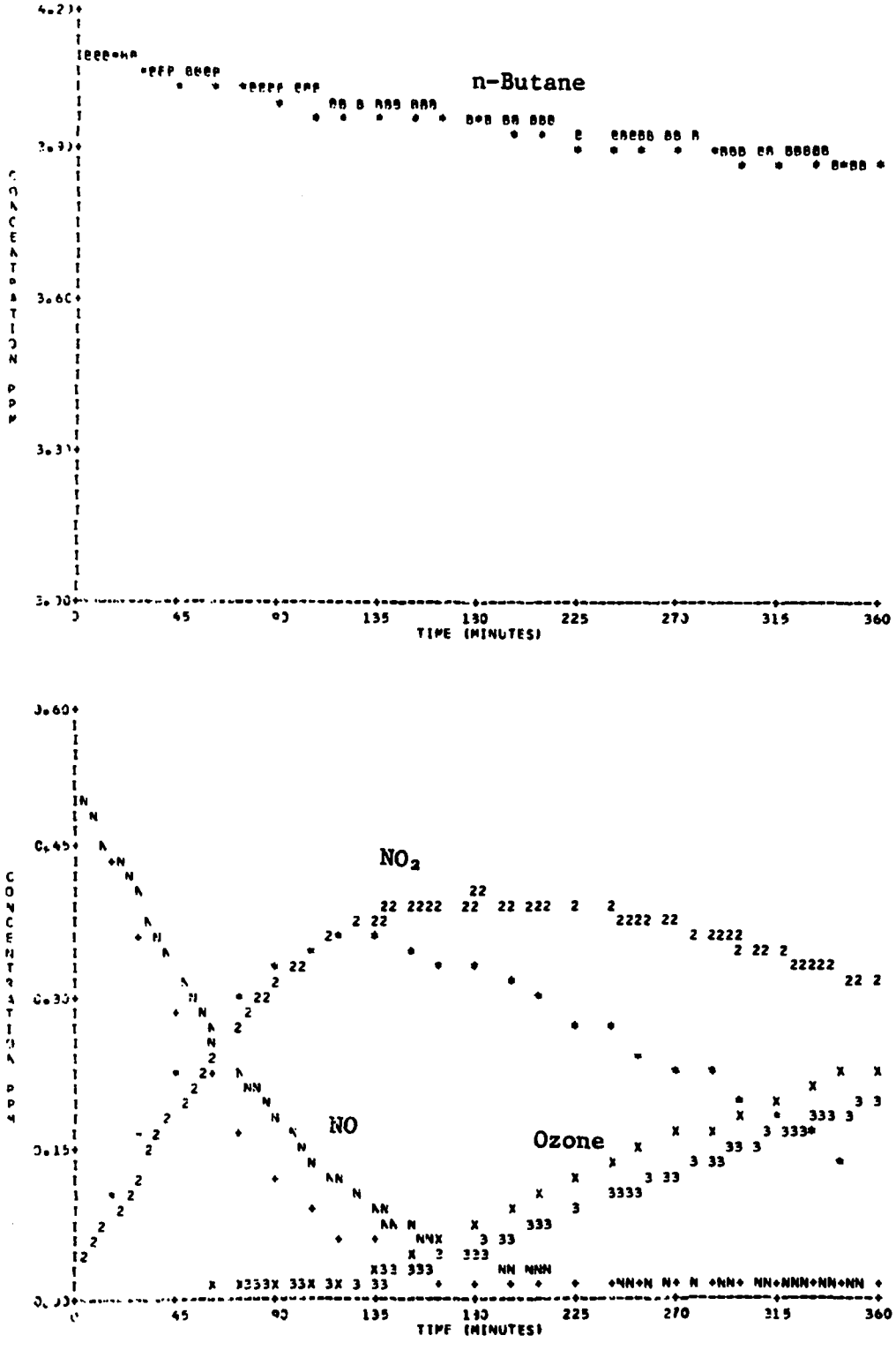

Figure B-7A. Simulation of SAPRC EC-46.
(Radical Addition Rate = 3 x 10^{-4} min^{-1})

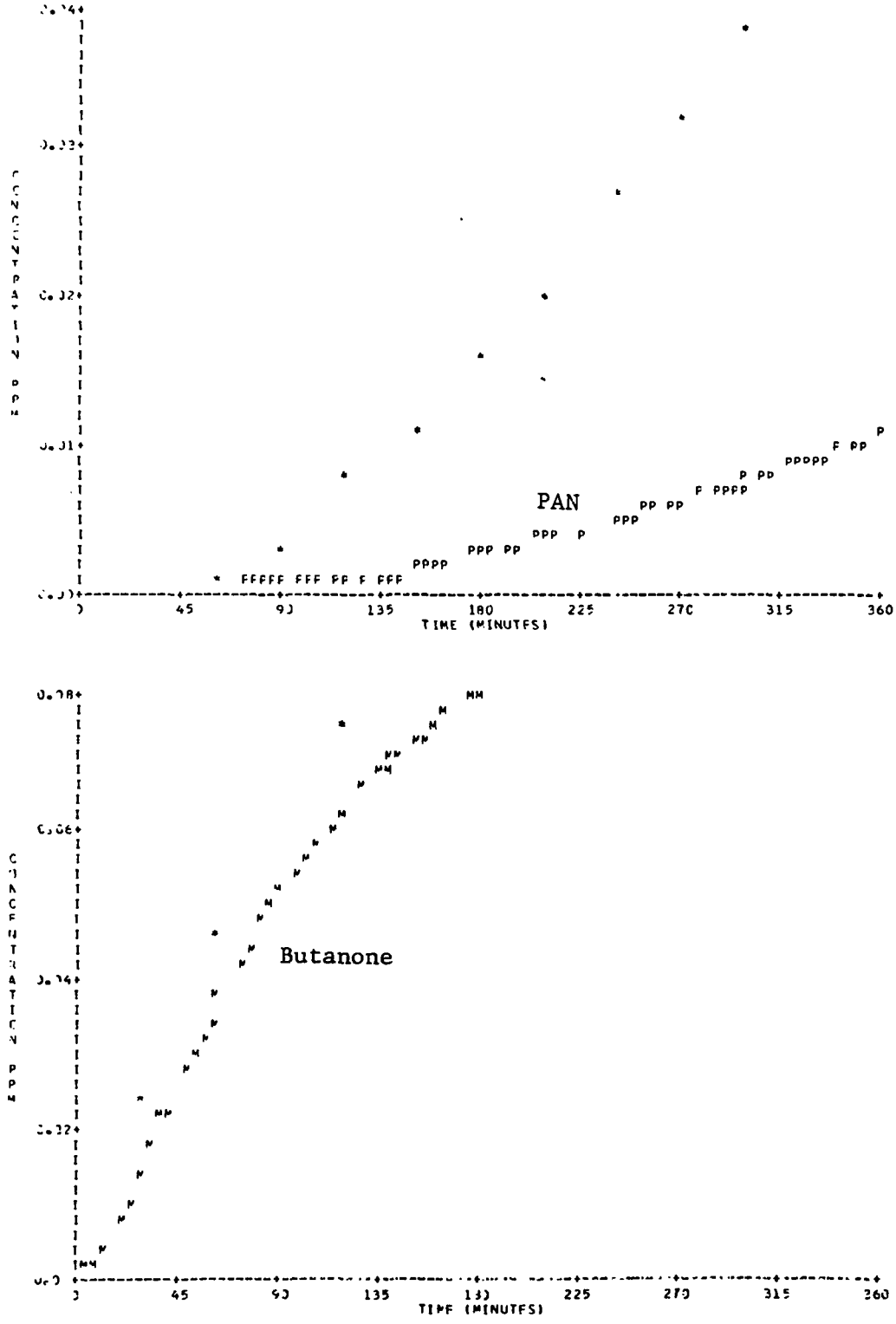

Figure B-7A. Simulation of SAPRC EC-46.
(Radical Addition Rate = 3 x 10^{-4} min^{-1}) (Continued).

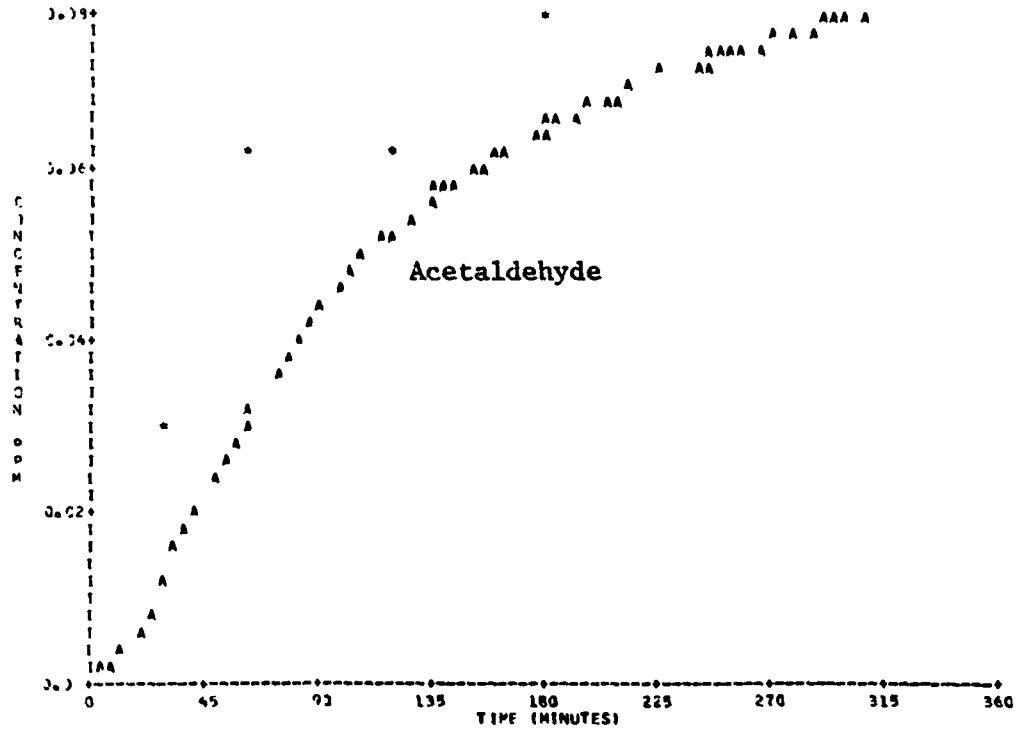

Figure B-7A. Simulation of SAPRC EC-46.
(Radical Addition Rate = 3 x 10^{-4} min^{-1}) (Concluded).

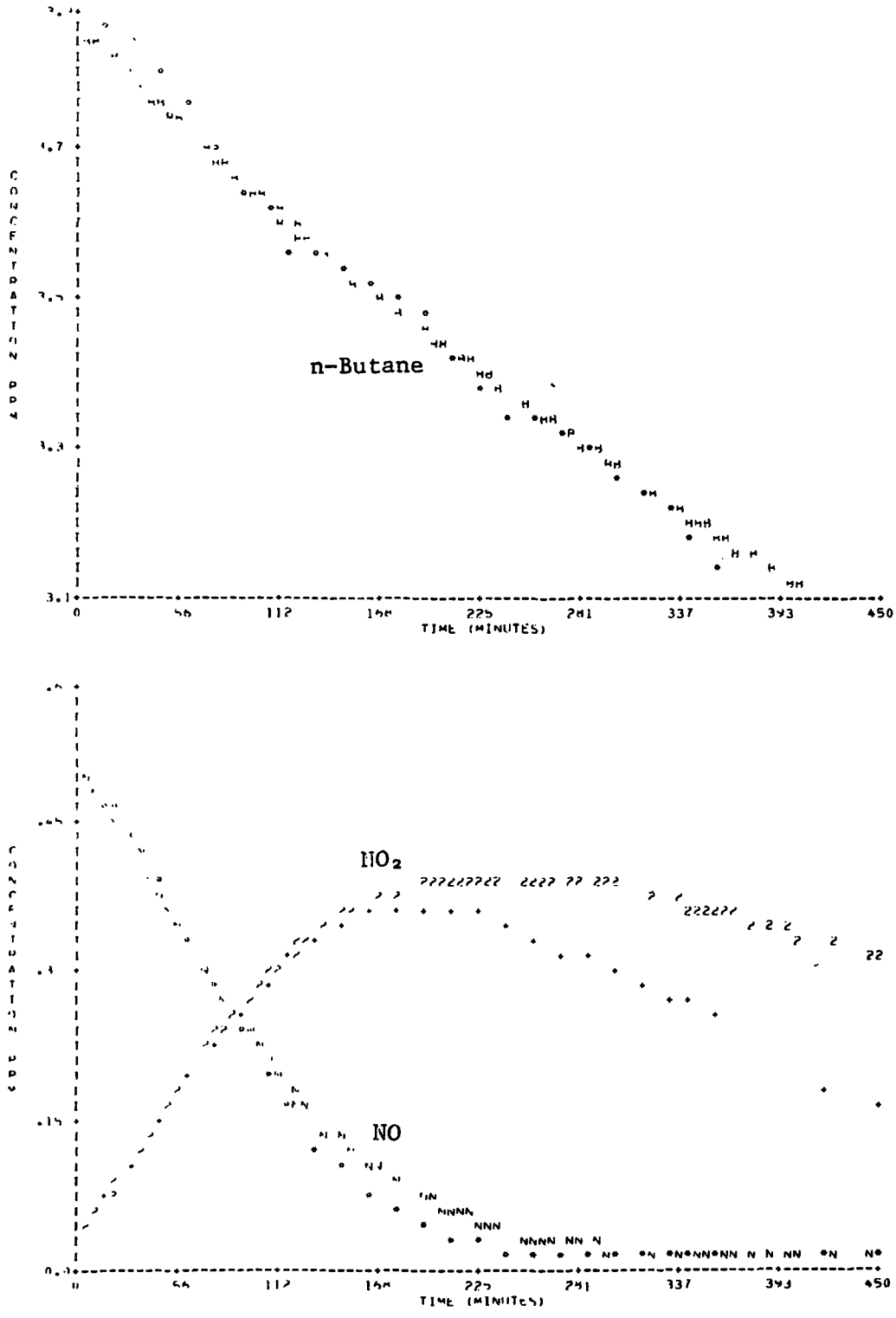

Figure B-8. Simulation of SAPRC EC-47.

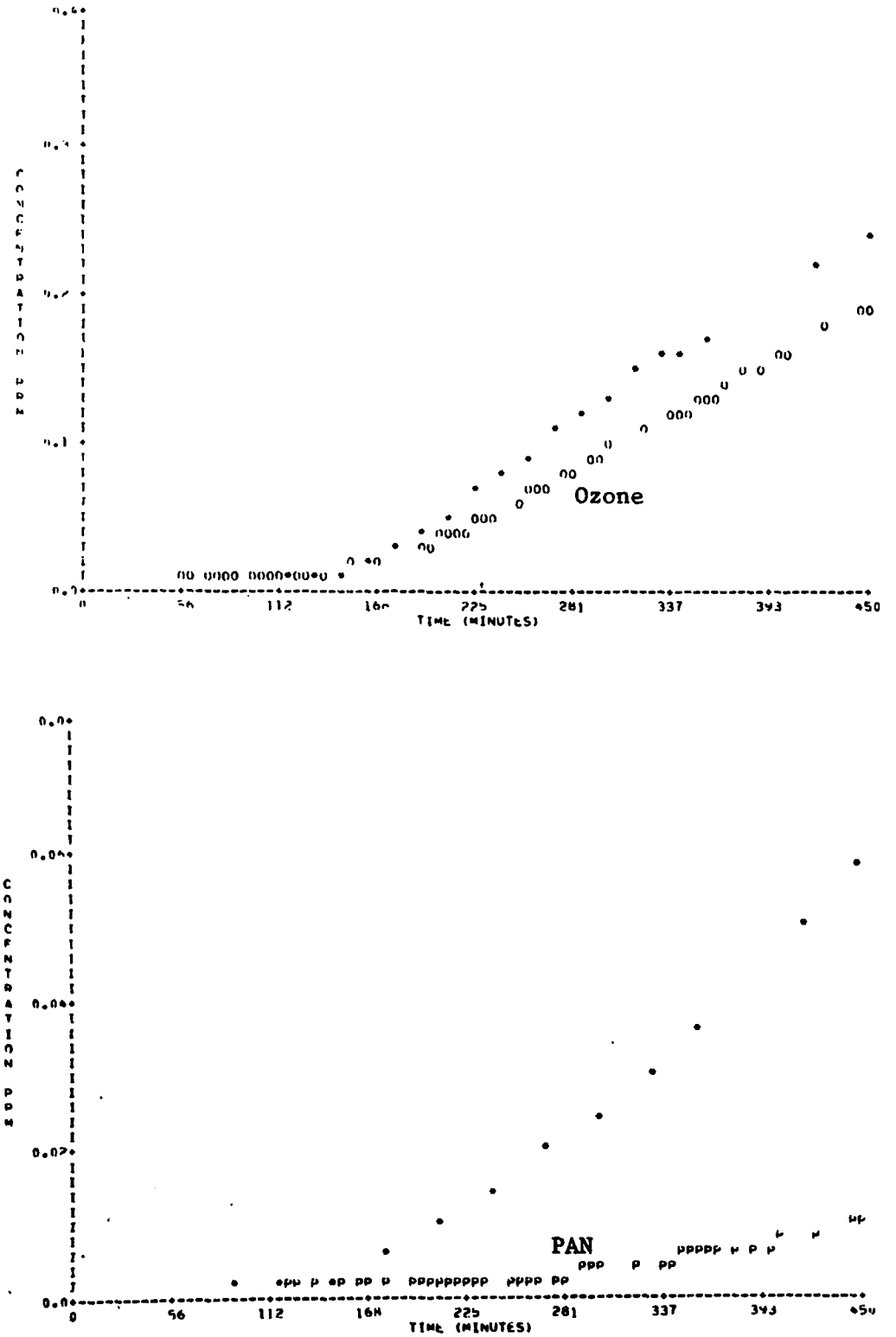

Figure B-8. Simulation of SAPRC EC-47 (Continued).

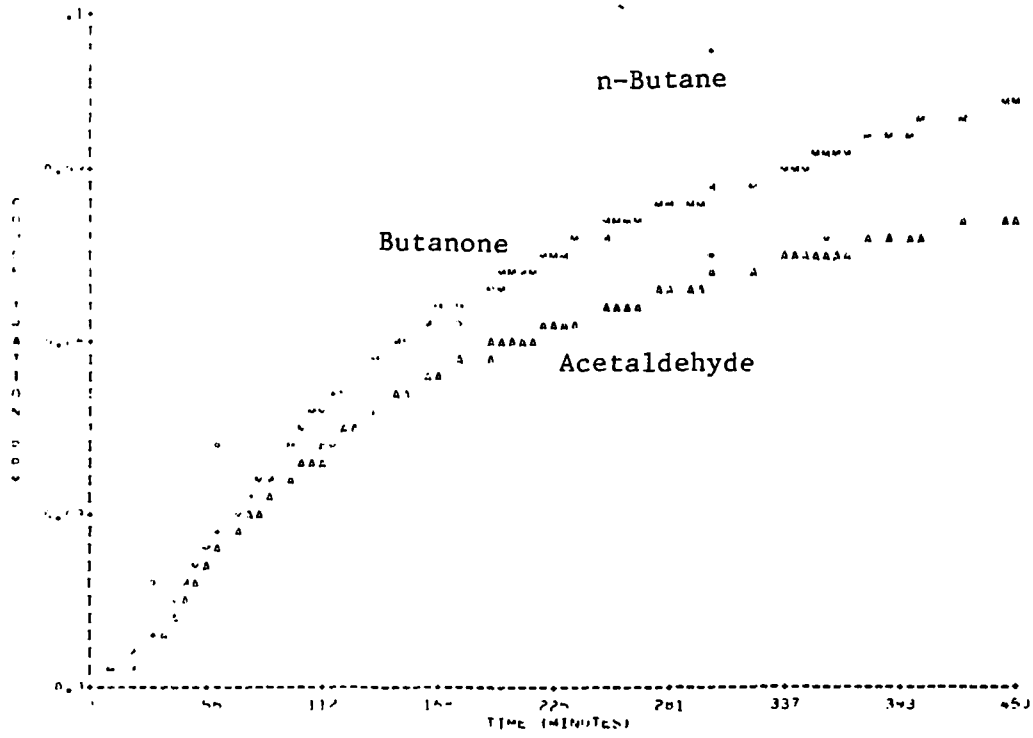

Figure B-8. Simulation of SAPRC EC-47 (Concluded).

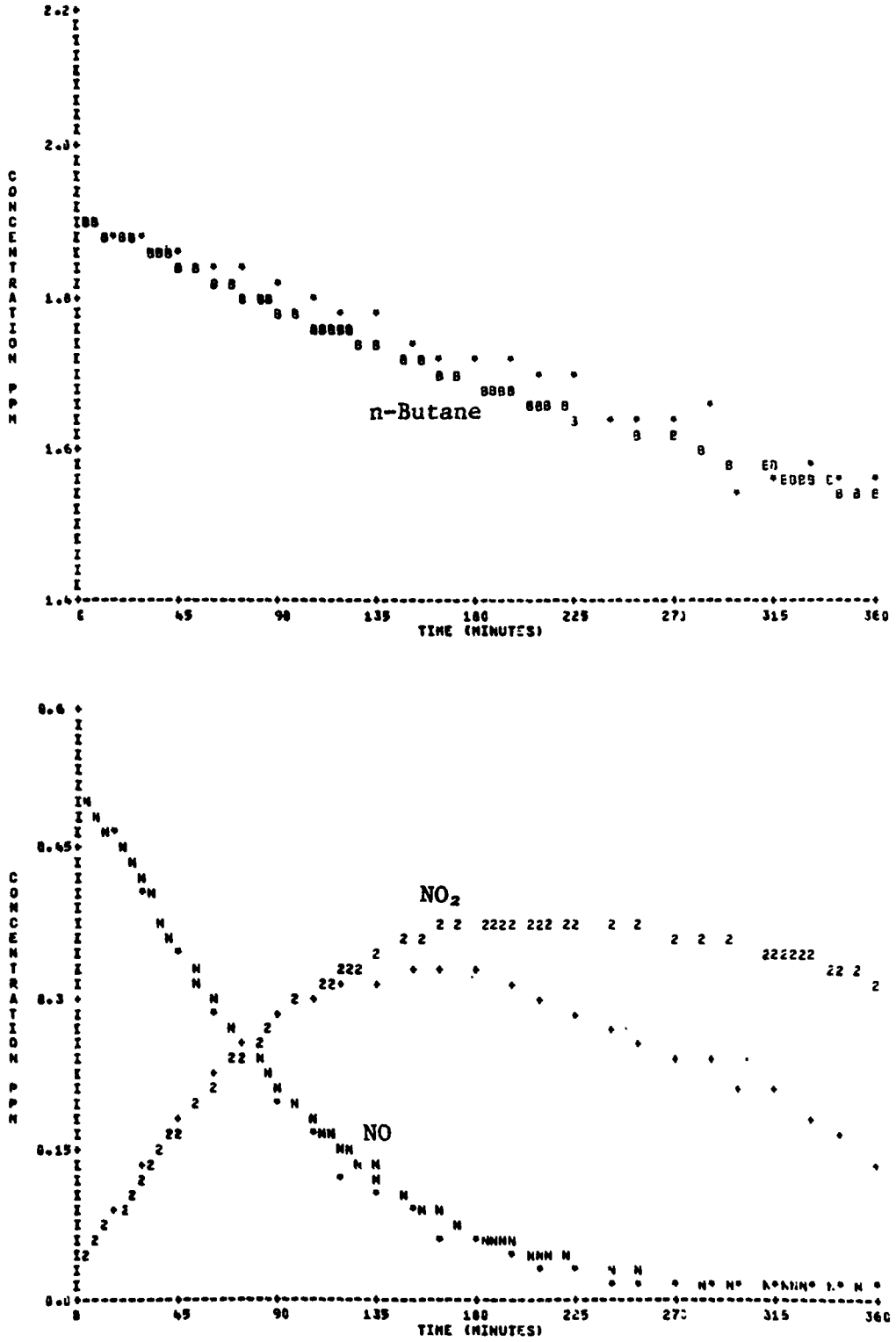

Figure B-9. Simulation of SAPRC EC-48.

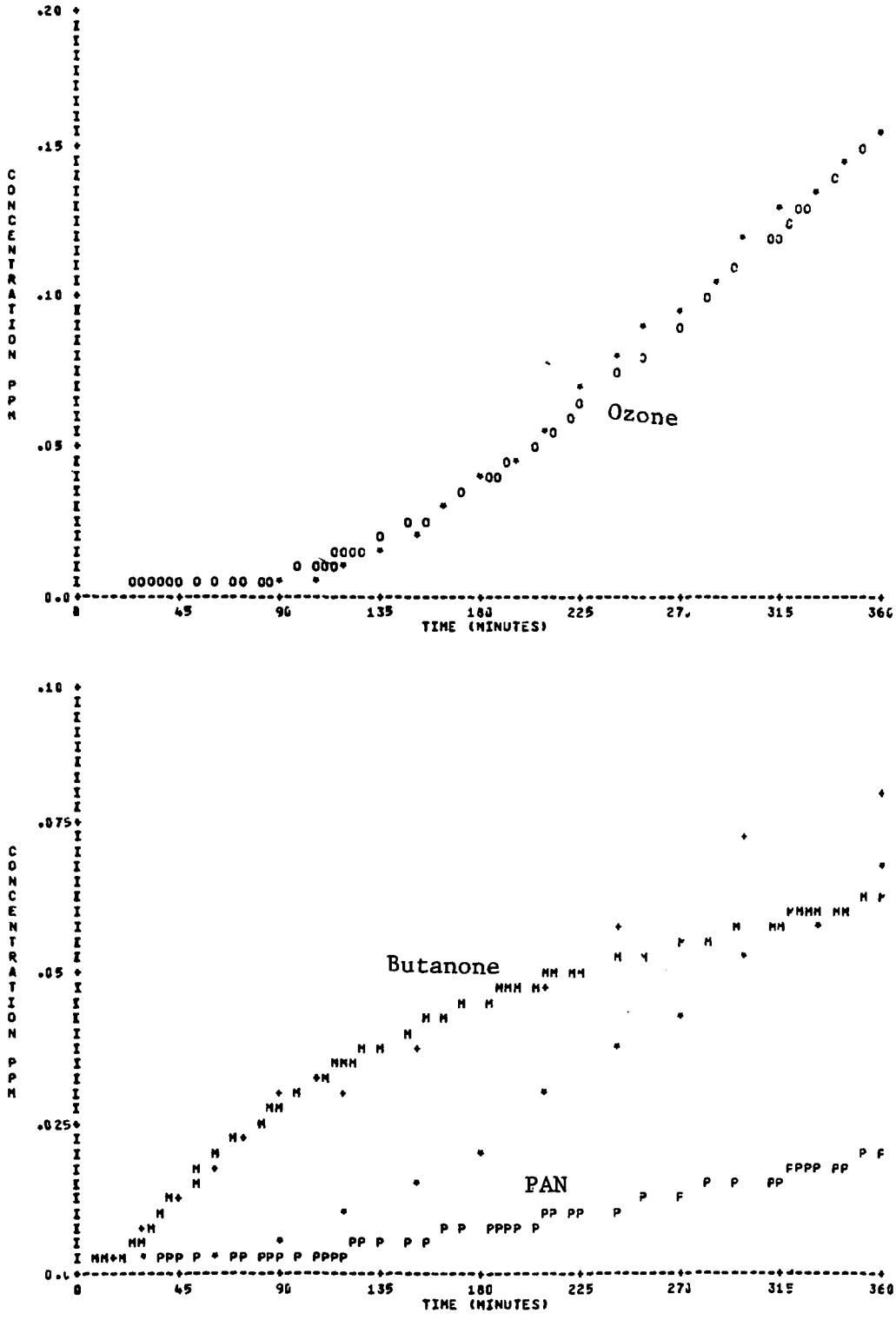

Figure B-9. Simulation of SAPRC EC-48 (Continued).

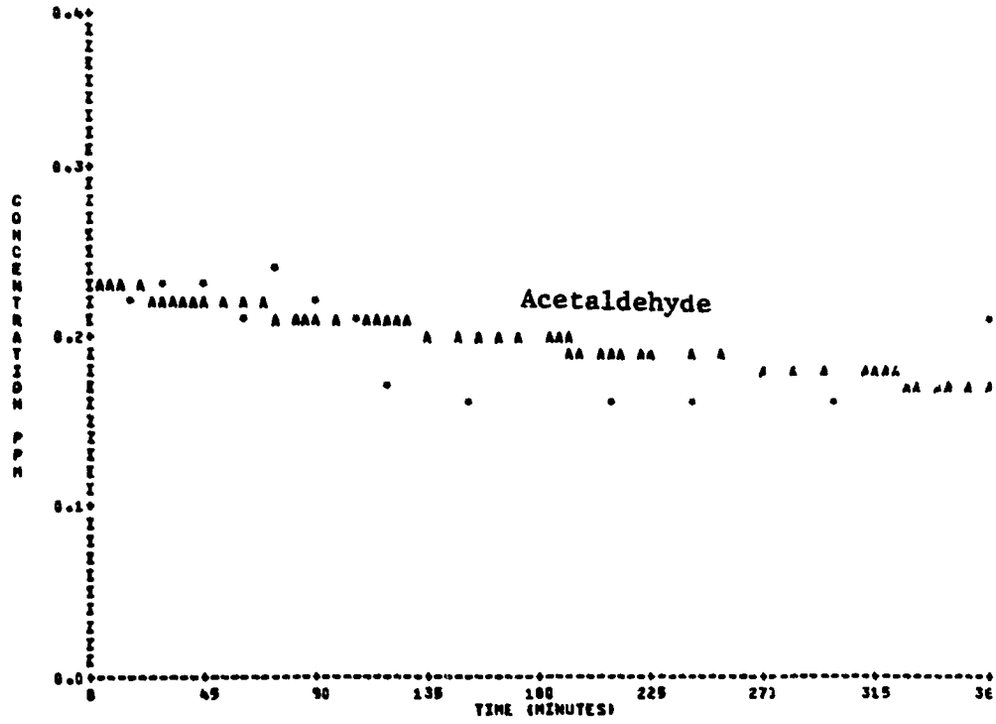

Figure B-9. Simulation of SAPRC EC-48 (Concluded).

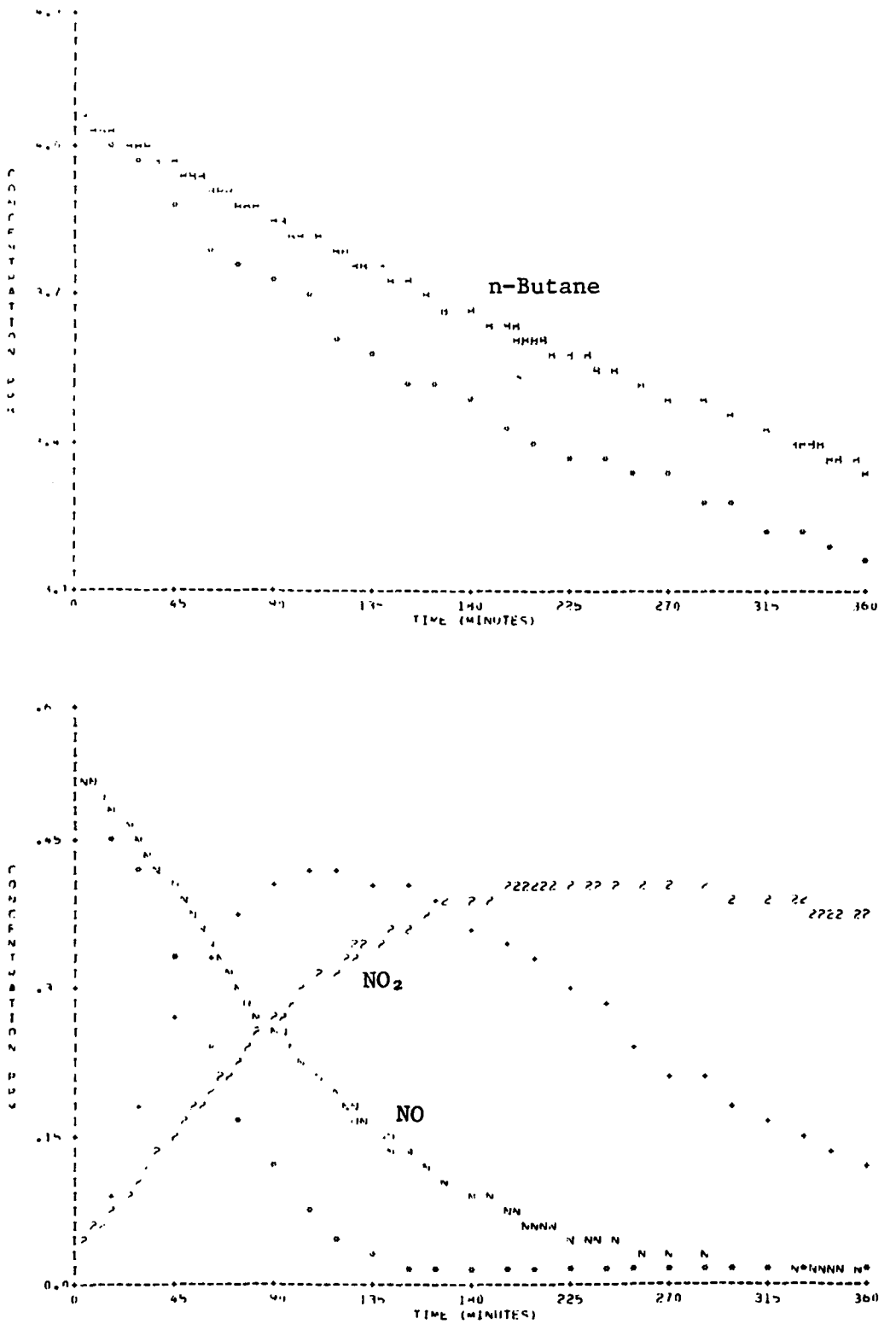

Figure B-10. Simulation of SAPRC EC-49.

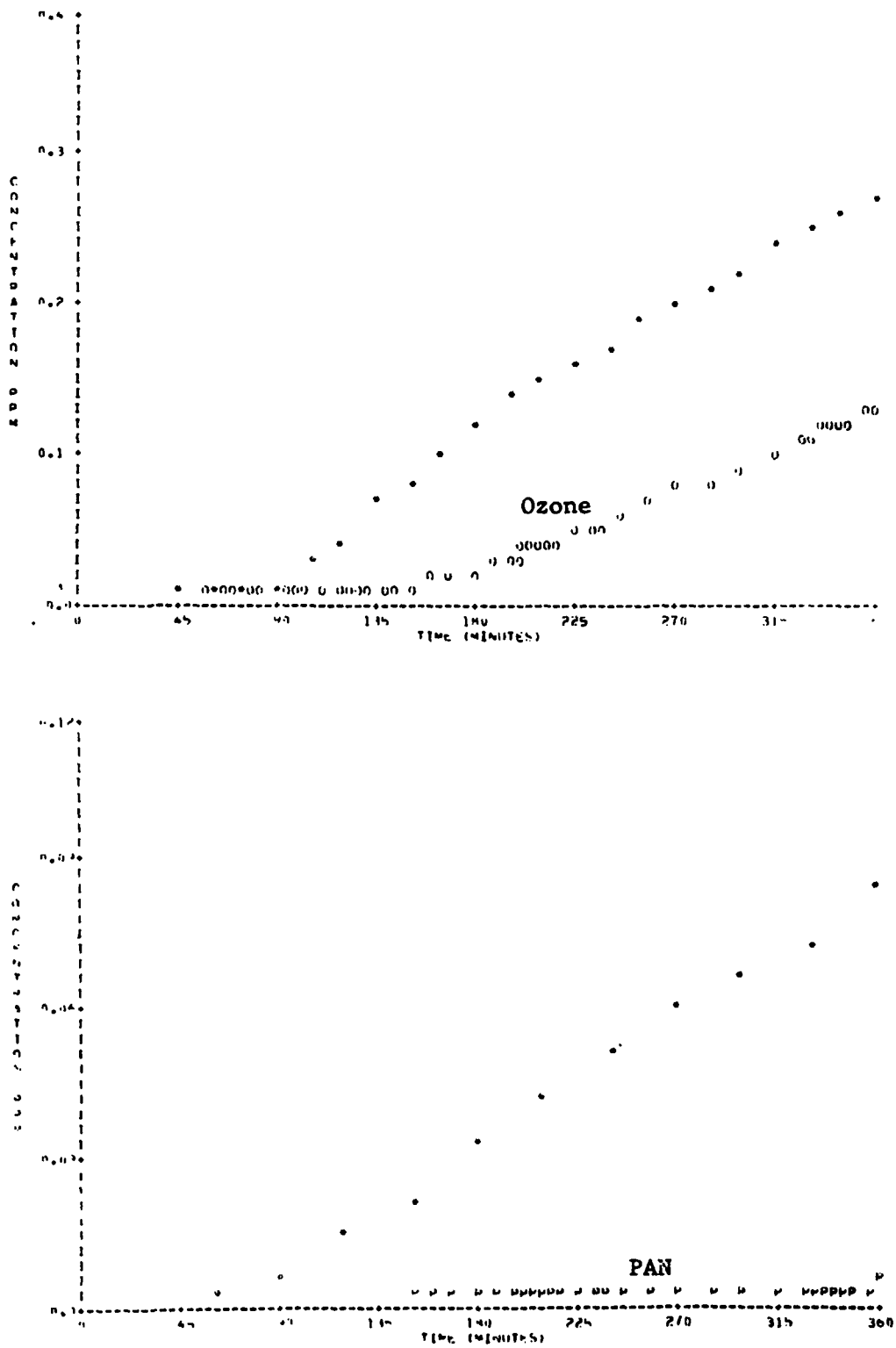

Figure B-10. Simulation of SAPRC EC-49 (Continued).

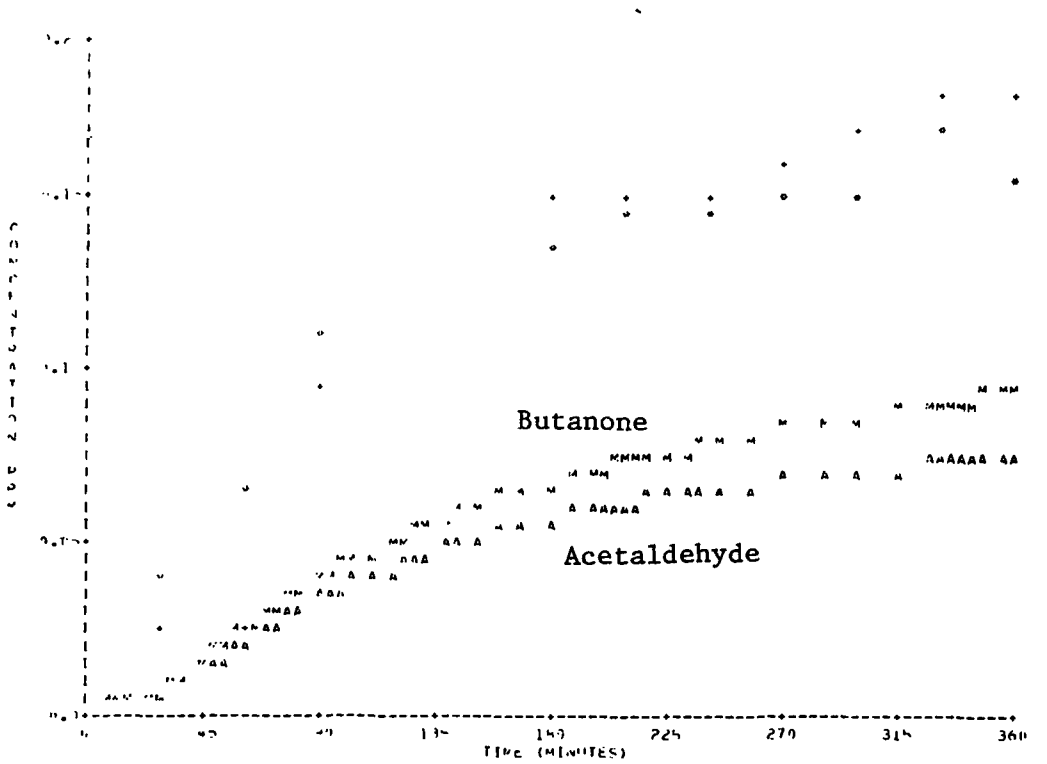

Figure B-10. Simulation of SAPRC EC-49 (Concluded).

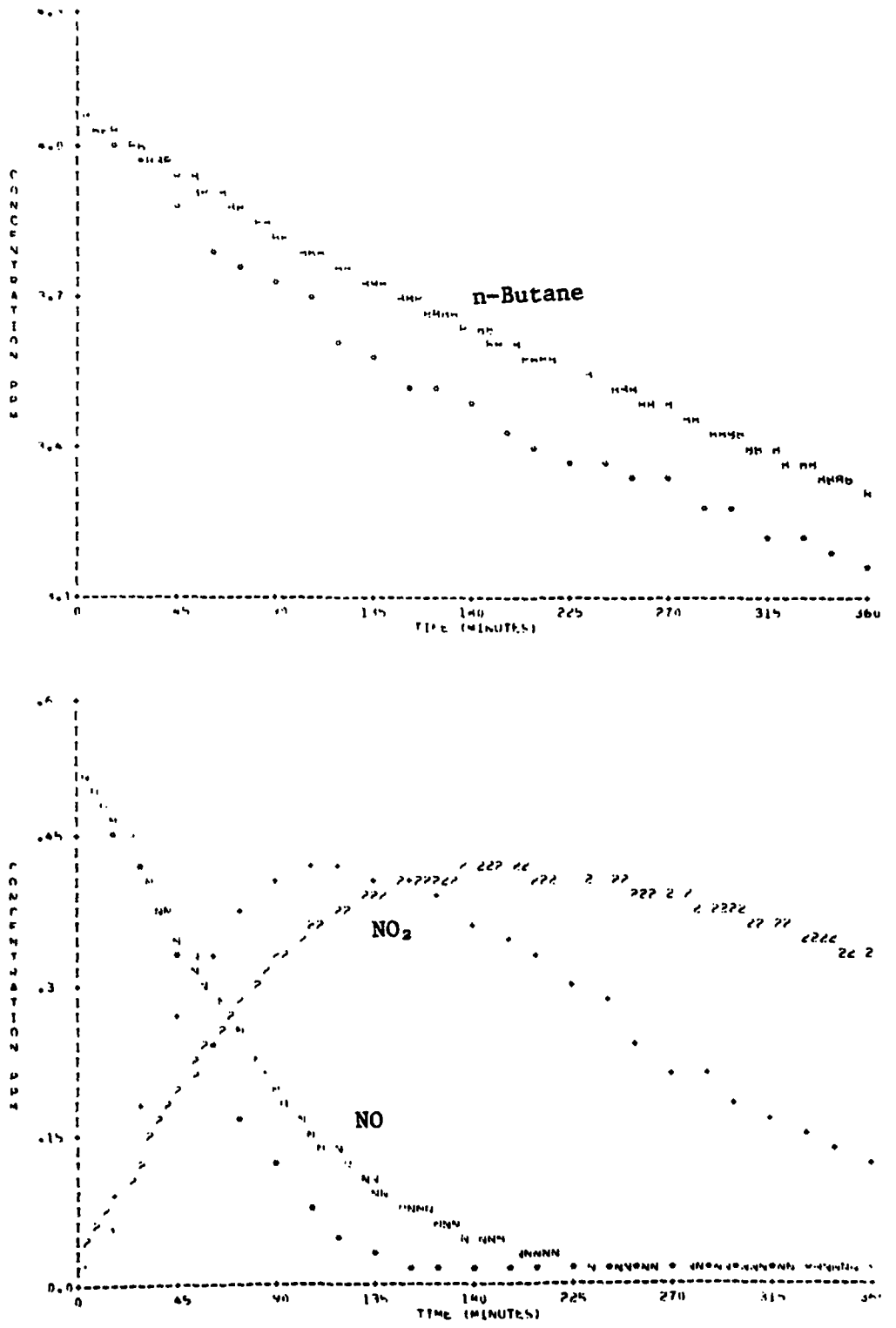

Figure B-10A. Simulation of SAPRC EC-49.
(Radical Addition Rate = 3 x 10^{-4} min^{-1})

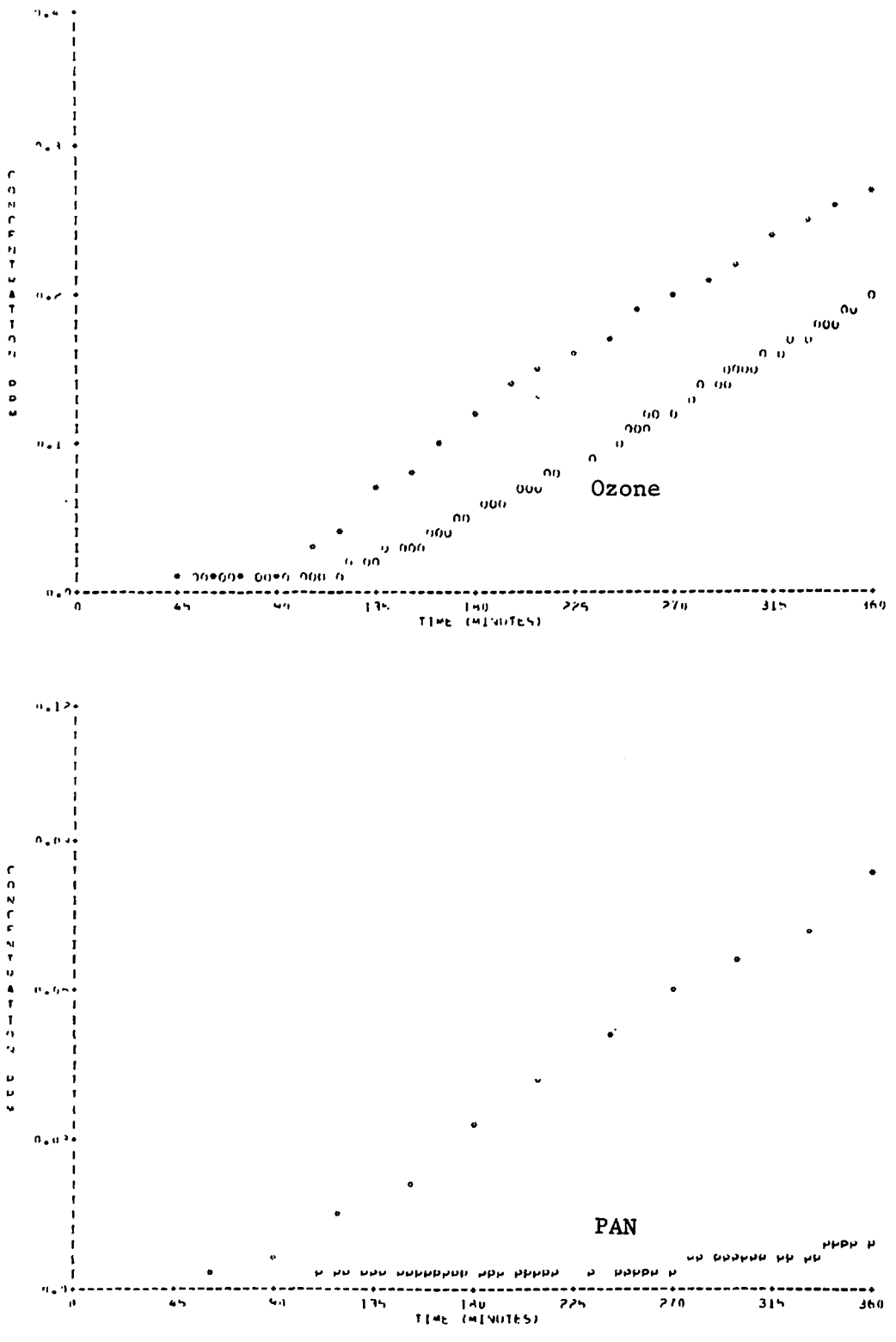

Figure B-10A. Simulation of SAPRC EC-49.
(Radical Addition Rate = 3 x 10^{-4} min^{-1}) (Continued).

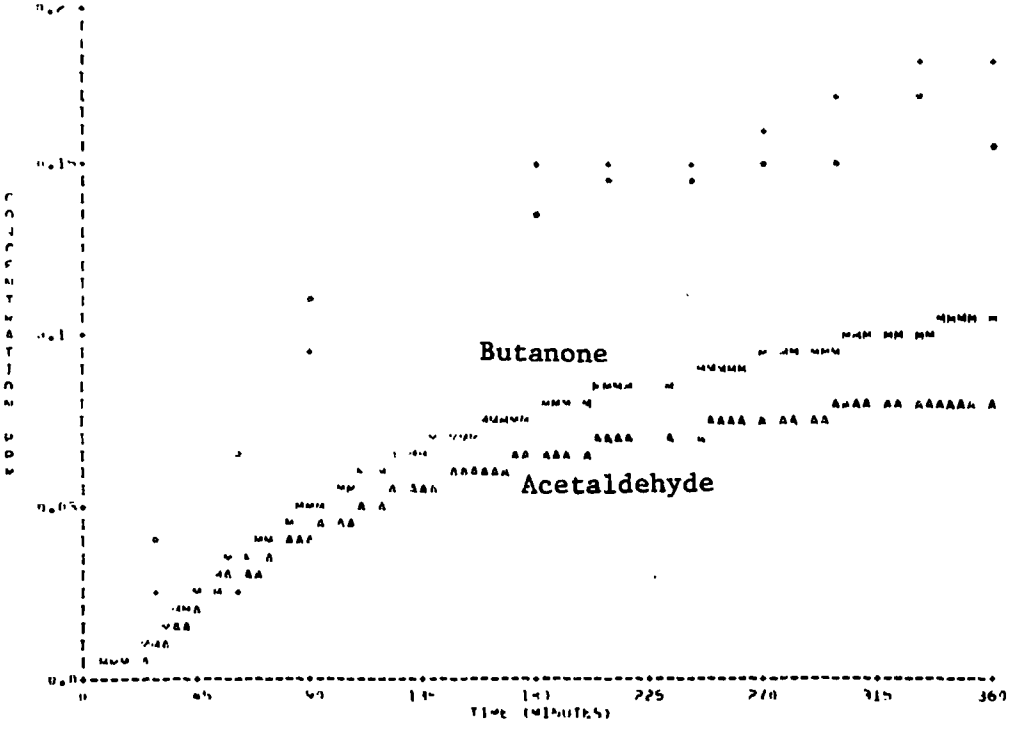

Figure B-10A. Simulation of SAPRC EC-49
(Radical Addition Rate = 3 x 10^{-4} min^{-1}) (Concluded).

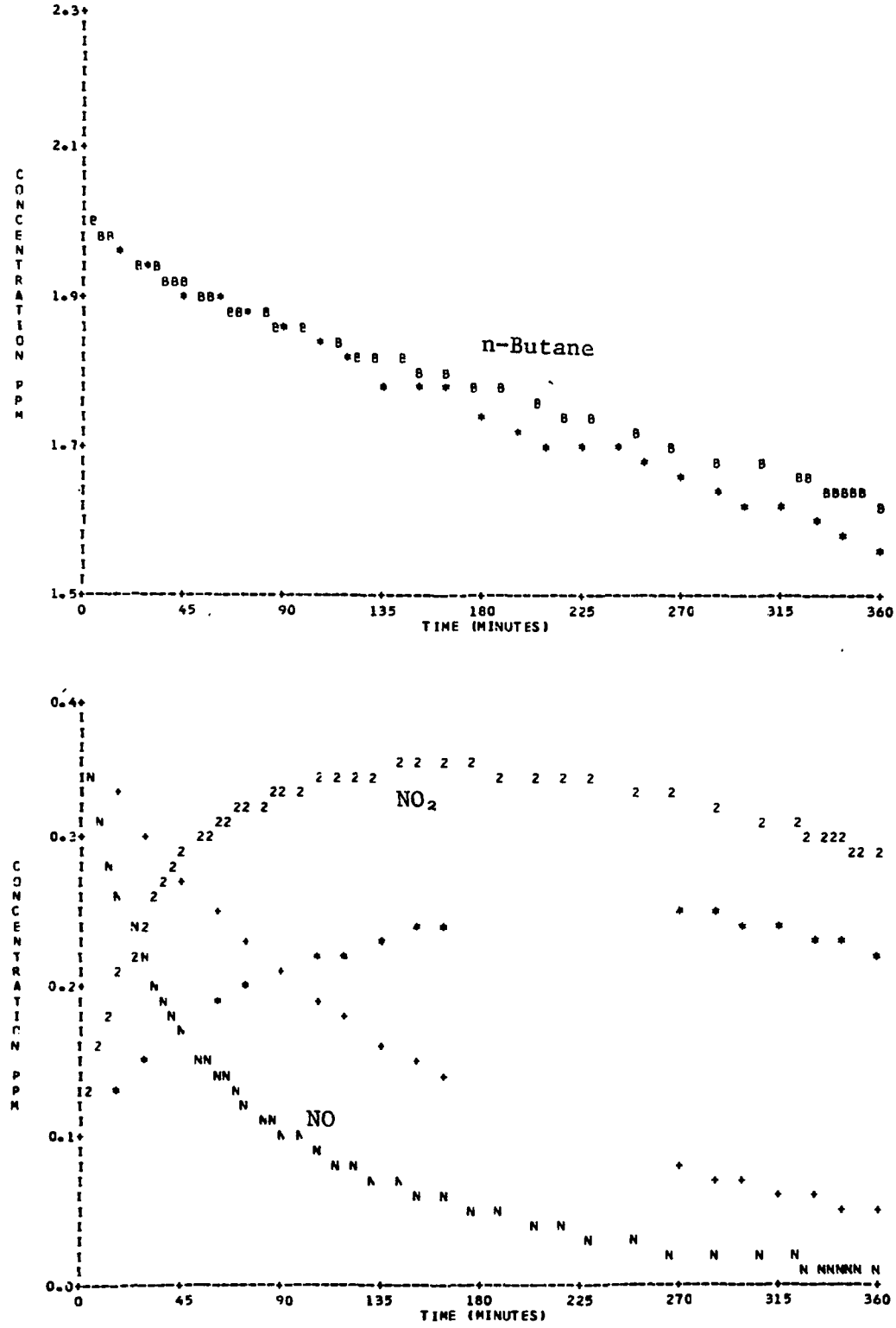

Figure B-11. Simulation of SAPRC EC-162.

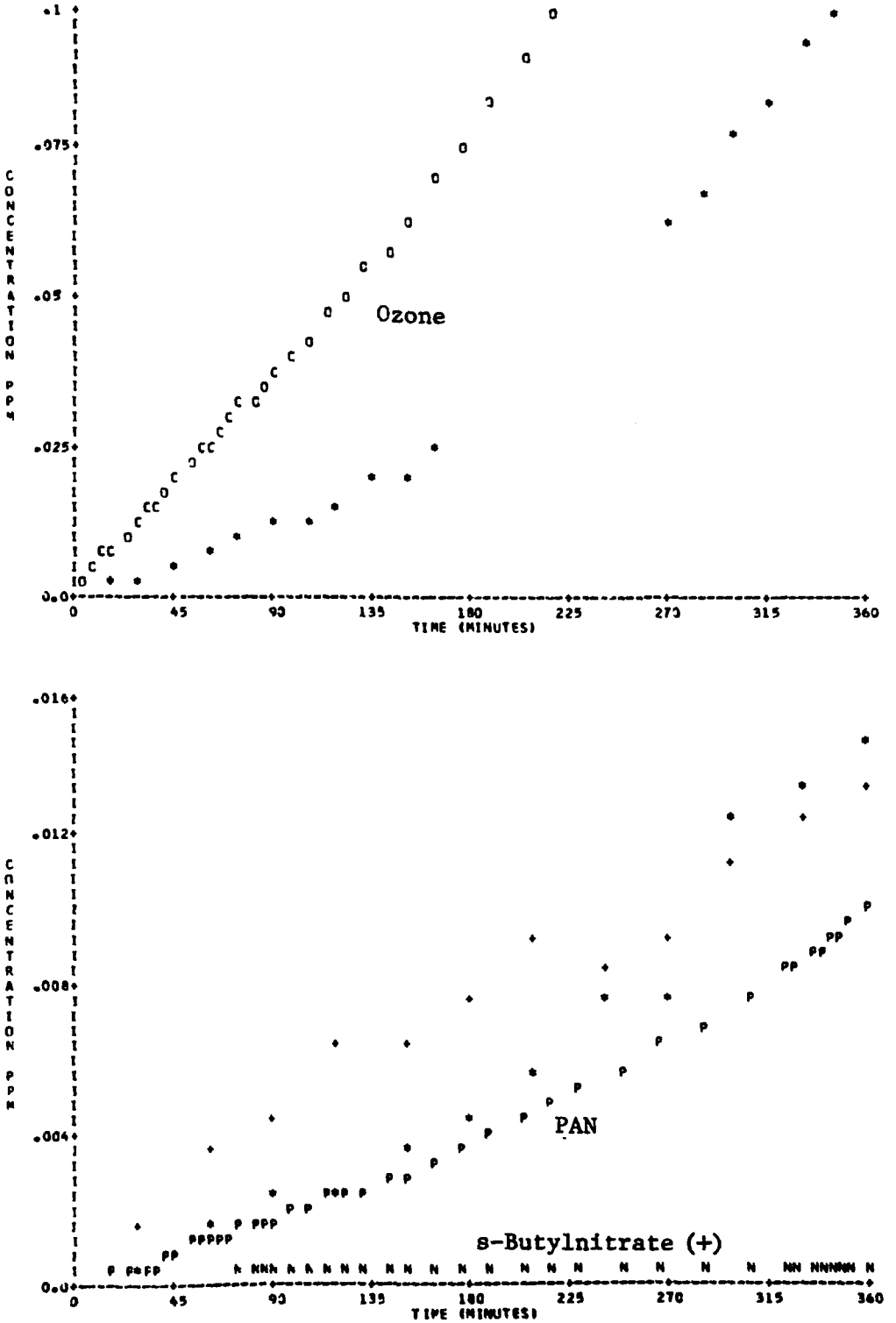

Figure B-11. Simulation of SAPRC EC-162 (Continued).

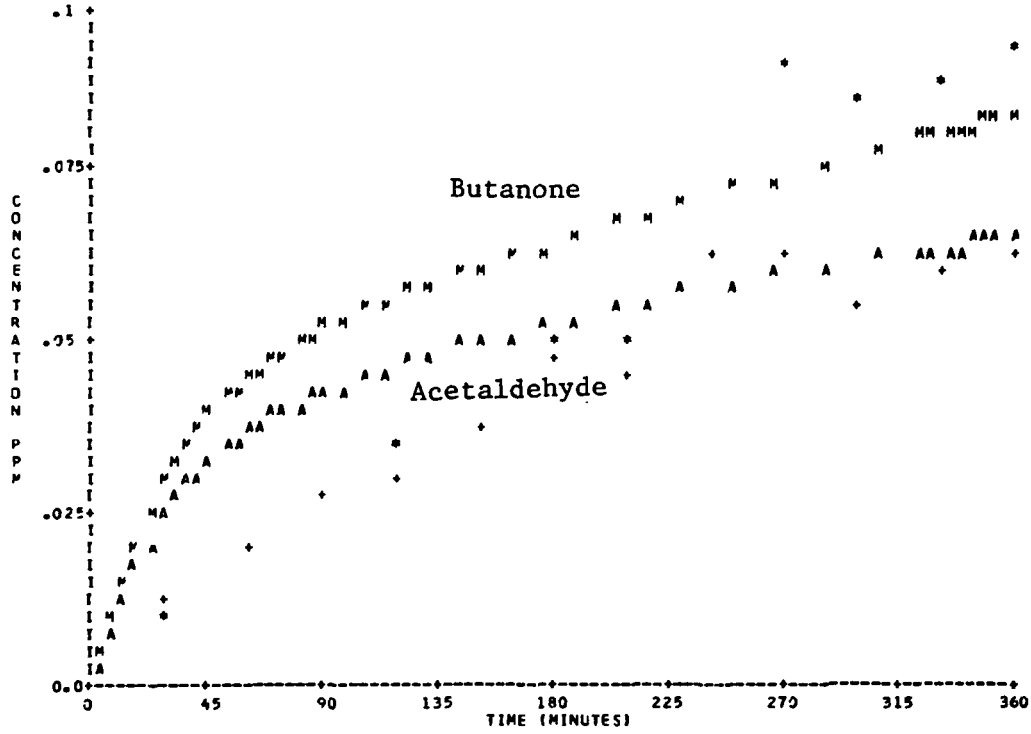

Figure B-11. Simulation of SAPRC EC-162 (Concluded).

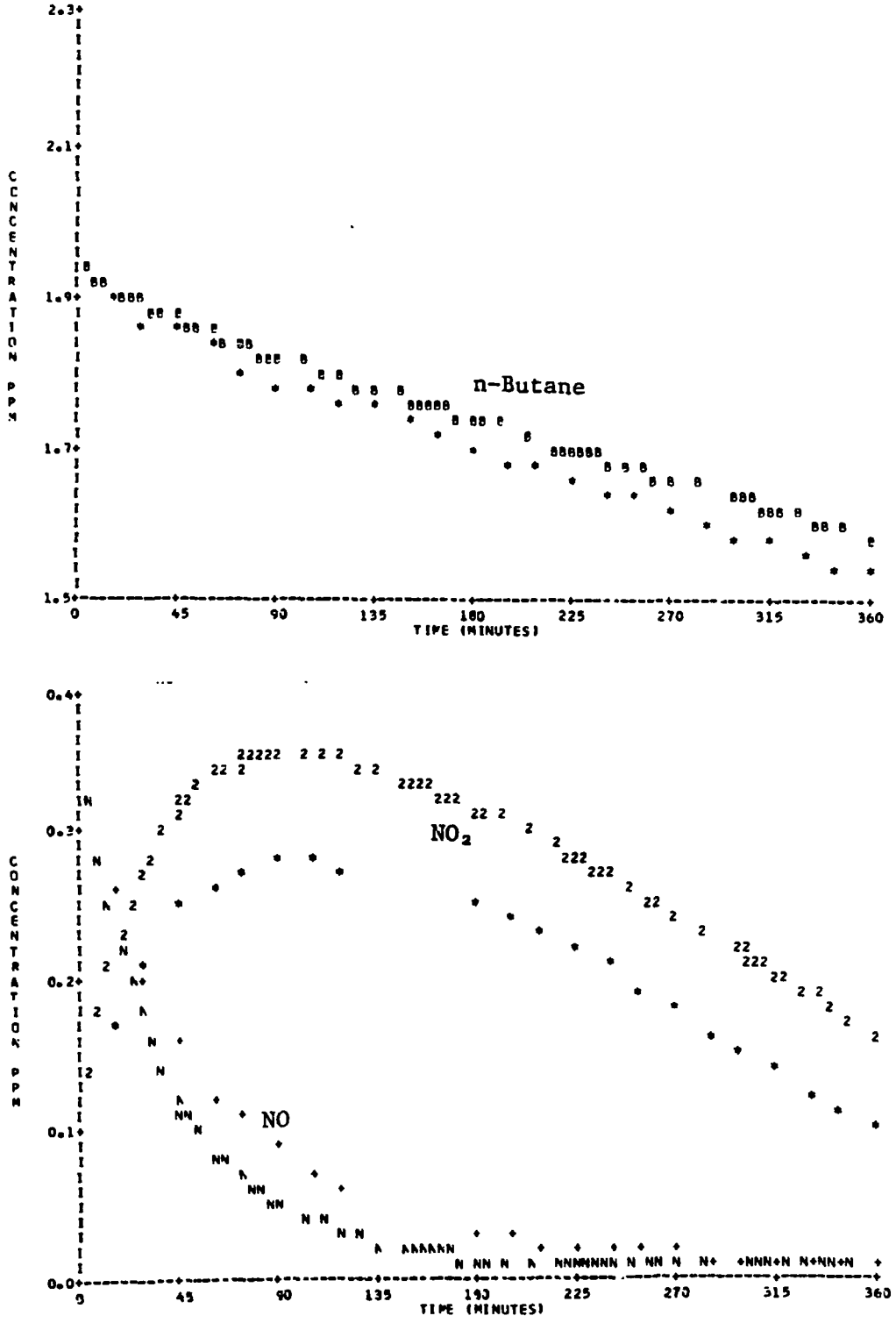

Figure B-12. Simulation of SAPRC EC-163.

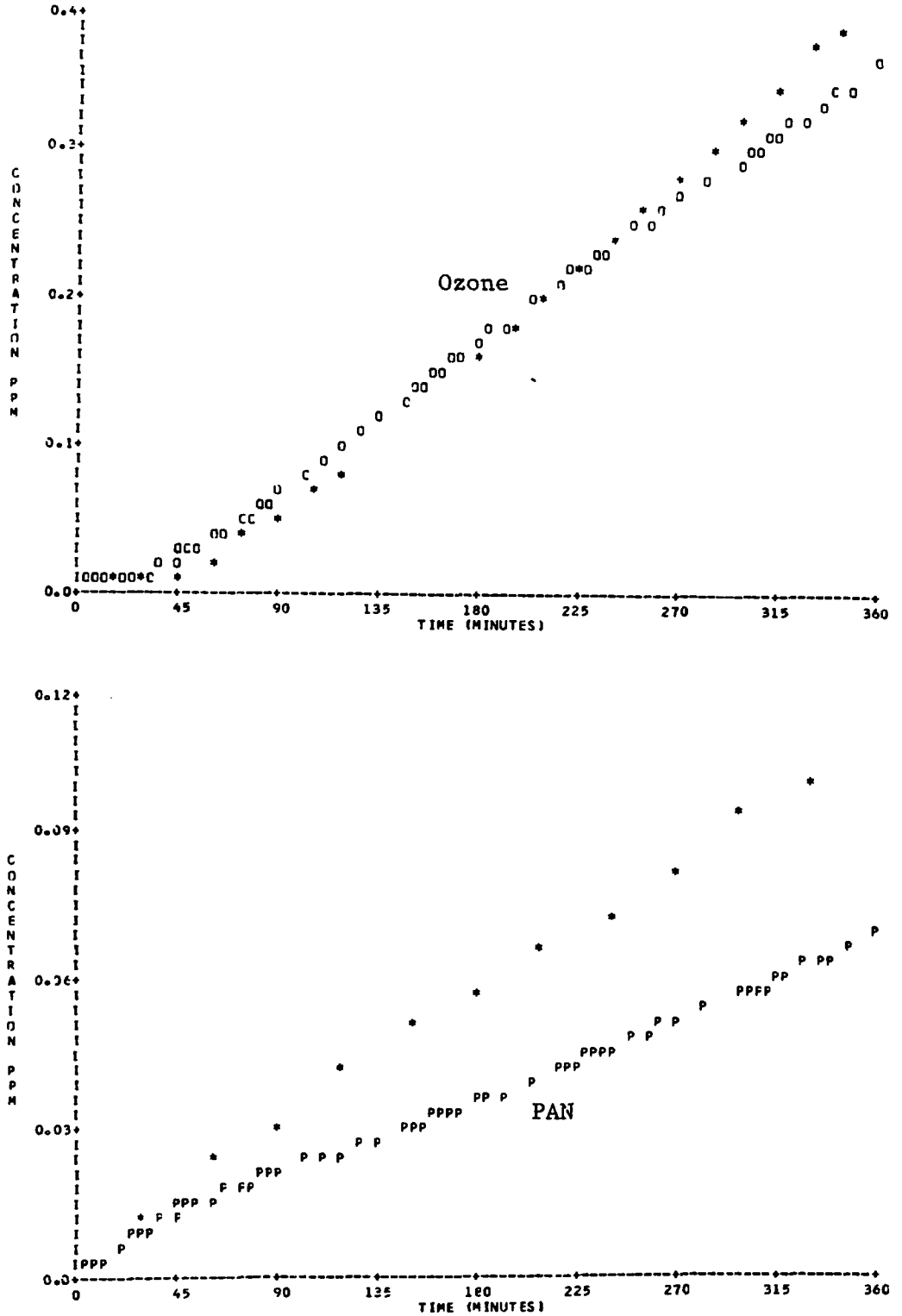

Figure B-12. Simulation of SAPRC EC-163 (Continued).

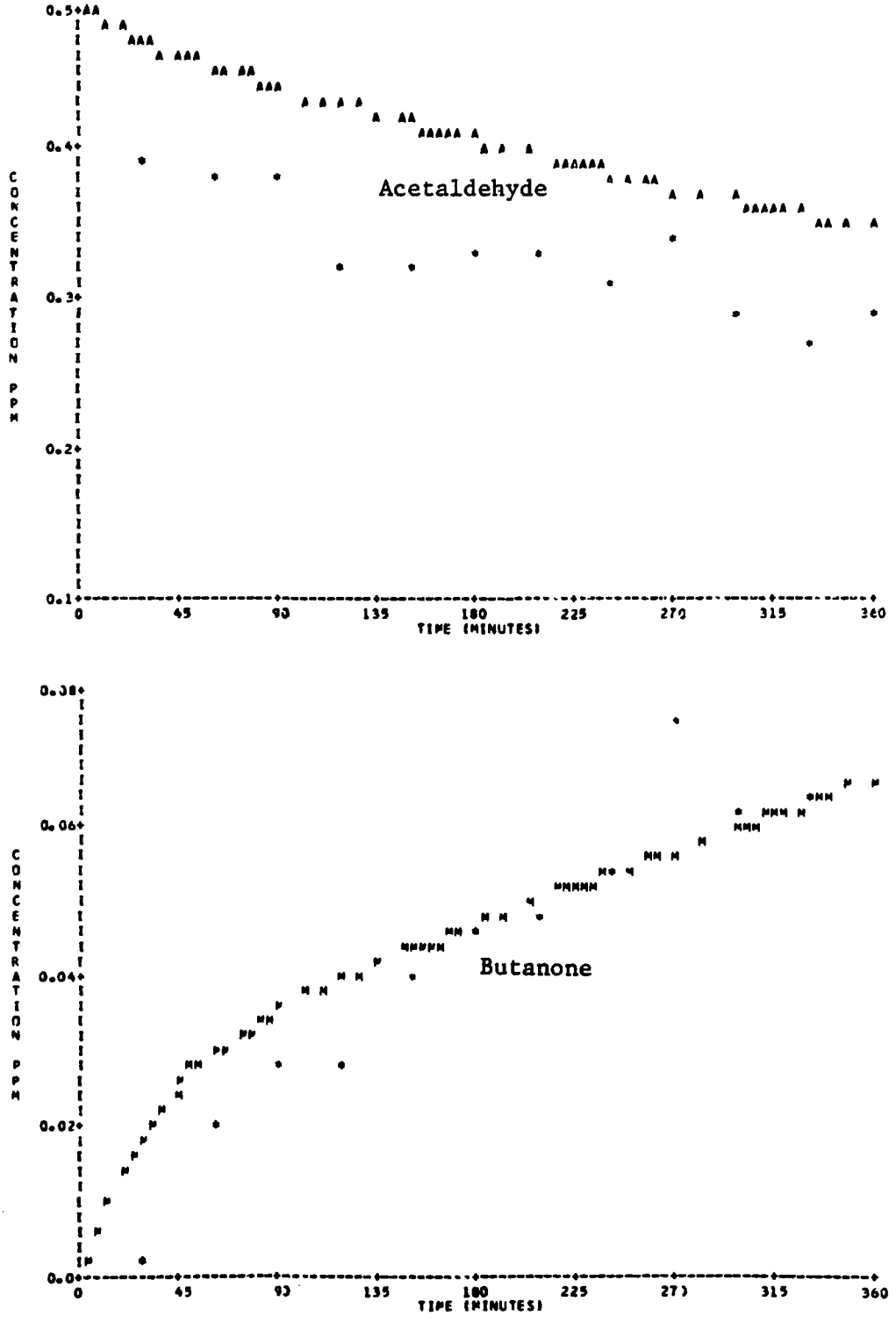

Figure B-12. Simulation of SAPRC EC-163 (Concluded).

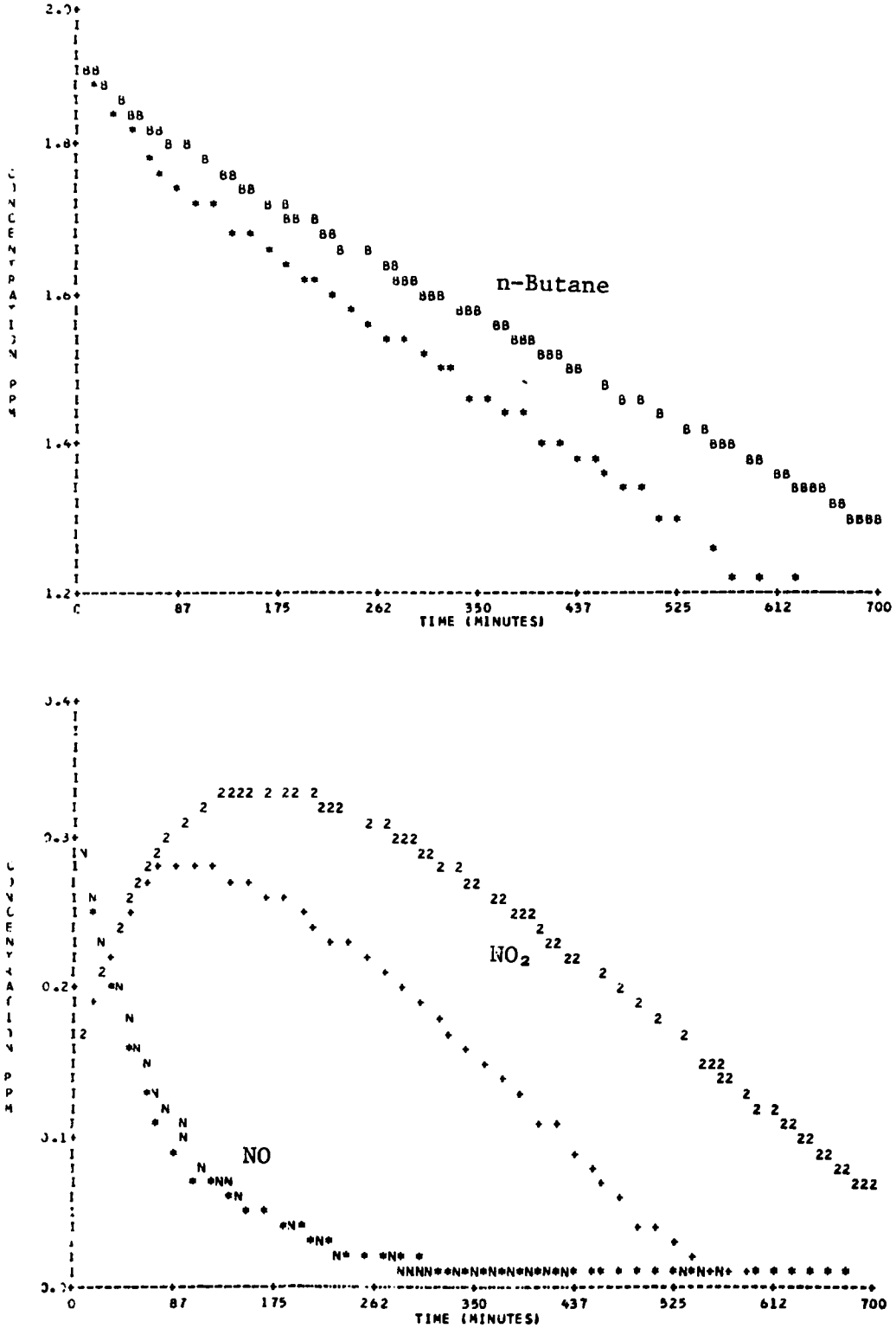

Figure B-13. Simulation of SAPRC EC-168.

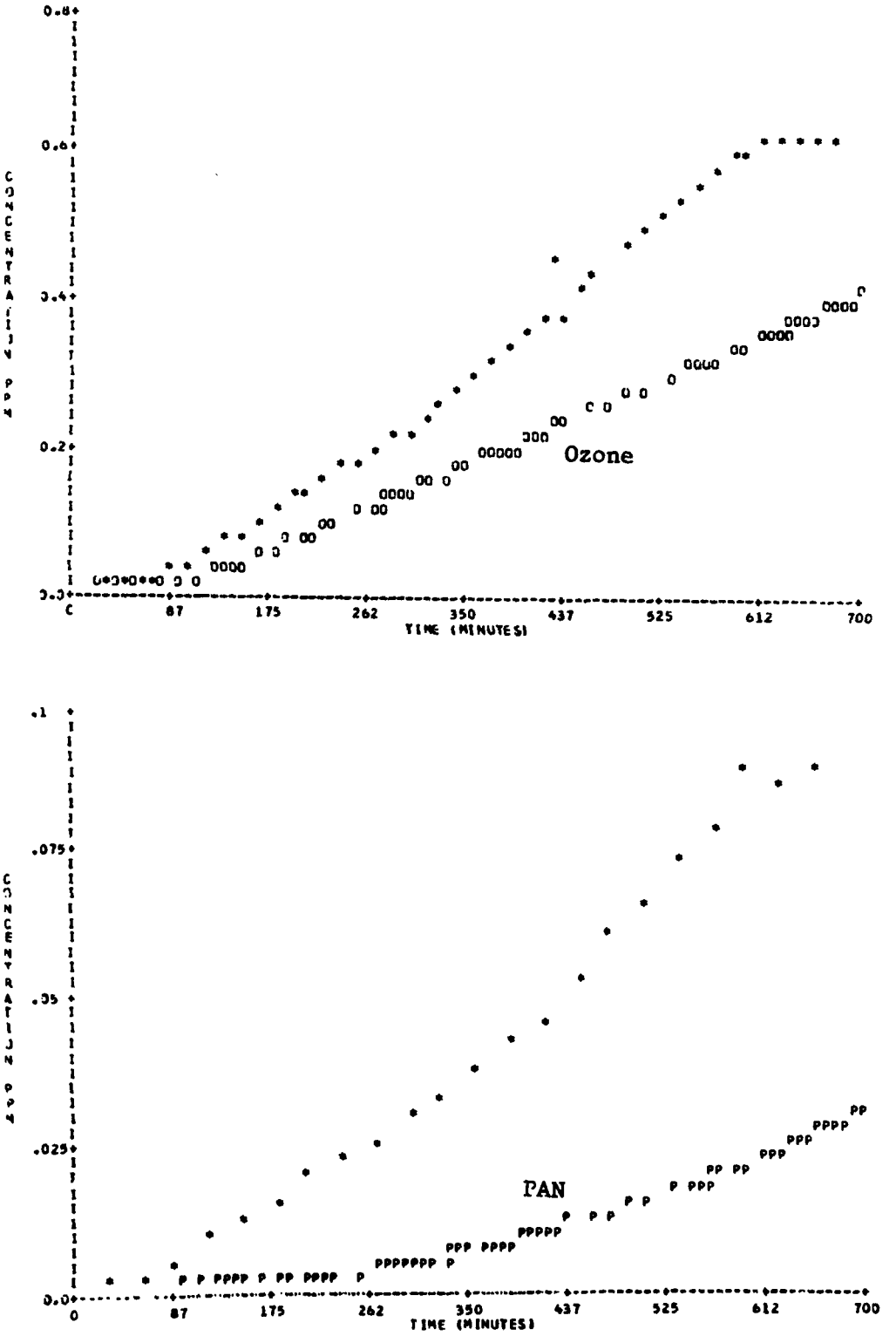

Figure B-13. Simulation of SAPRC EC-168 (Continued).

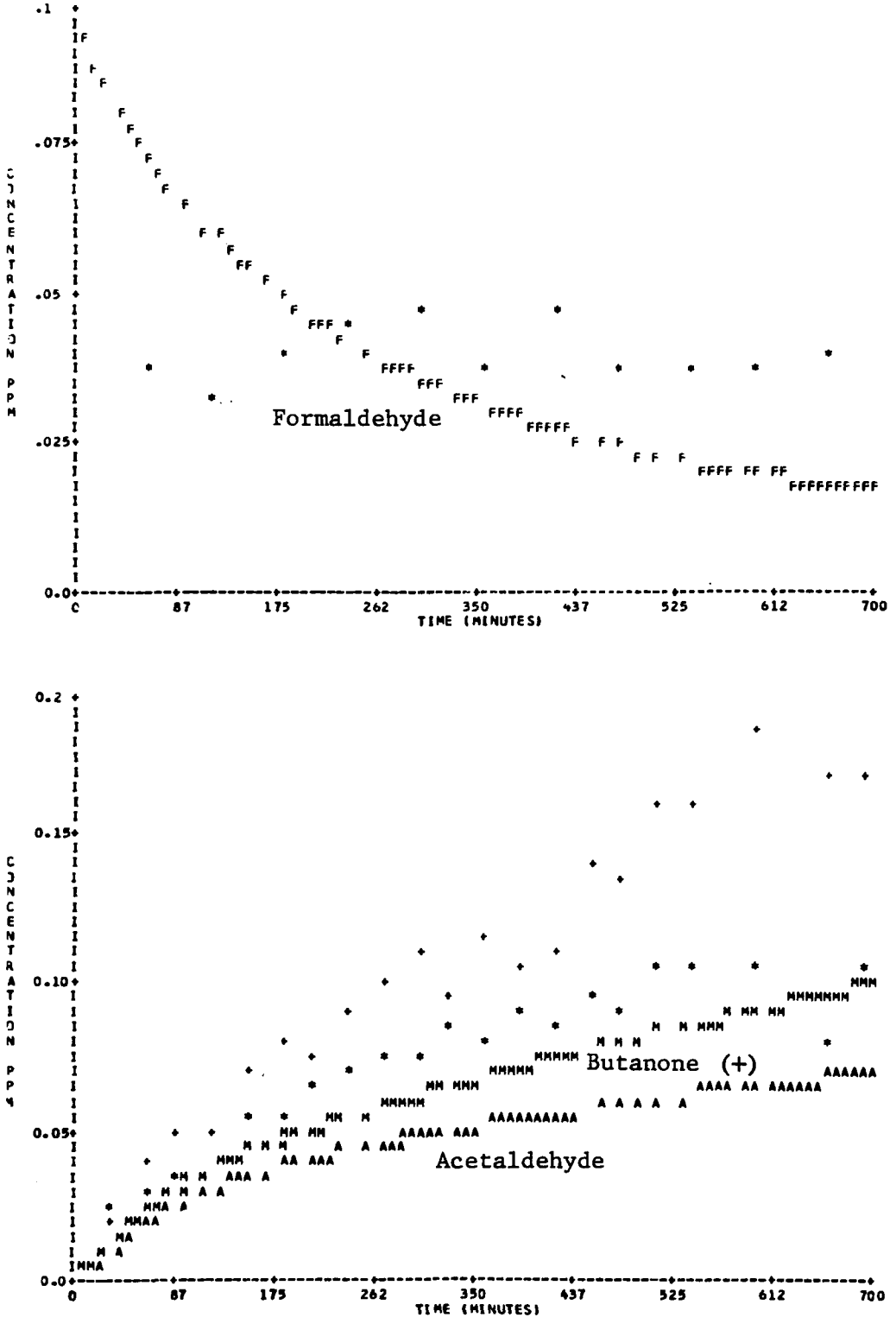

Figure B-13. Simulation of SAPRC EC-168 (Concluded).

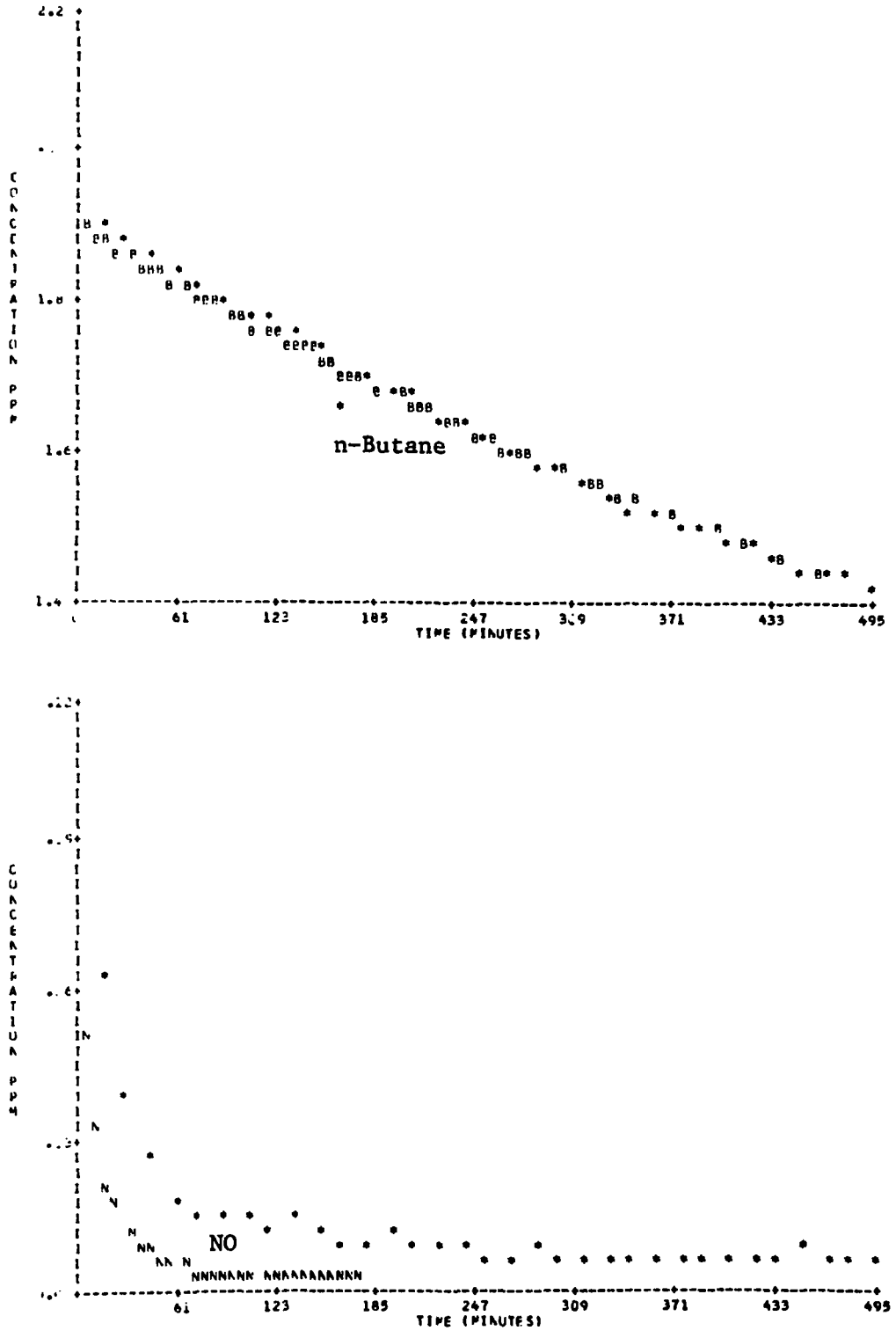

Figure B-14. Simulation of SAPRC EC-178.

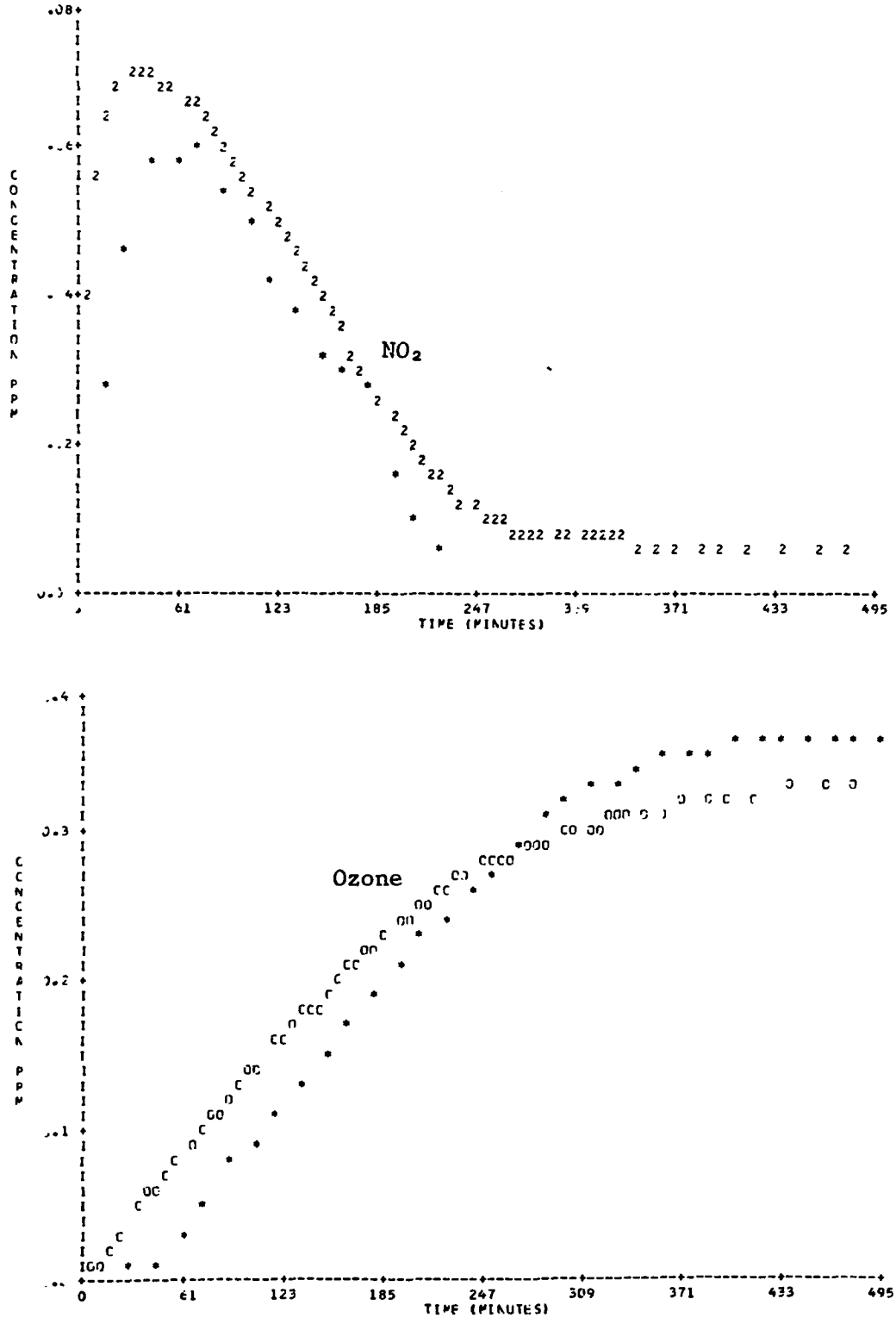

Figure B-14. Simulation of SAPRC EC-178 (Continued).

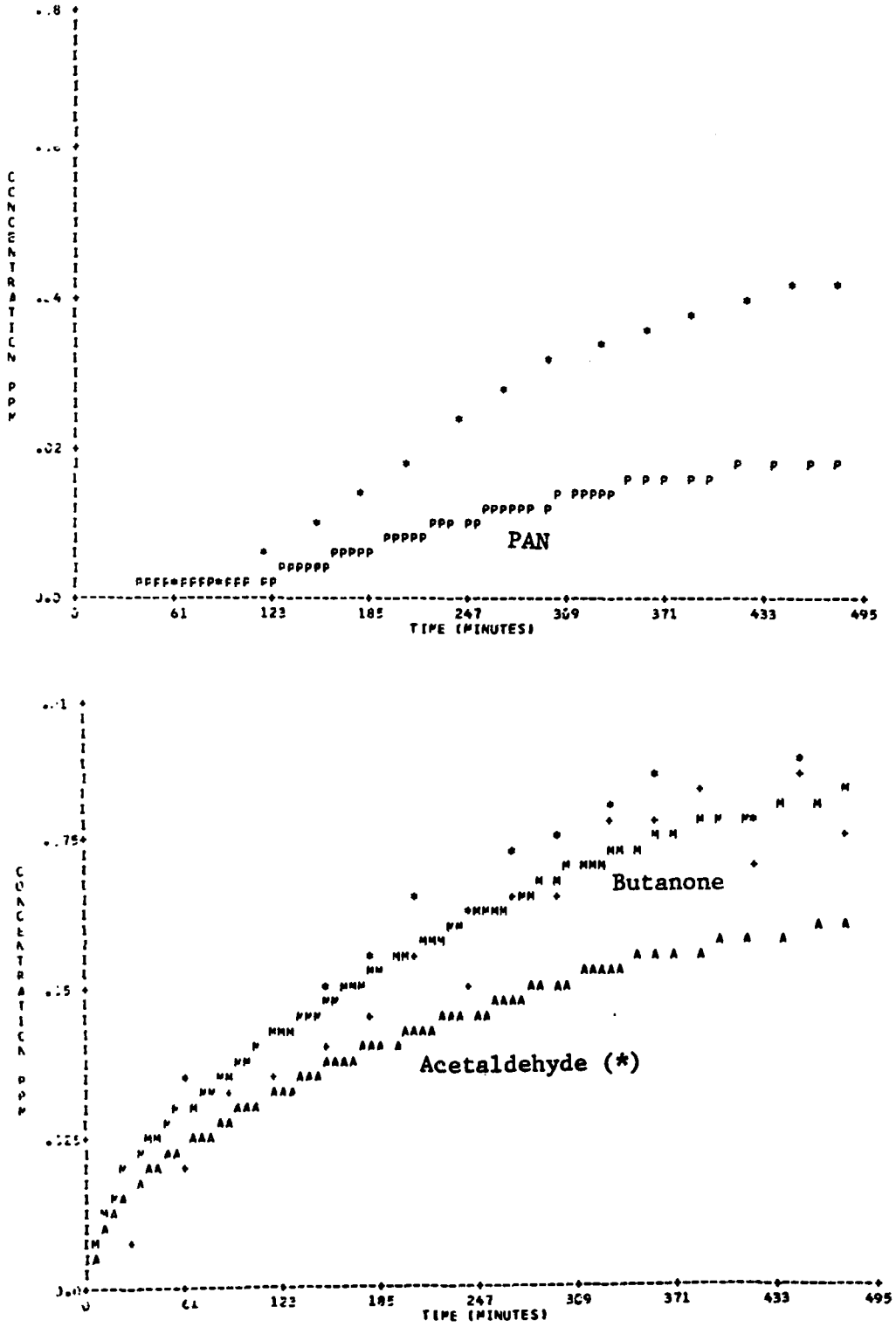

Figure B-14. Simulation of SAPRC EC-178 (Concluded).

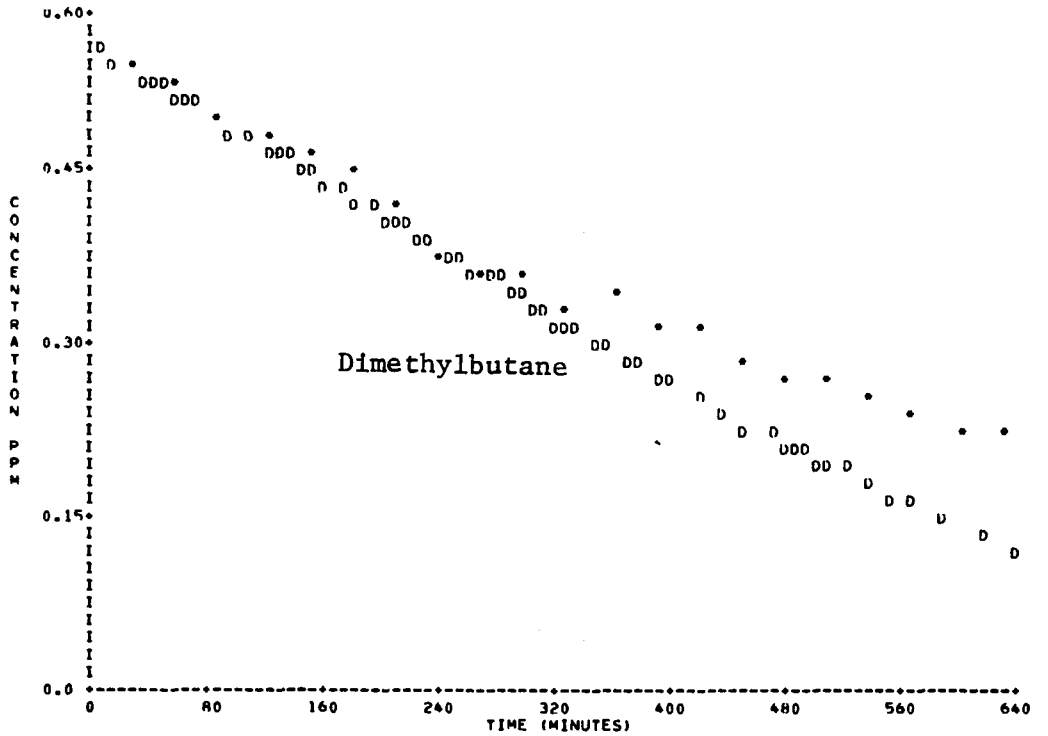

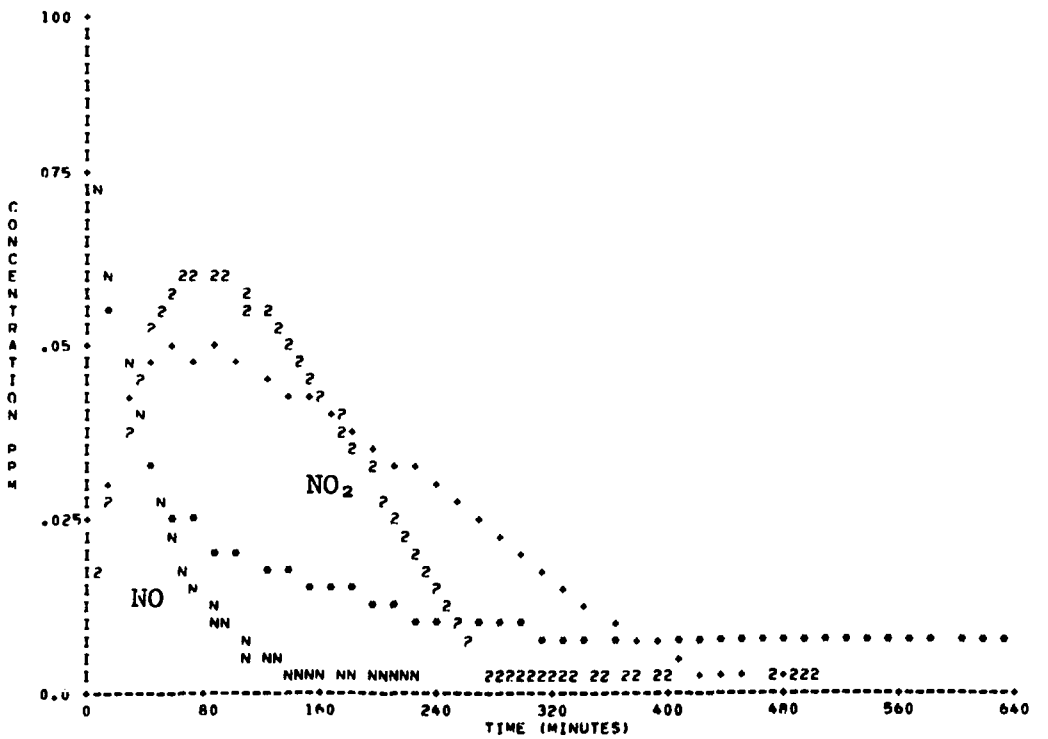

Figure B-15. Simulation of SAPRC EC-171.

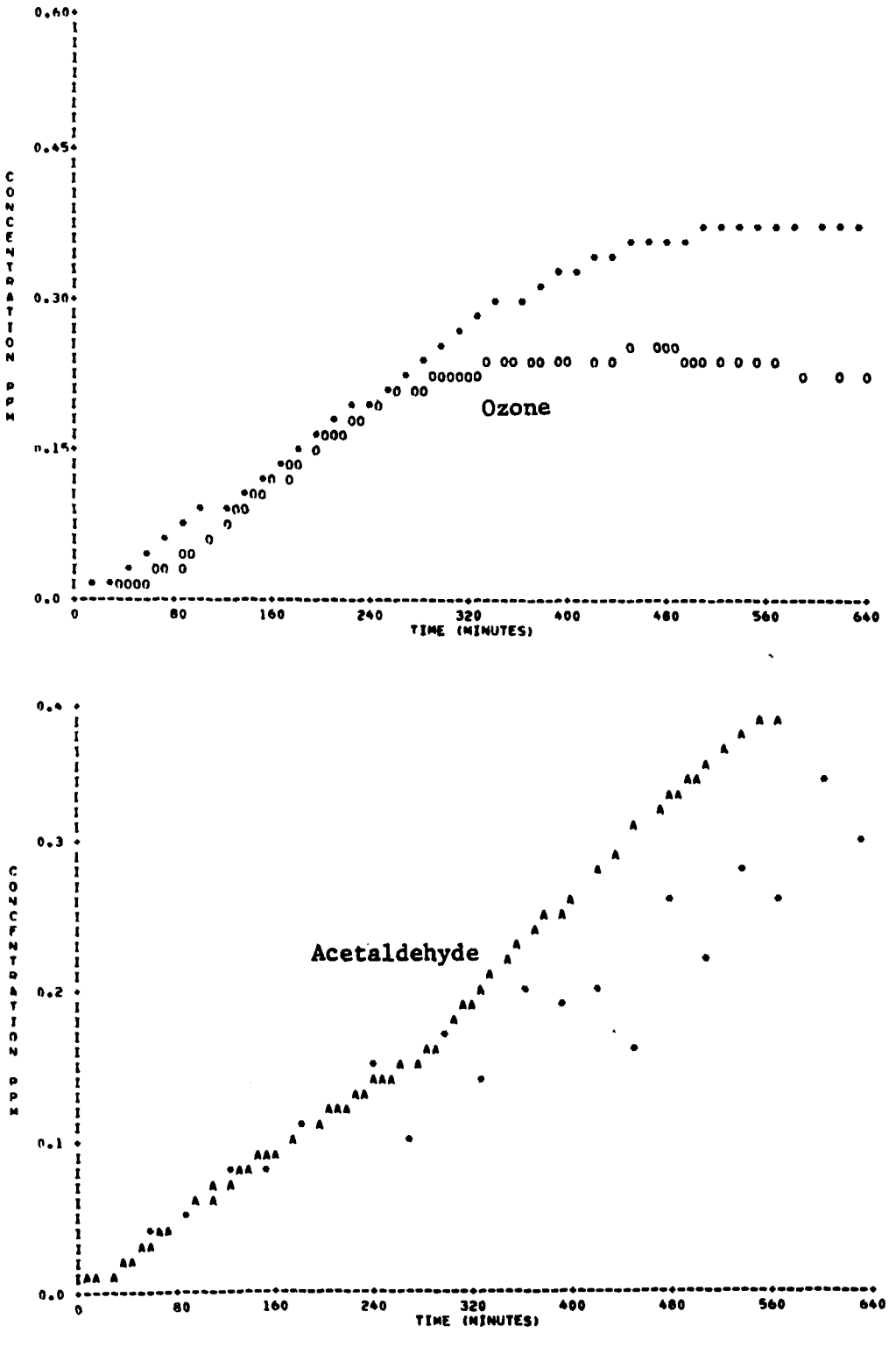

Figure B-15. Simulation of SAPRC EC-171 (Continued).

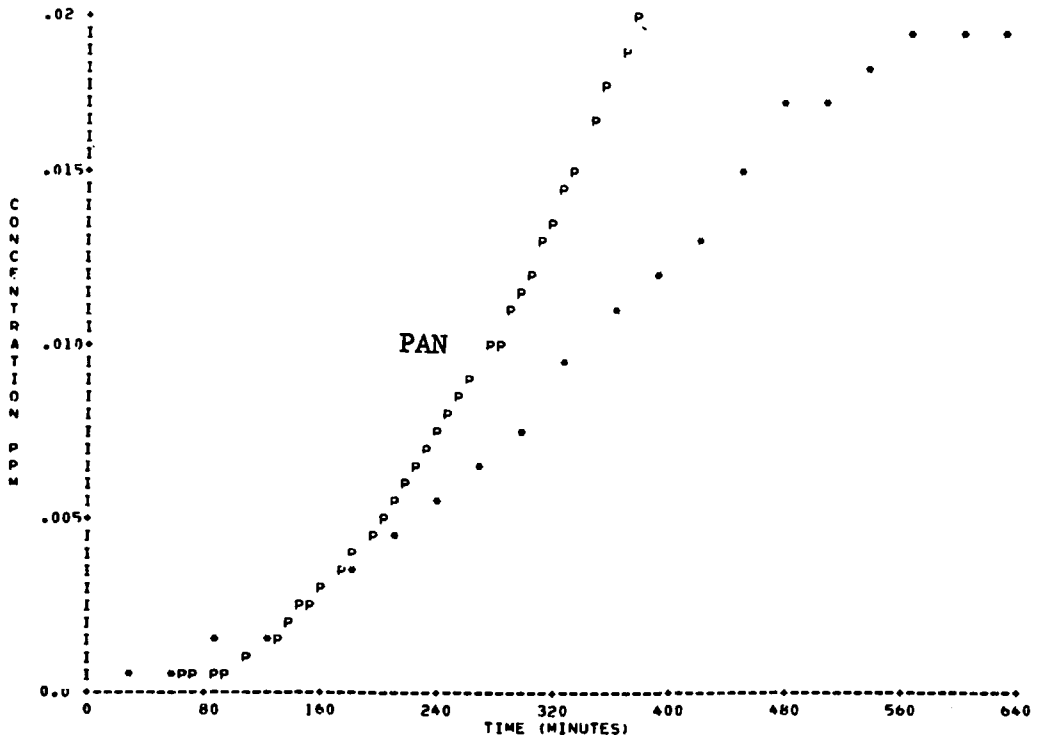

Figure B-15. Simulation of SAPRC EC-171 (Concluded).

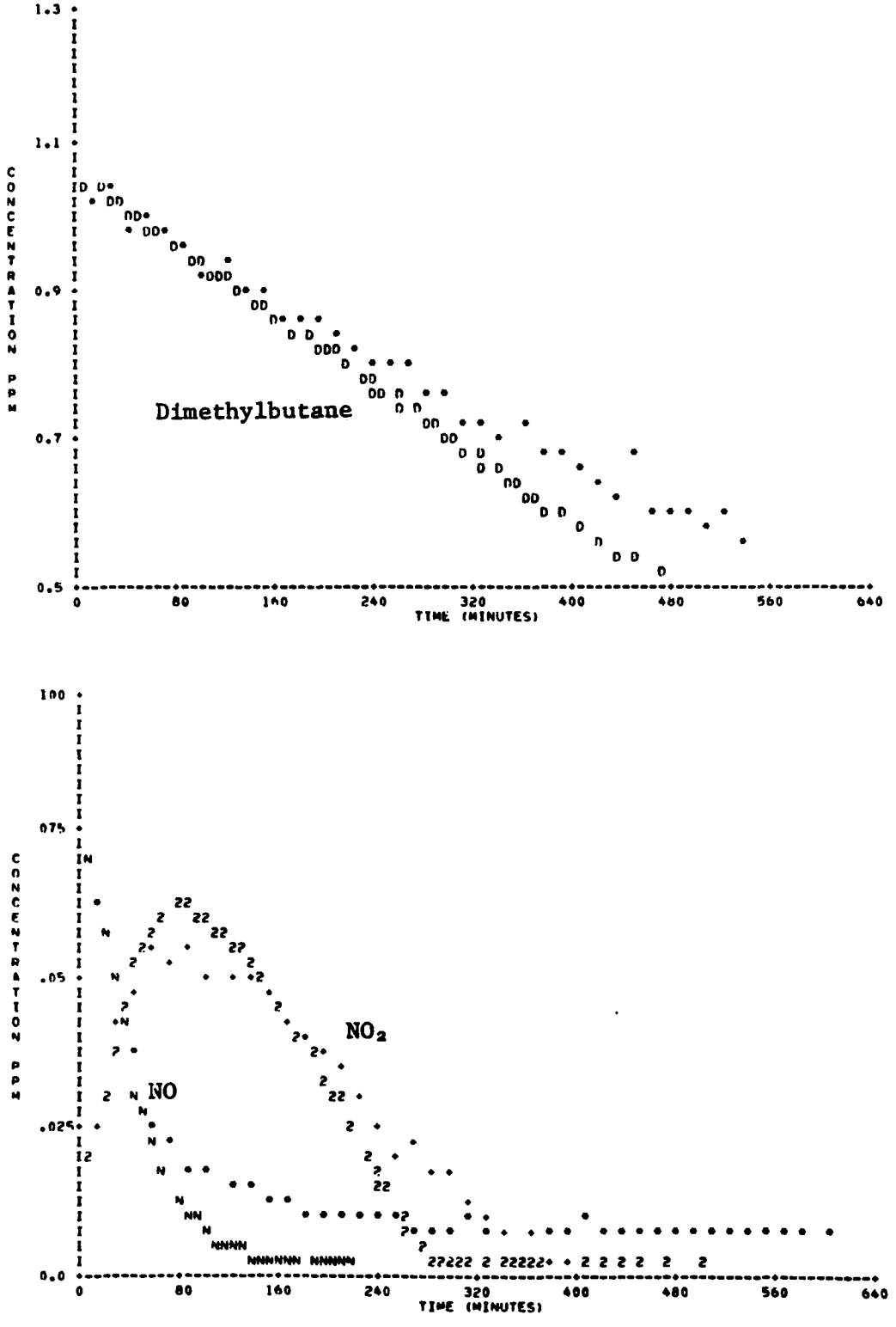

Figure B-16. Simulation of SAPRC EC-165.

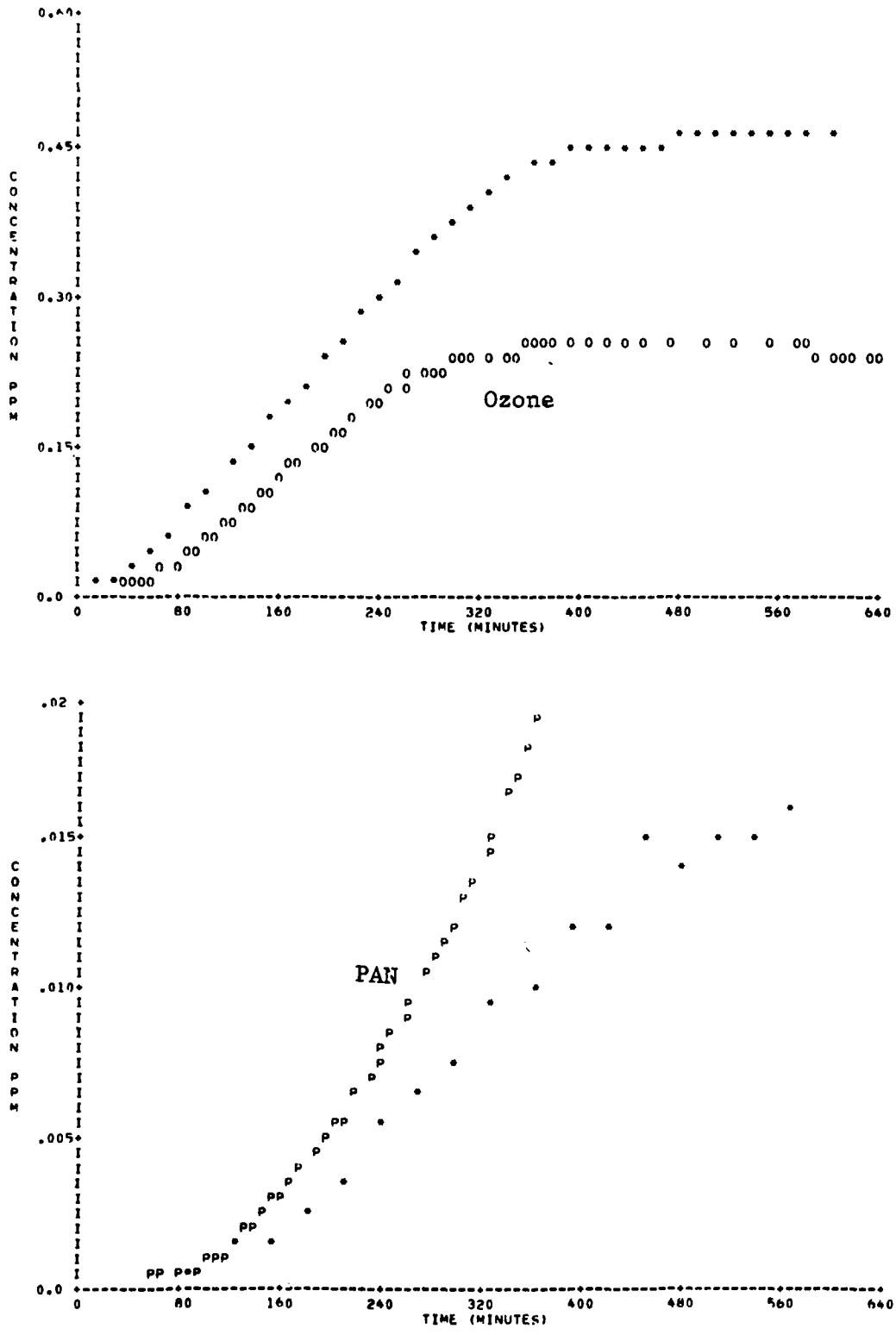

Figure B-16. Simulation of SAPRC EC-165 (Continued).

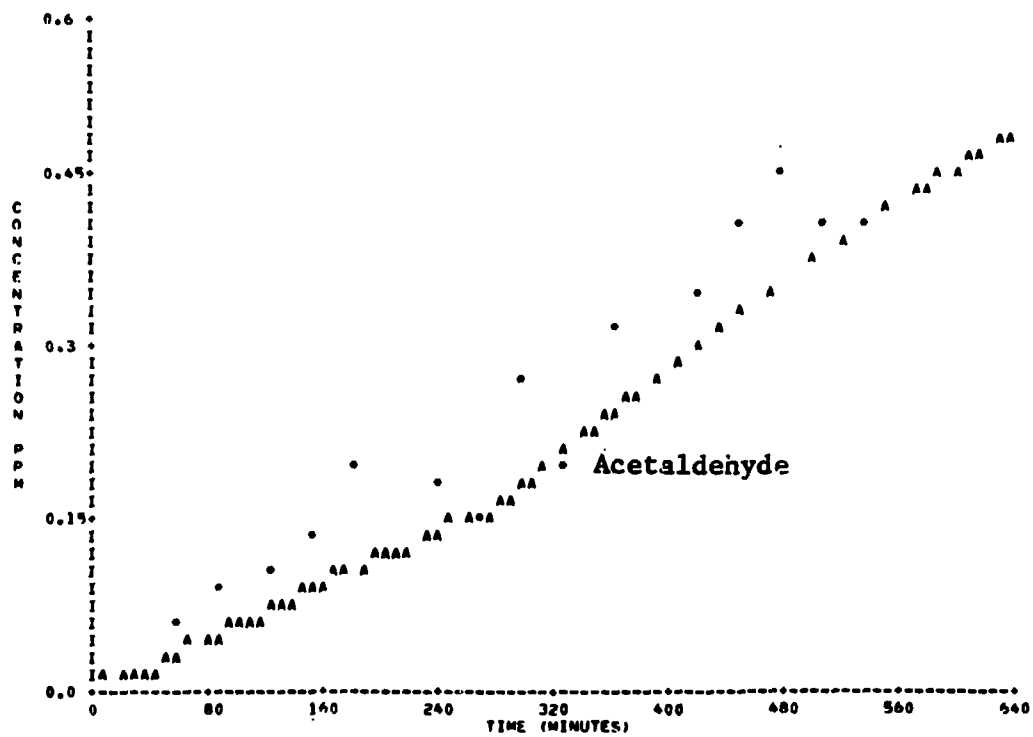

Figure B-16. Simulation of SAPRC EC-165 (Concluded).

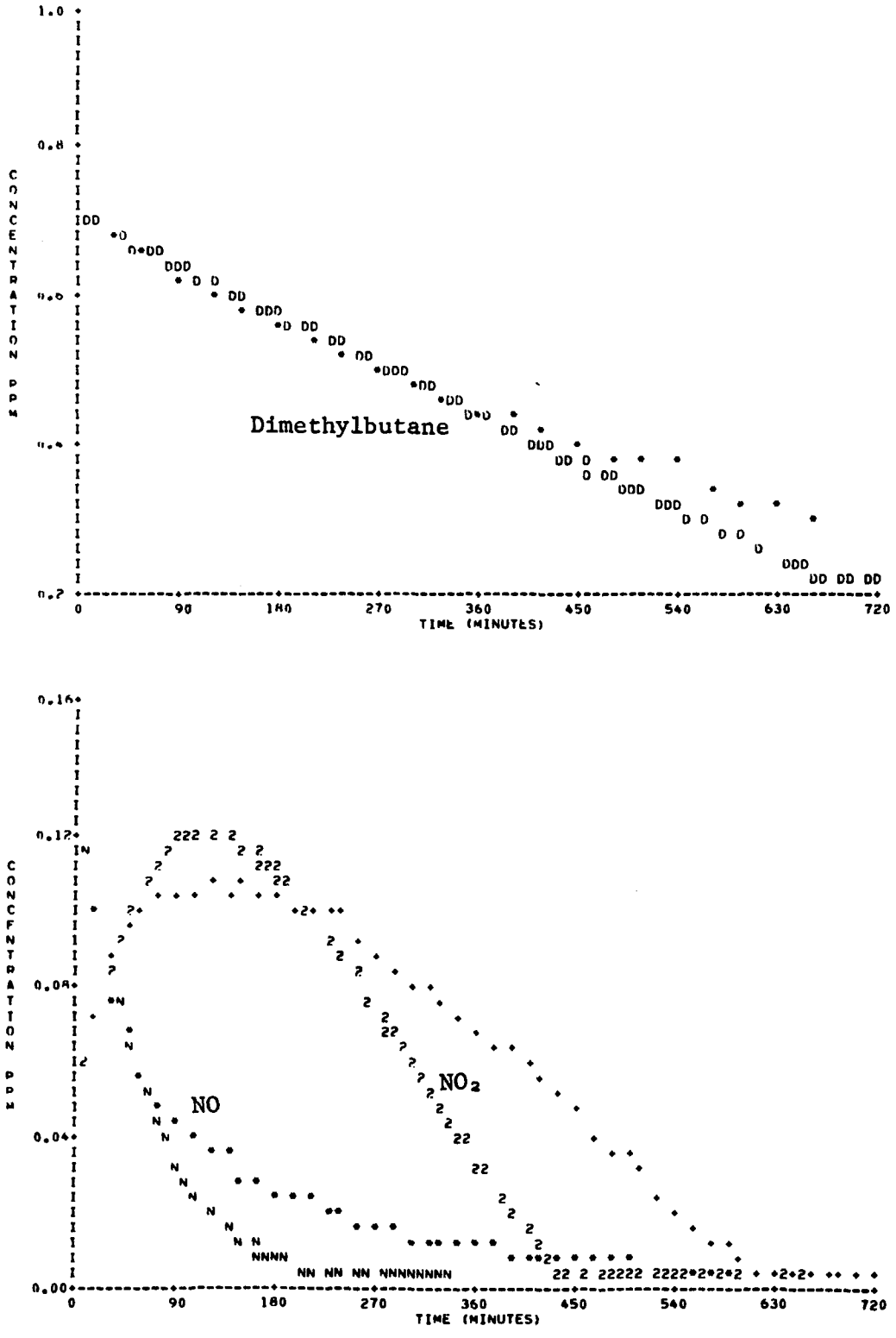

Figure B-17. Simulation of SAPRC EC-169.

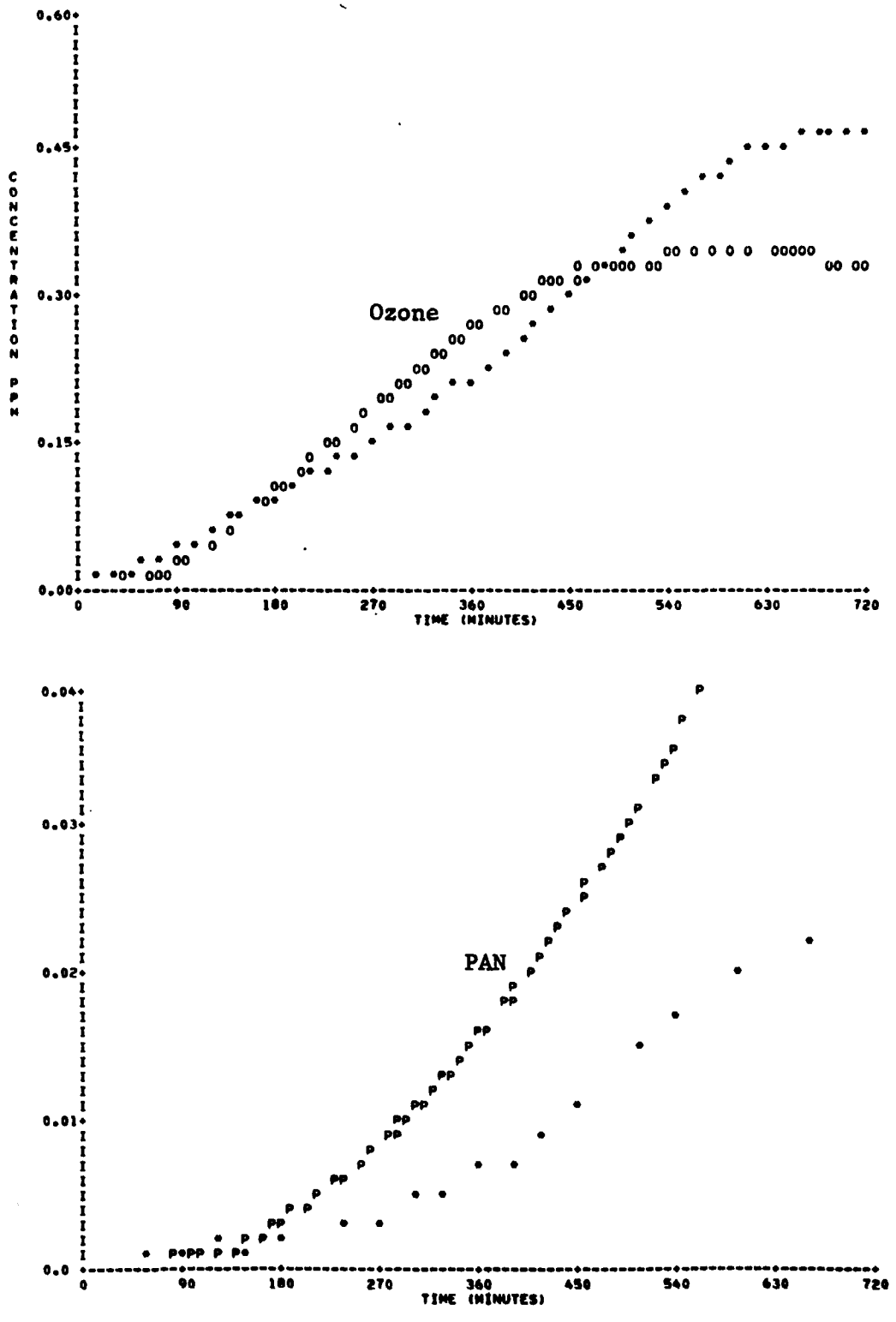

Figure B-17. Simulation of SAPRC EC-169 (Continued).

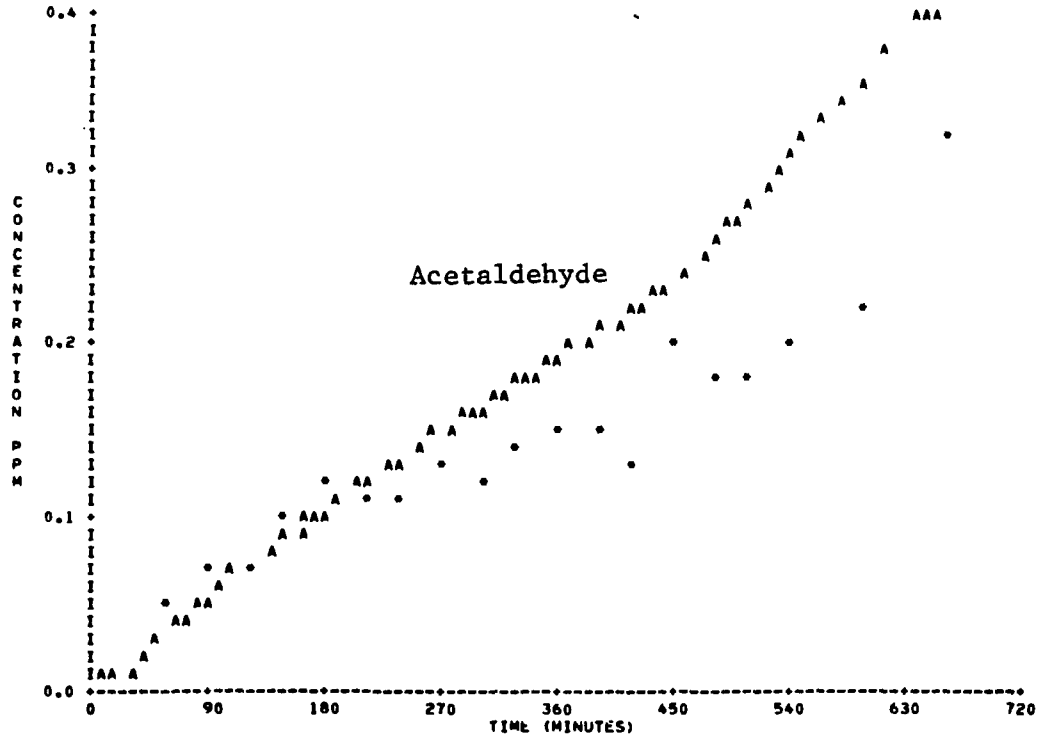

Figure B-17. Simulation of SAPRC EC-169 (Concluded).

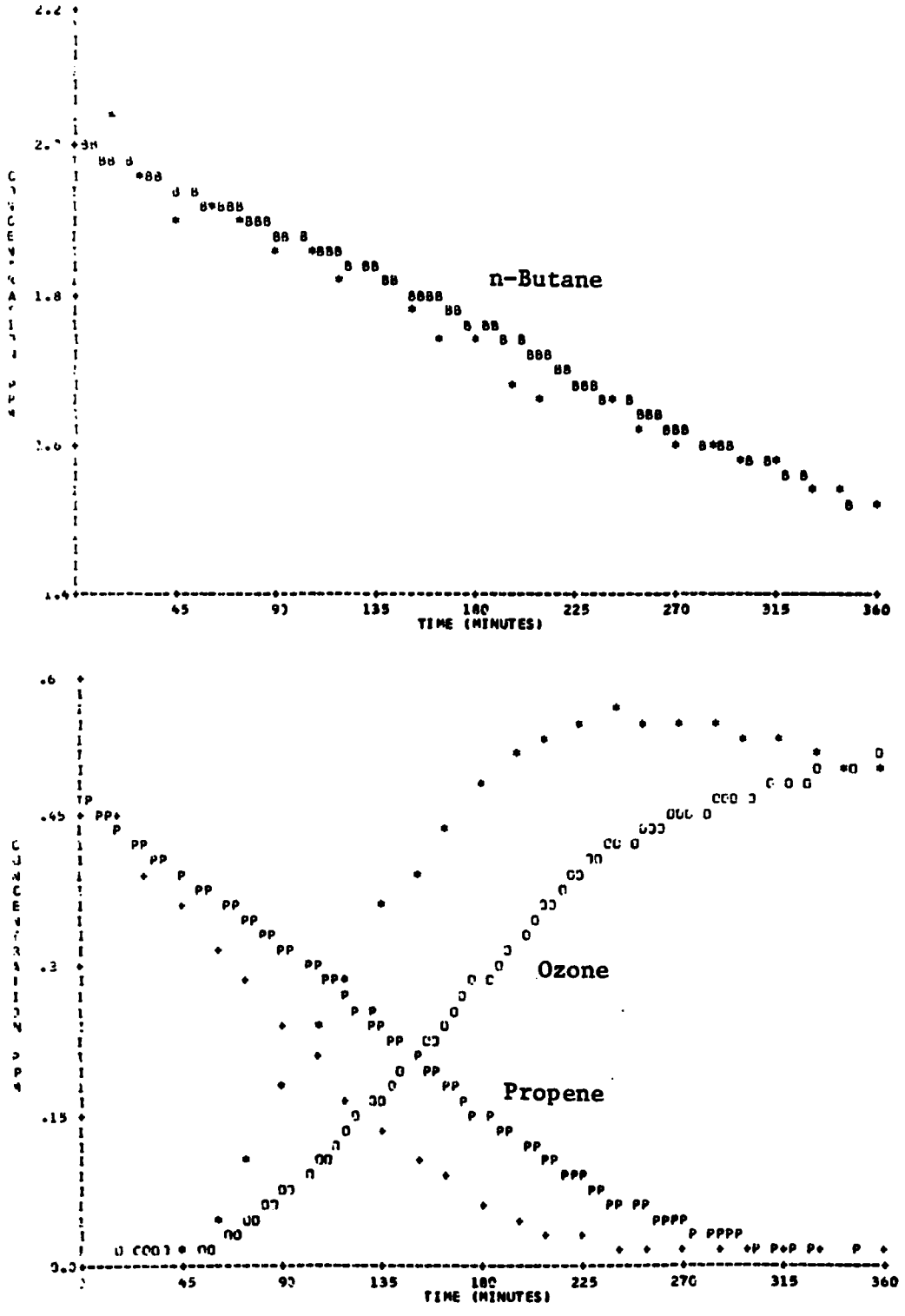

Figure B-18. Simulation of SAPRC EC-97.

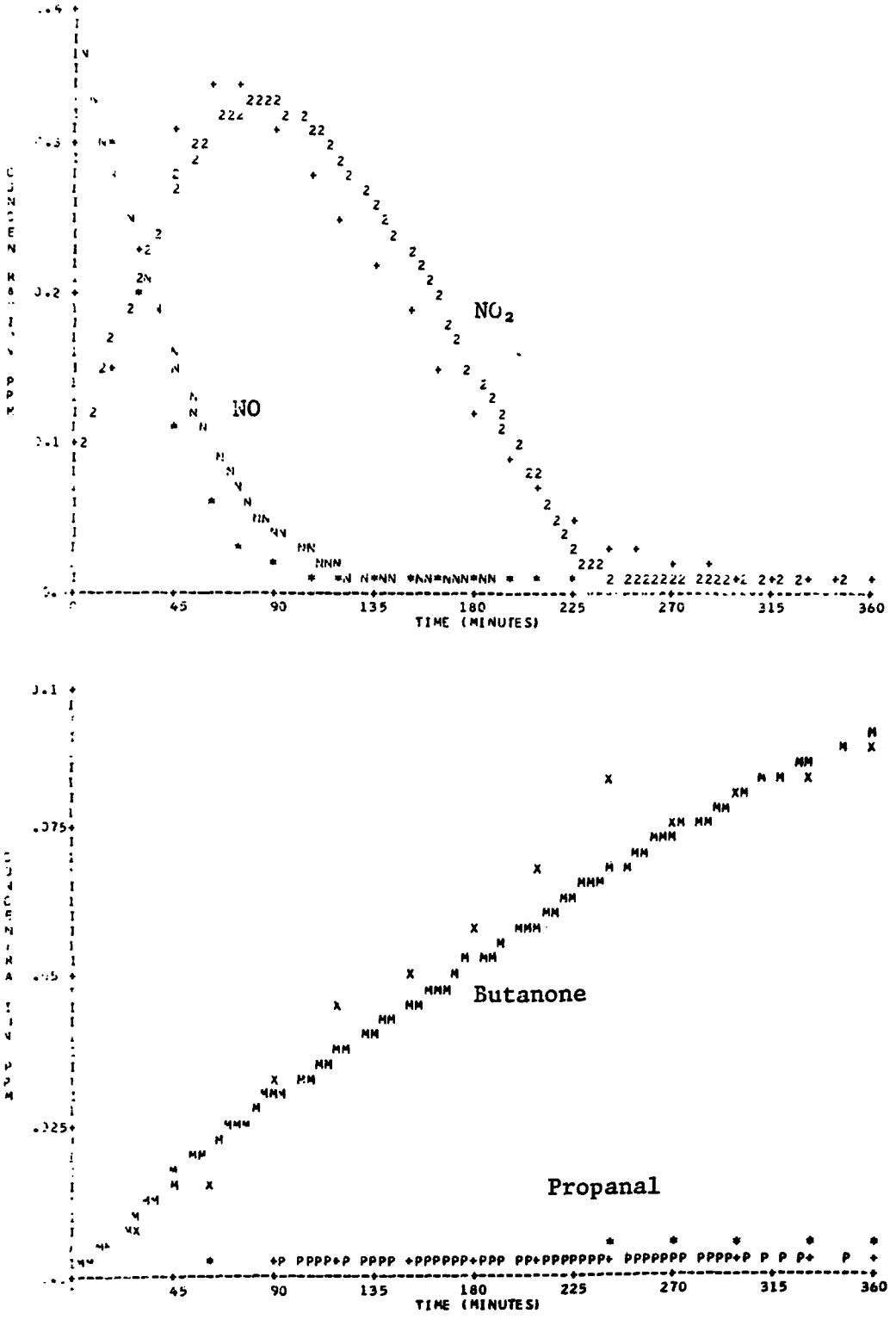

Figure B-18. Simulation of SAPRC EC-97 (Continued).

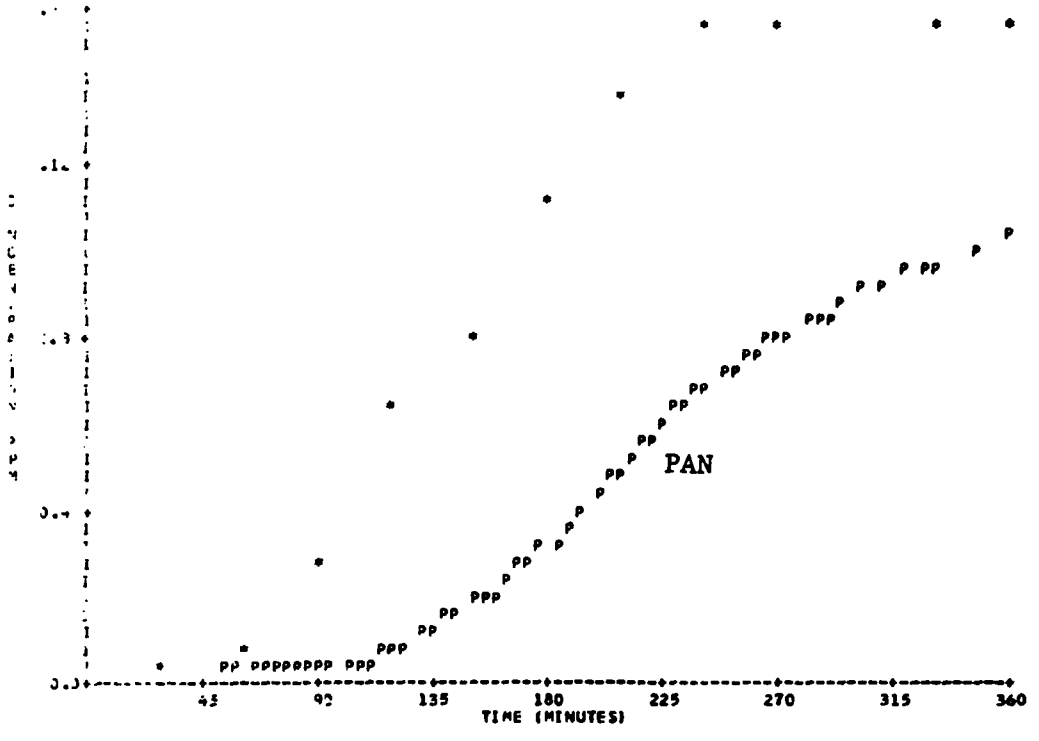

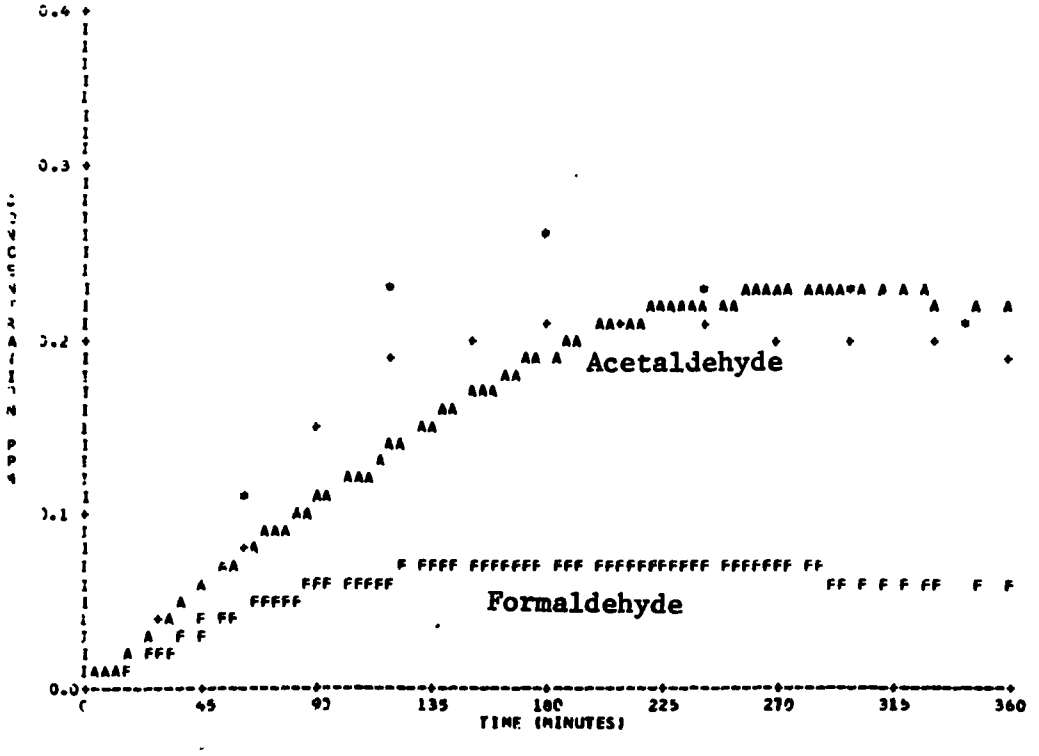

Figure B-18. Simulation of SAPRC EC-97 (Concluded).

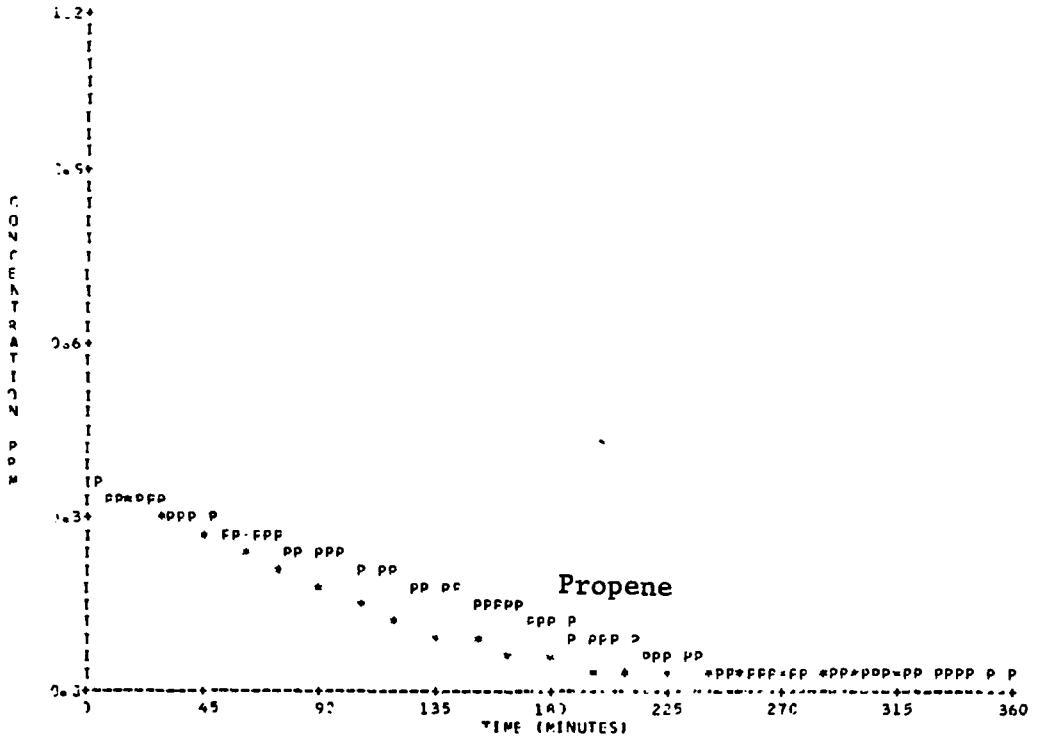

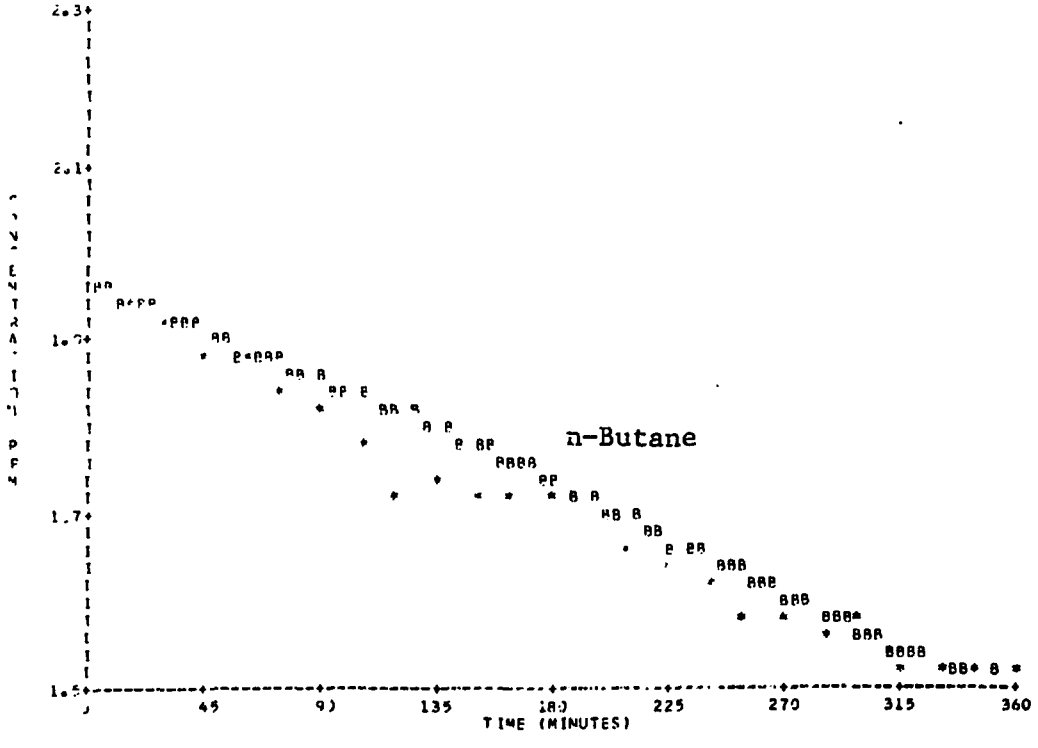

Figure B-19. Simulation of SAPRC EC-99.

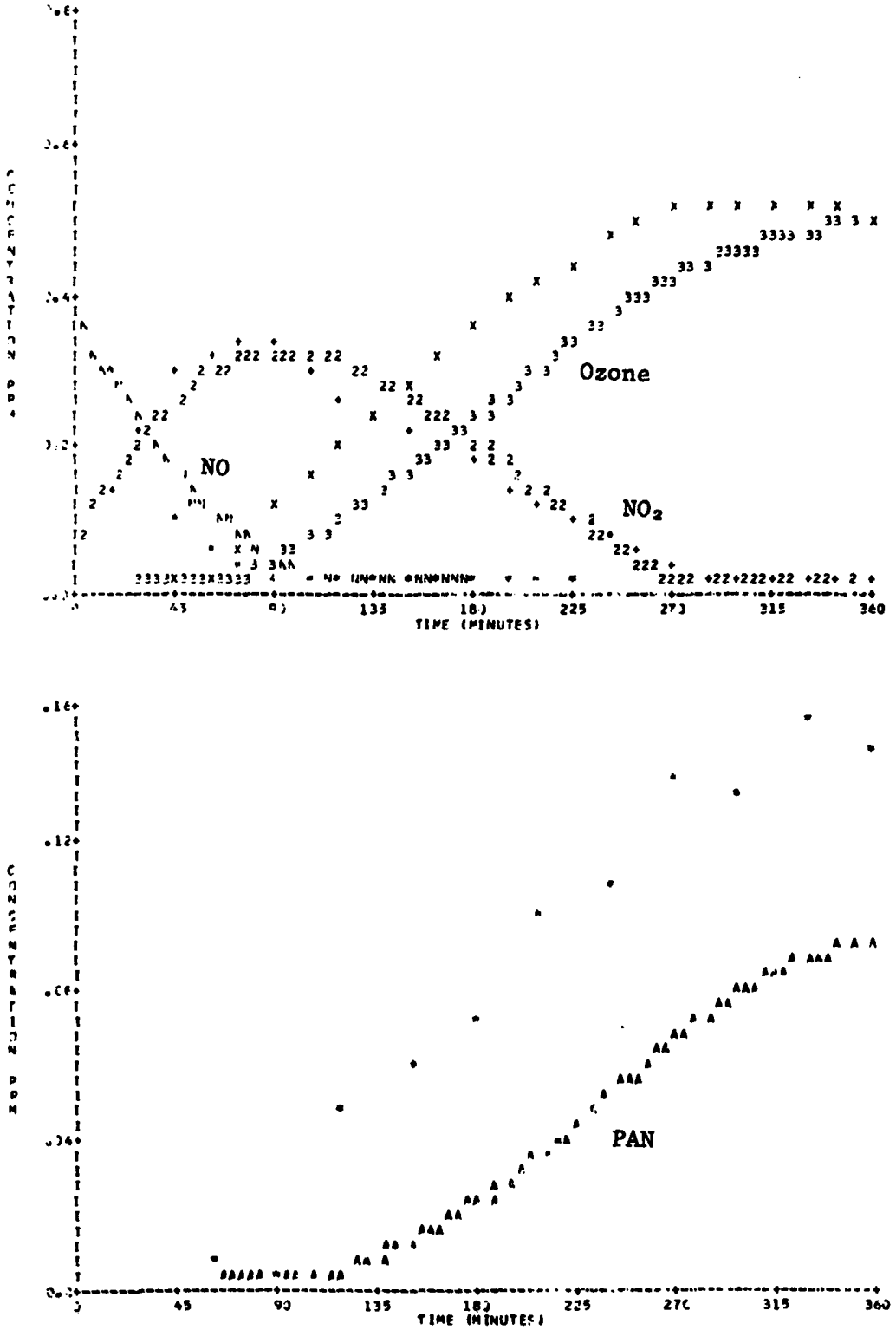

Figure B-19. Simulation of SAPRC EC-99 (Concluded).

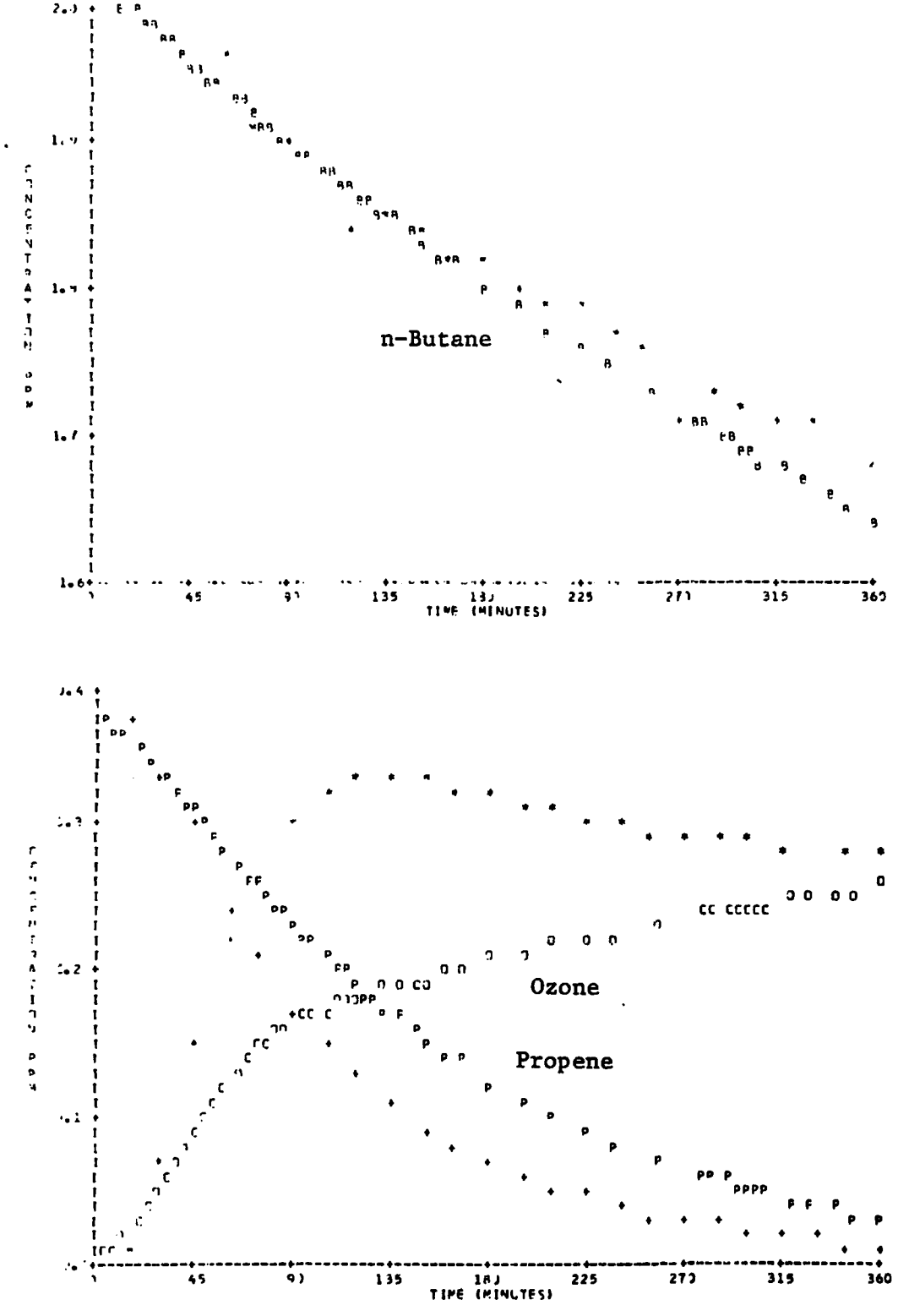

Figure B-20. Simulation of SAPRC EC-113.

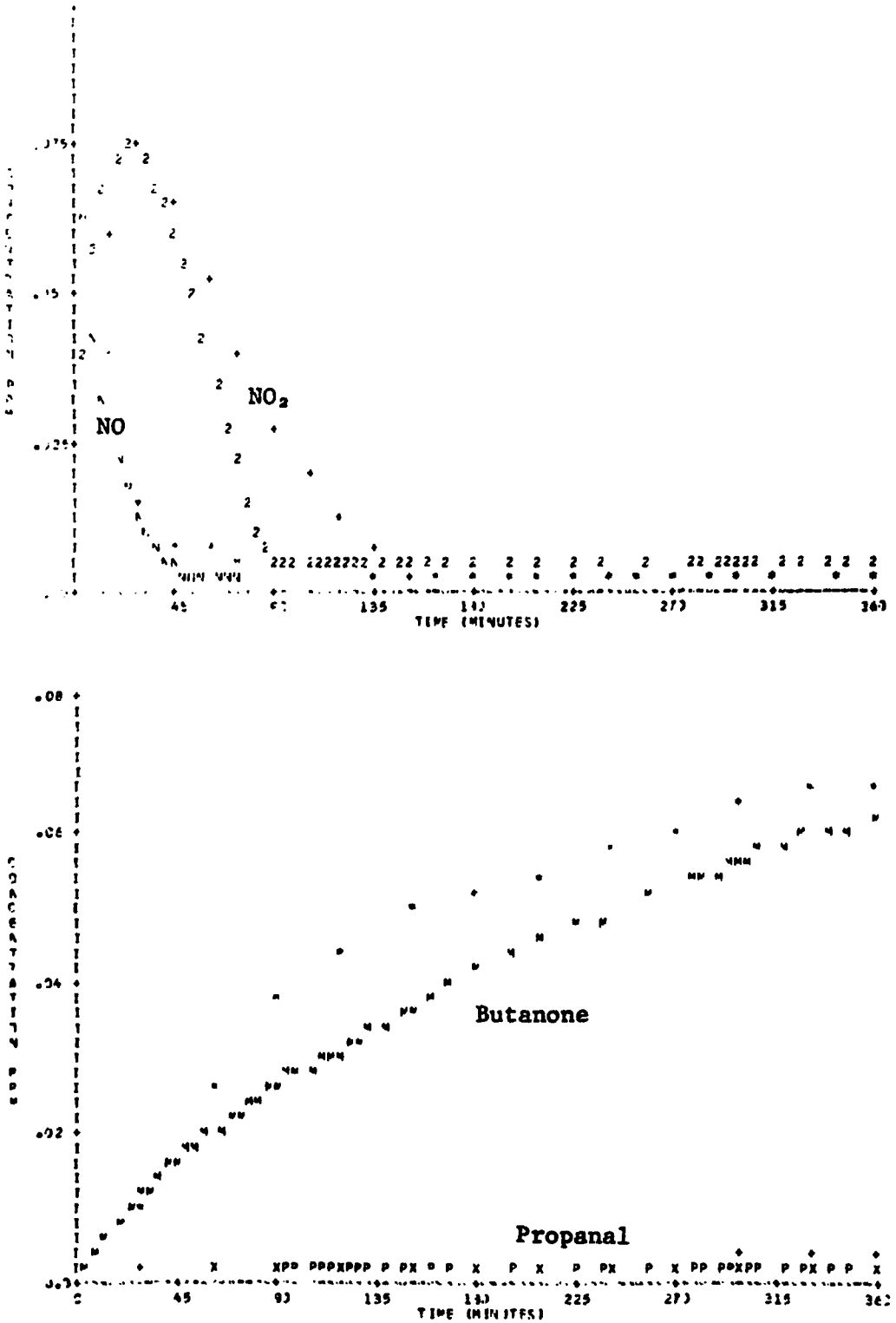

Figure B-20. Simulation of SAPRC EC-113 (Continued).

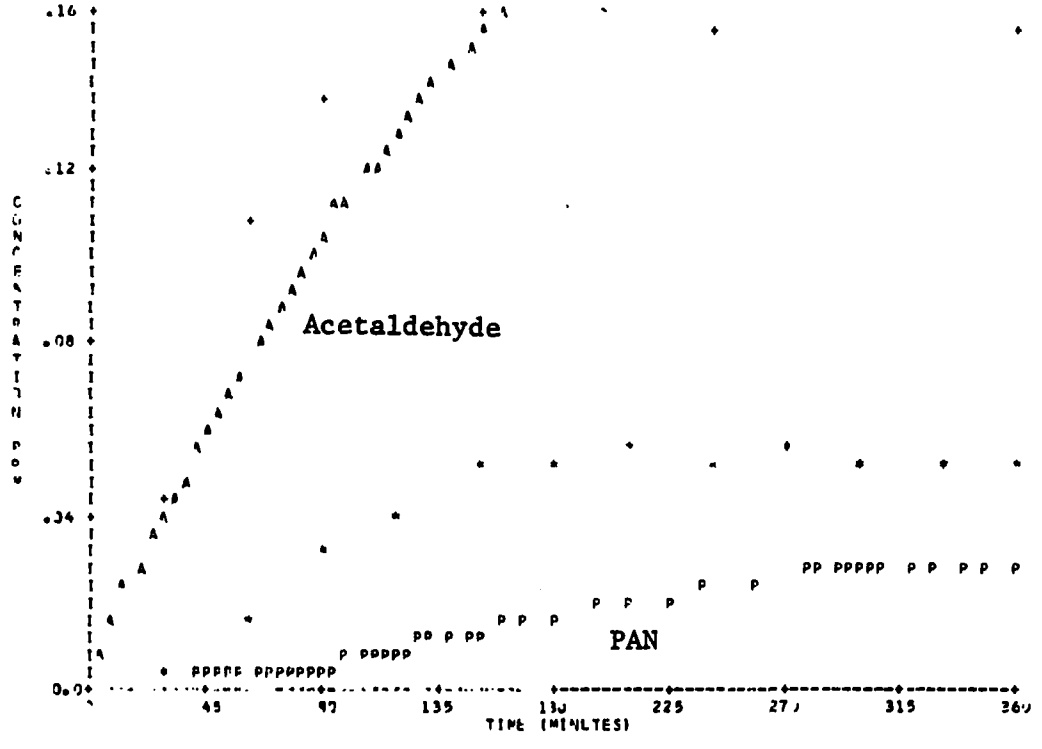

Figure B-20. Simulation of SAPRC EC-113 (Concluded).

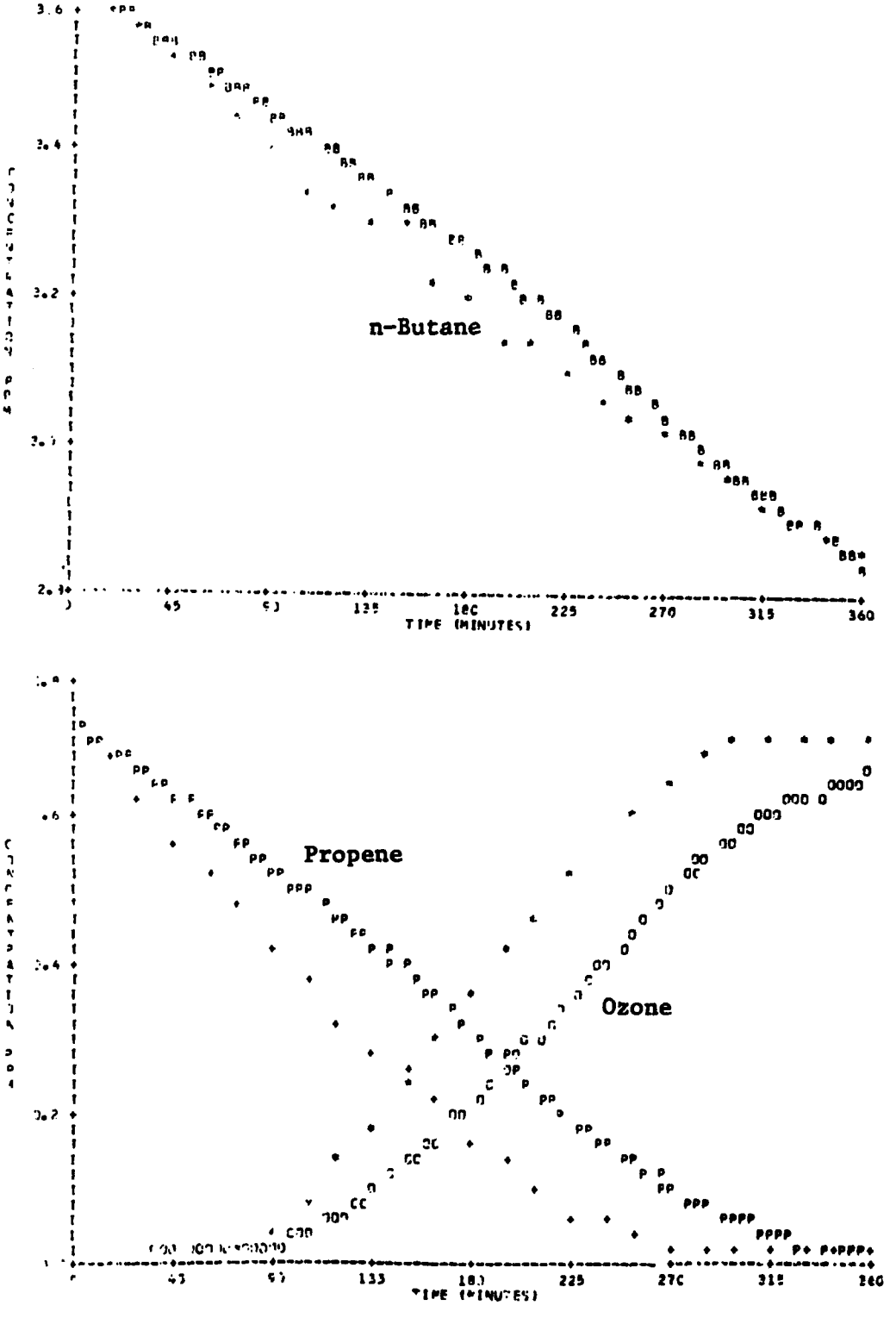

Figure B-21. Simulation of SAPRC EC-114.

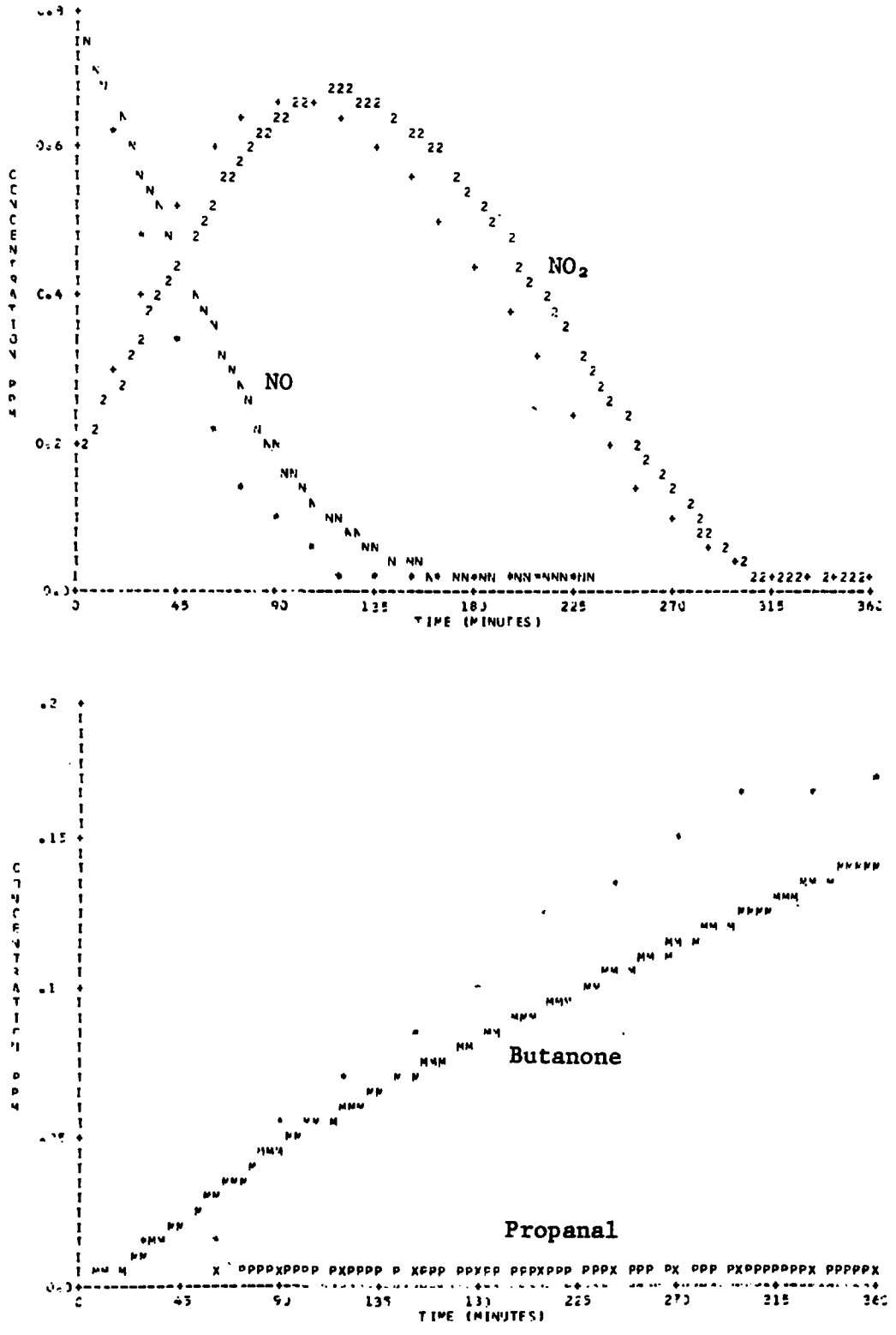

Figure B-21. Simulation of SAPRC EC-114 (Continued).

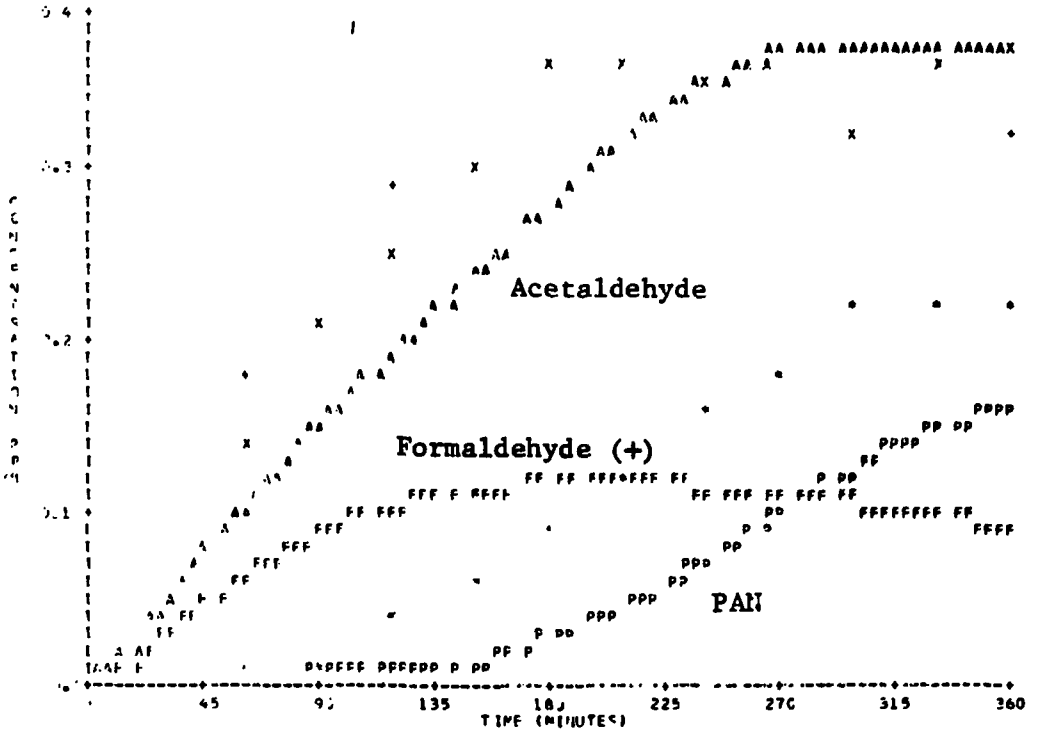

Figure B-21. Simulation of SAPRC EC-114 (Concluded).

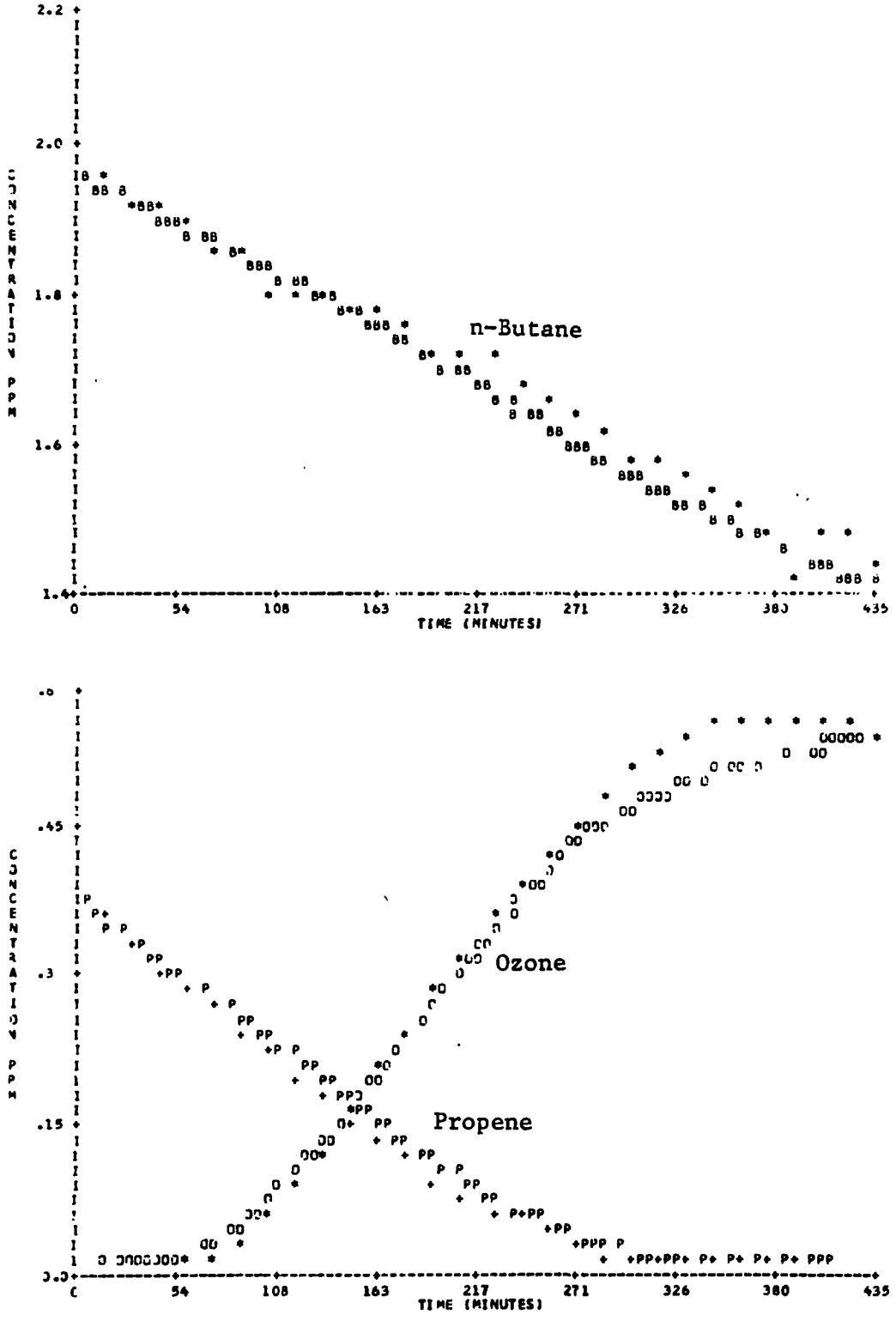

Figure B-22. Simulation of SAPRC EC-106.

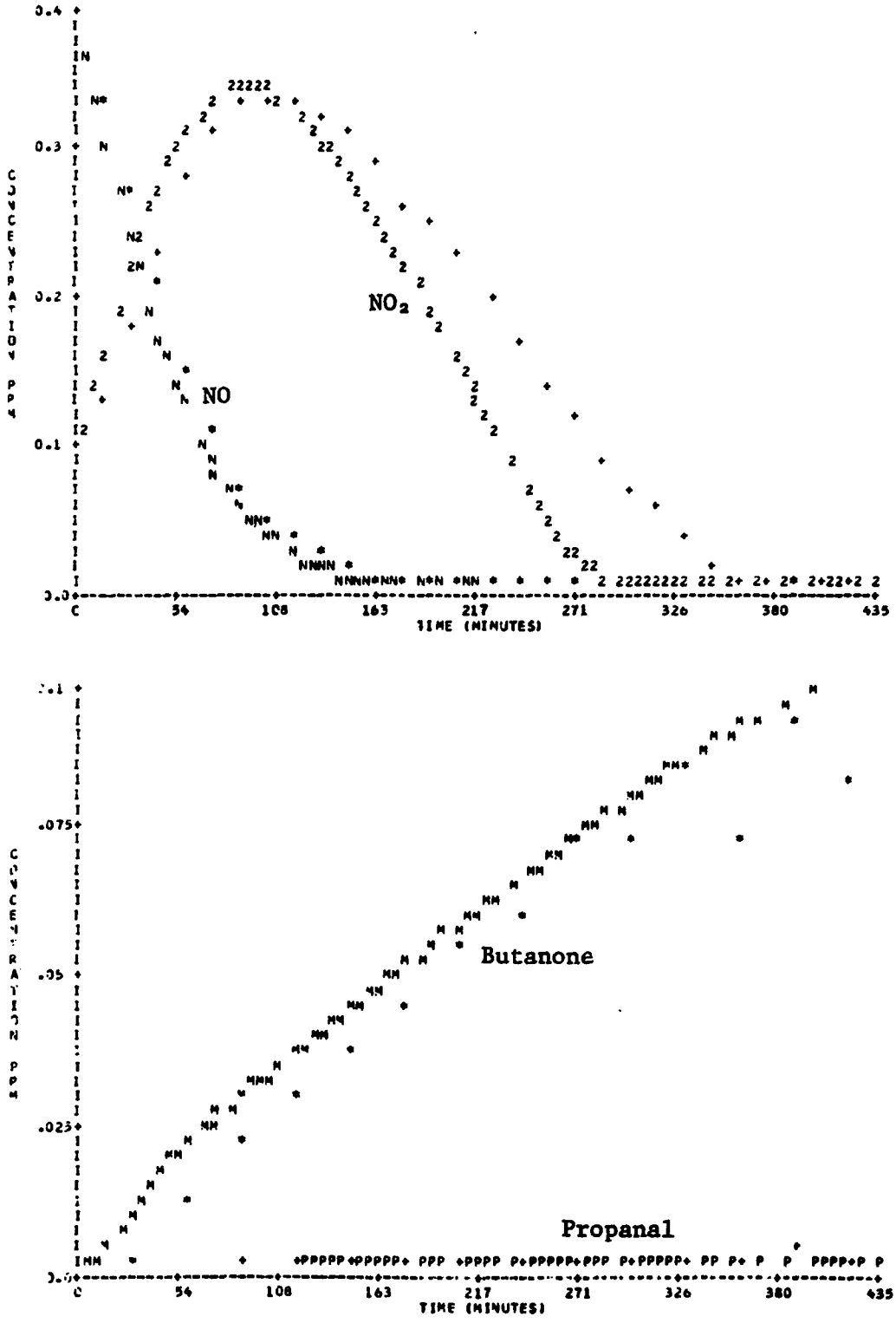

Figure B-22. Simulation of SAPRC EC-106 (Continued).

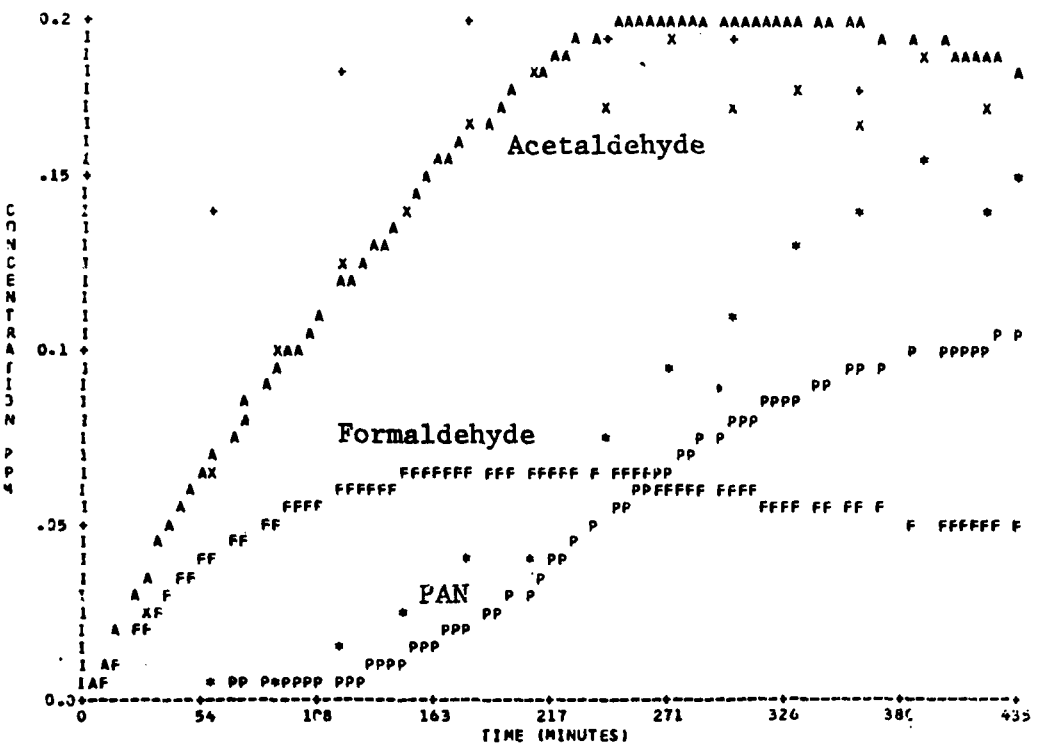

Figure B-22. Simulation of SAPRC EC-106 (Concluded).

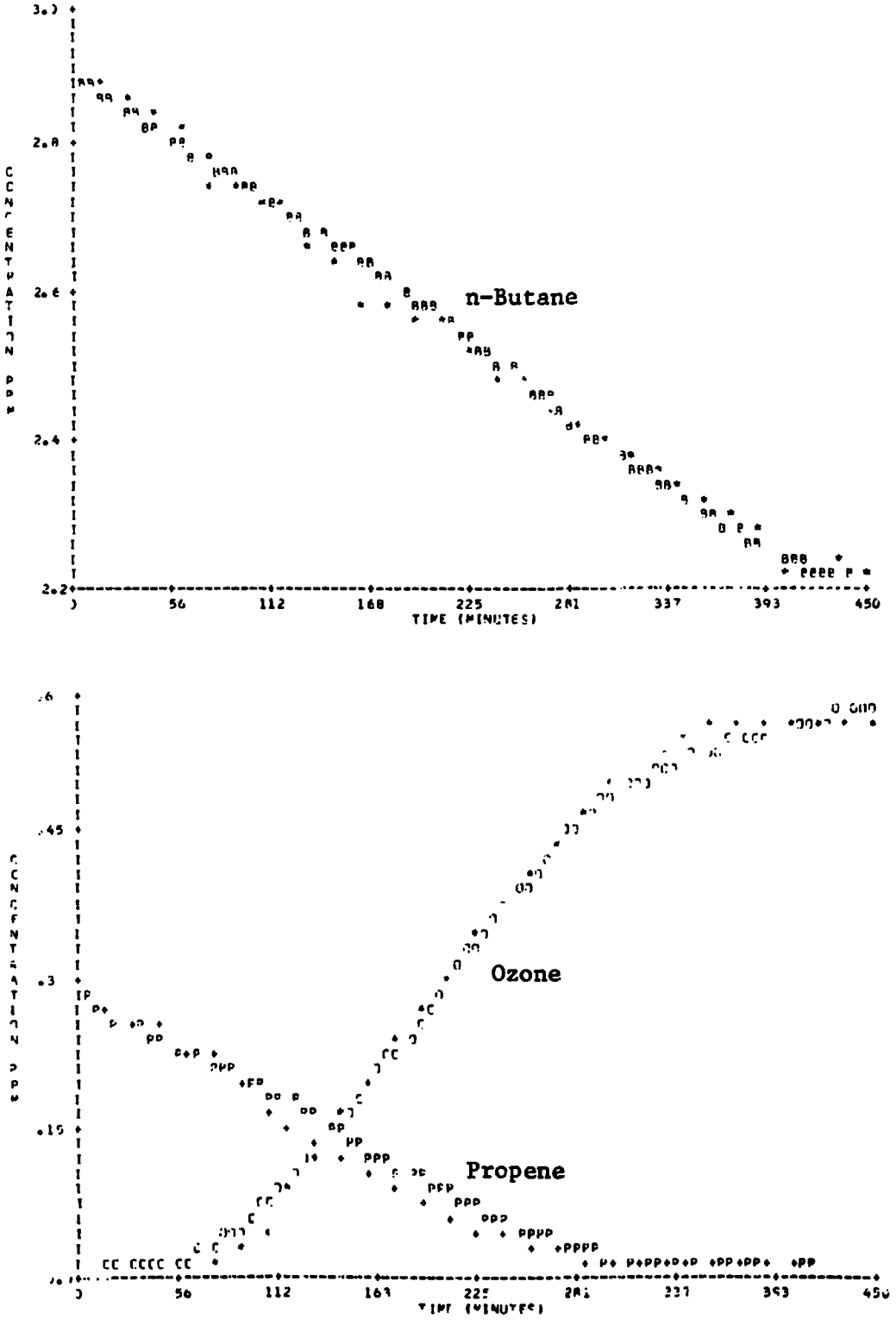

Figure B-23. Simulation of SAPRC EC-115.

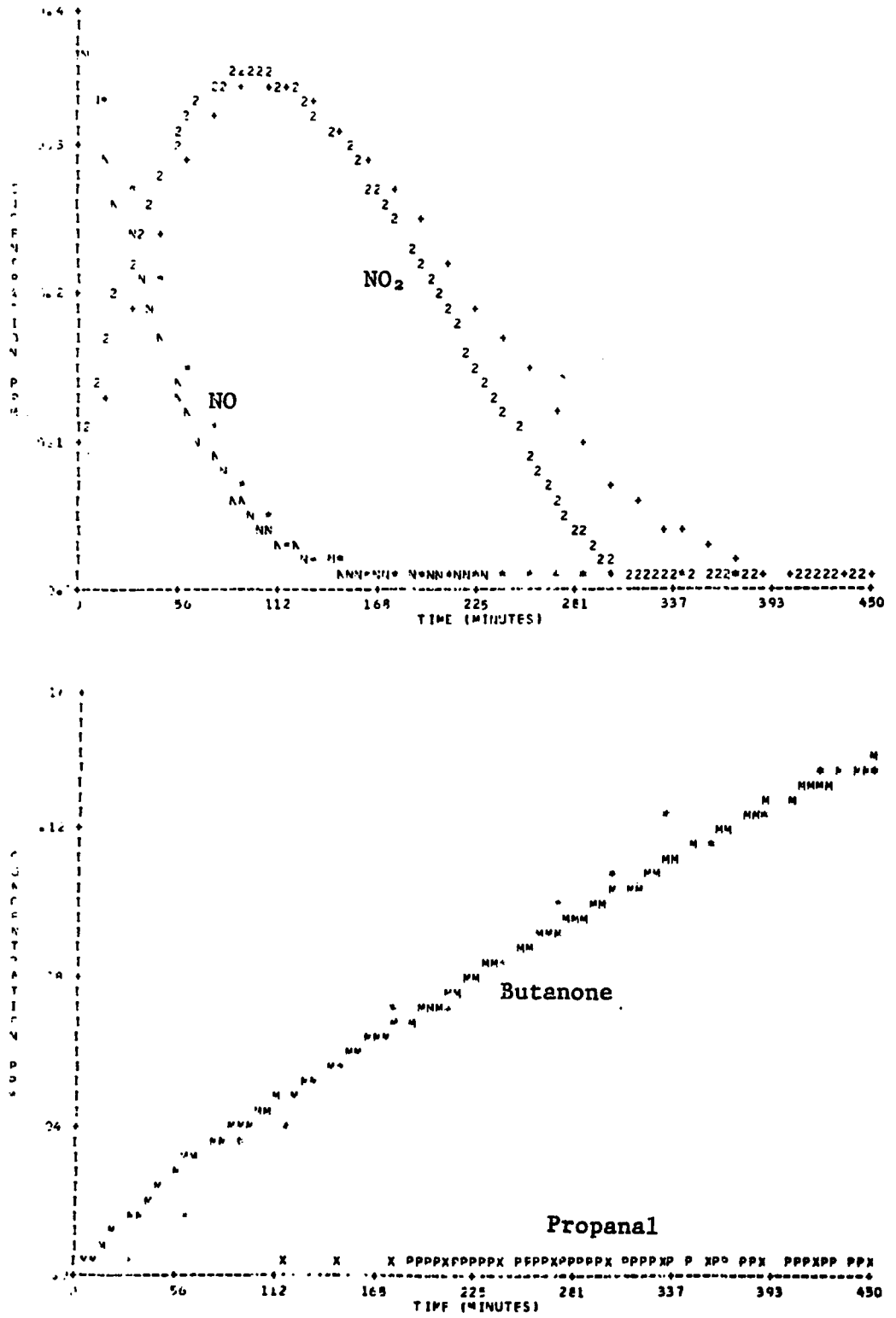

Figure B-23. Simulation of SAPRC EC-115 (Continued).

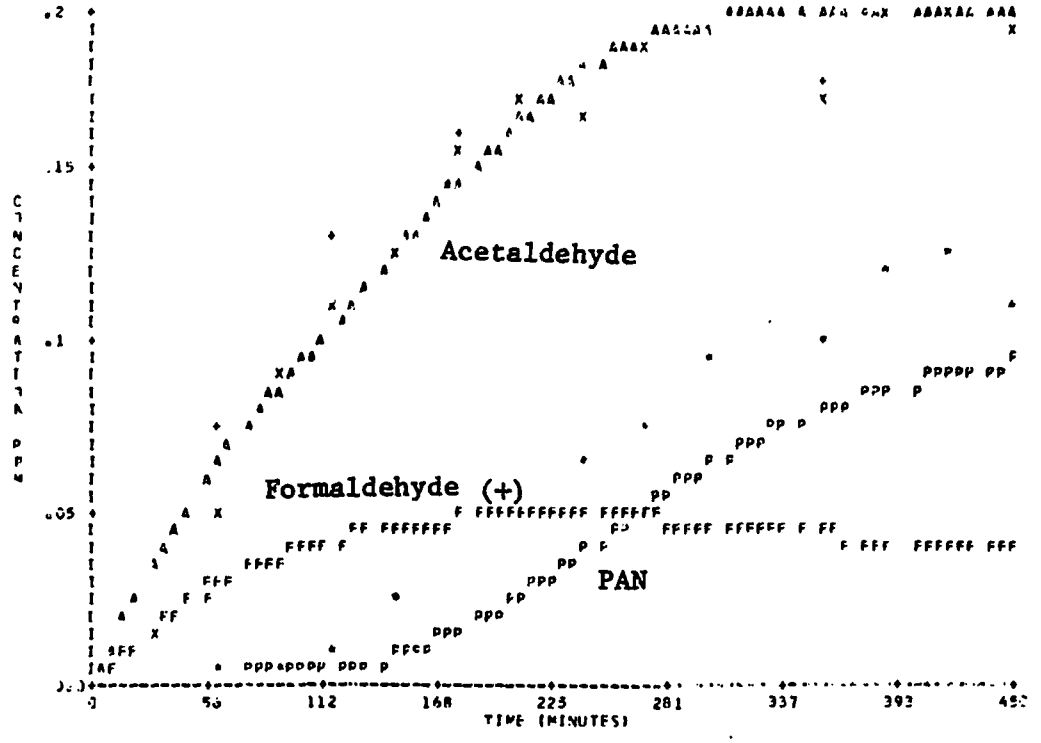

Figure B-23. Simulation of SAPRC EC-115 (Concluded).

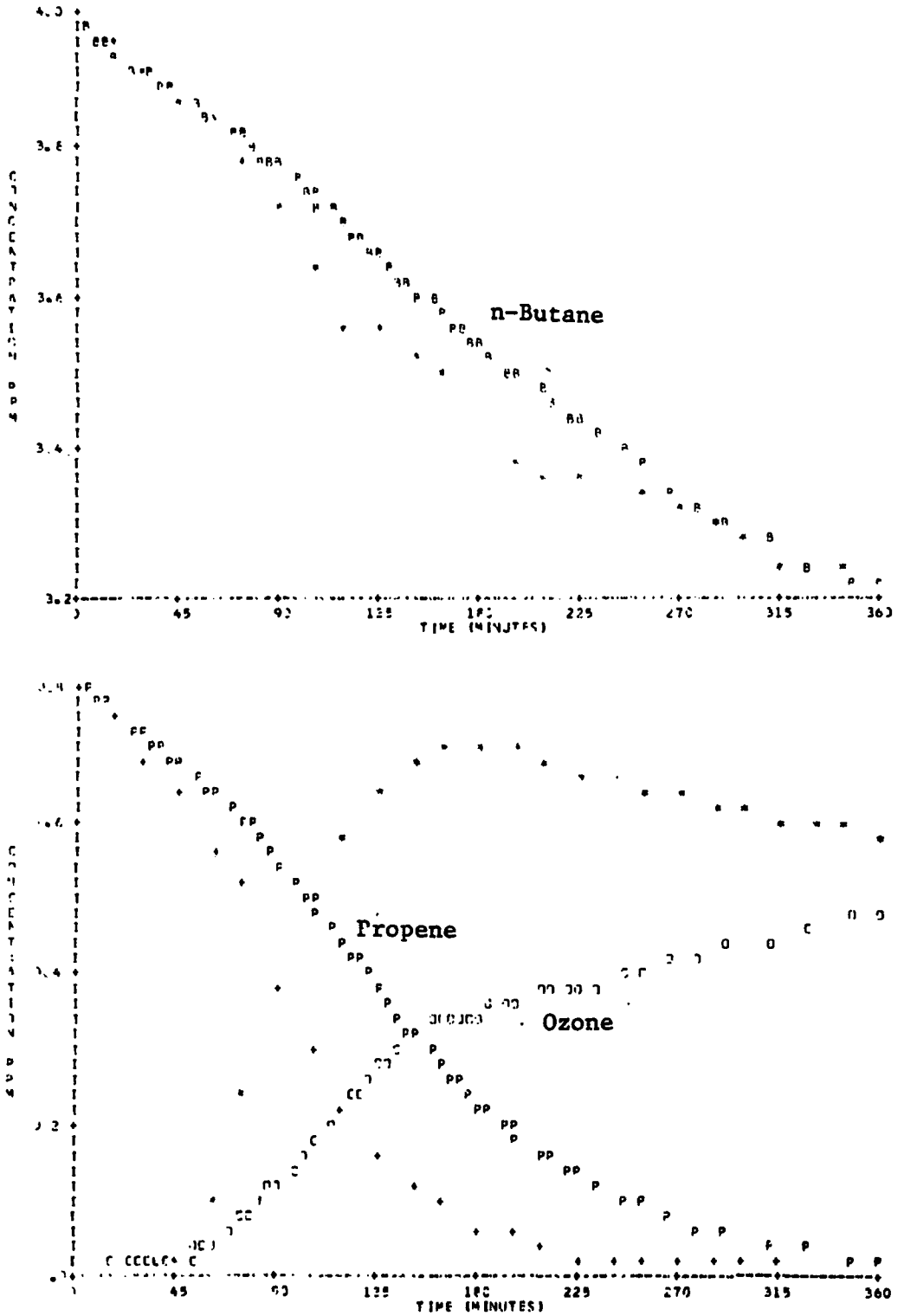

Figure B-24. Simulation of SAPRC EC-116.

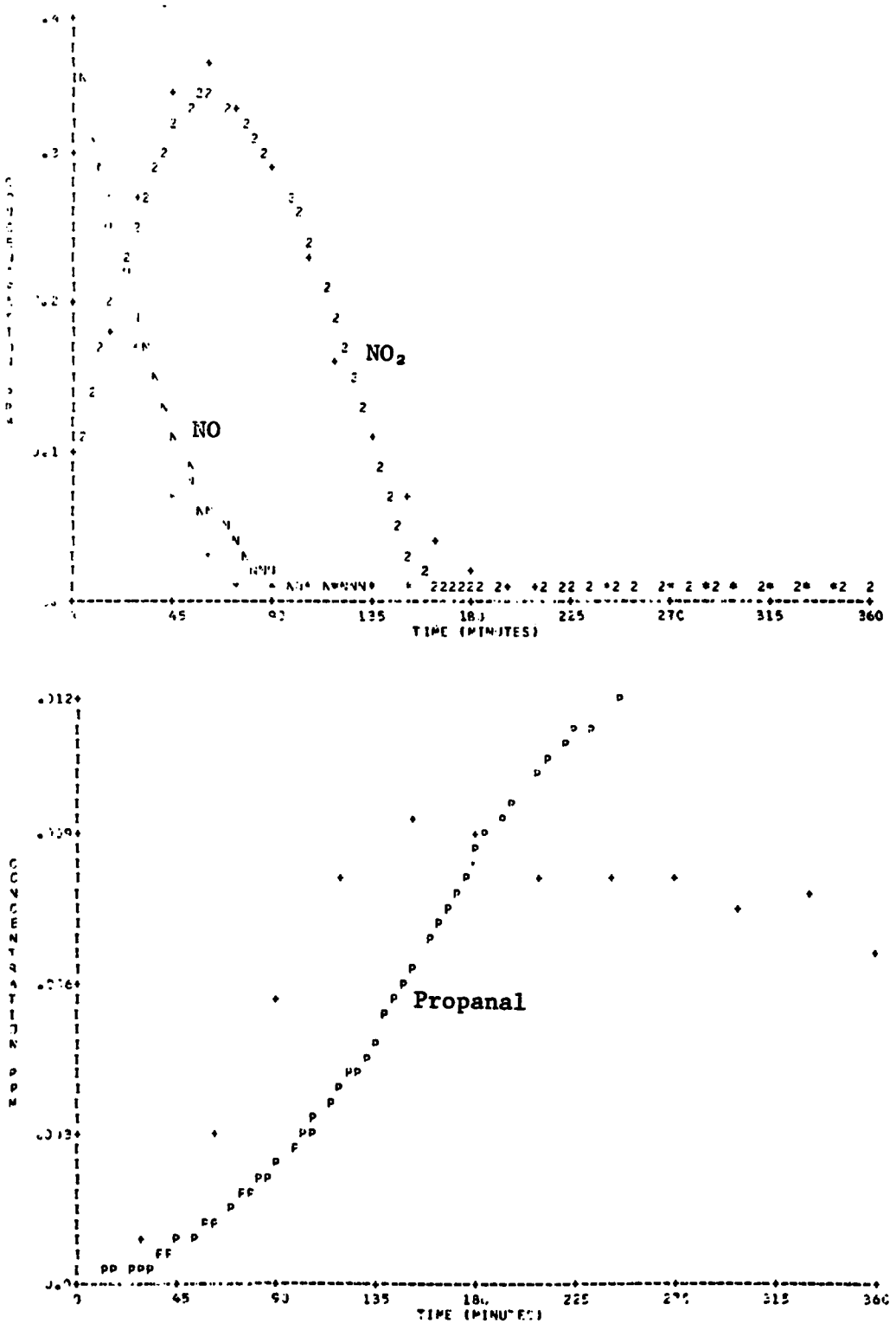

Figure B-24. Simulation of SAPRC EC-116 (Continued).

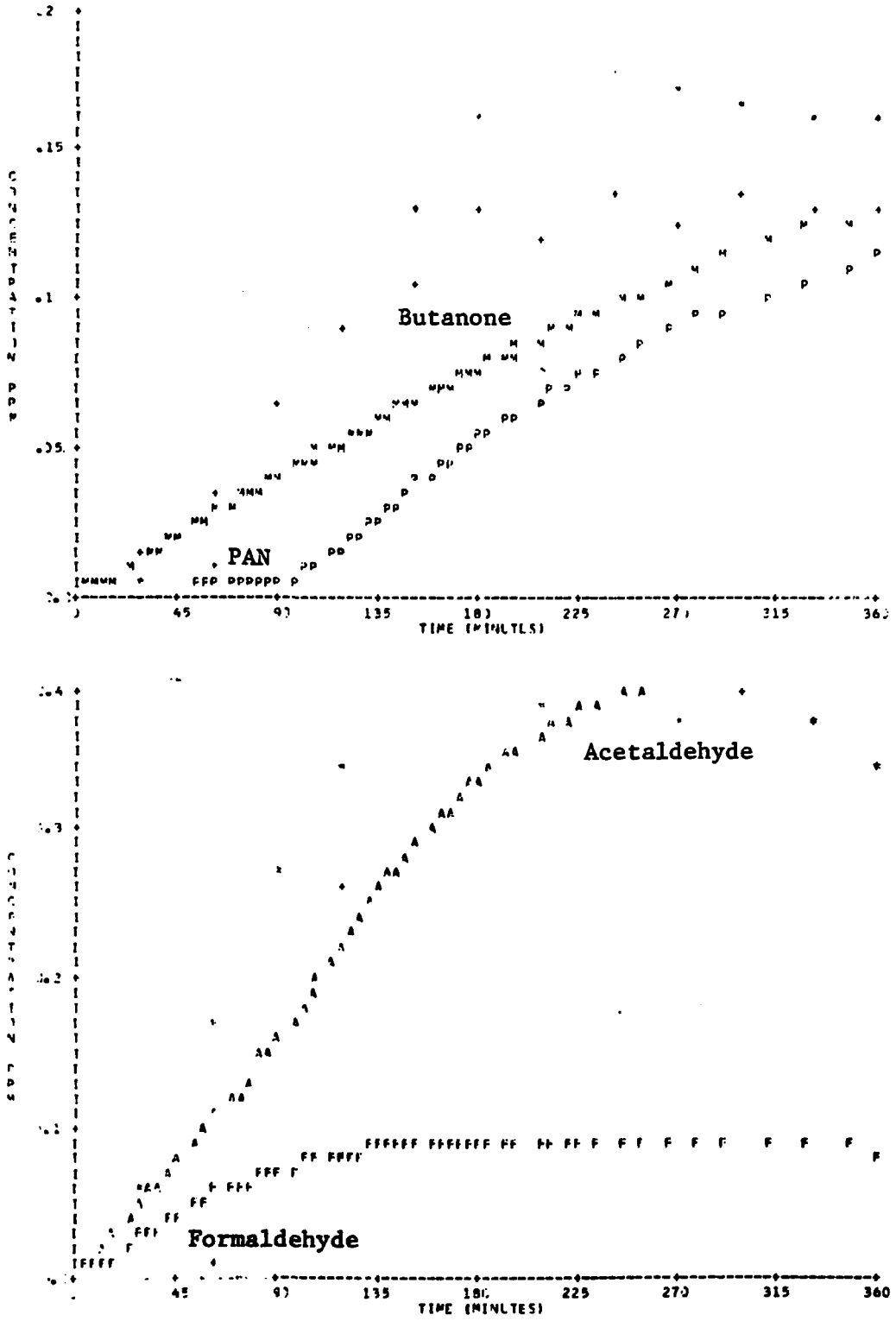

Figure B-24. Simulation of SAPRC EC-116 (Concluded).

APPENDIX C

Simulations of SAPRC Toluene Runs

TABLE C-1. INITIAL CONDITIONS OF TOLUENE CHAMBER RUNS

E.C. Number	INITIAL CONCENTRATION (ppm)					
	Toluene	NO	NO_2	HNO_2	H_2CO	PhCHO
77	0.276	0.518	0.058	0.005	0.003	0.0
78	0.210	0.069	0.032	0.001	0.0	0.0
79	0.976	0.080	0.019	0.020	0.011	0.0
80	1.02	0.401	0.095	0.020	0.0	0.0
81	1.96	0.408	0.094	0.020	0.0	0.0
82	1.88	0.679	0.337	0.030	0.001	0.0
83	5.63	1.363	0.664	0.02	0.0	0.016
84	0.968	0.388	0.080	0.001	0.007	0.032
85	1.92	0.431	0.092	0.005	0.00	0.005
86	1.09	0.407	0.080	0.001	0.161	0.0

TABLE C-2. PHOTOLYSIS RATE CONSTANTS FOR TOLUENE CHAMBER RUNS

E.C. No.	NO_2	HNO_2	H_2O_2	$O_3(^1D)$	$O_3(^3P)$	H_2CO (Rad)	H_2CO (molec)	PhCHO	$CH_3C(O)CHO$	HC(O)CHO
77-86	0.16	0.045	3.3×10^{-4}	1.2×10^{-3}	6.6×10^{-4}	5.0×10^{-4}	9.0×10^{-4}	5.0×10^{-3}	0.09	0.09

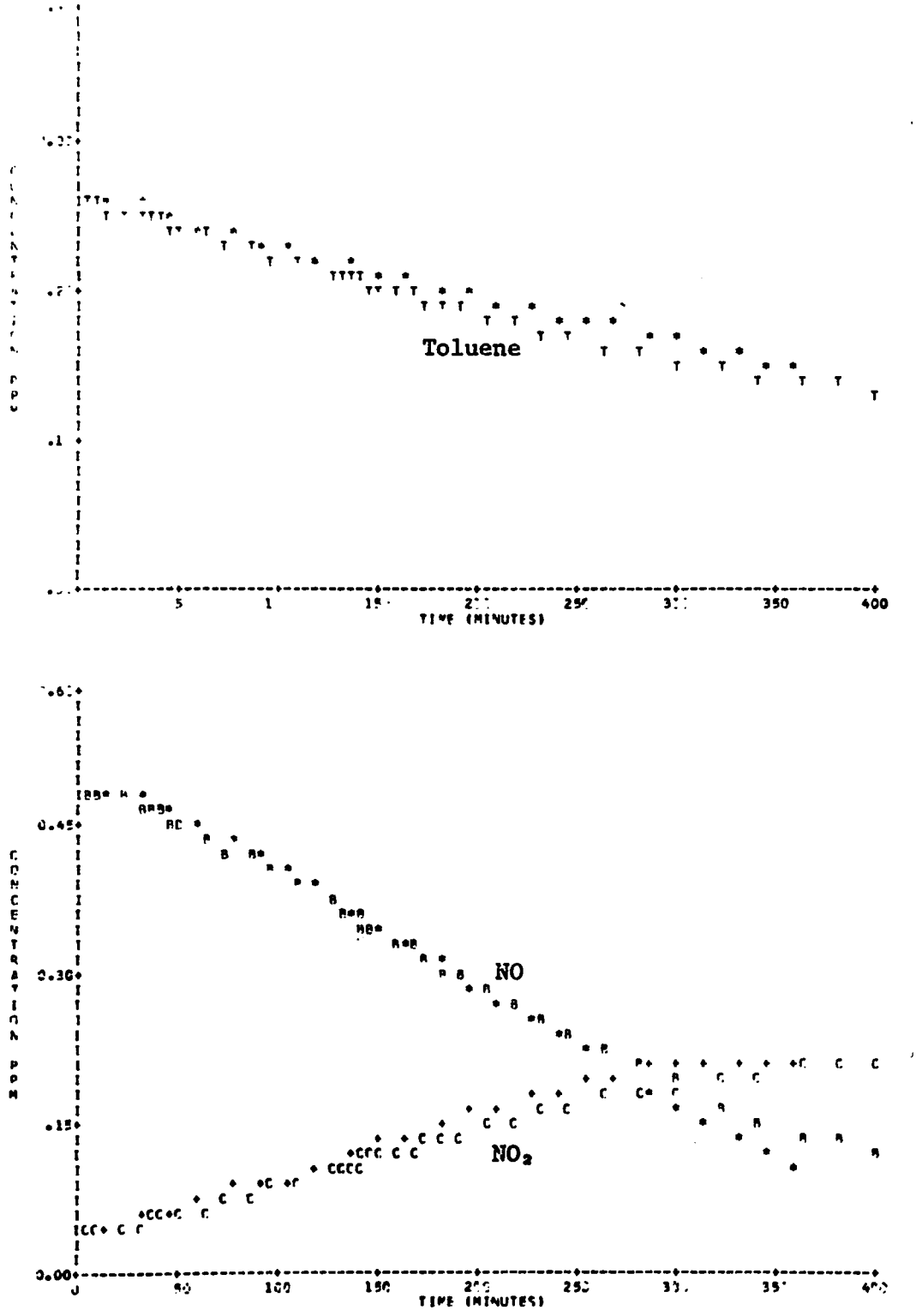

Figure C-1. Simulation of SAPRC EC-77.

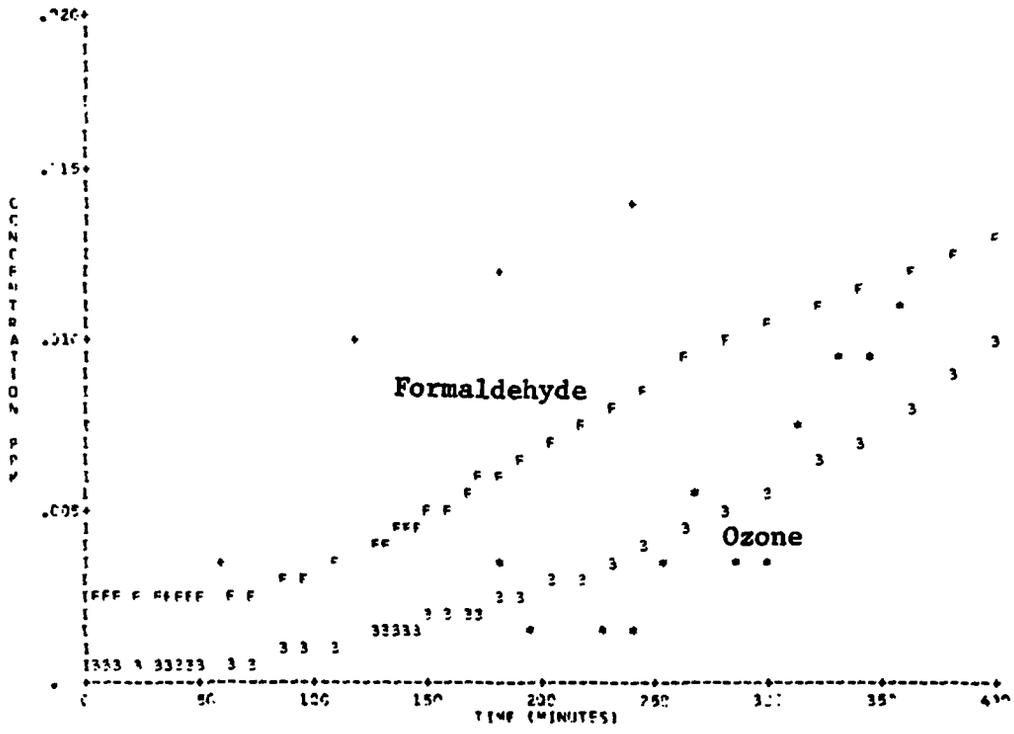

Figure C-1. Simulation of SAPRC EC-77 (Concluded).

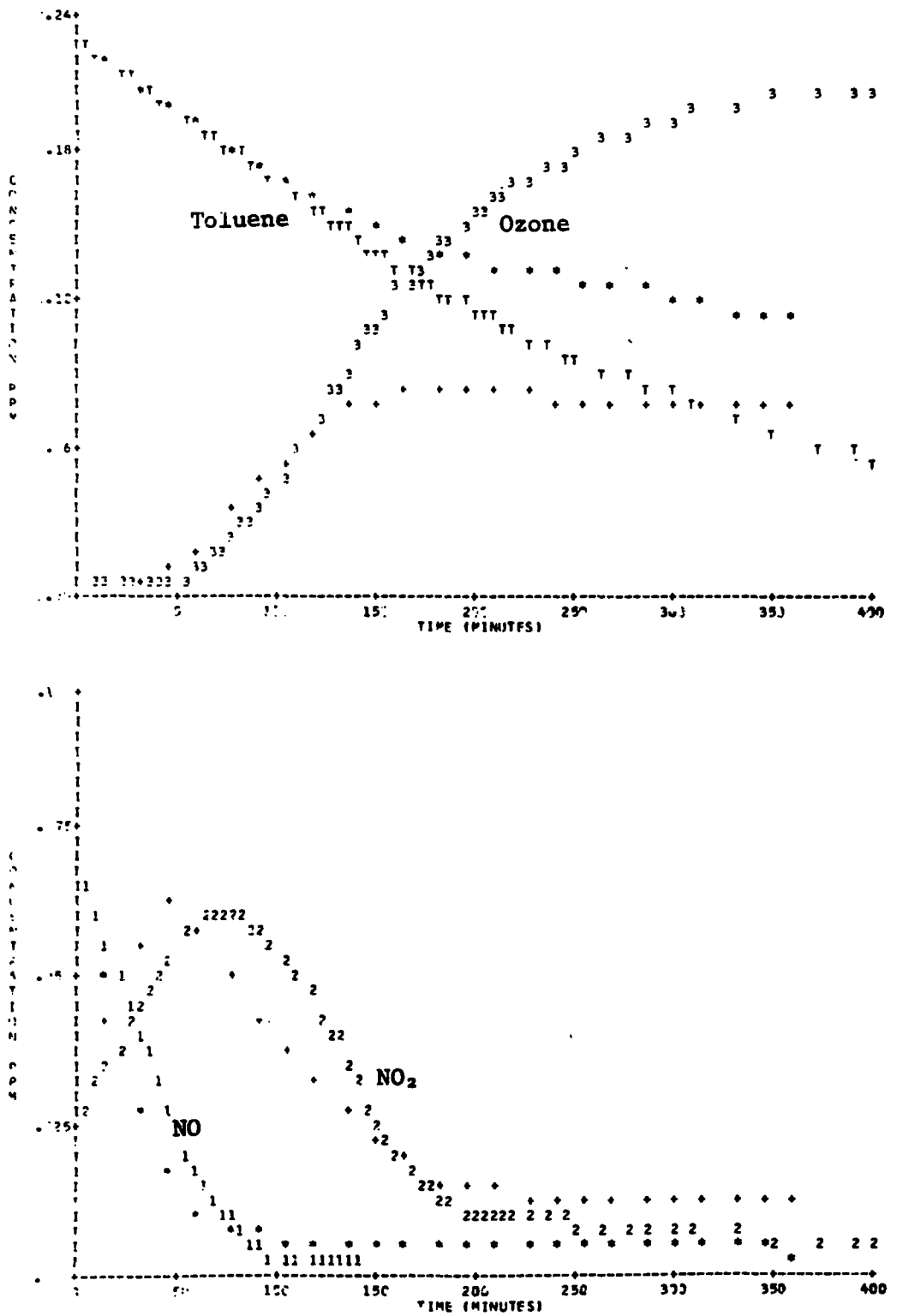

Figure C-2. Simulation of SAPRC EC-78.

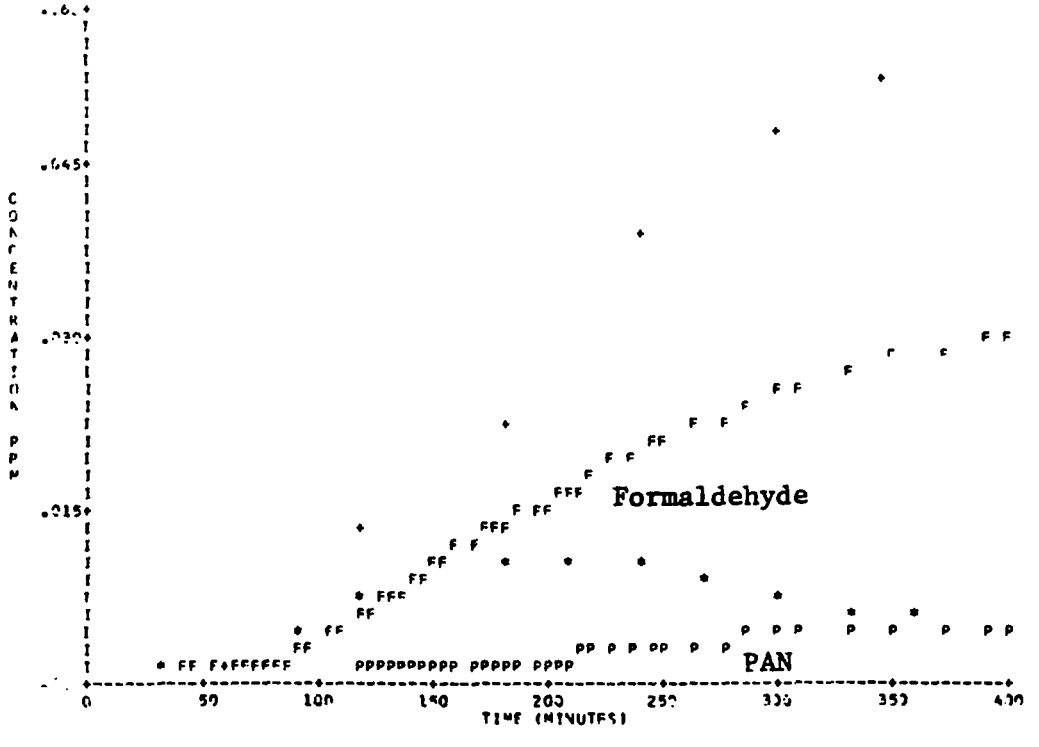

Figure C-2. Simulation of SAPRC EC-78 (Concluded).

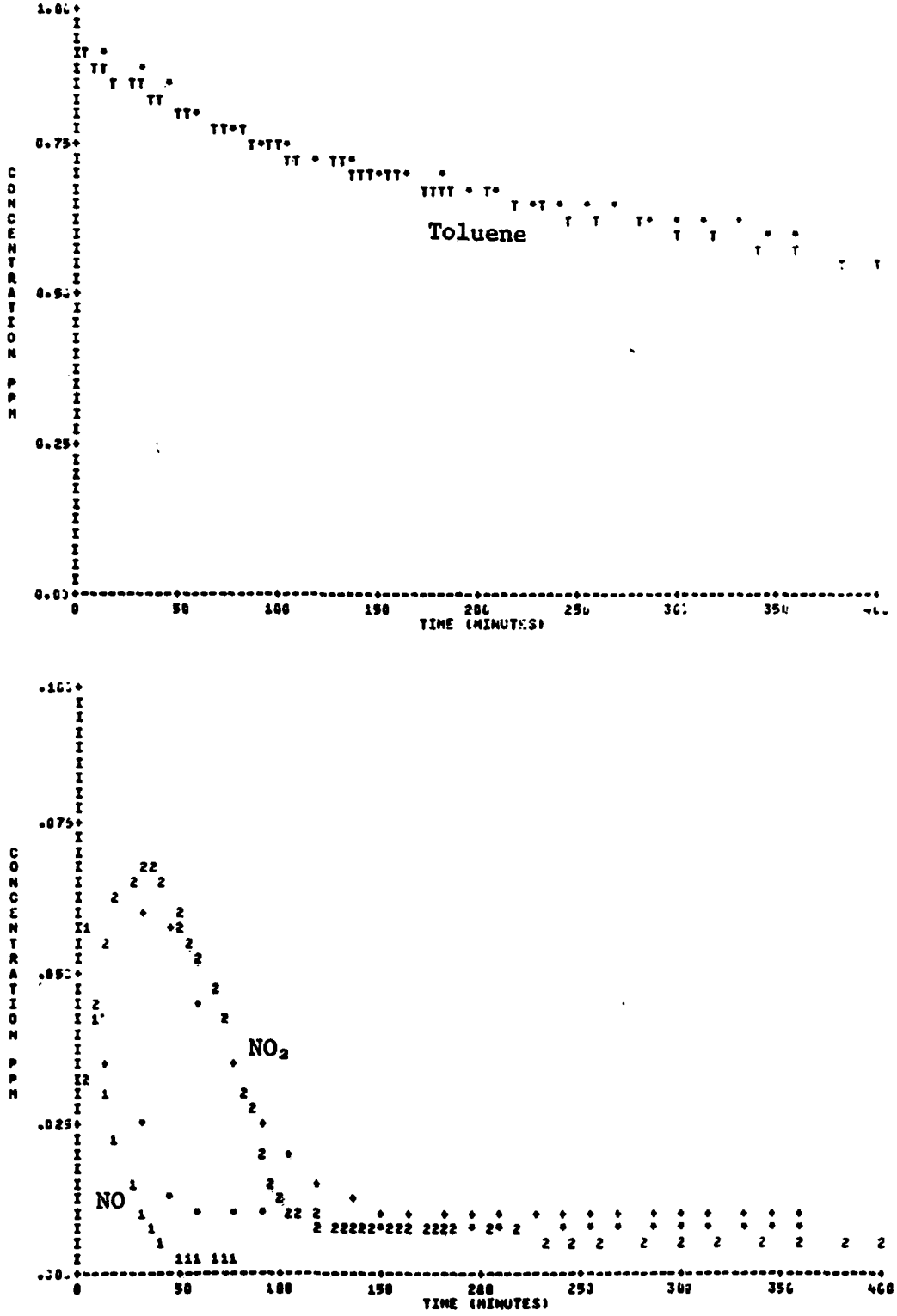

Figure C-3. Simulation of SAPRC EC-79.

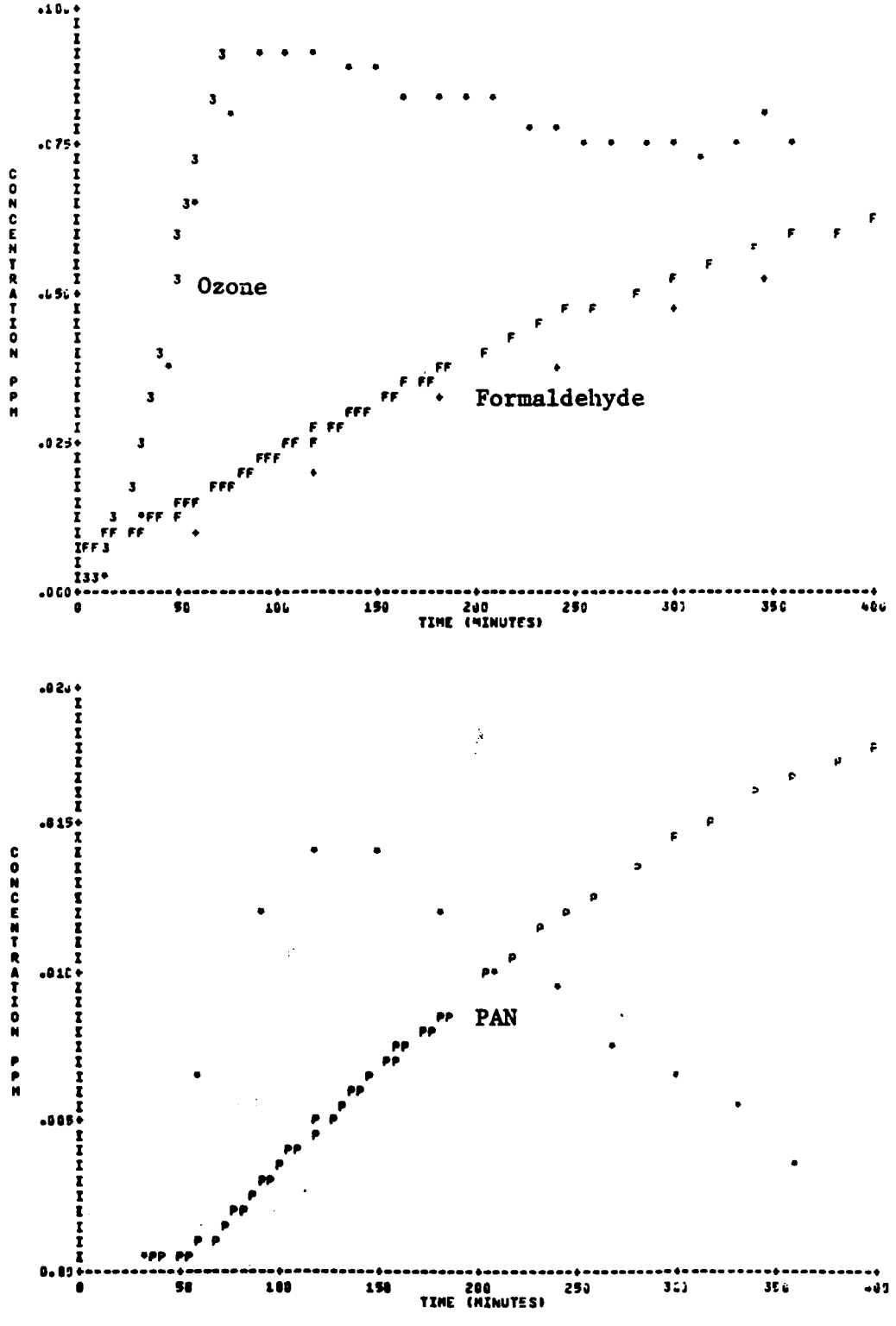

Figure C-3. Simulation of SAPRC EC-79 (Concluded).

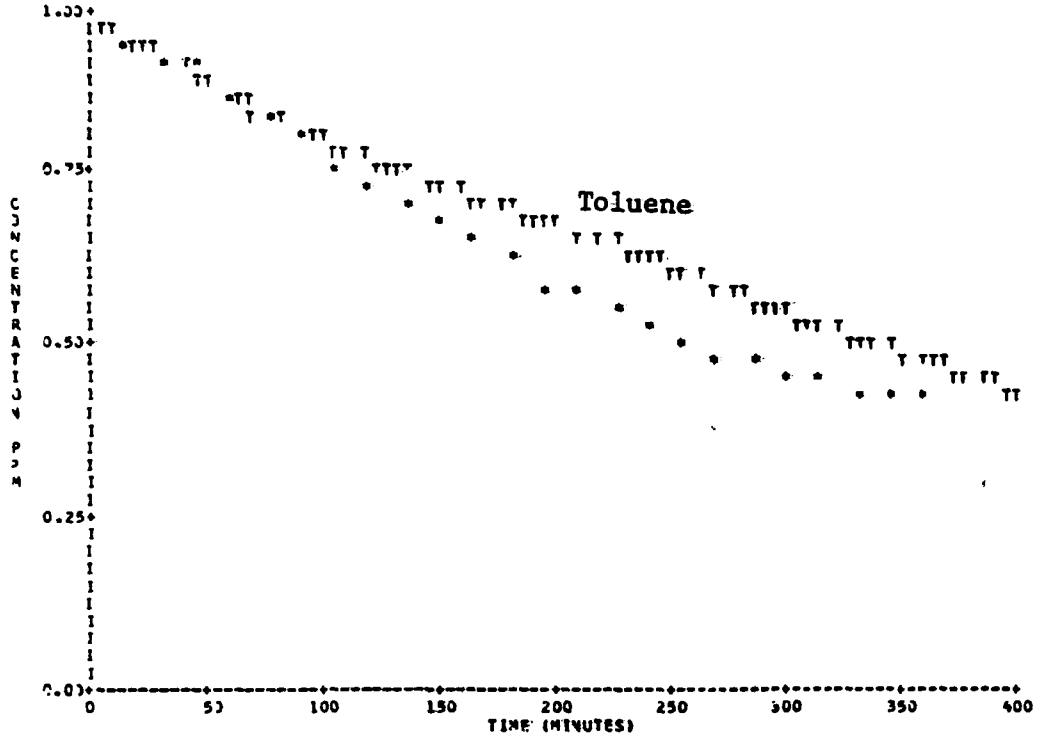

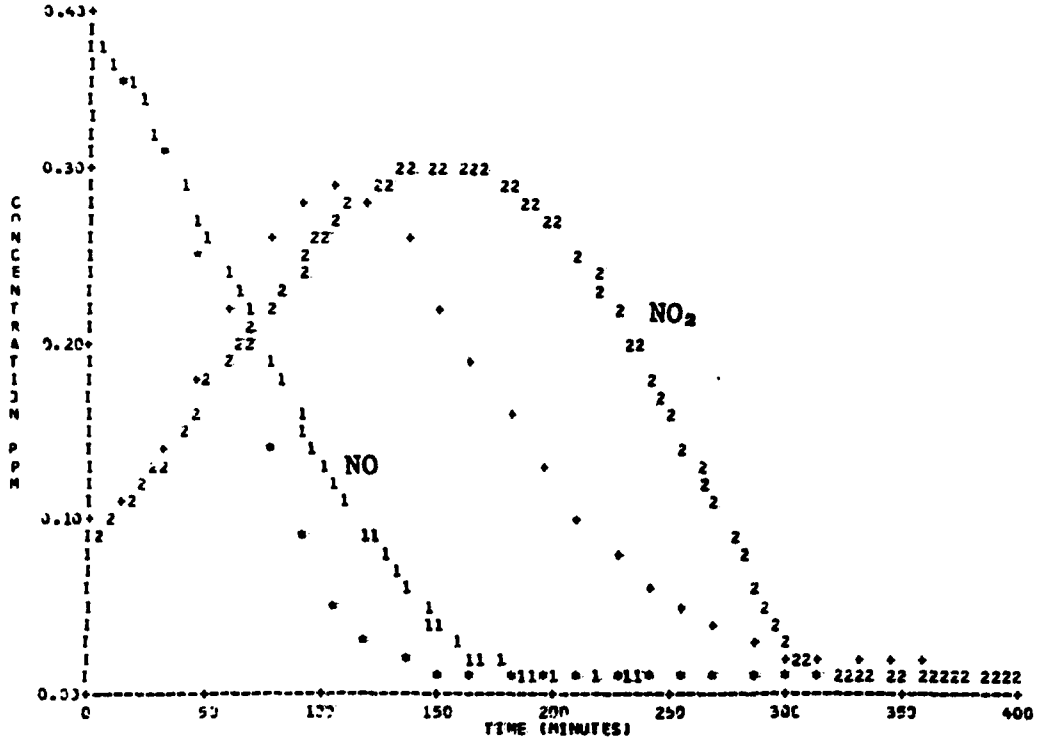

Figure C-4. Simulation of SAPRC EC-80.

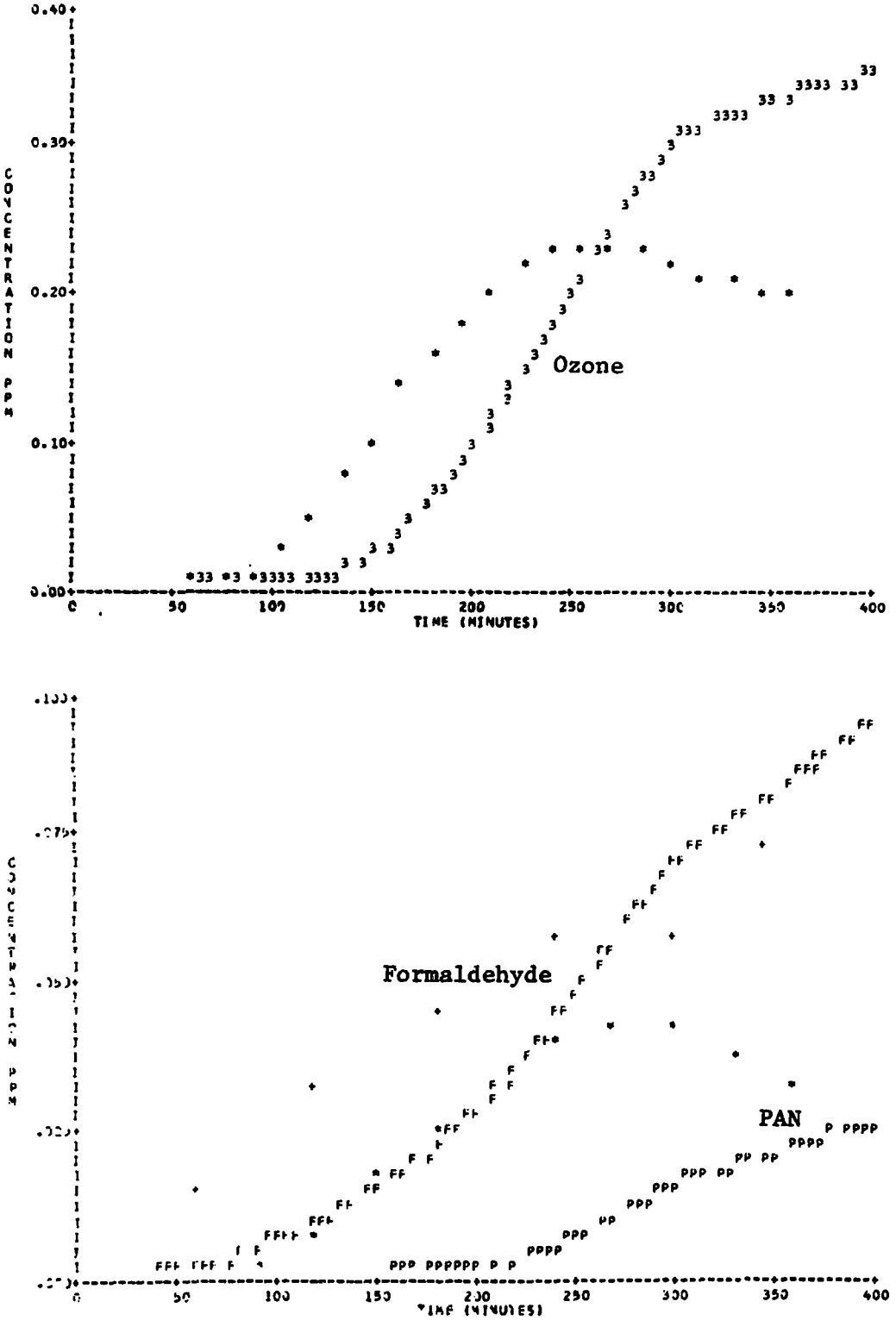

Figure C-4. Simulation of SAPRC EC-80 (Concluded).

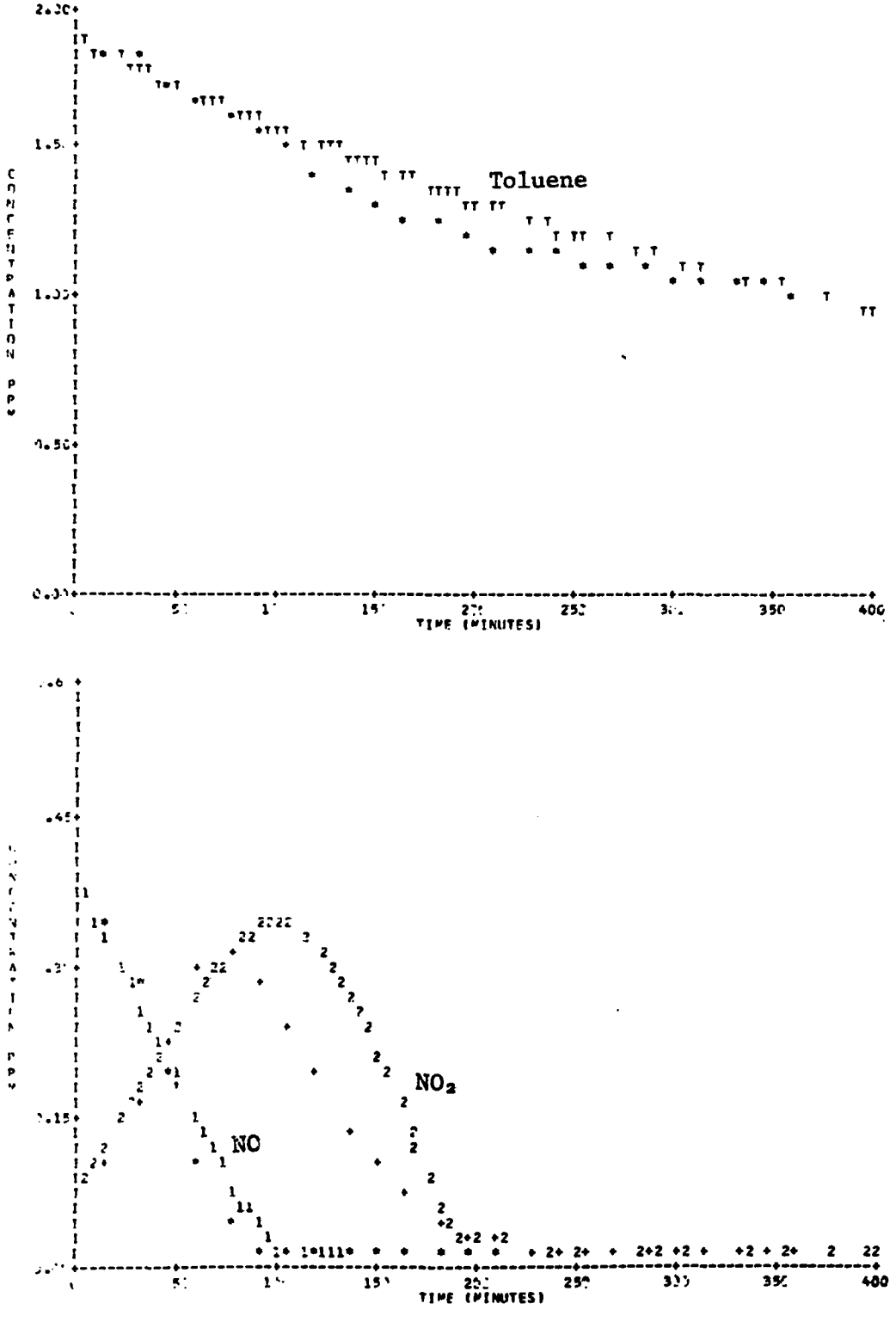

Figure C-5. Simulation of SAPRC EC-81.

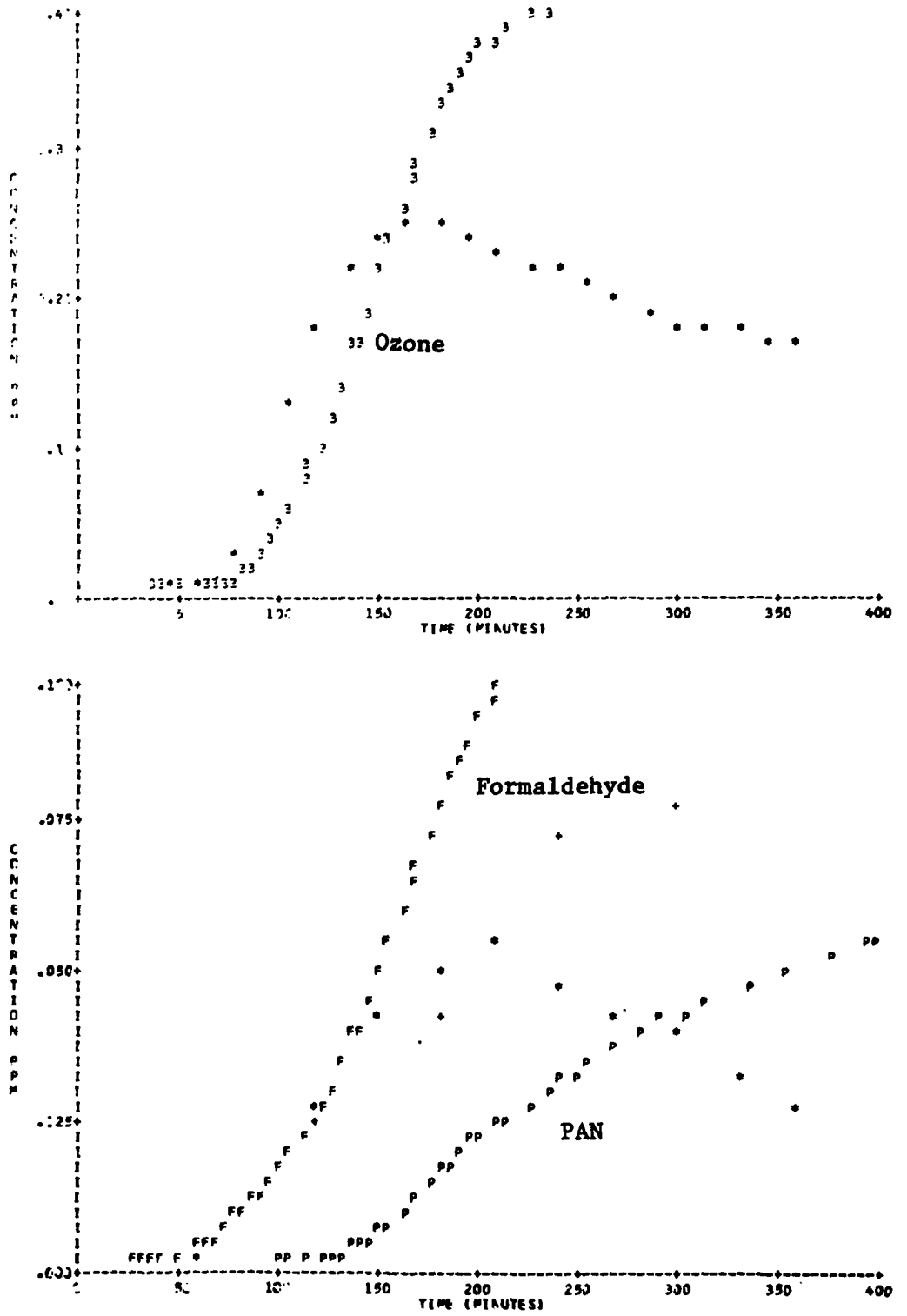

Figure C-5. Simulation of SAPRC EC-81 (Concluded).

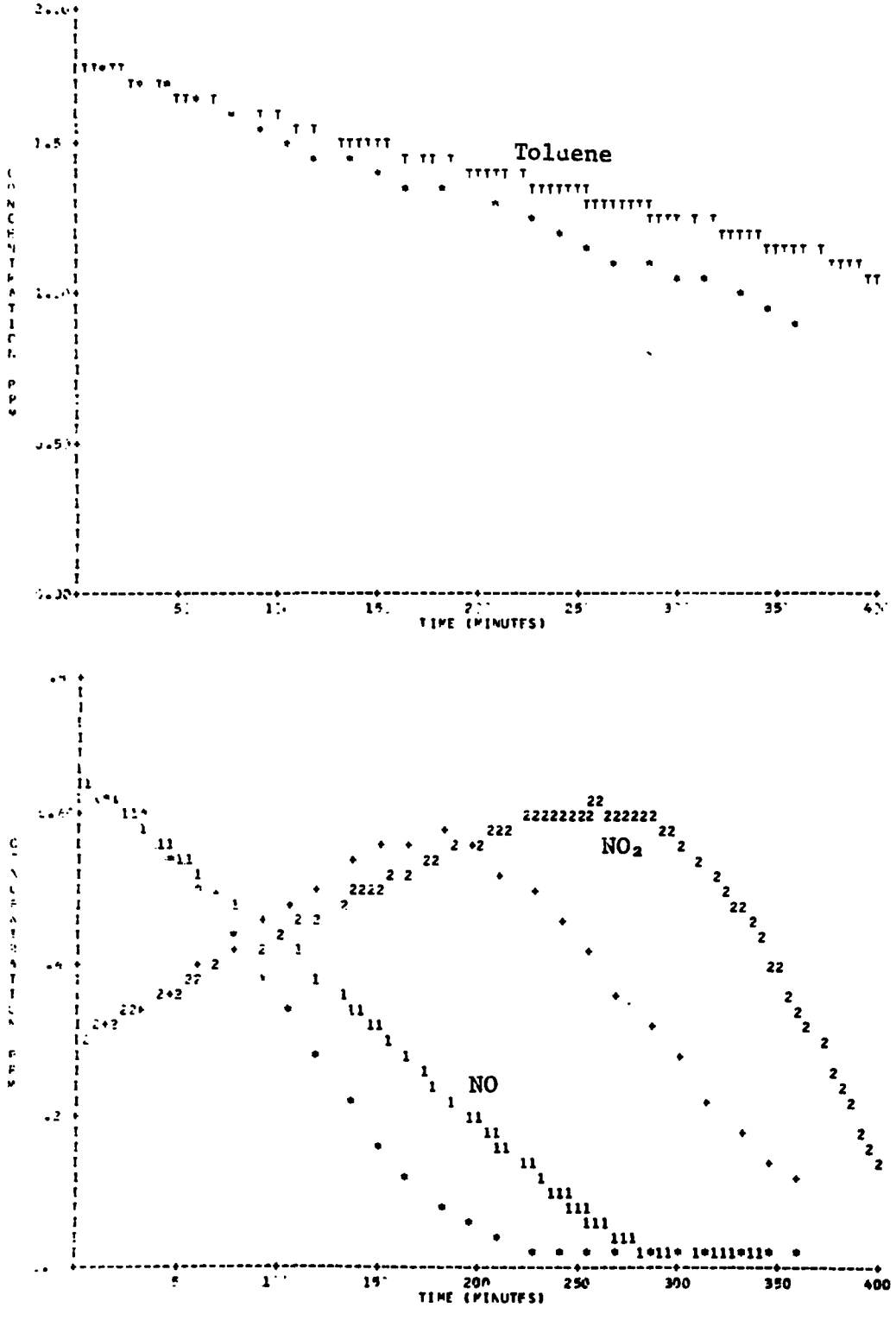

Figure C-6. Simulation of SAPRC EC-82.

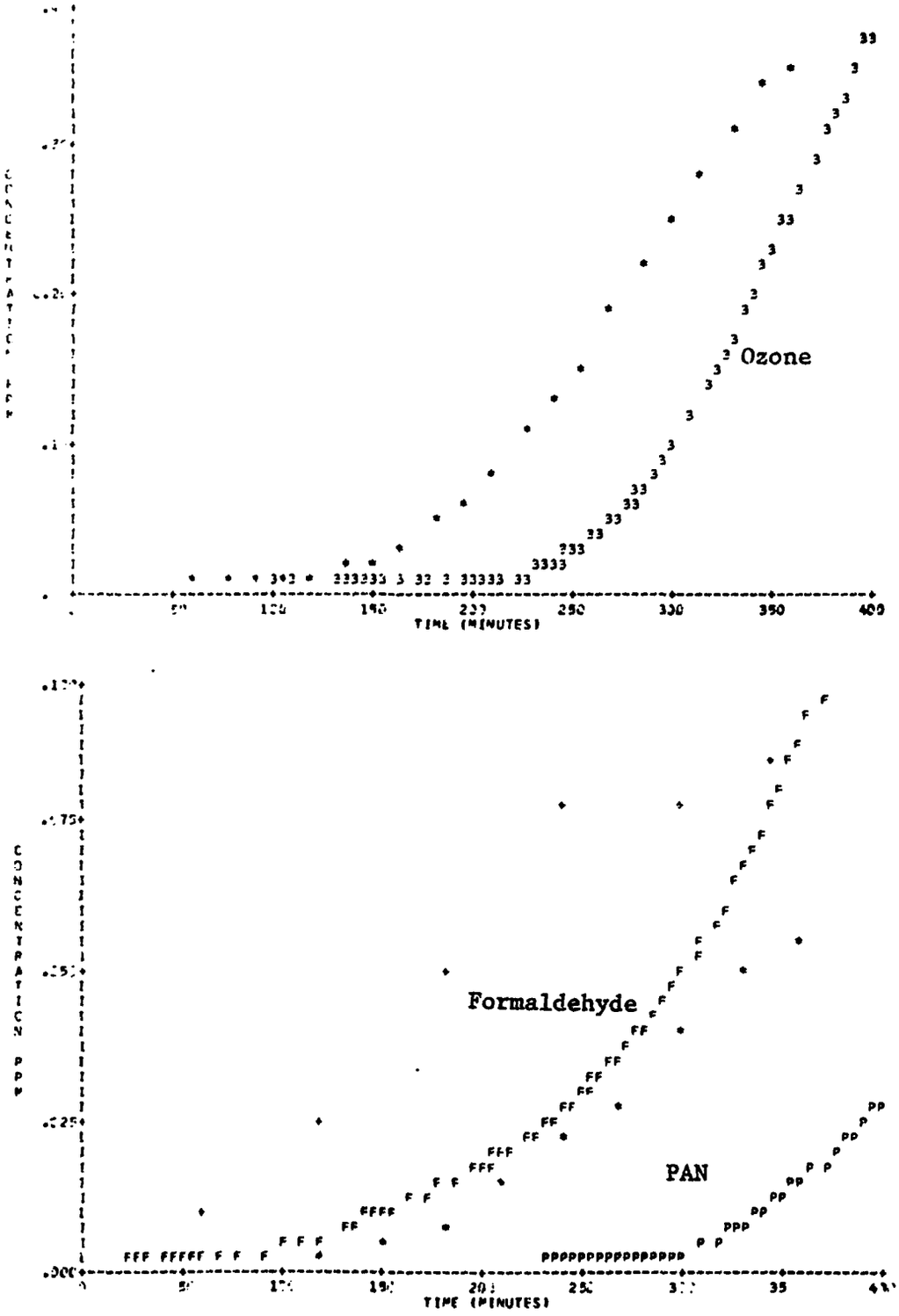

Figure C-6. Simulation of SAPRC EC-82 (Concluded).

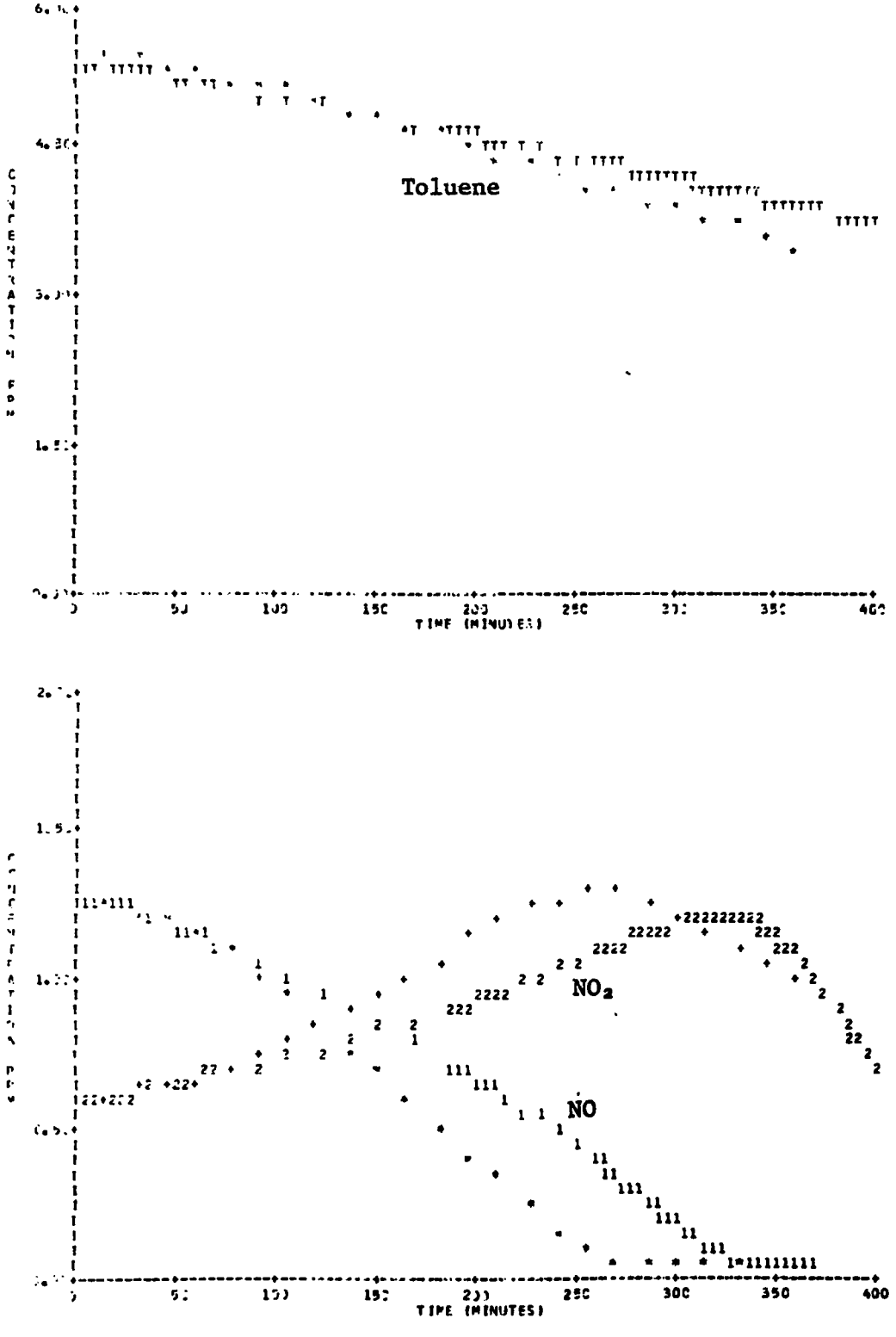

Figure C-7. Simulation of SAPRC EC-83.

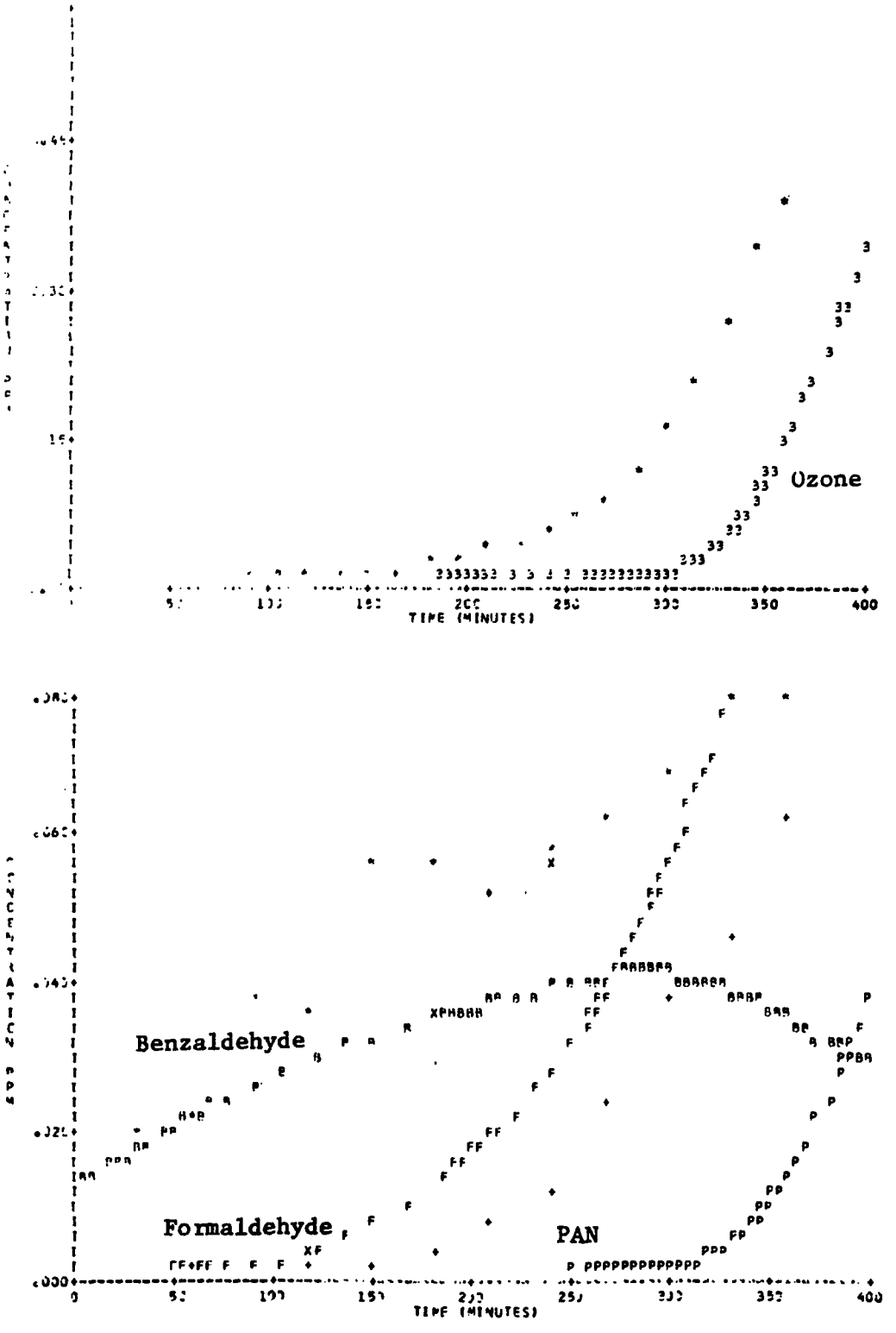

Figure C-7. Simulation of SAPRC EC-83 (Concluded).

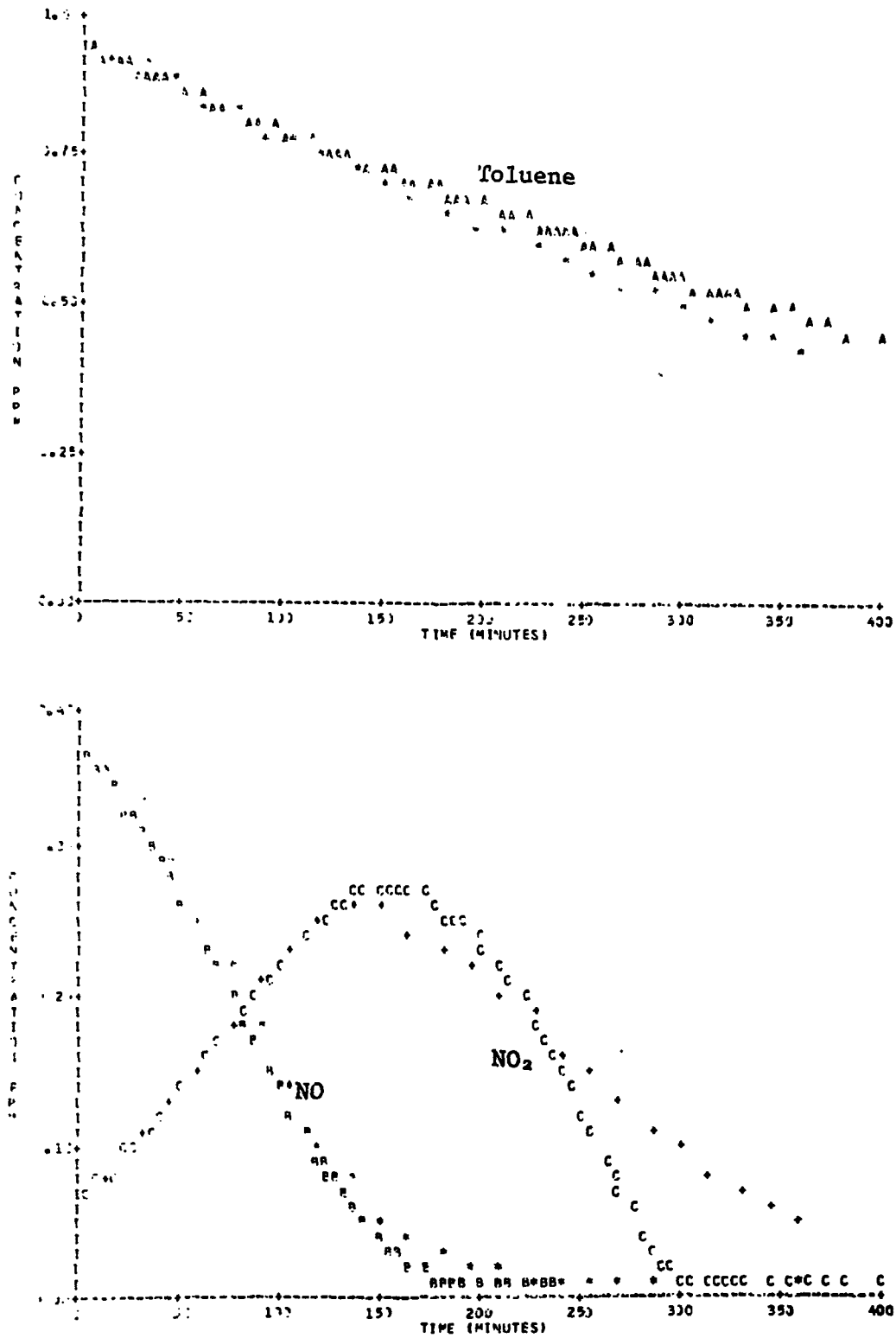

Figure C-8. Simulation of SAPRC EC-84.

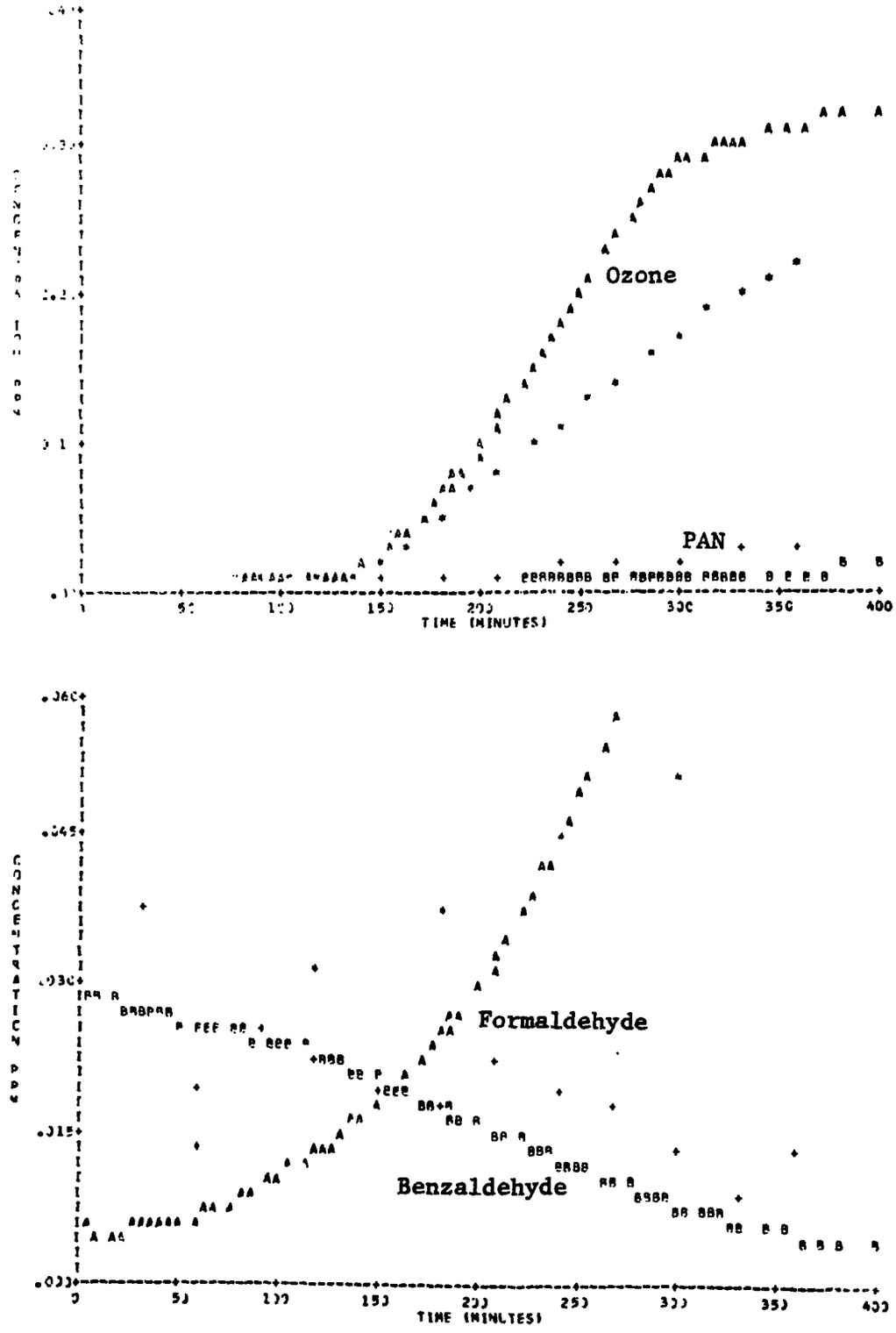

Figure C-8. Simulation of SAPRC EC-84 (Concluded).

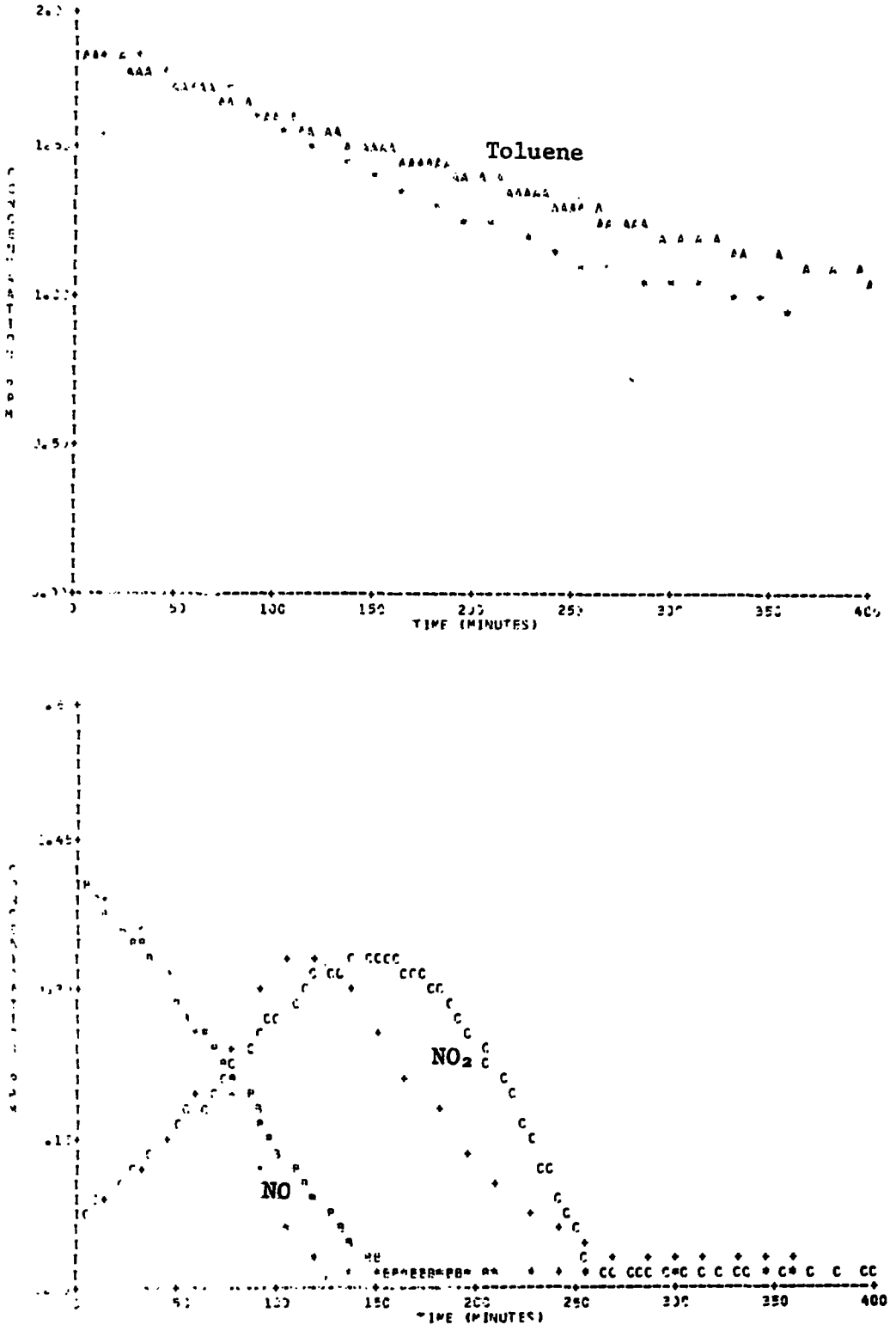

Figure C-9. Simulation of SAPRC EC-85.

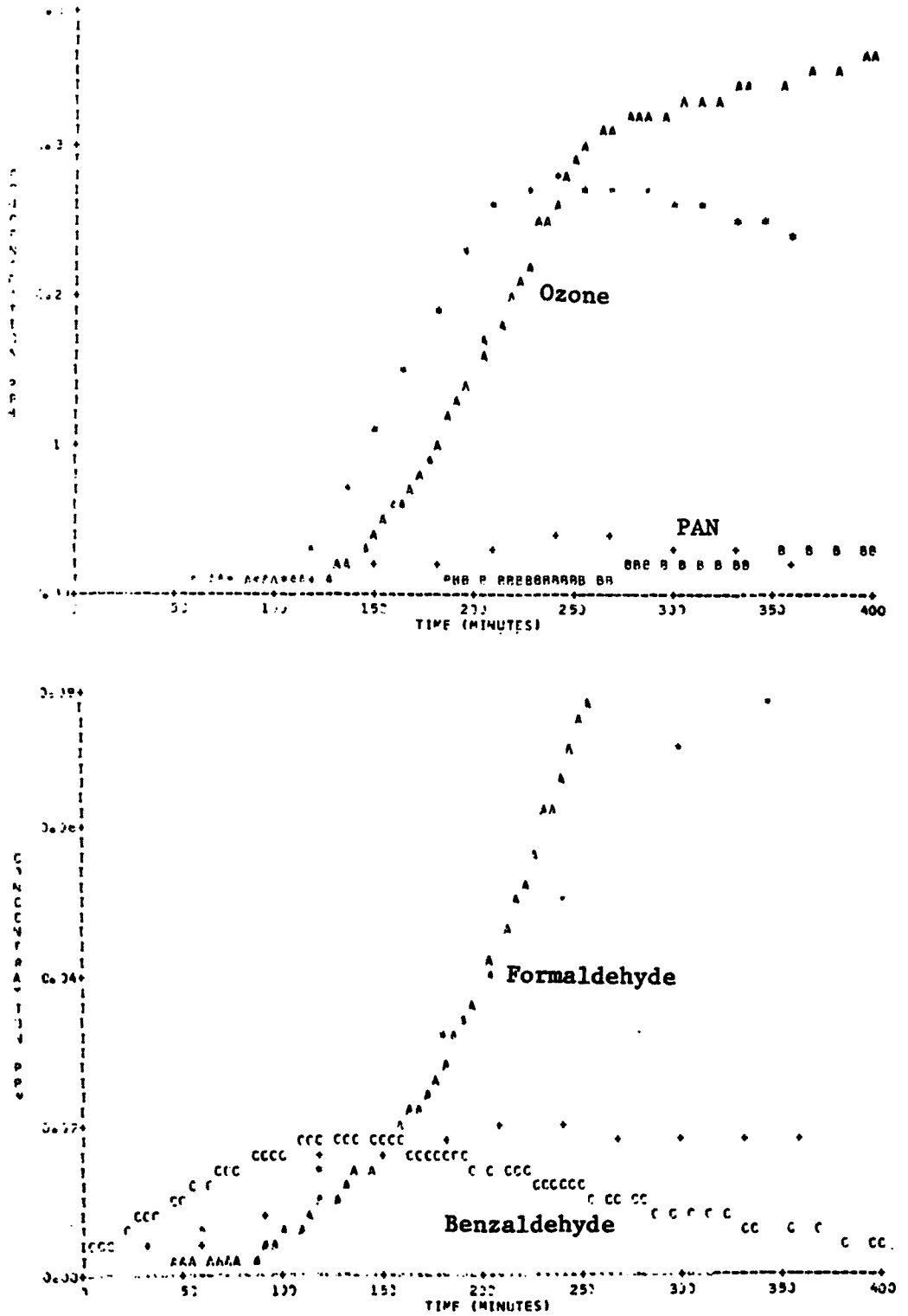

Figure C-9. Simulation of SAPRC EC-85 (Concluded).

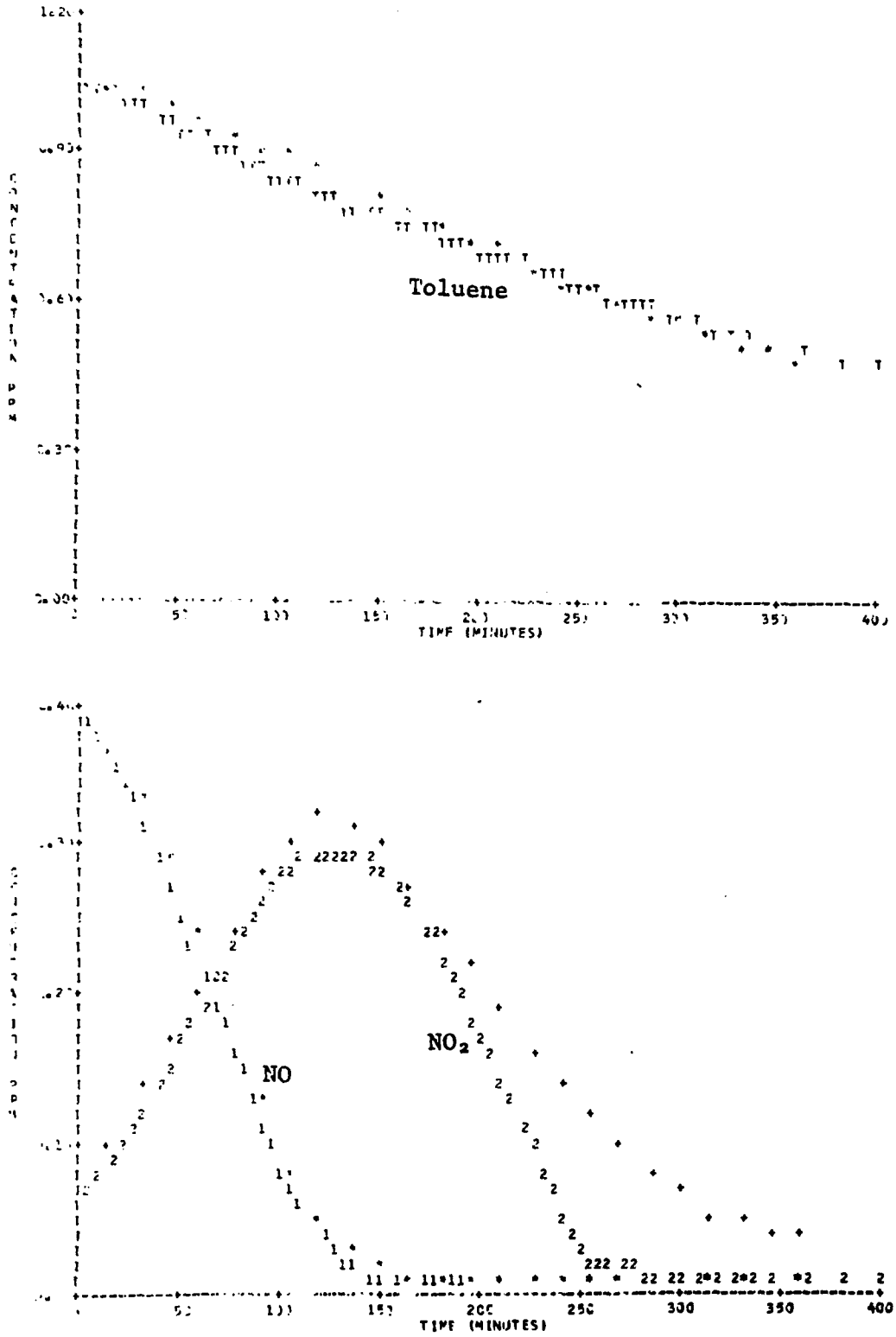

Figure C-10. Simulation of SAPRC EC-86.

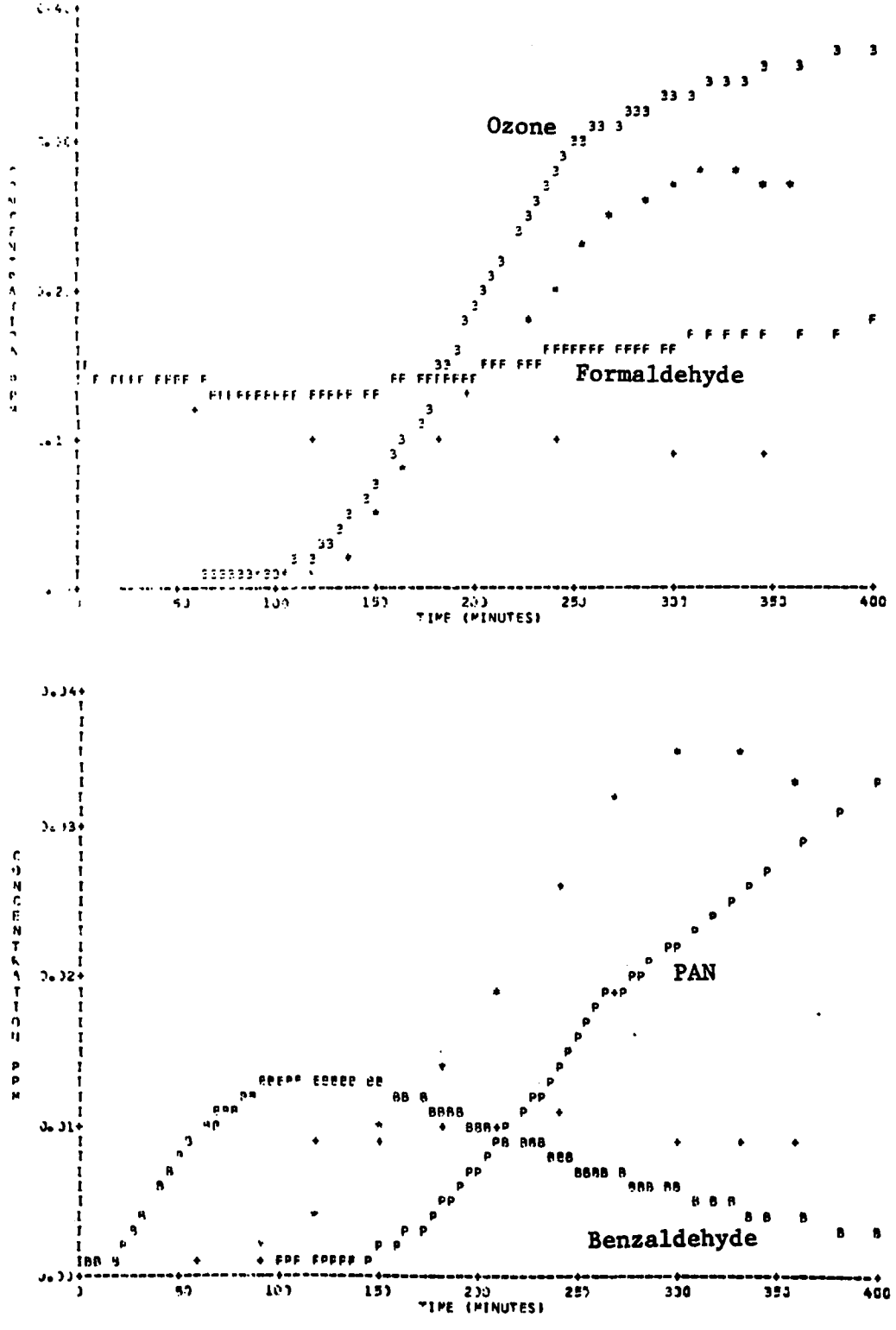

Figure C-10. Simulation of SAPRC EC-86 (Concluded).

REFERENCES

1. J. N. Pitts, Jr., et al., "Mechanisms of Photochemical Reactions in Urban Air," EPA Report 600/3-77-0146, February 1977, and subsequent Quarterly Reports.

2. K. L. Demerjian, J. A. Kerr, and J. G. Calvert, Adv. Environ. Sci., 4, 1 (1974).

3. H. Niki, E. E. Daby, and W. Weinstock, Adv. Chèm. Series, 113, 16 (1972).

4. T. A. Hecht, J. H. Seinfeld, and M. C. Dodge, Environ. Sci. Technol., 8, 327 (1974).

5. G. Z. Whitten and H. Hugo , "Mathematical Modeling of Simulated Photochemical Smog," EPA Report 600/3-77-011, January 1977.

6. M. C. Dodge, "Effect of Selected Parameters on the Prediction of a Photochemical Model," EPA Report 600/3-77-048, June 1977.

7. R. Overend, G. Paraskevopoulos, and C. Black, J. Chem. Phys., 64, 4149 (1976).

8. C. Anastasi, I.W.M. Smith, and R. Zellner, Chem. Phys. Letters, 37, 370 (1976); L. Anastasi, I.W.M. Smith, J. Chem. Soc. Faraday Trans II, 1459, (1976).

9. C. J. Howard, J. Chem. Phys., private communication.

10. P. L. Bevan and G.R.A. Johnson, J. Chem. Soc., Faraday Trans. I, 69, 216-277 (1973).

11. D. D. Davis, J. T. Herron, and R. E. Huie, J. Chem. Phys., 58, 530-535 (1973).

12. K. H. Becker, U. Schurath, and S. H. Seit, Int. J. Chem. Kinetics, 6, 725-739 (1974).

13. R. F. Hampton and D. Garvin, "Chemical Kinetic and Photochemical Data for Modeling Atmospheric Chemistry," NBS Technical Note 866, National Bureau of Standards, Washington, D.C., 1975.

14. W. B. DeMore, Science, 180, 735-737 (1973).

15. A. Harker and H. S. Johnston, J. Phys. Chem. 77, 1153-1156 (1973).

16. E. D. Morris and H. Niki, J. Phys. Chem., 77, 1929-1932 (1973).

17. W. H. Chan, R. J. Nordstrom, J. G. Calvert, and J. H. Shaw, Environ. Sci. Technol., 10, 674-682 (1976).

18. R. Atkinson, D. K. Hansen, and J. N. Pitts, Jr., J. Chem. Phys., 62, 3284 (1975).

18. R. Atkinson and J. N. Pitts, J. Chem. Phys., 62, 3284-3288 (1975).

19. T. T. Paukert and H. S. Johnston, J. Chem. Phys., 56, 2824 (1972).

19a. JANAF Thermochemical Tables, 2nd Ed., D. R. Stull and H. Prophet, Nat. Stand. Ref. Data Ser., Nat. Bur. Stand., 37 (June 1971).

20. F. Stull and H. Niki, J. Chem. Phys., 57, 3671-3677 (1972).

21. R. Walker, Chem. Soc., Spec. Publ. II.

22. L. Batt, R. T. Milne, and R. D. McCullough, Int. J. Chem. Kinetics, 9, 567-587 (1977).

23. D. G. Hendry and R. A. Kenley, J. Amer. Chem. Soc., 99, 3198 (1977).

24. D. M. Golden and G. Smith, Int. J. Chem. Kinetics, in press.

25. H. Niki, P. D. Maker, C. M. Savage, and L. P. Breitenbach, Chem. Phys. Letters, in press.

26. A. C. Baldwin, J. R. Barker, D. M. Golden, and D. G. Hendry, J. Phys. Chem., in press.

27. J. R. Barker, S. W. Benson, G. D. Mendenhall, and D. M. Golden, "Measurement of Rate Constants of Importance in Smog." EPA Report 600/3-77-110, October 1977.

28. S. W. Benson, Thermochemical Kinetics, 2nd ed. (John Wiley and Sons, Inc., New York, 1976).

29. J. R. Barker, S. W. Benson, and D. M. Golden, Int. J. Chem. Kinetics, 9, 31 (1977).

30. D. A. Parkes, Int. J. Chem. Kinetics, 9, 451-469 (1977).

31. G. E. Zaikov, J. A. Howard, K. U. Ingold, Can. J. Chem., 47, 3017 (1969).

32. J. T. Herron and R. D. Penzhorn, J. Phys. Chem., 73, 191 (1969).

33. E. D. Morris, Jr., and H. Niki, J. Chem. Phys., 55, 1991 (1971).

34. W. J. Braun, L. Rajbenbach, and F. R. Eirich, J. Phys. Chem., 66, 1591 (1962).

35. G. Emanuel, Int. J. Chem. Kinetics, 4, 591 (1972).

36. R. I. Martinez, Dissertation Abstracts International, 1976, 6193-B.

37. M. B. Colket, D. W. Naegeli, and I. Glassman, 16th Combustion Symposium, Paper No. 87 (1976).

38. G. Moortgat, private communication and Abstracts from Fifth International Symposium on Gas Kinetics, July 1977.

39. J. G. Calvert, J. N. Pitts, Jr., and D. D. Thompson, J. Amer. Chem. Soc., 78, 4239 (1956).

40. J. Weaver, J. Meagher, and J. Heicklen, J. Photochem., 6, 111, (1976/77).

41. H. S. Johnston and R. Graham, Can. J. Chem., 52, 1415 (1974).

42. R. A. Cox, J. Photochem., 3, 175 (1975).

43. H. S. Johnston and R. Graham, J. Phys. Chem., 77, 62 (1973).

44. H. C. Urey, L. H. Dawsey, and F. O. Rice, J. Amer. Chem. Soc., 51, 1371 (1929).

45. M. Gripps, J. of Chem. Phys., 49, 857 (1968).

46. E.C.Y. Inn and Y. Tanaka, J. Opt. Soc., Amer., 43, 870 (1953).

47. R. D. McQuigg and J. G. Calvert, J. Amer. Chem. Soc., 91, 1590 (1969).

48. J. G. Calvert and J. N. Pitts, Jr., "Photochemistry," (John Wiley and Sons, Inc., New York, 1967).

49. R. Overend and G. Paraskevopoulos, J. Chem. Phys., 67, 674 (1977).

50. R. Atkinson and J. N. Pitts, Jr., J. Chem. Phys., 63, 3591 (1975).

51. D. D. Davis, "Investigation of Important Hydroxyl Radical Reactions in the Perturbed Troposphere," EPA Report 600/3-77-111, October 1977.

52. S. M. Japar, C. H. Wu, and N. Niki, J. Phys. Chem., 78, 2318 (1974).

53. F. Stuhl and H. Niki, J. Chem. Phys., 55, 3904 (1971).

54. R. J. Cvetanovic, Adv. Photochem., 1, 115 (1963).

55. R. Atkinson and J. N. Pitts, Jr., J. Phys. Chem., 78, 1780 (1974).

56. S. M. Japar and H. Niki, J. Phys. Chem., 79, 1629 (1975).

57. H. Niki, E. E. Daby, and B. Weinstock, Advances in Chemistry Series, 113, American Chemical Society, Washington, D. C.

58. H. E. O'Neal and C. Blumstein, Int. J. Chem. Kinet., 5, 397 (1973).

59. J. Herron and R. E. Huie, J. Amer. Chem. Soc., 99, 5430 (1977).

60. N. R. Greiner, J. Chem. Phys., 76, 1919-1924 (1972).

61. A. C. Lloyd, K. R. Darnall, A. M. Winer, and J. N. Pitts, J. Phys. Chem., 80, 789-794 (1976).

62. J. T. Herron and R. E. Huie, J. Phys. Chem., 73, 3327-3337 (1969).

63. R. Atkinson and J. N. Pitts, Jr., J. Phys. Chem., 79, 295 (1975).

64. D. D. Davis, W. Bollinger, and S. Fischer, J. Phys. Chem., 79, 293 (1975).

65. R. A. Perry, R. Atkinson, and J. N. Pitts, Jr., J. Phys. Chem., 81, 296 (1977).

66. R. A. Kenley, J. E. Davenport, and D. G. Hendry, to be published.

67. R. J. O'Brien, unpublished data.

68. R. A. Perry, R. Atkinson, and J. N. Pitts, Jr., J. Phys. Chem., 81, 1607 (1977).

69. D. G. Hendry, unpublished data.

70. J. D. Bevington and J. Toole, J. Polym. Sci., 28, 413 (1958).

71. W.P.L. Carter and J. N. Pitts, private communication.

TECHNICAL REPORT DATA
(Please read Instructions on the reverse before completing)

1. REPORT NO.	2.	3. RECIPIENT'S ACCESSION NO.
EPA-600/3-78-059		

4. TITLE AND SUBTITLE	5. REPORT DATE
COMPUTER MODELING OF SIMULATED PHOTOCHEMICAL SMOG	June 1978
	6. PERFORMING ORGANIZATION CODE

7. AUTHOR(S)	8. PERFORMING ORGANIZATION REPORT NO.
D.G. Hendry, A.C. Baldwin, J.R. Barker, and D.M. Golden	

9. PERFORMING ORGANIZATION NAME AND ADDRESS	10. PROGRAM ELEMENT NO.
SRI International 333 Ravenswood Avenue Menlo Park, California 94025	1AA603 AC-20 (FY-77)
	11. CONTRACT/GRANT NO.
	Contract No. 68-02-2427

12. SPONSORING AGENCY NAME AND ADDRESS	13. TYPE OF REPORT AND PERIOD COVERED
Environmental Sciences Research Laboratory - RTP, NC Office of Research and Development U.S. Environmental Protection Agency Research Triangle Park, North Carolina 27711	Interim 9/76 - 9/77
	14. SPONSORING AGENCY CODE
	EPA/600/09

15. SUPPLEMENTARY NOTES

16. ABSTRACT

This report discusses continuing efforts to develop kinetic mechanisms to describe the formation of photochemical smog. Mechanisms were formulated for the ethene, propene, butene-1, trans-butene-2, n-butane, 2,3-dimethylbutane, and toluene/NO_x systems. Smog chamber data collected at the University of California, Riverside were used to test these mechanisms. The mechanisms are composed of critically evaluated kinetic data for the individual reactions to the extent possible. Where data on specific reactions were not available or were not at the appropriate temperature and pressures, thermochemical techniques were used to estimate or extrapolate existing data to obtain the desired rate data. Whenever thermochemical data were estimated to predict rate constants, error bounds were assigned to the estimates and the resulting rate constants. In only a relatively few cases was it necessary to vary the estimated rate constants within the error limits in order to optimize the agreement between computed and experimental concentration-time profiles. Given the kinetic information currently available, this general approach minimizes the need for adjustment of rate constants and produces mechanisms that are valid representations of the homogeneous gas-phase chemistry of each of these hydrocarbons in photochemical smog formation.

17. KEY WORDS AND DOCUMENT ANALYSIS

a. DESCRIPTORS	b. IDENTIFIERS/OPEN ENDED TERMS	c. COSATI Field/Group
* Air pollution		13B
* Reaction kinetics		07D
* Photochemical reactions		07E
* Mathematical models		12A
* Computerized simulation		14B

18. DISTRIBUTION STATEMENT	19. SECURITY CLASS *(This Report)*	21. NO. OF PAGES
RELEASE TO PUBLIC	UNCLASSIFIED	304
	20. SECURITY CLASS *(This page)*	22. PRICE
	UNCLASSIFIED	

EPA Form 2220-1 (9-73)